Romanian Committee on Large Dams

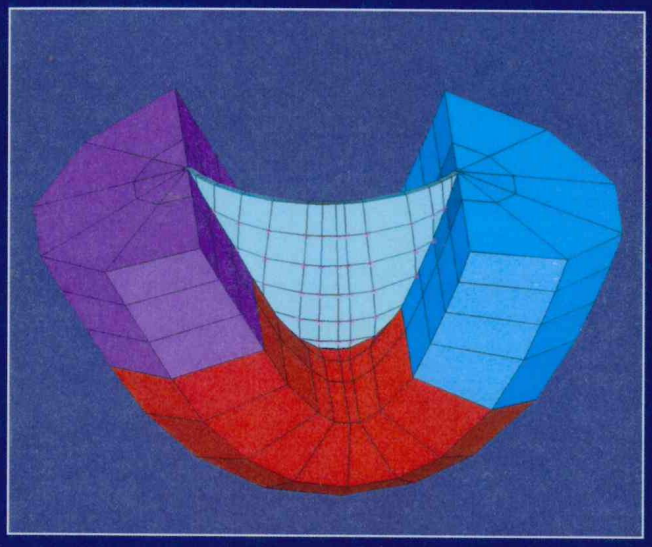

PROCEEDINGS
SEVENTH BENCHMARK WORKSHOP ON NUMERICAL ANALYSIS OF DAMS

Bucharest, Romania
September 24-26, 2003

Organized by

ICOLD
Ad-Hoc Committee on Computational Aspects of Analysis and Design of Dams

PROCEEDINGS
SEVENTH BENCHMARK WORKSHOP
ON NUMERICAL ANALYSIS OF DAMS

ROMANIAN COMMITTEE ON LARGE DAMS

PROCEEDINGS
SEVENTH BENCHMARK WORKSHOP
ON
NUMERICAL ANALYSIS OF DAMS

Bucharest, Romania
September 24-26, 2003

Organized by

I C O L D

Ad-Hoc Committee on Computational Aspects of Analysis and Design of Dams

Publishing coordinators:
ADRIAN POPOVICI and NICOLAE DASCALESCU

Cover figure: Finite Element Mesh for Vidraru Dam – Romania, seismic analysis

Descrierea CIP a Bibliotecii Naţionale a României
Proceedings of Seventh Benchmark Workshop on Numerical Analysis. – Bucureşti: Conspress, 2004
Bibliogr.
Index
ISBN 973-8165-88-1

626/627

Editura Conspress – Technical University of Civil Engineering Bucharest
Cover design & DTP: Press Image
Printing: Profile Graphics

Romanian Committee on Large Dams (ROCOLD)
Telephone: +40-21-307.61.83
Fax: +40-21-312.09.25
E-mail: office@rocold.ro
Web site: www.rocold.ro

FOREWORD

The Seventh Benchmark Workshop on Numerical Analysis of Dams was held on September 24..26 in Bucharest, Romania. This Workshop was the latest in a series of six workshops successfully organized by the ICOLD Ad-Hoc Committee on Computational Aspects of Analysis and Design of Dams and hosted in Bergamo, Italy (1991 and 1992), Paris, France (1994), Madrid, Spain (1996), Denver-Colorado, U.S.A. (1999) and Salzburg, Austria (2001).

The objective of the Benchmark-Workshops corresponds to some Ad-Hoc Committee's Terms of Reference as follows:

●Necessity of creating a stronger link between the observed and the modelled structural behaviour.

●Opportunity to promote numerical modelling improvements to approach safety-related dam problems that do not seem at present approachable in a reliable manner.

●Validation of computational approaches for dams and stimulation of the technical scientific community towards the solution of the problems mentioned in the previous item.

Moreover, the Benchmark-Workshops allow the dam professionals throughout the world, working in design, construction, operation, and also in the educational field to be informed about the most advanced numerical and statistical methods including associated software, to analyze the dams behaviour and to evaluate their safety state.

Consistent with previous Workshops, three themes were selected for the 7th Benchmark Workshop, referring to concrete dams (Theme A), RCC dams (Theme B) and, respectively embankment dams (Theme C). The problems provided for each of that three themes above mentioned were the followings: evaluation of the ultimate strength of gravity dams with curved shape against sliding (formulator: CESI Milan, Italy), thermal analysis of a RCC gravity dam (formulator: Coyne et Bellier, Bureau d`Ingénieurs Conseils, Genevilliers, France) and seepage through an earth dam – foundation system and piezometric level variation (formulator: Technical University of Civil Engineering, Bucharest, Romania).

All the proposed problems were of real interest for the participants in Workshop. A total number of 19 papers containing solutions of the problems, written by 41 authors were submitted to be debated and compared during Workshop works, respectively: 6 papers for Theme A, 7 for Theme B and 6 for Theme C. In the works of the Benchmark Workshop have participated 68 delegates, professionals in computation and design of dams from 12 countries: Austria, Bulgaria, Canada, France, Iran, Italy, Japan, Romania, Russia, Switzerland, United Kingdom and United States of America.

The solutions of the problems were performed using different computation methods as: numerical methods (FEM), statistical analysis, neural networks. Generally, the solutions given by participants were in good accordance with the monitoring data. Some participants could to improve after Workshop, their initial solutions.

This volume contains the formulation of problems, synthesis reports concerning the solutions, given to the problems and the papers submitted by participants. The keynote addresses referring to a topic of major interest in the domain of the analyzed problems are included, too. Some papers presented in the Workshop poster session are included in the last section of this volume.

It is hoped that the solutions presented in this Proceedings will become the terms of reference for the validation of some numerical, statistical, neural networks procedures and, at the same time, will be useful models for practical analyses.

SEVENTH BENCHMARK WORKSHOP
ON
NUMERICAL ANALYSIS OF DAMS

Bucharest, Romania
September 24-26, 2003

Scientific Committee

(Members, ICOLD Ad-Hoc Committee on
Computational Aspects of Analysis and Design of Dams)

G. Giuseppetti, Chairman (Italy)
C. Bossoney (Switzerland)
S. H. Chen (China)
M. Fanelli (Italy)
J. Köngeter (Germany)
Y. P. Liapichev (Russia)
G. Manueco (Spain)
G. Mazzà (Italy)
A. Carrère, Vice Chairman (France)
P. Obernhuber (Austria)
A. Popovici (Romania)
O. Ravaska (Finland)
S.N. Soheili (Iran)
R. Tinawi (Canada)
Y. Uchita (Japan)
C. H. Yeh (USA)

Organizing Committee

Mrs. **G. Giuseppetti** - ICOLD representative
A. Popovici - Romanian Committee on Large Dams
D. Stematiu - Chairman, Romanian Committee on Large Dams
N. Dascalescu - Romanian Committee on Large Dams
A. Abdulamit - Technical University of Civil Engineering of Bucharest
M. Fanelli - Italian National Committee on Large Dams
G. Mazzà - Italian National Committee on Large Dams
A. J. Carrère - Director for Science & Technology, Coyne et Bellier
Mrs. **Ch. Noret-Duchêne** - Chief Engineer, Coyne et Bellier

Remembering GABRIELLA GIUSEPPETTI
10-06-1945 - 17-09-2003

Gabriella was born in Pesaro, a nice small town in central Italy, on 10 June 1945.
She graduated, aged only 23, in Civil Engineering at the Bologna University. After a brief period of activity in Pesaro as a free-lance design engineer, in 1971 she entered the ENEL Centre for Hydraulic and Structural Research (CRIS), where her activity was directed to numerical analysis methods for use in dam safety assessment. In this capacity she showed at once a remarkable drive and attitude; these qualities, together with her sociable, lively nature which made teamwork easygoing, earned her the esteem of her supervisors as well as of her colleagues.
Her qualities brought her to take on ever more prominent assignments within the framework of CRIS, of which she became at last Director in 1995. In the intervening years many an international recognition of her qualities was forthcoming, in connection with her activity within several Technical Committees of ICOLD, in particular the T. C. for Dam Monitoring as well as the T. C. for Computational Aspects in Dam Analysis and Design; she became Chairperson of the latter in 1995. Under her guidance the 4th, 5th and 6th International Benchmark Workshops on Dam Analysis were organised. ICOLD recognised her outstanding contributions by awarding her the title of 'Honorary Member' in the year 2002. The cruel illness against which she struggled valiantly until the end prevented her from contributing in full to the organization of the 7th Benchmark Workshop, held in Bucharest in September 2003.
The years from 1995 to 2002 were difficult ones, coinciding with important changes in the organisation of ENEL, in parallel with analogous trends shown by the big energy corporations on the international scene. As always, Gabriella engaged herself strenuously in the defence of the autonomy and specificity of the CRIS researchers, in open and often tough confrontation with the societal decisions. Gabriella's loyal, open, unrelenting personality earned her, in these circumstances, not only the respect and affection of her colleagues, but also the esteem and recognition even of all those who, in obeisance to the societal decisions, had to act and argue in opposition to her reasons.
Recently, in May 2003, the President of Italian Republic and the Prime Minister of Italy awarded her the coveted title of 'Ufficiale dell'Ordine al Merito della Repubblica Italiana' for the results obtained in the course of her career as well as for the dedication with which she developed her professional activity.
During all those long, busy and often hectic years Gabriella –we like to call her simply by her first name, as she was wont to address all and sundry quite naturally– maintained even at the worst junctures, both societal and personal ones, her zest for life and her character of a serene, cheerful, communicative person. These qualities diffused goodwill and inspired feelings of affectionate friendship among all those –collaborators, colleagues and friends– who frequented her at the workplace or in everyday life. It was impossible to resist her keen sense of humour and her explosive, infectious laughter, and even in the darker hours a witty remark or a smile of hers was enough to relieve the tension.

We shall ever remember her this way, in the image of irrepressible youth of the spirit which for us is indissolubly tied to her personality so rich in strength, loyalty and passionate love for her work and for all aspects of life.

Acknowledgements

The Romanian Committee on Large Dams gratefully acknowledgements the support for organizing the 7th ICOLD Benchmark Workshop on Numerical Analysis of Dams from the following international magazines and Romanian universities and companies:

The International Journal on Hydropower & Dams
Hydro Review Worldwide
International Water Power & Dam Construction

Universitatea Tehnica de Constructii – Bucuresti
S.C. Hidroelectrica S.A.
Autoritatea Nationala "Apele Romane"
S.C. Hidroconstructia S.A. Bucuresti
S.C. Apasco S.A. Maneciu – Prahova
Institutul de Studii si Proiectari Hidroenergetice (ISPH) – Bucuresti
S.C. AquaProiect S.A. – Bucuresti
Institutul de Studii si Consultanta Energetica (ISCE) – Bucuresti

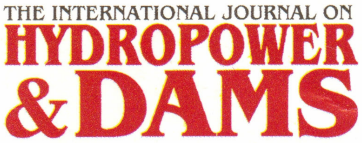
THE INTERNATIONAL JOURNAL ON
HYDROPOWER
&DAMS


HRW
CONNECTING
THE WORLDWIDE
HYDRO COMMUNITY


INTERNATIONAL
Water Power
& DAM CONSTRUCTION


UNIVERSITATEA TEHNICA
DE CONSTRUCTII BUCUREST


HIDROELECTRICA S.A.


APELE ROMÂNE


S.C. HIDROCONSTRUCTIA S.A.


apasco


ISPH


AP
AQUAPROIECT S.A.


ISCE

Table of Contents

7th BENCHMARK WORKSHOP ON NUMERICAL ANALYSIS OF DAMS
September 24-26, 2003 - Bucharest, ROMANIA

THEME A

EVALUATION OF ULTIMATE STRENGTH OF GRAVITY DAMS WITH CURVED SHAPE AGAINST SLIDING

Michele FANELLI
Consultant
'INVITED LECTURE' FOR THEME A OF THE 7th BENCHMARK-WORKSHOP ON COMPUTATIONAL PROBLEMS OF DAM ANALYSIS AND DESIGN
(BUCHAREST, 24-26 September 2003)

RE-ASSESSING OLD CONCRETE DAMS: THE CASE OF GRAVITY DAMS WITH CURVED PLAN

I- THE NEED FOR REASSESSMENT OF OLD DAMS

Dams more than some decades old constitute a sizable –and growing- percentage of the total number of existing dams. Such structures were designed on the basis of technical knowledge and codes of practice that may have become obsolete in the intervening time, thus posing the question whether their 'safety' is sufficiently guaranteed or should be assessed anew in the framework of the new criteria. Besides, the external actions they are called to withstand may be appraised, on the basis of recent developments, to be appreciably more taxing than it was supposed at the time of their initial conception. At last, the material they were built with may have suffered degradation due both to aging and to the action of aggressive agents.

In the way of examples of circumstances calling for re-assessment, suffice it to consider:

a) the case of the adoption of more stringent Regulations or Codes of practice, e. g. in respect of the resistance to sliding for gravity dams[1];
b) the revision of seismic zoning, as a consequence of which the dam may be called to withstand earthquakes where this action was not initially foreseen, or to withstand seismic ground motions more severe than anticipated in the original design;
c) the case of gravity dams designed without taking into account uplift pressures, while present Regulations call for their inclusion among the standard loads;
d) the case of drainage systems having become clogged or ineffective, so that the uplift pressures are substantially greater than they would have been in the presence of effective drains;
e) the case in which the reservoir has become heavily silted, so that the horizontal load on the upstream face of the dam has been substantially increased;
f) the case of materials having been damaged by leaching, erosion, scouring, adverse chemical reactions; etc.

In some cases, the dam in question may have been designed with overabundant reserves of strength, so that even after a reappraisal carried out with up-to-date criteria it will appear to qualify; but in many cases it will turn out that the dam –despite an observed flawless performance in the past- appears not to comply with the letter of present-day regulations. The problem then arises what to do, and in principle only a handful of options are open for the owner/operator of the dam:

-to reduce the operating as well as the maximum level of impoundment, so that it can be demonstrated that under these modified loading conditions the dam is in accordance with the official prescriptions;

-to plan a set of interventions on the dam body so as to recover the lacking reserves of strength or to lower the level of adverse actions (e.g. buttressing a gravity dam with additional concrete or with a downstream earthfill shoulder; re-drilling of drainage holes or erection of an upstream concrete shoulder provided with effective drains; installing vertical post-tensioned steel cables to improve the ratio between vertical and horizontal forces in the sliding safety evaluation; etc.).

-to effect additional analyses, with tools more refined than those of 'current practice' the Regulations or Codes of practice call for –remaining of course in consistency with demonstrable physical circumstances-, aiming at documenting that the dam is in fact 'safe' (this last course of action appears to be particularly reasonable in presence of a record of past satisfactory behaviour). Indeed, in many countries there is explicit mention in the Regulations that it is within the faculties of the designer –or the responsible for the dam

[1] In most countries, the official Regulations now prescribe that existing dams should be analysed and certified according to the current version of said Regulations, irrespective of the period of their design/construction.

'safety'- to use more sophisticated methods of analysis in producing the proof that the dam complies with the safety standards, the 'common practice' standard methods being considered as a sort of minimum –hence cautionary- requirement that can be superseded if more accurate evaluations can be effected. This explicit provision is clearly stated, for instance, in the text of the new Italian Regulations (Comma 11, 'Stability Analyses and Resistance Assessments', where it is explicitly foreseen that the method used may be '*not belonging to the common domain*' of professional practice, in which case the method in question must be '*thoroughly explained, illustrating it in detail, down to the final formulation*').
The first two options, anyway, entail grievous economic expenses, so that the third option is to be actively pursued whenever feasible. This brings the problem within the province of the Terms of Reference of our Working Group (see also footnote 3) and is the rationale underlying the choice of Theme A of the present B. W. This is a ground where the rational analytical methods are in tight interaction with the provisions of official Regulations and Codes of practice, highlighting the fact that our profession cannot operate purely within the 'ivory tower' of scientific research.

II- THE CASE OF GRAVITY DAMS WITH 'INSUFFICIENT' VERTICAL SECTION AND WITH CURVED PLAN

Restricting now our attention to the case of old concrete dams of the gravity type, it is to be remarked that not a few of these structures were designed and built with a longitudinal axis that is not rectilinear, but follows instead a curved plan; thus the body of the dam is a portion of a solid generated by a typical cross-section extruded not in a translatory mode (i. e. along a straight line normal to the typical section), but in a rotational mode (i. e. along a cylindrical surface to which the successive cross-sections are all perpendicular; the dam volume is thus delimited by the intersection of the foundation surface with the torus generated by the rotation of the typical triangular section around the axis of the reference cylinder).
This particular provision was adopted, often implicitly, in order to endow the dam with an additional resistance capacity which was not, however, explicitly taken into account in the original stability analyses (also for lack of the proper analytical tools at the time of dam design).
Moreover, many of these dams have a small ratio of crest length to height (often less than 2); this, combined with the huge base thickness, gives the dam body a compact shape. The last important factor (in the light of what follows) lies in the generally high ratio between the elastic modulus of concrete in respect of that of the foundation mass.
It turns out that many of these dams, if analysed with the normal criteria adopted for straight-axis gravity dams, do not comply with the up-to-date regulatory requirements in the matter of 'global stability' analyses, especially so as concerns the 'factor of safety against sliding', their cross-section being insufficient to satisfy the required criteria if analysed simply as a section of a rectilinear gravity dam; more accurately, the ratio $f = \frac{H}{V}$ of horizontal forces H to vertical ones V in such a 2-D analysis often exceeds the maximum value indicated as acceptable by the official Regulations (e. g. 0.75 for Italian Regulations, with some overshooting allowed for exceptional actions such as earthquakes).
The problem, in the light of the background illustrated in the preceding paragraph, is then in the first place to verify whether there are more refined criteria that can show an actual adequacy of the dam by taking into account, in a quantitative way, the contribution of the plan curvature to the dam stability.
The first –and simplest- idea that might come to mind, i. e. to analyse the dam as an arch-gravity structure, must be rejected for several reasons (at least as far as a linear-elastic analysis is contemplated; see § IX), among which:

- the high thickness-to-height and thickness-to-length ratios make the 'arches' from mid-height down very squat in shape, thus incapable to provide a supporting action without incurring in unacceptable (by Regulatory standards) horizontal tensile stresses;

- the joints between adjoining monoliths are not normally grouted in this type of dams[2], thus the monoliths would have to be displaced downstream before the arch supporting action can take place; etc.

Thus ad-hoc analytical tools should be developed to deal with the problem in hand. The preceding remarks suggest the following guidelines:

- the analysis should be of the non-linear type, taking into account both the possible presence of open joints and the possibility of monolateral contact along the foundation (and, if this is required, along the joints);
- it should take into account the fact of the axis curvature and the presence of joints;
- it should, as far as possible, be in harmony with the regulatory criteria normally used for the global stability analysis of straight-axis gravity dams; ideally, the ad-hoc tools in question should yield back these 'normal' regulatory criteria when the radius of curvature of the reference cylinder is made to tend to infinity (the curvature is made to tend to zero, the dam axis becoming rectilinear).

Probably there is not a unique conceptual framework (a unique 'model') satisfying the above requirements, and in this context it will be most interesting to compare the different approaches taken by the participants in Theme A of the present B. W., as well as to compare the final results of their analyses.

In the meantime, I propose to illustrate in the following a methodology (formulated initially by myself and later developed into a user-friendly software package with the help of many colleagues of mine, belonging to ENEL/CRIS and to ISMES) which appears to comply with the above-defined requirements and which has been, of late, applied to a number of ancient Italian dams of the type here considered, with satisfactory results. It is based on an original non-linear approach in which the dam and its constituent parts are treated as rigid bodies, while the foundation mass is modelled as an elastic semi-infinite space; it yields, as required, the usual stability criteria in the case of dams with rectilinear axis and it allows to obtain, in the framework of a unified procedure, also estimates of the contact stresses on the foundation, which must be checked against the prescribed upper limits. The procedure does not generate a unique solution[3], but provides instead a range of solutions, each one corresponding to a different value of the friction parameter f^* and to a different set of contact stresses; if an acceptable solution (both in terms of f^* and of contact stresses) lies within the domain of the multiple solutions found, the dam is to be considered safe. The global (rigid-body) equilibrium conditions can be checked not only for the dam as a monolithic body[4], but also separately for each monolith or for parts thereof [see § V].

III- THE CONCEPTUAL MODEL FOR A POSSIBLE RIGID-BODY ANALYSIS TAKING INTO ACCOUNT THE REAL GEOMETRIC AND MECHANICAL CONDITION OF THE WHOLE DAM, OR OF A DAM MONOLITH, IN A CURVED-AXIS GRAVITY DAM

Some of the dams here being considered, dating back to the first years of the 20th century, were built of stone masonry and without construction joints: they partake since their birth of the scheme of the monolithic body. Let us treat, however, the more common case of concrete dams with vertical (radial) construction joints between adjacent elements.

To begin with, the joints being radial ones (hence the joint planes converge downstream towards the curvature axis), if they are closed (or if they have been effectively grouted) the generic dam element would not be free to slide horizontally downstream independently of the

[2] It must be noted, however, that a few of these dams, built of stone masonry, were not provided with construction joints and thus are in principle monolithic bodies; irregular cracks, though, can alter this theoretical condition.

[3] This character (multiple solutions) could be considered as a theoretical drawback, insofar as intuition suggests that the equilibrium is reached in a single manner (and someone could also object that our W. G. should deal mainly with 'scientific' methodologies); however, the practical value of the method as a way of documenting the compliance of the structure with official prescription is not impaired (and it should be remembered, too, that our W. G. is concerned with every rational tool that can be of use to the profession) . Moreover, the method does give a unique solution in the case of a straight-axis dam with a plane foundation [see § VII], which is the case implicitly assumed in the Regulations for gravity dams; so no contrast is generated with the ordinary cases.

[4] Several dynamic-excitation tests carried out on dams of this type have consistently yielded frequencies and modal shapes that can only be interpreted under the assumption of monolithic behaviour, i. e. of mutual support actions transmitted across the joints between the dam elements.

others, as in the rectilinear-axis case. Indeed, it would find itself wedged between the adjacent elements, whose presence would provide a geometrical constraint impeding such a movement, unless the whole dam as a single three-dimensional body could slide 'en bloc' downwards.
If the joints are not grouted and the adjacent elements are not in mutual contact, the typical joint aperture being a, the radius of curvature R and the distance between two adjacent joints D, every single element would be allowed, from the kinematic point of view, only a limited freedom of radial movement. Indeed, after a downwards displacement of the order of $\frac{a.R}{D}$ (if the elements all should move simultaneously), or at most of $2.\frac{a.R}{D}$ (if only the element in question should slide)[5], it would enter into contact with the adjacent elements. Once all the elements are in contact, the dam body would then behave as a single 3-D body (see **FIG. 1**). First of all it is, therefore, necessary to examine the kinematic and static behaviour of such a solid body, and only in a second phase consider (as required by the Regulations) the stability of the tallest element (and, if the case be, also of the remaining elements and of the element parts).
The physical intuition, indeed, suggest to carry out the stability check in three steps:
-in the first step, an a-priori evaluation is made of the order of magnitude of the downwards displacements, if any, required in order to bring the elements into contact; if these displacements are restricted to some millimetres, or a few centimetres at most, they can be judged as tolerable without major dislocations;
-in the second step (supposing the first step has been passed with favourable results) the stability of the whole 3-D dam body is checked in respect of the downwards sliding and other possible movements. In this step the dam is treated as a rigid body on a compliant foundation, acted upon by deadweight, by the maximum hydrostatic thrust, by the uplift forces and by the seismic forces, if any;
-in the third step, starting from the results of the preceding step (see further on), the stability check of single dam parts can be performed (these parts being the single dam elements and parts thereof, e. g. the parts of a monolith above surfaces separating pouring concrete lifts).
In the following these qualitative criteria are developed according to the dictates of the kinematics, and of the static equilibrium conditions, of a rigid body reposing on a compliant medium.

IV- THE SYMBOLIC FORMULATION OF THE RIGID-BODY ANALYSIS OF THE WHOLE DAM, WITH PARTICULAR EMPHASIS ON THE SLIDING STABILITY CHECK

In the proposed analysis it is necessary (contrary to what happens in the usual 2-D analysis) to determine first of all the distribution of normal and tangential stresses over the 3-D contact surface between concrete and bedrock, because in the sliding safety check the active and the resistant forces must be projected along a direction which is not the same for all the tangential stresses, the latter being in general variously oriented. For the same token, also the normal stresses contribute, in general, to the sliding equilibrium equations. It becomes necessary, therefore, to formulate a plausible mathematical model allowing, as simply as possible, to evaluate this stress distribution. Moreover, this formulation must be compatible with the usual 2-D analysis for straight-axis gravity dams, in the sense that it should yield the usual global equilibrium criteria when applied to the latter type of dams [in this latter context see § VII].
The starting point is taken to be the equilibrium condition of a 3-D rigid body having the shape and the density of the dam under scrutiny, in monolateral, no-tension contact with an elastic, semi-indefinite body. The contact surface has of course the actual 3-D shape of the dam footprint on its foundation.
The assumption of a rigid-body behaviour, indisputably a limit schematisation, can be justified in the circumstances by the following considerations:
-the rigid body equilibrium conditions must in any case be satisfied by the dam as well as by all parts thereof;
-the compact shape of the dams in question, together with the generally low ratio between the YOUNG modulus of the bedrock and that of concrete, make the assumption of a rigid-body

[5] Since the orders of magnitude are as follows: $a = 0.5cm, \quad R = 100 \div 250m, \quad D = 15m,$ the downwards displacements required to close the joints are of the order of a few centimetres at most.

behaviour more acceptable for this type of dam than for other types (it is evident that such an assumption would be untenable, e. g., for arch or arch-gravity dams);
-the results of in-situ dynamic excitation tests carried out on several dams of this type showed a 'collective' behaviour of the different dam elements which is very nearly that of a monolithic body (see § VI); it is worth mentioning that such a behaviour has been found, sometimes, even for straight-axis gravity dams.
Let us see now how one could tackle the problem of determining the contact stresses distribution on the basis of the preceding considerations.

A)-THE KINEMATICS
An unconstrained 3-D rigid body is generally endowed with six degrees of freedom. With respect to a Cartesian reference trihedron (orthogonal axes $x,\ y,\ z$), let G be an arbitrarily chosen point rigidly tied to the body (e. g. its barycentre). The vector displacement of the point G , denoted by $\vec{u}(G)$ and assumed to be a small quantity of the first order, is defined by its three Cartesian components $u_x(G),\ u_y(G),\ u_z(G)$; every small rigid motion of the body is then defined by these three components together with the amount of three small rotations (one around each of the three axes) that we denote by $\omega_x,\ \omega_y,\ \omega_z$, which define a pseudo-vector $\vec{\omega}$ (again to be considered as an infinitesimal of the first order). These six quantities suffice to define the displacement of every other point of the body; in fact, for every such point P_j the relevant vector displacement is given by:

$$\vec{u}(P_j) = \vec{u}(G) + \vec{\omega} \wedge (P_j - G) \qquad \text{(IV.1)}$$

(The six degrees of freedom reduce to only three –two displacements and one rotation- in the case of a symmetrical dam on a geometrically and physically symmetrical foundation, see § VII and **FIG. 2**).
If P_j be now a point of the dam-foundation contact surface, and $\vec{n}$ be the unit vector perpendicular to that surface at P_j [6], it is possible to express the normal, respectively the tangential component of the local dam displacement at P_j in vector notation as follows:

$$u_n(P_j).\vec{n}(P_j) = \left|\vec{u}(P_j) \times \vec{n}(P_j)\right|.\vec{n}(P_j) \qquad \text{(IV.2)}$$

$$u_t(P_j).\vec{t}(P_j) = \vec{n}(P_j) \wedge \left[\vec{u}(P_j) \wedge \vec{n}(P_j)\right] \quad , \qquad \text{(IV.3)}$$

where $\vec{t}$ denotes a unit vector tangent at P_j to the contact surface and directed as the double vector product figuring in the right-hand side of eq. (IV.3)[7].
In the equations of equilibrium that follow the six degrees of freedom:

$$u_x(G),\ u_y(G),\ u_z(G)\ ,\ \omega_x,\ \omega_y,\ \omega_z \qquad \text{(IV.4)}$$

implicitly entering eqs. (IV.2), (IV.3) by virtue of eq. (IV.1), are to be regarded as the primary unknowns of the model in hand.

B)-THE CONTACT STRESSES; THE CHOICE OF 'CONSTITUTIVE EQUATIONS' FOR THE FOUNDATION
At this point it is necessary to postulate a relationship between the displacement components at the generic contact point and the local reaction (in terms of normal and tangential stress components) of the underlying foundation mass. Different options could be chosen; the simplest one is to admit the following 'constitutive laws', inspired by the well-known WINKLER hypothesis or by the VOGT treatment.

---

[6] It is assumed that $\vec{n}$ is directed from the dam body into the foundation mass; thus if $u_n(P_j)$ is positive it means that the dam stays in contact with the foundation at P_j , while if $u_n(P_j)$ is negative the dam tends to be detached from the foundation at P_j .

[7] Note that the direction of $\vec{t}$ is not known beforehand, depending on the solution of the equilibrium equations, see IV.C).

The normal component $F_n(P_j)$ of the local contact stress is taken to be proportional to the normal component of displacement $u_n(P_j)$, see (IV.2), whenever the latter is positive, and to be zero whenever it is negative (condition of monolateral contact):

$$\vec{F}_n(P_j) = -K.u_n(P_j)\vec{n}(P_j) \quad \text{when} \quad u_n > 0 \ , \tag{IV.5}$$

$$\vec{F}_n(P_j) = 0 \quad \text{when} \quad u_n < 0 \ ,$$

where K is a foundation stiffness parameter (see further on). Moreover, it can be assumed (under conditions of incipient sliding) that the tangential component of the local contact stress be directed in the opposite sense as the unit vector $\vec{t}$, see (IV.3), and its intensity be proportional to the normal component (IV.5) with a COULOMB-friction factor of proportionality, f^* :

$$\vec{F}_t(P_j) = -f^*.K.u_n(P_j)\vec{t}(P_j) \quad \text{when} \quad u_n > 0 \ , \tag{IV.6}$$

$$\vec{F}_t(P_j) = 0 \quad \text{when} \quad u_n < 0 \quad [\text{and consequently} \quad \vec{F}_n(P_j) = 0\,] \ . \tag{IV.7}$$

It should be noted that, as a consequence of the foregoing assumption (IV.6), the local resultant stress:

$$\vec{F}(P_j) = \vec{F}_n(P_j) + \vec{F}_t(P_j) \tag{IV.8}$$

lies in general along a direction different from that of the local vector displacement given by the vector sum of (IV.2) and (IV.3), although lying in the same plane: the plane normal to the contact surface and containing the direction of the vector displacement.

It can of course be contended that the assumption of a local normal stress of the form (IV.6), i. e. proportional to the normal component of displacement with a single factor of proportionality K, is not a realistic one. This is in principle true, and the assumption in question can indeed produce some errors in restricted areas close to the boundary of the contact surface; but it is known, in the light of the computations carried out using the VOGT compliance coefficients, that such an assumption leads to global results in good agreement both with experimental evidence and with more accurate analyses. Likewise, the VOGT treatment appears to justify –from a pragmatic, non rigorous point of view- the assumption that the normal stress components depend only from the normal components of displacement.

This choice, moreover, is not a strictly necessary one; it is always possible, as a more accurate alternative, to discretise the bedrock mass and to represent its compliance with a Finite Element-type formulation. This latter option would be, indeed, necessary in the case of a strongly heterogeneous foundation.

C)-THE EQUILBRIUM CONDITIONS OF THE RIGID BODY; THE SUCCESSIVE CHECKS OF COMPATIBILITY OF RESULTS WITH OFFICIAL PRESCRIPTIONS

It is now possible to write down the equilibrium equations of the rigid body under the action of the above-derived foundation reactions and of a system of external forces whose resultant be $\vec{\Phi}_e$ and whose moment (with respect to an arbitrary pole O) be $\vec{M}_e(O)$.

These equations can be cast in succinct vector form as follows:

$$\int_S \vec{F}(P_f)\,dS + \vec{\Phi}_e = 0 \tag{IV.9}$$

$$\int_S \left[(P_f - O) \wedge \vec{F}(P_f)\right] dS + \vec{M}_e(O) = 0 \quad , \tag{IV.10}$$

where S is the contact surface and P_f is the generic point thereof. This system of two vector equations gives rise, through projection of each equation on the three Cartesian axes, to six scalar equations containing implicitly the six unknowns $u_x(G),\ u_y(G),\ u_z(G)$, $\omega_x,\ \omega_y,\ \omega_z$ through eqs. from (IV.1) to (IV.7). The equations (IV.9), (IV.10) are non-linear ones, both because of the condition of monolateral contact along the dam-foundation interface and because the local direction of the tangential component of contact stress (unit vector $\vec{t}$) depends on the solution of (IV.9), (IV.10). The solution has therefore to be sought by an iterative numerical procedure, the details of which are not given here; suffice it to say that the

integrals can be replaced by sums after suitable discretisation of the contact interface[8] [see **FIG. 3**].
Once the equilibrium equations have been solved, yielding the values of the six unknowns of the rigid body motions [$u_x(G)$, $u_y(G)$, $u_z(G)$, ω_x, ω_y, ω_z], eqs. (IV.2), (IV.3) give the interface displacements and successively, through eqs. (IV.5), (IV.6), (IV.7) the contact stresses are obtained [see **FIG. 4**]. Of course the rigid motion must be such as to bring the dam elements into mutual contact (in other words, the motion should take place towards downstream); moreover, the areas of the interface where the dam body is detached from the underlying bedrock must be limited, so as not to allow to any of the dam elements the possibility of breaking loose.
It remains to be said that the solution does not depend, in terms of distribution and values of contact stresses, on the value chosen for K ; indeed, only the values of the displacements are dependent on K [9], being inversely proportional to said value. On the other hand, the field of displacements and stresses obtained from the solution depends on the value assigned to the friction coefficient f^* ; indeed, to every assumed value of f^* there corresponds a distinct solution of the problem [see **FIG. 5**], unless the dam axis is straight and the dam-foundation contact surface is plane, see § VII. Among these different solutions, some will correspond either to excessive values of f^* or to excessive values of the contact stresses; the solution in which the least value of f^* within the prescribed limit yields contact stresses that are everywhere within the admissible limits –if such a solution exists- can be assumed as a proof that an equilibrium satisfying the requirements can be achieved.
Evidently, a check carried out along these lines allows to assess, in the framework of a single procedure, the stability of the dam in relation not only to sliding, but also to overturning (the latter type of stability would be denied if the iterative procedure of elimination of the foundation areas where the dam tends to be detached from its footprint should fail to converge); at the same time, the checking of the admissibility of the contact stresses in relation to the bedrock resistance to crushing is obtained as a natural by-product of the procedure.

V- THE EXTENSION OF THE ANALYSIS TO THE STABILITY CHECK OF SEPARATE DAM MONOLITHS AND OF MONOLITH PARTS

Once obtained a satisfactory solution for the whole dam, it is possible to carry out the stability assessment for each one of the dam monoliths; successively, if required, also the checks of the stability of parts of a dam monolith can likewise be effected.
In order to achieve the first of these two objectives, let us begin by considering one of the two end elements of the dam (right or left bank). The forces transmitted to it through the foundation are known from the foregoing global stability analysis; on the other hand, if the rigid body equilibrium of the element is to be reached, these forces should be exactly counteracted by the external actions on the element (which are known) together with the forces transmitted to the element though the joint separating it from the next monolith. This last set of forces is unknown, but the rigid-body equilibrium conditions of the element obviously allow to determine it completely. It can then be assessed whether the ratio of the tangential component of the resultant of these mutual forces to their component orthogonal to the joint is within the admissible limit; and the distribution of the contact stresses on the joint surface can be derived too, taking into account if need be the condition of monolateral contact. Thus a complete check of the consistency of conditions across the joint with the mandatory prescriptions can be carried out.

[8] Over each element of the interface discretisation the integrals can be evaluated on the basis either of the single value of the integrand in the element barycentre or on the basis of the values in the Gauss points of the element; **FIG. 6** shows, moreover, that linear and parabolic elements are almost equivalent in terms of final results.
[9] However, by assigning to K a plausible value (such as e. g. it can be derived from VOGT-type formulas) the order of magnitude of the displacements will turn out to be approximately correct. This order of magnitude can then be used to evaluate a-posteriori whether the horizontal displacements are sufficiently large to close the joints (assuming their opening is known in the unloaded state).

Let us consider now the next element proceeding from the dam end towards the centre. It is evident that the above seen procedure can be readily extended, because now the forces transmitted from the end element to the next one are known, as are known the external actions and (from the global analysis) the forces acting on the element through the foundation interface. Thus the forces exchanged between this new element and its neighbour on the side of the dam centre can be determined, once again, from rigid-body equilibrium considerations; after which, all desired checks can be performed in a like manner as seen for the first element. Proceeding in this way from one element to the next, from bank to bank, all the monoliths can be individually checked for stability.
Actual applications of this type of procedure have shown that the ratio between tangential and normal components of the forces transmitted though joint interfaces (i. e. the friction coefficient on the joints) presents a minimum near the dam centre and increases steadily proceeding from the central joints towards either bank.
It remains to be seen how to assess the stability of parts of a single dam monolith, e. g. the part overlying a given plane of concrete pour (such checks are often requested, albeit a greater upper limit of the friction coefficient –e. g. $f^* = 1$ in place of $f^* = 0.75$- is usually admitted in the sliding stability checks along these planes, in comparison with the maximum value allowed at the dam-foundation interface). Consistently with all the foregoing, also these checks can be carried out by means of rigid-body equilibrium considerations. Indeed, let us assume that in the foregoing analysis of the dam monoliths stability the distribution of the contact stresses on all the joint surfaces has been determined; then the forces generated by these distributions over the two portions of a monolith's joints lying above the horizontal plane on which the partial stability check is to be effected can be determined by numerical integration. Now the forces acting on the part of monolith above the chosen plane are all known, so that the sliding and overturning stability checks can be performed; also the distribution of normal and tangential stresses over the section plane can be assessed. All the checks prescribed by official norms can therefore be made within the framework of the proposed model.

VI- THE INDICATIONS OF SOME IN-SITU DYNAMIC TESTS

As already mentioned, several in-situ dynamic excitation tests were carried out on some Italian dams of the type considered, with the aim of determining the eigenfrequencies and the corresponding modal shapes and of ascertaining, by back-analysis, whether these dynamic properties could be interpreted in the framework of a definite structural model.
The modes that it was possible to identify were at least the first three or four modes of natural vibrations (in order of ascending frequencies).
In all cases the back-interpretation of experimental results showed that the dynamic behaviour was very nearly that of a monolithic body. In other words, the contact across the joints was sufficiently effective as to impede relative motions of the monoliths, producing instead their collective motion as a rigidly connected whole. This was observed even in cases where the curvature was very slight (e. g. with a ratio of the reference cylinder radius to dam height of about 5.7).
This 3-D dynamic behaviour was observed also for a straight-axis gravity dam in which the joints were not real construction joints predisposed in the traditional manner, but were instead cut in the fresh concrete layers, the latter having been uniformly poured and compacted in a way not unlike the successively developed RCC technique. [This last experience suggests that RCC gravity dams designed according to the traditional 2-D check criteria may be actually endowed with supplementary margins of resistance].
From the above a substantial confidence can be derived that the proposed scheme is not an artificial conceptual construct, but reflects instead a real property of the class of dams being investigated.

VII- THE CONSISTENCY OF THE PROPOSED METHODOLOGY WITH THE REGULATORY PRESCRIPTIONS FOR RECTILINEAR-AXIS GRAVITY DAMS

If the above conceptual model is applied to a straight-axis dam (e. g. one with plane facings parallel to the y axis), subjected to external actions all perpendicular to its axis, the rigid-body degrees of freedom that can produce work with such external forces are reduced to only

three: u_x, u_z, ω_y . Correspondingly, the equilibrium equations are now only three (see **FIG. 2**):
-translational equilibrium in the vertical (z) direction;
-translational equilibrium in the horizontal (x) direction normal to the dam axis;
-rotational equilibrium in the vertical plane perpendicular to the dam axis (plane $x-z$).
[Indeed, the remaining three equations are identically satisfied by null values of u_y, ω_x, ω_z; as a consequence, no contact stresses are generated save those that are contained in the plane x-z perpendicular to the dam axis].
It is evident that, in the case of a plane contact surface between the dam and the bedrock, the mathematical formulation adopted in the 3-D case yields now a linear distribution of the normal stresses along the contact surface; in the admitted scheme, where the tangential stresses are proportional to the normal ones through the friction factor f^*, the same type of distribution would then hold for the shear stresses along the contact line. Then in the equilibrium equation along a direction parallel to the contact line only the resultant of these contact shear stresses would be present, and in the equilibrium equation along a direction normal to the contact line only the resultant of the contact normal stresses would appear. [The first of these resultants is obviously proportional, under the assumptions made, to the second one through the friction factor f^*]. Thus the magnitude of the maximum normal stress would be decoupled from the choice of f^*, contrary to what happens in the 3-D case, and the sliding check would simply depend on the comparison of the $\frac{H}{V}$ ratio with the admissible maximum value of f^* (H being the resultant of the external forces parallel to the contact line and V the resultant of the external forces normal to the contact line); in other words, the sliding check becomes now identical with the usual 2-D formulation for gravity dams. On the other hand, the resistance check of the foundation rock in regard to crushing assumes as well the usual form of the 2-D case, under the assumption that the contact section remains plane and disregarding the stress concentrations near the ends of the contact line. The overturning check is satisfied if the no-tension portion of the contact line remains shorter than the full contact length.
Moreover, the general framework of the proposed analysis shows that in the case of a straight-axis dam on a non-plane foundation surface the usual 2-D checks are in principle defective, and resort should be made again to a formulation of the type described in the above paragraphs, albeit with a reduced number of rigid-body degrees of freedom. In such a case the problem is again a coupled, non-linear one as in the full 3-D case.
It can be concluded that the proposed 3-D rigid-body model not only appears to be a valid one in the general case, but is able to generate, for the particular case of straight-axis dams on a plane foundation, the usual 2-D stability check criteria. Therefore the proposed methodology is fully consistent with the dictates of the official regulations for gravity dams, while taking advantage, for dams with curved axis, of the mutual support between adjacent monoliths, as in some cases the regulations in question explicitly allow[10].

VIII- APPLICATIONS OF THE PROPOSED METHODOLOGY

This 3-D, rigid-body model has been applied to the stability checks of a number of old Italian gravity dams with curved axis (Salto, Turano, Scandarello, Scalere…) which if checked with the usual criteria for straight-axis dams would have been found defective, especially so in regard of the sliding check. In every one of said cases the new approach showed that the stability criteria are satisfied if account is taken –in the way illustrated in the above paragraphs- of the 'wedge effect' provided by the axis curvature. Besides, for some of these dams it has been possible to document an actual 3-D behaviour through back-analysis both of their in-service behaviour (quantitative interpretation of observed displacements under static loads) and of the results of in-situ dynamic excitation tests. [As already mentioned, also a straight-axis gravity

[10] Italian Regulations, § 4.2.2.3.1: '*…it will be allowed, if [geometrical and physical] circumstances justify it, to take into account resistant contributions external to the single dam monolith…*'

dam (Alpe Gera, built with a technology close to the RCC method of construction) such a 3-D static and dynamic behaviour was observed].
It appears, therefore, that a sufficient experience has been accumulated in order to state with confidence that the proposed procedure is adequate to deal, in a realistic way, with the reappraising needs often arising for structures of the described type.

IX- CONCLUSIONS

The methodology here summarily illustrated is, beyond doubt, a compromise between the partially conflicting exigencies of a rigorous approach, of easy checking against the official prescription dictates and of simplicity of formulation[11].
There is no doubt that the 'royal highway' to a fully satisfactory mathematical modelling would lie in a non-linear analysis starting from a complete F. E. discretisation of both the dam and the foundation mass, with the insertion of 'joint-type' elements both along the real joints and along a sizable upstream strip of the dam footprint. However, this approach would probably meet with remarkable computational difficulties, given the high number of non-linear elements that would become necessary.
In this context, it would be of considerable interest to effect a comparison, in a 'simple' case with only a few joints separating the dam monoliths and with moderate $\frac{H}{V}$ ratio (so that only along a limited upstream strip of the footprint would the dam be likely to be detached from the underlying bedrock), between a 'rigorous' analysis of the type just mentioned and an approximate analysis such as the one illustrated in the preceding paragraphs (or another similarly simplified approach). It is to be hoped that such comparisons be carried out in the near future, not only to help practising dam engineers in their evaluations of the safety of old dams, but also to encourage the control Authorities to evolve more comprehensive checking criteria. This interaction between applied research and regulatory activities appears indeed to become, more and more, a vital necessity. Our ICOLD W. G. could (and should, in my opinion) stimulate whenever possible, within the limits of its action, this interchange; I do not think that this would run contrary to the ICOLD policy of not intervening in the regulatory field, because there would be no direct participation of ICOLD members in the formulation of official prescriptions, but only their active promotion of a more effective circulation (and 'justification') of ideas apt, in the long run, to best serve the interests of every dam professional.

BIBLIOGRAPHIC REFERENCES

F. VOGT: "Ueber die Berechnung der Fundamentdeformation", Noske Videnskaps-Akademie, Oslo 1925

Proceedings of the XVIIth ICOLD Congress on Large Dams, 17-21 June 1991, pagg.319-320

M. FANELLI: General Report on Q. 68 (Safety Assessment and Improvement of Existing Dams), ICOLD XVIIIth Congress on Large Dams, Durban, 1994

M. FANELLI: Arch dams: Models and Methods of Analysis (Part 2 of the book "Arch Dams: Designing and Monitoring for Safety"- series by CISM, Udine, Courses and Lectures n°367, 4-8 Sept, 1995) - v. Fig. 8, pag.91

[11] It can be remarked, by way of criticism, that nowhere in the presented approach does the curvature of the dam axis explicitly enter the mathematical analysis. However, the relevance of the axis curvature does come into play in the a-posteriori check of the amount of the downstream displacements vs. those requested to close the joints (the latter displacements, indeed, are inversely proportional to the axis curvature). Besides, as mentioned in the text, the proposed approach could be relevant also for some dams with straight axis if these should exhibit a decidedly 3-D behaviour. In this connection, it is interesting to note that in straight-axis RCC gravity dams, where the joints are cut after concrete pouring and compacting, it could pay to cut the joints accordino to downstream-converging planes instead of along paralle planes; in this way, indeed, a wedging effect would be introduced leading to increased resistance to sliding.

M. FANELLI, G. MAZZA', G. RUGGERI, P. PALUMBO: "Gravity dams: safety evaluation against sliding with a 3-D rigid body formulation", Proceedings of the Meeting on Research and Development in the Field of dams", Crans-Montana (Switz.), Sept. 7-9, 1995, pagg. 253-264

ISMES – Rapporto interno REL-DPD-381/89: "Prove di vibrazione forzata sulla diga di Suviana"

ISMES - Rapporto interno RAT DMM 5190 , Diga di Alpe Gera, Interpretazione del comportamento strutturale mediante modello deterministico, 1989

ISMES – Rapporto interno RAT- DMM- 646/90: "Diga del Salto: Verifiche di stabilità con un metodo che considera l'effetto di curvatura geometrica", 1990

ISMES – Rapporto interno RAT- DMM- 907/90: "Diga di Turano: Verifiche di stabilità con un metodo che considera l'effetto di curvatura geometrica", 1990

ISMES – Rapporto interno RAT- DMM- 394/95: "Diga di Scandarello: Verifica di stabilità allo scorrimento in condizioni sismiche con un modello 3D", 1995

ISMES – Rapporto interno RAT- STR-2387/97: "Diga delle Scalere: Verifica delle condizioni di sicurezza statica e sismica", 1997

ISMES – Rapporto interno RAT- STR-1204: "Diga delle Scalere: Revisione dei calcoli di verifica statica e sismica", 1999

NORME TECNICHE PER LA SICUREZZA DELLE DIGHE DI SBARRAMENTO- Allegato al REGOLAMENTO ITALIANO PER LA COSTRUZIONE E L'ESERCIZIO DELLE DIGHE DI RITENUTA- Bozza 1999

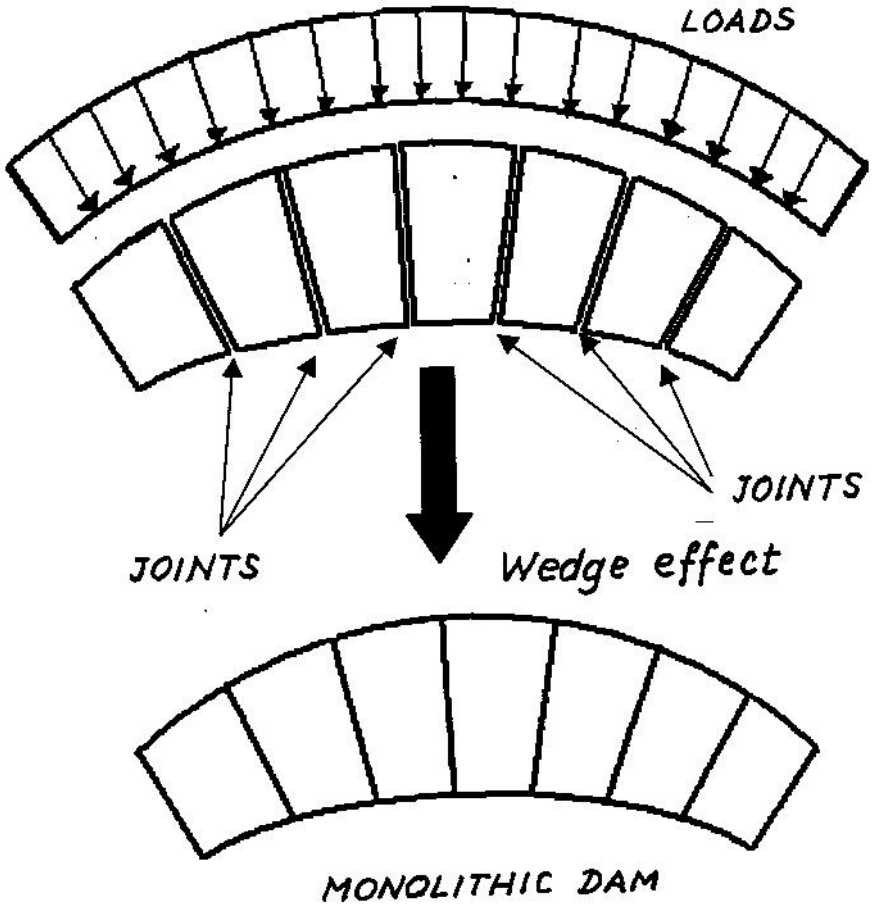

FIG. 1

Schematic illustration of the wedge effect for gravity dams with curved axis.
The figure represents schematically the footprint of the several monoliths making up the dam, separated by construction joints.
Starting from an initial condition with convergent open joints, a small displacement downwards bring the joint surfaces into contact and the dam elements wedge against each other; any further downstream displacement has the dam behaving as a monolithic body.

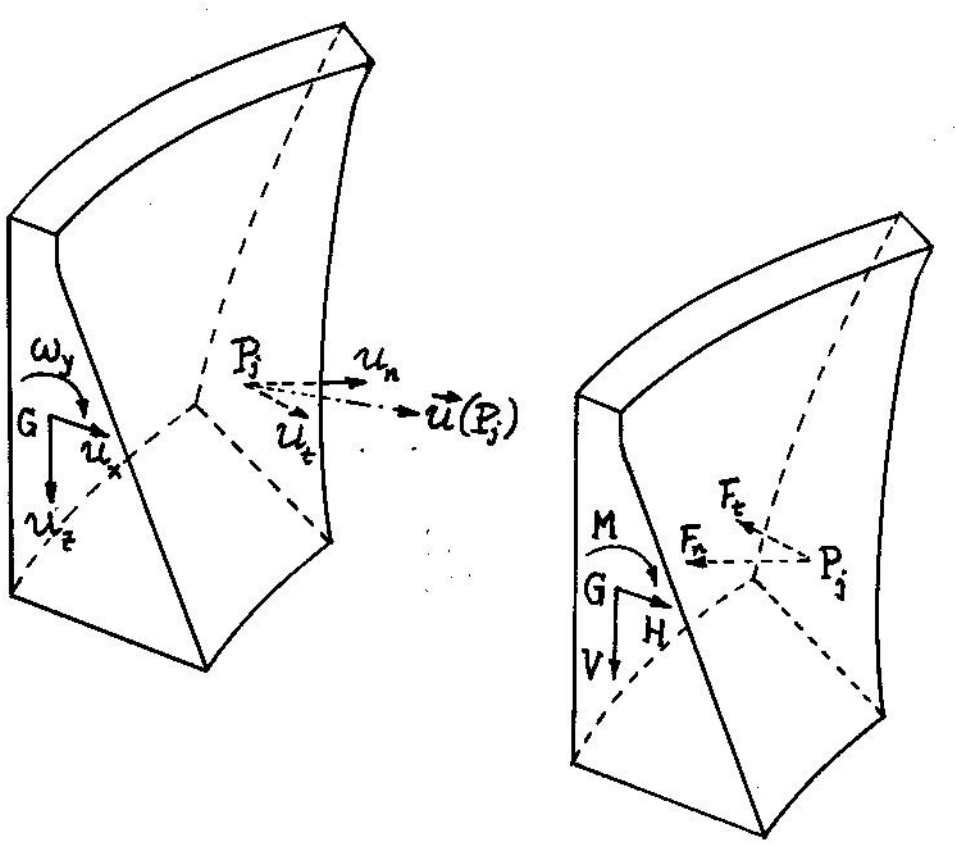

FIG. 2

Schematic illustration of the rigid-body 3-D equilibrium of a compact, symmetric gravity dam with curved axis on a compliant foundation (only half of the dam is shown for greater clarity).

At left: illustration of the three degrees of freedom of the rigid-body motion in the particular case of a symmetric dam on a physically symmetric elastic foundation. (In the general case three more degrees of freedom have to be considered: the bank-to-bank translation and two rotations, one around a vertical axis and one around a horizontal axis pointing from upstream to downstream); also the local components of the displacement at the dam-foundation contact surface are shown.

At right: the three components of external forces acting on the dam (in the particular case of a symmetric dam) and of the local reactions of the elastic foundation.

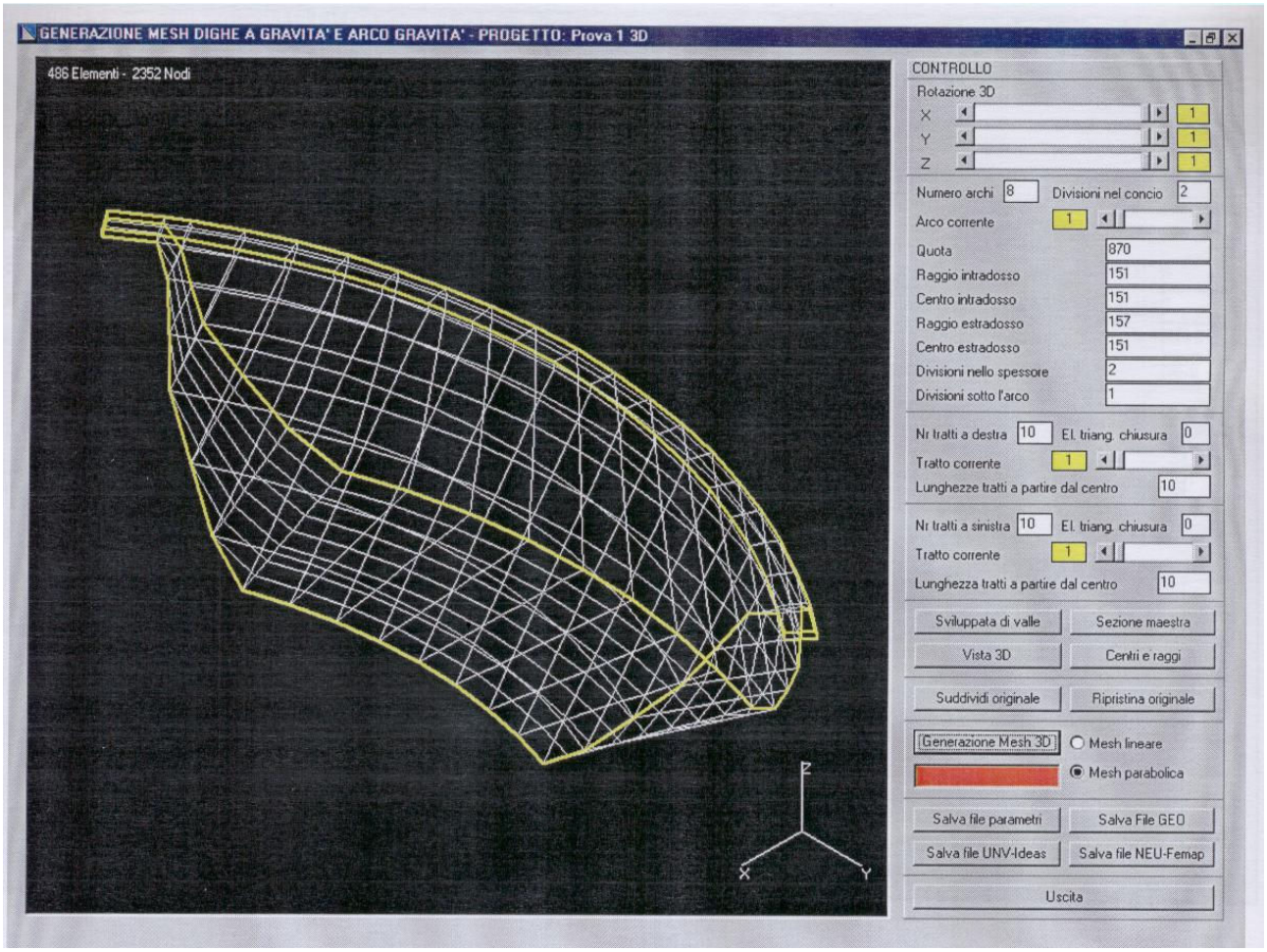

FIG. 3

The input of the rigid-body analysis software: the dam mesh, allowing the discretisation of the contact surface and the subdivision of the dam volume into separate parts for successive analysis of the equilibrium of single elements and parts thereof.

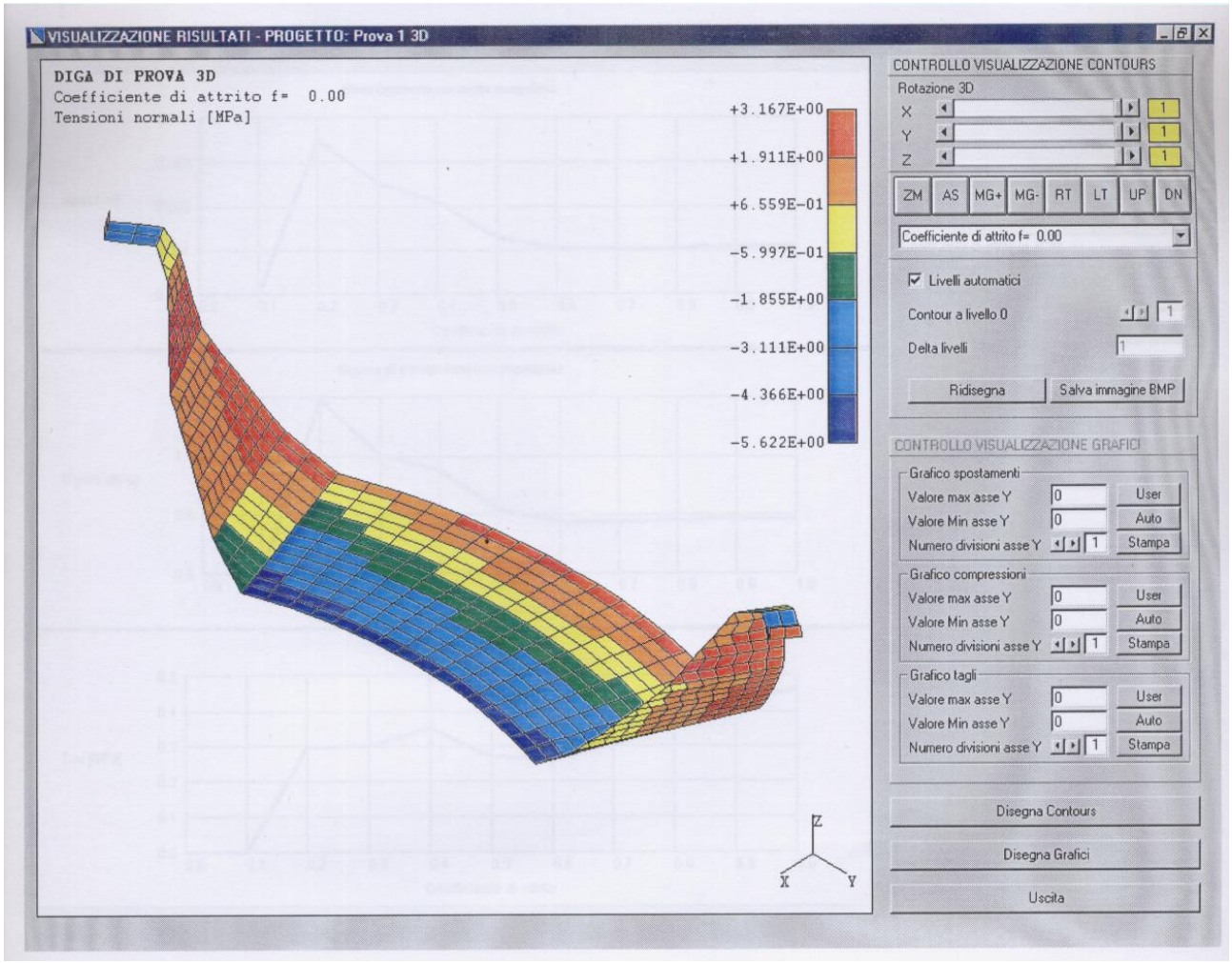

FIG. 4

Output of the rigid-body analysis software: a colour-coded representation of the contact stress distribution along the foundation surface.

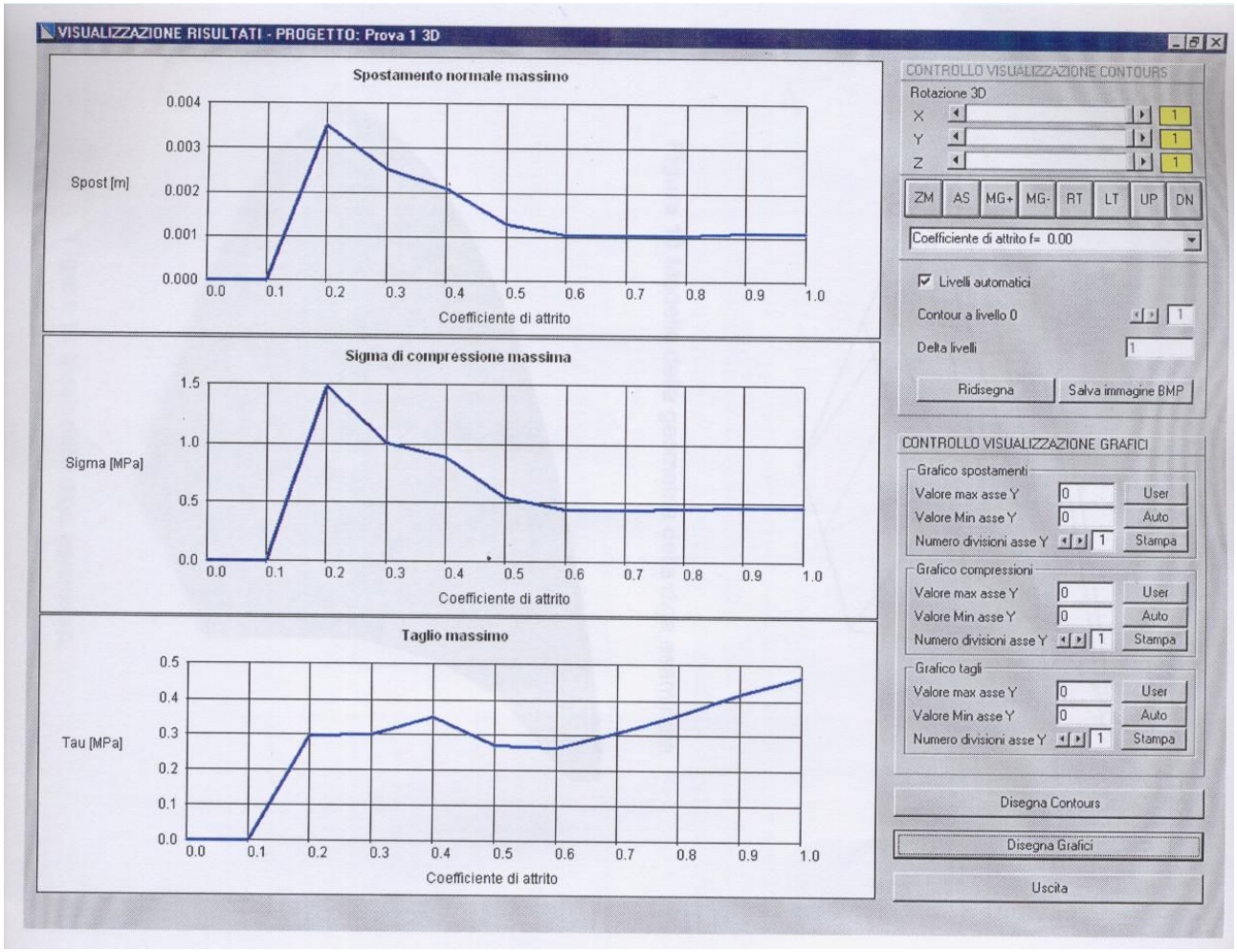

FIG. 5

Output of the rigid-body analysis: the max. displacements and contact stresses as functions of the assumed friction coefficient, f^* .

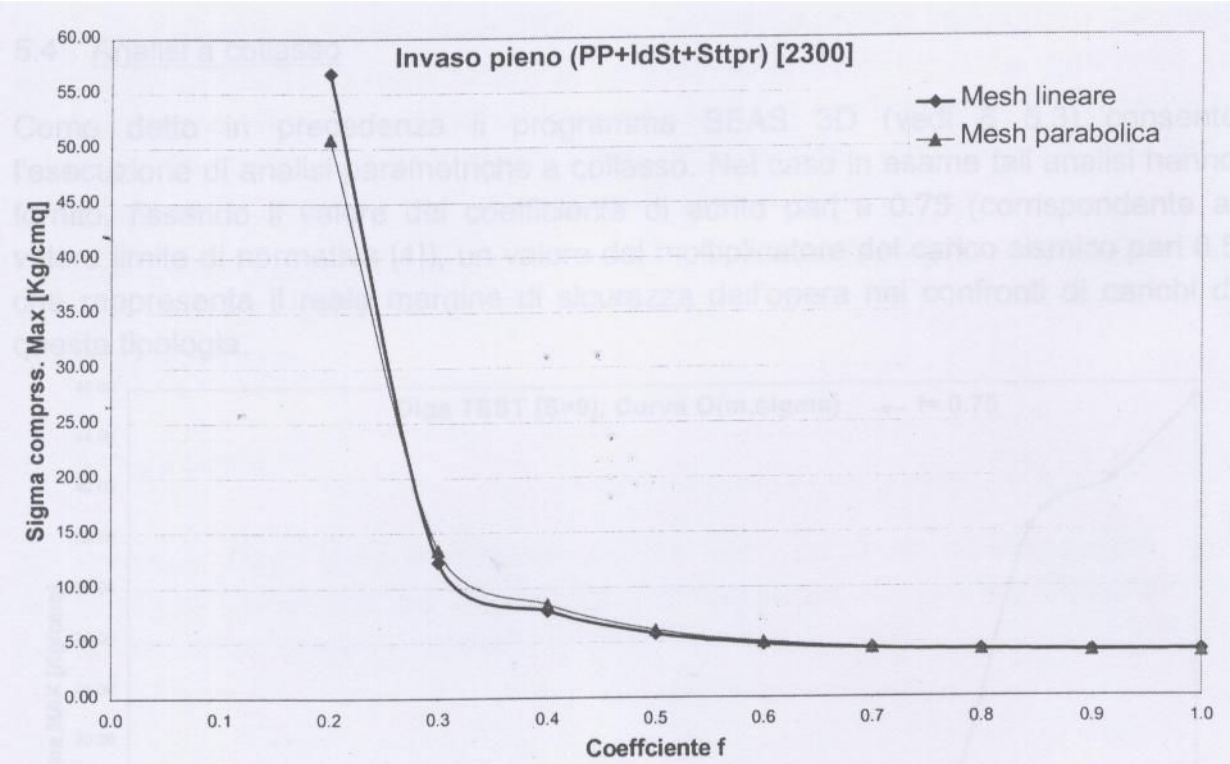

Figura 14 Verifica sismica tridimensionale: condizioni di carico ordinarie

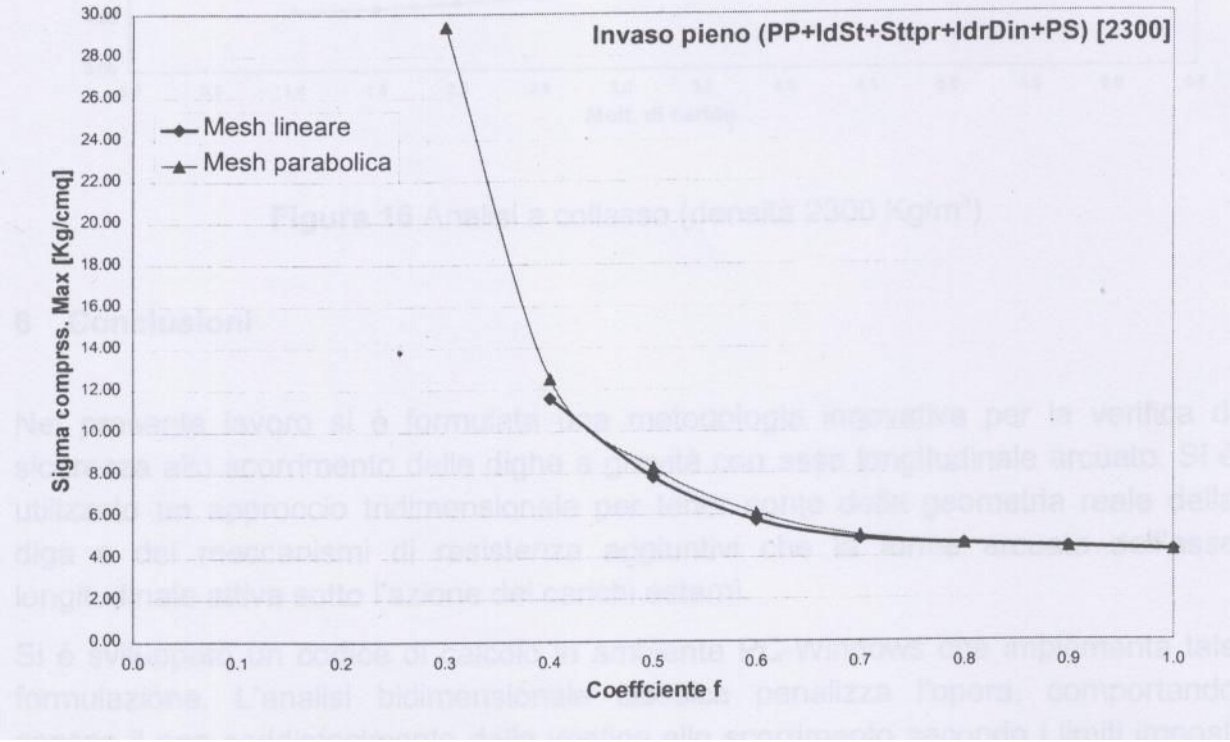

FIG. 6

Output of the rigid-body analysis: variation of the max. contact stress as a function of the friction coefficient, f^* , under two load conditions:

-upper diagram: ordinary loads
-lower diagram: exceptional loads (including earthquake),
and with two different types of surface elements along the foundation: linear elements (thick lines) and parabolic elements (thin lines).

7th Benchmark Workshop on Numerical Analysis of Dams
September 24-26, 2003 – Bucharest, ROMANIA

EVALUATION OF ULTIMATE STRENGTH OF GRAVITY DAMS WITH CURVED SHAPE AGAINST SLIDING

Prepared by
G. Giuseppetti, G. Mazzà, M. Meghella, CESI S.p.A., Milan, Italy
M. Fanelli, Consultant, Milan, Italy

FORWARD

Very often both concrete and masonry gravity dams have been built with a slightly curved shape. This designers' choice was generally due to the implicit assumption that the curved shape could allow, in case of adverse conditions, to rely on an additional strength mechanism - in particular against sliding which is the most critical failure mechanism for this dam typology - due to the arch effect generally ignored in the safety sliding evaluation which is usually carried out by means of a 2-dimensional approach.

In the frame of the 7th Benchmark Workshop promoted by the ICOLD "ad hoc" Committee on Computational Aspects of Analysis and Design of Dams, ***Theme A – Concrete Dams*** will be devoted to the numerical analysis of a gravity dam which was built with a slightly curved axis. The proposed exercise asks for the evaluation of the ultimate strength against sliding taking into account the actual dam shape and making an estimate of the increase of the ultimate strength in comparison with the traditional 2-dimensional approach.

In the present case, Scalere dam (a structure whose owner is ENEL Produzione, Italy, that has kindly allowed to use this dam as the test-case for the benchmark) has been proposed as a case history on which different experts in the field of numerical investigations could prove the effectiveness of their skill and software.

In the exercise, the capabilities of the computer codes used for the analyses and the main aspects of the methodologies/approaches adopted by the participant have to be described and the results requested by the formulator have to be presented according to the scheme suggested in order to allow the comparison of the results.

The exercise is proposed to point out the different strategies of analysis instead of the ***Validation*** [1] of software moving, hence, towards the ***Justification*** of engineering methodologies adopted in the dam safety assessment.

1 SOME GENERAL CONSIDERATIONS ON THE BEHAVIOUR OF GRAVITY DAMS WITH A CURVED AXIS

Gravity dams represent a rather numerous population all around the world and in several cases their shape is slightly curved. The idea of the designers, as mentioned in the Forward, was clearly addressed to give to such structures an additional strength, due to the arch effect, with respect to the strength of isolated blocks. The supplementary resistant mechanism due to the arch effect is not sufficiently put into evidence by means of 3-dimensional linear elastic analyses [2], which tends to emphasize the existence of local tensile stress concentrations with little meaning for the ultimate strength of the structures. Moreover, these stress concentrations are not completely realistic, considering the influence of the interface between dam body and rock foundation and of the vertical construction joints, which the structures are normally provided of, which can be partially (or sometimes completely open) according to the environmental conditions.

On the other hand, sometimes it is necessary to carry out a structural safety reassessment because during the dam life several changes can take place, among which: a) reduction in the effectiveness of the drainage system; b) change in the seismic zoning of the area in which the dam is located (from a non seismic zone to a seismic one or a recognized increase in the seismic intensity of the area); c) change of the physical-mechanical characteristics of the materials (dam body and rock foundation) which induce the need to re-evaluate the dam safety; etc.

A new method on the evaluation of arch effect for gravity dams with curved axis based on a rigid body formulation, and an application to a real case can be found in [3 and 4].

For these reasons the ICOLD "ad hoc" Committee on Computational Aspects of Analysis and Design of Dams has considered of some interest the evaluation of the actual ultimate strength of gravity dams that can be considerably increased thanks to the above cited curved shape. The aim of the exercise proposed as ***Theme A-Concrete Dams*** for the 7th Benchmark Workshop on Numerical Dam Analysis is the ***Evaluation of Ultimate Strength of Gravity Dams with Curved Shape Against Sliding*** which represents the most critical failure mechanism for this dam typology.

2 SHORT DESCRIPTION OF SCALERE

Scalere dam (see Figs. 1, 2, and 3) is a large solid gravity structure in concrete located in the centre-north of Italy [5]. The construction works took place in the period 1910-1911. The foundation rock, excellent in every respect, consists of stratified Eocene sandstones dipping upstream. The faces of the dam, unlined owing to the great impermeability of the structure, are in blocks laid in regular courses. The dam has not been provided with contraction joints. The drainage system does not comply with the requirements of the current Italian Standards, so no reduction of the uplift pressures have been considered in the analysis developed so far and, analogously, in the exercise proposed for the B-W. The trend of the measurements carried out by the monitoring system installed on the dam has always been normal, showing displacements well correlated to the seasonal thermal variations with a small hydrostatic component.

The main features of the dam are:

Crest elevation	*830.50 m a.s.l.*
Height above the general foundation plane	*34.00 m*
Length of the crest	*158.00 m*
Volume of the dam	*40,000 cu. m.*

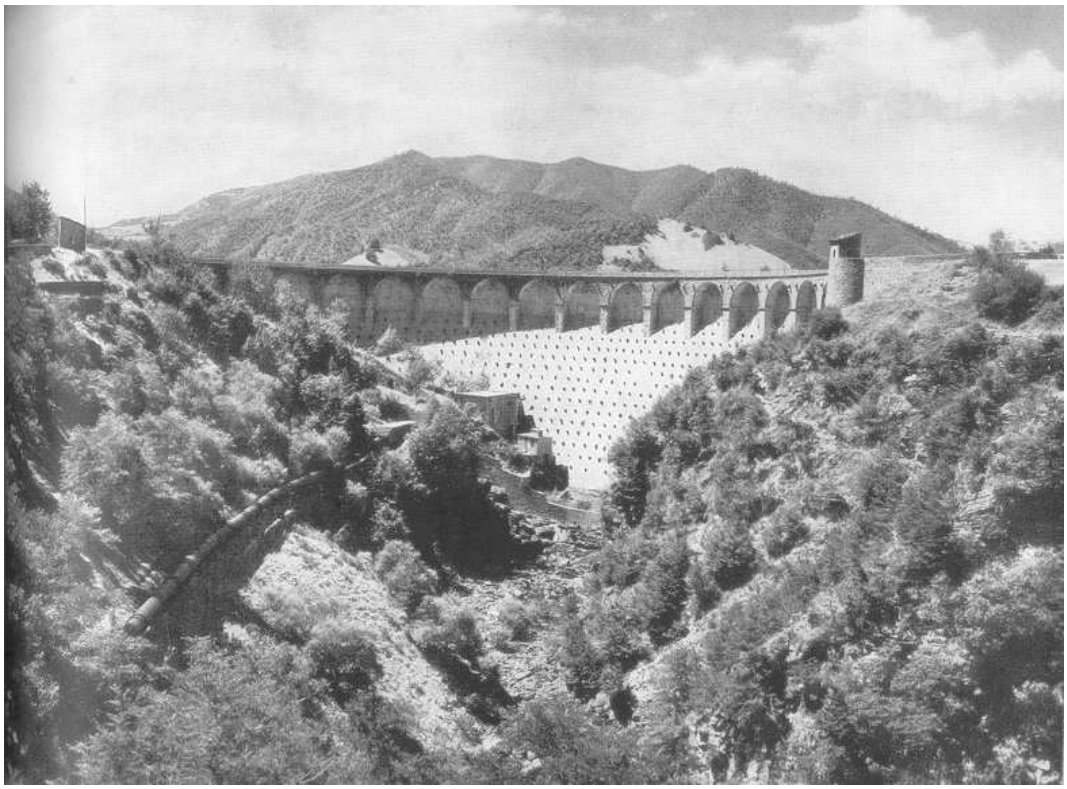

Fig. 1 Downstream view of Scalere dam

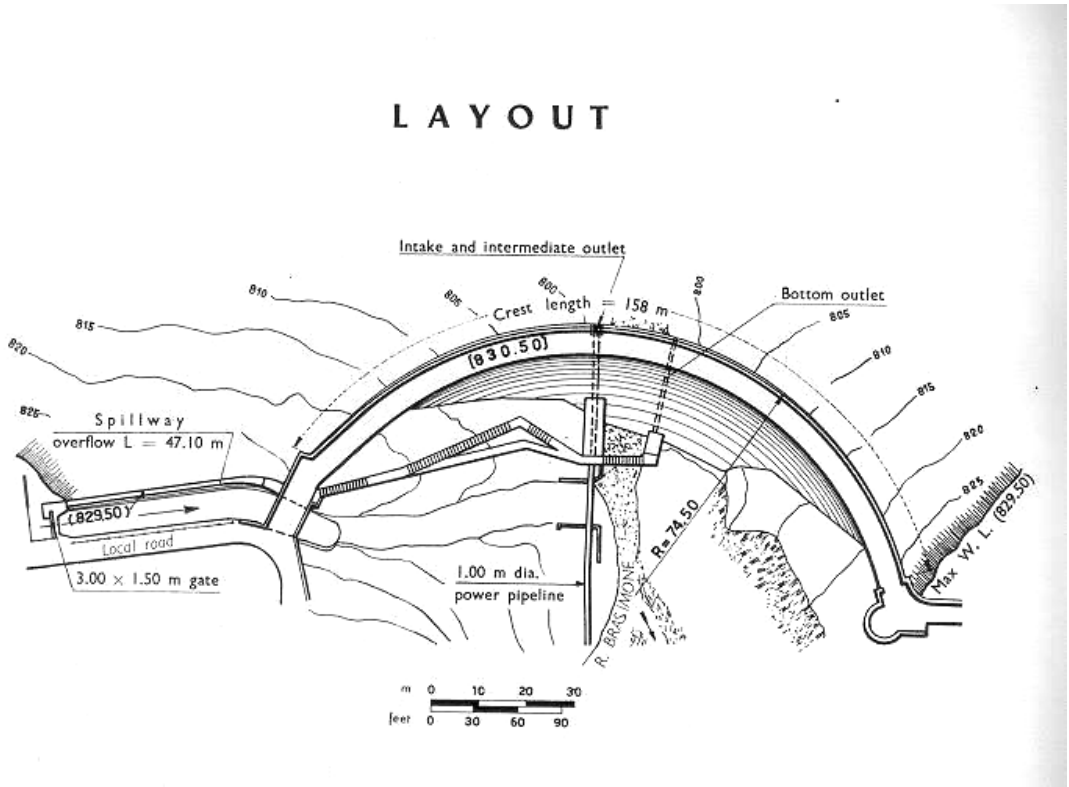

Fig. 2 Plan of the dam

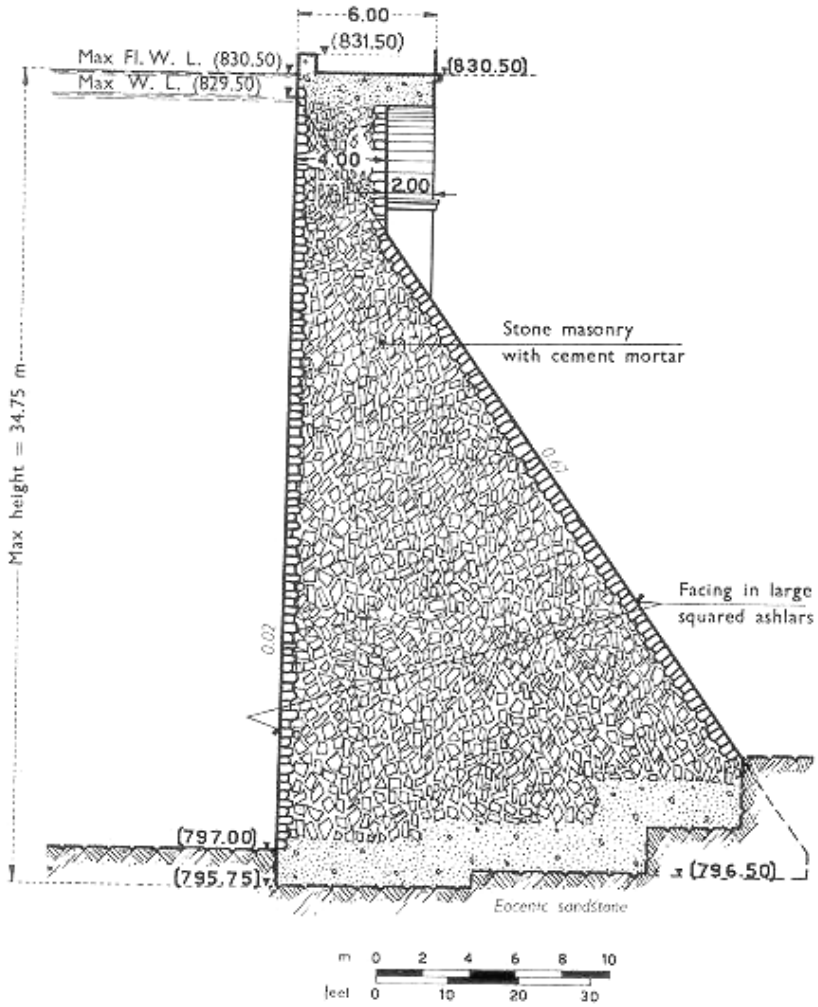

Fig. 3 Main vertical section of the dam

3 PREPARATION OF THE EXERCISE

Each participant to the workshop will be provided with the following information (reported in the Annex):

a) Data Set of the geometry of the dam, including dam-rock interface; (important note: the dam-rock interface to be considered in the calculations is not the real one represented in figure 3, but the idealized one according to the geometry provided in the attached "*Solids.zip"* file)

b) Physical-mechanical parameters of dam body and rock foundation, i.e. elastic moduli, specific weights, compressive and tensile strengths of concrete and rock foundation (these parameters have to be considered as reference values for the B-W; in fact, no direct measurements are available);
c) Physical-mechanical parameters of the dam-foundation interface (i.e. friction angle, cohesion as basic parameters to be considered as reference values);
d) Loading conditions: for sake of simplicity the hydrostatic pressures and dead weight only will be considered, assuming the maximum water level as the reference value (hence, thermal

variations and seismic loads will be ignored); of course, the uplift pressures related to the water in the reservoir have to be included in the analysis according to the adopted method. As already stated in paragraph 2, participants have not to consider the presence of a drainage system.

The analysis to evaluate the ultimate strength of the dam against sliding could be carried out making reference to the numerical (or analytical) methodology/approach decided by the participant which basic assumptions have to be clearly stated in the paper presented at the workshop.

In order to have the minimum uncertainties in the way to carry out the analyses and to make results comparable (even if the adopted methodologies could be different), it is suggested to evaluate the ***ultimate strength of the dam against sliding*** in terms of a coefficient of the maximum hydrostatic load expressed as a multiplier of the height of the water in the reservoir starting from the reference value (maximum water level)[1].

4 PRESENTATION OF THE RESULTS

As already said in the Forward, the present exercise is rather free from the point of view of the method to be used to evaluate the ultimate strength of the dam against sliding (as defined in the previous paragraph). This means that the basic result to be provided is represented by the multiplier coefficient of the water height in the reservoir, which determines a limit equilibrium condition starting from the strength parameters assigned to materials and discontinuities.

In addition, participants are also asked to provide, for the above cited limit condition, an accurate distribution of the normal and shear stresses on the dam-rock interface, on the main cross vertical section of the dam and on a horizontal arch as defined in the Annex.

5 FINAL COMMENTS

The exercise here proposed represents a second, more complex step of the exercise examined in the 5th Benchmark Workshop in which a plane scheme of an ideal gravity dam was considered.

The present exercise should be, however, more interesting from the engineering point of view because it makes reference to an actual dam. The results obtained by the participants, critically discussed during the workshop, could allow dam engineers to examine under different points of view which is the most rational way to carry out the safety assessment of gravity dams with arched shape against sliding.

The critical examination of the results could be of some benefit also for national and international organisms which are entrusted to issue and to apply standards and guidelines.

[1] Alternatively, the limit equilibrium condition could be achieved reducing the strength values of the materials and discontinuities in order to obtain the lower bound value, but this approach, even more meaningful from the engineering point of view, appears more complex in terms of comparison of the results because it is tightly linked to the model adopted by each participant (e.g. if a 3-D rigid body model with an interface between dam and rock is assumed, it can be controversial to decide which strength parameter has to be reduced - cohesion or friction angle, or both – in order to evaluate the limit condition).

REFERENCES

1. **ICOLD,** Bulletin n°. 94. *Computer software for dams. Validation. Comments and proposals.* 1994.
2. **P. Londe,** ICOLD, *Transactions*. Proceedings of the Seventeenth International Congress on Large Dams. Vienna, 17-21 June 1991, pp. 319-320.
3. **ENEL S.p.A, ISMES S.p.A.,** *Seismic Reassessment of ENEL Dams*. Proceedings of the Eighteenth International Congress on Large Dams, Durban (South Africa), Vol. 1, Q. 68, R. 64.
4. **M. Fanelli, G. Mazzà, G. Ruggeri, P. Palumbo,** *Gravity Dams: Safety Evaluation Against Sliding With A 3-D Rigid Body Formulation*. Proceedings on Research and Development in the field of Dams, Crans Montana (Switzerland), 7-9 Sept., 1995.
5. **ANIDEL.** Dams for hydroelectric power in Italy. Volume n°. 4, 1952.

ANNEX

List of data for the preparation of
Theme A: EVALUATION OF ULTIMATE STRENGTH OF GRAVITY DAMS WITH CURVED SHAPE AGAINST SLIDING

a) Data Set of the geometry of the dam, including dam-rock interface:

Solid geometry included in attached "Solids.zip" file (containing 3 different international standard graphic formats: IGES, STEP, VRML)

b) Physical-mechanical parameters of materials:

Concrete

- elastic modulus: 20000 MPa
- mass density: 2300 Kg/m^3
- Poisson coefficient: 0.2
- compressive strength: 11.6 Mpa
- tensile strength: 1.0 MPa

Rock foundation

- elastic modulus: 10000 ÷ 15000 MPa
- compressive strength**:** 10 ÷ 15 MPa

c) Physical-mechanical parameters of the dam-foundation interface

- friction angle: 37 degrees
- cohesion: 0 ÷ 0.2 MPa

d) Loading conditions:

- hydrostatic pressures assuming the maximum water level at 830.50 m a.s.l.
- dead weight
- uplift pressures related to the water in the reservoir (participants have not to consider the presence of a drainage system)

The analysis to evaluate the ultimate strength of the dam against sliding could be carried out making reference to the numerical (or analytical) methodology/approach decided by the participant which basic assumptions have to be clearly stated in the paper presented at the workshop.

7th Benchmark Workshop on Numerical Analysis of Dams
September 24-26, 2003 – Bucharest, ROMANIA

EVALUATION OF ULTIMATE STRENGTH OF GRAVITY DAMS WITH CURVED SHAPE AGAINST SLIDING

Synthesys of results

Prepared by
G. Mazzà, CESI S.p.A., Milan, Italy

INTRODUCTION

In the frame of the 7th Benchmark Workshop promoted by the ICOLD "ad hoc" Committee on Computational Aspects of Analysis and Design of Dams, ***Theme A – Concrete Dams*** has been devoted to the numerical analysis of a gravity dam which was built with a slightly curved axis. The proposed exercise asks for the evaluation of the ultimate strength against sliding taking into account the actual dam shape and making an estimate of the increase of the ultimate strength in comparison with the traditional 2-dimensional approach.

Scalere dam (a structure whose owner is ENEL Produzione, Italy) has been proposed as the case history on which different experts in the field of numerical modelling have proved the effectiveness of their skill and software.

In the Figure 1 below the finite element mesh proposed by the participants is shown.

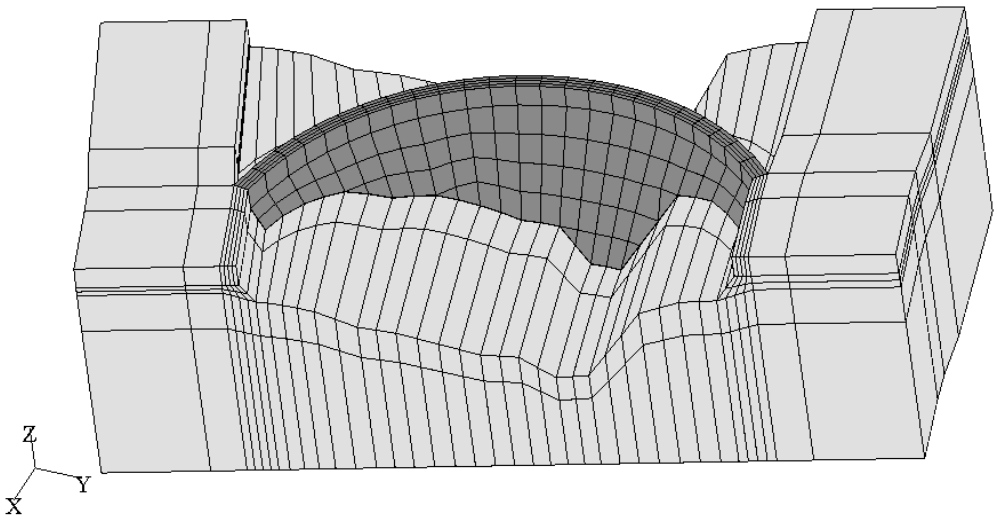

Figure 1. Finite element mesh proposed to carry out the analyses

The capabilities of the computer codes used for the analyses and the main aspects of the methodologies adopted by each participant has been described in the reports and the results have been presented according to the requests of the formulators in order to allow a fruitful comparison.

1 PRESENTATION OF THE RESULTS

In order to have the minimum uncertainties to carry out the analyses and to make results comparable (even if the adopted methodologies and computer codes could be obviously different), it has been requested to evaluate the ***ultimate strength of the dam against sliding*** in terms of a ***load factor*** of the maximum hydrostatic level expressed as a multiplier of the maximum water level in the reservoir.

In addition, participants are also asked to provide, for the above cited limit condition, the distribution of normal and shear stresses on the dam-rock interface, on the main cross vertical section of the dam, and on a horizontal arch as defined in the Annex.

All participants have presented the results in terms of load factors vs. displacements. The stress distributions in the dam body and on the dam-rock interface has been presented according to the different post-processors available, either commercial or own-developed.

The results expressed in terms of load factor vs. displacements are directly comparable and have been summarized in Table 4. On the contrary, the computed stresses in the different dam locations need a huge editing work to be compared. For this reason, in the present synthesis just some general considerations about stress values and distributions are summarized. Those who want to examine deeper this aspect can refer directly to the papers included in the proceedings.

1.1 COMMENTS ON RESULTS

The main aspects of the different papers and the most important results are summarized in 4 Tables. In the 5th Table the main topics discussed during the technical session have been collected.

The content of the Tables is briefly commented here below.

1.1.1 TABLE 1

In the table 1 the list of the participants is shown. Six papers have been presented by scientist, specialists of numerical modelling, and engineers coming from several countries: Romania, Bulgaria, United States of America, Japan, France, and Italy.

In the Table 1 an Identification number (ID) has been assigned to each participant/s. The same ID is adopted in the other tables and in the comments to the results.

1.1.2 TABLE 2

Table 2 shows, with reference to each participant, some general information about methods and models adopted to carry out the analyses.

In particular, the most meaningful aspects are summarized here below.

Finite element models have been used to carry out all the 3-dimensional analyses as requested; two participants have adopted a commercial code (ANSYS), while the others made resort to own-developed codes (ID1-FERC, ID2-BETHY, ID3-CANT-SD, ID6-MERLIN). Moreover, participants ID3 and ID6 have also carried out 2-dimensional finite element analyses, and finally participant ID5 has also adopted the classical Trial Load Method.

Different material models have been used for concrete and rock (ID1, ID4, and ID5 linear elastic; ID2, ID3, and ID6 non-linear, making reference to different constitutive laws). Accordingly, basic parameters proposed by the formulators have been adopted by ID1, ID4, and ID5, while additional parameters were needed by ID2, ID3, and ID6 models; these additional parameters have been assumed directly by the participants and the choice has been justified in the papers.

With reference to the dam-rock interface, joint different models has been used: ID2, ID3, and ID4 have adopted the well known Coulomb criteria, while the other participants made resort to particular models which characteristics have been specified in the papers. Uplift distributions have been assumed accordingly with the chosen joint models.

1.1.3 TABLE 3

Table 3 summarizes some aspects related to both numerical and mechanical criteria of the analyses carried out by the participants. In particular, 5 participants (ID1, ID2, ID3, ID5, and ID6), have carried out the analyses up to the attainment of non-convergence of the analyses. Participant ID4 has based the analysis on the attainment of the limit tensile stress state in the dam body in order to establish a failure criteria (see Table 4).

It is worthwhile noting that 3 participants (ID2, ID3, and ID5) have put into evidence that the failure mechanism starts at the right bank (this aspect is fully related to the adverse slope – downstream bending – of the dam-rock interface of that area given by the formulators in order to make more "unstable" the numerical process).

A second interesting aspect, related to the assumption just mentioned above, has been put into evidence by participants ID3, ID5, ID6 who have emphasized the importance of cohesion in the attainment of the limit equilibrium condition even for water levels below the crest of the dam.

Finally, participants ID1, ID2, and ID4 have made important comments on the turning of the dam behavior from a gravity resisting mechanism to an arch resisting mechanism according to the

variation of the water level in the reservoir: in particular, it has been put into evidence that for a level of the water in the reservoir below the maximum, the gravity mechanisms is strongly predominant.

1.1.4 TABLE 4:

In the Table 4 the most interesting aspects of the benchmark can be found. Two aspects have been considered: the different values of load factors computed in the numerical analyses and the failure criteria assumed by the participants.

Load factor

Two values of the load factor have been considered: the start of sliding and the generalised sliding.

With reference to the start of sliding, three participants have put into evidence this aspect (ID2, ID3, and ID6). The load factors ranges between 0.9 and 1.1 (displacements can not be directly comparable).

With reference to the generalised sliding, in spite of the different criteria and models adopted for materials and dam-rock interface, the load factors ranges in a rather narrow band, i. e. 1.18 and 1.33.

Failure criteria

From the point of view of the failure criteria, participants have considered both physical-mechanical aspects as well as the numerical non-convergence of the analyses. In particular, a displacement of 10 mm at the dam-rock interface level has been considered as a physical failure condition by participants ID2, ID3, and ID5 (the corresponding load factors ranges between 1.20 and 1.26). Other participants has assumed as the physical failure condition the full mobilization of shear strength on the dam-rock interface (ID1) and the overcome of the limit tensile stress in the concrete (ID4).

1.1.5 TABLE 5:

In the Table 5 a synthesis of the main topics examined during the discussion is reported.

1.1.6 Comments on stress distribution

As far as the stress distribution, as mentioned in the paragraph 1, a direct comparison of the stresses in the dam body and foundation is rather complex, and would need a huge editing work that is out of the scope of the present synthesis.

Here below, just some general comments are reported.

First of all, compressive stresses for all analyses performed by the participants remains well below the defined limit value (11.6 Mpa). In general, the maximum is attained at the downstream dam toe, and the values reaches about 1.5-2.0 Mpa. Tensile stresses attain values comparable with the limit strength of 1.0 Mpa only in very narrow locations, in the downstream dam face, close to the zone where sliding occurs. Participants who have carried out analyses assuming a non-linear behavior for materials (ID2, ID3, ID6) have clearly stated the negligible influence of a limited tensile strength on the overall sliding load factor. In fact, the failure mechanism is clearly related to the sliding of the dam body (and in particular of its right part) along the dam-rock interface. Of course, the limit state can be also based on the achievement of the limit tensile stress in the dam body (as stated by participant ID5); in this case the load factor which give rise to a partial or global sliding of the structure can not be obtained.

Readers particularly interested to examine deeper the distribution of stresses can refer directly to the papers included in the proceedings.

TABLE 1

ID	Authors	Company
1	*B. Brand*	*Fed. Energy Regulatory Commission, USA*
2	*A. Carrère*	*Coyne et Bellier, Paris (France)*
	M. Béraud	*Coyne et Bellier, Paris (France)*
3	*M. Meghella*	*CESI Spa, Milan (Italy)*
	G. Mazzà	*CESI Spa, Milan (Italy)*
4	*I. Michael*	*University of Timisoara (Romania)*
	G. Lazar	*University of Timisoara (Romania*
5	*A. Popovici*	*Tech. Univ. of Civil Eng., Bucharest (Romania)*
	R. Sarghiuta	*Tech. Univ. Of Civil Eng., Bucharest (Romania)*
	N. Dimitrov	*Energoproekt, Sofia (Bulgaria)*
6	*T. Shimpo*	*Tokyo El. Power Service Co. (Japan)*
	Y. Uchita	*Tokyo El. Power Co. (Japan)*
	V. Saouma	*Univ. Of Colorado (USA)- Politecnico of Milan (Italy)*

TABLE 2

Authors/ Company (ID)	Method of analysis	Material Model	1.1.1.1.1 Joint model	Uplift	Parameters
1	Variational nonlinear 3-D FEM *FERC code*	Linear elastic	Triangular Failure Element	Tringular, variable with water level	Basic parameters
2	3-D FEM *BETHY code*	Poroplastic (biphasic porous media)	No Joints; Weaker joint layer	According to plasticization in a weaker rock layer	Additional parameters required
3	3-D FEM *CANT-SD code* 2-D Analytical conventional analyses	Lade for concrete and rock	Coulomb; No-tension with limit opening	Tringular, variable with water level	Additional parameters required
4	3-D FEM *ANSYS code*	Linear elastic	Coulomb	Tringular, variable with water level	Basic parameters
5	3-D FEM *ANSYS code* Trial Load Method	Linear elastic	Coulomb	Tringular, variable with water level	Basic parameters
6	2-D and 3-D FEM *MERLIN code*	Drucker-Prager (compr.) Smeared crack (tension)	Interface Crack Model (Fract. Mech.); Dilatancy	Variable with crack propagation	Additional parameters required

TABLE 3

Authors/ Company (ID)	Analyses carried out	Comments and notes
1	3-D FEM analysis up to full mobilization of shear strength at the dam-rock interface (non-convergence)	Assuming weak abutments above 820 m asl leads to limit equilibrium for water level below crest; arch effect develops with strong abutments
2	Fully 3-D FEM analysis up to non-convergence; Simulation of the construction process	Gravity resisting mechanism below max water level; Arch resisting mechanism starts at higher levels; Failure starts at the right bank
3	2-D analytical (Chopra) limit equilibrium analysis; Fully 3-D FEM analysis up to non-convergence	When cohesion is not considered, limit equilibrium condition is reached for water level below crest; Failure starts at the right bank Different material parameters does not show great influence
4	Fully 3-D FEM analysis to evaluate effective shear strength on dam-rock interface	Quantitative estimate of arch contribution to prevent sliding
5	Trial Load Method + FEM for the main block; Fully 3-D FEM analysis up to non-convergence	When cohesion is not considered, limit equilibrium condition is reached for water level below crest; Failure starts at the right bank
6	2-D FEM up to non-convergence 3-D FEM for the main block up to n. - c. Fully 3-D FEM up to n.- c. Fully 3-D with vertical joints up to n.- c.	When cohesion is not considered, limit equilibrium condition is reached for water level below crest;

TABLE 4

Authors/ Company (ID)	Load factor Kh		Failure criteria	
	Start of sliding	Generalised sliding IFF (Imminent failure flood)	Physical	Numerical
1		Kh = 1.33 Displacement not defined	Full mobilization of shear strength	
2	Kh = 1.06 - 1.11 Displ. = 2 - 3mm (cross section, crest)	Kh = 1.18 - 1.21 Max displacement (right bank) > 10mm	Displacement of 10mm at dam-rock interface (Kh = 1.2)	Non-convergence of the analysis
3	Kh = 1.07 Displ. < 1mm (right bank, bottom)	Kh = 1.3 Max displacement (right bank, bottom) > 25mm	Start of sliding (Kh = 1.26 when 10mm displacement is reached at dam-rock interface)	Non-convergence of the analysis
4		Kh = 1.2 Max displacement = 2.4mm (cross section, crest), = 0.35mm (cross section, bottom)	Overcome of limit tensile stress in the concrete	
5		Kh = 1.28 Displ. = 13mm (right bank, crest) Displ. = 11mm (right bank, bottom)	10mm at dam- rock interface (Kh = 1.26)	Non-convergence of the analysis
6	Kh=0.89 - 0.95 for 2-D and 3-D models respectively (opening of interface)	Kh=1.05, Displ.=6.5mm (3-D block) Kh=1.27, Displ.= 4mm (3-D model)		Non-convergence of the analysis

TABLE 5

DISCUSSION			
	RESULTS	*OPEN QUESTIONS*	*COMMENTS FROM THE AUDIANCE*
1	*Load Factor Kh ranges between 1.18 - 1.33, Displacements ranges between 4mm - 25mm*	*Can be results considered comparable?*	*The evaluation of the Load Factors is based on the equilibrium of all forces applied to the structure. This aspect is, obviously, safeguarded by all method of analyses and this explains the rather good comparison in terms of Load Factors. The evaluation of displacements depends on the different material and joint models adopted by each participant and this can give rise to some differences in terms of displacements.*
2	*Failure:* • *10mm displacement at the dam base* • *tensile stresses or shear strength overcome* • *start of sliding* • *non-convergence of the analysis*	*Which of the previous conditions can be considered failure?*	*Different aspects have to be considered contemporaneously and none of them should be ignored, in particular when safety assessment has to be carried out (see next point). What can be defined failure is debatable. From the numerical point of view, it is undeniable that it has to be identified with the lack of convergence of the analysis. From the physical point of view criteria based on defined displacement and stress values should be assumed as "intermediate limit states". Also the start of sliding could be considered as an "intermediate limit state".*

3	***Failure criteria and safety***	***Which is the relationship between failure criteria and safety?***	***Safety engineering judgement has to be based mainly on physical considerations. Experience, of course, play a predominant role. However, numerical models capable to analyse complex scenarios which effects can not be predicted by simplified or conventional approaches could be of the utmost importance to address the engineering judgement and to avoid choices that could be over- as well as under-conservative.***
4	***Reliability of numerical modelling***	***On the basis of the comparative good performance of the different computer codes, which is the judgement on the reliability of numerical modelling?***	***Reliability of numerical models can not be based just on comparative terms (i.e. the fact that different computer programs give similar results simply means that algorithms are correctly implemented in the code, and the differences have to be ascribed to the different models of materials and interfaces). Reliability has also to be based on the capability of the models to represent the physical-mechanical behaviour of materials and structures. Moreover, for real cases, reliability of the analyses has to be based on the availability of data on the past dam behaviour in order to allow a "calibration" of the models (by means of back-analyses) that can be adopted to support the dam safety assessment.***

2 CONCLUSIONS

The case proposed as Theme A – Concrete Dams as obtained a good success in terms of numbers of participants and keeping into account the quality of the papers. Most of the participants, moreover, have carried out more than the specific analysis requested by formulators. This aspect can allow to make a comparison not only in terms of differences between 2-D vs. 3-D analyses in the evaluation of load factors associated to sliding, but also to examine the influence of different mechanical parameters and models on the results.

The critical examination of the results obtained for Theme A could be of some benefit also for national and international organisms which are entrusted to issue and to apply standards and guidelines.

REFERENCES

1. **ICOLD,** Bulletin n°. 94. *Computer software for dams. Validation. Comments and proposals.* 1994.
2. **ICOLD,** Bulletin n°. 122. *Computational procedures for dam engineering.* 2001.
3. **P. Londe,** ICOLD, *Transactions*. Proceedings of the Seventeenth International Congress on Large Dams. Vienna, 17-21 June 1991, pp. 319-320.
4. **ENEL S.p.A, ISMES S.p.A.,** *Seismic Reassessment of ENEL Dams*. Proceedings of the Eighteenth International Congress on Large Dams, Durban (South Africa), Vol. 1, Q. 68, R. 64.
5. **M. Fanelli, G. Mazzà, G. Ruggeri, P. Palumbo,** *Gravity Dams: Safety Evaluation Against Sliding With A 3-D Rigid Body Formulation*. Proceedings on Research and Development in the field of Dams, Crans Montana (Switzerland), 7-9 Sept., 1995.

ANIDEL. Dams for hydroelectric power in Italy. Volume n°. 4, 1952.

Generalization of Classical Limit State Analysis Using a Variational Finite Element Approach

Bruce Brand
Federal Energy Regulatory Commission (USA)

SUMMARY: The term "Non-Linear Analysis" typically refers to analyses in which deflection is not a linear function of load. Historically, dam and foundation engineering has been dominated by non-linear assumptions. Rock wedge analyses, slip circle slope stability analyses, and gravity dam sliding and overturning analyses, are all examples of non- linear analysis. The widespread use of the finite element method over the past 30 years has muddied what used to be the clear understanding of the need to identify and evaluate failure mechanisms. It has been my experience that linear finite element analyses often give a very precise answer to the wrong question. In response to this problem, the Federal Energy Regulatory Commission (FERC) has generalized traditional limit state analysis into a family of finite element codes. This paper discusses a variational solution technique which easily accommodates concrete cracking and shearing, and yields unique solutions to non-linear problems.

RÉSUMÉ : Le terme "Analyse non-linéaire" se réfère habituellement aux analyses où les déflexions ne sont pas une fonction linéaire du chargement. Historiquement, l'ingénierie des barrages et des fondations a été domineer par des hypothèses de comportements non-linéaires. Les analyse de stabilité de blocs de roc, les cercles de glissement dans les talus et le glissement et renversement des barrages-poids sont tous des exemples d'analyses non-linéaires. L'utilisation à grande échelle de la méthode des elements finis pendant les 30 dernières années a assombri ce qui était auparavant une compréhension claire de la nécessité d'identifier et d'évaluer les mécanismes de défaillance. Mon expérience m'indique que l'utilisation d'analyses linéaires par éléments finis donne le plus souvent une réponse précise à la mauvaise question. En réponse à ce problème, la Commission Fédérale de Régulation de l'Énergie (FERC) a généralisé les techniques d'analyses limites traditionnelles à l'aide d'une famille de logiciels d'éléments finis. Cet article discute d'une technique de resolution variationnelle qui permet de tenir compte facilement de la fissuration du béton, de l'endommagement en cisaillement et qui permet d'obtenir une solution unique pour les problèmes non-linéaires.

1. HISTORICAL BACKGROUND

Although it may not be thought of in these terms, the conventional gravity dam stability analysis, checking for sliding and overturning, is in fact non-linear analysis. Inherent in these traditional analyses are the stress strain relationships depicted in Figure 1. It has always been assumed that while shear stress, τxy will increase linearly with shear strain γxy to some limiting value which is function of normal stress. Also, the no-tension-at-the-base criteria means that the linear relationship between vertical compressive stress σyy, and strain ,εyy, is interrupted as soon as the base goes into tension.

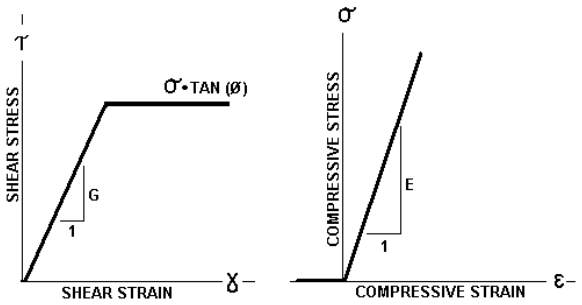

Fig. 1 Assumed stress/strain curves

These assumptions have been regarded as common sense dam engineering for over a century. They underlie the United States Bureau of Reclamation's and U.S Army Corps of Engineers guidelines for gravity dam stability. This traditional limit equilibrium approach simply and un-ambiguously addresses dam gravity stability. The problem with this traditional approach however, is that it can not be used to model arch dams, gravity dams that are not straight, gravity dams on non-planar foundations, or any other situation where there is significant structural redundancy.

Over the past 30 years, this limitation has been addressed through finite element modeling. In the great majority of analyses that the FERC has received, the finite element models have been linear elastic models. These models solve the problem of structural redundancy, but they can not model failure. Because of this, there is no rational way of computing a safety factor against failure.

Non-linear finite element techniques capable of accounting for concrete cracking and shearing are now quite common. They are typically stiffness matrix based. Non-linearities are accounted for by application of structural loads in small increments and a continual modification of the stiffness matrix. as individual elements are softened or removed. The limitations of a linear stiffness matrix are thus overcome by turning the non-linear problem into a series of piecewise linear problems.

2. THE VARIATIONAL TECHNIQUE

2.1 DEPARTURE FROM STANDARD METHODS

The variational technique that the FERC is currently using for non-linear structural analysis is unique becasue it is not a matrix method. Because of this, it can more easily handle material and geometric non-linearities.

Variational principles are very often used in the formulation of element stiffness matrices. The relationship between nodal forces and nodal deflections are derived using the fact that for the "correct" set of nodal displacements given an applied force

vector, the energy produced by differential movement (dU) of an applied force will be exactly offset by a corresponding change in the internal strain energy of the element. This is known as the theorem of minimum stationary potential energy. It can be expressed as follows:

$$\iiint (\sigma \frac{d\varepsilon}{dU}) dxdydz \quad - FdU \quad = 0 \qquad Eq.\ 1$$

Typically, once the individual element stiffness relationships are established using Equation 1, they are assembled into a global structural stiffness matrix. The matrix is then solved for displacements give applied loads. These displacements are then back substituted into the element stiffness matrices to calculate element stresses.

In the FERC's global variational technique, a structural stiffness matrix is not used. Rather, the variational principles commonly used to formulate individual element load - displacement relationships are applied to the structure as a whole. For a given set of nodal displacements, the change in the potential energy of the entire structural system due to a differential change of a single degree of freedom represents the slope of the potential energy surface with respect to that degree of freedom.

Consider the following illustrative example using a 2 degree of freedom model made up of constant strain triangles (Figure 2). A force "F" will be applied to node 6 in the positive X direction. Nodes 5 and 6 are free to move in the X or Y direction, but the symmetry of the problem assures that there will be no motion in the Y direction. All other nodes are fixed. U_5 and U_6 then are the magnitudes of deflection in the X direction at nodes 5 and 6 respectively. For this case, the potential function for the system can be expressed as a function of the 2 degrees of freedom, U_5 and U_6 as follows:

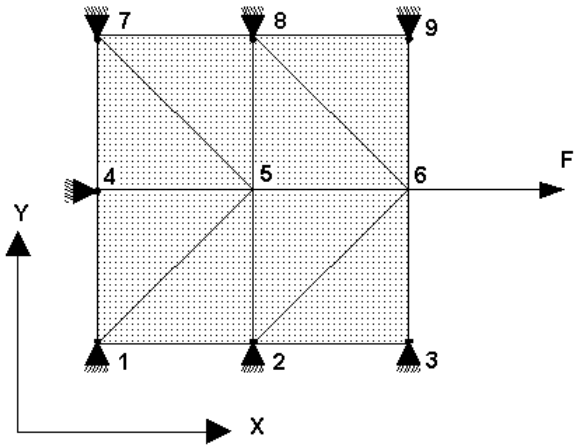

Fig. 2 Example

$$\prod = \sum_{i=1}^{8} A_i \left(\int_0^{\varepsilon_x} \sigma_x d\varepsilon + \int_0^{\varepsilon_y} \sigma_y d\varepsilon + \int_0^{\gamma_{xy}} \tau_{xy} d\gamma \right) - F_6 U_6 \qquad Eq.\ 2$$

The summation in Equation 2 is over the 8 elements in the model. Ai is the element area. The strains are functions of U_5 and U_6 through the element displacement fields as follows:

$$\begin{pmatrix} \varepsilon_x \\ \varepsilon_y \\ \gamma_{xy} \end{pmatrix}_i = \begin{pmatrix} b_{11} & b_{12} \\ b_{21} & b_{22} \\ b_{31} & b_{32} \end{pmatrix}_i \begin{pmatrix} U_5 \\ U_6 \end{pmatrix} \qquad Eq.\ 3$$

The b_{ij} in Equation 3 are the standard constants dependent only on the geometry

of the element being considered. In the case of linear, plane stress, the stresses in each element are functions of the strains as shown in equation

$$\begin{pmatrix}\sigma_x\\ \sigma_y\end{pmatrix}_i = \frac{E}{(1-\upsilon^2)}\begin{pmatrix}1 & \upsilon\\ \upsilon & 1\end{pmatrix}_i\begin{pmatrix}\varepsilon_x\\ \varepsilon_y\end{pmatrix}, \quad \tau_{xy} = G\gamma_{xy} \qquad \textit{Eq. 4}$$

Combining equation 2 and 4 results in the following expression:

$$\prod = \sum_{i=1}^{8} A_i\left[\frac{E}{2(1-\upsilon^2)}(\varepsilon_x^2 + \varepsilon_y^2 + 2\upsilon\varepsilon_x\varepsilon_y) + \frac{G}{2}(\gamma_{xy}^2)\right]_i - F_6U_6 \qquad \textit{Eq. 5}$$

Equation 5 is plotted with respect to U_5 and U_6, in Figure 3. The surface formed has a minima which corresponds to the displacement state at which a differential movement in either the U_5 or U_6 direction causes no change in the potential. The solution represents not only the point on the potential surface where a differential change produces no effect, but also the bottom of the potential energy surface. Because of this, a gradient following numerical solution technique corresponding to Newton's method in N dimensions can be employed to find the correct displacement vector.

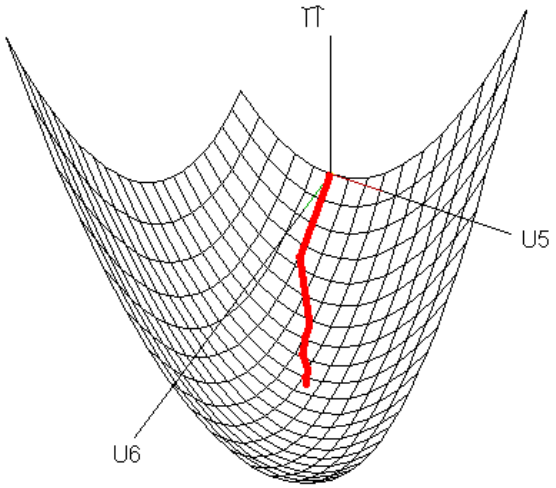

Fig. 3 Potential energy surface

2.2 THE NATURE OF THE POTENTIAL ENERGY SURFACE

The nature of the potential surface can be seen in Figure 3 as well as the path taken to the minima by the solution technique (heavy line). The potential surface depicted in Figure 3 has one and only one relative minima. This guarantees the uniqueness of the solution. In order to demonstrate this fact, equation 6 must be re-written in terms of U_5 and U_6. Inserting Equation 3 into Equation 5, the potential energy surface is of the following form:

$$\prod = \sum_{i=1}^{8} A_i(K_{1i}U_5^2 + K_{2i}U_6^2 + K_{3i}U_5U_6) - F_6U_6 \qquad \textit{Eq. 6}$$

Where for each element i,:

$$K_1 = \frac{E}{2(1-\upsilon^2)}(b_{11}^2 + 2\upsilon b_{11}b_{21} + b_{21}^2) + \frac{G}{2}(b_{31}^2)$$

$$K_2 = \frac{E}{2(1-\upsilon^2)}(b_{12}^2 + 2\upsilon b_{12}b_{22} + b_{22}^2) + \frac{G}{2}(b_{32}^2)$$

$$K_3 = \frac{E}{2(1-\upsilon^2)}(b_{11}b_{12} + b_{21}b_{22} + \upsilon(b_{11}b_{22} + b_{21}b_{12})) + G(b_{31}b_{32})$$

It is clear by inspection that there is only one (U_5,U_6) which satisfies the criteria that the derivative of the potential function with respect to U is zero, It can also be seen that K_1 and K_2 are always positive. If K_3 is greater than $(K_1K_2)^{1/2}$, the surface could be a saddle, however it can be shown that for $v^2 < 1/2$ K_3 is always less $(K_1K_2)^{1/2}$ which guarantees that the this unique displacement vector represents a true minimum. This makes physical sense since if this were not the case, there would be a displacement vector that would produce negative strain energy.

2.3 THE EFFECT OF MATERIAL NON-LINEARITY ON THE POTENTIAL SURFACE

The effect of non-linear material behaviour such as cracking, yielding, or frictionfull shearing is to de-couple stress and strain so that stress is constant (or zero) with respect to strain. Equation 5 is effected by the addition of first order strain terms. This produces first order deflection terms in Equation 6 and diminishes the second order terms. These first order terms do not change the concave up character of the surface and therefore, do not destroy the uniqueness of the solution. If cracking and yielding progresses to a point where one or more of the second order terms vanish, a solution does not exist. This corresponds to structural failure.

To illustrate the effect of yielding on the shape of the potential surface, again consider the structure depicted in Figure 2 A Von-Mises yield criteria will be assumed.

$$\sqrt{\sigma_1^2 - \sigma_1\sigma_2 + \sigma_2^2} \le \sigma_{yield}$$

The force applied at node 6 is increased to structural failure. This potential surface is depicted in Figure 4. Notice that the curvature with respect to the U_6 direction vanishes as U_6 becomes large. In this region, the variational strain energy of continued displacement in the U_6 direction is exactly offset by the variational displacement energy of the applied load F. This corresponds to yielding.

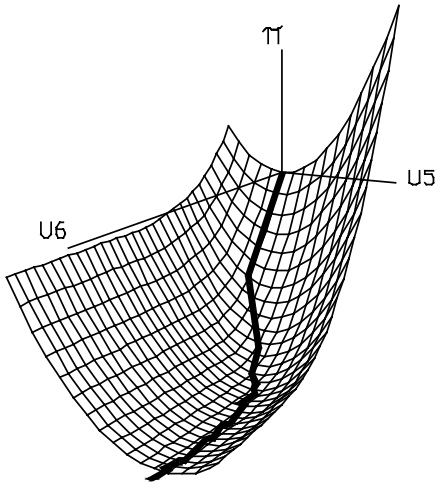

Fig. 4 Effect of yielding on energy surface

The potential surface can be thought of as a n dimensional bowl. The effect of applied loads is to tilt the bowl. If the bowl has positive curvature in all directions, no

amount of tilting could cause a ball to role out of the surface. However, if there is a direction along which the curvature becomes zero, tilting the bowl in that direction will eventually produce a situation in which a ball can roll out. This corresponds to structural failure.

2.4 THE ADVANTAGE OF THE VARIATIONAL TECHNIQUE

Current practice in non-linear finite element modelling of structures requires the load to be applied gradually, (load stepped), and at each load increment, all elements must be checked to see if a failure or yield criteria has been exceeded. If it has, the cracked or yielded element must be removed from the stiffness matrix, or its effect offset by a fictitious load in the load vector. Many iterations are required at each load step to achieve a solution. In addition, convergence becomes load step dependent.

The advantage of this technique over standard matrix methods is that there is no requirement for linearity, even piecewise linearity, in the material constitutive relationships or the relationships linking strain to displacement. All non-linearity is accounted for in the shape of the potential energy surface. Load stepping is not necessary. In addition, if the stress-strain relationship is one to one, the solution, if found, it is unique.

3. THE TRIANGULAR FAILURE ELEMENT

Generalizing the traditional limit state assumptions so that limit state analysis can be performed on 3 dimensional structures of arbitrary geometry requires that non-linearity be introduced into the finite element model in the same manor as it is used in traditional limit state analysis.

Figure 5 depicts the typical limit state assumptions. The triangular failure element (TFE) must have all of the same features:

1) Planar normal stress distribution.
2) No tension allowed.
3) Shear limited to normal stress times a friction coefficient.

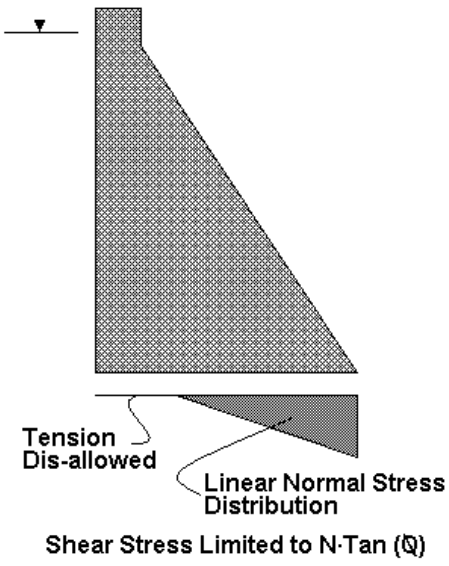

Fig. 5 Traditional limit state assumptions

3.1 FORMULATION OF THE TFE

The TFE is defined by 6 nodes. The element is formulated assuming a unit thickness, ie the distance normal to the failure plane, between i and l, j and m , and k and n is one unit, The local axes, R and S are as shown in Figure 6. The element displacement field is planar. Since the element is formulated assuming unit thickness, the resulting strain (and stress) fields are also planar. Distortion of the ijk plane or the lmn plane by itself does not produce any internal stress. It is only relative deformation between the top and bottom element planes that results in internal stress. The relative normal and shear displacement fields are of the following form:

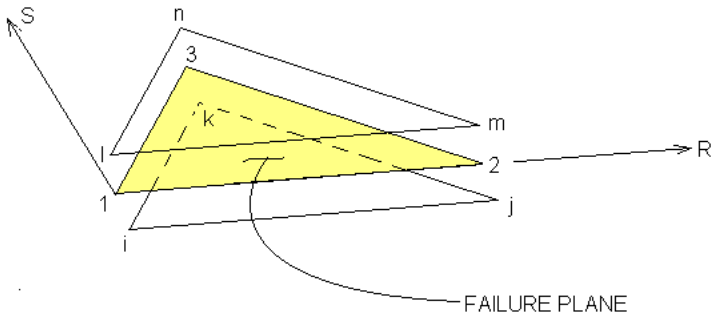

Fig. 6 Triangular Failure Element (TFE)

$$U = U_1\left(-R/R_2 + \left(R_3/R_2 - 1\right)\left(S/S_3\right) + 1\right) + U_2\left(R/R_2 - \left(R_3/R_2\right)\left(S/S_3\right)\right) + U_3\left(S/S_3\right) \qquad \text{Eq. 7}$$

Where: $U_1 = (U_l - U_i)$; $U_2 = (U_m - U_j)$; $U_3 = (U_k - U_n)$

Strain energy in the element is directly integrated. With respect to stresses normal to the failure plane, the element only resists compression. Regions of tensile strain, are omitted from the strain energy computation. Energy due to shear strain is also computed by integrating only over the portion of the failure plane in compression. Resulting nodal shearing forces are further limited to a friction coefficient (Tan(φ)) times the compressive nodal force.

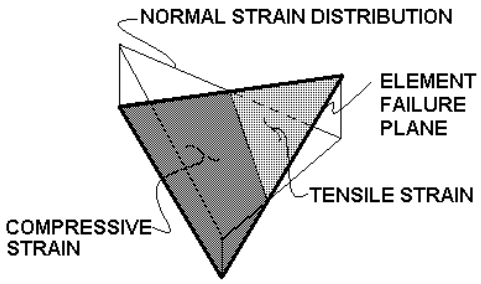

Fig. 7 TFE planar strain field

The variational solution scheme described in Section 2 easily accommodates the TFE.

3.2 PERFORMANCE OF THE TFE

The goal of this type of non-linear modelling is to generalize the traditional limit state analysis to 3 dimensional structures of arbitrary geometry. A non linear analysis of a two dimensional gravity dam on a rigid foundation

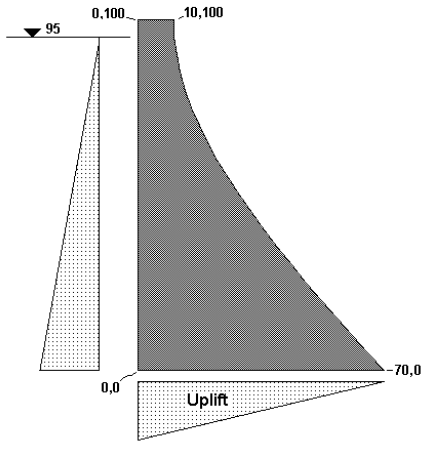

Fig.8 Two dimensional example

using a finite element model with TFE's should duplicate the results of a conventional gravity analysis. Consider the gravity dam example shown in Figures 8 and 9.

Figure 9 shows the non-linear finite element solution. The foundation contact is modelled with 4 TFE's, one pair overlapping the other pair. While 2 TFE's would have been sufficient, 4 were used in this example. With 4 TFE's, each of the 4 base nodes of the dam has 2 TFE nodes attached to it. This guarantees that nodal stiffness does not vary in the third dimension. The dam body is modelled with 8 node brick elements with a linear stress strain relationship.

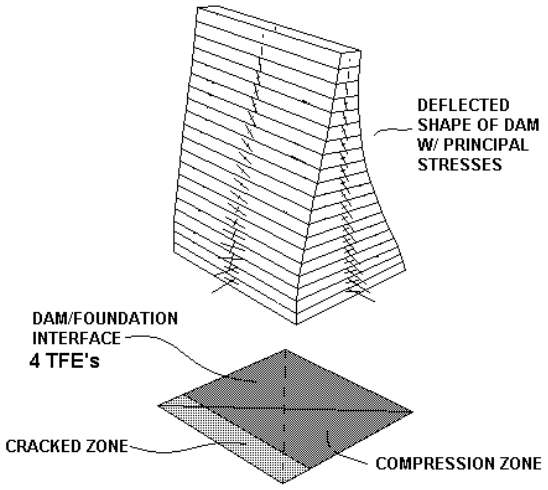

Fig. 9 Non linear finite element solution

Ideally, the amount of base cracking, and the fraction of mobilized foundation shear strength resulting from the non linear finite element solution should be the same as that calculated by traditional limit state gravity dam analysis. The results of the non-linear finite element analysis are as follows:

Portion of base cracked	23%
Friction angle required	45.6°

The table below shows the results of a standard gravity dam analysis.

GRAVITY DAM ANALYSIS USING STANDARD TECHNIQUES UNITS kN, M

FORCE DESCRIPTION	F->	ARM	F^	ARM	M @ 0,0 (heel)
DAM WEIGHT-->			-76613.98	21.52	1648732.82
RESERVOIR LOAD-->	44222.50	31.67			1400526.58
UPLIFT-->			32585.00	23.33	-760316.67
TOTAL FORCE =	44222.50		-44028.98		2288942.73

RESULTANT AT	51.99
CRACK LENGTH	15.96
% BASE CRACKED	22.8
FRICTION ANGLE REQUIRED	45.13°

This comparison shows that the non-linear technique described above duplicates standard gravity dam analysis quite well.

4. APPLICAITON OF VARIATIONAL NON LINEAR SOLUTION TECHNIQUE TO THEME A PROBLEM

Now that the classical limit state analysis technique has been incorporated into a general 3 dimensional finite element model through the use of the TFE and the variational energy method, limit state analysis can be performed on 3 dimmensinal structures of arbitrary geometry. The Theme A problem is solved below subject to 2 different assumptions.

1) Weak abutment assumption. First, because it is not clear whether or not there is anything to resist arch thrusts above elevation 820, the dam was analysed assuming that there is no means of resisting arch thrusts above this elevation.

2) Hard abutment solution. This analysis assumes hard vertical abutments from elevation 820 up to the top of the dam. (Elevation 830.5)

In these two analyses the flexibility of the foundation is ignored. Again, this is an attempt to be faithful to the assumptions that underlie the traditional limit state method. In addition, the dam will be modelled with only 1 layer of linear 8 node brick elements through the dam thickness. Because the linear 8 node brick elements and the TFE's have linear stress variation, the linear base pressure distribution that is typically assumed in traditional limit state analysis will be preserved in this technique.

Uplift pressure is applied to the dam base assuming a linear variation from full reservoir pressure upstream to zero downstream. The uplift pressure distribution is not altered by base cracking. In 2 dimensional analysis it is often assumed that an open crack is pressurized to full reservoir head, and that no pressure reduction occurs. This assumption is based on the idea that the compression zone downstream of the crack tip will be much less pervious and therefore prevent water flow tin the crack. When the foundation crack is 3 dimensional, water can flow around compression zones, and therefore the flow/pressure situation in the crack is much more complicated. For this reason, linear variation of uplift pressure is also assumed in cracked areas.

4.1 ANALYSIS ASSUMING NO SUPPORT ABOVE ELEVATION 820

Assuming no support above elevation 820, the dam is found to be at incipient failure with a load factor of 1.0. The adverse orientation of the foundation contact over much of the dam's base combined with a relatively low friction angle (35°) results in failure under normal reservoir conditions. (Figure. 10) This begs the question, "Why has the dam stood there for 80 years?". The reason is probably a combination of higher than assumed friction at the base due to rock asperities, and some support above elevation 820.

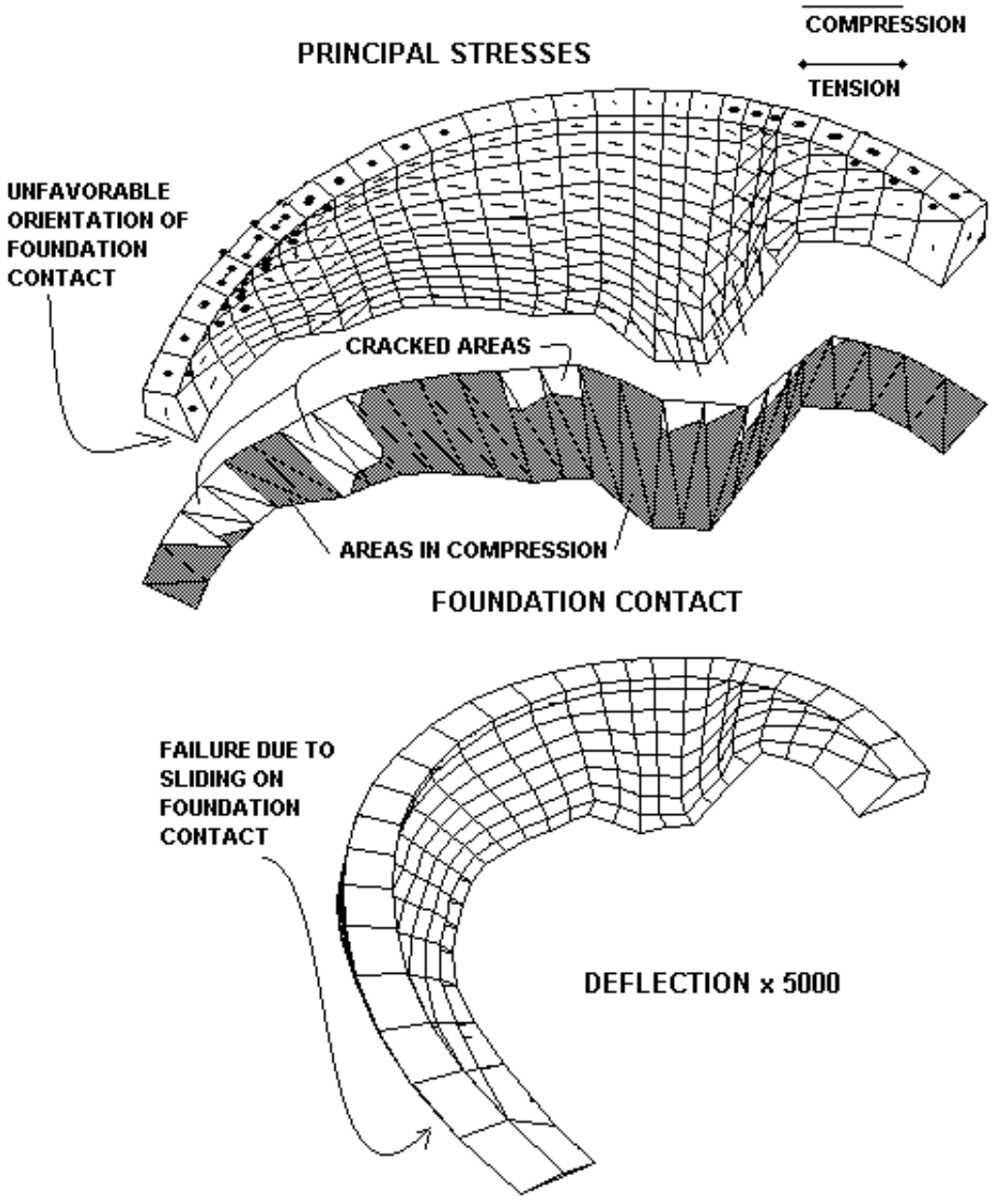

Fig. 10 Dam unsupported above elev. 820

4.2 ARCH THRUSTS RESISTED TO TOP OF DAM

Figure 11 shows the results of the assumption of hard abutments above elevation 820, load factor of 1.0. When this assumption is made, the adverse orientation of the contact planes on the base of the dam becomes unimportant as arch thrust redistributes load to the vertical abutments above elevation 820.

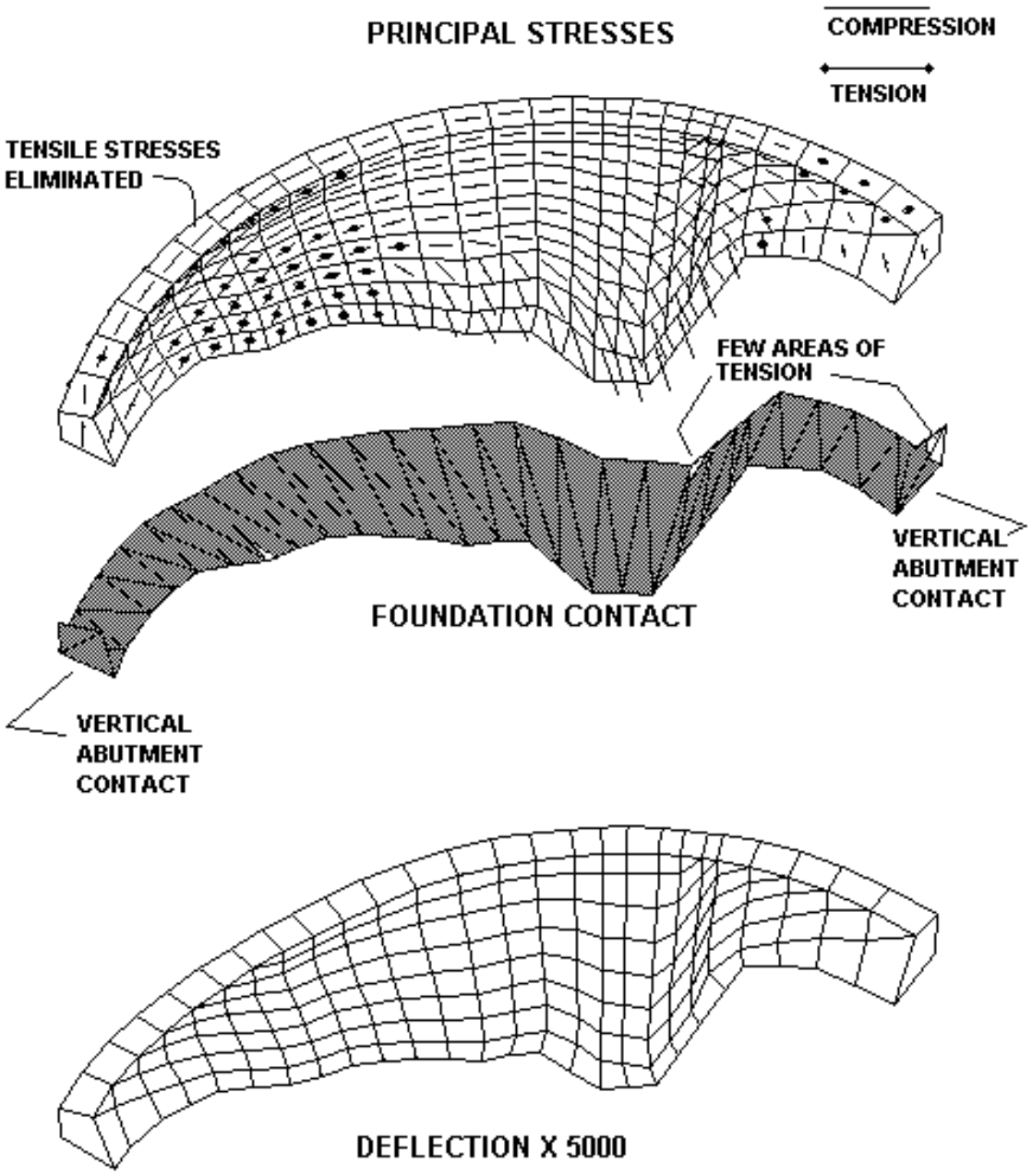

Fig. 11 Dam with hard abutments above elev. 820

4.3 FAILURE MODE OF THE DAM WITH HARD VERTICAL ABUTMENTS ABOVE ELEVATION 820

For the rest of this exercise, we will consider only the hard abutment case and increase the reservoir elevation until failure.

4.3.1 *Monolithic dam loaded until tensile strength limit is exceeded*

Figure 12 shows the state of the dam with the reservoir at elevation 842, 11.5 meters over the crest. The shear strength of the base of the dam is fully mobilized. Note that very little of the base is under compression as the load drives the dam downstream and uplift forces reduce the compressive contact between the dam and the foundation. The dam is equalibriated by arch thrust into the vertical abutments.

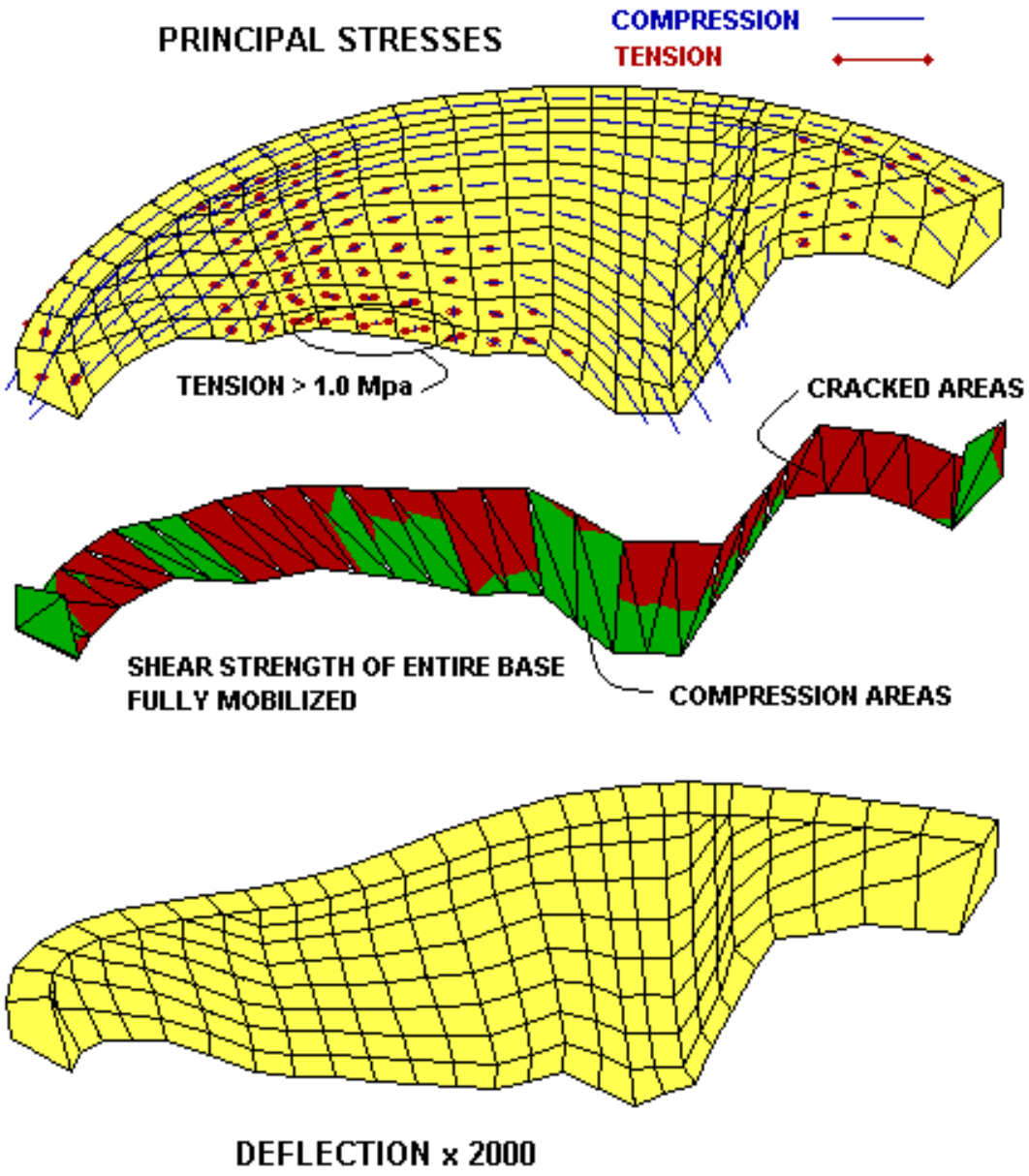

Fig. 12 Monolithic dam with reservoir @ 842

Note that the tensile strength limit of 1.0 Mpa is starting to be exceeded in the arch direction on the downstream face near the base.

The tension limit exceedence can be handled in several ways. For example, it can be assumed a single crack initiates at the location of peak tensile stress and then propagates through a homogeneous elastic monolith according to principles of fracture mechanics. The author will take a different approach. It will now be assumed that the dam is pre-cracked by vertical joints. While no information was provided as to the location of pre-existing cracks or vertical construction joints, the author regards the existence of pre-existing vertical or near vertical cracks within a few meters of any arbitrary point a virtual certainty.

4.3.2 *Dam with vertical joints*

Figure 13 shows the state of the dam with the reservoir at elevation 842, 11.5 meters over the crest, assuming arch tensile stress relief by vertical joints. The joints are modelled using TFEs in the same way the foundation contact is modelled. It is assumed that the friction angle on vertical joints is 55°. Hydraulic pressure is applied to the vertical joints in the same manor as it is applied to the foundation. Note the joint opening in the area of high arch tension stress shown in Figure 12.

There is no kinematically admissible failure mechanism for the dam as long it is in contact with the abutments. The only way the dam can fail without crushing concrete is to float upward due to uplift forces so that it is no longer in contact with the abutments. This is unlikely. Since the variational technique is robust and continues to converge as the reservoir level rises, failure will be governed by material strength exceedence rather than kinematic sliding.

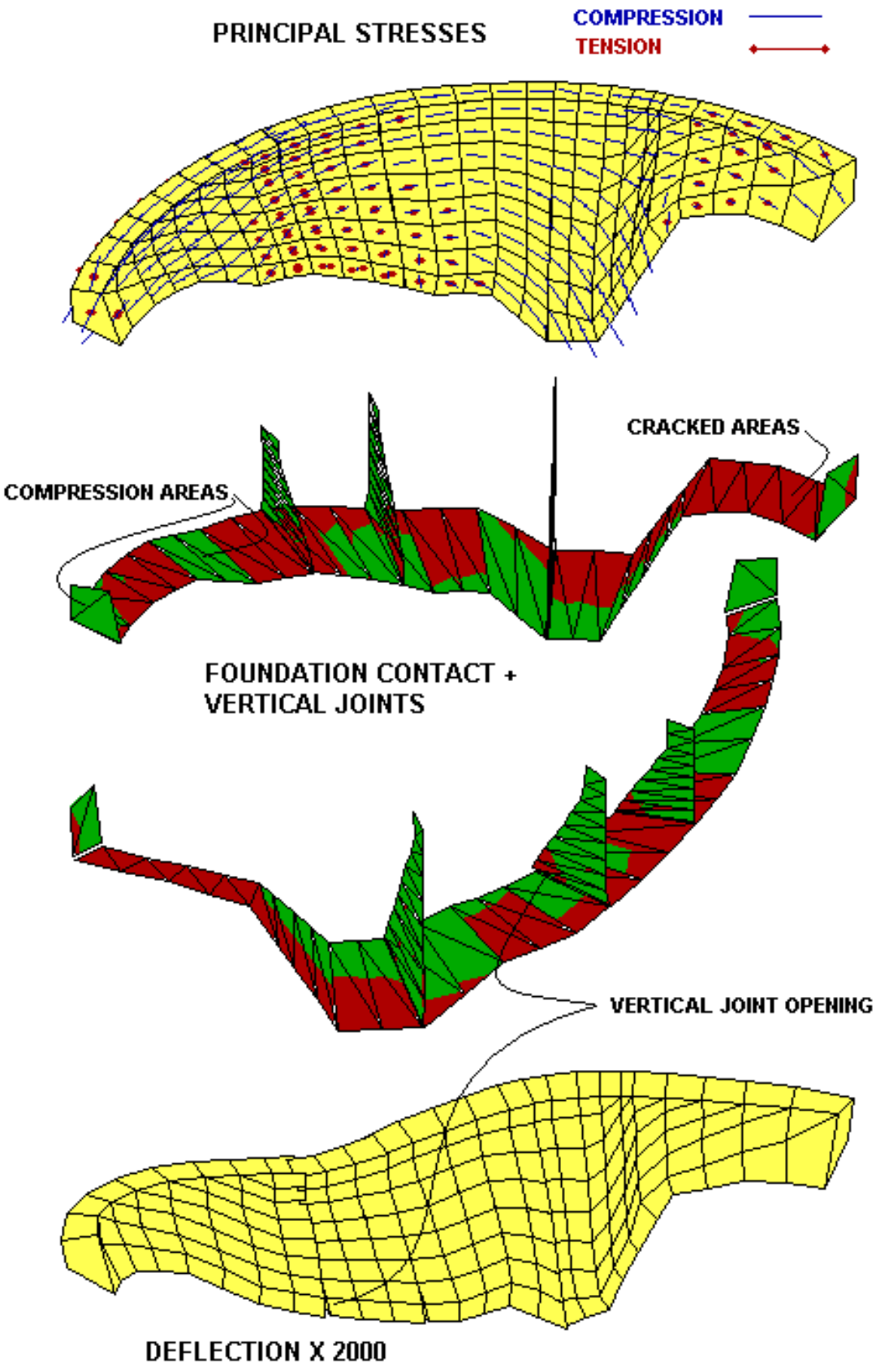

Fig. 13 Dam with vertical joints. Reservoir @ 842

4.3.3 *Limit state of dam, Reservoir at Elevation 854*

Figure 14 shows the limit state of the dam. At reservoir elevation of 854, the compressive strength of the concrete begins to be exceeded in the arch direction. In addition, the compressive stress on the vertical abutments approaches the upper limits of abutment strength. While additional joints could be added to relieve areas of high tensile stress, the fact that compressive strengths are being exceeded means that redistribution of additional load into arch compressive stress is no longer possible.

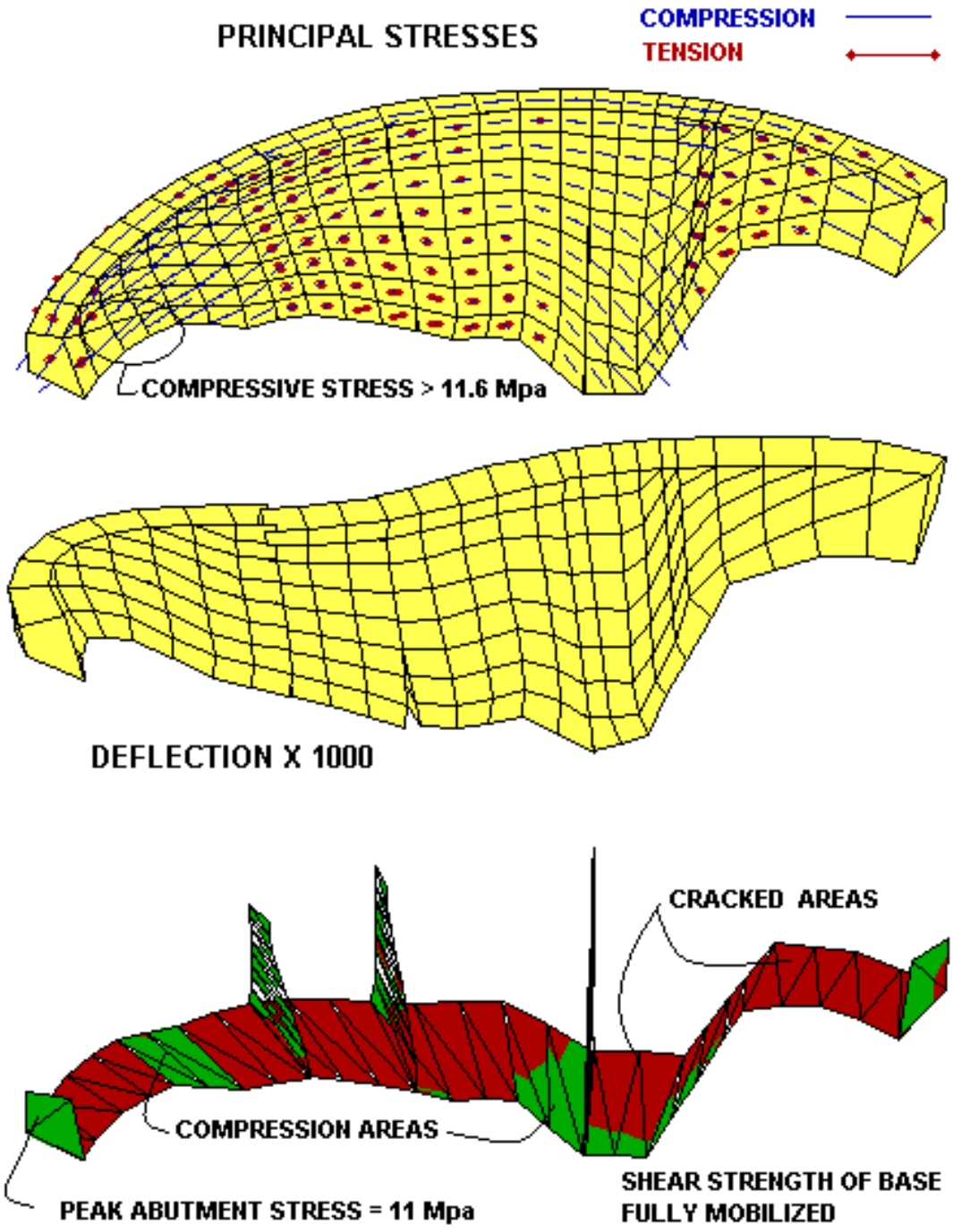

Fig. 14 Limit state of dam. Reservoir @ 854.

5. CONCLUSION

The model presented in this paper is deliberately crude. The model assumes linear stress distributions through the dam's thickness, and ignores the principles of fracture mechanics. Its purpose is not the precise modelling of stresses. What is intended is a generalization of the classical limit state analysis techniques of dam engineering to allow the modelling of 3 dimensional structures of arbitrary geometry. As a result, stability analyses performed using this technique can be compared directly to results from classical analysis.

EFFECT OF THE CREST CURVATURE ON THE ULTIMATE STABILITY OF GRAVITY DAMS *

Alain Carrère, Matthieu Béraud
Coyne et Bellier, Bureau d'Ingénieurs Conseils, Gennevilliers, FRANCE

SUMMARY: The behaviour of SCALERE dam, a concrete dam with a standard gravity profile and a strongly curved crest, is analysed when loaded with an artificially exaggerated hydrostatic loading, increased until instability is evidenced. The exercise has made use of the poroplastic model, a mechanical-hydraulical coupled model, able to reproduce plasticity and cracking of materials, plus resulting pore pressure variations. The calculations were carried out with BETHY, a FEM code dedicated to arch dams design and check. The first main resisting scheme, which is that of a gravity dam, was found stable as long as the loading remains below the normal level, then plunging arches start efficient action. When the water level is about 10 metre above normal level, then right abutment of plunging arches start sliding along their foundation, displacements increase dramatically and materials damage generalises. However at this stage there still exist resistance resorts especially at crest level which the analysis could not catch out.

RÉSUMÉ: Le comportement du barrage de SCALERE, un barrage poids en béton fortement arqué, est analysé lorsqu'il est soumis à une charge hydrostatique artificiellement exagérée jusqu'à la mise en évidence de la rupture. L'étude a fait appel au modèle poroplastique, un modèle couplé mécanique-hydraulique capable de représenter la plasticité, la fissuration des matériaux, et les changements de sous-pression qui en résultent. Le code aux éléments finis BETHY, dédié au dimensionnement et à la vérification des barrages voûtes, a été utilisé. Le mécanisme résistant principal, qui est celui du barrage poids, résiste tant que le chargement ne dépasse pas la cote de chargement normale, ensuite les arcs plongeants prennent efficacement le relais. C'est pour une surcharge d'environ 10 mètres d'eau qu'on voit l'extrémité droite de ces arcs glisser sur leur fondation, en même temps que les déplacements augmentent et que l'endommagement se généralise. Il existe cependant encore à ce stade des réserves de résistance notamment en crête, que l'analyse n'a pas réussi à mettre en défaut.

* Rôle de la courbure de la crête des barrages poids sur leur stabilité ultime.

1. SELECTION OF METHODS, TOOLS, PARAMETERS AND PROCEDURES

1.1 SELECTION OF THE METHOD OF ANALYSIS

The profile of SCALERE dam [1] is that of a slightly insufficient gravity dam with the sum of face slopes equal to 0.69, it is therefore believed that it will react as a pure gravity dam when the water level remains below or close to the crest level. This is the first resisting mechanism of this structure, and the more rigid one. However, should the crest alignment be straight, the stability of the crown section would become quickly hazardous, since drainage is provided neither inside the dam body nor in the foundation. Moreover, the artificial increase of the hydrostatic load above the crest level will definitely win the gravity mode resistance rather soon.

The very sharp curvature in plane certainly favours the development of resisting arch forces, but these can appear only if displacements are made possible, which is not the case when the gravity scheme still resists. The arching effect is therefore only a second level resisting scheme, at maximum.

The shape of the foundation on the banks may limit the resistance of the dam and may particularly make the abutments of the arches sliding, therefor limiting the arch capability to resist excessive loads. The gentle slope on the Right abutment in the bank-to-bank direction may allow movement upward, and also the downstream sloping of the foundation may additionally lead to sliding towards downstream. Only the top arches in the top 10 metre have a sound foundation (at least in the model provided).

This leads to the belief that not one single sudden failure will be observed when the hydrostatic load is progressively increased, but a succession of local ruptures, which will allow spare equilibriums to appear when the initial ones are exceeded. In such conditions, it has been considered that the numerical approach to be used should be able to take into consideration the deformations of the structure and its foundation, and should be able to represent all local failures progressively according to the modifications of the global equilibrium.

The most common numerical tools which are able to do that are finite elements with non-linear constitutive laws of the materials. They proceed with iterative calculations to adjust deformations to stress levels. This allows easy adjustment of the equilibrium when only local failures occur. But when the failure criteria violation becomes general, the iterative process is not able to converge and the stability cannot be reached. Observation of convergence rates is therefore part of the results, and a lack of convergence is then to be interpreted as infinite displacements.

The tool which has been selected to solve the proposed problem is BETHY, a finite element code which is able to consider complex constitutive laws for rock and concrete. It is based on the theory of poroplasticity [3] [4], and it has been mainly used to date for the dimensioning and the safety evaluation of large arch dams.

1.2 MAIN FEATURES OF POROPLASTIC MODELS

Poroplasticity is a constitutive model for geomaterials that takes into consideration non-linear phenomena which may enter into action, plus the influence of their water saturation. It has been developed by B. FAUCHET during a Doctorate thesis [3] [4] prepared in Coyne et Bellier. Poroplasticity is based on the theory of poro-elasticity developed by BIOT in 1972, which has been extended in the non-linear field by COUSSY in 1989. The porous medium is described as biphasic. The first phase is composed of the connected voids, which are saturated by a fluid (water or air); the second one is the complement, i.e. the solid part or matrix. Any stress component applied to the porous medium is decomposed into one part applied to the fluid and one part applied to the matrix. The second one is named effective stress. The concept of poroplasticity is therefore a coupled approach, which is an extension of the pore pressure concept in Soil Mechanics. The equation is

$$\sigma_{el}' = \sigma - b * p$$

where

σ'_{el} is the effective stress

σ is the total stress

p is the fluid pressure,

b is the Biot coefficient, the value of which is between the initial material porosity and 1; this coefficient quantifies the fraction of a volumetric deformation that affects the connected volume of voids in the elastic field.

A similar equation links stresses in the plastic field:

$$\sigma_{pl}' = \sigma - \beta * p$$

A plastic constitutive law is given to the solid phase, which links volumetric and deviatoric deformations to the effective stress state. It can be the Hoek-Brown or the Drücker-Präger laws. In the present case the William-Warnke criterion is preferred since it better fits the behaviour of concrete in the field of low confining stresses.

Finally the permeability of the medium is modified as a function of porosity variations. It is assumed that all volumetric plastic deformations correspond to the opening of cracks, and the permeability is increased in the direction of cracks as a crack permeability.

BETHY software performs in a coupled way the mechanical calculation on the matrix phase and the seepage analysis on the fluid phase. Water pressure interacts with effective stresses, corresponding deformations interact with permeability.

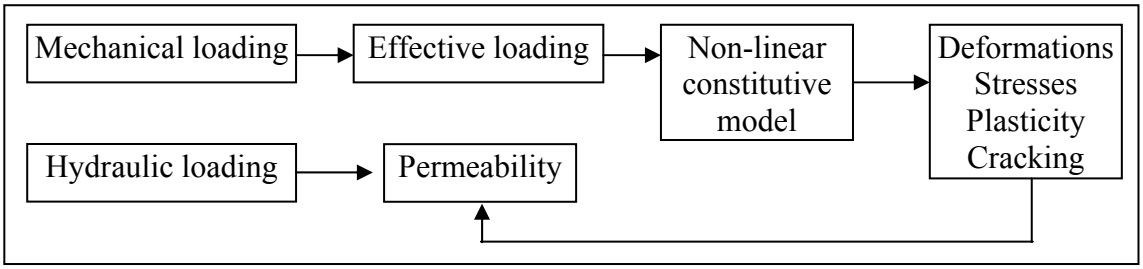

1.3 PREPARATION OF THE NUMERICAL MODEL

The preparation of the model started with the definition of the mesh. The mesh was prepared for use with second-degree isoparametric elements, in which the distribution of displacements is supposed to be parabolic. The Formulators provided the general shape of the dam, the foundation and the rock-concrete contact surface. Starting from this information, the mesh for the dam body was elaborated, as shown on figure 1. The dam volume is divided in vertical and horizontal alignments of elements, with 2 to 5 elements along the thickness.

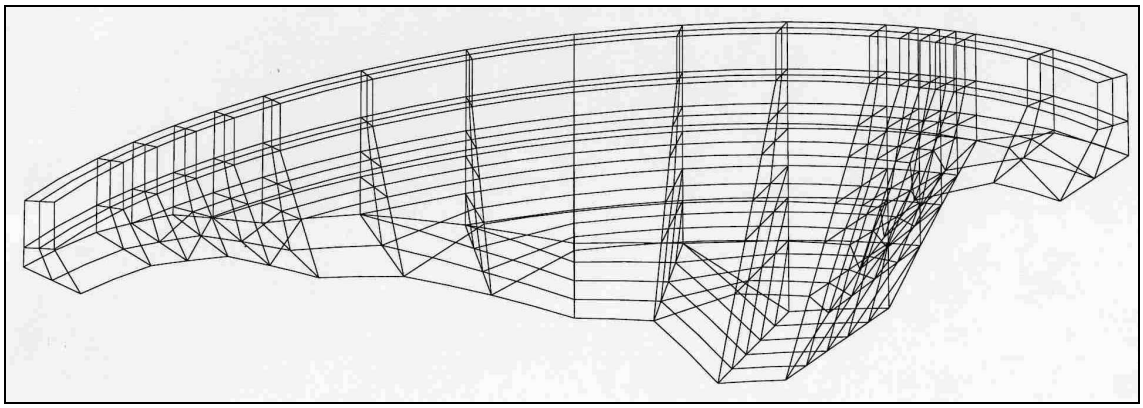

Figure 1: The Finite Elements mesh – Dam only

In the concept of poroplasticity, the damaging of materials, either deviatoric deformation or opening of cracks, is a result of the analyses, i.e. it has not to be arbitrarily localised along predetermined surfaces. For this reason, no use has been made of joint elements. However it was necessary to represent the weaker sliding resistance as defined by the Formulators. This was achieved by incorporating into the model a special layer of weaker rock. Figure 2 shows A), the general arrangement of the foundation around the dam; B), the whole rock volume, in which the weakened rock is shown just below the dam; C) gives the standard cross section.

The parameters for concrete and rock have been selected as given by the Formulators. However additional parameters are required by the William-Warnke constitutive law and by the poroplastic model. Those have been defined according to the past experience on similar models. The values used are collected in Table 1 below. Selected parameters shown in the 3rd column of the table correspond to the artificially weakened rock, in order to match a shear angle of 37 degrees and a cohesion of 0.2 MPa (the equivalence has been adjusted after tests). This selection of parameters translates the intent of having most of the non-linear behaviour occurring in the close foundation below the contact, not in concrete above.

Mechanical boundary conditions for the model consist in fixing in the 3 directions all nodes located at the lower, upstream and downstream limits of the model. On the hydraulic point of view, the lower, upstream and downstream limits of the model are supposed to be watertight (no flow). On the upstream side of the dam and upstream foundation surface, the water pressure is either the reservoir pressure or 0 above water level. On the top and downstream face of the dam as well as on the downstream foundation surface the water pressure is nil or no-flow.

Material	Concrete	Rock	Rock-concrete Interface
Suggested parameters	E=20 GPa ρ=2 300 kg/m3 ν=0.2 Rc=11.6 MPa Rt=1.0 MPa	E=10 - 20 GPa Rc=10 - 15 MPa	ϕ=37 degrees C=0 – 0.2 MPa
Selected parameters for BETHY	E=20 GPa ρ=2 300 kg/m3 ν=0.2 Rc=11.6 MPa Rt=1.0 MPa Rbiaxial=11.6 MPa b=0.4 β=0.9 $K=10^{-9}$ m/s $\omega=10^{12}$ m/s	E=15 GPa ρ=2 500 kg/m3 ν=0.18 Rc=15 MPa Rt=0 MPa Rbiaxial=infinite b=0.8 β=1 $K=10^{-7}$ m/s $\omega=10^{12}$ m/s	E=15 GPa ρ=2 500 kg/m3 ν=0.18 Rc=5 MPa Rt=0 MPa Rbiaxial=infinite b=0.8 β=1 $K=10^{-7}$ m/s $\omega=10^{12}$ m/s

Table 1: Parameters for materials

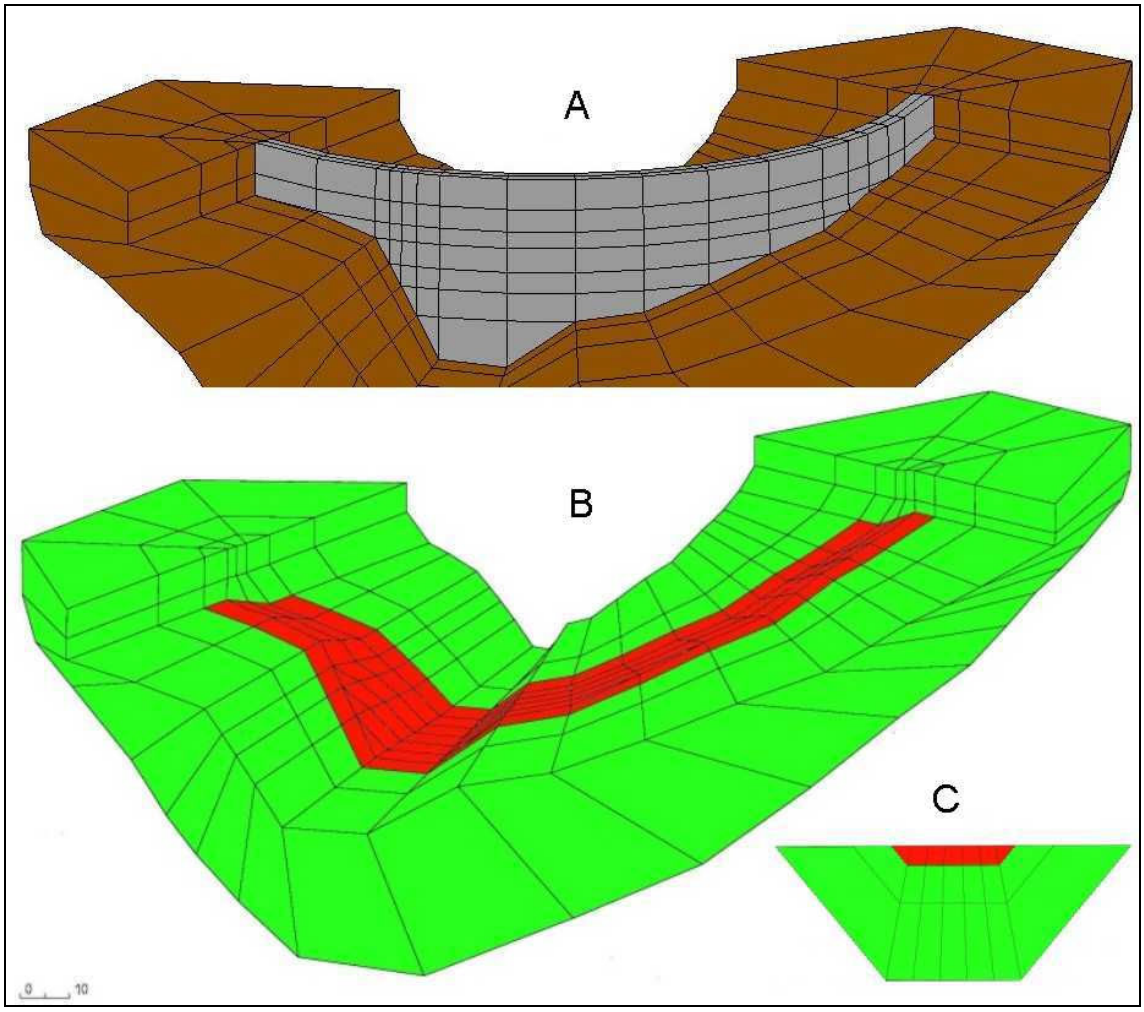

Figure 2: The Finite Elements mesh – Dam and foundation – Normal and weakened rock

2. ANALYSES CARRIED OUT

Preliminary analyses were first carried out in order to generate the initial stress field. The dead weight of the whole rock mass was applied in one step and non-linear process was allowed in order to release local stress concentrations close to the model limits. Then the dead weight of the dam was applied, analysing independently odd and even cantilevers then adding both stress fields, in order to simulate the construction process with independent cantilevers. In the same time the hydraulic pressure field was initialised, with the water level being uniformly at the river level.

The progressive hydraulic loading was applied progressively, with a water height increased from 0 to 42 metre during 50 successive stages of 0.84 metre each. Each loading stage is characterised by the water height and the reservoir level (the bottom being supposed to be at El. 795.75). The loading factor Kh has also been defined as the relative water height, i.e. as the ratio between the water height at a given stage and the maximum water height, which is 34.75 metre. The loading factor therefore varies during the analyses between zero and 1.21 for the last loading stage. The loading was stopped after stage n°50 with a water height of 42 metre, where numerical convergence could hardly be obtained, as explained below.

3. ANALYSIS OF RESULTS

A very large number of results have been obtained which require careful interpretation. They are described and commented in the following sections by themes, starting with the crown cantilever equilibrium, the arching effect, the behaviour of the foundation, and finally consideration of convergence of numerical calculations.

3.1 EQUILIBRIUM OF THE CROWN CANTILEVER

Figure 3 gives the pore pressure distribution across joint 8, located 25 metre on the right of the crown cantilever, where pore pressure starts first to increase at the heel when the hydrostatic load increases. A) corresponds to a moderate loading although higher than the crest level, B) is the ultimate loading being applied.

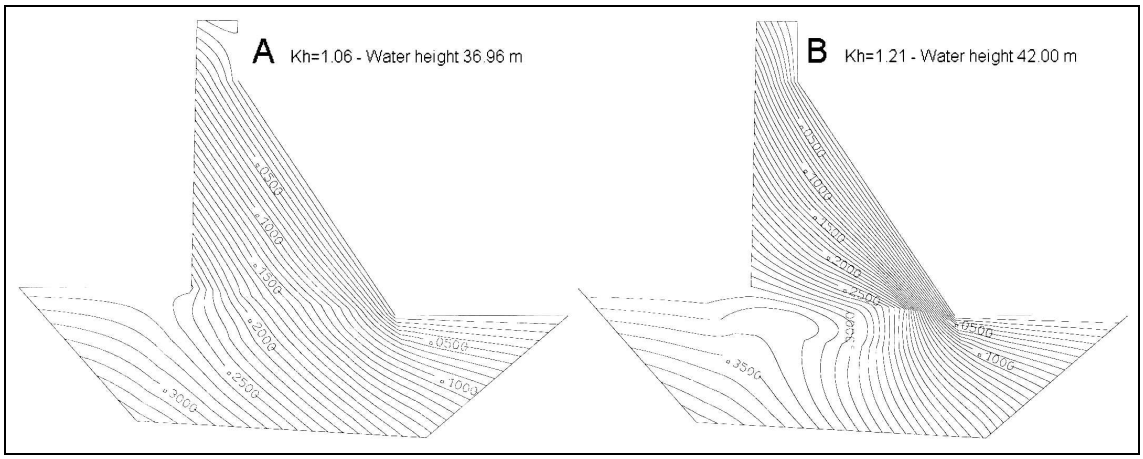

Figure 3: Distribution of uplift in Joint 8 for normal and extreme loadings

Figure 4 gives stresses inside the crown cantilever at the same two load stages. While in A) stresses are well distributed and moderately inclined, for extreme case B) stresses are concentrated on the downstream half of the contact and near to zero upstream, just where pore pressure has become maximal.

Both pore pressure and stress distributions show that case A) is not far from the stability limit of the central sections, in terms of gravity criteria.

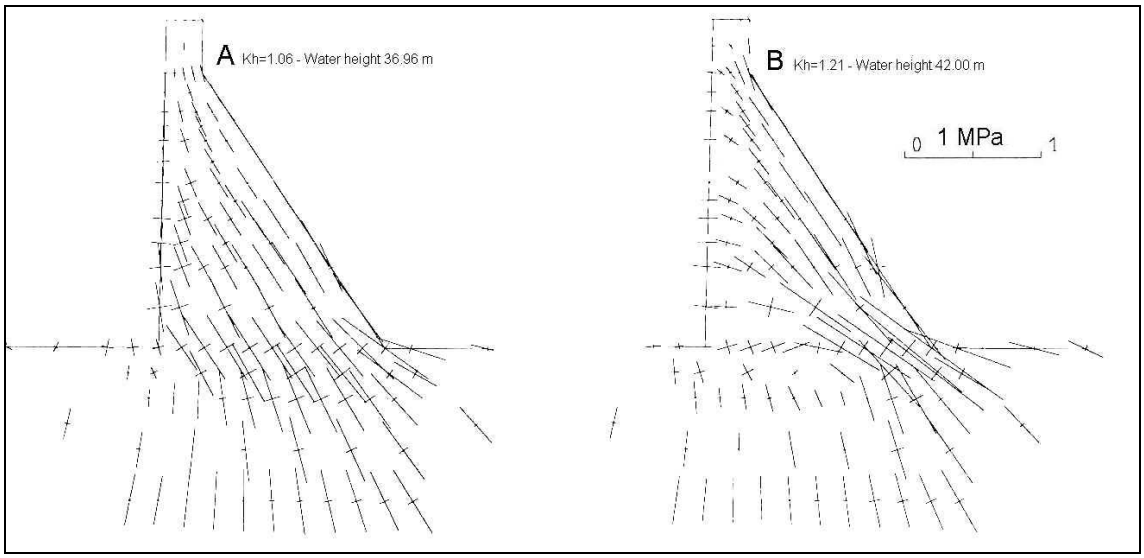

Figure 4: Stresses in the crown cantilever for normal and extreme loadings

3.2 ANALYSIS OF ARCH EFFECTS

Principal stresses along the dam downstream face are presented on Figure 5. For Kh=1.06 the major principal stresses draw active plunging arches which are more or less well centred around the valley and the base of the Right Bank. Stress values are very low, in the range of 0.25 MPa. This, together with the very low deflection at crest (less than 3 mm, see Figures 7 and 8) indicates that the contribution of the arching affect in the global reaction to water thrust is still low.

For higher hydrostatic loadings, arch stresses increase up to 0.85 MPa, which is still limited. Figure 6 shows that the increase of arch stresses is quite progressive. In the same way deflections at the top of the crown cantilever increase very progressively, up to 5 mm for the maximum loading.

The most important feature to be noticed is that both stresses and displacements become more dissymmetric for higher loads: arch stresses now tend to bridge the lower part of the Right Bank (Figure 5B), and at the same time the maximum deflection at crest moves from the crown to the top of right Bank (Figure 7). Figure 8B shows the importance of the dissymmetry.

These observations strongly suggest that something has been happening to the Right Bank foundation during the loading increase.

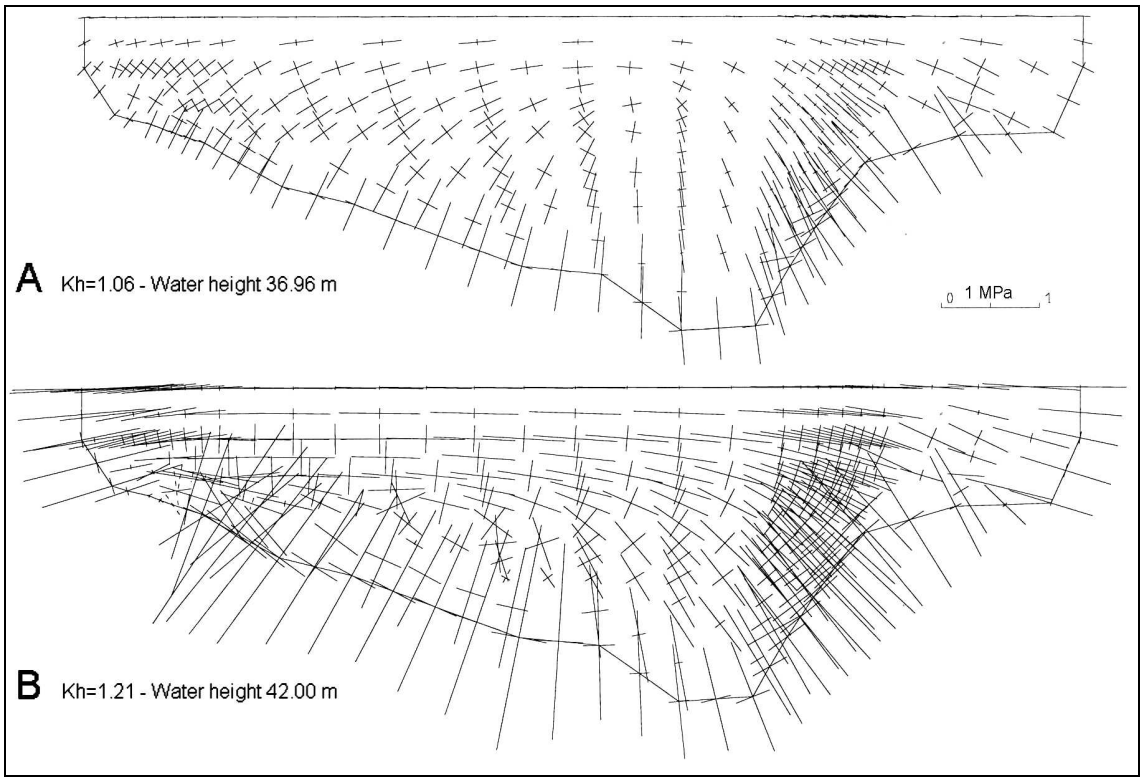

Figure 5: Principal stresses on the downstream face for normal and extreme loadings

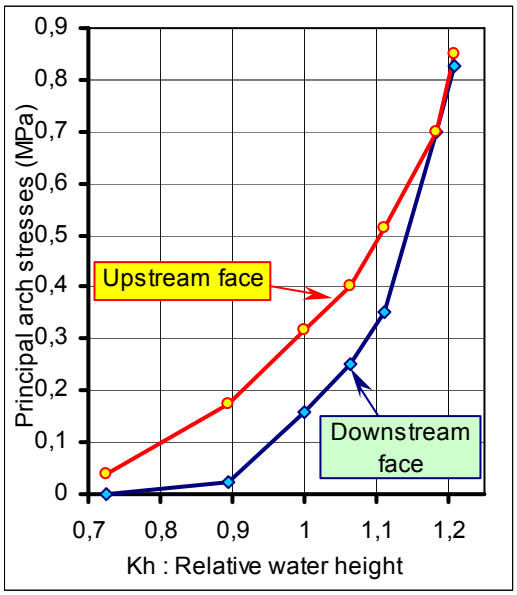

Figure 6: Arch stresses at El. 825 Vs Load factor Kh

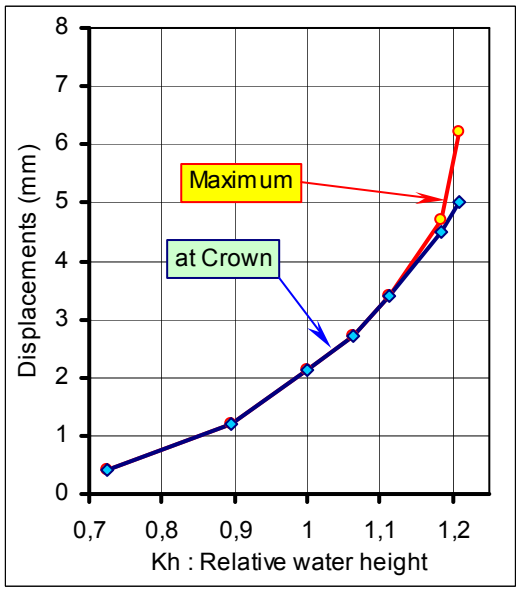

Figure 7: Displacements Vs Load factor Kh

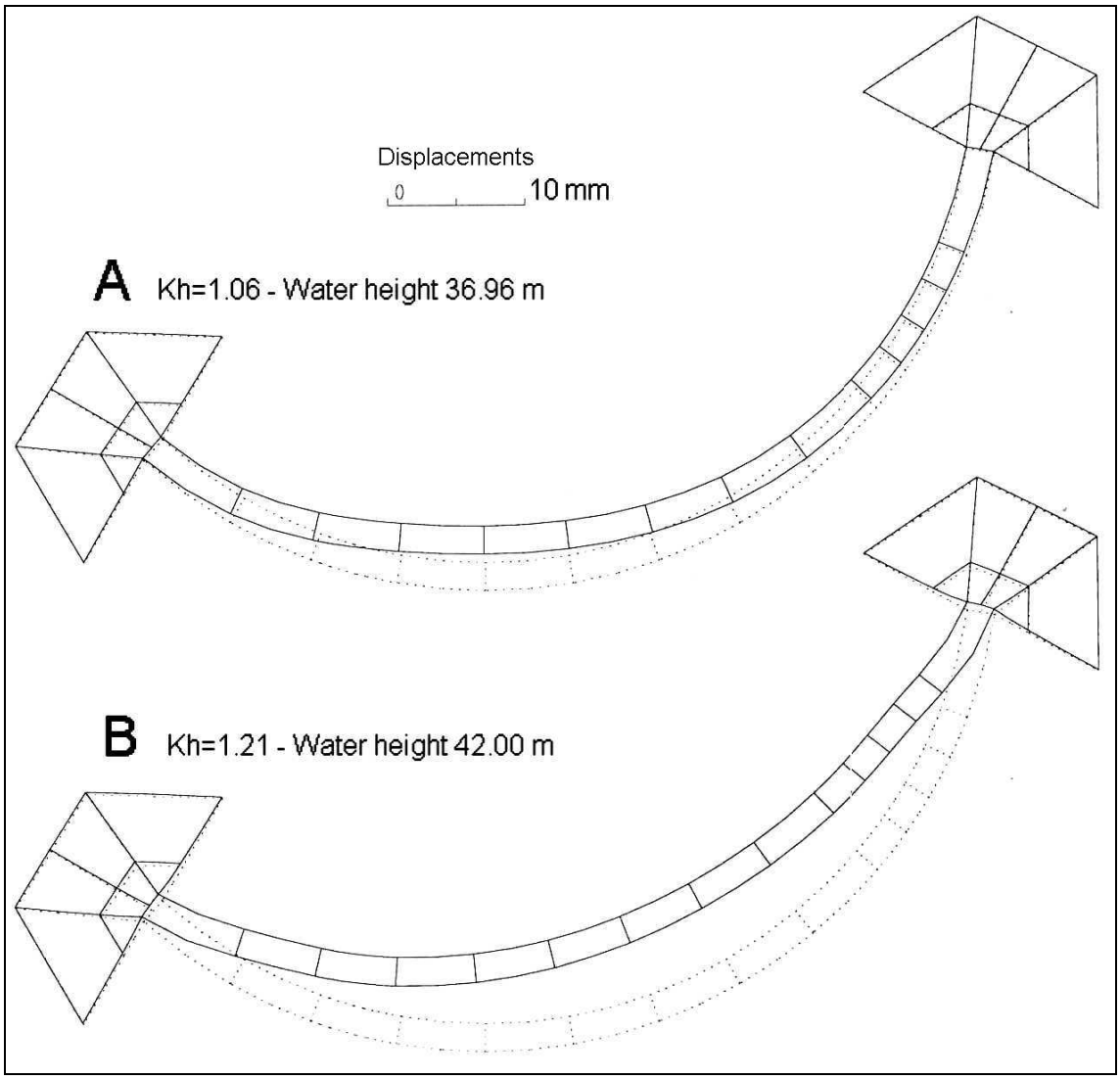

Figure 8: Deformation of the crest for normal and extreme loadings

3.3 BEHAVIOUR OF THE FOUNDATION

Figure 9 presents 4 maps of the foundation where plastic porosity has been presented in coloured zones. Plastic porosity is equivalent to the density of cracking, which in turn corresponds to an increase in rock permeability and more penetration of uplift. Maps referenced A, B, C and D correspond respectively to Kh=1.06, 1.11, 1.18 and 1.21.

In the two first cases the uniform colour indicates that there is virtually no cracking, except a slight trend at the heel of cantilevers located at 25 metre both sides of the crown. This means that full water pressure does not penetrate substantially the foundation, except locally at the heel of side cantilevers. When the load factor reaches Kh=1.18 (map C), plastic porosity develops on the upstream side of both banks. Finally when Kh=1.21, the one situated on the Right Bank dramatically increases and deepens. The phenomenon is quite sudden, since the difference in water height between Kh=1.18 and Kh=1.21.

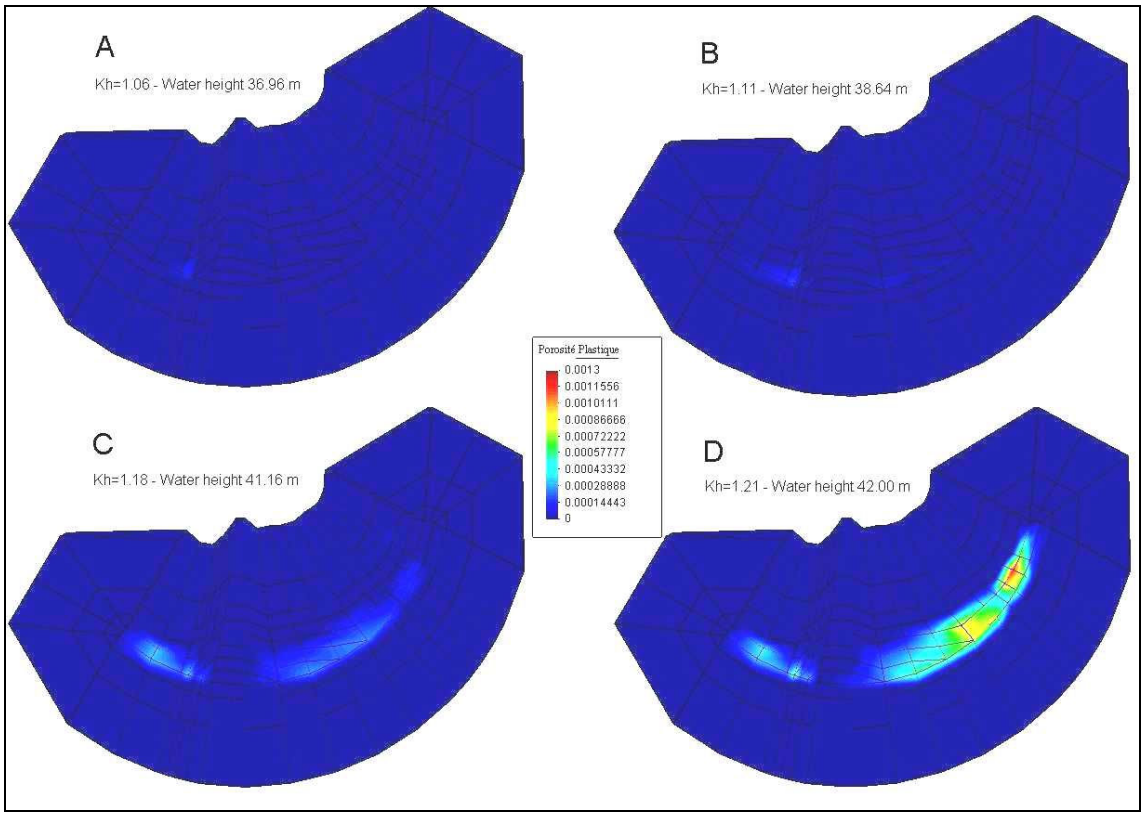

Figure 9: Development of poroplasticity in the foundation as the loading is increased

Displacements of the foundation surface (Figure 10) give a similar indication and confirm that there is a sudden change in the behaviour of the foundation at the top of Right Bank. The movement at the heel of the crown cantilever is very progressive, with only a slight acceleration for highest loading stages. On the opposite, the horizontal movement at the top of Right Bank remains very low until Kh=1.11, and then it strongly accelerates at Kh=1.18 and changes its order of magnitude at Kh=1.21, with more than 1 cm.

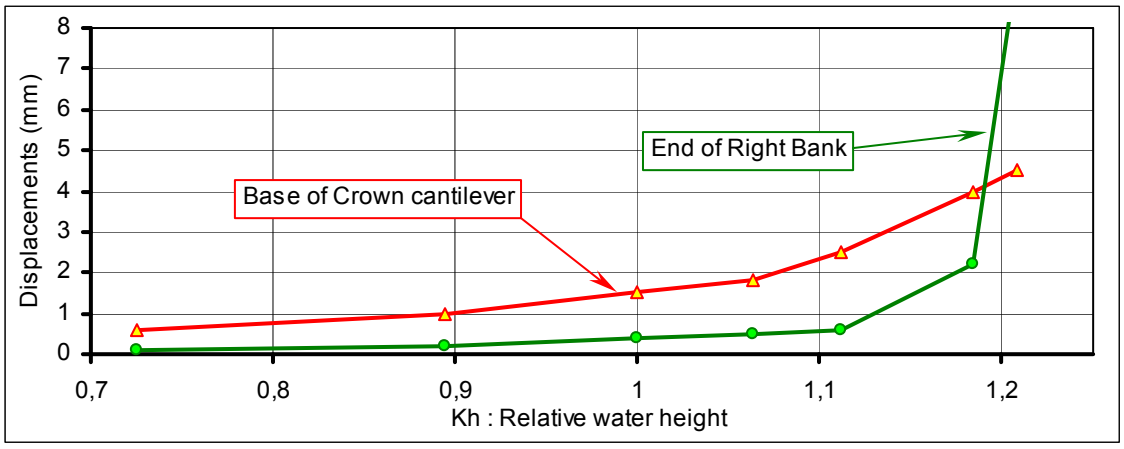

Figure 10: Displacements in the close foundation Vs Load factor Kh

Figure 11 provides two maps of the foundation where stresses applied to the contact surface have been plotted. Case A corresponds to Kh=1.06 and case B to Kh=1.21. The graphic convention is to give the normal stress as a circle (scale for radius given), and the tangential stress is presented with an arrow. Scales are such that an incidence of 37 degrees corresponds to having the arrow just on the circle.

In case A, normal stresses are compressive nearly along the whole surface except the very upstream areas on the banks. Incidences of stresses are higher than 37 degrees, but the excess corresponds roughly to the cohesion of 0.2 MPa, which has been included in the parameters of the weakened rock below the dam. One exception is observed on the Left Bank.

Case B shows a quite different feature. Stresses virtually disappear from more than the upstream half, except on the lower part of Left Bank. Normal stresses concentrate on the downstream portion. Tangential stresses also concentrate on the same downstream portion of the surface, and allowable incidences are exceeded by far. This observation is consistent with the development of plastic porosity and the high displacements at the top of Right Bank, which all indicate that this area is no more in equilibrium.

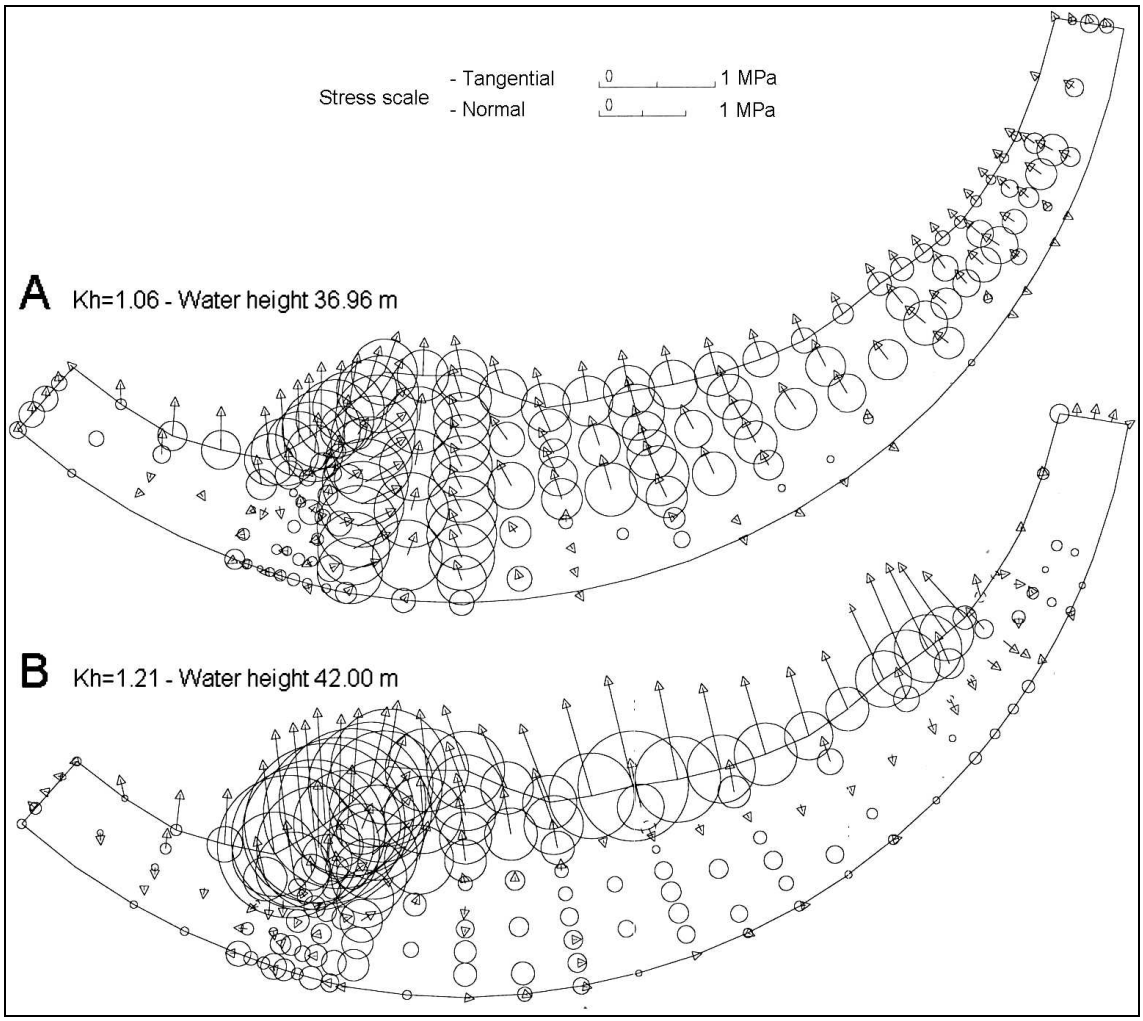

Figure 11: Normal and tangential stresses for normal and extreme loadings

Figure 12 presents a plot of normal and tangential stresses in MOHR diagrams, which gives a more detailed vision of the incidences. Stresses located just along the downstream edge of the rock-foundation contact are given in Diagram A. The cohesion required to prevent sliding is around 0.1 MPa for Kh=1.0 or Kh=1.06. For Kh=1.18 the mobilised cohesion is around 0.4 MPa, and it is 0.5 for Kh=1.21.

It is generally accepted that stresses given by F.E. models at a geometrical kick are exaggerated, because of extrapolation rules used to calculate stresses at nodes. For this reason, stresses located at the first line upstream of the edge have also been plotted on Figure 12b. This second graph indicates that the cohesion mobilised for Kh=1.06 is still around 0.1 MPa, but the one needed for most extreme loadings is only 0.2 MPa.

In any case, assuming zero cohesion does not even allow reaching the crest level. With the assumed cohesion of 0.2 MPa, it is clear that sliding is occurring for higher water levels, when Kh becomes higher than 1.18.

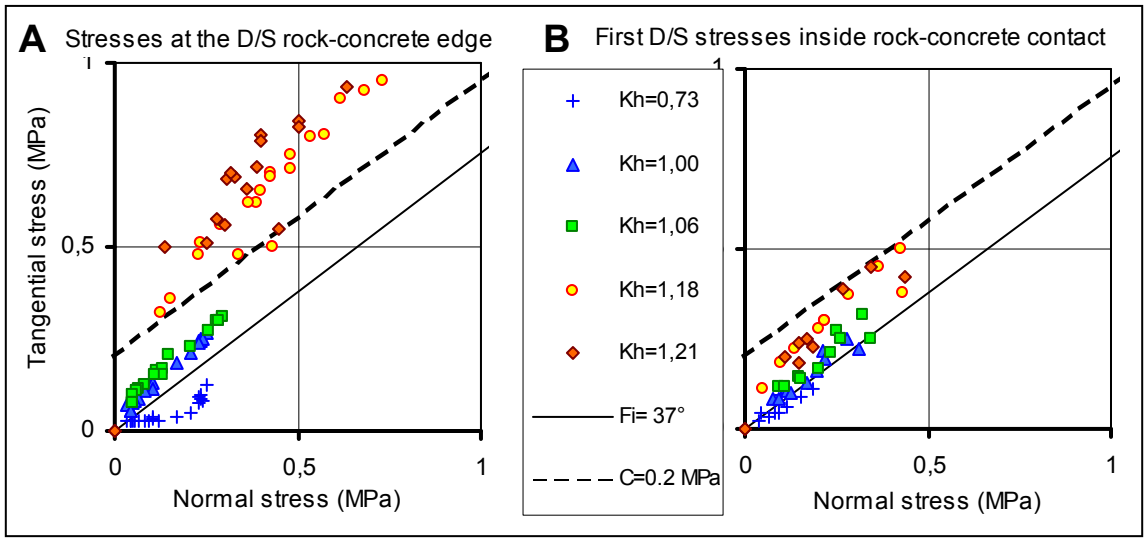

Figure 12: MOHR diagrams with stresses on the foundation for different loadings

Figure 13 has been plotted to see where cohesion is required to prevent sliding along the Right Bank. Figure 13a corresponds to stresses situated just at the downstream rock-concrete edge, and Figure 13b corresponds to the first line just upstream of the edge. This shows that sliding seems to start first at mid-height of the bank (sections B-C at Kh=1.11), and then develops all along the Right Bank when Kh reaches 1.18. For the ultimate loading (Kh=1.21) the required value surprisingly falls to zero at the top of Right Bank. It has not been possible to clarify whether this is due to a full opening of the contact surface, or it is due to the imperfect convergence of the calculation at this ultimate stage.

To summarise the stress condition along the Left Bank, Figure 14 gives the maximum cohesion mobilised for each load factor along the foundation. This clearly shows that sliding is starting when Kh exceeds 1.11, and generalises when Kh=1.21. This explains why displacements dramatically increase at this time.

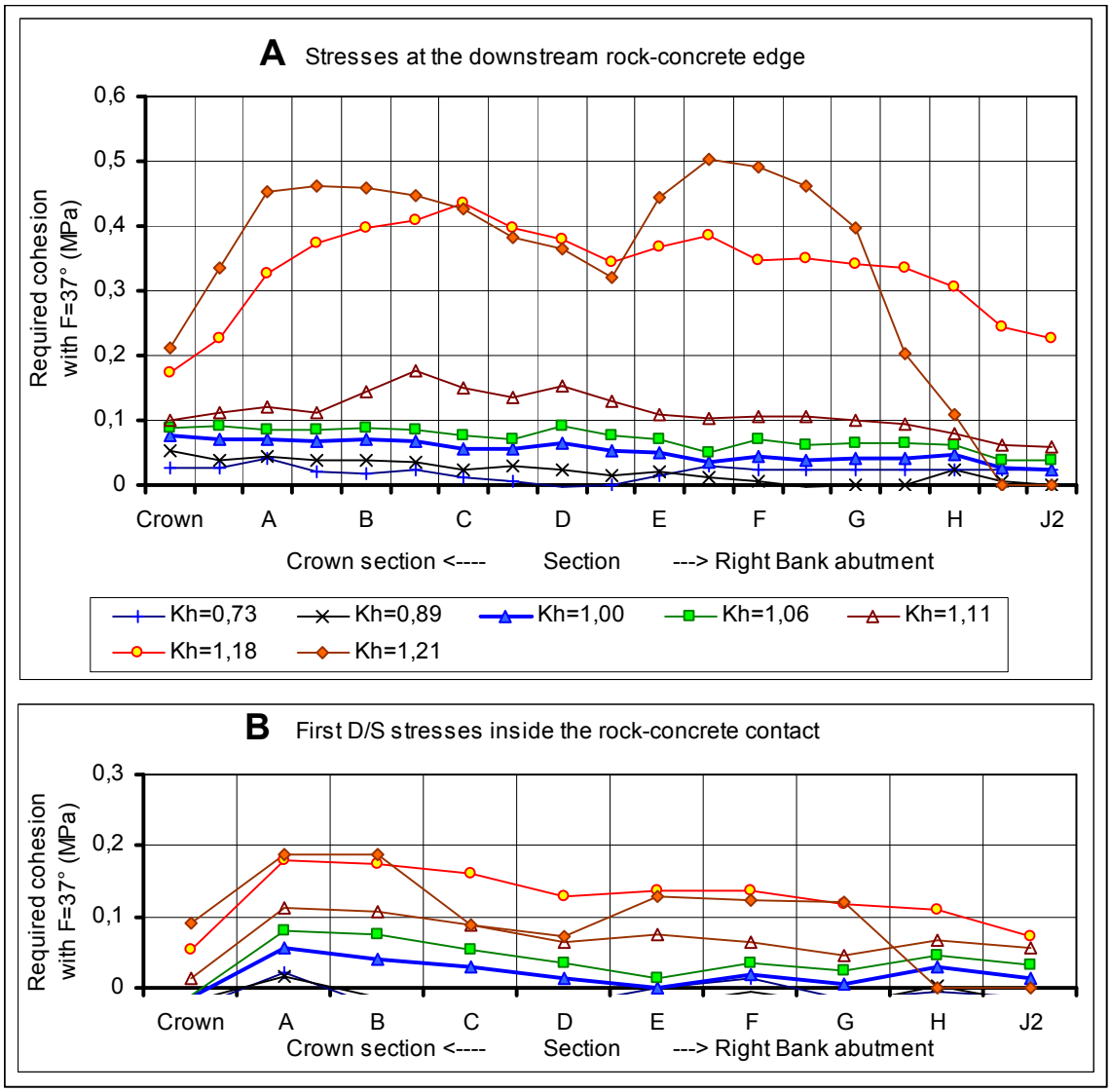

Figure 13:Cohesion required to prevent sliding along the Right Bank foundation surface

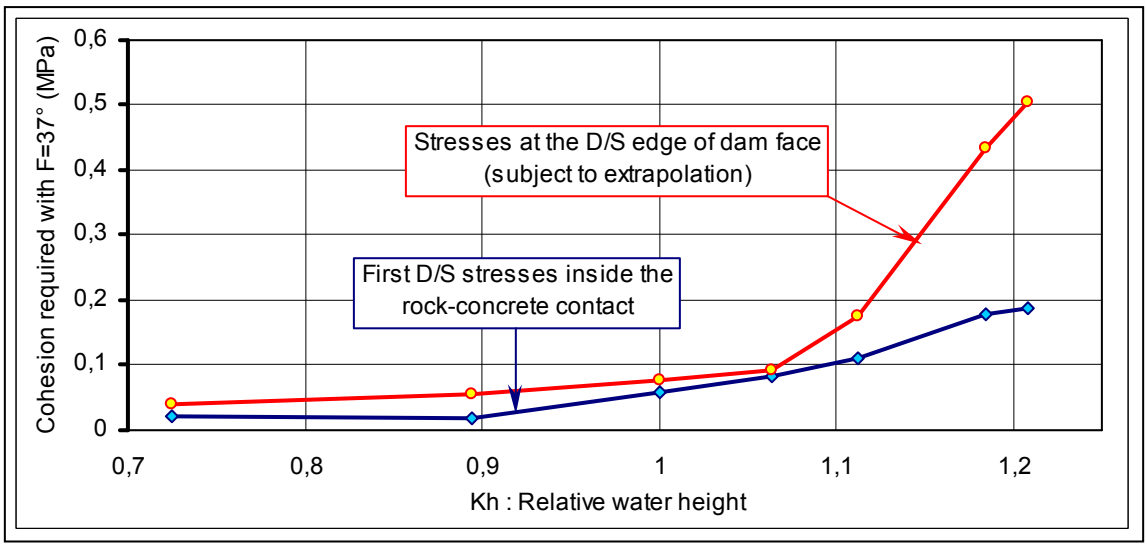

Figure 14:Cohesion required to prevent sliding Vs Load factor Kh

3.4 ASSESSMENT OF NUMERICAL CONVERGENCE

The BETHY software automatically runs iterations until several stability criteria are met. The convergence can be checked by analysing curves giving the controlled parameters with iteration numbers, as shown on figure 15. In the present case the additional displacements for each iteration should be less than 10^{-6} m and the overall force imbalance should be less than 10^{-2} MN (one metric ton). The latter Criterion (on the Left of Figure 15) was the leading one.

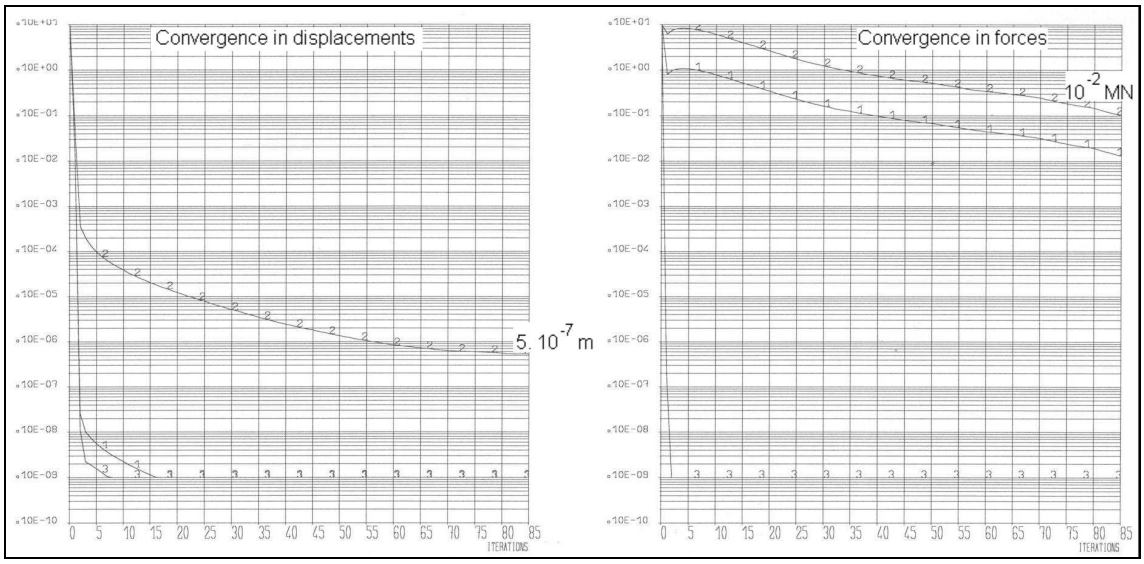

Figure 15:Example of convergence curves for Kh=1.11

Figure 16 below gives the number of iterations that were needed for each loading step, i.e. each time the water level was increased by 0.84 m.

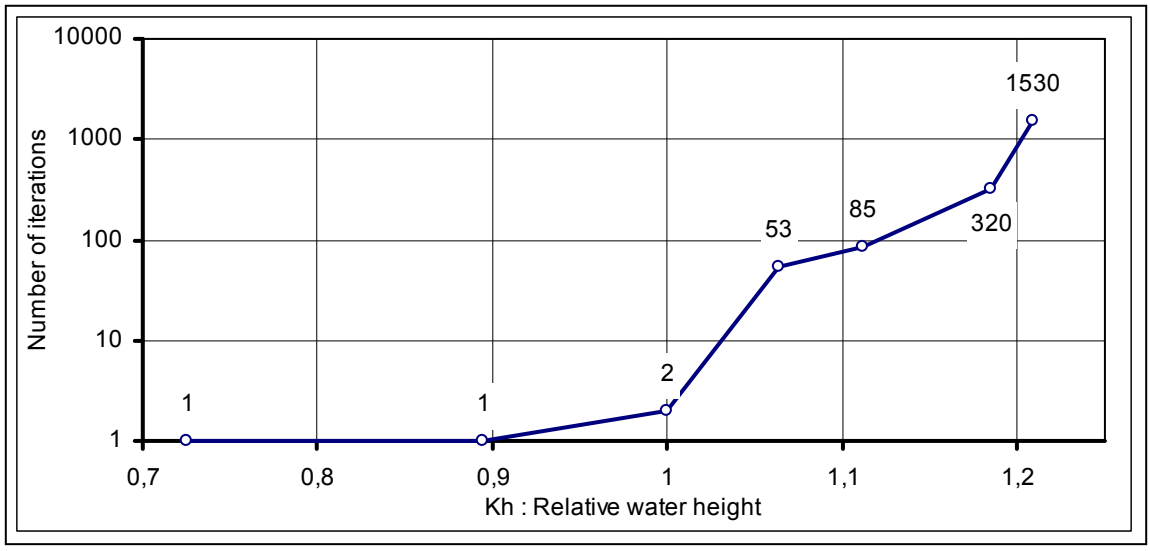

Figure 16:Convergence : number of iterations to reach the criteria Vs Load factor Kh

One can see that:

- the equilibrium is obtained immediately until Kh=1, and is still obtained rather easily up to 1.05 with a rather important non-linear process ; this corresponds to the development of poroplasticity at the base of both banks,
- between Kh=1.05 and 1.15 some stabilisation seems to appear, however the sliding along the banks still develops,
- for Kh= 1.18 the stability can hardly be obtained and at Kh=1.21 this becomes really impossible; this corresponds to the sliding / failure of the upper Right Bank.

4. CONCLUSIONS

What is the ultimate strength is in fact debatable each time failure is not purely brittle, and the criterion for deciding that failure has occurred has often to be decided in a rather fuzzy way [2]. The Table below tries to summarise all relevant indices as a function of the load factor. Uplift first starts extending towards downstream, then stresses along the foundation start reaching locally the limits, but sliding generalises only when the water height is between 41.16 and 42 metre of water. The question that could not be solved is whether a further equilibrium can be found after the lateral blocks have been sliding along their foundation, or if the movement is going to become infinite. In any case, a sliding movement of more than 1 centimetre along the foundation would make the dam definitely unsound for further operation.

Water height	25,20	31,08	**34,75**	36,96	38,64	41,16	42,00
Reservoir level	820,95	826,83	**830,50**	832,71	834,39	836,91	837,75
Loading factor	0,73	0,89	**1,00**	1,06	1,11	1,18	1,21
Uplift extension downstream (J8)							
Crest deflection increase (R/B)							
Foundation sliding at top R/B							
Poroplasticity development at R:B							
Required cohesion >0.2 MPa - at D/S edge – along 2nd line							
Lengthy convergence of stage							

REFERENCES

[1] Giuseppetti, G., Mazzà, G., Meghella, M., Fanelli, M., 'Evaluation of Ultimate Strength of Gravity Dams with curved shape against sliding', Theme A for the 7th Benchmark Workshop on Analysis of Dams, ICOLD, Milan, 2003

[2] Carrère, A., Tardieu, B., Ozanam, O., 'Uses and misuses of realistic numerical models in dam safety evaluation', International workshop on Dam Safety Evaluation, Grindelwald, Switzerland, 1993

[3] Fauchet, B., 'Analyse poroplastique des barrages en béton et de leur fondation', Thèse de doctorat, Ecole Nationale des Ponts & Chaussées, Paris, Septembre 1991.

[4] Fauchet, B.,- 'Poroplastic analysis of concrete dams and their foundation', Dam Engineering, vol. 2, Issue 3, London, August 1991.

[5] Carrère, A., 'Arch dams, uplift and design criteria – Are heel base joints useful ?', The International Journal on Hydropower & Dams, vol. 1, Issue 666, London, November 1994

SAFETY EVALUATION AGAINST SLIDING OF A GRAVITY DAM WITH CURVED SHAPE

Massimo Meghella, Guido Mazzà
CESI Spa, ITALY

SUMMARY: In the frame of the 7th Benchmark Workshop on numerical analysis of dams, the proposed Theme A on the evaluation of the ultimate strength of concrete gravity dams with curved shape against sliding has been approached by using the finite element method. Several analyses have been carried out in order to investigate the influence of materials and joint/interface parameters. Comparison with the results of conventional 2D sliding stability analyses has been made and the additional strength due to the arch effect has been critically evaluated and discussed.

RÉSUMÉ: Dans le cadre du 7iéme atelier sur l'analyse numerique des barrages, le Thème A sur l'évaluation de la résistance limite au glissament des barrages poids avec l'axe planimetrique courbe, a été approchée avec la méthode des élément finis. Différentes analyses ont été exécutées au but de déterminer l'influence des paramètres des matériaux et des joints. Une comparison avec les resultats des analyses 2D conventionalles a été effectuée et la resistance additionnale dû à l'effet de la courbure a été évalué et discuté.

1. INTRODUCTION

According to the purpose of Theme A of the 7th Benchmark Workshop on numerical analysis of dams [1], in the present paper the results of the evaluation of the ultimate strength against sliding for the proposed case history are presented and discussed.

In a preliminary stage of the study, the authors' intention was to adopt a methodology based on a rigid formulation for the dam body, which, in the light of the results provided further on, has been replaced by a deformable formulation based on the finite element method.

Different material constitutive laws for the dam body, the rock foundation and the dam-rock interface have been considered and a parametric study has been carried out in order to investigate the influence of the different model parameters. Finally, the

results have been compared with those provided by the conventional 2D approach on the main vertical section and the additional strength due to the arch effect has been assessed.

The geometric data, the physical-mechanical parameters and the loading conditions which have been provided for the dam under examination are summarized in the following table:

Geometry			
Crest elevation [m a.s.l.]	830.5	Dam Height [m]	36.55
Crest length [m]	158.0	Dam Volume [m^3]	40,000
Materials			
Parameter	*Concrete*	*Rock foundation*	*Dam Rock interface*
Elastic Modulus [MPa]	20,000	10,000 ÷ 15,000	-
Mass Density [Kg/m^3]	2,300	-	-
Poisson Coefficient [-]	0.2	0.2	-
Compressive Strength [MPa]	11.6	10.0 ÷ 15.0	-
Tensile Strength [MPa]	1.0	-	-
Friction Angle [Degrees]	-	-	37
Cohesion [MPa]	-	-	0.0 ÷ 0.2
Loads			
Dead Weight	Hydrostatic Pressure at max. water level: 830.5 m a.s.l		Uplift pressures

Tab. 1. Theme A input data.

2. METHODOLOGIES AND MODELLING ASSUMPTIONS

Starting from the digitally provided geometry, a FEM mesh of the dam-rock foundation system has been created (Fig. 1). The mesh consists of 5764 nodes, 416 parabolic brick elements for the dam, 560 parabolic brick elements for the rock foundation and 124 joint elements (§ 2.1.2.).

The analyses have been carried out by means of CANT-SD, a FEM program for dam analysis developed by CESI [2].

Loads have been properly accounted for, according to the input specifications. In particular the uplift pressure has been assigned to the dam-rock interface in order to act with the classic triangular variation, from the actual hydrostatic pressure value at the upstream side to zero at the downstream side. The dead weight and the maximum hydrostatic pressure have been assigned through 4 load steps each and the subsequent increment of the maximum water level has been modeled by means of additional increments of 1 m each, up to the limit condition, namely when the last balanced and stable solution is achieved, according to the assigned convergence parameters.

2.1 MATERIALS MODELS

In order to investigate the influence of the materials behaviour on the dam global stability and on the stress patterns within the dam body and the rock foundation, two constitutive models have considered both for concrete and rock: a) linear-elastic; b) elasto-plastic (Lade, 1988 [3]).

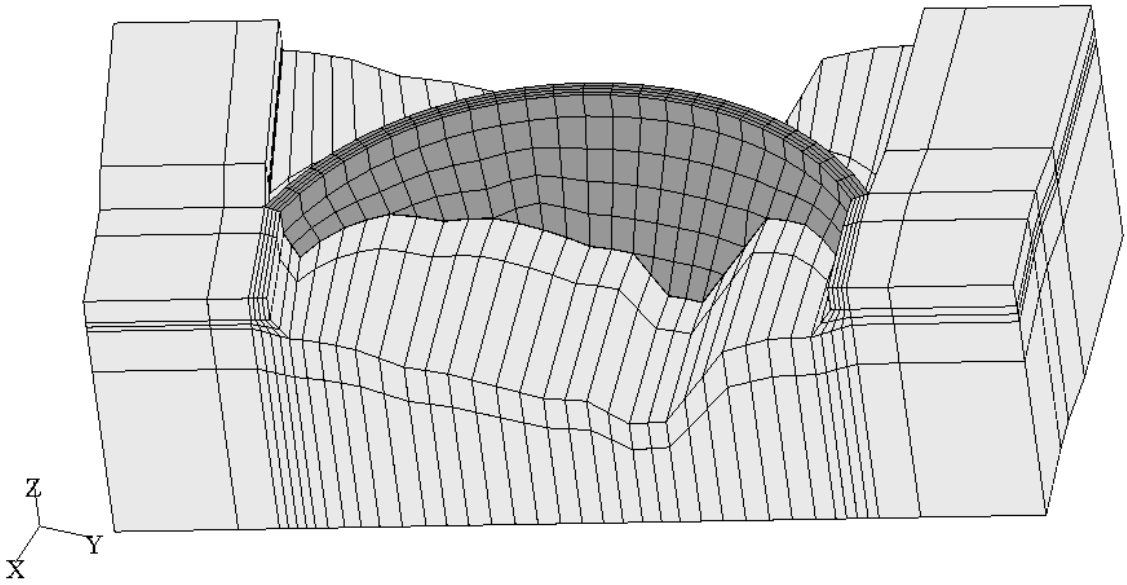

Fig. 1. FEM mesh of the dam- rock foundation model.

2.1.1 *Concrete and foundation rock*

The parameter values of Tab. 1 have been assumed for the linear elastic models. In particular, for the rock foundation, the mean value of the elastic modulus (12,500 MPa) and a Poisson ratio of 0.2 have been assumed.

The elastoplastic model (Lade, 1988 [3]) adopted in this study is the most suitable for materials having different tensile and compressive behaviours, such as concrete, rock and soil, among those implemented in CANT-SD.

The definition of the model for a given material requires the identification, starting from the assigned tensile and compressive strengths (Tab. 1), of 13 adimensional parameters: 3 are related to the non-linear elastic behaviour; 1 is related to the tensile strength, 7 are related to the elasto-plastic behaviour in presence of deviatoric stress, 2 are related to the elasto-plastic behaviour in the isotropic compressive condition. Such parameters, based on the concrete strengths, are summarized in Table 2, and have been also extended to the rock foundation in Case Set 5 (§ 2.1.3).

K = 2 E 5	$\mu_1 = 3.45$
n = 0	h = 1.666
$\nu = 0.2$	$\alpha = 1.65$
a = 10	C = 0.475E-9
m = 0.992 ($\psi_1 = 1.566E-3$)	p = 2.93
$\psi_2 = -2.93$	$\eta_1 = 30876$

Tab. 2. Lade elasto-plastic model parameters.

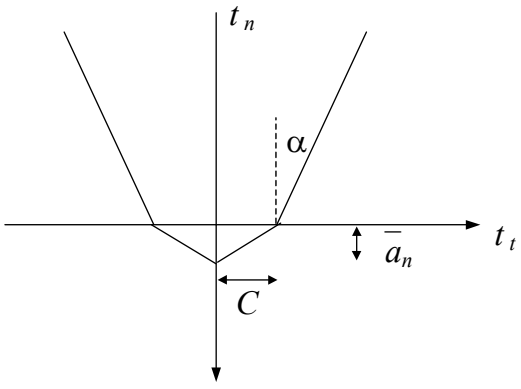

Fig.2 . Base joint model.

2.1.2 *Dam-foundation interface*

The dam-rock foundation interface has been modeled by using thin elements with a friction-cohesion, no-tension behaviour [2].

For the formulation of the model (Fig. 2), three different situations are considered: the closed state ($a_n < 0$), the open state below the opening limit ($0 < a_n < \bar{a}_n$) and the open state above the opening limit ($a_n > \bar{a}_n$). The normal contact surface force t_n is compressive in the closed state and equal to zero in the open state (no-tension models): a non softening tensile strength can be simulated by adding an initial compressive term t_n^i. The elastic part of the behaviour is governed by the two parameters E and G (E/h and G/h define the normal and shear stiffnesses, being h the distance between the two faces of the joint). A sufficiently high value of normal stiffness avoids any significant penetration between the two faces of the joint.

In the closed state ($a_n < 0$), the constitutive law is elastic perfectly plastic and reproduces the Coulomb friction behaviour with cohesion (shear strength for zero compressive stress) and without dilatancy.

In the open state below the opening limit ($0 < a_n < \bar{a}_n$) the normal contact surface force t_n is equal to zero, while the shear strength linearly decreases from C (at $a_n = 0$) to zero (at $a_n = \bar{a}_n$).

2.1.3 *Parametric analysis*

The provided input data and some preliminary analysis led to the choice of 6 case sets, whose parameters are summarized in Tab. 3.

For all case sets, the value of $\bar{a}_n = 5$ mm has been assumed.

Case set	Material Constitutive Laws		Dam-Rock Interface Parameters		
	Concrete	Rock	Friction angle [°]	Cohesion [KPa]	Tensile strength [KPa]
0	Lin.-elastic	Lin.-elastic	37	100	0
1	Ela-plastic	Lin.-elastic	37	100	0
2	Ela-plastic	Lin.-elastic	37	100	100
3	Ela-plastic	Lin.-elastic	37	200	100
4	Ela-plastic	Lin.-elastic	37	0	100
5	Ela-plastic	Ela-plastic	37	100	0
6	Ela-plastic	Lin.-elastic	37	0	0

Tab. 3. 3D Analysis case sets description.

3. CONVENTIONAL 2-D MODEL RESULTS

According to the common practice for the evaluation of the sliding stability of concrete gravity dams, a parametric conventional 2D analysis of the highest vertical section, accounted for as a rigid body, have been carried out, considering the limit equilibrium condition between the external acting loads and the resistant forces acting

along the base joint. The same 3D case sets (but not considering those involving the material constitutive laws) have been analyzed.

The multiplier coefficient is obtained by dividing the reservoir height at the limit condition by the maximum height (36.55 m).

The stress calculation has been done by using the beam theory, allowing tensile stress to develop up to the tensile strength, with the consequent redistribution of compressive stresses along the base joint [4]. The results are summarized in Tab. 4.

Case Set	Highest vertical section			
	Water elevation [m a.s.l.]	Multiplier coefficient	Max Principal Stress [KPa]	Min Principal Stress [KPa]
0	830.0	0.99	0.0	-1,212
2	830.5	1.00	100	-1,231
3	832.5	1.05	100	-1,727
4	828.5	0.95	-127	-760
6	826.2	0.88	-248	-746

Table 4 Conventional 2D stability and stress analysis results.

It can be noticed that the limit equilibrium condition is reached with water levels below the maximum for all case sets, with the exception of case set 2 (cohesion = 100 KPa, tensile strength = 100 Kpa), for which the water level reachs the maximum, and case set 3 (cohesion = 200 KPa, tensile strength = 100 Kpa), for which the water level goes 2 m above it. As expected, the dam-rock interface parameters influence significantly the results. The stress analysis at the limit condition provides principal stress values well below their respective material strengths.

4. FEM 3-D MODEL RESULTS

In Fig 3 the top-bottom displacement of the highest vertical section is illustrated for all case sets, except for case set 6, for which no equilibrium solutions can be found over the maximum water level. For all other case sets the analyses converged to a solution with water level increases up to a range of 19 ÷ 27 m, providing displacements ranging between 0.050 ÷ 0.062 m at collapse.

From the same figure it can be noted that the sliding initiation threshold, or failure point, is not easily definable, being the transition between different slopes parts within the curves quite smooth. For such a reason, the sliding curves relevant to the dam rock interface elements are more helpful and representative.

4.1. SLIDING STABILITY

In Fig. 4 the sliding curves relevant to the base joint are shown. As anticipated above, the transition between different slopes parts is definitely sharper and the failure point can be singled out with sufficient accuracy, by zooming around it (Fig 5).

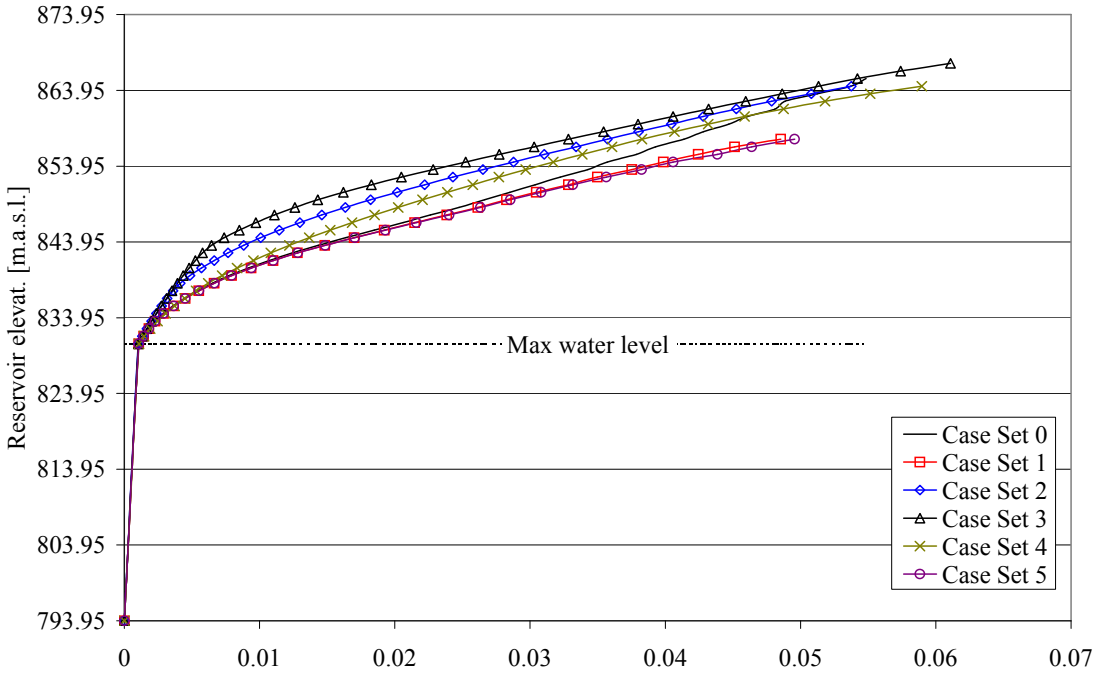

Fig 3. Top-bottom lateral displacement [m]– highest vertical section.

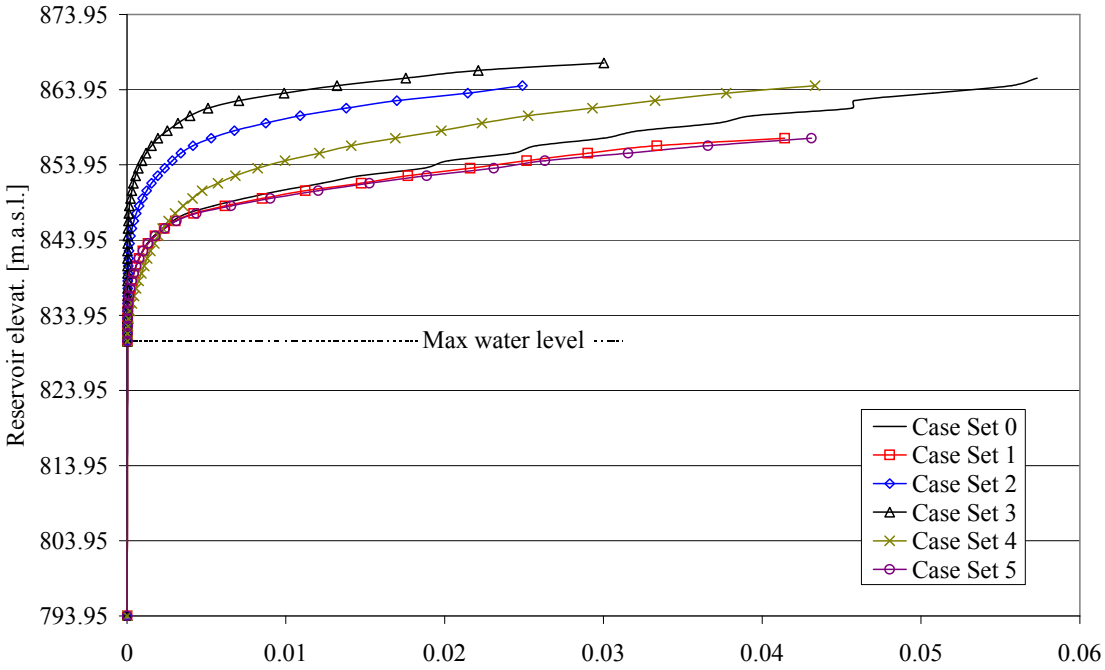

Fig 4. Sliding [m] – highest vertical section.

Looking carefully at the sliding contour around the failure point (Fig. 6), it is easy to note that the right portion of the dam starts to slide before the highest central part. See also (Fig. 7) the deformed shape of the dam at different water level increments for case set 0 (the deformed shapes are very similar for all case sets). The corresponding sliding curves are shown in Figs. 8, 9.

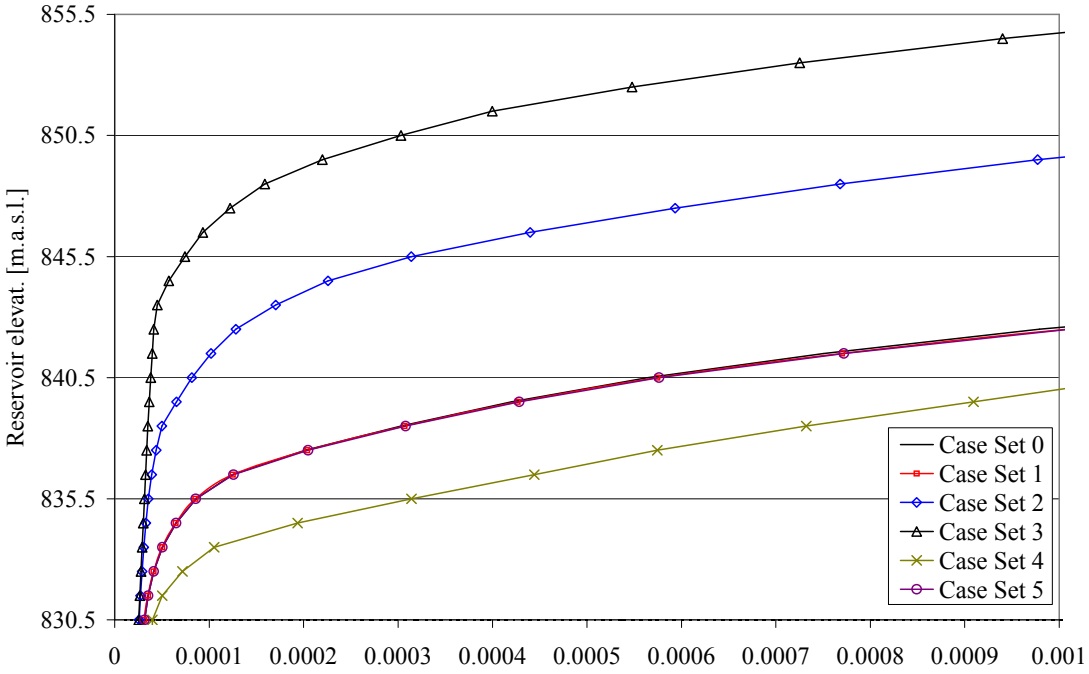

Fig 5. Sliding [m]– highest vertical section -zoom.

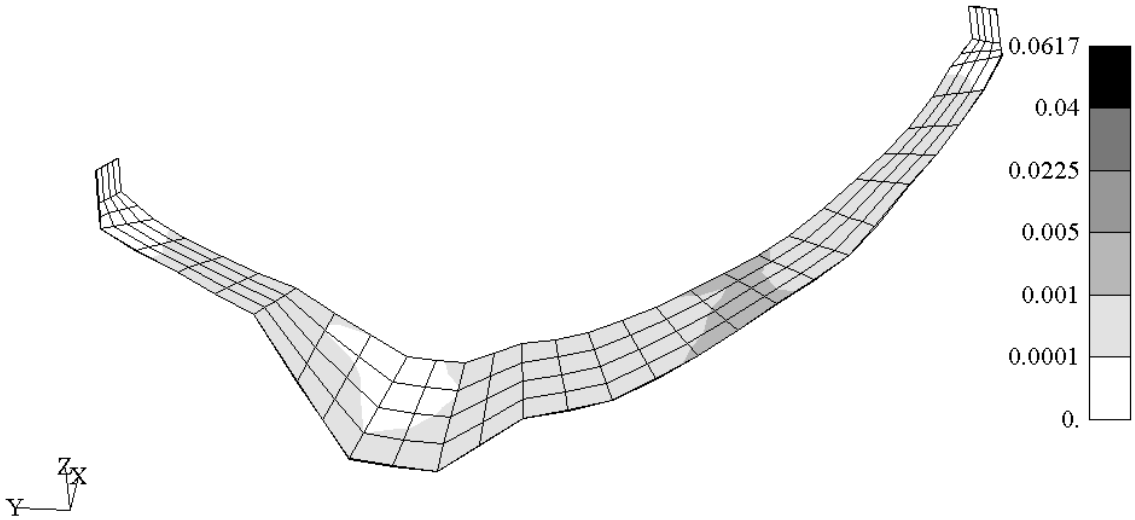

Fig 6. Case Set 0 - Sliding contour [m] along the dam-foundation interface.

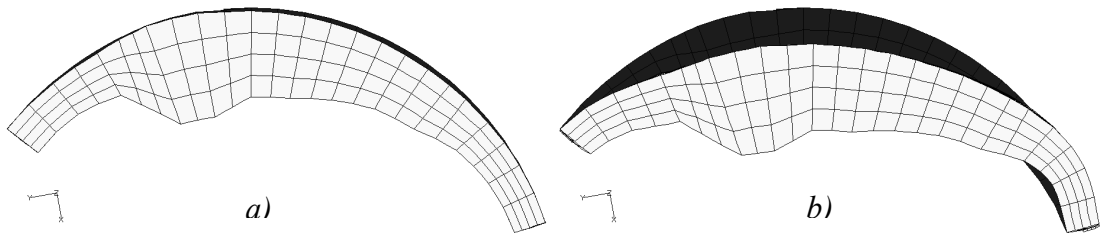

Fig. 7. Case Set 0 - Deformed shape at: a) 3rd increment (833.5 m a.s.l); b) last increment (865.5 m. a.s.l).

This fact highlights the first important result, namely that any rigid body approach brings to misleading conclusions about the definition of the failure point and might be due to the slopes of the lateral parts of the base joint that are unusually in favour of the sliding displacements under the acting loads.

In order to better investigate this important outcome, the base joint surfaces have been modified, making them laying horizontally, as usually it is in many common situations (of course counter-slope joint surfaces would be preferable for the sliding stability) and an additional analysis has been carried out for the case set 0. Well then, the same trend is confirmed (Fig. 10), even if fewer differences occur between failure points of central and right vertical sections (and possibly the trend would be inverted in case of counter-slope joint surfaces).

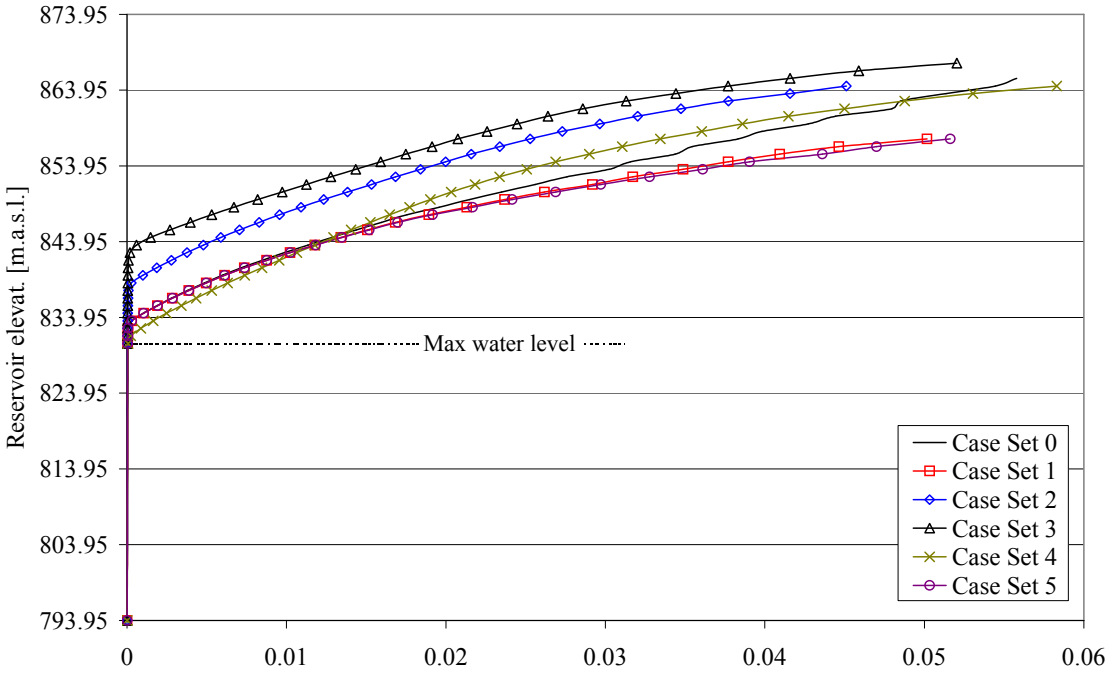

Fig 8. Sliding [m]– right side vertical section.

Another important outcome from the analyses results is that the different material constitutive laws have a very low influence on the global behaviour of the dam, thus allowing the use of linear-elastic models (more practical, cheap and diffused within dam engineers) to carry out this type of analysis.

Conversely, all displacement curves show a strong influence, higher then 2D conventional analysis, of joint parameters in the sliding stability. In particular the cohesion, whose existence is reasonably justifiable due to the asperity of the joint surfaces, plays the most important role (the existence of any residual tensile strength on joints might be questionable and the friction angle depends on the type of materials in contact, and usually its experimental values result not much scattered, being so easier to be identified with respect to cohesion).

In Tab. 5 the ultimate strength against sliding expressed by means of multiplier coefficients, according to their definition as provided in § 3, are summarized, both for the higher vertical section and for the right vertical section.

By comparison with Tab. 4, it can be noticed the additional strength provided by the 3D arch effect for all comparable case sets.

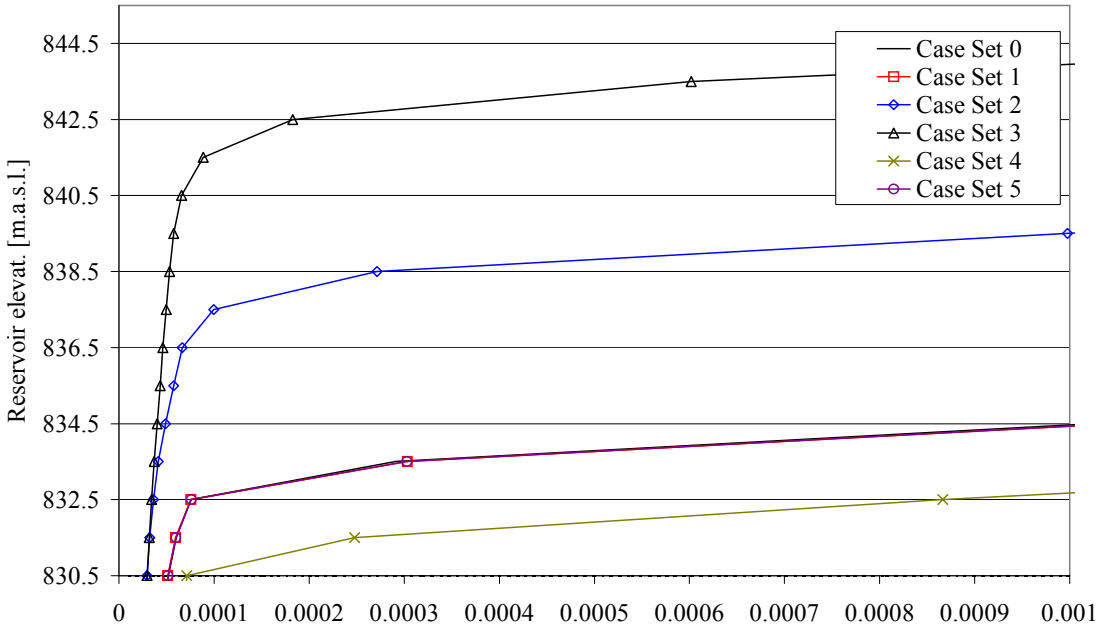

Fig 9. Sliding [m]– right side vertical section -zoom.

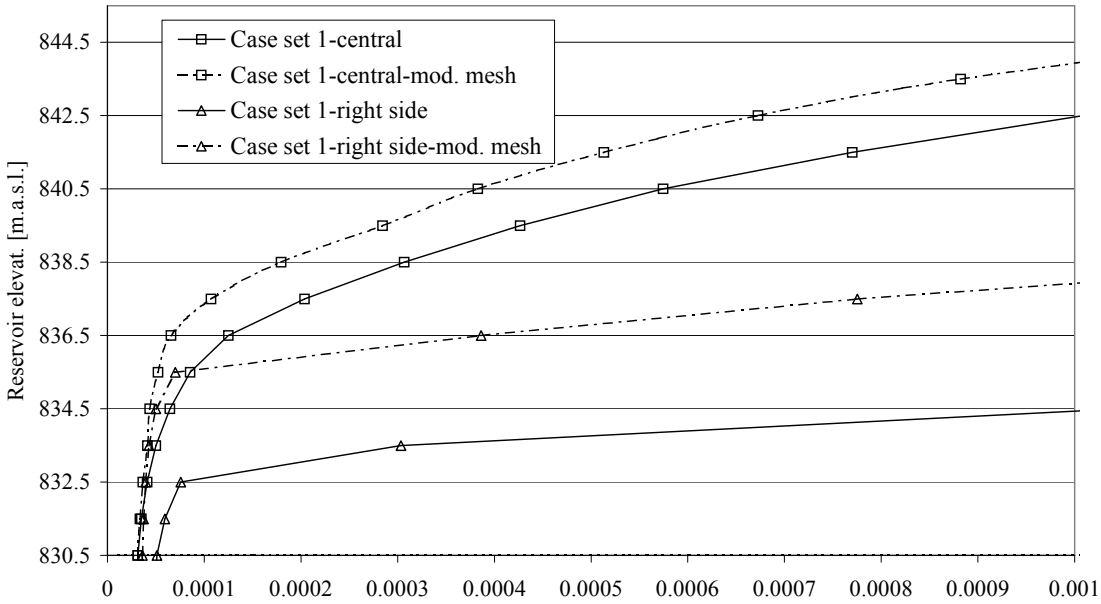

Fig 10. Sliding [m]– Actual joint vs. modified joint.

4.2. STRESS RESULTS

The stress results corresponding to the failure points exhibit low values (well below of the respective strength) of principal stresses for all case sets, with very little differences between case sets. In particular, for case set 0 principal stresses within the dam body are shown in Fig 11 ÷ 14.

In the highest vertical section no tensile stresses occur and compressive stresses do not exceed 1,215 KPa. Tensile stresses, up to 115 Kpa, occur on the lateral part of the dam and compressive stresses results lower than for the highest section.

Case Set	Highest vertical section		Right side vertical section	
	Water elevation [m a.s.l.]	Multiplier coefficient	Water elevation [m a.s.l.]	Multiplier coefficient
0	833.5	1.09	832.5	1.07
1	833.5	1.09	832.5	1.07
2	838.5	1.23	836.5	1.18
3	843.5	1.37	840.5	1.29
4	831.5	1.04	830.5	1.00
5	833.5	1.09	832.5	1.07
6	830.5	1.00	830.5	1.00

Tab. 5. Ultimate sliding strength – multiplier coefficients.

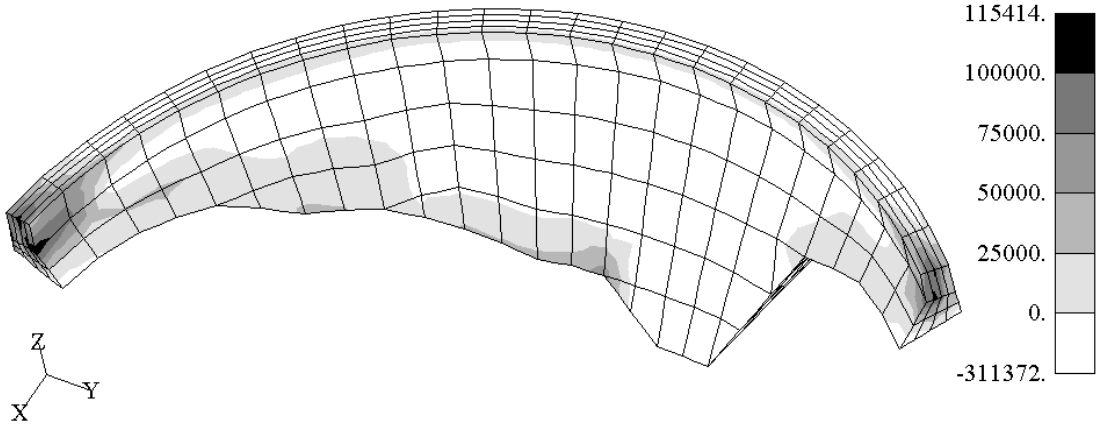

Fig. 11. Max. Principal stresses [Pa] at 833.5 m water elevation – downstream/top.

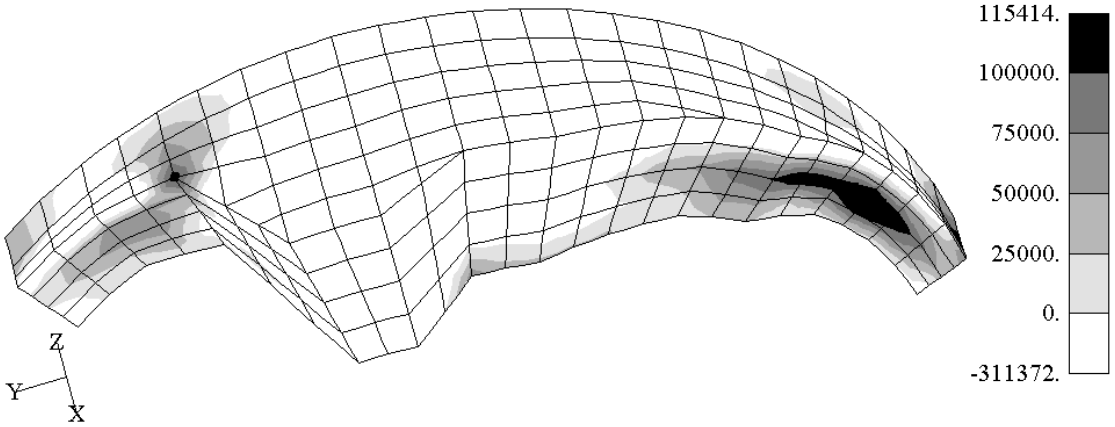

Fig. 12. Max. Principal stresses [Pa] at 833.5 m water elevation – upstream/bottom.

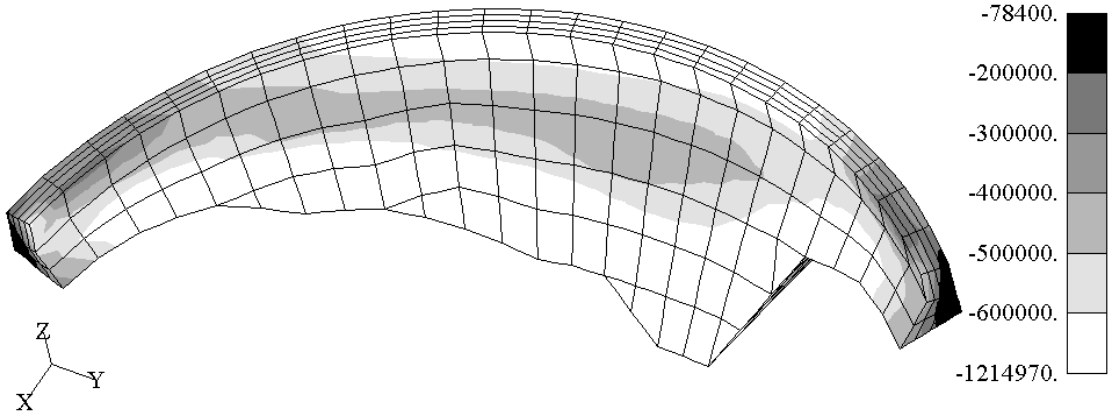

Fig. 13. Min. Principal stresses [Pa] at 833.5 m water elevation – downstream/top.

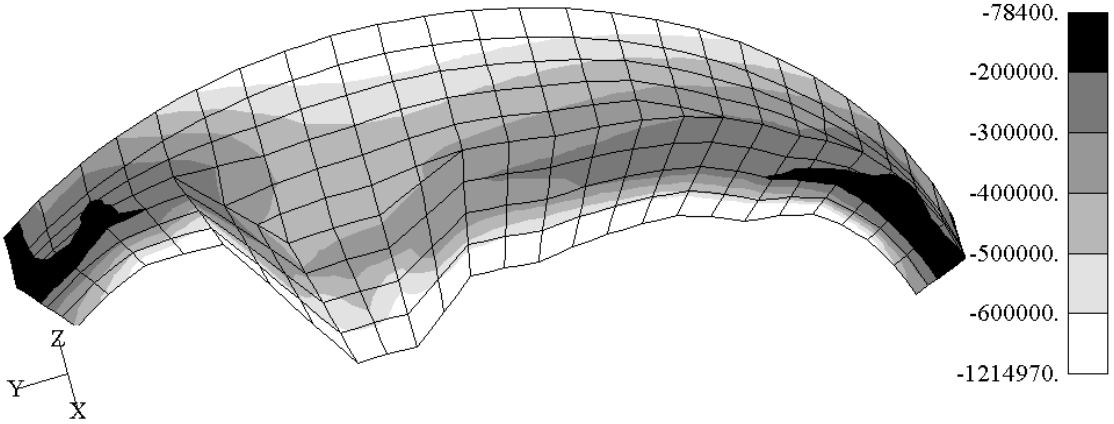

Fig. 14. Min. Principal stresses [Pa] at 833.5 m water elevation – upstream/bottom.

The highest arch section exhibits its higher values of tensile stress (not exceeding 100 KPa) at the abutments (Figs. 11, 12), while compressive stress do not exceed 800 KPa in the middle part (Figs. 13, 14).

Finally, for the same case set, normal stresses and shear stresses on the dam-rock interface are shown in Figs. 15 and 16 respectively.

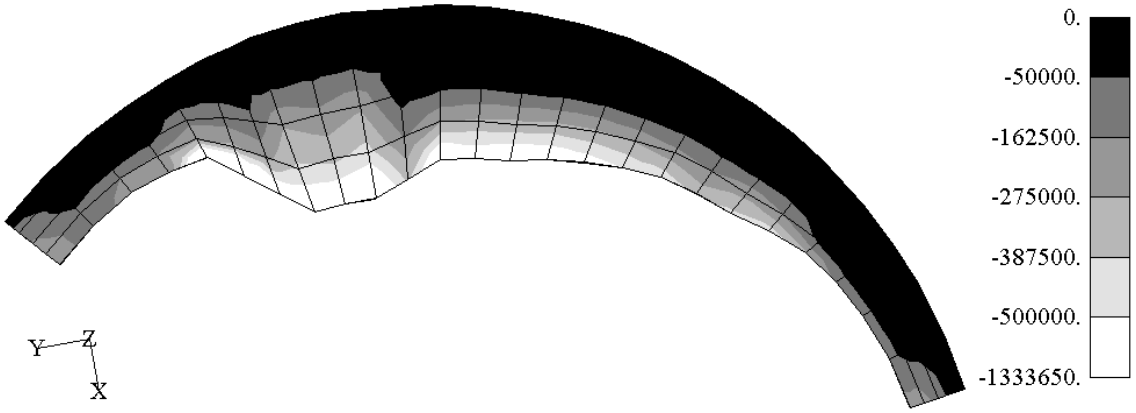

Fig. 15. Normal stresses on dam-rock interface at 833.5 m water elevation – bottom.

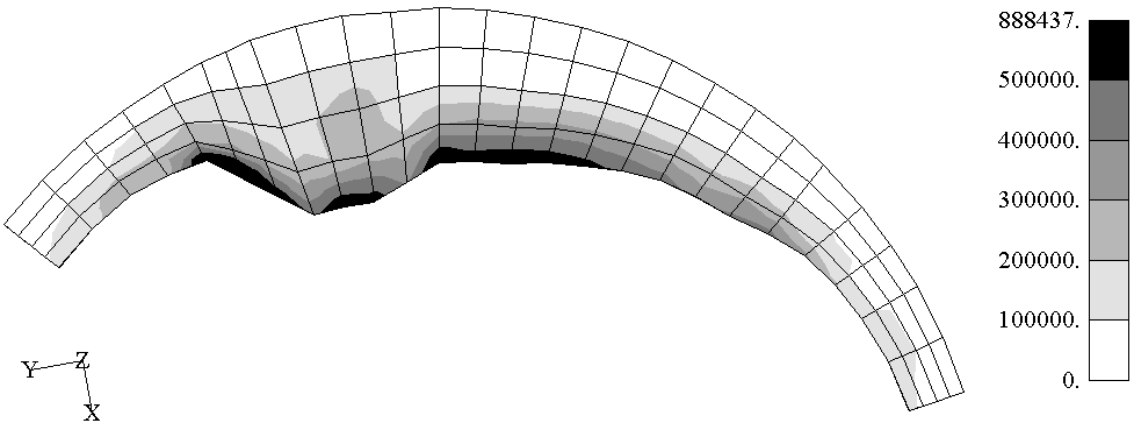

Fig. 16. Shear stresses on dam-rock interface at 833.5 m water elevation – bottom.

Such distributions shows that low normal and shear stresses are transferred to the rock foundation, confirming the scarce influence of the material constitutive law on the sliding stability of the dam under examination.

5. CONCLUSION

Theme A of the 7th Benchmark Workshop on numerical analysis of dams has been approached by using the finite element method. Parametric analyses have been carried out in order to investigate the influence of materials and joint/interface parameters. Comparison with the results of conventional 2D sliding stability analyses has been made and the additional strength due to the arch effect has been critically evaluated.

The most important results can be summarized as follows:

- 2D conventional and 3D rigid body approaches are inappropriate, in this particular situation, to determine the failure point, since FEM analysis shows that sliding first occurs on the lateral parts of the dam, even modeling the base joint to lay horizontally, as it would be expected in more usual situations;
- the different material constitutive laws have a very scarce influence on the global behaviour of the dam, thus allowing the use of linear-elastic models to carry out this type of analysis;
- the stress results in correspondence of failure points exhibit low values (well below of the respective strength and comparable with 2D stresses) of principal stresses for all case sets, with very little differences between case sets; normal and shear stresses transferred to the rock foundation exhibit the same trend;
- all sliding curves up to collapse show a strong influence, higher then 2D conventional analysis, of joint parameters in the sliding stability;
- the additional strength provided by the 3D arch effect for all comparable case sets is significant.

REFERENCES

[1] Giuseppetti, G., Mazzà, G., Meghella, M., Theme A formulation (Evaluation of ultimate strength of gravity dams against sliding), 7th Benchmark Workshop on Numerical Analysis of Dams, Bucharest, September, 2003.
[2] Masarati, P., Meghella, M., The FEM computer code CANT-SD for non-linear static and dynamic analysis of dams. Enel.Hydro rep. n. 6045, Milan, 2000.
[3] Lade P.V., Kim, M.K. Single hardening constitutive model for frictional materials. II. Yield criterion and plastic work contours, Computers and Geotechnics, 6, 13-29, 1988.
[4] Léger, P., Tinawi, R., Leclerc, M., CADAM Computer Analysis of concrete gravity Dams, version 1.4.11,Ecole Polytecnique de Montrèal, Canada, July, 2002.

ACKNOWLEDGEMENT

The authors wish to thank Renato Cadei and Piero Masarati for the valuable contribution they provided in all phases of this study.

ESTIMATION OF THE ULTIMATE SLIDING STRESS FOR A CURVED – WEIGHT DAM BY THE FINITE ELEMENT METHOD

Michael ION, prof.dr.eng., E-mail: michael@mail.dnttm.ro
Gheorghe LAZAR, ass.prof.dr.eng., E-mail:gh_lazar@hidro.utt.ro
"Politehnica" University of Timisoara, ROMANIA

SUMMARY: The sliding stress for the curved – weight dam is determined by the finite element method using the ANSYS program facilities. For meshing the structure and the foundation soil, 3D finite elements (SOLID 92) are used. At the concrete-foundation soil contact zone, connection elements (CONTACT 174) were employed. From the finite element analysis, results the shear stresses in the contact elements and the resultant friction force.

Considering that the sliding stability is at the limit ensured (the safety ratio being equal with1), the following loads are employed: hydrostatic pressure, gravity weight, uplift pressure, and a component due to the arch effect.

Taking into account the fictitious water levels, corresponding to the 830.50 + Δh elevations, and by simulating the stress state in the studied domain, it came out that the limit sliding stress state is reached when over passing the admitted stress values in the concrete or the foundation rock. This situation appeared for a value of 1.202 of the ratio between the fictitious water level and the dam toping elevation.

1. GENERAL CONSIDERATIONS

According to the proposed theme A [1], in order to determine the stress and strain state occurring in the Scalere Dam (Italy) - concrete gravity dam with a slightly arch shape – the following data were given: the 3D geometry of the dam including the structure – foundation rock connecting zone, the characteristic physical and mechanical parameters for the materials (concrete, foundation rock), loading and boundary conditions. Besides the dam geometry, given by the "solid.igs" file, in the present study the foundation rock was modeled by extending the attached geometry with about 5 m. This extending aims to emphasize the dam – rock interaction. The boundary conditions were so translated at the bottom limit of the extended domain.

Following the suggestion mentioned by the given theme, the discontinuities owned to the vertical interfaces delimitating the concrete blocks were not considered.

2. DOMAIN MESHING

Considering the proposed subject, the figure 1 presents several views of the meshed Scalere Dam: an upstream view, an aerial view, and a detail of the foundation rock (sub domain obtained by the mentioned extending).

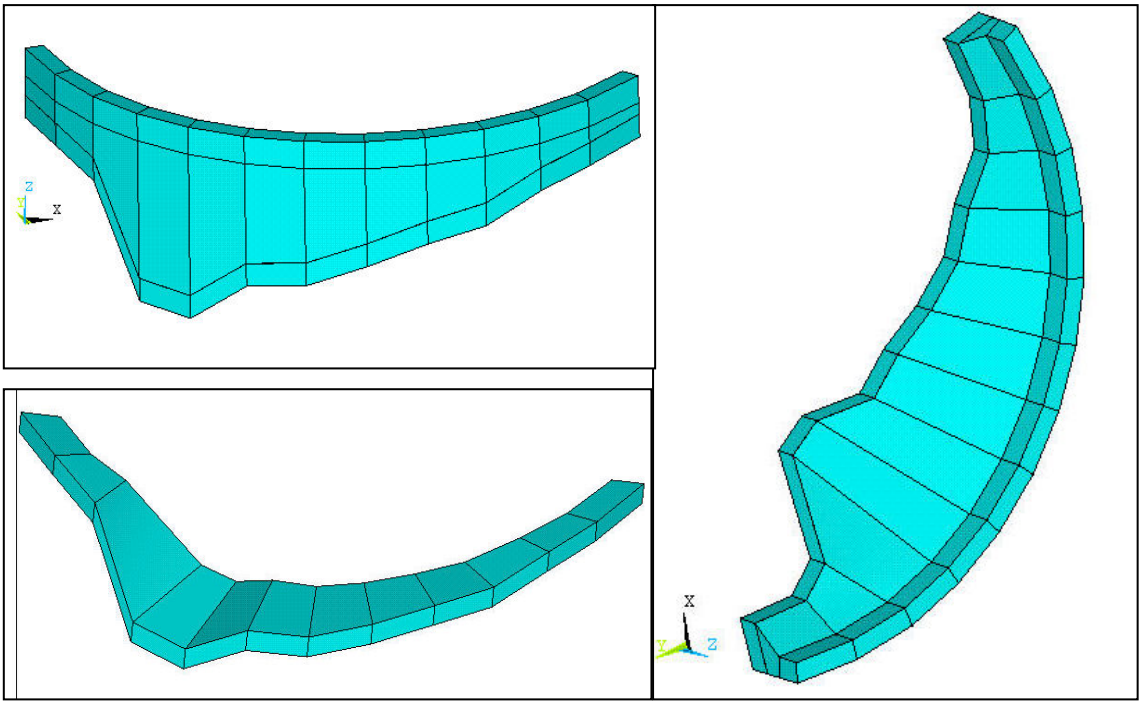

Figure 1 General views of the meshed geometry for the Scalere Dam and its foundation rock

The dam and the foundation rock were meshed considering 3D finite elements type SOLID 92 [4, 5], the specific properties corresponding to the two materials. The cohesion and the friction for the concrete – foundation rock interface was modeled by 3D finite elements type CONTACT 174 [5]. The used elements are given by the ANSYS package of programs.

The figure 2 presents the considered spatial meshing option, the upstream view being presented on the right side. There are visualized the two types of materials – concrete and foundation rock.

The physical and mechanical parameters for the considered materials, together with their values, are presented in table 1.

Table 1

Element type	Material type	E [daN/m^2]	ρg [daN /m^3]	μ	$f=tg(\Phi)$	c [daN/m^2]
SOLID 92	1- concrete	2.0e+09	2300	0.2	-	-
	2 – rock	1.5 e+09	0	0.35	-	-
CONTACT 174	interface	-	-	-	0.75	2.0e+05

The following loads were considered as acting on the Scalere Dam: concrete gravity weight (the foundation rock weight being not considered), the hydrostatic pressure and the uplift pressure (at the concrete – rock interface), these two corresponding to the fictitious upstream water level. It is mentioned that the dam toping corresponds to an elevation level of 830.50 m.

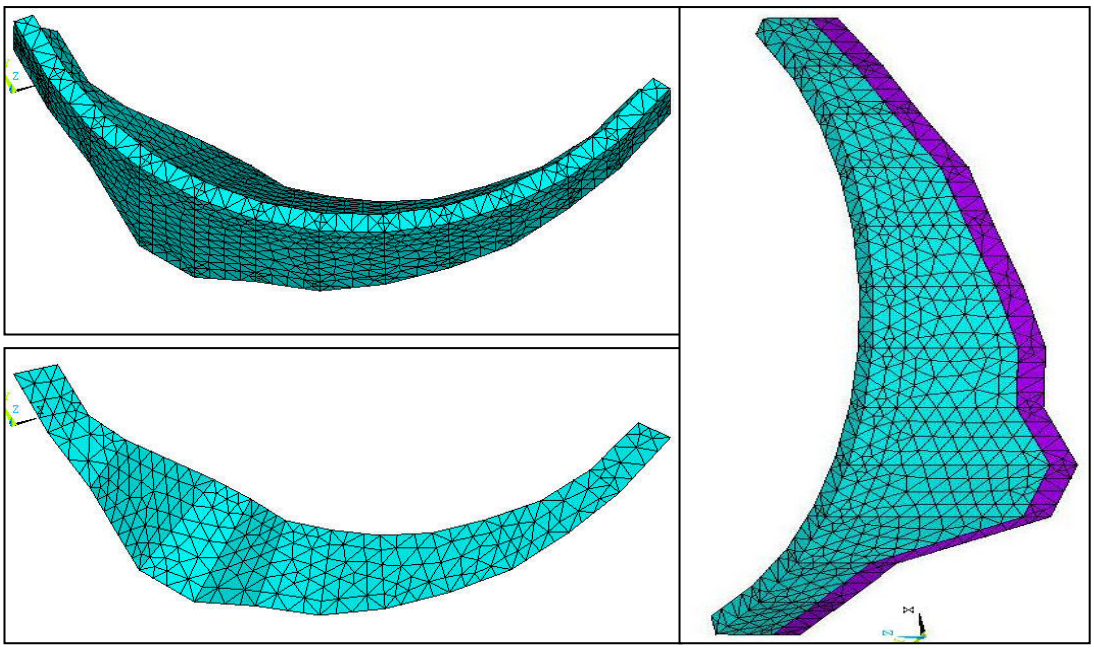

Figure 2 Domain meshing by SOLID 92 and CONTACT 174 elements blue – concrete, mauve – foundation rock

As an example, the figure 3 presents the distribution for both the hydrostatic pressure against the upstream face and the uplift pressure at the concrete - rock interface, the two corresponding to a fictitious water level in the reservoir of 840.5 m (Δh = 10m).

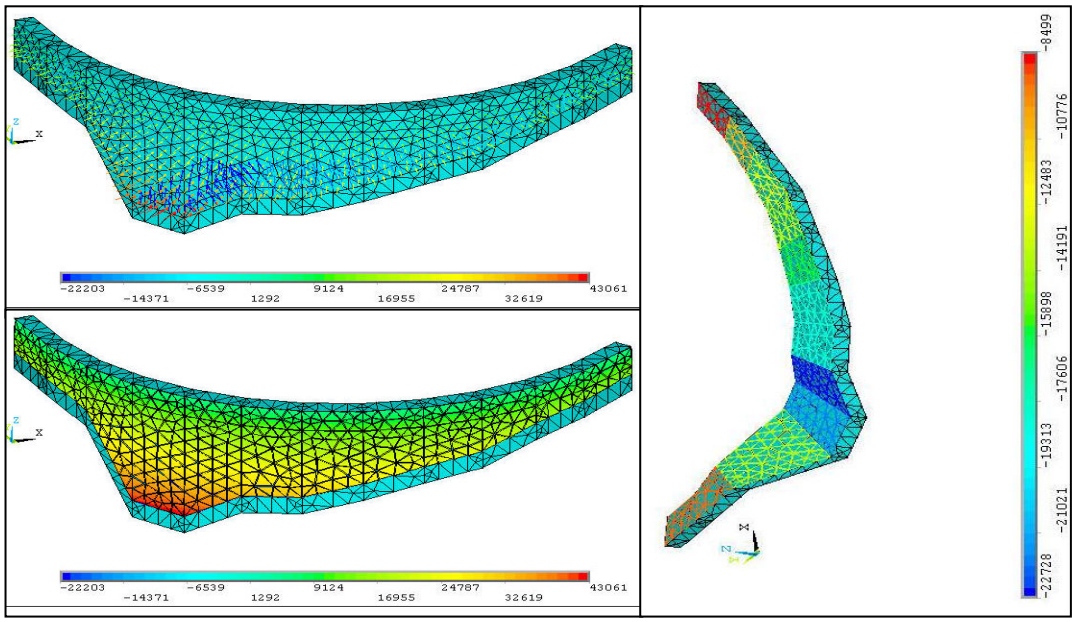

Figure 3 Arrows and contour type representation of the hydrostatic and uplift ressures

3. SLIDING LIMIT STATE EVALUATION

The sliding of a massif concrete dam placed on a rocky foundation site occurs when the sum of the horizontal forces overturns the sum of the friction forces appearing at the concrete – foundation rock interface. At limit, the following balance can be written [2, 3]:

$$k_s \sum H = f \sum V \quad (1)$$

where:

k_s – safety coefficient at sliding;

ΣH – sum of the horizontal forces;

ΣV – sum of the vertical forces;

$f = tg(\Phi)$ – friction ratio at the concrete – rock interface.

When considering the cohesion at the concrete – rock interface, and also the dam arch shape effect, for a safety coefficient of a value 1, the limit sliding stability condition for a concrete block presents the following expression:

$$1 = \frac{f \sum V + cA}{\sum H} + \frac{1}{\sum H} P_a \quad (2)$$

where:

c – specific cohesion, (daN/m^2);

A – area of the sliding surface at the concrete – rock interface, (m^2);

P_a – resultant force of the reactions acting lateral due to the arch effect, obtained in the sliding surface, (daN).

The resultant force expression is accepted as $P_a = a \times \Sigma H$, where a is a loading coefficient for the arch. The formula for this coefficient can be determined from the condition 2:

$$a = 1 - \frac{f \sum V + cA}{\sum H} \quad (3)$$

The loading coefficient for sliding of the concrete gravity dam at the concrete – rock interface can be consequently defined:

$$k = \frac{f \sum V + cA}{\sum H} = 1 - a \quad (4)$$

By the finite elements method, using specific contact elements for the concrete – foundation rock interface, the resultant effective force determined by friction and cohesion can be obtained by summing (integrating) the effective shear stresses occurring on the interface.

It is known that the hydrostatic pressure and the uplift pressure are determined by the water level considered in the reservoir. If the reservoir water level is increased at a fictitious value by Δh with respect to the level indicated by the study theme (830.50m), the boundary conditions regarding the hydrostatic pressure and the uplift pressure need to be changed for each analyzed situation (fictitious water level).

4. EVALUATION METHODOLOGY FOR THE LIMIT SLIDING STATE

For a given fictitious hydrostatic level (830.50 + Δh), the ANSYS program allows, when using a pressure gradient by the vertical direction (along the OZ axis, $\delta p/\delta z$ = -1000 daN/m^3) [5], an automatic calculation of the forces representing the hydrostatic pressure acting against the upstream face.

The equivalent forces representing the uplift pressure acting at the concrete – rock interface are established in a spreadsheet by the EXCEL program. The uplift pressure was obtained as mean values for the foundation level of each concrete block. These forces are to be updated by the user in the entering data file with respect to each analyzed situation. For each concrete block, the uniformly distributed load obtained by EXCEL is adopted in the ANSYS program in order to establish the corresponding uplift forces acting in the meshing nodes at the concrete – foundation rock interface.

In the developed numerical modeling, the displacement's three components (u_x, u_y, u_z) where considered as blocked for the nodes attached to the bottom surface of the hole considered domain.

By the numerical simulation the displacements of all considered domain nodes are obtained. Through several post-processing operations upon the mentioned results, the stress state is obtained in the concrete structure, in the foundation rock, and at the concrete – rock interface. By integrating the effective shear stresses occurring at the concrete – rock interface, the effective resultant force due to friction and cohesion is obtained. Consequently, the arch loading coefficient *a* and the loading coefficient for sliding of the concrete gravity dam *k* are estimated for a specific concrete block, as an outcome of the usual loads previously mentioned.

At the limit state, the sum of the horizontal forces corresponding to a concrete block is balanced by the resultant forces determined by the friction and cohesion effect as well as by the arch effect. It is noticed that the values of *a* and *k* coefficients are below 1**. The limit state of the considered model, comprised from a massif concrete dam with a slightly arch shape supported by a rock of good quality, is reached when the maximum admitted value of the stress (tension or compression) is reached in the concrete structure or the foundation rock.**

In order to reach the limit state, **the concrete dam is successively loaded, besides by its own weight, by the hydrostatic pressure at the upstream face and the uplift pressure at the concrete – rock interface according to the several fictitious water levels in the reservoir, until the maximum admitted value for the tension or compression stress is reached in at least one of the two materials.**

The fictitious water level in the reservoir is considered with respect to the initial reference level of 830.50 m. The maximum values admitted for the considered materials are: 10 daN/cm^2 for the concrete tension stress, 116 daN/cm^2 for the concrete compression stress, and 100 – 150 daN/cm^2 for the rock stress respectively.

4. RESULTS PRESENTATION

For the previously mentioned conditions, regarding the analyzed domain, the boundary conditions and the meshing characteristics, the following four computation assumptions were considered in order to determine the stress state in the structure and the foundation rock, ensuring the limit sliding state:

Ass.1 – reference level at 830.50 m;

Ass.2 – reference level at 830.50 m, loading level 830.50 + Δh. Δh =10 m., the water level varies fictitious in between 830.50 m and 860.50 m;

Ass.3 – reference level at 830.50 m, loading level 830.50 + Δh. Δh =2.5m., the water level varies fictitious in between 830.50 m and 838.00 m;

Ass.4 – reference level at 838.00 m, loading level 830.50 - Δh. Δh = 0.5m., the water level varies fictitious in between 838.00 m. and 837.50 m.

Following the successive simulations developed based on the considered assumptions, the tension stress σ_y corresponding to the fictitious water level of 837.50 m. is coming close to the maximum admitted value σ_{adm} = 10 daN/cm^2. In the case of the fictitious water level of 838.0 m, the tension stress σ_y overpass the considered maximum admitted value. So, it is considered that the sliding limit state for the Scalere concrete dam with a slightly arch shape is reached for the fictitious water level in the reservoir of 837.50 m.

The figure 4 presents the σ_x stress variation for the concrete – foundation rock model, together with a detail at the arch spring on right bank. It can be noticed that at the right bank spring, upstream face, the maximum tension stress value of 6.97 daN/cm^2 occurs. The maximum compression stress reaches -18.03 daN/cm^2.

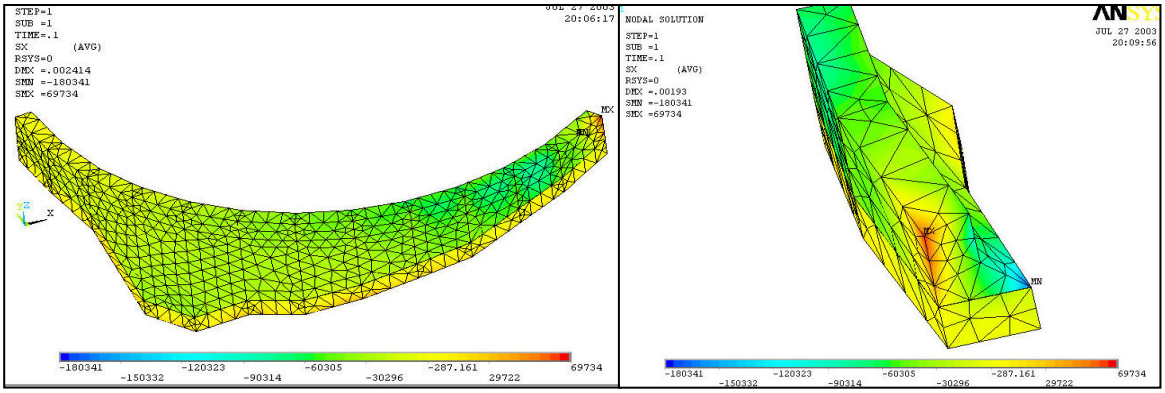

Figure 4 σ_x stress spectrum in the concrete structure and the foundation rock, detail at the arch spring on the right bank. H_f=837.50 m.

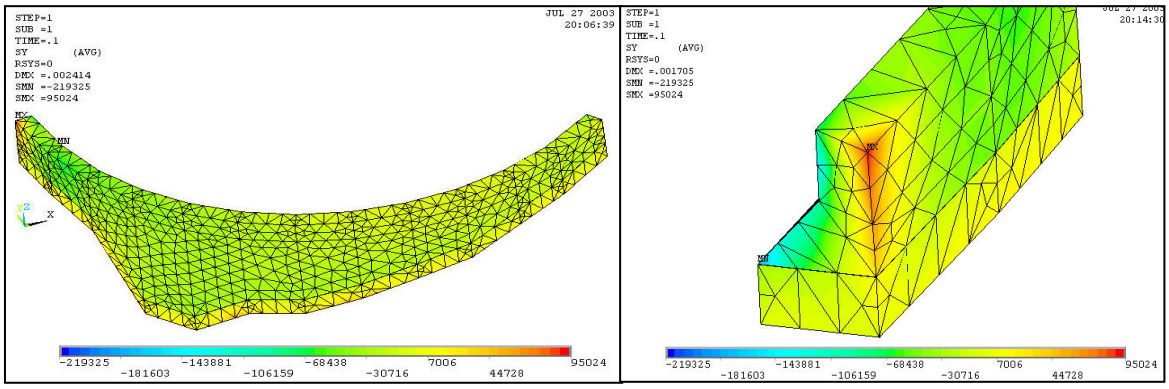

Figure 5 σ_y stress spectrum in the concrete structure and the foundation rock, detail at the arch spring on the left bank, , H_f=837.50 m.

The figure 6 presents the variation of the σ_z stress. The maximum tension value is 7.99 daN/cm^2, appearing in the foundation rock at the upstream bottom edge, and the maximum compression value is -16.30 daN/cm^2, downstream bottom edge.

The figure 5 presents the σ_y stress variation for the concrete – foundation rock model, together with a detail at the arch spring on left bank. It can be noticed that at the left bank spring, upstream face, the maximum tension stress value of 9.50 daN/cm^2 occurs. The maximum compression stress reached downstream is -21.93 daN/cm^2.

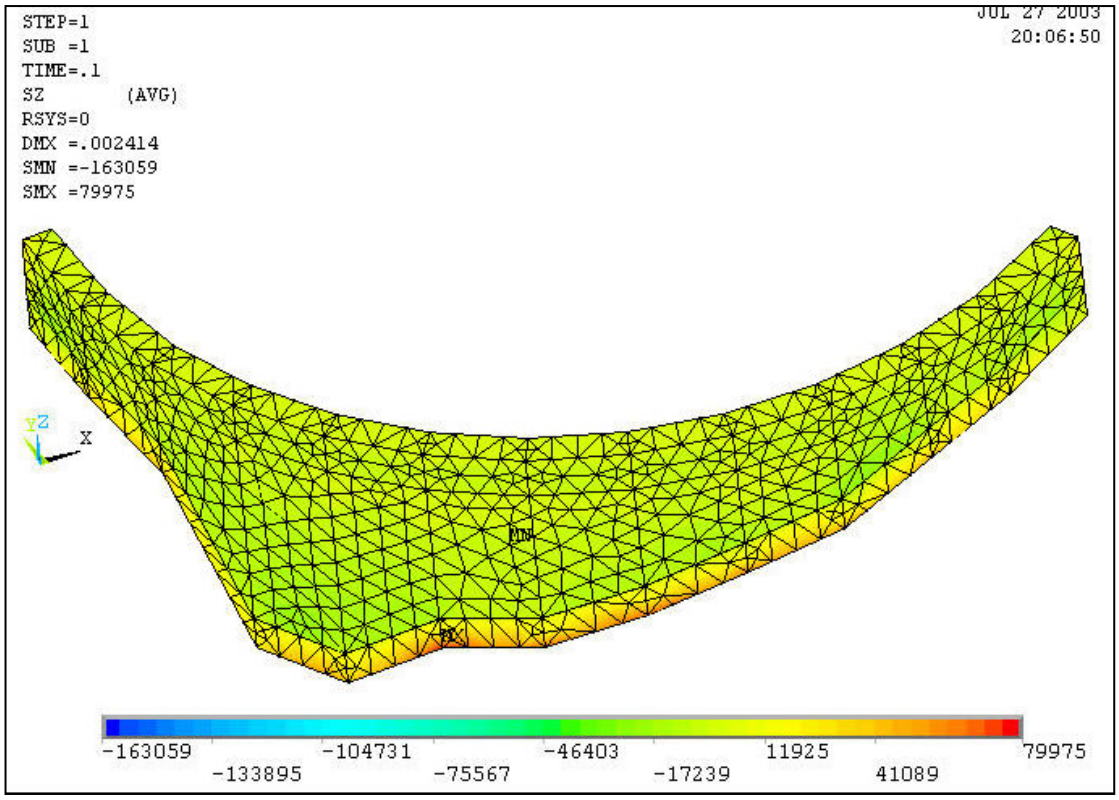

Figure 6 σ_z stress spectrum in the concrete structure and foundation rock, , H_f=837.50 m.

In the figure 7, the effective shear and normal stresses variations are presented at the contact surface, for the several water levels of: 830.50 m, 835.50 m, 838.00 m, and 837.50 m. In the figure 8, the same stresses are presented at the contact surface for the highest concrete block, corresponding to the four mentioned water levels.

From the figures 7 and 8, it can be noticed that the upstream shear and normal stresses decrease till the value of zero, with the increase of the fictitious water level. The spreading zone of the studied stresses at the dam bottom increase with the fictitious water level increase.

The normal and shear stresses increase in value and redevelop on the new compresses area. By increasing the fictitious water level, the maximum shear stress presents the following values (fig.8): 1.58 daN/cm^2, 1.72 daN/cm^2, 1.93 daN/cm^2, and 2.85 daN/cm^2. In the same time the maximum normal stress presents the following values: 3.87daN/cm^2, 4.42 daN/cm^2, 4.81 daN/cm^2, 5.49 daN/cm^2.

The shear effective stresses on the bottom surface of the highest block were integrated according to the theme notification, in order to establish the loading coefficients *a* and *k*, for the hole range of fictitious water level corresponding to the assumption 1 to 4.

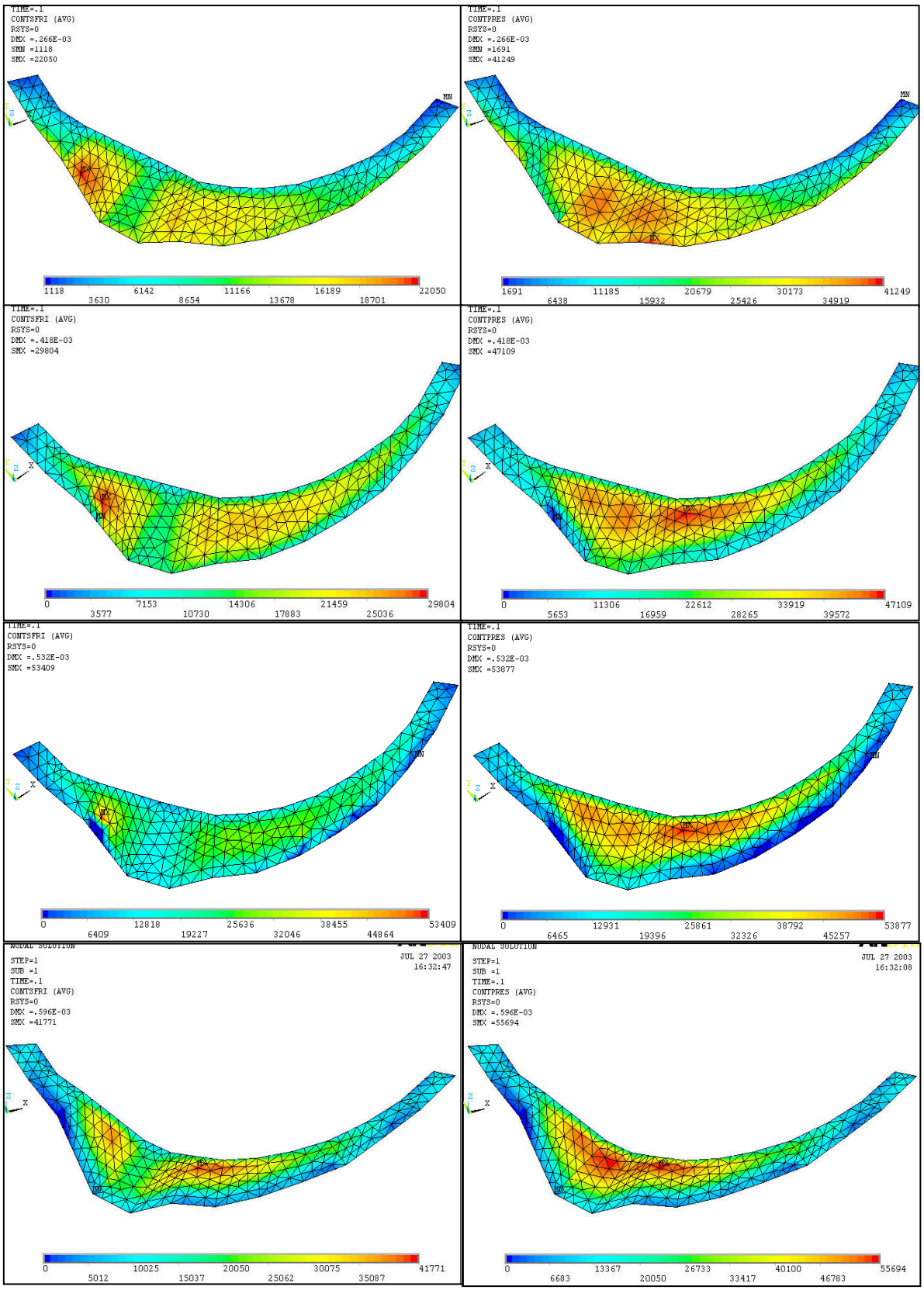

Figure 7 Shear and normal stresses spectrum at the concrete – rock interface, for the fictitious water levels of: 830.50m, 835.50m, 838.00m, 837.5m

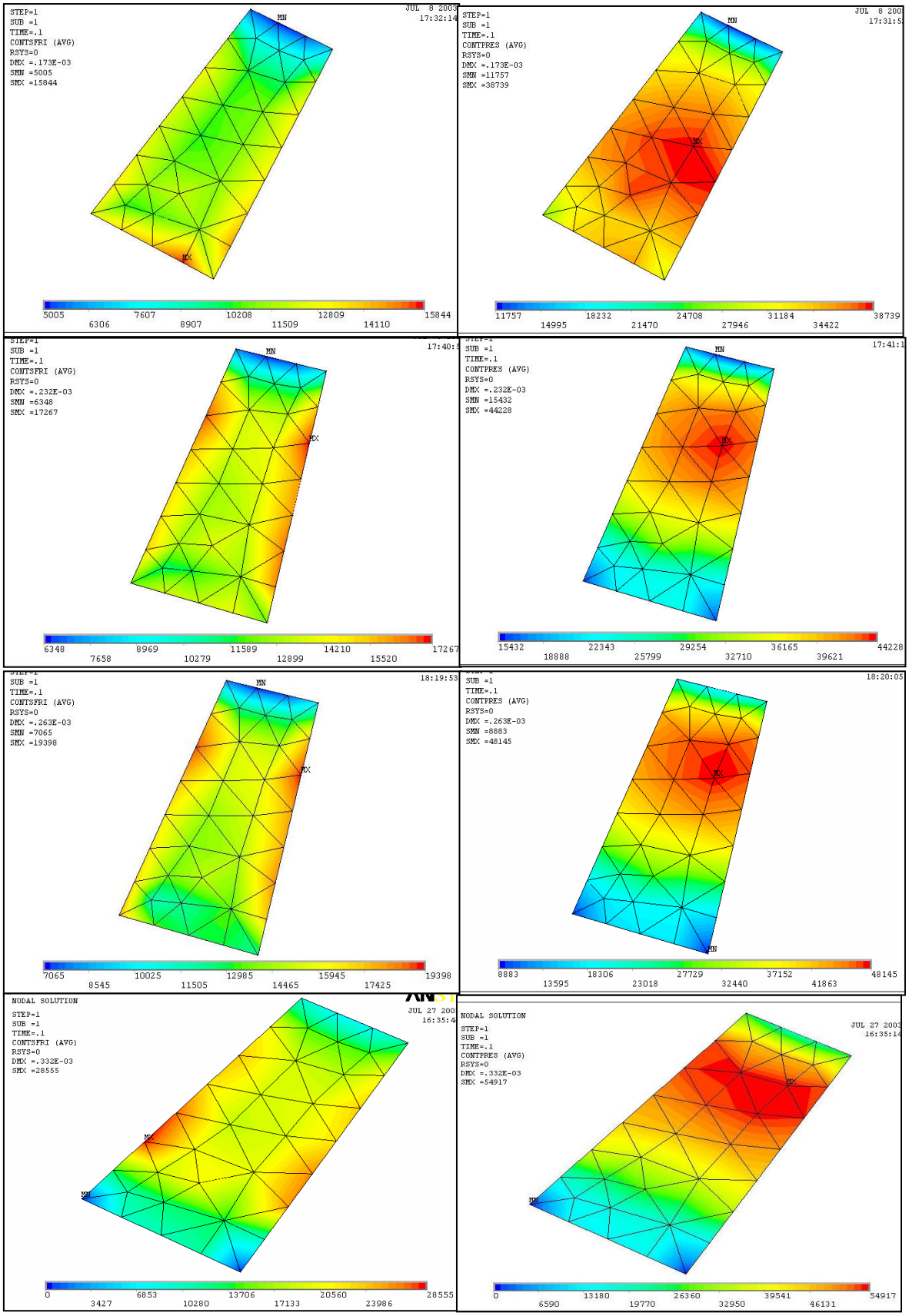

Figure 8 Shear and normal stresses spectrum at the concrete – rock interface of the highest concrete block, for the fictitious water levels of: 830.50m, 835.50m, 838.00m, 841.5m

The development of the obtained *a* and *k* values with the normalized fictitious level (ratio between the fictitious water level and the reference level) is presented by the figure 9.

It is noticed that by increasing the normalized fictitious level, the arch loading coefficient increases from 0.6014 to 0.65 and after that decreases to 0.55, while the sliding loading coefficient decreases from 0.3986 to 0.35 and after that increases to 0.45.

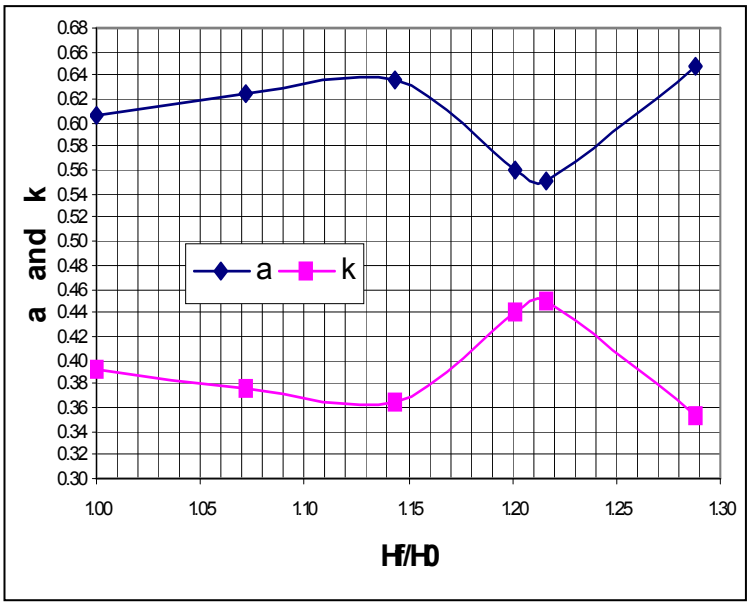

Figure 9 Variations of the arch *a* and sliding *k* loading coefficients with the normalized fictitious level

For all the analyzed cases, the strain state for the concrete dam – foundation rock model was also determined. As required through the theme notifications, in order to face up the obtained results with results obtained by other analysis, there were considered two edge nodes on the upstream face of the meshed Scalere Dam: dam toping – node 5964, dam bottom – node 6201, both for the highest concrete block.

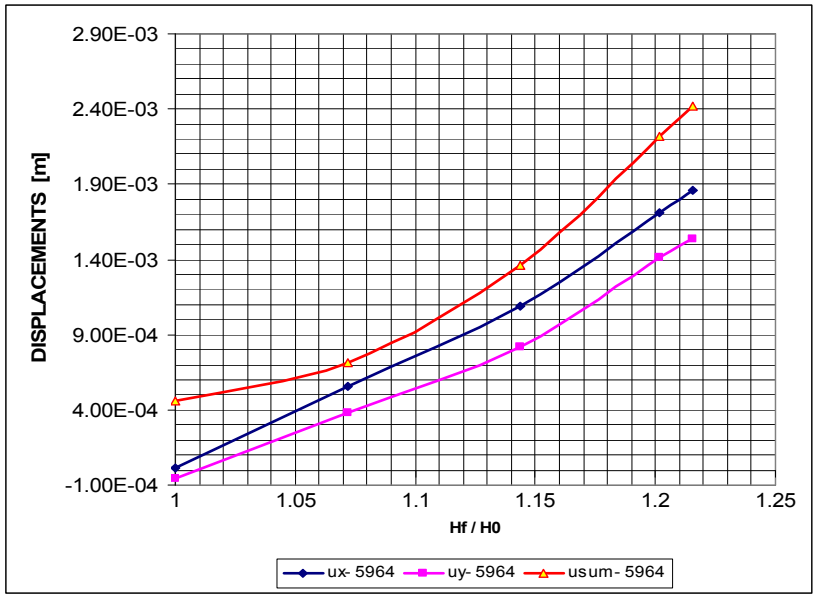

Figure 10 Dam toping node 5964 displacements development with the normalized fictitious level

The figures 10 and 11 present the variations with the normalized fictitious level of the ux, uz and usum displacements for the two specified nodes.

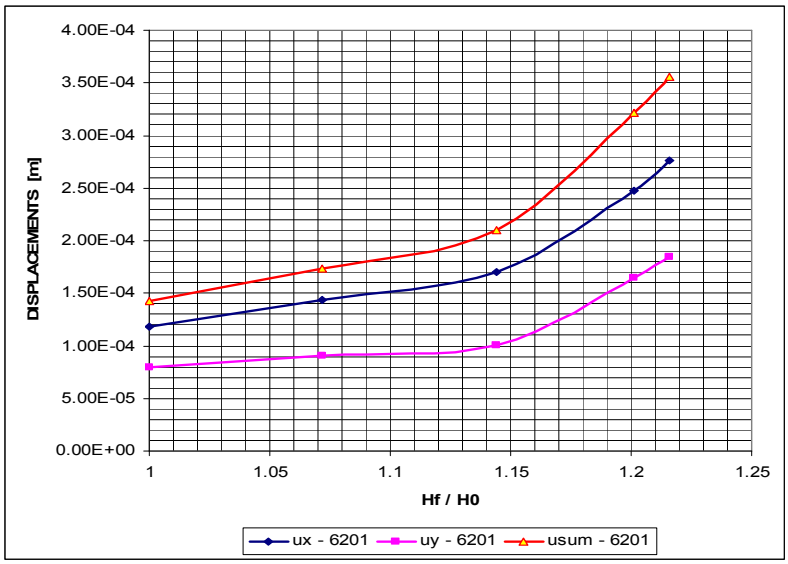

Figure 11 Dam bottom node 6201 displacements development with the normalized fictitious level

In conclusion, according to the theme requirement, it can be acknowledged that the limit value of the equivalent overloading coefficient, given by the ratio between the fictitious water height in the reservoir (H_f = 837.50 – 796.00 = 41.50 m) and the reference dam height (H_0 = 830.50 – 796.00 = 34.50 m), presents the value of 1.202.

REFERENCES

[1] G.Giuseppetti, & al – "Evaluation of ultimate strength of gravity dams with curved shape against sliding", 7th Benchmarck Workshop on Numerical Analysis of Dams, September 24-26, 2003 – Bucharest, ROMANIA
[2] Radu PRISCU – "Construcţii hidrotehnice", vol.1, Ed. Tehnică, Bucureşti, 1974
[3] Adrian POPOVICI, Calin POPESCU – "Baraje pentru acumulari de apa", vol. I, Ed. Tehnica, Bucuresti,1992.
[4] Michael ION – "Calculul structurilor hidrotehnice", Curs, Tipografia IPT, Timisoara, 1982
[5] **** - "ANSYS/ED" - Student Edition, Release 5.3, Copyright 1971, 1978, 1982, 1985, 1987, 1989, 1992-1996 by SAS IP - ISO 9001- 1994.

ULTIMATE STRENGTH AGAINST SLIDING OF A GRAVITY CURVED DAM*

Adrian Popovici, Radu Sarghiuta
Technical University of Civil Engineering of Bucharest, ROMANIA
Netzo Dimitrov
Energoproekt-PLC Hydropower Division, Sofia BULGARIA

SUMMARY: The evaluation of the ultimate strength against sliding of Scalere dam (Italy) is presented. This dam with 36.50 m maximum height is a concrete gravity structure with insufficient cross section but slightly curved in plan. The analysis is performed with ANSYS computer code. The dam body is discretized with three-dimensional SOLID95 elements and, respectively rock interface is modelled with CONTA174 elements. The failure mechanism to sliding is achieved by fictitious successively increase of the reservoir water level over dam crest. The following failure mechanism are analysed:

- sliding of the dam independent central cantilever evaluated by standard analysis; the portion of the hydrostatic pressure acting on cantilever is calculated according to TLM (Trial Load Method);
- excessive increase of displacements along the dam-rock interface (≥ 10 mm);
- sliding because of the overtake of the allowed limits between shear force and normal force on some areas from dam foundation.

RÉSUMÉ: L'évaluation de la résistance ultime au glissement du barrage Scalere (Italie) est présentée. Ce barrage avec la hauteur maximum de 36.50 m est une structure en béton poids avec la section central insuffisante mais légèrement arquée dans le plan. L'analyse est exécutée avec le code aux éléments finis ANSYS. Le corps du barrage est discrétisé avec des éléments tridimensionnels SOLID95 et, respectivement l'interface de roche est modelée avec des éléments CONTA174. Le mécanisme de rupture est accompli par successivement l'augmentation fictive du niveau d'eau de réservoir au-dessus de la crête de barrage. Les mécanismes de rupture suivantes sont analysés:·

- glissement de la console central indépendant de barrage évalué par analyse standard; la partie de la pression hydrostatique agissant sur la console central est calculée selon TLM (Trial Load Method);·
- augmentation excessive des déplacements le long de l'interface de barrage-roche (≥ 10 mm);
- glissement en raison du dépassement des limites permises entre la force de cisaillement et la force normale sur quelques secteurs de la fondation.

* La résistance ultime au glissement d'un barrage poids arqué

1. INTRODUCTION. FAILURE MECHANISM

Scalere Dam (Fig. 1) is a concrete gravity structure with insufficient cross section but slightly curved in plan. The main features of the dam are the followings:

Year of commissioning	1911
Maximum height above foundation	36.50 m
Length of the crest	158.00 m
Quality of the foundation rock	excellent
Contraction joints	no
Drainage in the foundation or dam body	no
Behaviour in operation	normal

In the problem proposed for Theme A – Concrete Dams from 7th ICOLD Benchmark Workshop on Numerical Analysis of Dams, it is asked to evaluate the ultimate strength against sliding of Scalere dam in terms of the ratio between maximum fictitious reservoir level corresponding to the sliding critical state and maximum reservoir water level considered in design (830.50 maSL, reservoir reference depth 36.50 m) [1].

Concerning Scalere dam, it is evident that in the standard bidimensional sliding stability analysis, the conclusion would be this dam could not withstand to sliding because of its insufficient cross section [2]. However due to relative narrow gorge of the dam site and especially, due to dam plan curvature, it has additional reserve of resistance and it has been operating in normal conditions for over 90 years.

a b

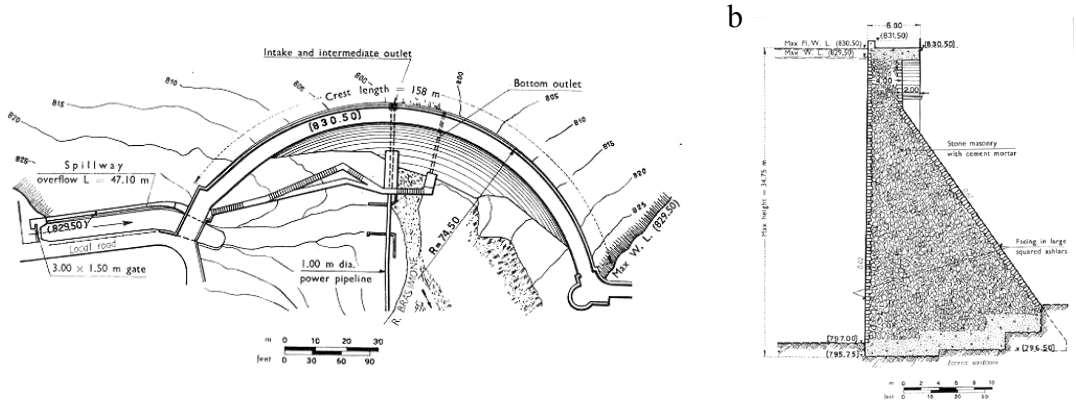

Fig. 1. Scalere dam: a - plan view; b – main cross section

Based on the above mention remarks, the followings failure mechanism by sliding of the dam were taken into account:

• According to Trial Load Method (TLM) the dam body can be discretized in a number of independent arches and cantilevers connected in the common nodes. The portion of the hydrostatic pressure acting on independent cantilever is then evaluated equalizing its displacements with the corresponding ones from arches-cantilevers discretized system. In a similar manner can be evaluated the portion of the hydrostatic pressure acting on independent arches. Usually, in the allotment of the hydrostatic pressure on independent arches and cantilevers is sufficient to take into account only the radial displacements of the system. In the site with steeped banks, the torsional (twist) effect between adjacent cantilevers may be also significant. Further, knowing the hydrostatic pressure repartition for different reservoir levels on the central cantilever, its ultimate strength against sliding is evaluated by standard sliding stability equation [3].

• The higher rates of increase of displacements versus reservoir water level increase on the dam-foundation interface can be interpreted as a sign that the failure mechanism by sliding was started. This parameter is analysed together with the maximum allowed displacement on the dam-foundation interface for normal operation of the dam. So, the maximum allowed displacement on the contact is considered limited to 10 mm. Displacements over 10 mm on contact will provoke unacceptable shear cracks on contact and loss of the dam stability.
• The overtake of the friction and cohesion forces possible to be mobilised on some areas from dam foundation by effective shear force on that areas is another criterion taken into account.

The criteria above-mentioned are successively used in order to evaluate the ultimate strength against sliding of Scalere dam. The results of the analysis are presented in the following paragraphs.

2. DESCRIPTION OF THE MATHEMATICAL MODEL

The mathematical model was built in compliance with ANSYS computer code [4]. The dam body was automatically meshed with SOLID95 finite element, defined by 20 nodes. A total number of 4166 tetrahedral elements resulted for dam body.

The dam-foundation interface was modelled with CONTA174 3-D surface-to-surface contact element (Fig. 2).

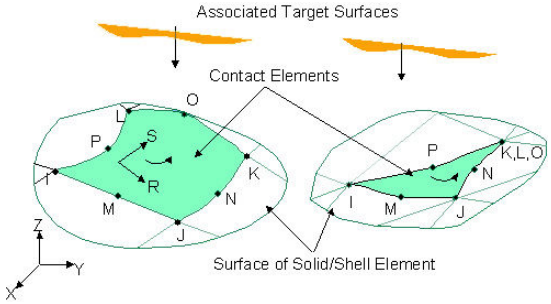

Fig. 2. CONTA174 3-D Surface-to-Surface Contact Element [4]

This element is used to represent contact, gap and sliding between 3-D "target" surfaces (TARGE170) deformable surface, defined by this element. It is located on the surfaces of 3-D solid elements, and has three degrees of freedom at each from its corner nodes: translations in the nodal x, y, and z directions. The element has the same geometric characteristics as the solid element face with which it is connected. Contact occurs when the element surface penetrates one of the target segment elements, on a specified target surface. Coulomb and shear stresses friction is allowed. A total number of 192 contact elements, respectively 192 “target” surfaces were used to model dam-foundation interface.

In the Figure 3 can be seen a general view of the Scalere dam finite element mesh, which was considered in analyses.

In the Table 1 are presented the main material parameters considered in analysis.

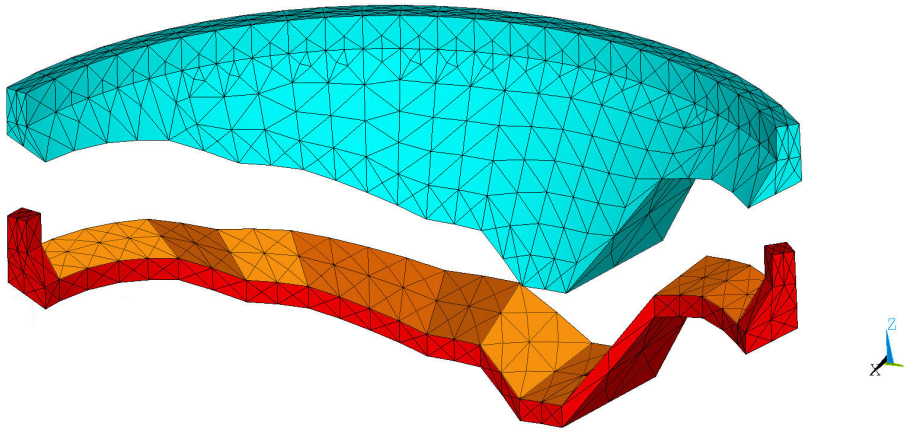

Fig. 3. General view of the Scalere dam finite element mesh

Table 1

Parameter	Material type		
	Concrete	Rock	Rock-concrete interface
Young's Modulus E [MPa]	20000	15000	
Poisson ratio ν	0.2	.18	
Density [kg/m^3]	2300	-	
Friction angle φ			37º
Cohesion c [MPa]			0.2

3. SLIDING STABILITY ANALYSIS OF THE INDEPENDENT CENTRAL CANTILEVER

The contact elements from dam-foundation interface were eliminated in this analysis. The translations on x, y, z directions of the nodes from dam foundation interface were blocked.

The analysis was performed in the linear elastic field. The dead weight was transferred only to cantilevers.

The hydrostatic pressure for different reservoir elevation (830.50, 837.80 and 845.10 maSL) was applied in the finite element discretized system. The uplift pressure diagram had triangular shape; the uplift pressure was equal with water column weight at the dam upstream toe and respectively nought at the downstream toe. The diagrams of the radial displacements in the dam central cantilever due to hydrostatic pressure computed from finite element dam model (FEM) are presented in the Figure 4.

Four independent arches with the shapes corresponding to the dam horizontal sections from 827.50, 818.20, 813.15 and, respectively 803.57 maSL elevations were built.

They were loaded with radial uniform pressure in order to find the values of the hydrostatic pressure, which generate in the arches central section radial displacement equals with those computed in the dam finite element mesh.

In this way, the hydrostatic pressure could be divided on the dam arches and central cantilever (Fig. 4). Further the sliding stability of the central cantilever, considered as the dam critical section for sliding risk, was computed by standard sliding analysis.

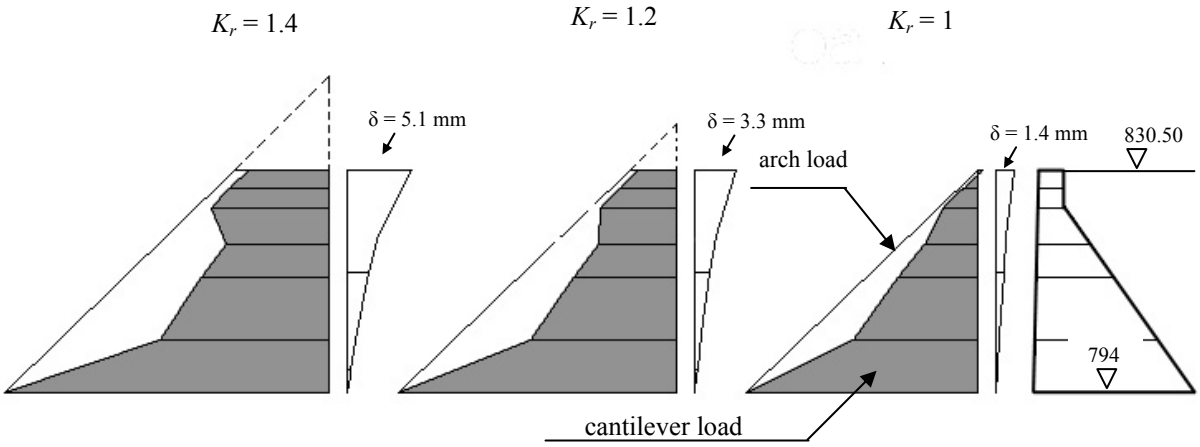

Fig. 4. Scalere dam: distribution of the hydrostatic pressures on independent arches and central cantilevers and diagrams of the radial displacements in the central cantilever due to hydrostatic pressures (computed from FE dam model)

The sliding stability coefficient (K) is evaluated according to standard relations:

$$K = \frac{f\left(\sum G - S\right) + c\Omega}{\sum H} \qquad (1)$$

where
- f is frictional coefficient at sliding (tanφ=tan37º=0.753);
- $\sum G$ - cantilever weight (γ_c = 23 kN/m^3);
- S - uplift force acting on cantilever foundation;
- c - cohesion (0.00…0.20 MPa);
- Ω - foundation area of the cantilever;
- $\sum H$ - hydrostatic force on horizontal direction acting on cantilever.

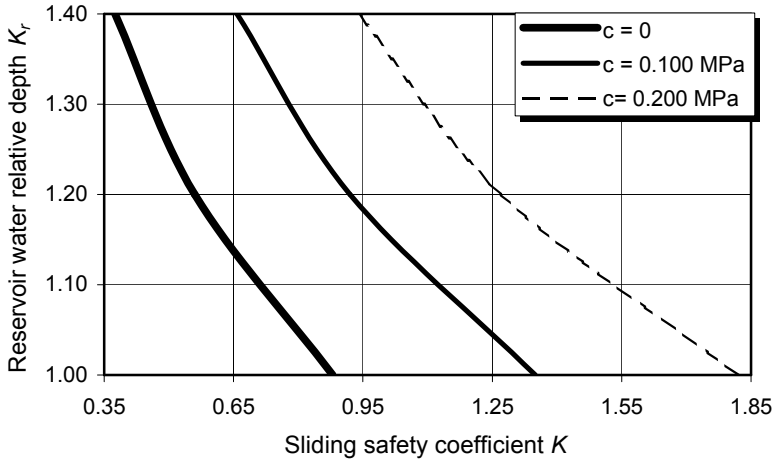

Fig. 5. Scalere dam – Sliding safety coefficient (K) for different reservoir levels according to TLM (friction angle tanφ = 37º, cohesion c = 0.0 … 0.2 MPa)

The results of the central cantilever sliding stability analysis performed with relation (1) are illustrated in the Figure 5. The following remarks can be pointed out about results:

- the cohesion (c) is a very important parameter for the sliding stability; it can be seen that for $c = 0$ the structure results to be unstable for reservoir at the crest level (830.50 maSL); instead the sliding stability coefficient, $K = 1.82$ for $c = 0.20$ MPa and reservoir at the same level; generally this conclusion is valid in the case of all dams with small or medium height, like Scalere dam.
- the relative influence of the dam curvature on the sliding stability becomes higher in ratio with the increase of the reservoir water level; for instance when the reservoir surface is at elevation 830.50 maSL, 19.8% from hydrostatic load is transferred to arches; instead for reservoir surface at the fictitious elevation 845.10 maSL, 26% from hydrostatic load is transferred to arches; this results can be explained, the relative contribution of arches in taking over a bigger portion from hydrostatic load versus increase of the reservoir water level is due to the increasing of dam displacements response.
- noting the relative water depth K_r as the ratio between reservoir depth and reference depth (reservoir at the crest level), the ultimate strength of the dam against sliding in terms of K_r are as follows:

$K_r = 0.95$ for $\varphi = 37^o$; $c = 0.0$ MPa
$K_r = 1.16$ for $\varphi = 37^o$; $c = 0.1$ MPa
$K_r = 1.34$ for $\varphi = 37^o$; $c = 0.2$ MPa

Assuming the analysed cantilever is the most exposed to the sliding risk, the results above mentioned can be extended to the whole dam.

4. ULTIMATE STRENGTH AGAINST SLIDING RESULTING FROM NONLINEAR FINITE ELEMENT ANALYSIS

The finite element mesh was presented in the Figure 3. The CONTA174 was used to model dam-foundation interaction. The crest arch of the dam was connected directly to banks, free of contact elements, in order to improve the convergence of the iterative solutions and for a better mathematical modelling of the physical behaviour. The nonlinearity of the model was due to contact elements, dam body having linear elastic behaviour.

The loads were applied step by step, the strain and stress states depending on loads time history. The dead weight was applied initially, after model calibration. The hydrostatic pressure was applied progressively in each new step the reservoir water level being considered with 3.65 m higher. The uplift pressure corresponding to hydrostatic pressure was considered with triangular shape. The reservoir water level has increased progressively as high as the convergence of the solution could be obtained.

According to the formulator suggestion a coefficient of water relative depth K_r was considered as follows:

$$K_r = \frac{\text{current reservoir water depth}}{\text{reference reservoir water depth (36.50 m)}} \qquad (2)$$

Note: the reference reservoir water depth of 36.50 m is in compliance with the set of geometry of the dam provided by formulator.

Some results obtained in the above described analysis model are presented in the Figures 6…11.

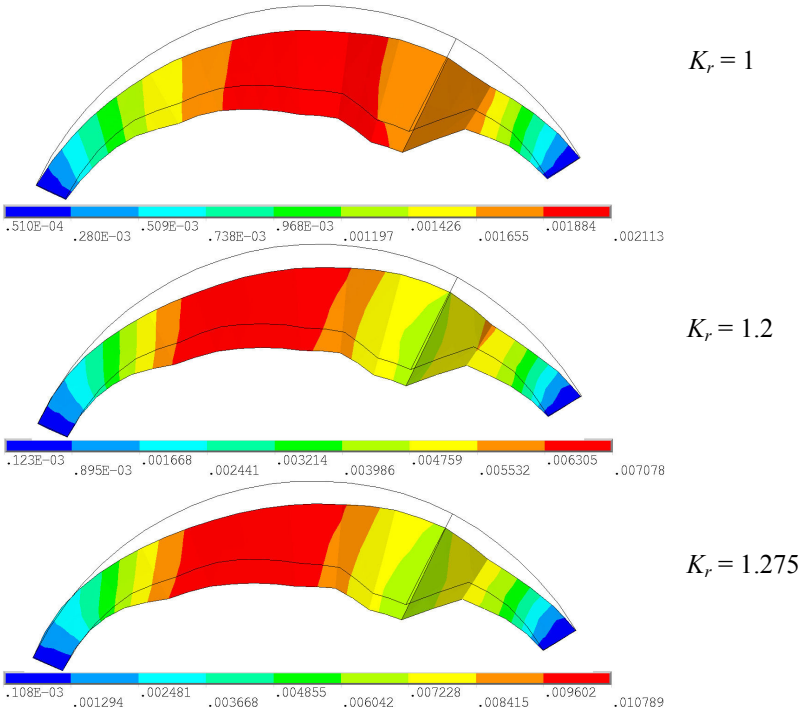

Fig. 6. Upstream-downstream displacements contours on the dam-foundation contact for different fictitious reservoir levels

It can be remarked that the last step for which convergence could be obtained corresponded to $K_r = 1.275$.

The contours of total displacements on the dam foundation contact for different fictitious reservoir levels are presented in Figure 6. Based on interpretation of displacement contours, it may point out the zone of the dam situated on the right bank near central section having the biggest relative displacements is the most exposed to sliding.

The variation of the crest and dam-foundation contact maximum displacements versus K_r can be seen in the Figure 7.

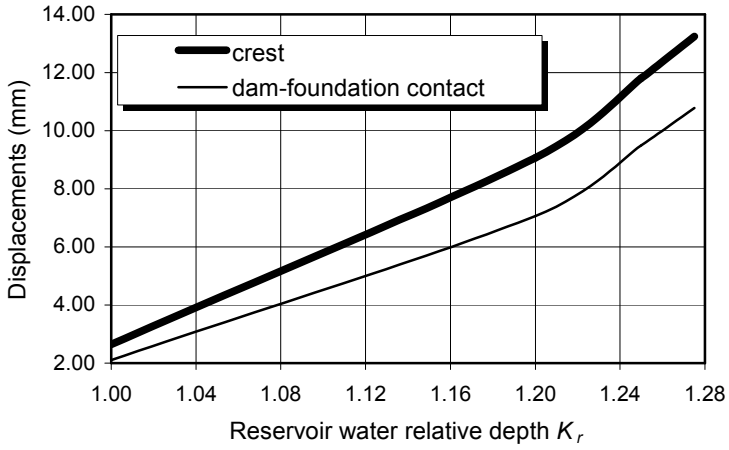

Fig. 7. The variation of the maximum displacements from crest and dam-foundation contact with relative reservoir level.

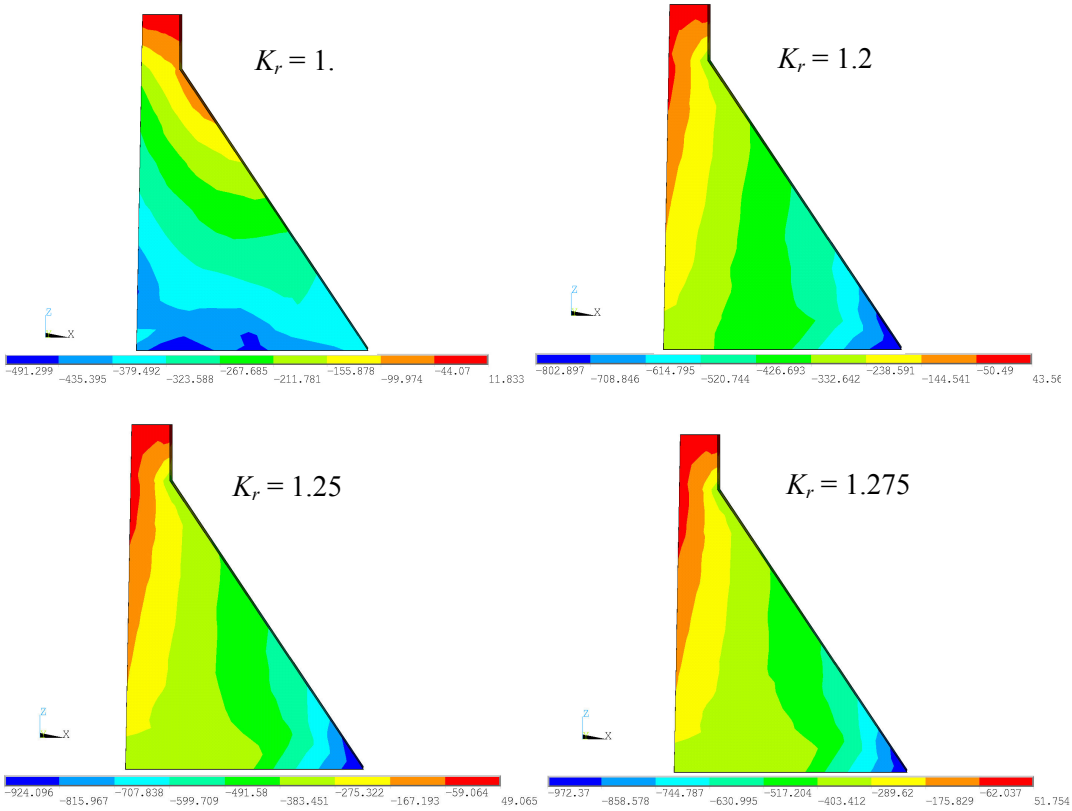

Fig. 8. Scalere dam – central cross section: Contours of vertical stresses due to dead weight + hydrostatic pressure + uplift pressure for different fictitious reservoir levels (in KPa)

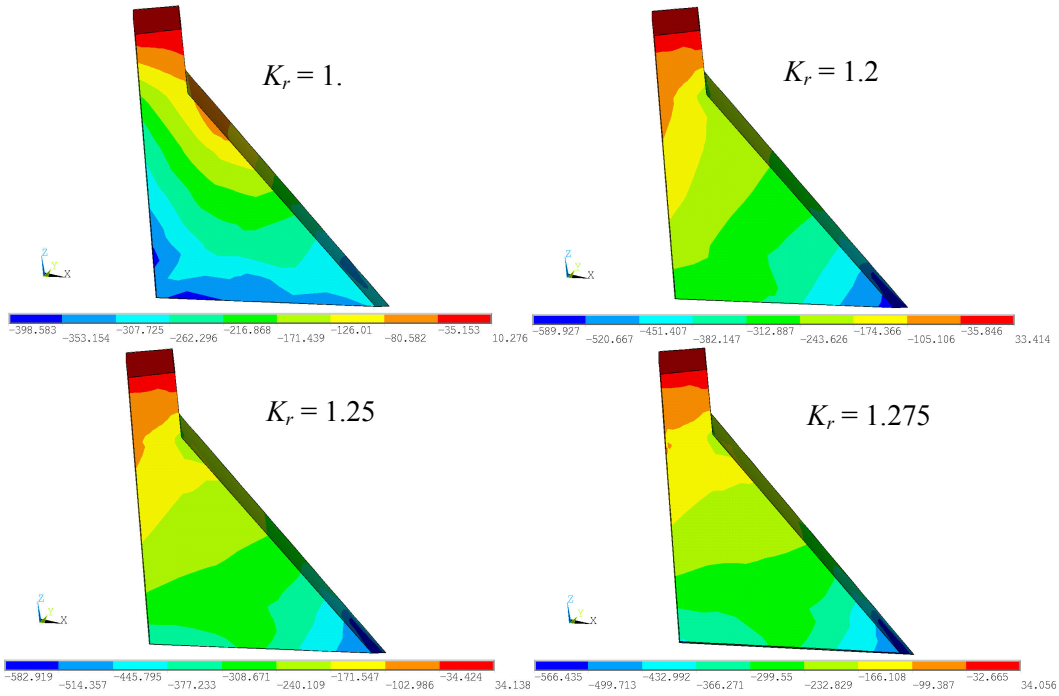

Fig. 9 Scalere dam – cross section in the sliding zone: Contours of vertical stresses due to dead weight + hydrostatic pressure + uplift pressure for different fictitious reservoir levels (in KPa)

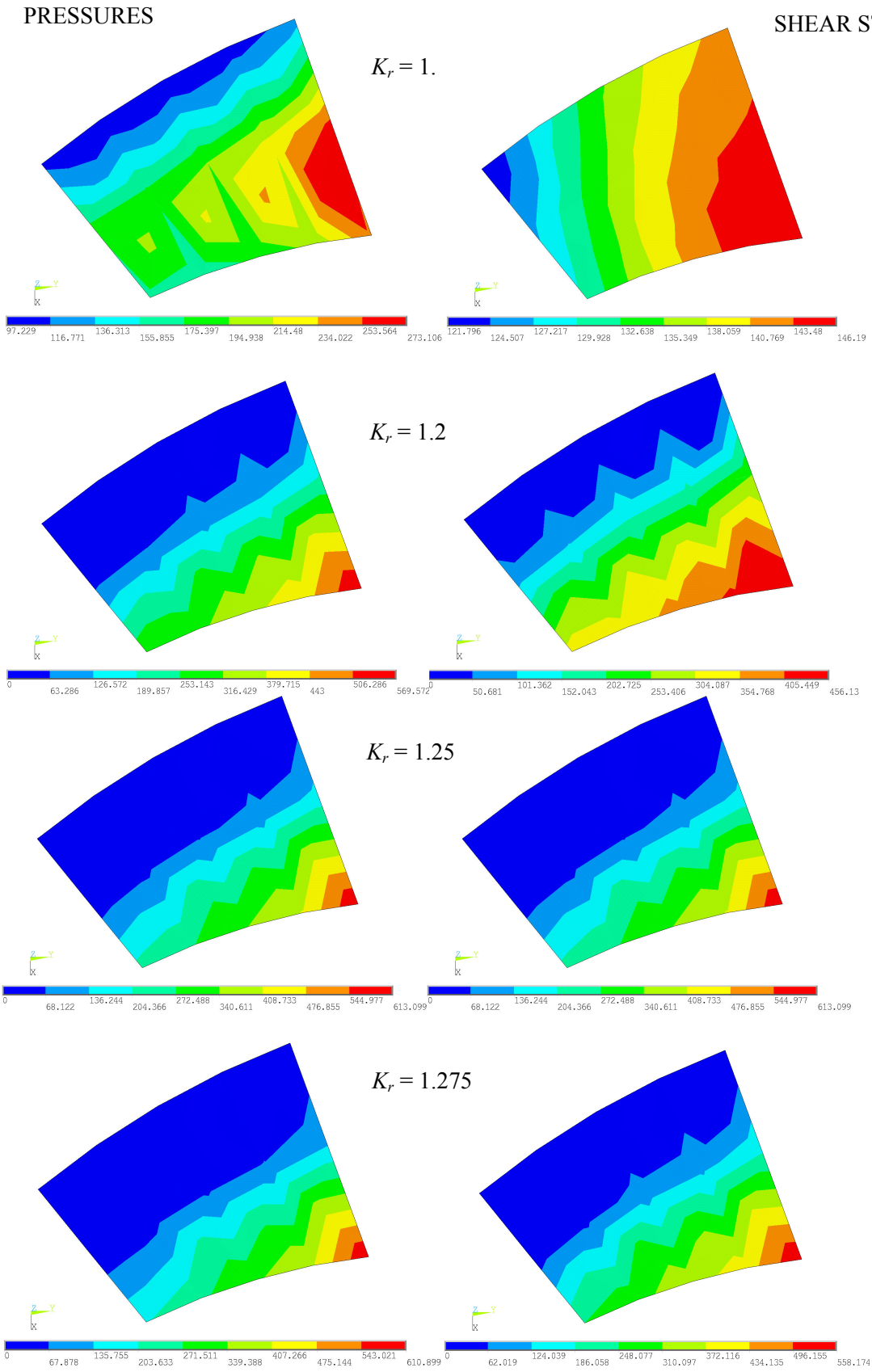

Fig. 10. Scalere dam-foundation contact in the sliding zone: Contours of pressures and shear stresses on contact elements for different fictitious reservoir levels (in KPa)

The maximum displacements on dam-foundation contact as were illustrated in the Figure 6, are on the dam zone situated on the right bank near central section. If for functional reason the maximum displacement allowed on contact was limited to 10 mm, then the reservoir water critical relative depth (K_r) results 1.258.

The contours of the vertical stresses versus K_r in the dam central section and cross section in the most exposed zone to sliding (see Figure 6) are presented in the Figures 8 and 9. The vertical stresses are compression in all the analysed cases except a local zone at the dam crest. The values of the compressive stresses reaches 0.97 MPa at the downstream toe of the central section. The stresses have evident tendency to increase versus dam downstream toe when $K_r > 1$. However, the stresses remain permanently smaller than compressive strength of rock foundation provided by formulator (10...15 MPa).

The low rate of increase of the vertical stresses with K_r, suggests the more important transfer of the hydrostatic loads on dam plunging arches. This conclusion resulted also by TLM analysis, presented at the previous paragraph.

The failure mechanism may be initiated by excessive ratio between global shear stresses (shear force) and global normal pressures (normal force) on the dam-foundation contact in the critical zones. With a view to analysing this aspect in the Figure 10 are illustrated the contours of the pressures and of the stresses versus K_r on contact elements for a cut out dam foundation zone, corresponding to the most exposed to sliding (see Figure 6).

The ratio between shear force ($\sum T$) and normal force ($\sum N$) on the cut out foundation zone is used to check up the sliding stability of this zone considered as independent one. The sliding stability coefficient (K) is calculated from limit equilibrium equation, as follows:

$$K\sum T = f\sum N + c\Omega \qquad (3)$$

where f, c were already defined at the paragraph 3 and Ω is the area of the cut out foundation in which doesn't exist gap in the contact elements.

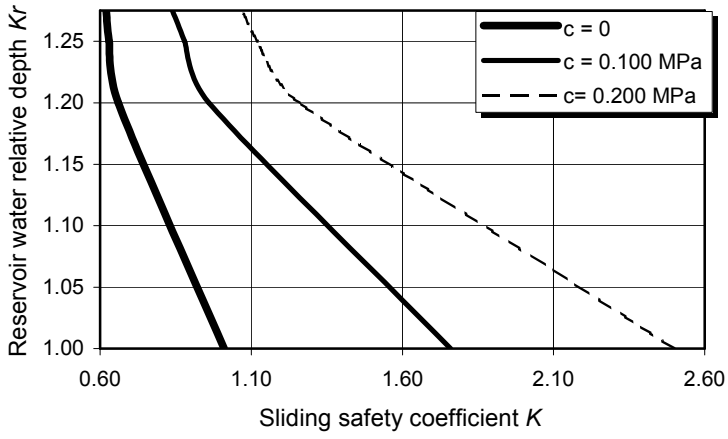

Fig. 11. Scalere dam – Sliding safety coefficient (K) for different reservoir levels according to nonlinear finite element analysis (friction angle tanφ = 37°, cohesion c = 0.0 … 0.2 MPa)

The results of the analysis performed with relation (3) are presented in the Figure 11. If the cohesion on the dam-foundation contact is neglected, the considered block would slide if the reservoir level increase over reference level (dam crest

elevation). However this block is connected with the rest of the dam body and shear stresses against sliding developed on the lateral face of the block will probably stop its sliding. Again, it is emphasized the significant contribution of the cohesion on dam-foundation interface. The sliding safety coefficient (K) of the block is bigger than one ($K > 1$) for all the fictitious reservoir levels taken into account (K_r = 1.00 … 1.275) if c = 0.200 MPa.

Finally, based on the results provided by nonlinear finite element analysis, K_r = 1.258 can be considered as critical value for ultimate strength against sliding of Scalere dam. In this case, the displacements on the dam-foundation interface reach unacceptable values (≥10 mm), generating interface cracks with important increase of the seepage and of the uplift pressure and successively initiating sliding mechanism.

5. CONCLUDING REMARKS

The failure mechanisms to sliding of the Scalere dam were analysed by three different procedures, as follows:

- dividing the hydrostatic pressure on the dam independent arches and cantilevers and further, evaluating the sliding stability of the central cantilever by standard relations;
- interpreting the evolution of displacements rate and value on the dam-rock interface in correlation with reservoir water level;
- interpreting the effective global stresses (normal forces, shear forces) versus corresponding maximum potential forces mobilised on the dam-rock interface.

The analyses were performed with ANSYS computer code. A three dimensional surface to surface contact element was used to model gap/sliding on the dam-rock interface.

The ultimate strength against sliding is expressed in terms of relative reservoir depth versus reference depth (K_r, where reference depth is H= 36.50 m with reservoir surface at the crest level 830.50 maSL).

The following remarks may be pointed out based on the results of the analyses:

To indicate a value for K_r is a very difficult task. Different model analyses conducted to different values for K_r.

Generally, it seems that for $K_r \leq 1.20 \ldots 1.25$ the dam withstands to corresponding loads.

The most exposed zone of the dam to sliding resulted to be the portion on the right bank situated close to central section of maximum height.

For $K_r \geq 1.25 \ldots 1.30$ it is difficult to appreciate if the dam has additional capacity to withstand or inevitably local damage which appeared (cracks, big leakage, increased uplift pressure) will initiate the dam sliding.

REFERENCES

[1] Giuseppetti, G., Mazzà, G., Meghella, M., Fanelli, M., Evaluation of ultimate strength of gravity dams with curved shape against sliding, 7th ICOLD Benchmark Workshop on Numerical Analysis of Dams, Bucharest, 2003.

[2] Popovici, A., Popescu, C. Dams for Water Storage (in Romanian) Editura Tehnica, Bucharest, 1992

[3] Design of gravity dams – Bureau of Reclamation, A Water Resources Technical Publications, Denver-Colorado, 1976

[4] ANSYS Element Reference. Tenth Edition, SAS IP, Inc ®, 1998

FULL NON LINEAR ANALYSIS OF AN ARCH GRAVITY DAM USING MERLIN*

Takashi Shimpo, Yoshihisa Uchita, Victor Saouma
Tokyo Electric Power Service Company; Tokyo Electric Power Company; University of Colorado/Politecnico di Milano

SUMMARY: An extensive nonlinear parametric study of an arch-gravity (Scalere) dam using Merlin is reported. Effects of vertical (between monoliths) and horizontal (between rock and concrete) joint opening/sliding, modeled by a specially formulated interface element, are examined. In the context of the required non-linear incremental analysis, uplift is automatically adjusted to reflect crack openings, and the imminent failure flood (IFF) is determined when lack of numerical convergence occurs.

RÉSUMÉ: Une série d'analyses non linéaire d'un barrage voûte-poid (Scalere) avec le logiciel Merlin est reportée. Les effets des joints verticaux (entre les monolithes), et ceux horizontaux (entre la roche et le béton), modélisés a travers une formulation d'un élément d'interface, sont examinés. Dans le contexte de l'analyse non linéaire incrémentale, les sous pressions sont automatiquement ajustées afin de refléter la variation temporaire et spatiale de l'ouverture des fissures, et enfin la charge maximale est déterminée quand il y'a un manque de convergence numérique.

1. INTRODUCTION

Whereas the linear elastic design of an arch-gravity dam can be deceptively simple, its non linear analysis to determine the imminent failure flood (IFF) can be particularly tricky if one does not recognize all the modeling subtleties. These include first and foremost the treatment of joints and discontinuities, but also handling of the uplift pressures. Joints, discontinuities or cracks must be modeled in such a way to account for both mode I and (mostly) mode II displacements and induced failure through the tensile strength, cohesion, angle of friction, dilatancy, and fracture energy. The uplift which is initially linear along the uncracked ligament must gradually revert to a trapezoidal one as the crack propagates due to the incremental increase in pool elevation. As a vehicle for the IFF determination, we examine closely Scalere dam which has been assigned by the organizers of the 7th Benchmark Workshop on Numerical Analysis of Dams.

* Analyse non linéaire d'un barrage voûte-poid avec le logiciel MERLIN.

2. PROGRAM DESCRIPTION

The analysis reported has been conducted using a specialized set of software specially developed for the three dimensional non linear seismic analysis of concrete dams. At the core of this computational environment is the MERLIN [1] finite element code which was originally developed for the Electric Power Research Institute (EPRI, Palo-Alto) [2], and more recently we have extended its capabilities to include dynamic analysis, development of the mesh generator, and much improvements to the graphical postprocessor.

Some of the major features of the code include: seismic analysis (Alpha method; explicit version under development); Non-Linear fracture (both discrete and smeared crack models); Automatic adjustments of (Static and dynamic) uplift; Extensive library of elements and constitutive models; numerous nonlinear algorithms (including indirect control and Arc-length methods). To accompany MERLIN, we have developed a model generator (mesh, loads, material properties, boundary conditions) KUMONOSU, and a graphical postprocessor, SPIDER. Finally, an external driver, CRACKER enables MERLIN to perform crack propagation with automatic remeshing for 2D problems. All three codes operate in a Window environment.

An essential component of Merlin is its interface crack model (ICM) which is used to model both joints (between monoliths, and between the rock and concrete), and cracks. Hence, in our approach we clearly adopt the so-called discrete crack model to represent cracks/joints by inserting interface elements along the mesh discontinuities. If needs be, non-linear continuum elements, with Drucker-Prager type model for compression, and Rankine (thus smeared cracks) in tension can also be adopted; these are very seldom needed for dam analysis, where the major source of nonlinearity is the presence of joints/cracks whose behavior is governed by the constitutive model for the ICM.

The major premises upon which the model is developed are:

1. Shear strength depends on the normal stress.
2. Softening is present both in shear and tension.
3. There is a residual shear strength due to the friction along the interface, which depends on the compressive normal stress.
4. Reduction in strength, i.e. softening, is caused by crack formation.
5. There is a zero normal and shear stiffness when the interface is totally destroyed.
6. Under compressive normal stresses neither the shear and nor the normal stiffnesses decrease to zero. In addition, should a compressive stress be introduced in the normal direction following a full crack opening, two faces of the interface come to contact, and both tangential and normal stiffnesses become nonzero.

7. Irreversible relative displacements are caused by broken segments of the interface material and by friction between the two crack surfaces.
8. Roughness of the interface causes opening displacements (i.e. dilatancy) when subjected to sliding displacements.

9. The dilatancy vanishes with increasing sliding or opening displacements.

Hence, the following hyperbolic law is proposed for the strength of the interface

$$F = \left(\tau_1^2 + \tau_2^2\right) - 2c\tan(\phi_f)(\sigma_t - \sigma) - \tan(\phi_f)^2(\sigma^2 - \sigma_t^2) = 0$$

Where σ and τ_i are the normal and shear stresses (in 3D), c and ϕ_f are the cohesion, angle of friction respectively and σ_t is tensile strength. In this formulation, both the cohesion and the tensile strength are a function of the effective inelastic displacements.

The shape of the failure function in two-dimensional case is shown in Fig. 1. The general three-dimensional failure function is obtained by mere rotation around the σ -axis.

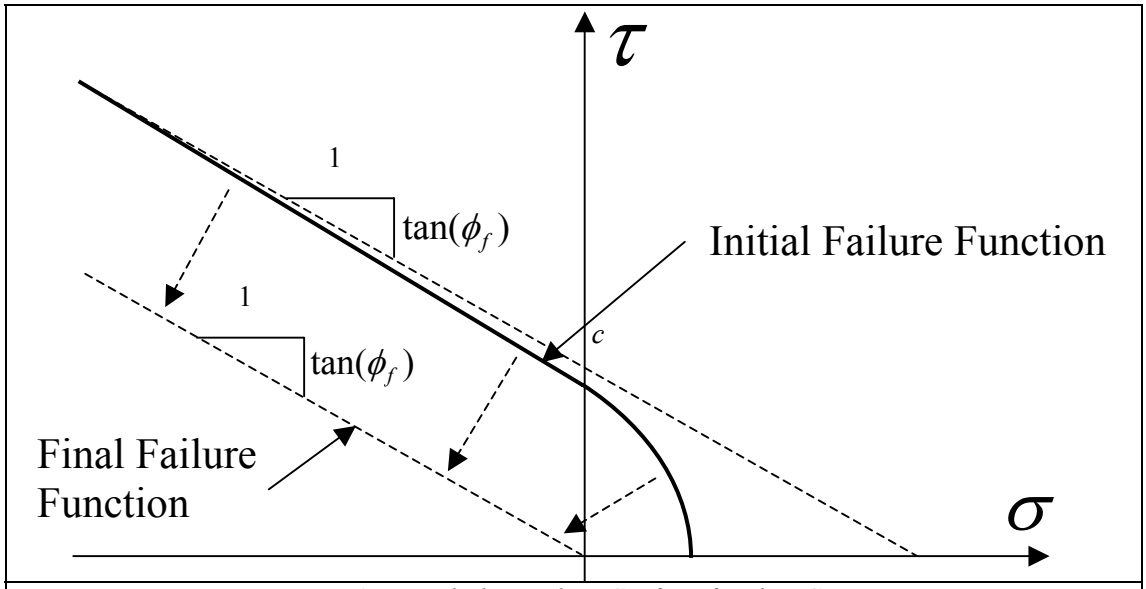

Fig. 1 Hyperbolic Failure Surface for the ICM.

The evolution of the failure function is based on a softening parameter u^{ieff} which is the norm of the inelastic displacement vector $\boldsymbol{u}^i$. The inelastic displacement vector is obtained by decomposition of the displacement vector $\mathbf{u}$ into an elastic part $\mathbf{u}^e$ and an inelastic part $\mathbf{u}^i$ .The inelastic part can subsequently be decomposed into plastic (i.e. irreversible) displacements $\boldsymbol{u}^p$ and fracturing $\boldsymbol{u}^f$ displacements. The plastic displacements are assumed to be caused by friction between crack surfaces and the fracturing displacements by the formation of microcracks.

$$F = F(c, \sigma_t, \phi_f), \quad c = c(u^{ieff}), \quad \sigma_t = \sigma_t(u^{ieff})$$

$$\boldsymbol{u} = \boldsymbol{u}^e + \boldsymbol{u}^i; \quad \boldsymbol{u}^i = \underbrace{\boldsymbol{u}^p}_{Irreversible} + \underbrace{\boldsymbol{u}^f}_{Fracturing}$$

$$u^{ieff} = \left\| \boldsymbol{u}^i \right\| = \left(u_x^{i^2} + u_y^{i^2} + u_z^{i^2} \right)^{1/2}$$

In this work both linear and bilinear relationship are used for c^{ieff} and σ_t^{ieff}

$$
\left.
\begin{aligned}
c(u^{ieff}) &= c_0 + u^{ieff}\,\frac{s_{1c} - c_0}{w_{1c}} \quad \forall\ u^{ieff} < w_c \\
c(u^{ieff}) &= s_c\left(1 - \frac{u^{ieff} - w_{1c}}{w_c - w_{1c}}\right) \quad \forall\ u^{ieff} \in \langle w_{1c}, w_c \rangle \\
w_c &= \frac{2G_F^{IIa} - (s_{1c} - c_0)\,w_{1c}}{s_{1c}}
\end{aligned}
\right\} \text{Bi-Linear for cohesion}
$$

$$
\left.
\begin{aligned}
\sigma_t(u^{ieff}) &= \sigma_{t0} + u^{ieff}\,\frac{s_{1\sigma} - \sigma_{t0}}{w_{1\sigma}} \quad \forall\ u^{ieff} < w_{1\sigma} \\
\sigma_t(u^{ieff}) &= s_{1\sigma}\left(1 - \frac{u^{ieff} - w_{1\sigma}}{w_{\sigma t} - w_{1\sigma}}\right) \quad \forall\ u^{ieff} \in \langle w_{1\sigma}, w_\sigma \rangle \\
w_\sigma &= \frac{2G_F^{I} - (s_{1\sigma} - \sigma_{t0})\,w_{1\sigma}}{s_{1\sigma}}
\end{aligned}
\right\} \text{Bi-Linear for tensile strength}
$$

where G_F^I and G_F^{IIa} are mode I and II fracture energies. s_{1c}, w_{1c} and $s_{1\sigma}$, $w_{1\sigma}$ are the coordinates of the breakpoint in the bi-linear softening laws for cohesion and tensile strength respectively. The critical opening and sliding corresponding to zero cohesion and tensile strength are denoted by w_σ and w_c respectively, and they are determined from the condition that the area under the linear or bilinear softening law must be equal to G_F^I and G_F^{IIa} respectively. The significance of these symbols can be best explained through Fig. 2

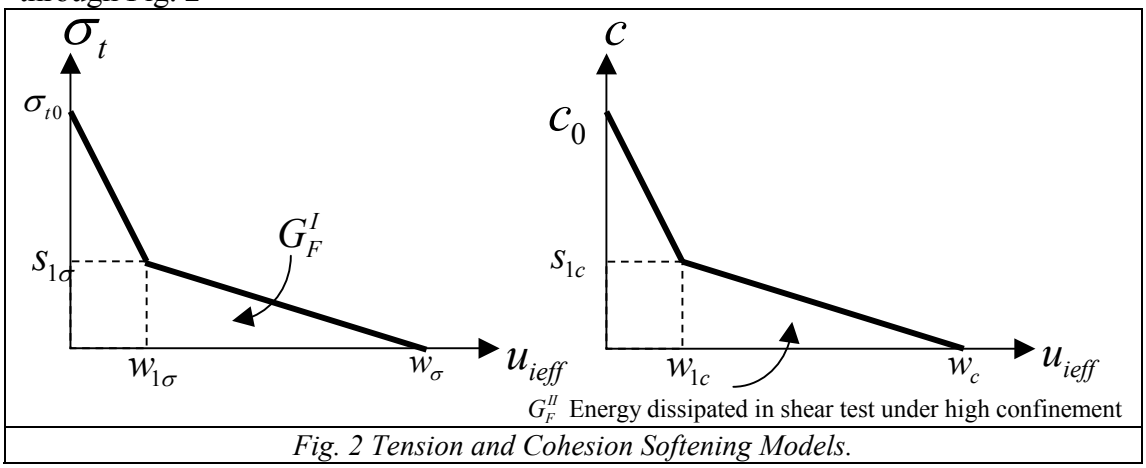

Fig. 2 Tension and Cohesion Softening Models.

It should be noted that G_F^{IIa} is not the pure mode II fracture energy (i.e. the area under a $\tau - u_x$), but rather is the energy dissipated during a shear test with high confining normal stress. This representation seems to be more favorable to the pure mode II fracture energy G_F^{II}. The determination of G_F^{II} would require a pure shear test without confinement, which is extremely difficult to perform. Alternatively, a G_F^{IIa} test requires a large normal confinement, and is therefore easier to accomplish. Furthermore, if G_F^{II} is used, the whole shear-compression region of the interface model would be an extrapolation from the observed behavior, whereas the second approach represents an interpolation between the upper bound G_F^{IIa} and the lower bound G_F^I. The residual shear strength is obtained from the failure function by setting both c and σ_t equal to 0, which corresponds to the final shape of the failure function in Fig. 1 and is given by:

$\tau_1^2 + \tau_2^2 = \tan^2(\phi_f)\sigma^2$

Stiffness degradation is modeled through a damage parameter, $D \in \langle 0,1 \rangle$ which is a relative measure of the fractured surface. Thus, D is related to the secant of the normal stiffness K_{ns} in the uniaxial case: $D = \frac{A_f}{A_0} = 1 - \frac{\mathbf{K}_{ns}}{\mathbf{K}_{n0}}$ where $\mathbf{K}_{n0}$ is the initial normal stiffness of the interface; A_0 and A_f are the total interface area and the fractured area respectively. It is assumed, that the damage parameter D can be determined by converting the mixed mode problem into an equivalent uniaxial one (Fig. 3).

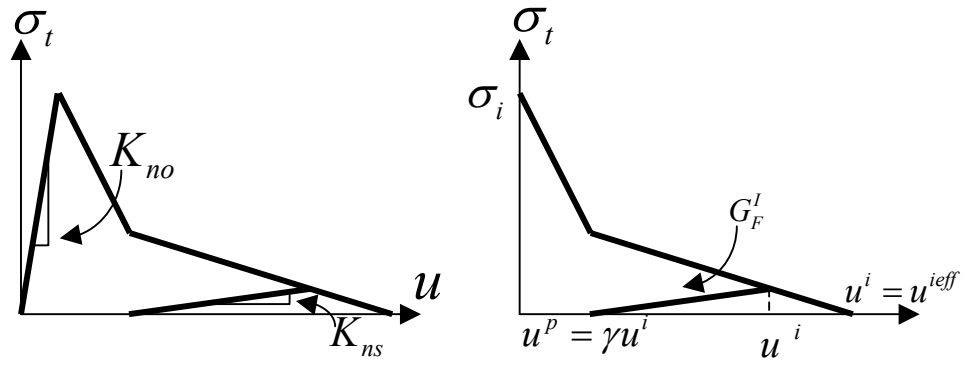

Fig. 3 Stiffness Degradation in the Uniaxial Case.

In the equivalent uniaxial problem the normal inelastic displacement is set equal to u^{ieff} . Then, the secant normal stiffness can be determined from:

$$\mathrm{K}_{ns} = \frac{\sigma}{u - u^p} = \frac{\sigma_t(u^{ieff})}{u^e + u^p + u^f - u^p} = \frac{\sigma_t(u^{ieff})}{\frac{\sigma_t(u^{ieff})}{\mathrm{K}_{no}} + (1-\gamma)u^{ieff}}$$

where γ is the ratio of irreversible inelastic normal displacement to the total value of inelastic displacement. Experimentally, γ can be determined from a pure mode I test through: $\gamma = \frac{u_p}{u_i}$ where u_i is the residual displacement after unloading and u_i is the inelastic displacement before unloading. For concrete, γ is usually assumed equal to 0.2-0.3. Then, the evolution of the damage parameter D is defined by formula:

$$D = 1 - \frac{\sigma_t(u^{ieff})}{\sigma_t(u^{ieff}) + (1-\gamma)u^{ieff} K_{n0}}$$

The stress-displacement relationship of the interface is expressed as:

$\boldsymbol{\sigma} = \alpha \mathbf{E}(\mathbf{u} - \mathbf{u}^p)$ where $\sigma = \{\tau_1, \tau_2, \sigma\}^T$ is the vector of tangential and normal stress at the interface. α is the integrity parameter defining the relative active area of the interface, and it is related to the damage parameter D, and $\alpha = 1 - \frac{|\sigma| + \sigma}{2|\sigma|} D$ It should be noted that α can be different from 1 only if the normal stress σ is positive (i.e. the interface is in tension). In other words, the damage parameter D is activated only if the interface is in tension. In compression, the crack is assumed to be closed, and there is full contact between the two crack surfaces. The activation of D is controlled through the fraction

$\frac{|\sigma|+\sigma}{2|\sigma|}$ which is equal to one if σ is positive, and is zero otherwise. $\mathbf{E}$ is the elastic stiffness matrix of the interface.

$$\mathbf{E} = \begin{bmatrix} K_{t0} & 0 & 0 \\ 0 & K_{t0} & 0 \\ 0 & 0 & K_{n0} \end{bmatrix}$$

It should be noted, that the off-diagonal terms in the elastic stiffness matrix $\mathbf{E}$ of the interface are all equal to zero, which implies that no dilatancy is considered in the elastic range. The dilatancy is introduced later after the failure limit has been reached through the iterative solution process. The dilatancy of the interface is given by dilatancy angle ϕ_D, which is again assumed to be a function of u^{ieff} .In the proposed model, a linear relationship is assumed:

$$\phi_d(u^{ieff}) = \phi_{d0}\left(1 - \frac{u^{ieff}}{u_{dil}}\right) \forall u^{ieff} \le u_{dil}$$

$$\phi_d(u^{ieff}) = 0 \qquad \forall u^{ieff} > u_{dil}$$

where u_{dil} is the critical relative displacement after which, the interface does not exhibit the dilatancy effect any more, and ϕ_{D0} is the initial value of the dilatancy angle.

2. MODEL DESCRIPTION

Scalere dam is a large solid gravity structure in concrete located in the centre-north of Italy. The construction works took place in the period 1910-1911. The foundation rock, excellent in every respect, consists of stratified Eocene sandstones dipping upstream. The faces of the dam, unlined owing to the great impermeability of the structure, are in blocks laid in regular courses. The dam has not been provided with contraction joints. The drainage system does not comply with the requirements of the current Italian Standards, so no reduction of the uplift pressures is allowed. The trend of the measurements carried out by the monitoring system installed on the dam has always been normal, showing displacements well correlated to the seasonal thermal variations with a small hydrostatic component. The crest elevation is at 830.5 m, maximum height 34.0 m, and crest length 158.0 m [3], Fig. 4.

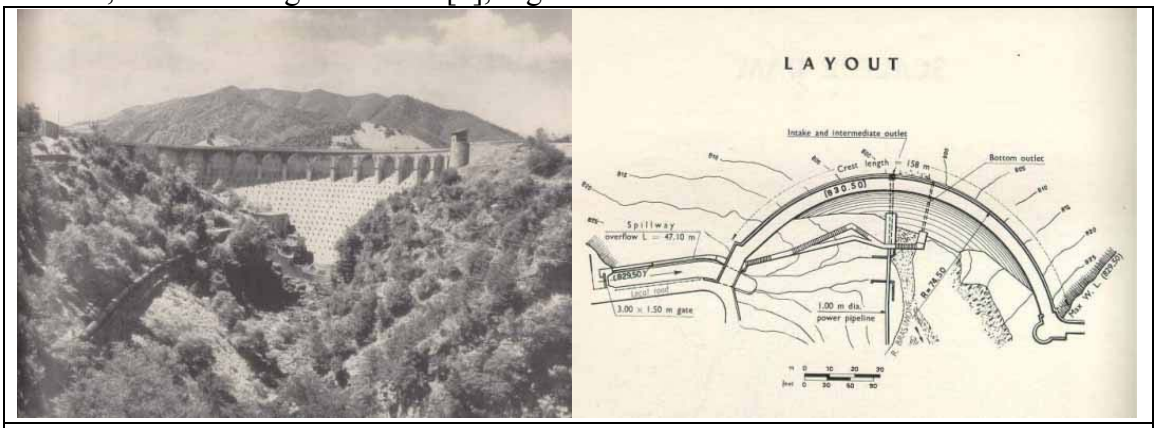

Fig. 4: Scalere Dam [4]

Whereas the organizers have provided us with data files for the 3D mesh (without interface elements), we decided to regenerate the mesh with Kumo as this would have greatly facilitated the parametric investigation which included the effects of joints.

The Boundary description of Scalere dam is shown in Fig. 5.

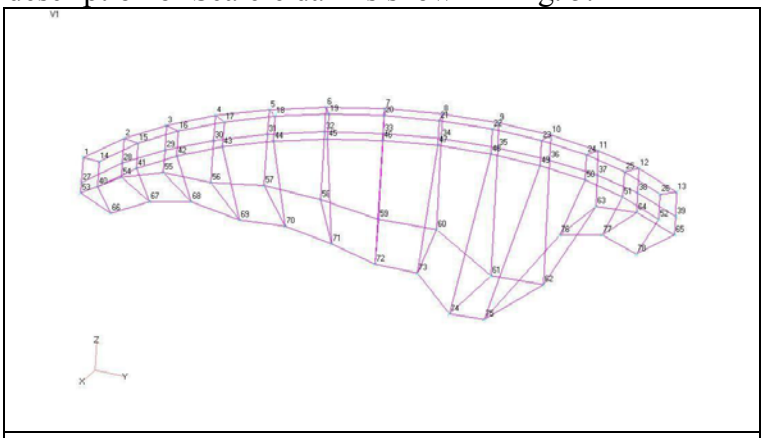

Fig.5 Boundary definition of Scalere Dam.

For the dam body, Elastic modulus was set to 20,000 MPa, mass density to 2,300 kg/cm^3, Poisson coefficient: 0.2, Compressive strength: 11.6 MPa, Tensile strength: 1.0MPa; The rock foundation had an elastic modulus: 10,000 – 20,000 MPa, and a compressive strength: 10–15 MPa, and a zero mass density and Poisson's coefficient. The dam foundation interface had a friction angle of 37 degrees and a cohesion ranging from 0 to 0.2 MPa. Finally, the loading consisted of the dead weight (applied in one increment), hydrostatic pressures induced by a pool elevation of up to 830.5 m, and the corresponding uplift pressures. In all 2D and single block 3D analyses, pool elevation was raised by increments of 5 m. for the first 30 m., and then by one meter at a time. For the full 3D analysis, pool was raised by 5 m for the first 25 m, and then by 2 m.

The interface elements (rock-concrete, and joint-joint), the following reference characteristics were assigned: G_F^I ranging from 25 to 200 J/m^2, and $G_F^{II} = 10G_F^I$. In all cases we first identify the pool elevation at which a crack opens at the heel, and the one for which dam failure (IFF) occurs.

3. ANALYSIS RESULTS

Early on, it was decided to use this dam as a model for a detailed, and extensive parametric study using Merlin. The objective was to assess the importance and overall importance of each input parameter on the overall results. Hence, we will first report detailed results of some of those parametric studies, and will conclude with what we consider our Engineering assessment of the failure load of the dam.

3.1 2D INVESTIGATION

The insertion of an interface element to properly model the rock/concrete joint being necessary, the interface element as formulated (see above) being quite general, it was first necessary to assess the relative importance of some of the key parameters

which can not be easily determined from tests. Those include: cohesion and tensile strength, and mode I and II fracture energies, Table 1 and 2.

t	0.1	m	Interface thickness	Assumed
Gmax	100	mm	Maximum aggregate size	Assumed
f_c	1.16E+07	MPa	Compressive Strength of Concrete	Assumed
E	2.00E+10	MPa	Young's modulus	Assumed
C	2.00E+05	Pa	Cohesion	Provided
Φ_f	37	degree	Friction angle	Provided
f_t	1.00E+05	Pa	Tensile strength	Assumed
K_t	2.00E+11	Pa	Tangential stiffness	Assumed : E/t
K_n	2.00E+11	Pa	Normal stiffness	Assumed : E/t
Φ_D	0	degree	Dilatancy angle	Assumed
G_F^I	100	N/m	Fracture energy Mode I	Assumed
G_F^{II}	1000	N/m	Fracture energy Mode II	Assumed : $10*G_F^I$
γ	0		Relative value of irreversible deformation	Assumed
u_{Dmax}	0	m	Maximal displacement for dilatancy	Assumed
s_1	0.00E+00	Pa	Tensile stress at the break-point	Assumed
sw_1	0.00E+00	m	Crack opening displacement at the break- point	Assumed
c_1	0.00E+00	Pa	Cohesion at the break-point	Assumed
cw_1	0.00E+00	m	Crack sliding displacement at the break-point	Assumed

Table 1:Material Properties of Interface crack model (Case 8)

Case	Analysis Conditions (Parametric stadies of interface material Properties)					Pool elevation at crack initiation and dam sliding			
						Absolute (EL. m)		Multiplier coefficient to dam height (36.55m)	
	Cohesion	Friction Angle	Tensile Strength	Fracture Energy Mode I	Fracture Energy Mode II	Crack Initiation	Failure (Sliding)	Crack Initiation	Failure (Sliding)
Effect of Cohesion and Tensile Strength									
1	1.7 MPa	37	1.0 MPa	159 N/m	G_F^I*10	828.5	834.5	0.95	1.11
2	0.2 MPa	37	0.1 MPa	159 N/m	G_F^I*10	826.5	830.5	0.89	1.00
3	0.1 MPa	37	0.05MPa	159 N/m	G_F^I*10	826.5	830.5	0.89	1.00
4	0.05MPa	37	0.025 MPa	159 N/m	G_F^I*10	826.5	827.5	0.89	0.92
Effect of Fracture Energy I									
5	1.7 MPa	37	1.0 MPa	200 N/m	G_F^I*10	828.5	834.5	0.95	1.11
6	1.7 MPa	37	1.0 MPa	100 N/m	G_F^I*10	828.5	834.5	0.95	1.11
7	0.2 MPa	37	0.1 MPa	200 N/m	G_F^I*10	826.5	832.5	0.89	1.05
8	0.2 MPa	37	0.1 MPa	100 N/m	G_F^I*10	826.5	830.5	0.89	1.00
9	0.2 MPa	37	0.1 MPa	50 N/m	G_F^I*10	826.5	829.5	0.89	0.97
10	0.2 MPa	37	0.1 MPa	25 N/m	G_F^I*10	826.5	830.5	0.89	1.00
Effect of Fracture Energy II									
11	0.2 MPa	37	0.1 MPa	100 N/m	G_F^I*20	826.5	830.5	0.89	1.00
12	0.2MPa	37	0.1 MPa	100 N/m	G_F^I*5	826.5	830.5	0.89	1.00
Effect of ratio of tensile strength to cohesion									
13	0.2 MPa	37	0.14MPa	100 N/m	G_F^I*10	826.5	831.5	0.89	1.03
14	0.2MPa	37	0.12MPa	100 N/m	G_F^I*10	826.5	831.5	0.89	1.03
15	0.2 MPa	37	0.08 MPa	100 N/m	G_F^I*10	826.5	830.5	0.89	1.00

Table 2: 2D Parametric Study

Fig. 6 illustrates the uplift pressure distribution for Case 1, and we observe that the crack forms at increment 7, E.L.826.5m and the dam fails soon after increment 11, E.L.830.5m. Crest displacements in terms of water elevation are shown in Fig. 7.

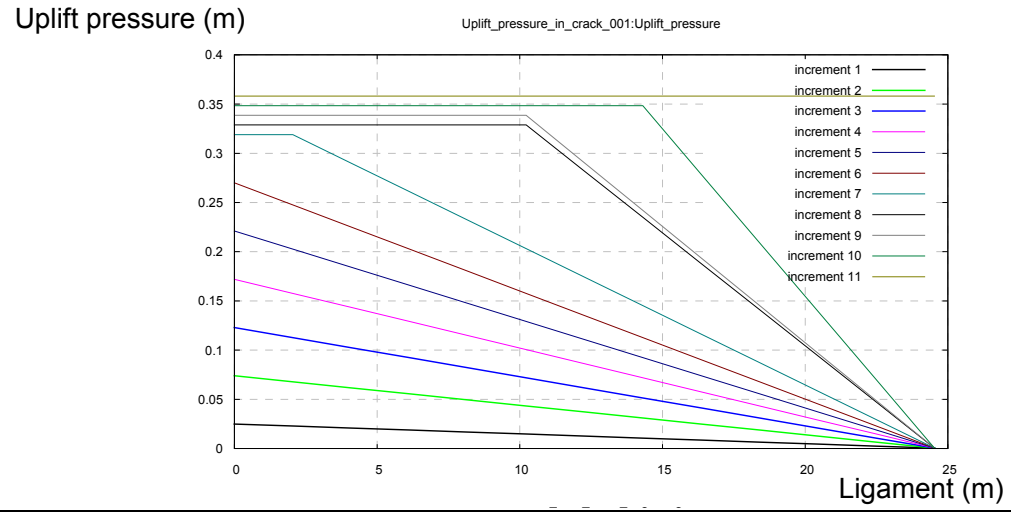

Fig. 6: Uplift Pressure Distribution.

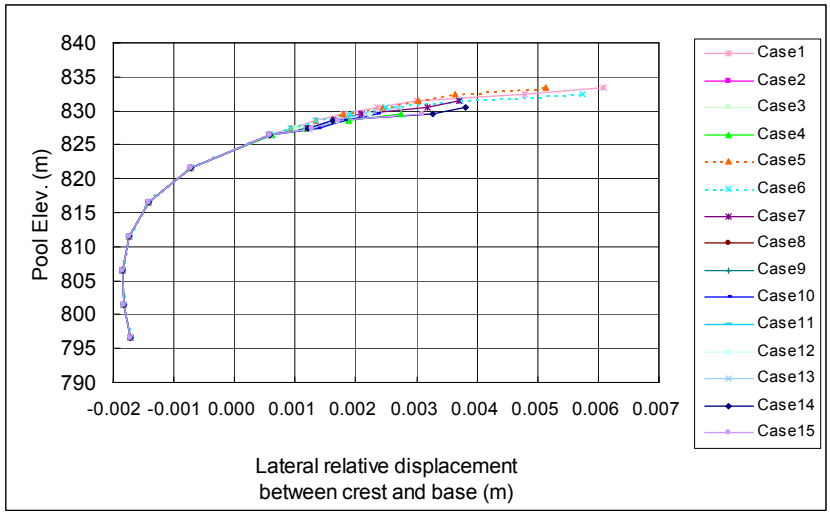

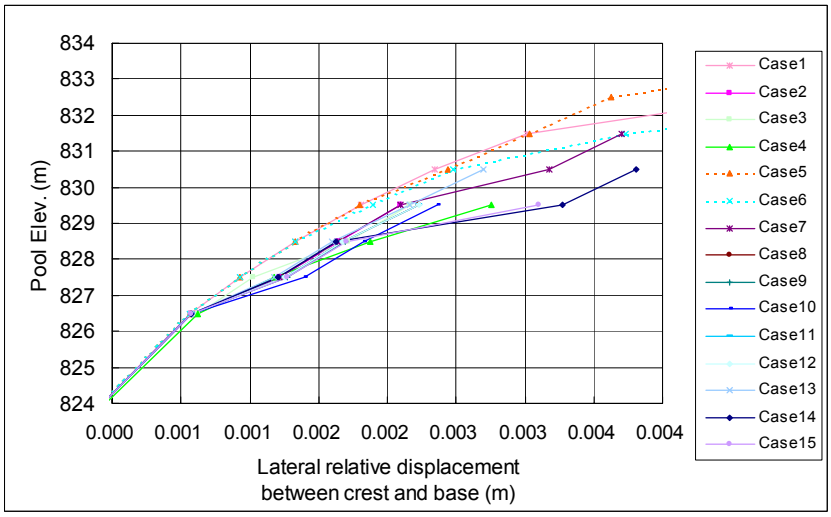

Fig. 7. Crest Displacements

3.2 3D SINGLE MONOLITH

Following the preliminary 2D investigation, we focused on the 3D analysis of a single 3D monolith for the maximum section, shown in Fig. 8, to further investigate the effect of uplift pressures. Results are shown in Fig. 9.

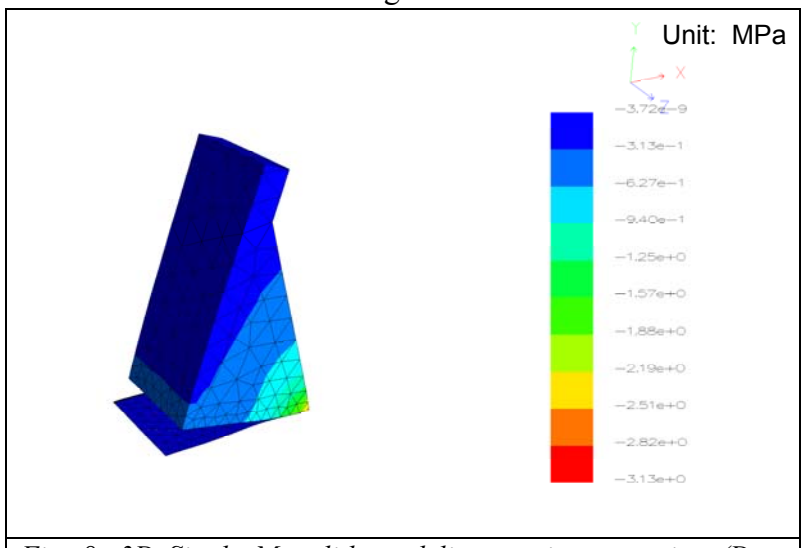

Fig. 8: 3D Single Monolith modeling maximum section (Dam and Interface elements only are shown)

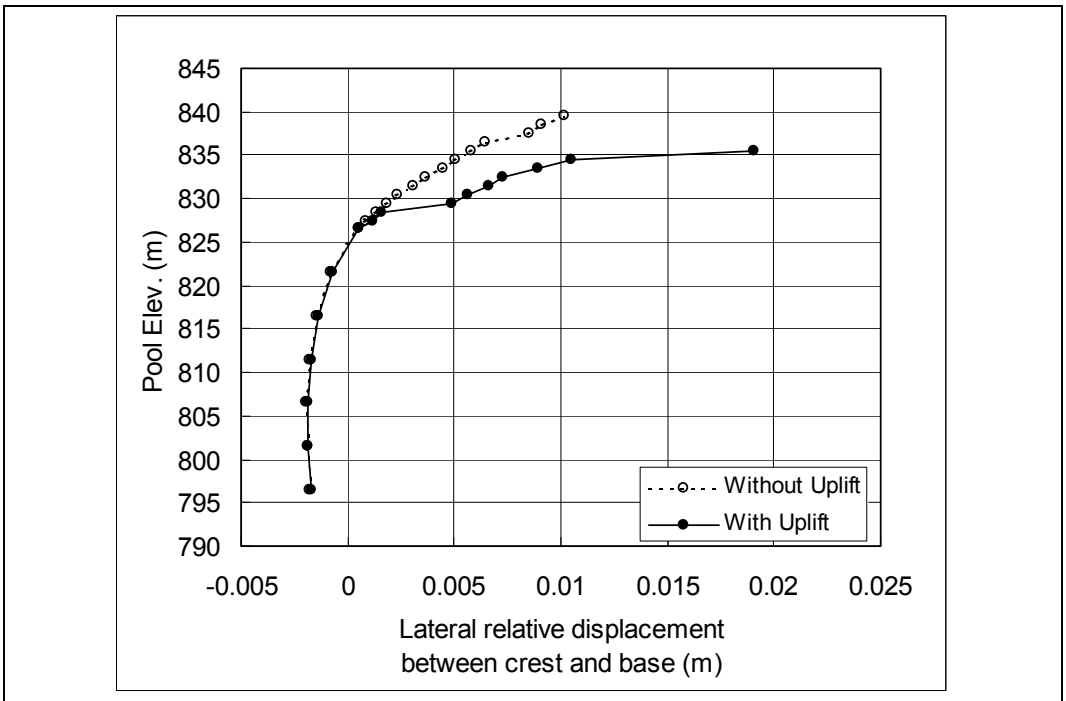

Fig.9: Effect of Uplift on the 3D Single Monolith

From Fig. 9, it is apparent that even in an arch-gravity dam uplift plays a non-negligible role. Finally, through the SPIDER post-processor we show in Fig. 10 various plots associated with the crack between the dam base and the foundation. A mere inspection of this figure can shed some light on the actual behavior of this jointed structure. In particular, we note the quasi-linear crack opening, and the full uplift

applied when the crack opens, and then the linear transition to the downstream hydrostatic pressure.

Distribution of Crack Opening Displacements	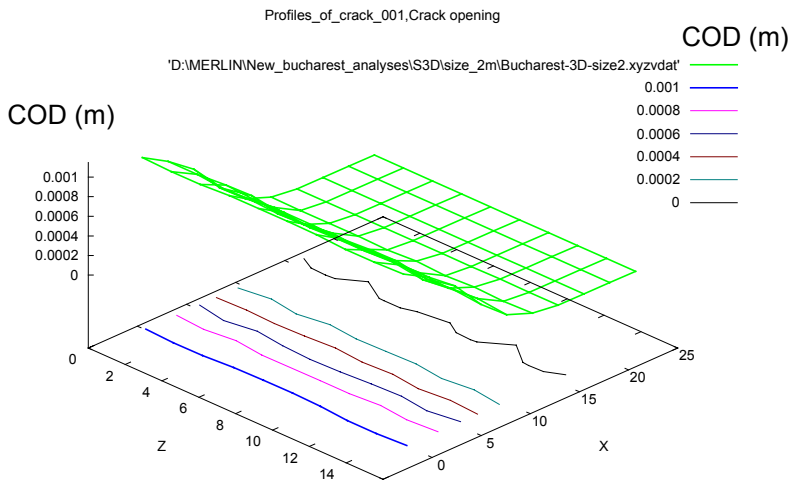
Distribution of Crack Sliding Displacements	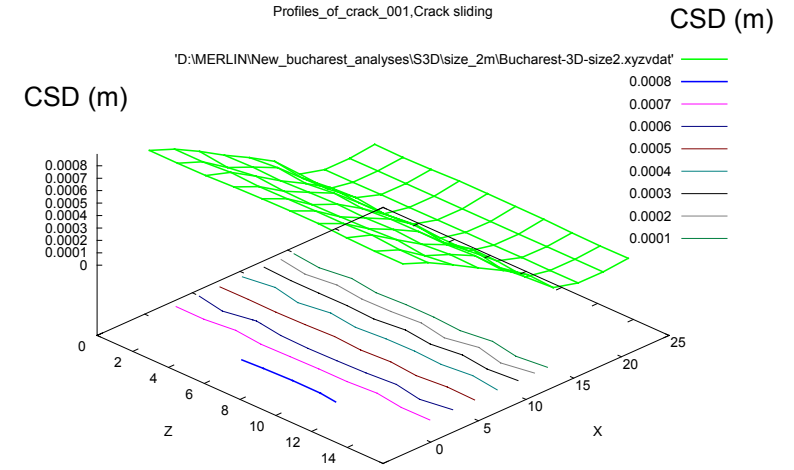
Distribution of Uplift Pressures	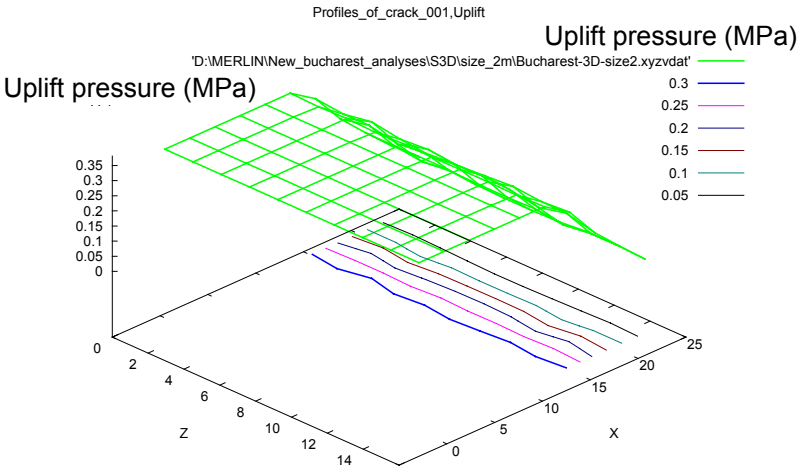

Fig. 10: Crack Data For Pool Elevation 829.5 m

3.3 3D FULL DAM MODEL

Finally, a full 3D analysis of the entire dam is conducted. The mesh boundary Description was provided by the organizers, this information was then used to generate the mesh with Kumo, Fig. 11. Two analyses were performed, one without vertical joints (albeit with horizontal ones between dam and rock), and another with vertical joints.

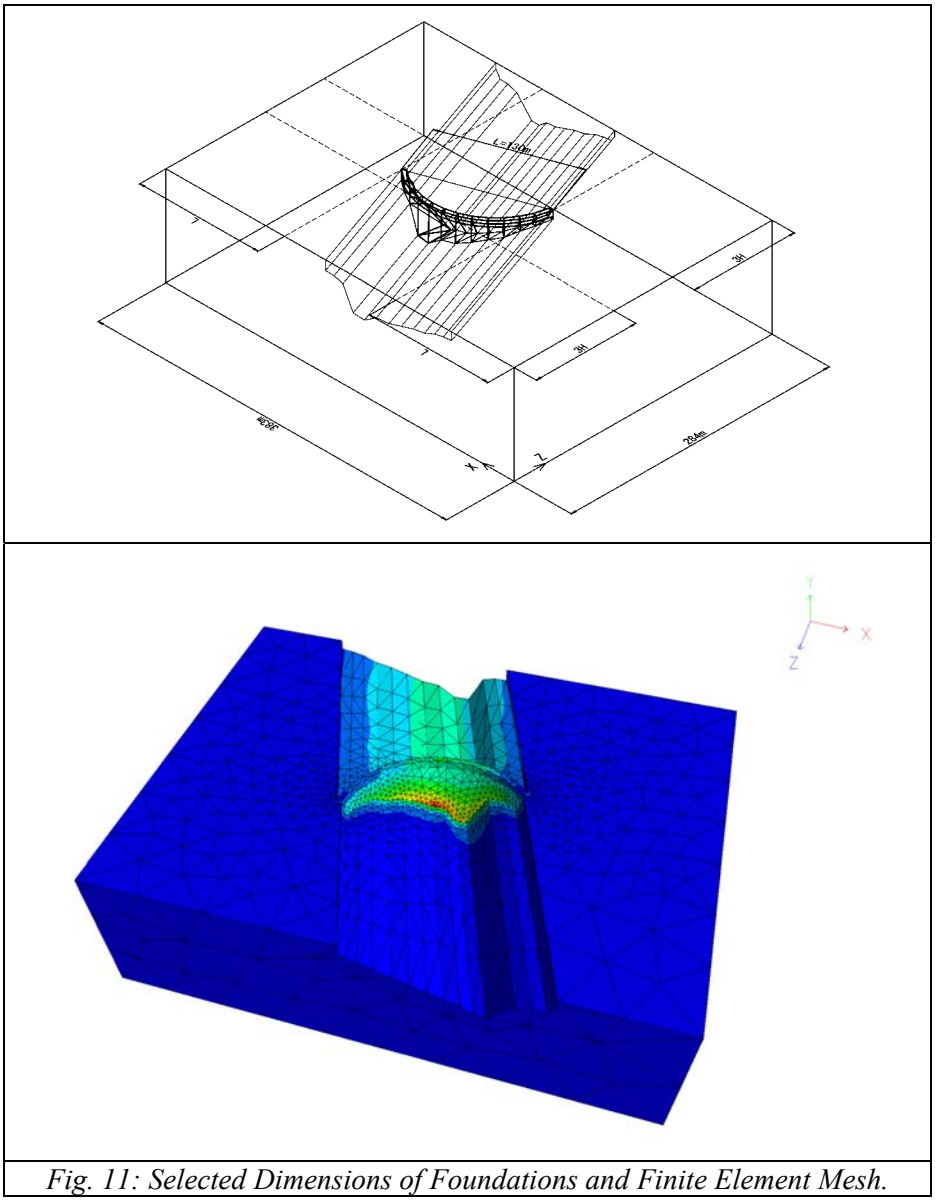

Fig. 11: Selected Dimensions of Foundations and Finite Element Mesh.

3.3.1 Full 3D No Joints

The full 3D analysis, without joints was performed next, and results are tabulated in Table 3 and shown in Fig. 12. Fig. 13 illustrates the crest displacements in terms of the pool elevations for the simple 3D block and the full 3D model with and without uplift. We note that for the case with uplift, the full 3D model has a lower maximum pool elevation than for the simple 3D monolith.

Case	Analysis Conditions (Parametric stadies of interface material Properties)					Pool elevation at crack initiation and dam sliding			
						Absolute (EL. m)		Multiplier coefficient to the dam height (36.55m)	
	Cohesion	Friction Angle	Tensile Strength	Fracture Energy Mode I	Fracture Energy Mode II	Crack Initiation	Failure (sliding)	Crack Initiation	Failure (sliding)
2D	0.2 MPa	37	0.1 MPa	100 N/m	G_F^I*10	826.5	830.5	0.89	1.00
3D Single	0.2 MPa	37	0.1 MPa	100 N/m	G_F^I*10	826.5	832.5	0.89	1.05
Full 3D	0.2 MPa	37	0.1 MPa	100 N/m	G_F^I*10	828.5	840.5	0.95	1.27

Table 3: Comparison Between 2D and 3D Analyses without Joints

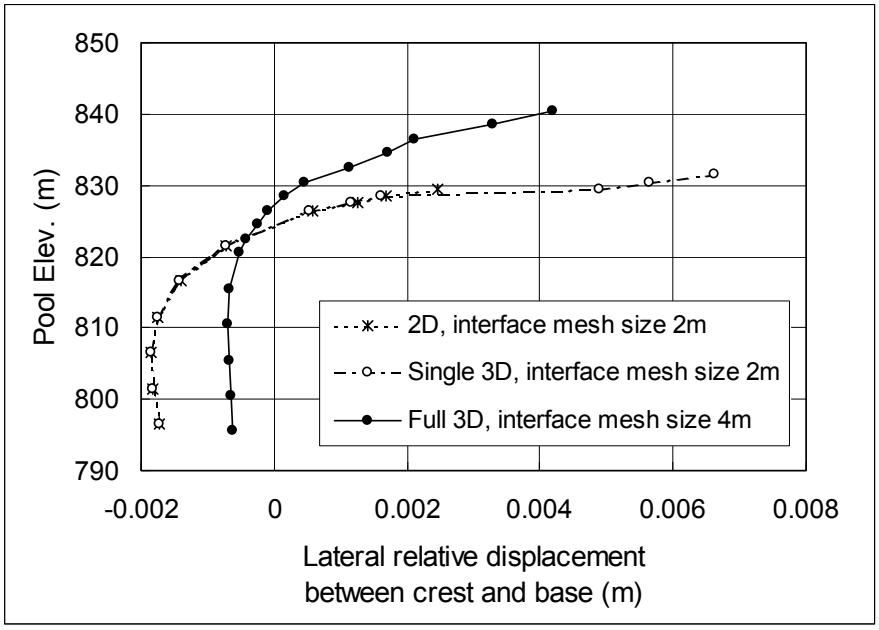

Fig. 12 Crest Displacement comparison among different analyses with different mesh sizes

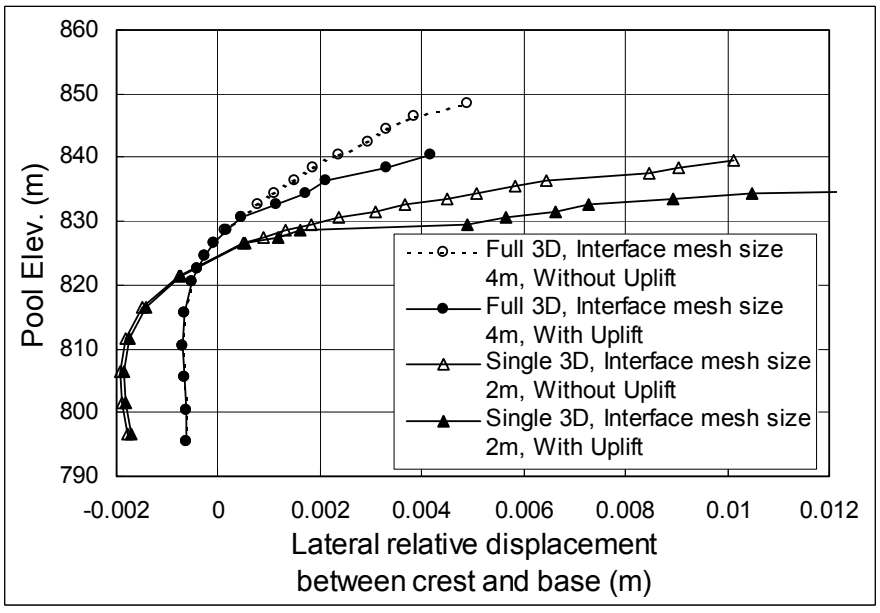

Fig. 13 Crest Displacements for Single and Full 3D Models With and Without Uplift

3.3.2 Full 3D with Joints

Finally, the last analysis consisted of the full 3D dam with vertical joints. Fig. 14 shows all the joint elements used in the model, the vertical ones between the monoliths, and the horizontal ones between the dam and the rock. The effects of the joints are shown in Fig. 15 and Table 4. We observe that depending on the joint properties, the dam response may be stronger or weaker than the case in which the joints are not modeled.

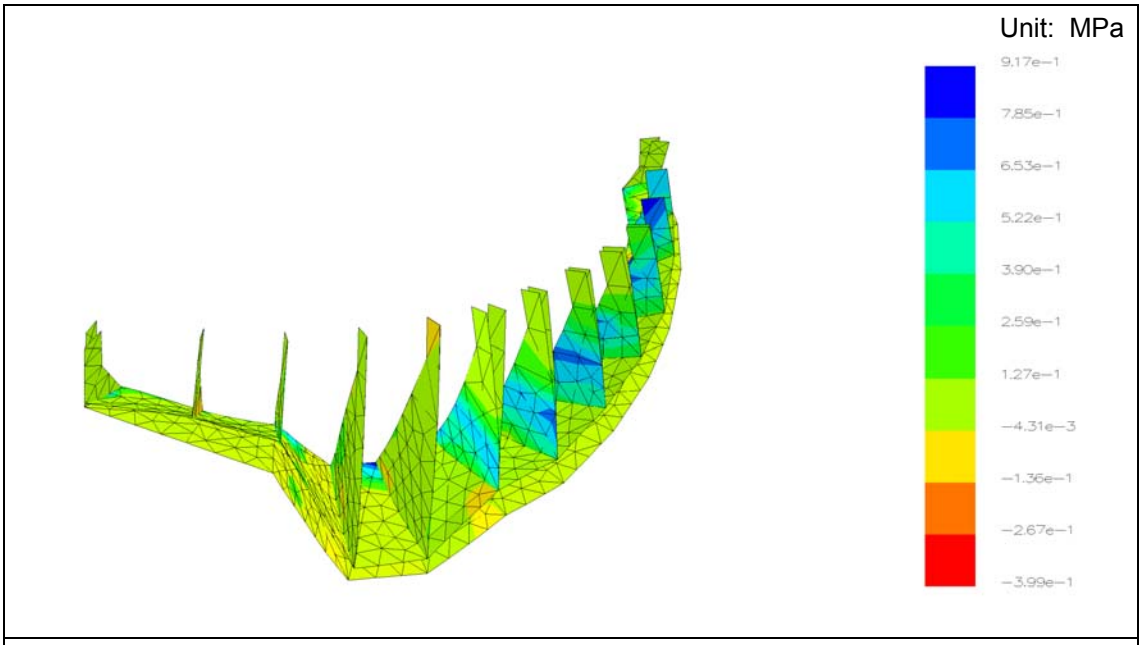

Fig. 14: Interface Elements Between Monoliths, and Dam/Foundation.

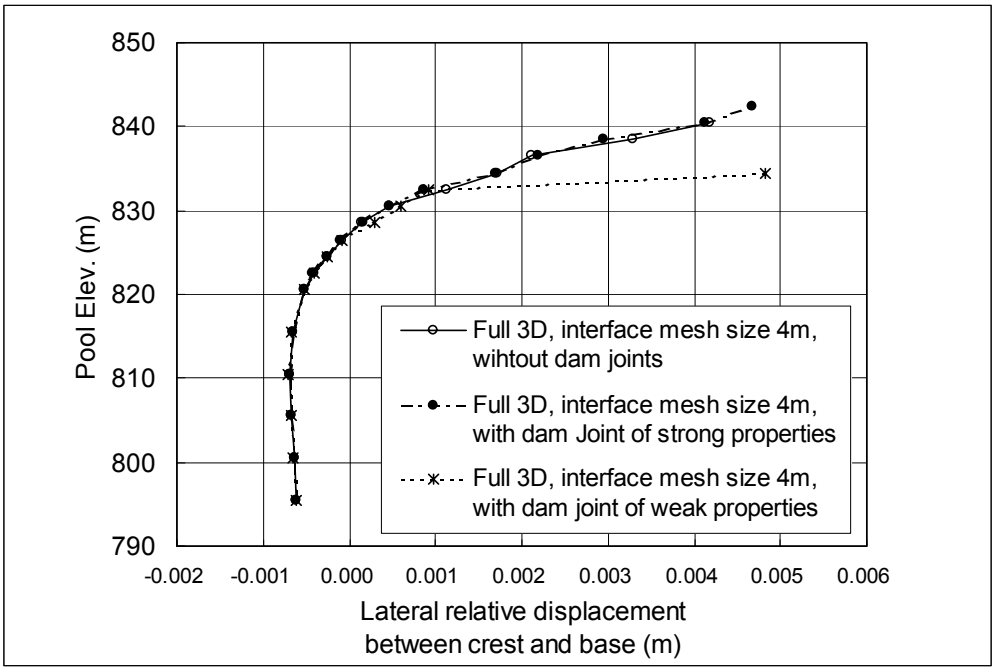

Fig. 15 Crest Displacements for Full 3D Models and Effect of Vertical Joints

State of Vertical Joints	Analysis Conditions (Parametric stadies of interface material properties for Vertical joints)					Pool elevation at crack initiation and dam sliding			
						Absolute (EL. m)		Multiplier coefficient to the dam height (36.55m)	
	Cohesion	Friction Angle	Tensile Strength	Fracture Energy Mode I	Fracture Energy Mode II	Crack Initiation	Failure (sliding)	Crack Initiation	Failure (sliding)
No	-	-	-	-	-	828.5	840.5	0.95	1.27
Strong	1.7 MPa	37	1.0 MPa	100 N/m	G_F^I*10	828.5	842.5	0.95	1.33
Weak	0.2 MPa	37	0.1 MPa	100 N/m	G_F^I*10	828.5	834.5	0.95	1.11

Table 4: Effect of Vertical Joints in a Full 3D Dam Model

4. CONCLUSIONS

In summary, through the extensive parametric study undertaken for Scalere dam (full set of results can be found in [4]), we can conclude that:

1. The value of the tensile strength of the rock/concrete interface may be important, however a tenfold increase resulted in a relatively minor increase of the IFF.
2. The value of the fracture energy plays a relatively minor role in assessing the IFF. Hence, one may conclude that its exact determination for dam analysis is not that important.
3. Analyzing a single monolith as a 3D structure, as opposed to a 2D one, results in a 10% increase in the IFF, but in both cases, crack initiate at the same pool elevation.
4. Failure to account for the uplift load may result in unacceptable overestimate of the IFF.
5. A full 3D analysis, without vertical joints, resulted in a good 27% increase of the IFF.
6. Accounting for the vertical joints in a 3D analysis can provide results which brackets the one without joint, depending on the joint properties.

ACKNOWLEDGMENTS

The authors would like to thank Mr. Y. Yagome, and Ms. S. Fortuna for their invaluable technical assistance, and Mr. S. Tsuruta, and Mr. H. Noguchi for their support of the project.

REFERENCES

[1] http://civil.colorado.edu/~saouma/Merlin

[2] McCarron, B. and Saouma, V.E., ``Merlin Analysis of Leesville Dam", EPRI Technical Report 1000165, prepared by Schnabel Engineering, 2000.

[3] Giuseppetti, G., Mazza, G., Meghella, M., Fanelli, M., "Evaluation Of Ultimate Strength Of Gravity Dams With Curved Shape Against Sliding", 7th Benchmark Workshop on Numerical Analysis of Dams.

[4] Shimpo, T., Yagome, Y, Saouma, V.E., "Full Nonlinear Analysis of an Arch-Gravity Dam", Tokyo Electric Power Service Company, Internal Report, Sept. 2003.

THEME B

THERMAL ANALYSIS OF RCC GRAVITY DAM

RCC Dam Construction State of the Art in 2003

Bernard Bouyge, Consulting Engineer, Montpellier, France
e-mail: Bernard.Bouyge@free.fr, phone: + 33 6 22 12 80 10

Roller compacted concrete

Abstract

RCC dams have been developed all over the world within the 20 last years. From an innovative technique, it has come to reach the status of confirmed technique that can be used by all designers and built by all contractors. Simplified and faster construction offered by this technique can significantly reduce overall construction costs.

The present trend is to standardize the design and construction of RCC dams, as it has happened for other types of dams, particularly concrete dams. This trend is most obvious in the fields of mix design and temperature control. Should this trend lead to new severe design considerations and technical specifications, then the economical advantage of RCC construction will be less significant.

I Introduction

Approximately 250 large Roller Compacted Concrete dams have been built since the early 1980 and about 30 are being built. Longtan dam, in South China, presently under design, will reach a height of 218m and will have a volume of 7.5M $m^{3.}$ When constructed, it will be the tallest RCC Dam in the world.

RCC dams, which have been built in all parts of the world, are – these days - often considered as an alternative to Conventional Concrete (CVC) Gravity dams, Embankment dams and Concrete Faced Rockfill (CFRD) dams. It could even be said that these RCC dams are in fashion. In general they present the advantages of being competitive in terms of costs and construction time.

Today, the RCC dams tend to replace the conventional concrete dams. The comparative economic interest of RCC dams is based on following elements :

-less cementitious materials content,
-less processed aggregates,
-less formwork (transversal joints are not formed),
-high production rates (100,000 m^3/month is not unusual) and reduced construction time.

It is interesting to note that the concept of RCC dams remains still open:

-this technique is in evolution with innovative methods of construction,
-this technique allows for adaptation of the design to suit site conditions.

A common point of all RCC dams is that they are all constructed in multiple layers (Lifts). Therefore, the main concern of RCC design is the watertightness of the structure, and the bonding between the lifts:

- crack control of the dam is achieved by controlling raise of internal temperature (parameters will be type and content of cementitious materials, limitation of concrete temperature when placed, and limitation of placing during periods of high ambient temperatures)
- correct bonding between layers is important to assure watertightness and shear resistance. The permitted time lapse between successive lifts without need for grouting between layers determines the DT factor.

The answers to these concerns will be further detailed.

The designer needs to understand that the contractors will be able to make a better job of construction if he makes a “Contractor-Friendly” design - resulting in a higher quality Dam.

II RCC mixes

The techniques of building dams in RCC have been developed in different parts of the world, and with different principles :

-lean RCC, with less than 100kg/$m^3$of cementitious materials: dams built in this way need a watertightness system separate from the dam body,

-RCD techniques and dams developed and built in Japan, limited to this country, only: the RCD contains 120-130 kg/$m^3$of cementitious materials out of which 30% is fly ash; the RCD is encircled in thick conventional concrete faces with cold joints between all lifts;

-high-paste content RCC dams with cementitious material exceeding 150kg/m^3 cementitious materials are based in great part on pouzzolanic materials

-medium paste RCC with cementitious materials between 100 and 150kg/m^3

-hard-fill dam: similar to cement-stabilised soil concrete-faced dam, suitable for bad quality foundations, and/or when only bad material is available for construction

Today, the most commonly used technique is “high paste” RCC that provides good workability and ease of construction to the contractor. This technique allows for a wide range of applications - from very high performance of RCC to structures that are easy to build (in sense of obtaining quality and better guarantee).

In practice, a RCC mix design starts with looking for (wet) density that is frequently understood as being between 2.4 and 2.45 (dependant upon aggregate density) and workability (values looked for are in order of 15-20 s measured by Vebe tests).

Knowing that:

-cohesion or bonding is controlled in principle by the percentage of fines (less than 80µ), content of water and presence of fly ash or pozzolan,

-segregation is influenced by the MSA and shape (roundness), proportion of sand/coarse aggregates, content of fines and water, and granulometric curve shape,

-workability (compactability) is primarily controlled by the content of sand and water, the amount of fly ash or pozzolan and hydration speed,

-strengths are tied to content of cementitious materials, and to C/W ratio, and they are influenced by content of sand (less than 5mm) and fines.

It results in following most common guidelines for RCC :

-the granulometric curve excluding cement should be of type P= (d/MSA)exp(1/2 to ¼), considering pozzolan as fines,

-the percentage of fines + cementitious materials should be between 12 and 14% of the dry weight of RCC,

-the paste content, by volume, should be between 19 and 21% (paste includes all elements less than 80µ : fines of sand and gravel, cementitious materials, water and air)

-the percentage of sand should be between 35 and 50% (in general 40-45% is better) of the mix (sand + dry aggregates).

The second and forth of these conditions are the most important.

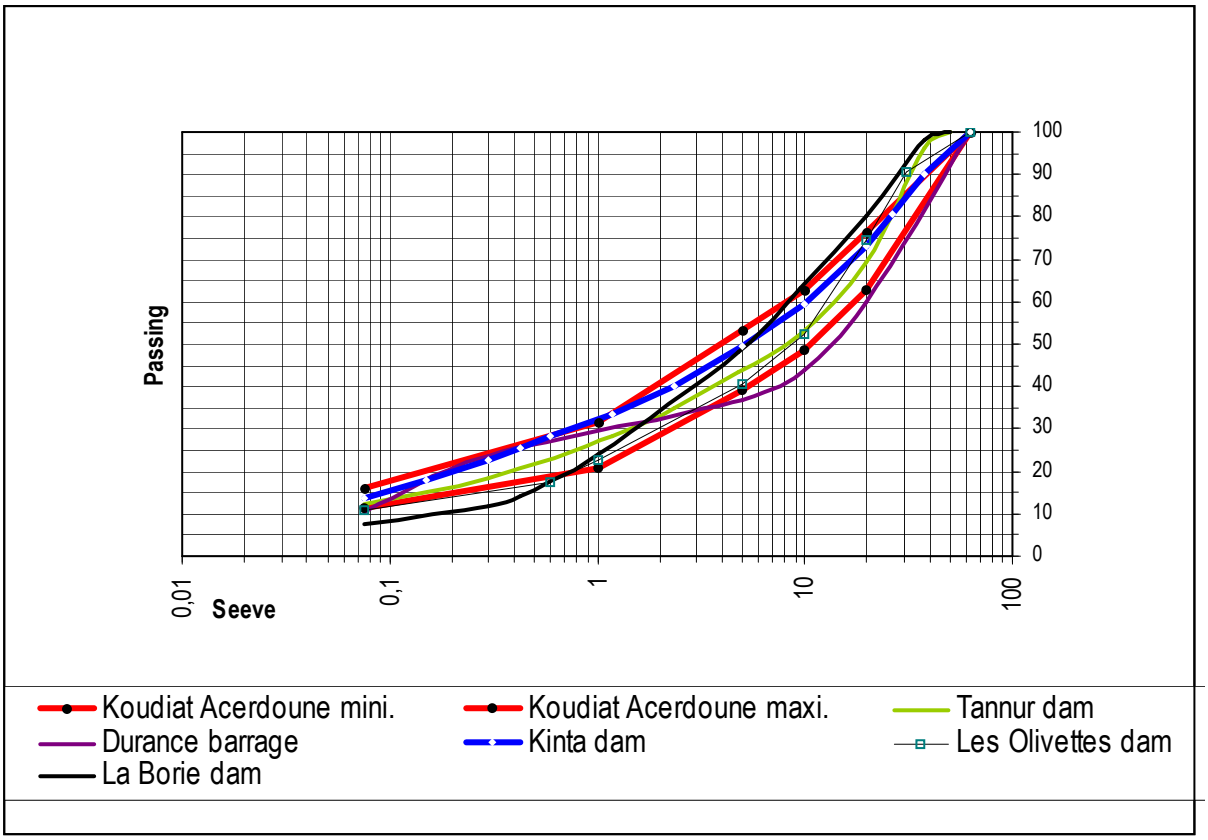

Some granulometric RCC curves (including cementitious materials)

III RCC construction methods

III.1 Construction methods

The RCC has been developed from Soil Cement techniques to benefit from high production rates. Production rates with RCC are expressed in hundreds of m^3/h, and not anymore in tens of m^3/h : on recent large dams built, or in construction, the rates reach often 400-500m^3/h (and more than an average of 100,000m^3/month).

Of course, in RCC placing there are dump trucks, bulldozers and vibratory roller compactors.

The necessary means of production as well as the material supply should be adjusted according to these rates.

RCC will be produced with large capacity plants :

-batching plants (discontinuous process of mixing), above all used when cooling with ice should be applied,

-or continuous mixing plants, more economical, producing concrete of equal quality.

The transport of RCC to and on the dam can be done in various ways :

-by dump trucks travelling on access roads following the progress of the works ; access onto the dam is a critical point that requires a permanent treatment and constitutes a strong constraint,

-by conveyor belts : conveyors can load trucks on the dam for final distribution and placement on the lift, or connect to a placing device (crawler placer) that eliminates dump trucks travelling on the surface of the lift,

-by chute, in case the abutment slopes are steep (over 45 degrees), to load dump trucks on the lift for final distribution and placement.

Then RCC is spread and compacted.

Example of all conveyor delivery system

III.2 Upstream facing watertightness

The upstream faces of RCC dams may be classified into four types :

-conventional concrete placed simultaneously with RCC against formworks,
-slip-formed conventional concrete placed in advance to RCC,
-grout enriched RCC,
-geo-membrane acting as watertight barrier.

The first two types are classic : they both consist of a layer of conventional concrete, few tens of cm wide between the RCC and face. Therefore we will here describe only the principles of use of GeRCC and use of geo-membrane (that are equally used in rehabilitation of old structures)

GeRCC

The GeRCC Concept, set up in China and Australia, has been developed in order to improve the bonding between RCC dam body and the facing. In this process, there is no more internally vibrated facing concrete but RCC is laid against the formwork; and, near the formwork, in an area about 40cm wide, cement grout is added: the resulting GeRCC is then compacted with a vibrating poker. The success depends upon the ability of the grout to soak into the RCC.

The difficulties in implementing this process are:

-avoiding any previous compaction of GeRCC area which would hamper grout penetration into the mother material,

-limiting the vibration to the minimum to avoid resurfacing of grout, which would consequently increase the work of preparation of surfaces and reduce the RCC placing output,

-GeRCC is implemented just before RCC placing, and any delay to this task would slow down RCC placing,

-GeRCC has a lower or equal compressive strength compared to mother RCC. GeRCC density is a little bit lower than that of RCC.

This method brings the following advantages:

-there is a continuity between the dam body and the facing, as it can be checked from numerous core samples taken on the dams where GeRCC is used,

-quality surface finish of the facings,

-GeRCC can be also used to treat :

-contact with rock foundation in abutments,

-contact with various openings within the dam (galleries and similar),

and therefore there is no need for a conventional concrete team when placing layers.

By using this method, there is only one material being placed on the working surface: the operating advantage is less equipment and less workers.

Geomembrane

The means to achieve the imperviousness of the upstream face are to provide water-tightness to the dam by a separate independent watertight element attached to the upstream face. The water-tightness function is then separated from the stability function. This can be achieved with a synthetic membrane:

-exposed drained membrane (most often PCV),

-covered synthetic membrane embedded in pre-cast facing elements.

The arguments in favour of the use of geomembranes can be summarized as follows : in RCC dams, there is often more cementitious materials than that strictly required for strength. These additional quantities are there mainly to improve imperviousness of the dam body along the horizontal joints (It is known that early RCC dams have experienced significant seepage through these joints).

If there is another means to achieve imperviousness of the joints, then the cementitious content may be reduced; furthermore, if there is a mean of achieving imperviousness of the upstream face of the dam, uplift and therefore stresses within the dam body will be reduced, the minimum required strength will be lowered and the cementitious content will be consequently reduced. RCC strength will be lower, but will still be enough to cope with the actual stresses in the dam body. The lift joints will be allowed to be more pervious, but imperviousness will be no more relevant as the water from the reservoir will be unable to penetrate the dam due to the imperviousness of the upstream face.

III.3 Horizontal joints

The RCC is usually placed in 30 cm thick layers that thus create horizontal joints that become a critical point in terms of structure and watertightness at every 30 cm of dam's height. Therefore, bonding in between successive layers is of major concern of designers and contractors.

Generally, no RCC should be placed before the surface has been cleaned from:

-bad quality RCC, poorly compacted, deteriorated, too wet, segregated, etc…

-all other materials and substances like : dust, clay, oils and other petroleum products, curing compounds, various residuals from cleaning operation, etc…,

-water puddles.

The equipment that complies the best with these requirements is a truck mounted vacuum cleaner.

In addition to vacuum cleaning of the surface, usual surface preparation procedures are:

-blowing the surface with air under pressure,

-washing the surface with a mix of air and water under pressure of at least 0.5 MPa.

Whichever procedure is selected for surface preparation, it has to be performed in a way that secures that aggregate is not dug out from the layer's surface and cleans only the exposed surface of the aggregate.

The idea that prevails in RCC specifications is that the ideal situation is when the time required to cover one layer with another is less than the final setting time of RCC.

The technical specifications that translate this idea into procedures generally define 3 types of horizontal joints :

-cold joint of type A in case of covering higher than defined by factor DT that is equal to XX°C*h (XX being in the range of 250 to 500),

- cold joint of type B defined by YY (often in the range of 36) hours

-hot joints: joints created out of any of the above 2 criteria

The DT factor is the multiplication of the time that joint was not covered by and average ambient temperature during that period. For a given average ambient temperature this factor defines the maximum exposure time that affects the surface of the layer prior to being covered with the next layer. The maximum value of this factor is set at an established limit that is based upon results of trial tests and depends upon the type of cementitious material selected.

Hot joints are not to be treated, unless travelled on, in which case the treatment is minimal, usually not more than vacuum cleaning.

A type cold joints are subject to vacuum cleaning and treatment with bedding mix in the upstream areas of the layer.

B type cold joints are subject to green cutting on the whole surface and treatment with mortar on a very big portion of the surface of the layer.

The slump of mortar used to increase the bonding between layers is 20 cm so it can penetrate the surface of compacted layer and coat the largest aggregates of the layer being placed.

In all areas where RCC is spread over a layer of mortar it has to be completed before setting of the mortar (generally 45 minutes)

To efficiently address the problem of proper bonding between layers, above all when placing RCC in hot climate conditions, two new solutions exist, and both have been successful :

-sloped (inclined) layers method, invented in China, also applied in Australia and Jordan, among others, enables covering the layers in a very short period of time,

-using retarders to increase the final setting time.

These two solutions do not contradict each other; they can even be applied simultaneously, if necessary.

The use of retarder is an interesting solution if the economic conditions are favourable, which can be analysed by comparing the over cost of using bedding mortar to savings when reducing bedding mortar quantities and maintaining continuous placing rates of RCC.

Use of retarder

This solution is often used in China, using residual products from agro industry that are not expensive(1/3 of the usual price). Chinese products are selected based on ambient temperatures. This is Calcium Lignosulfate or Calcium Carbohydrate or organic acids for high temperatures, like tartaric acid, citric acid or glucose. These products can increase the setting time to 6-8 hours with content less than 1%.

Products used by European companies and tested on Miel dam in Colombia for example, have showed the following results :

-dosage: 1% of weight of cement,

-Increase of compression strength of more than 15% after 28 days, and near 20% after 56 days (allowing decreased amount of cement, resulting in lower hydration temperatures),

-setting time increases from 3-4 hours to 12-16 hours, which is considerable and allows a very important relaxation of DT criteria.

Price of these additives are in range of 1€/kg.

Of course, the use of retarders should be based on preliminary studies at the jobsite laboratory to determine the correct dosage and resulting properties to check compatibility with aggregates and cementitious materials used.

Sloped layers

The sloped layer method was first set up in China (Jiangya dam, 131m high).

Instead of building the dam in successive horizontal layers of 30 cm thick, the dam is built in thick horizontal lifts equivalent to n times 30 cm thick layers.

Each of those lifts are made of a succession of layers inclined a few degrees going from one abutment to the another: each of those inclined layers are of low volume representing a production of 1-2 hours of mixing plant. These layers are getting covered in a very short time and DT criteria widely assured.

Depending on the width of the dam and the height of the lift (linked to the height of the form of the facing) and of the discharge rate of the mixing plant, the slope of the inclined layers may vary between 1% and 10% or more .

The benefit of this solution is obvious: it reduces the number of layer surface treatment; also, with time of coverage from 1-2 hours it assures higher quality of bonding ; this quality has been largely proved with test cylinders extracted from the dams built this way.

This attractive solution is in the same time delicate to implement compared to horizontal layers:

-to place inclined layers, laser cannot be used: the bulldozer operator has to be skilled and some “tricks” like marking the layers on the forms have to be used,

-creation of thin edges of RCC layers should be avoided by cutting if necessary,

-additional stresses to formwork: along a piece of formwork, the elevation of RCC (and therefore of concrete facing or GeRCC) may reach 3 metres within a few hours. The resulting thrust on formworks therefore far exceeds the ones usually encountered, and formworks and their anchorages should be sized accordingly,

-cold joint treatment (every n times 30cm): whereas the number of cold joints is significantly reduced, these surfaces are uneven and require additional work, which can however be carried out in parallel to RCC placement.

The compaction of inclined layers does not represent a big problem for layers inclined less than approximately 10%.

The angle of layer inclination should be defined based on production of RCC and size of the dam at level of works: the reasonable goal to aim is to cover the layer in less than 2 hours; usual slopes are between 1 and 10%.

The following advantages are brought by the method:

-the time limit criteria for overlapping layers are successfully met,

-the surfaces to be treated (green cutting, cleaning, mortar laying) are reduced: within a 3 meters slice, for example, layers follow each other fast, and the treatments are minimum, or even no more necessary,

-the quality of the contact between successive layers is therefore significantly increased and the concern with horizontal joints bonding drastically reduced,

-the height of lift of 2.7-3m is very interesting (upstream forms are usually of this height); when not possible, for reason of availability of forms or downstream face design, layers of 1.2 m can be made; supposing that 1.2 m high downstream steps will be authorized,

-the downstream and upstream concrete faces should be made in the same way.

Regarding the operating management of the dam: when planning the RCC dam construction, selecting the size of plants and equipment (m^3/h of aggregate, mixing, cooling, and placing systems) is based on criteria of production i.e. total time available (scheduled, allowed) for placing RCC, and criteria of "cold joint" placing requirements. Whichever is the bigger, that is the one you should go with.

Therefore, the sloped layer technique's actual and main advantage is the possibility of building the dam with lower placing capacity installed. This means that for parts of the dam where "cold joint" requirement for horizontal layers is higher than "production" requirement (very often the case when layer surface is large) switching to placing the RCC in sloped layer system rather than sizing the plants and equipment based on that high "cold joint" requirement can result in considerable savings.

IV Thermal problems in RCC dams

Like all concrete dams, RCC dams are also exposed to temperature rise : but, this rise even being moderate (in the range of 15 degrees C) due to low cement content, tend to become an important concern of the designers

When temperature is of concern it is most often expressed as : "maximum temperature when placing RCC should not exceed T ".

The experience shows that temperature raise between time of mixing and placing in the layer can reach dT=4 °C.

The target is then to limit temperature raise (dt) during transportation on one side, and find means to produce the RCC at temperature T-dt at the mixing plant on the other side.

The ways to control temperature can vary: it can be also very expensive. The contractors, when answering to the tender, will be looking for the least expensive method to

provide the required result. To estimate the technical proposal the contractors should know the so called: "wet bulb temperature" and this figure is very rare to find (almost never) in the specifications of the tender. This is creating false competition between the contractors.

There are numerous ways to control the temperature of concrete:

-means depending on jobsite organization:

. spraying aggregates with water to take benefit from evaporation to cool down the aggregates,

. painting aggregate bins and cementitious storage silos in white,

. covering conveyor belts,

. in hot periods using stocks made during cold periods and then protected,

. placing RCC by night,

. paying attention to curing concrete: different systems exist that may require lots of water; by "Fogging" (creating a mist over the layer) the contractor will reduce considerably the amount of water needed, and maintain atmosphere saturation right above the layer, thus reducing the ambient temperature by 3-5 degrees C.

-ways that require specific investments:

.-use of water chilled down to 1-4 °C reduces RCC temperature by 1.5 to 2 °C. Cold water is made by classical refrigerating plants. It can also be made by using liquid azoth (cost: 1 €/m^3),

. introducing flake ice in the mixer: dosage of ice and time needed by ice to melt requires a batching type plant. Substituting 30kg of ice to 30 litres of water leads to gain 5°C (this gain becomes 6.5°C if 40kg are substituted. The limitation of the volume substituted is determined by the minimum volume of water requested for the mix design, and the required production rate per week

. pre-cooling coarse aggregates using a wet belt running in an insulated tunnel in which aggregates are sprayed with cooled water during 1 – 2 minutes. This method requires a post screening process of the aggregates but allows to use continuous mixing plants.

. pre-cooling coarse aggregates by refrigerated air circulation, within insulated storage silos (time required: 40 minutes)

The above refrigerating costs may represent 15 to 20% of the unit cost of RCC.

Compared to these means, the simplest and cheapest way to limit cracking due to thermal origin constraints could be to use closer spaced transversal joints.

These joints are cut after compaction of RCC; they are made by pushing a metallic blade into the layer and then introducing material (PVC sheet, iron sheet, sand…) preventing the faces of the joint to stick again.

The thermal calculation methods are presently enough developed to give the designer a precise knowledge of the strengths induced in the dam. With this knowledge the designer becomes able, so as to optimise the total cost of the dam, to ask for the strictly required thermal specifications. It is clear that these calculations methods are of utmost importance: it is hoped that they will be able to supersede approximate and conservative (and expansive) specifications.

It can be forecast that, based on precise thermal calculations, maximising the use of transversal joints and using simple methods (as spraying aggregates with water…) will be enough in most cases and will reduce the need for heavy and costly equipments.

V Conclusion

RCC Dam building has proved to be very interesting and its present growth shows that it is true all around the world.

It has to be kept in mind that this technique has superseded conventional concrete dam construction which did not evolve regarding design mix and which has become more and more rigid as complementary technical specifications, not always necessary, were added along tens of years. RCC has given the opportunity to build new construction technique, looking for each project not to require more specifications that strictly necessary.

Given these considerations, conditions for success are simple:

-a design which will allow the contractor to work quickly on a continuous way,

-looking for a non segregating mix

-allowing for the implementation of an industrial working organisation: the construction of a RCC dam needs that several jobs are done simultaneously, as in a factory: formworks, cleaning, bedding mortar, facing concrete, spreading RCC, compacting RCC, curing RCC, cutting the joints..

-choosing a contractor with a management team able to implement the above mentioned organisation.

The risky way is that projects are no more studied as individual projects but result from copying what has been done elsewhere and adding complementary technical specifications.

This can be observed for an increasing number of projects: the result is a project which is not adapted to the site conditions, more expensive and harder to build, without any benefit for the owner.

Concerning thermal problems and their consequences regarding the bonding of the layers or induced cracking, simple and not expensive means allow not to use heavy and costly methods. Proven calculation methods are to be implemented to minimize construction costs.

References:

B. Forbes: The sloped layer method and other techniques for improving quality and productivity on modern RCC dams. RCC 2002- April 7th-10th – Irbid – Jordan

E. K. Schrader: Experiences and lessons learned in 30 years of design, testing, construction and performance of RCC dams quality. RCC 2002- April 7th-10th – Irbid – Jordan

M. Dunstan: The state of the art of RCC dams at the end of 2001. RCC 2002- April 7th-10th – Irbid – Jordan

F. Andriolo: RCC-materials availability, properties and practices in different regions. RCC 2002- April 7th-10th – Irbid – Jordan

L. GuangTing, L. PengHui and X. ShuNan: Research and practice of roller compacted concrete arch dams. RCC 2002- April 7th-10th – Irbid – Jordan

M. Dunstan: Recent developments in roller compacted concrete dam construction. Water Power and Dam Construction Annual Handbook. 39-47. 1989. London

B. Bouyge: Fifteen years of experience in RCC dam construction. RCC 2002- April 7th-10th – Irbid – Jordan

B. Bouyge and B. Forbes : Tannur dam in Jordan: adapting the project to site conditions and specific construction methods. RCC 2002- April 7th-10th – Irbid – Jordan

A. Scuero, G.L. Vaschetti and J.A Wilkes: State of the art of geomembrane facing systems for RCC dams. RCC 2002- April 7th-10th – Irbid – Jordan

INTERNATIONAL COMMISSION ON LARGE DAMS
AD Hoc Committee on Computational Aspects of Analysis and Design of Dams

COMMISSION INTERNATIONALE DES GRANDS BARRAGES
Comité Ad Hoc des Méthodes de Calcul pour les Barrages

7th Benchmark Workshop on Numerical Analysis of Dams
September 24-26, 2003 – Bucharest, ROMANIA

Theme B – RCC dams

THERMAL ANALYSIS OF A RCC DAM BODY

DURING CONSTRUCTION

Formulator : Coyne et Bellier, Bureau d'Ingénieurs Conseils

A.J. Carrère, Coyne et Bellier,
9 allée des Barbanniers,
92632 Gennevilliers, France
alain.carrere@coyne-et-bellier.fr

The information package for the preparation of contributions to Theme B consists of :

- the present description — ThemeB.doc
- the cross section drawing — ThemeB.dwg
- the input date Excel file — ThB_data.xls
- the template file for results — ThB_ResXXXX.xls

1. INTRODUCTION

The 7th Benchmark Workshop promoted by the ICOLD "Ad Hoc" Committee on Computational Aspects of Analysis and Design of Dams proposes a new field for computation, besides those of concrete and earthfill dams which have been extensively explored during the previous BWs : this new subject is that of thermal analyses in the body of dams. ***Theme B*** is devoted to the prediction of temperature during construction of a RCC dam, one of the most popular type of dams in the recent years.

The problem consists in predicting the temperature field in the heart of a thick RCC dam, whose variations influence the stress field and may therefore induce cracks after several years, if no adequate system of joints has been incorporated into the design.

The bases for the analyses are quite simple, they rely mainly on dissipation of the cement hydration heat through conduction laws in the material, plus consideration of adequate limits conditions.

The main practical difficulty is the need to consider the frequent changes of the body geometry and limit conditions, due to the rate of placement of successive RCC lifts, which is typically daily. The influence of the construction schedule has proven to highly influence long-term concrete temperature.

Another general difficult aspect of such problems is that the hydration heat curve is not easily known, since the accuracy of standard laboratory methods is very low for heat production after the first week, which only special and expensive tests are able to measure adequately. However this obstacle will be avoided here, and a single heat development curve, which is partly based on special tests, is suggested to be used by all Participants.

The proposed exercise is inspired from construction conditions of one of the largest RCC dams presently under construction, with a height of about 100 metres and a total RCC volume of several million cubic metres. The dam is located in a country with a tropical climate. Because of the exceptional size of the works, a special construction procedure has been used, with series of 10 RCC layers being placed at a daily rate, and standby sequences between series. This makes the simulation of construction still more complex.

Considering the size and thickness of the dam, most of the hydration heat developped during construction will migrate through the RCC vertically, and the contribution of heat dissipation towards the damfaces is marginal on the short term. For this reason, a 1-D vertical analysis can be used to carry out the simulation with a rather good approximation. However data are provided for those who wish to make 2-D (vertical and upstream-downstream) analyses. The 3rd direction (bank-to-bank) must obviously be completely disregarded.

All Participants are kindly requested to provide a paper with 15 pages maximum, in which all assumptions are clearly exposed (especially as regards initial and boundary conditions). For comparison purpose, they must also give their key results under a prescribed format, in a EXCEL file derived from the **ThB_ResXXXX.xls** provided, where they will replace XXXX by an acronym of their organisation.

Compulsory results to be provided are the temperature in the heart of the dam body at different instants and at differant levels (coming either from 1-D or from 2-D analyses).

Participants who will carry 2-D analyses must also provide upstream-downstream temperature profiles at different instants and levels.

2. INPUT DATA

All detailed information on input data is provided in the **ThB_Data.xls** file.

2.1. Dam geometrical definition

The dam vertical cross section is shown on Figure 1 below (see also file ThemeB.dwg). The profile is defined by a triangle whose top is at el. 110, with a vertical upstream face and a downstream face sloping at 0.8h/1v. Below el. 55.00 the upstream face starts sloping at 0.4h/1v. The crest is 8 metre wide and its elevation is 112. The deepest foundation level is just below el. 20.00.

Figure 1 : Dam cross section and position of instruments

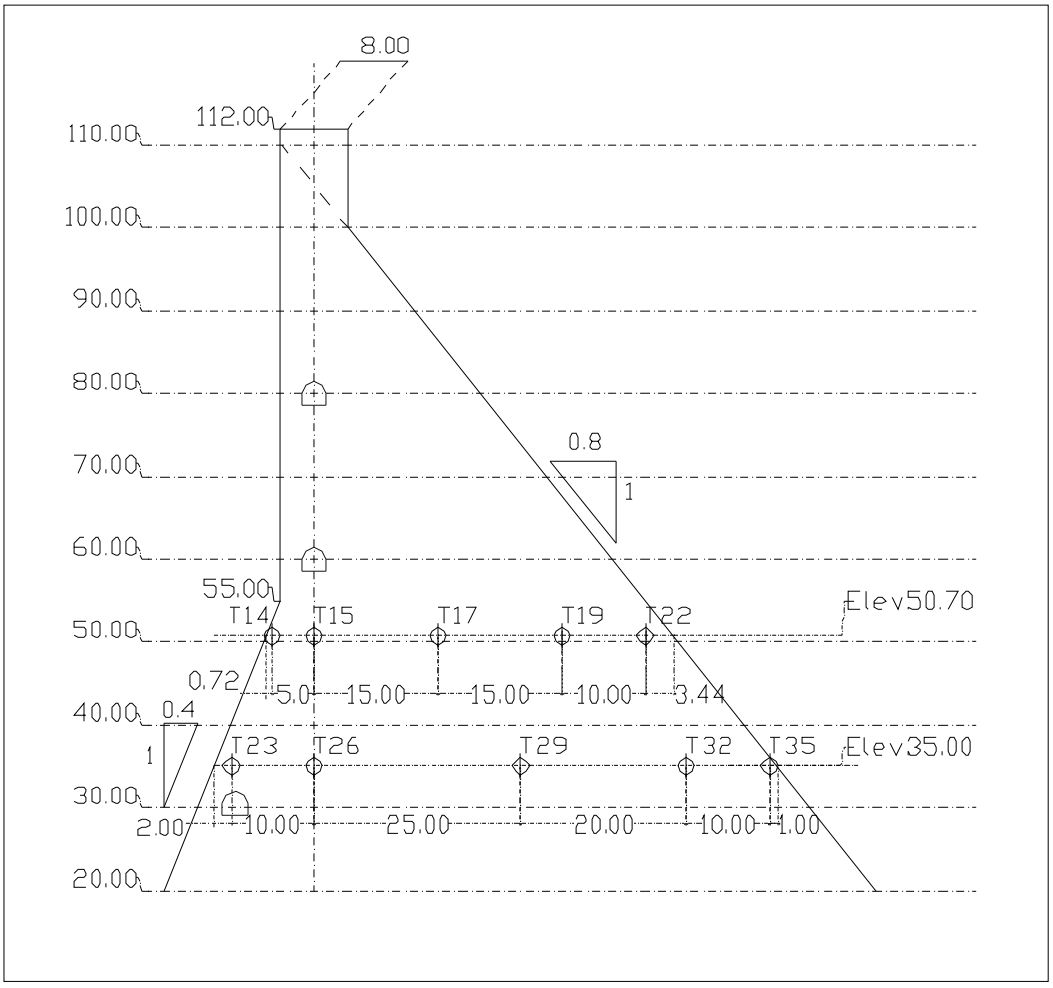

The dam is mainly composed of RCC, which is placed in 0.30 metre thick layers as explained below more in detail . Both dam faces are made of conventional vibrated concrete (CVC) as shown on Figure 2. The limit between CVC and RCC has a Christmas tree shape due to the placement method : conventional concrete is placed first, then the RCC is placed above and vibrated, and finally the CVC is vibrated (this system is adopted with the purpose of having an optimal bonding between materials).

Figure 2 : Detail of dam faces construction

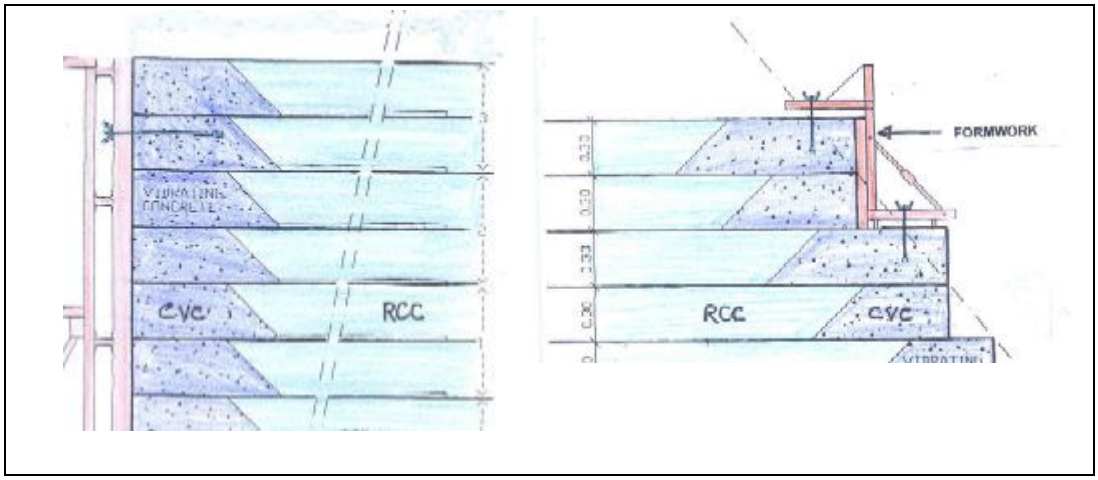

2.2. Construction procedures and schedule

The time of placement of RCC Vs time is shown on Figure 3. Basically the rate of placement is 1 lift a day, which corresponds to the steepest segments of the curve. Typically 10 layers are placed at this rate, then a standby is observed locally, during which RCC is placed in other sections. The exact placement schedule is given in the ThB_data.xls file.

Figure 3 : Detailed construction schedule of the RCC section

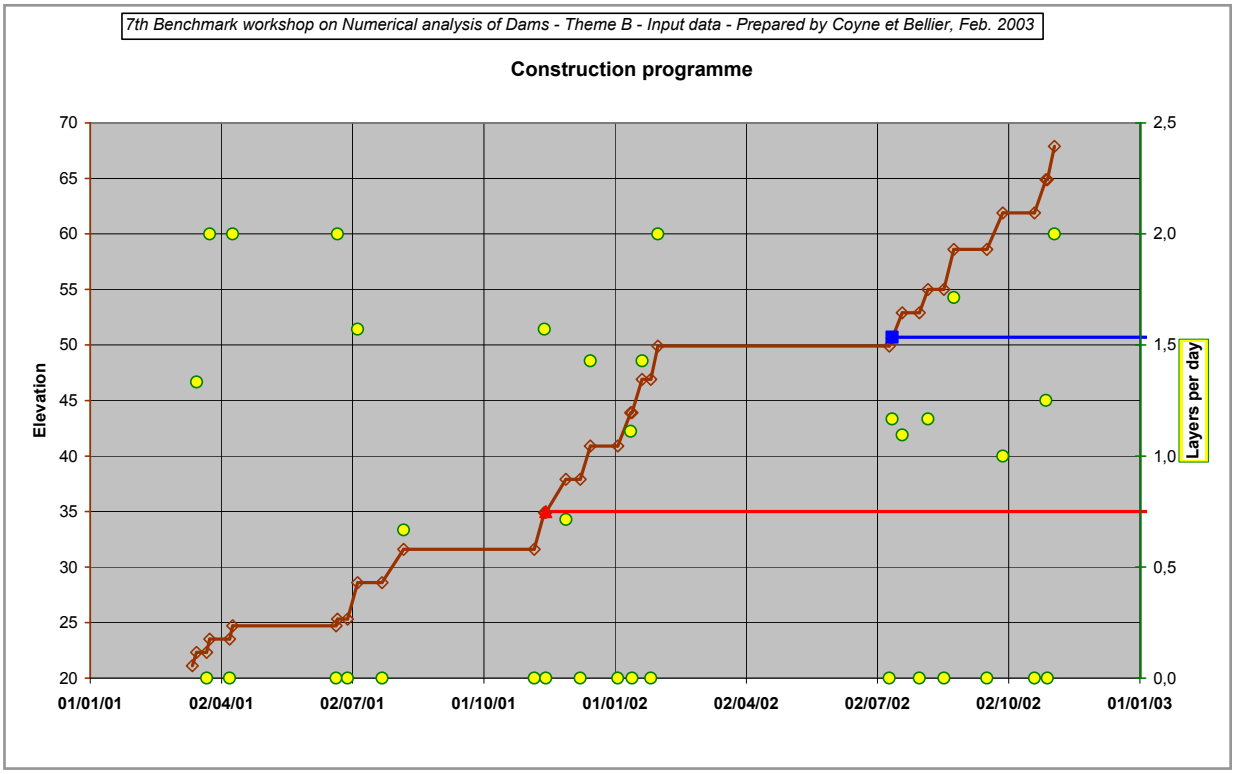

2.3. Characteristics of materials

The characteristics of RCC are given in Table A below.

Table A : Properties of RCC material

Variable	Symbol	Value	Unit
Unit weight	ρ	2380	kg/m^3
Specific heat	C	1.0	kJ/kg/°C
Conductivity	λ	10.0	kJ/m/h/°C
Diffusivity	a	0.0042	m^2/h

The cementitious material incorporated into the RCC is a mix of Portland cement (STC) and pouzzolanic fly ashes (PFA), with 100 kg and 90 kg of PFA per cubic metre of RCC.

The hydration heat of the STC+PFA mix in the given proportions is given in Figure 4. Values are expressed in Joules per gramme of cementitious material (STC+PFA). The detail are given in the ThB_Data.xls file. Experimental ploints are plotted in red. It is suggested to use the curve plotted in brown for hydration heat production beyond the first week.

Figure 4 : Hydration heat curves for RCC and CVC

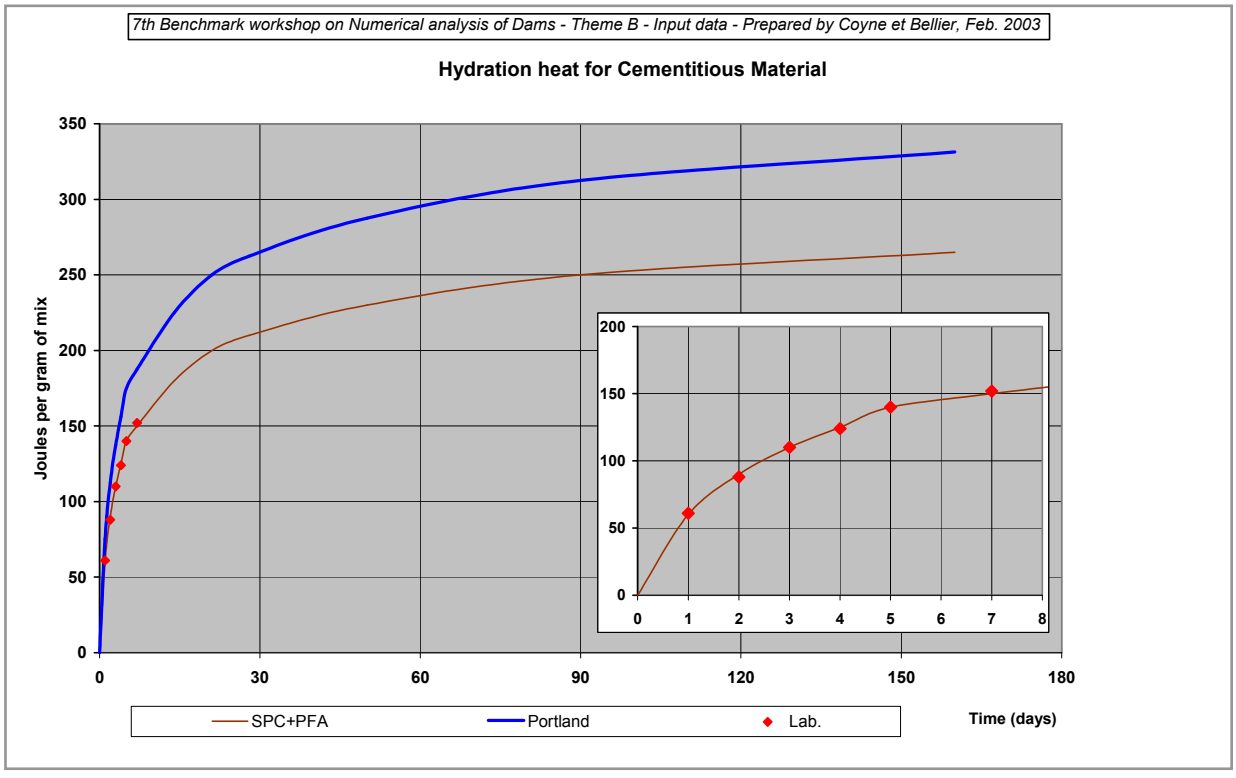

The conventional vibrated concrete used along the dam faces includes 350 kgs of Portland cement. No hydration heat curve is available for this material. If the Participants wish to incorporate CVC in their model, it is suggested to use the curve 'Portland' plotted in blue on Figure 4, which has been obtained simply by multiplying the one of the RCC mix by a factor of 1.25.

2.4. Instrumentation and readings

Electric thermo-couples have been placed inside RCC layers in several sections and elevations. Figure 1 shows the typical position of instruments at el. 35.00 and el 50.70. Other thermo-couples have been placed at different places outside the dam which give the ambient temperature Vs time.

Temperature of RCC and atmosphere have been recorded at uneven time intervals, from the time of RCC placement onwards.

2.5. Initial and limit conditions

Ambient temperature at site is given in Figure 5. It has been measured close to the dam faces at irregular dates. Details of readings are incorporated into the ThB_data.xls file. Except otherwise specified readings have been taken at 9:00 pm.

Initial RCC temperature, measured in the fresh material at the batching plant, is also given in Figure 5, as well as a few initial temperatures of RCC layers at the time of their placement. These data seem to indicate that the temperature of fresh RCC at the time of placement is substantially higher than that measured at the bartching plant. In faxct initial RCC temperature seem to be not far from that of air at the same time. It is therefore suggested to use ambient temperature as the initial RCC temperature wherever direct initial measurements are not provided.

Participants are free to consider the limit conditions of their choice at the foundation level, at the top of construction and along dam faces. The following may be of some help :

- the convection+radiation surface coefficient may be taken as α = 100 kJ/m²/h/°C
- the upstream face of the dam is facing the east

Figure 5 : Initial temperature RCC and air temperature

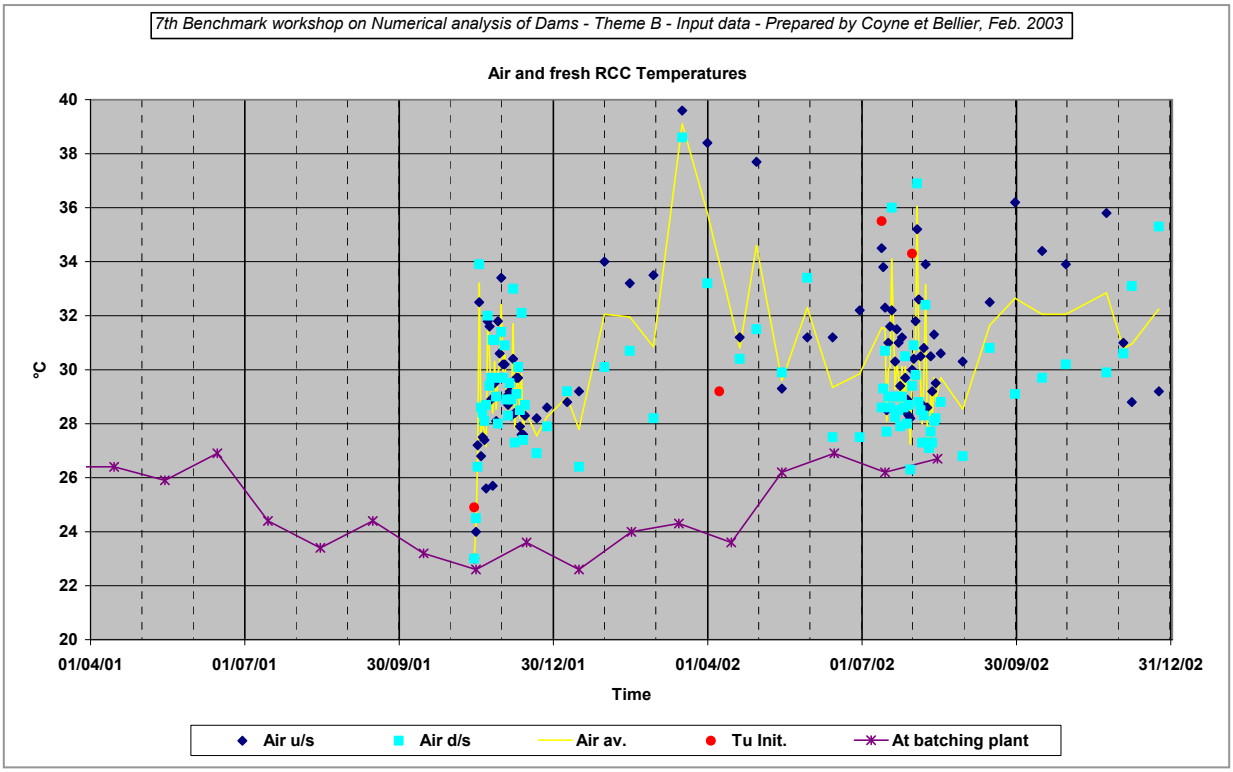

3. REQUESTED RESULTS

All Participants are kindly requested to provide a paper with 15 pages maximum, in which all assumptions are clearly exposed (especially as regards initial and boundary conditions). For comparison purpose, they must also give their key results under a prescribed format, in a EXCEL file derived from the **ThB_ResXXXX.xls** provided, where they will replace XXXX by an acronym of their organisation.

3.1. For all participants

Temperature in the heart of the dam vertical cross section at different levels and instants : fill the table in sheet '**Resu_1D**' of ThB_ResXXXX.xls (the table is reproduced below as Table B), at least the yellow lines and columns.

Table B : 1-D Results to be provided *(in sheet 'Resu_1D' of ThB_ResXXXX.xls)*

7th Benchmark workshop on Numerical analysis of Dams - Theme B - Results prepared by participant

Please fill the yellow cells *If possible do **not** modify the blue ones*

Results at center of horizontal sections

Center - Results Vs time			
Date	Value at center at el 35.00 participant	Date	Value at center at el. 50.70 participant
14/11/01		**13/07/02**	
17/11/01		20/07/02	
24/11/01		27/07/02	
01/12/01		03/08/02	
08/12/01		10/08/02	
15/12/01		17/08/02	
22/12/01		24/08/02	
29/12/01		31/08/02	
05/01/02		07/09/02	
12/01/02		14/09/02	
19/01/02		21/09/02	
26/01/02		28/09/02	
02/02/02		05/10/02	
09/02/02		12/10/02	
16/02/02		19/10/02	
23/02/02		26/10/02	
02/03/02		02/11/02	
09/03/02		09/11/02	
16/03/02		16/11/02	
23/03/02		23/11/02	
30/03/02		30/11/02	

Center - Results Vs elevation			
Elevation	Value at center on 27/07/02 participant	Value at center on 10/08/02 participant	Value at center on 28/12/02 participant
62,10			
61,50			
60,90			
60,30			
59,70			
59,10			
58,50			
57,90			
57,30			
56,70			
56,10			
55,50			
54,90			
54,30			
53,70			
53,10			
52,50			
51,90			
51,30			
50,70			
50,00			

3.2. Optional 2-D results

Temperature profiles along horizontal sections through the dam body, at 2 different levels and at 2 different instants : fill the table in sheet '**Resu_2D**' of ThB_ResXXXX.xls (the table is reproduced below as Table C), at least the yellow cells.

Table C : 2-D Results to be provided *(in sheet 'Resu_2D' of ThB_ResXXXX.xls)*

2-D results

2-D results Vs time			
Date	Value at T23 sensor (u/s, el 35.00) participant	Date	Value at T22 sensor (d/s, el. 50.70) participant
14/11/01		**13/07/02**	
17/11/01		20/07/02	
24/11/01		27/07/02	
01/12/01		03/08/02	
08/12/01		10/08/02	
15/12/01		17/08/02	
22/12/01		24/08/02	
29/12/01		31/08/02	
05/01/02		07/09/02	
12/01/02		14/09/02	
19/01/02		21/09/02	
26/01/02		28/09/02	
02/02/02		05/10/02	
09/02/02		12/10/02	
16/02/02		19/10/02	
23/02/02		26/10/02	
02/03/02		02/11/02	
09/03/02		09/11/02	
16/03/02		16/11/02	
23/03/02		23/11/02	
30/03/02		30/11/02	
06/04/02		07/12/02	
13/04/02		14/12/02	

2-D results Vs elevation			
Elevation	Value at 2 m from u/s face on 27/07/02 participant	Value at 2 m from d/s face on 10/08/02 participant	Value at 4 m from d/s face on 28/12/02 participant
62,10			
61,50			
60,90			
60,30			
59,70			
59,10			
58,50			
57,90			
57,30			
56,70			
56,10			
55,50			
54,90			
54,30			
53,70			
53,10			
52,50			
51,90			
51,30			
50,70			
50,00			
49,40			
48,80			

Horizontal profiles				
participant				
Elevation 50.70				
Cell	X=	27/07/02	10/08/02	28/12/02
u/s	-5,72			
T14	-5,00			
T15	0,00			
T17	15,00			
T19	30,00			
T22	40,00			
d/s	43,44			
participant				
Elevation 35.00				
Cell	X=	27/07/02	10/08/02	28/12/02
u/s	-12,00			
T23	-10,00			
T26	0,00			
T29	25,00			
T32	45,00			
T35	55,00			
d/s	56,00			

INTERNATIONAL COMMISSION ON LARGE DAMS
Ad Hoc Committee on Computational Aspects of Analysis and Design of Dams

COMMISSION INTERNATIONALE DES GRANDS BARRAGES
Comité Ad Hoc des Méthodes de Calcul pour les Barrages

7th Benchmark Workshop on Numerical Analysis of Dams
September 24-26, 2003 – Bucharest, ROMANIA

Theme B – RCC dams

THERMAL ANALYSIS OF A RCC DAM BODY

DURING CONSTRUCTION

SYNTHESIS

Final Version – January 2004

Formulator : Coyne et Bellier, Bureau d'Ingénieurs Conseils

A.J. Carrère, Coyne et Bellier,
9 allée des Barbanniers,
92632 Gennevilliers, France
alain.carrere@coyne-et-bellier.fr

Contents

1. FORMULATION OF THE PROBLEM

1.1 Introduction

The 7th Benchmark Workshop promoted by the ICOLD "Ad Hoc" Committee on Computational Aspects of Analysis and Design of Dams proposes a new field for computation, besides those of concrete and earthfill dams which have been extensively explored during the previous BWs : this new subject is that of thermal analyses in the body of dams. ***Theme B*** is devoted to the prediction of temperature during construction of a RCC dam, one of the most popular types of dams in the recent years.

The problem consists in predicting the temperature field in the heart of a thick RCC dam, whose variations influence the stress field and may therefore induce cracks after several years, if no adequate system of joints has been incorporated into the design.

The bases for the analyses are quite simple, they rely mainly on dissipation of the cement hydration heat through conduction laws in the material, plus consideration of adequate limits conditions.

The main practical difficulty is the need to consider the frequent changes of the body geometry and limit conditions, due to the rate of placement of successive RCC lifts, which is typically daily. The influence of the construction schedule has proven to highly influence long-term concrete temperature.

Another general difficult aspect of such problems is that the hydration heat curve is not easily known, since the accuracy of standard laboratory methods is very low for heat production after the first week, which only special and expensive tests are able to measure adequately. However this obstacle will be avoided here, and a single heat development curve, which is partly based on special tests, is suggested to be used by all Participants.

The proposed exercise is inspired from construction conditions of one of the largest RCC dams presently under construction, with a height of about 100 metres and a total RCC volume of several million cubic metres. The dam is located in a country with a tropical climate. Because of the exceptional size of the works, a special construction procedure has been used, with series of 10 RCC layers, each layer being placed at a daily rate, and standby sequences between series. This makes the simulation of construction still more complex.

Considering the size and thickness of the dam, most of the hydration heat developed during construction will migrate through the RCC vertically, and the contribution of heat dissipation towards the damfaces is marginal on the short term. For this reason, a 1-D vertical analysis can be used to carry out the simulation with a rather good approximation. However data are provided for those who wish to make 2-D (vertical and upstream-downstream) analyses. The 3rd direction (bank-to-bank) must obviously be completely disregarded.

Compulsory results to be provided by all Participants are the temperature in the heart of the dam body at different instants and at different levels (coming either from 1-D or from 2-D analyses).

Participants who will carry 2-D analyses must also provide upstream-downstream temperature profiles at different instants and levels.

A presentation paper is also requested, to expose the main methods and assumptions used.

1.2 Input Data

All detailed information on input data is provided in the **ThB_Data.xls** file.

1.2.1. Dam geometrical definition

The dam vertical cross section is shown on Figure 1 below (see also file ThemeB.dwg). The profile is defined by a triangle whose top is at el. 110, with a vertical upstream face and a downstream face sloping at 0.8h/1v. Below el. 55.00 the upstream face starts sloping at 0.4h/1v. The crest is 8 metre wide and its elevation is 112. The deepest foundation level is just below el. 20.00.

The dam is mainly composed of RCC, which is placed in 0.30 metre thick layers as explained below in more detail. Both dam faces are made of conventional vibrated concrete (CVC) as shown on Figure 2. The limit between CVC and RCC has a Christmas tree shape due to the placement method: conventional concrete is placed first, then the RCC is placed above and vibrated, and finally the CVC is vibrated (this system is adopted with the purpose of having an optimal bonding between materials).

1.2.2. Construction procedures and schedule

The time of placement of RCC Vs time is shown on Figure 3. Basically the rate of placement is 1 lift a day, which corresponds to the steepest segments of the curve. Typically 10 layers are placed at this rate, then a standby is observed locally, during which RCC is placed in other sections. The exact placement schedule is given in the ThB_data.xls file.

Figure 1 : Dam cross section and position of instruments

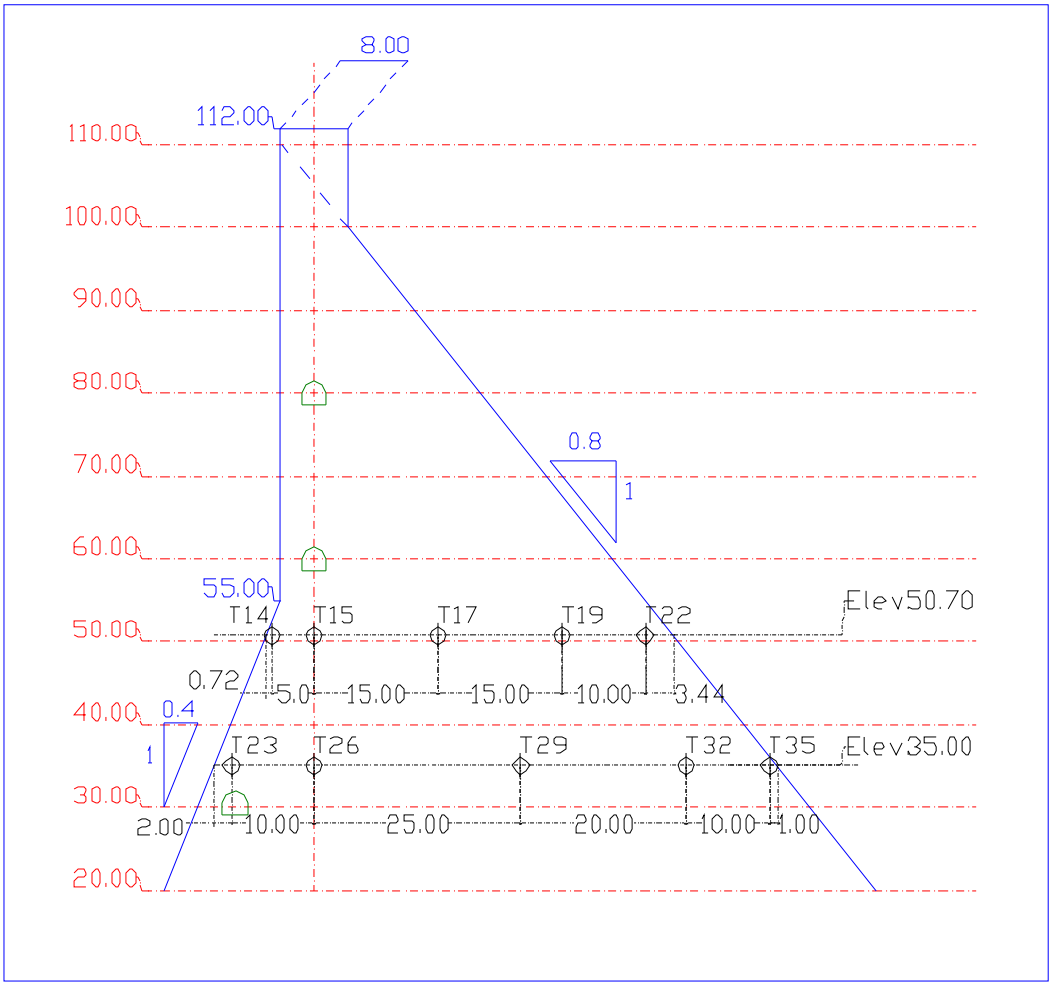

Figure 2 : Detail of dam faces construction

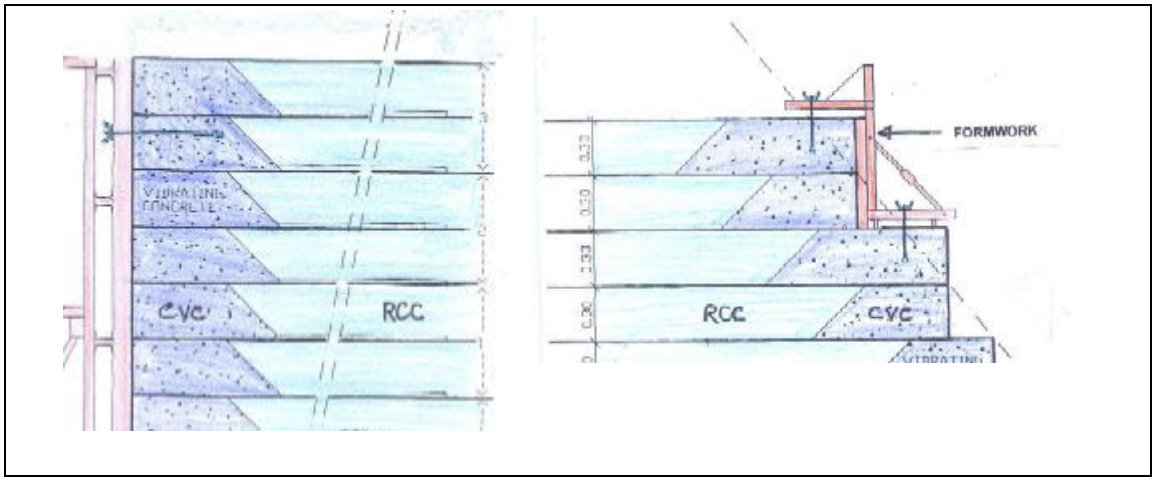

Figure 3 : Detailed construction schedule of the RCC section

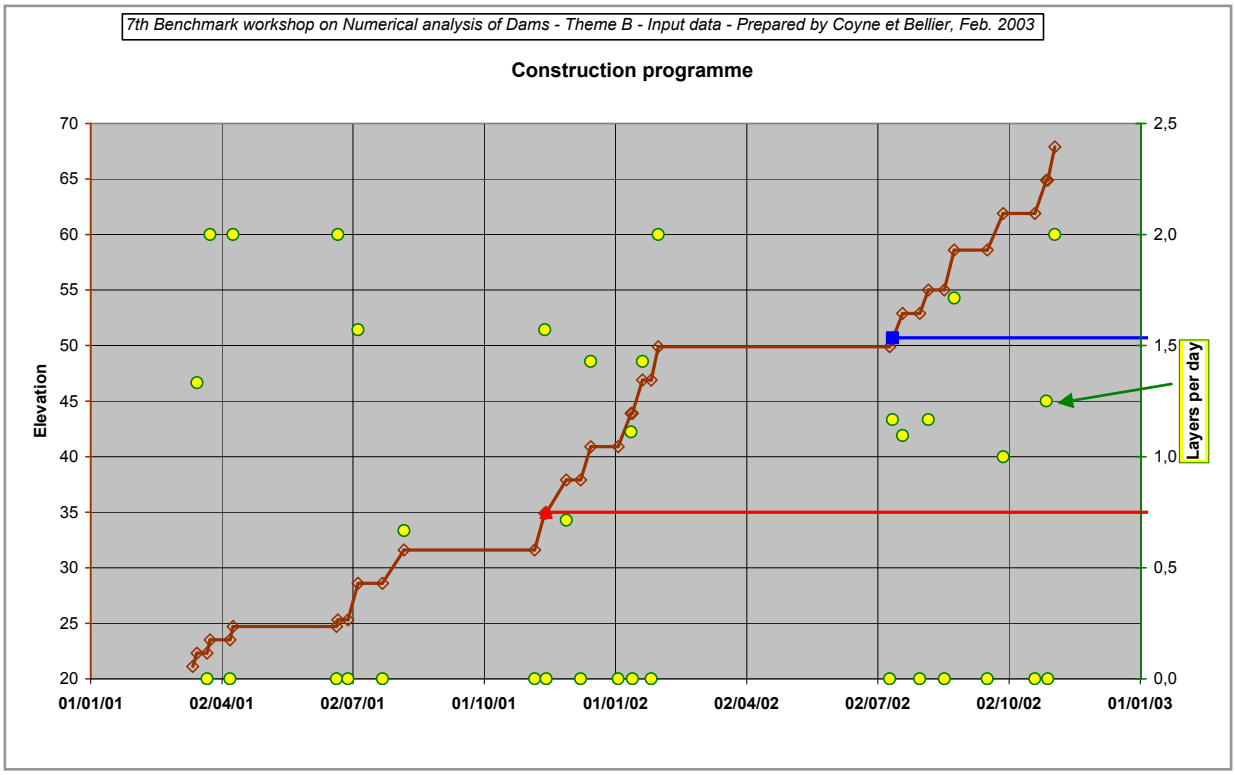

1.2.3. Characteristics of materials

The characteristics of RCC are given in Table A below.

Table A : Properties of RCC material

Variable	Symbol	Value	Unit
Unit weight	ρ	2380	kg/m^3
Specific heat	C	1.0	kJ/kg/°C
Conductivity	λ	10.0	kJ/m/h/°C
Diffusivity	a	0.0042	m²/h

The cementitious material incorporated into the RCC is a mix of Portland cement (STC) and pouzzolanic fly ashes (PFA), with 100 kg of cement and 90 kg of PFA per cubic metre of RCC.

The hydration heat of the STC+PFA mix in these proportions is given in Figure 4. Values are expressed in Joules per gramme of cementitious material (STC+PFA). The details are given in the ThB_Data.xls file. Experimental points are plotted in red. It is suggested to use the curve plotted in brown for hydration heat production beyond the first week.

Figure 4 : Hydration heat curves for RCC and CVC

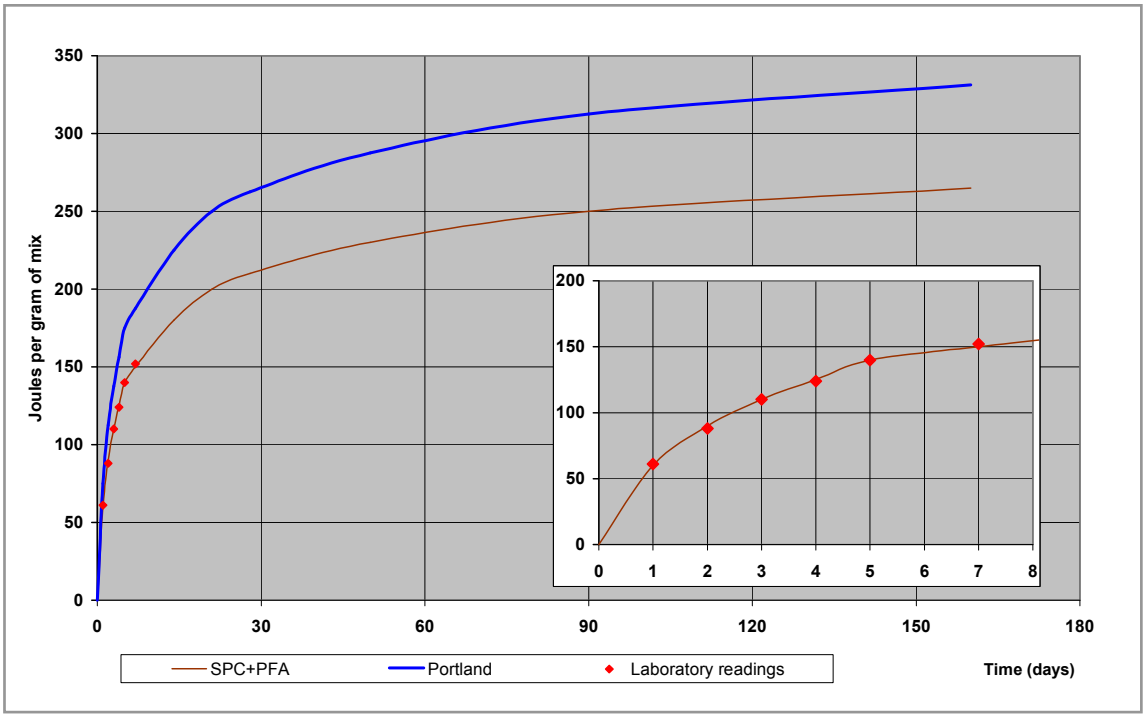

The conventional vibrated concrete used along the dam faces includes 350 kgs of Portland cement. No hydration heat curve is available for this material. If the Participants wish to incorporate CVC in their model, it is suggested to use the curve 'Portland' plotted in blue on Figure 4, which has been obtained simply by multiplying the one of the RCC mix by a factor of 1.25.

1.2.4. Instrumentation and readings

Electric thermo-couples have been placed inside RCC layers in several sections and elevations. Figure 1 shows the typical position of instruments at el. 35.00 and el. 50.70. Other thermo-couples have been placed at different places outside the dam which give the ambient temperature Vs time.

Temperatures of RCC and atmosphere have been recorded at uneven time intervals, from the time of RCC placement onwards.

1.2.5. Initial and limit conditions

Ambient temperature at site is given on Figure 5. It has been measured close to the dam faces at irregular dates. Details of readings are incorporated into the ThB_data.xls file. Except otherwise specified readings have been taken at **9:00 am.**

Initial RCC temperature, measured in the fresh material at the batching plant, is also given in Figure 5, as well as a few initial temperatures of RCC layers at the time of their placement. These data seem to indicate that the temperature of fresh RCC at the time of placement is substantially higher than that measured at the batching plant. In fact initial RCC temperature seems to be not far from that of air at the same time. It is therefore suggested to use ambient temperature as the initial RCC temperature wherever direct initial measurements are not provided.

Participants are free to consider the limit conditions of their choice at the foundation level, at the top of construction and along dam faces. The following may be of some help:

- the convection+radiation surface coefficient may be taken as α = 100 kJ/m²/h/°C
- the upstream face of the dam is facing the east.

Figure 5 : Initial temperature RCC and air temperature

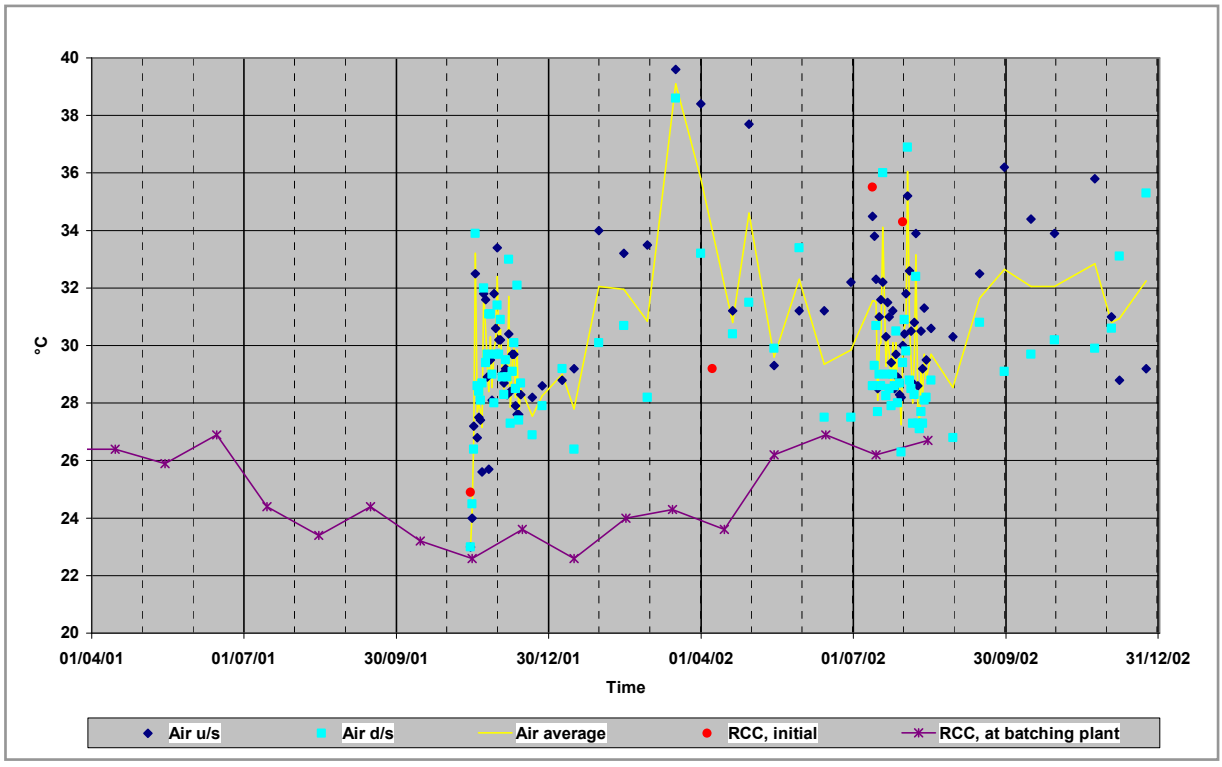

1.3 Requested Results

All Participants are kindly requested to provide a paper with 15 pages maximum, in which all assumptions are clearly exposed (especially as regards initial and boundary conditions). For comparison purposes, they must also give their key results under a prescribed format, in a EXCEL file derived from the **ThB_ResXXXX.xls** provided, where they will replace XXXX by an acronym of their organisation.

1.3.1. For all participants

Provide temperature variations in the heart of the dam vertical cross section at different levels and instants: fill the table in sheet '**Center_Results**' of ThB_ResXXXX.xls (the table is reproduced below as Table B), at least the yellow lines and columns.

Table B : Results to be provided along the dam centreline

(in sheet 'Center-Results' of ThB_ResXXXX.xls)

7th Benchmark workshop on Numerical analysis of Dams - Theme B - Results prepared by participant

Please fill the yellow cells *If possible do* ***not*** *modify the blue ones*

Results at center of horizontal sections

Center - Results Vs time			
Date	Value at center at el 35.00 participant	Date	Value at center at el. 50.70 participant
14/11/01		**13/07/02**	
17/11/01		20/07/02	
24/11/01		27/07/02	
01/12/01		03/08/02	
08/12/01		10/08/02	
15/12/01		17/08/02	
22/12/01		24/08/02	
29/12/01		31/08/02	
05/01/02		07/09/02	
12/01/02		14/09/02	
19/01/02		21/09/02	
26/01/02		28/09/02	
02/02/02		05/10/02	
09/02/02		12/10/02	
16/02/02		19/10/02	
23/02/02		26/10/02	
02/03/02		02/11/02	
09/03/02		09/11/02	
16/03/02		16/11/02	
23/03/02		23/11/02	
30/03/02		30/11/02	

Center - Results Vs elevation			
Elevation	Value at center on 27/07/02 participant	Value at center on 10/08/02 participant	Value at center on 28/12/02 participant
62,10			
61,50			
60,90			
60,30			
59,70			
59,10			
58,50			
57,90			
57,30			
56,70			
56,10			
55,50			
54,90			
54,30			
53,70			
53,10			
52,50			
51,90			
51,30			
50,70			
50,00			

1.3.2. Optional 2-D results

Provide temperature profiles along horizontal sections through the dam body, at 2 different levels and at 2 different instants: fill the table in sheet '**Resu_2D**' of ThB_ResXXXX.xls (the table is reproduced below as Table C), at least the yellow cells.

Table C : 2-D Results to be provided *(in sheet 'Resu_2D' of ThB_ResXXXX.xls)*

2-D results

2-D results Vs time			
Date	Value at T23 sensor (u/s, el 35.00) participant	Date	Value at T22 sensor (d/s, el. 50.70) participant
14/11/01		**13/07/02**	
17/11/01		20/07/02	
24/11/01		27/07/02	
01/12/01		03/08/02	
08/12/01		10/08/02	
15/12/01		17/08/02	
22/12/01		24/08/02	
29/12/01		31/08/02	
05/01/02		07/09/02	
12/01/02		14/09/02	
19/01/02		21/09/02	
26/01/02		28/09/02	
02/02/02		05/10/02	
09/02/02		12/10/02	
16/02/02		19/10/02	
23/02/02		26/10/02	
02/03/02		02/11/02	
09/03/02		09/11/02	
16/03/02		16/11/02	
23/03/02		23/11/02	
30/03/02		30/11/02	
06/04/02		07/12/02	
13/04/02		14/12/02	

2-D results Vs elevation			
Elevation	Value at 2 m from u/s face on 27/07/02 participant	Value at 2 m from d/s face on 10/08/02 participant	Value at 4 m from d/s face on 28/12/02 participant
62,10			
61,50			
60,90			
60,30			
59,70			
59,10			
58,50			
57,90			
57,30			
56,70			
56,10			
55,50			
54,90			
54,30			
53,70			
53,10			
52,50			
51,90			
51,30			
50,70			
50,00			
49,40			
48,80			

Horizontal profiles				
participant				
Elevation 50.70				
Cell	X=	27/07/02	10/08/02	28/12/02
u/s	-5,72			
T14	-5,00			
T15	0,00			
T17	15,00			
T19	30,00			
T22	40,00			
d/s	43,44			
participant				
Elevation 35.00				
Cell	X=	27/07/02	10/08/02	28/12/02
u/s	-12,00			
T23	-10,00			
T26	0,00			
T29	25,00			
T32	45,00			
T35	55,00			
d/s	56,00			

2. SOME ADDITIONAL INFORMATION ON THA-DAN DAM IN THAILAND

The problem proposed for Theme B is closely inspired from THA DAN dam, now under construction in Thailand. This dam was designed by Coyne et Bellier for the Royal Irrigation Department. The project's function is to improve irrigation development in the Region, which has periodically suffered from drought and flooding. It is located on a tributary of Nakon Nayok River about 120 km North east from Bangkok.

The dam is a RCC gravity dam, with a crest length of 2 600 m and a maximum high of 92 m. With a total volume of concrete of 5.5 10^6 m^3, of which 5 10^6 m^3 is RCC and 5 10^5 m^3 is conventional concrete, it will be the world's largest RCC dam in terms of volume. The upstream and downstream dam faces of the dam are constructed with horizontally slip-formed facing element which provide a durable external face and construction support for RCC placement. Conventional vibrated concrete poured between the upstream facing element and the RCC is the waterproof component of the dam. The RCC mix, which is made with Portland cement, fly-ash and crushed aggregates produced at site, has an average compressive strength at 91 days of 18 MPa.

The construction supervision Engineers for Tha Dan Project are Coyne et Bellier working with Asdecon Corporation and Team Consulting Engineer (both of Thailand). The RCC placing has started on March 2001. The maximum monthly placing rate has reached 200 000 m^3 while the average placing rate is 135 000 m^3 per month. The RCC is produced by two continuous mixing plants having a total capacity of 2 400 tons per hour, and is transported by belt conveyors and dump trucks.

Figure 6 - Thadan RCC dam under construction (end 2002)

The hydration curve of the cementitious mix was measured using the LANGAVANT method, which gives reliable results only in the first 5 to 7 days. The development of heat after the first week is considered negligible for standard concrete structures, but it is of great importance for thick sections such as gravity dams. The only reliable means to estimate it is to make large test blocks on site, at least 4 metre wide and high. This was

unfortunately not possible at Tha Dan, so the hydration heat curve at long term was unknown. For this reason, the curve that has been provided as input data had to be calculated by adjustment with the temperature development readings. In other terms, the Formulator had to carry out the reverse exercise. This has been done using TetaBCR, a software especially developed for temperature prediction in concrete and RCC structures during construction.

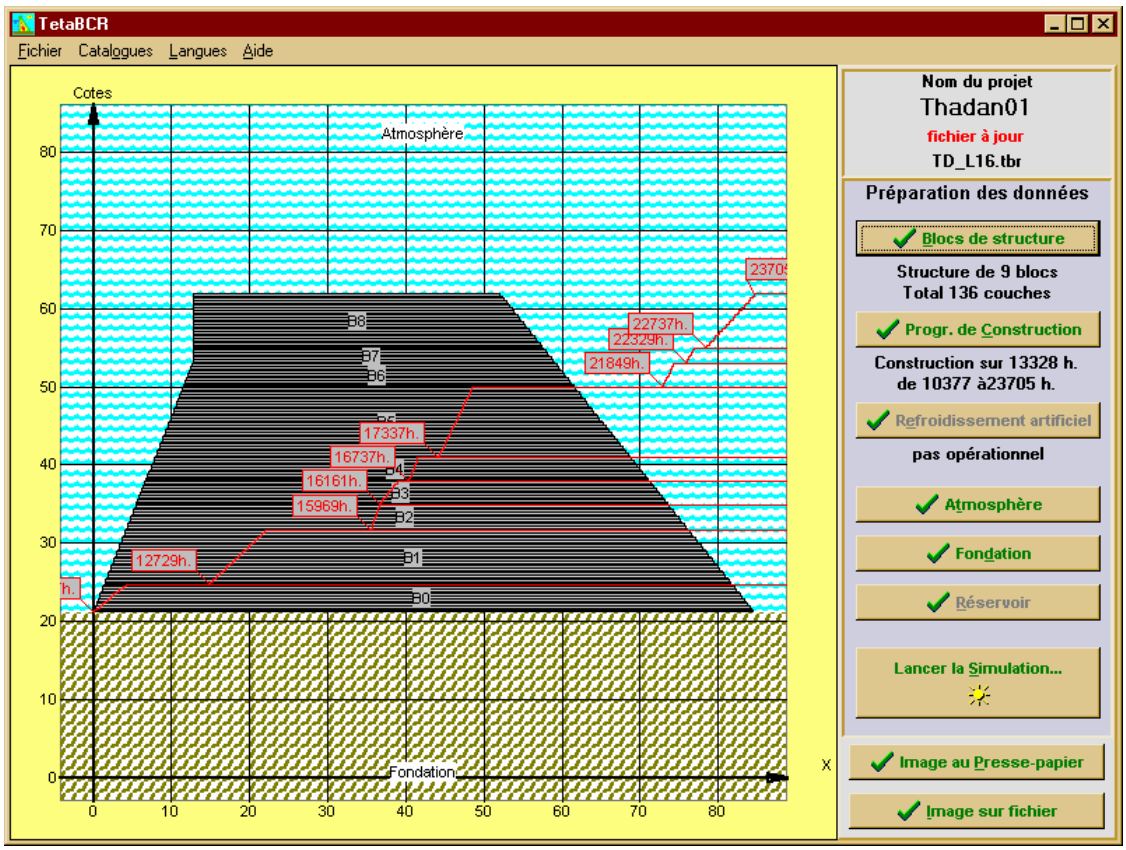

Figure 7 - Thadan model with TetaBCR

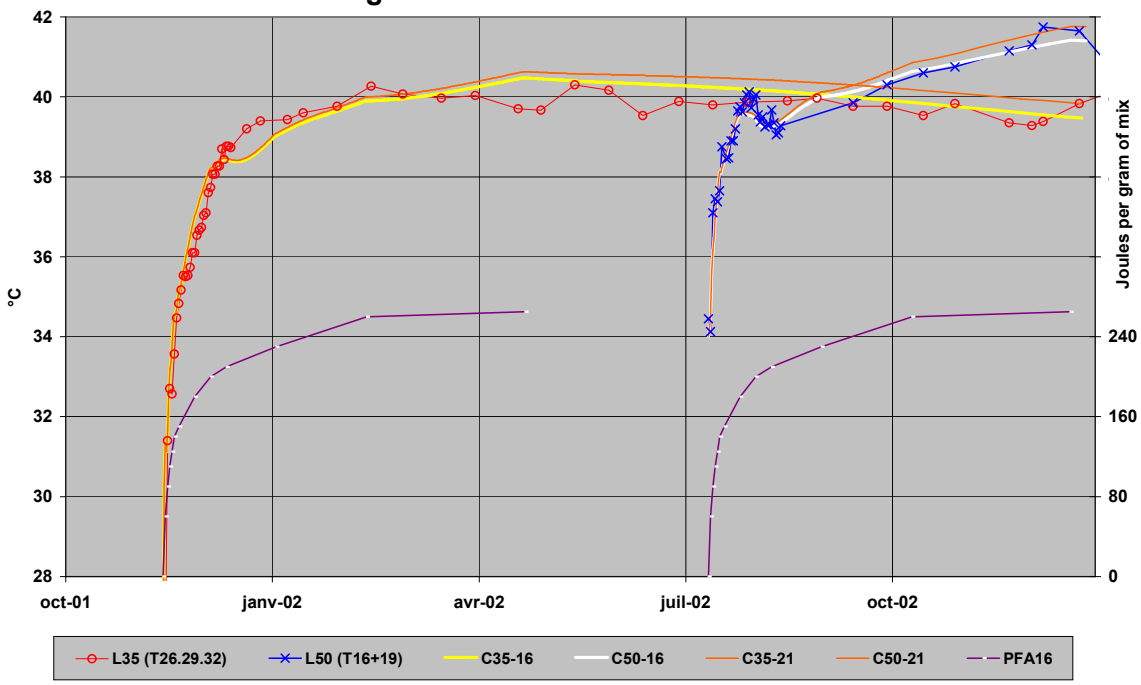

Figure 8 - Adjustment of hydration curve with site readings

3. PARTICIPANTS TO THE EXERCISE

Seven participants have proposed results. Their names are given below in the order of reception of their contributions (*1*).

P1 Thermal analysis of a RCC dam during construction using FLAC

by António Tavares de Castro (LNEC),
Teresa Santana (New University of Lisbon),
Noemí Schclar Leitão (LNEC), Lisbon, Portugal

P2 Thermal analysis of an RCC gravity dam during construction by bi-dimensional solution proposed by Stucky-Comsa

by Jean-Luc Sarf, ComSA Consulting Engineering,
Alexandre Wohnlich, STUCKY Consulting Engineers Ltd, SWITZERLAND

P3 Thermal analysis of an RCC dam body during construction

by Mojtaba Farrokh, Sharif University, Teheran,
Gholamreza Khoshrang, Mahab Ghodss Consulting Engineers, Teheran, Iran

P4 Thermal analysis of a RCC dam during construction

by Francesco Amberg, Lombardi Engineering Ltd, Switzerland

P5 Stress and strain state 2D modeling by the finite element method in a RCC dam acted by the cement hydration heat during the construction period

by Gheorghe Lazar,
Serban Nicoara,
Albert Titus Constantin, University of Timisoara, Romania

P6 Bidimensional thermal analysis of a RCC dam during construction

by Lucian Ilie, Labora Consulting, Paris, France,
Adrian Popovici, Radu Sârghiuta, Altan Abdulamit, Cornel Ilinca,
Technical University of Civil Eng. of Bucharest, Romania

P7 Thermal analysis of a RCC gravity dam

by Franz Perner, Verbundplan GmbH, on behalf of Verbund-Austrian Hydro Power, Salzburg, Austria

---

1 *A paper without a solution to the problem was also received from S. Ginsburg and al. "Parameter identification in mathematic model of temperature regime of rolled concrete dams during construction"*

All of them have carried out 2-D analyses, and Participant n°7 carried out also a 1-D vertical analysis. Two of them also gave the stress field resulting from the temperature variations, using additional assumptions on the mechanical properties of the materials. The Table D below gives a summary of the contributions.

Table D

Participant	Software	Observations
P1	FLAC	T air sinus function - Foundation 10 m
P2	Z_Soil	Adiab. foundation – Stress analysis
P3	ANSYS	Foundation at 30°C
P4	owner	Specific convection model at top
P5	ANSYS	Stress elastic analysis
P6	ANSYS	Foundation at constant temperature
P7	ABACUS	1-D and 2-D analyses

Note : During the Workshop, Participants were invited to propose minor amendments to their results if they found it useful, and to send them before the end of the year. This final version of the Synthesis on Theme B takes into consideration modifications to initial results received to date, as follows :

- Participant n°3 made a correction to their initial 2-D results, which were originally confused with their 1-D results,
- Participant n°6 carried out a new analysis whose results are completely different from those presented at the Workshop.

4. COMPARISON OF RESULTS AND SITE READINGS

Results provided by Participants are plotted together on following Figures 9 to 21, together with readings where applicable.

4.1 Temperature variations along the central line

See Figures 9 and 10.

Participant n°5 did not provide results on the dam centreline.

Participant n°7 provided results of both 1-D and 2-D analyses along the centreline. It has been noticed that the difference at any place and time is never higher than 0.2°C.

Most of results provided fit rather well with site readings and with the adjustment curve calculated to calibrate the hydration heat curve on the long term.

At elevation 35, the maximum temperatures given by Participants range between 39 and 42.5°C, while the measured maximum is 40.5°C. The temperature raise in the first 5 months is well reproduced, except by Participants P6, and P7 to a lesser extent. The differences are likely to be due to the shape of the hydration curve they used. Differences are also due to assumptions on the initial RCC temperature at placement time, for which some degree of uncertainty was left in the problem formulation.

At elevation 50.70 all curves are very similar, with offsets clearly due to different assumptions on the initial RCC temperature. Participants n°2, 3, 4 and 7 give a realistic shape of the first temperature peak after 20 days.

4.2 Temperature distribution Vs elevation along the central line

See Figures 11 to 13.

Site readings are available at only 2 levels, which are plotted as red circles. The curves calculated for calibration are also given. The shapes of most curves are similar with some offsets probably resulting from initial conditions.

One can also notice that the lower part of curves is more different than in elevation, especially in July and August. This results from different methods used to model the foundation (adiabatic, constant temperature, incorporated in the model or not). The calibration analysis has been done with integral equations.

In July, all curves reproduce the minimum temperature at El. 48 and the peak value at El. 50.70. Participant n°7 gives colder values close to the top, which suggests that the dissipation from the top level be overestimated. On the opposite Participant n°4 is on the high side.

In August, curves given by Participants n°1, 6 and 7 are again on the low side.

4.3 Temperature variations close to dam faces

See Figures 14 and 15.

Results close to the dam faces are more dispersed than those along the centreline.

The reason comes likely from:

- different ways of modelling the boundary conditions,
- consideration or not of the CVC as such, which dissipates more heat than the RCC,
- consideration or not of the shuttering transmittivity.

At Elevation 35 for cell n°23 placed at 2 metre from the upstream face, the maximum temperatures given by Participants range between 33.5 and 39°C, while the reading gives 41°C (probably because of the proximity to the CVC layer). Final temperatures calculated range between 30 and 33.5°C, while the reading is 34°C. Curves provided by Participants n°2, 3 and 4 reproduce rather well the first peak at around 2 weeks, as well as Participant n°7 at a lower level.

At Elevation 50.70 for cell n°22 placed at 3.44 metre from the downstream face, most of curves except that of Participant P6 are parallel to the readings. Participants n°2, 3 and 4 provide the best predictions. Curves from P5 and P7 are quite much lower than readings.

4.4 Temperature distribution Vs elevation close to dam faces

See Figures 16 to 18.

Points from site thermometers are plotted for reference with their distance to the face. Only at elevation 35 the sensor position corresponds to the requested distance of 2 metre (Figure 16).

The curve given by Participant n°3 for the distribution of temperature at 2 metre behind the downstream face on 10/08/02 in their presentation at the Workshop was similar to that on the dam centreline. This mistake has been corrected on the present Figure 17.

Except for simiulations done by Participant n°5, all curve present similar shapes for each key date. It is noticed that the dispersion is more for downstream results (August and December) then for the upstreapm side (July).

4.5 Temperature U/S to D/S profiles

See Figures 19 to 21 corresponding to the 3 key dates.

Experimental points are plotted in red (dark) circles on these graphs. Except for curves given by Participant n°5, sections given by calculations fit rather well with the readings. Only the strong increase of temperature on the upstream side in July and August at el. 50.70, which is due to the proximity of the CVC, has not been reproduced.

All these curves clearly show that the heat dissipation in the horizontal direction has only a marginal influence on the temperature distribution in the centre of the dam.

5. DISCUSSION AND CONCLUSION

This Theme B attracted the attention of not less than 7 Participants, and actually 9 different thermal analyses were carried out, since Participant n°7 presented two simulations (1-D and 2-D) at the workshop, and Participant n°6 made a second analysis after the meeting. In this respect, this exercise is one of the most successful among those proposed from the beginning of the Benchmark workshops of the Ad-Hoc Committee on Numerical analysis of Dams.

Even if most of results are not so far from readings made on the reference dam, not all simulations have given similar results. Differences as large as 8°C between results may be found at some places and instants of the simulations. This is not negligible, if one reminds that the total adiabatic temperature rise in the problem formulation is about 21°C. It is therefore worthwhile to investigate where such discrepancies come from.

1 Theory

Equations of thermal exchanges inside a solid body and at its boundaries with air and/or water are perfectly known, including convection and radiation. There is therefore no uncertainty coming from this aspect.

2 Numerical formulation

Algorithms and equations representing conduction and convection generally refer to an explicit/implicit finite-difference scheme in the time dimension. The main problem with such equations is that of unstability, which is easily identified and easily solved by adopting small enough time steps. There is no evidence of any such unstability in any of the results provided.

Another less evident problem may come from the mesh fineness, which must be fine enough to match the high gradients close to the exposed faces and give adequate estimation of the face dissipation. But since the time step is linked to the spatial distance between nodes, one is reluctant to excessively reduce it. One participant tested two mesh finenesses, with dimensions of 30 and 3 cm, corresponding to time steps of 1 and 0.01 hour. Only a small difference was observed at the very beginning of the simulations.

Simplifications

One difficulty of the exercise was the large number of RCC layers to be placed successively upon each other, with the consequence that the model boundaries change each time. All participants rejected any simplification in this respect, and all faithfully followed the construction programme described in the data, although it was not regular and therefore not prone to easy automation of loading. The time of cover of each RCC layer was therefore well represented, which was essential since most of the heat dissipates upwards.

Simplifications were made on the dam faces and relevant boundary conditions, which did not influence much the results except close to the faces.

More debatable simplificative assumptions were also made on the lower boundary of the model, for which Participants were free to adopt boundary conditions of their choice. Some used adiabatic or isotherm conditions, while others included some part of the foundation in their model. Significant differences in the first 10 metres above the ground level are shown, which are likely to come from these different assumptions.

Selection of parameters

Two major parameters have a strong influence on the temperature field, which are the hydration curve on the one side, and the initial RCC temperature on the other.

While basic thermal parameters of materials (density, specific heat, and conductivity) can be rather well determined with careful laboratory tests, it is very difficult to measure the hydration heat of cement after some days. The only way to obtain reliable values is to prepare a concrete test block of a reasonable size (say at least 4 x 4 x 4 metre) with a good instrumentation. Such test was not available for the construction of THA DAN dam and a hydration heat curve was derived from a back analysis, to avoid Participants to be confronted with this question. However the importance of even small differences in hydration heat values appears clearly.

Regarding the initial temperature of RCC at the time of placement of each layer, the information provided by the works was neither complete nor accurate, and Participants were therefore given some flexibility to select what they felt to be the best assumption. A large part of the difference between results likely comes from this degree of freedom.

As a conclusion…

The thermal analysis, which was the subject of Theme B, is only the first part of a more global problem, which should be continued with the corresponding mechanical analysis. Some participants tentatively carried out such analysis with approximate mechanical parameters. Here again, the main uncertainty comes from the difficult determination of mechanical parameters such as deformability, creep, and tensile resistance as a function of time or maturation. But this is another story, which might be the subject for a next Benchmark Workshop…

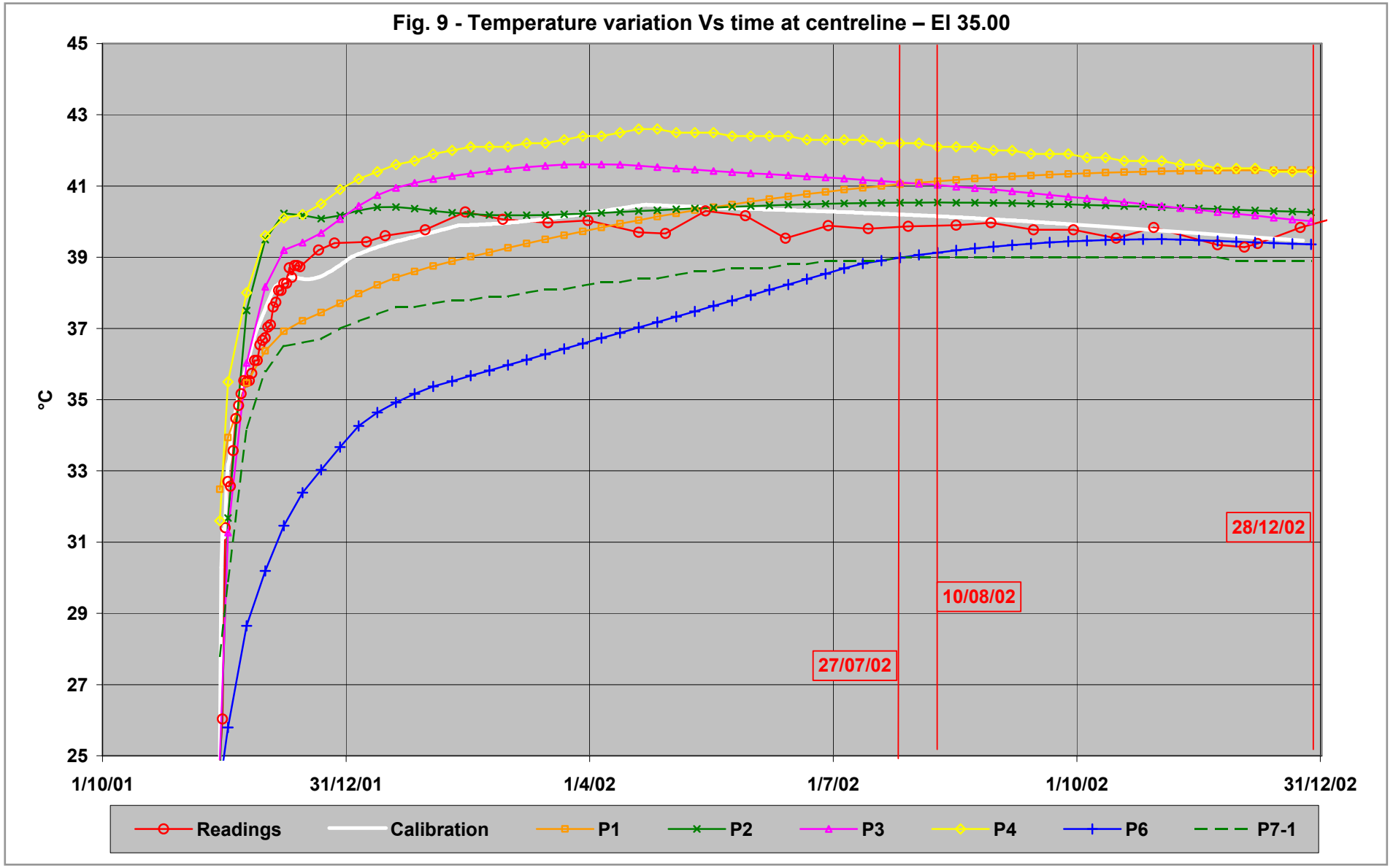
Fig. 9 - Temperature variation Vs time at centreline – El 35.00
°C
45
43
41
39
37
35
33
31
29
27
25
1/10/01
31/12/01
1/4/02
1/7/02
1/10/02
31/12/02
27/07/02
10/08/02
28/12/02
Readings
Calibration
P1
P2
P3
P4
P6
P7-1

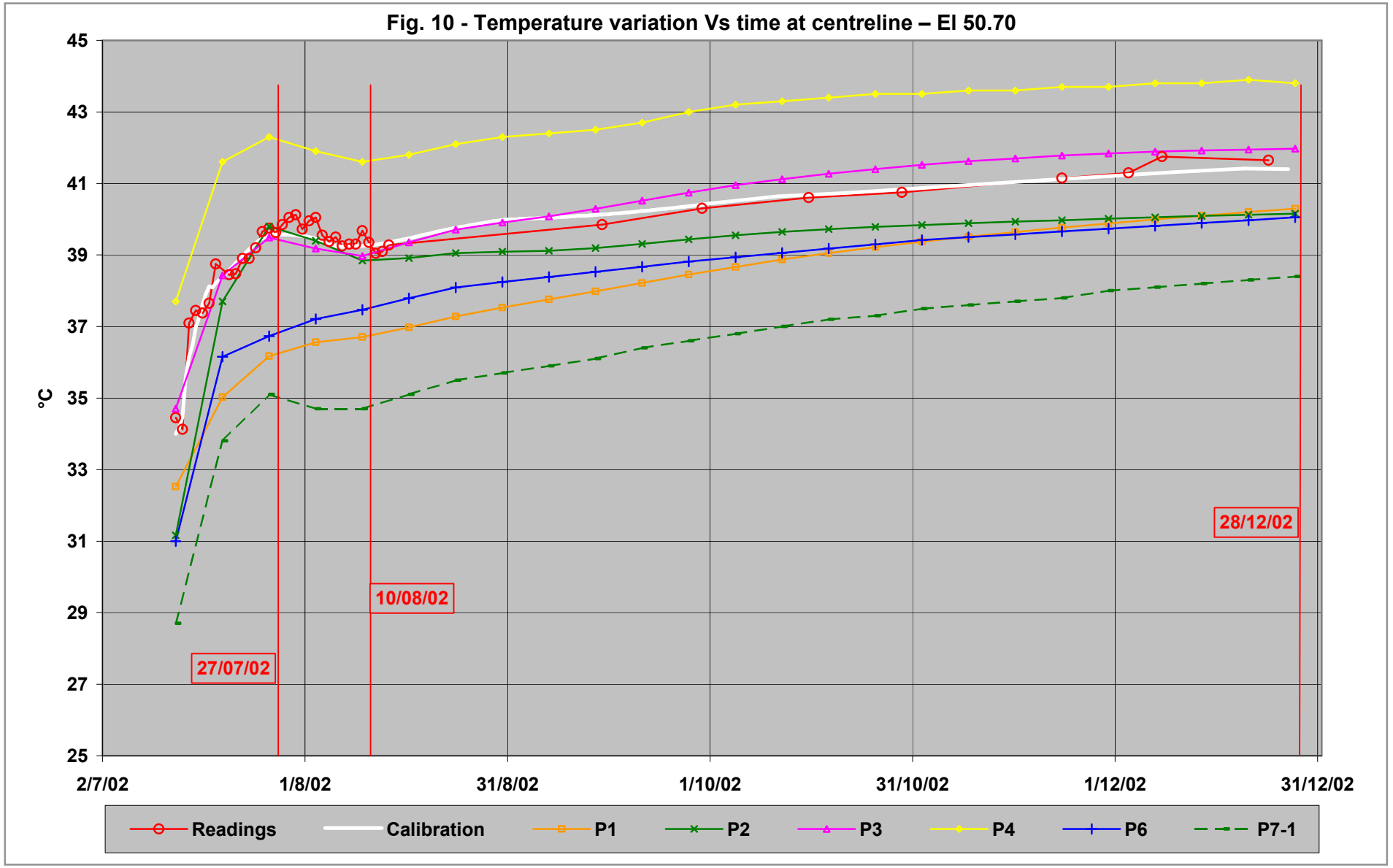
Fig. 10 - Temperature variation Vs time at centreline – El 50.70
°C
45
43
41
39
37
35
33
31
29
27
25
2/7/02
1/8/02
31/8/02
1/10/02
31/10/02
1/12/02
31/12/02
27/07/02
10/08/02
28/12/02
Readings
Calibration
P1
P2
P3
P4
P6
P7-1

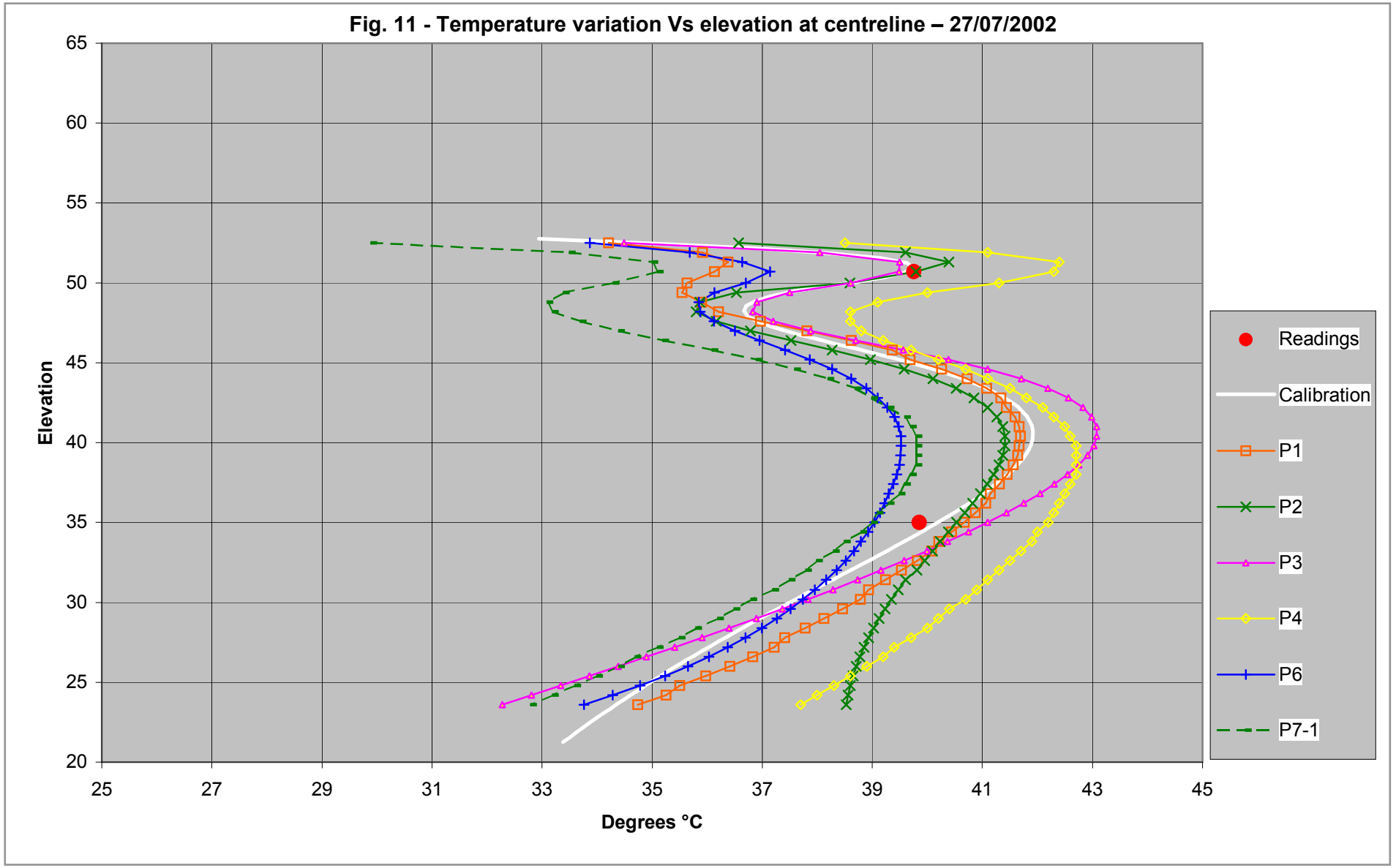
Fig. 11 - Temperature variation Vs elevation at centreline – 27/07/2002
Elevation
65
60
55
50
45
40
35
30
25
20
25
27
29
31
33
35
37
39
41
43
45
Degrees °C
Readings
Calibration
P1
P2
P3
P4
P6
P7-1

Fig. 12 - Temperature variation Vs elevation at centreline – 10/08/2002

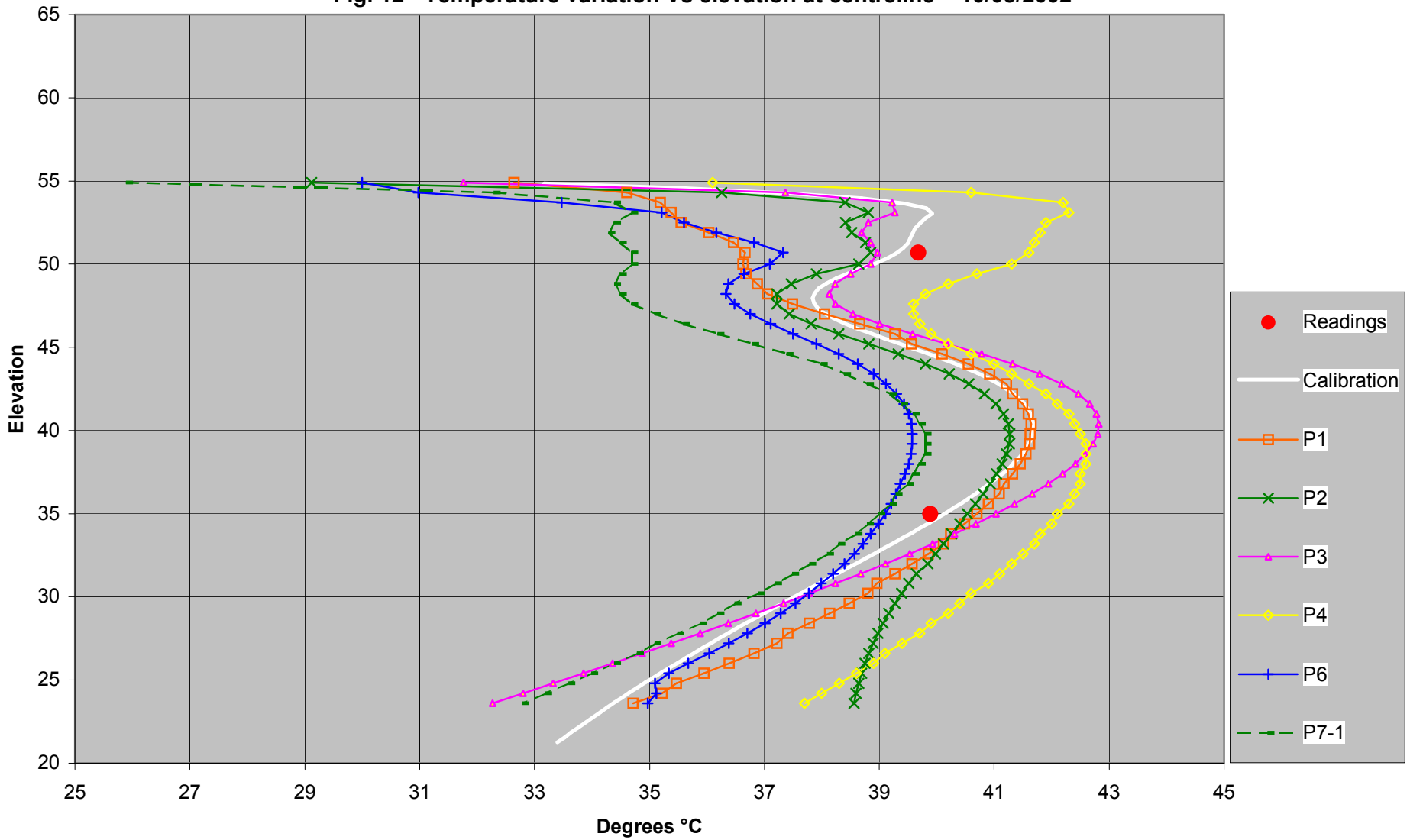

Fig. 13 - Temperature variation Vs elevation at centreline – 28/12/2002

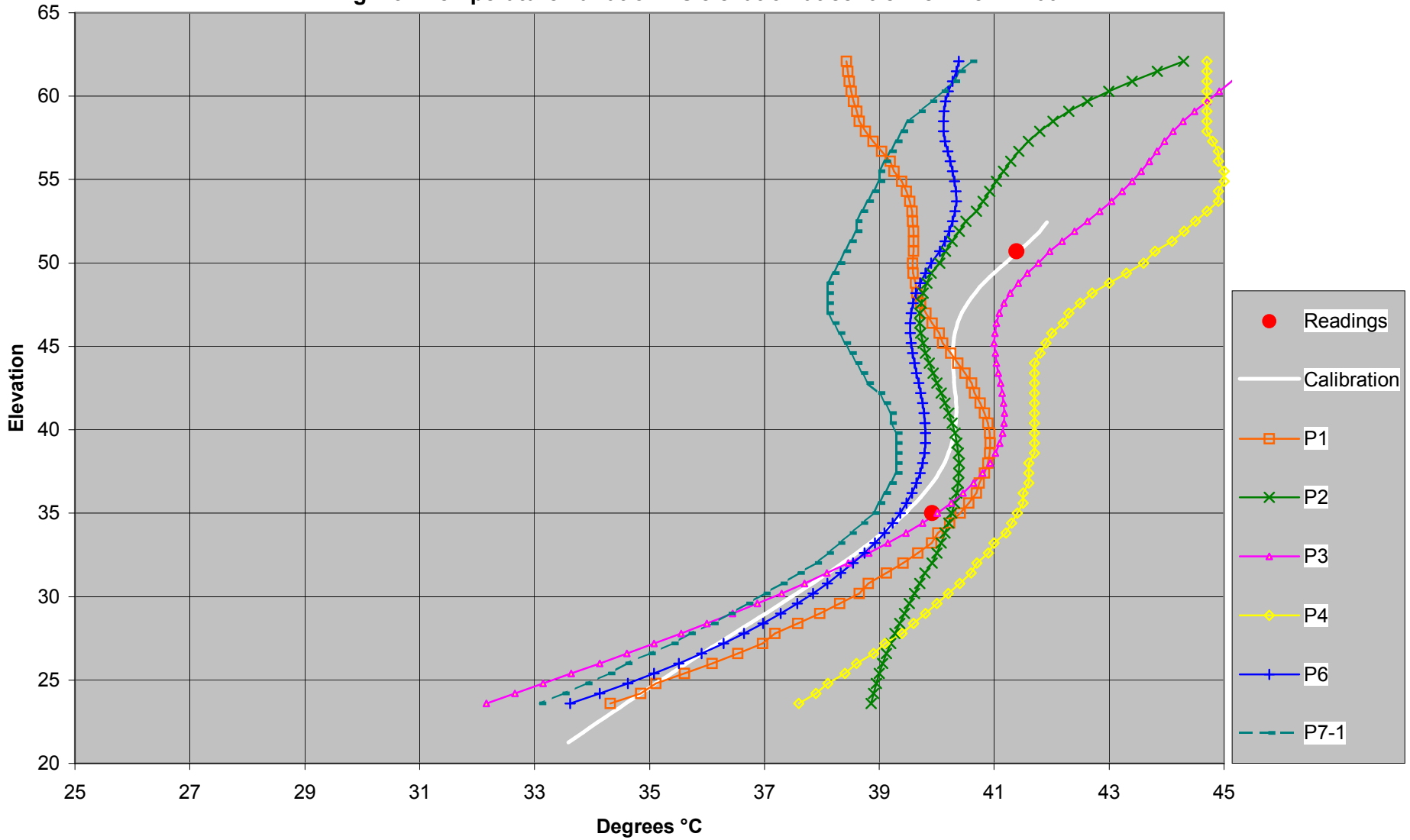

Fig. 14 - Temperature variation Vs time at cell n°23 (2 m from the upstream face) – El 35.00

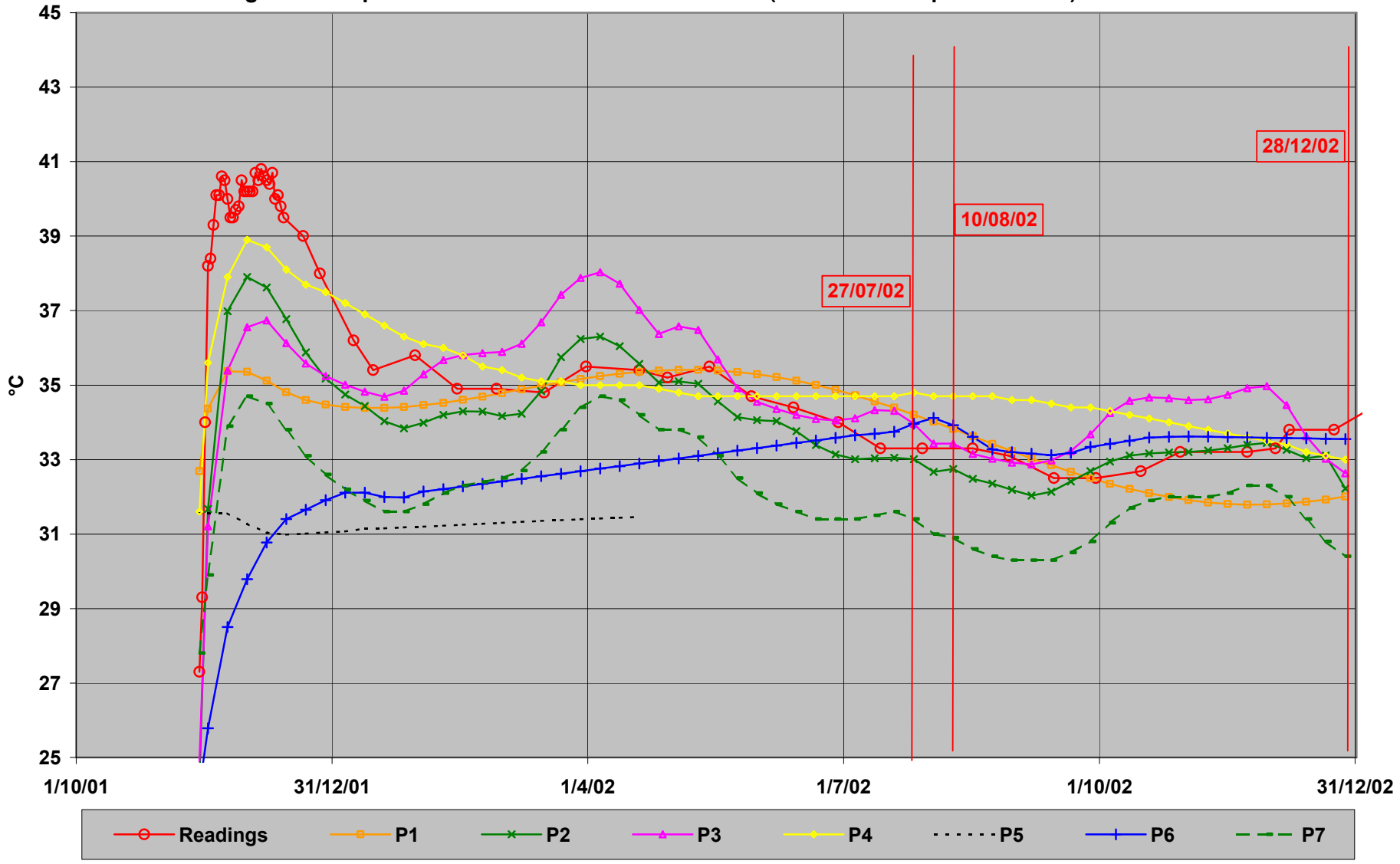

Fig. 15 - Temperature variation Vs time at cell n°22 (3.44 m from the downstream face) – El 50.70

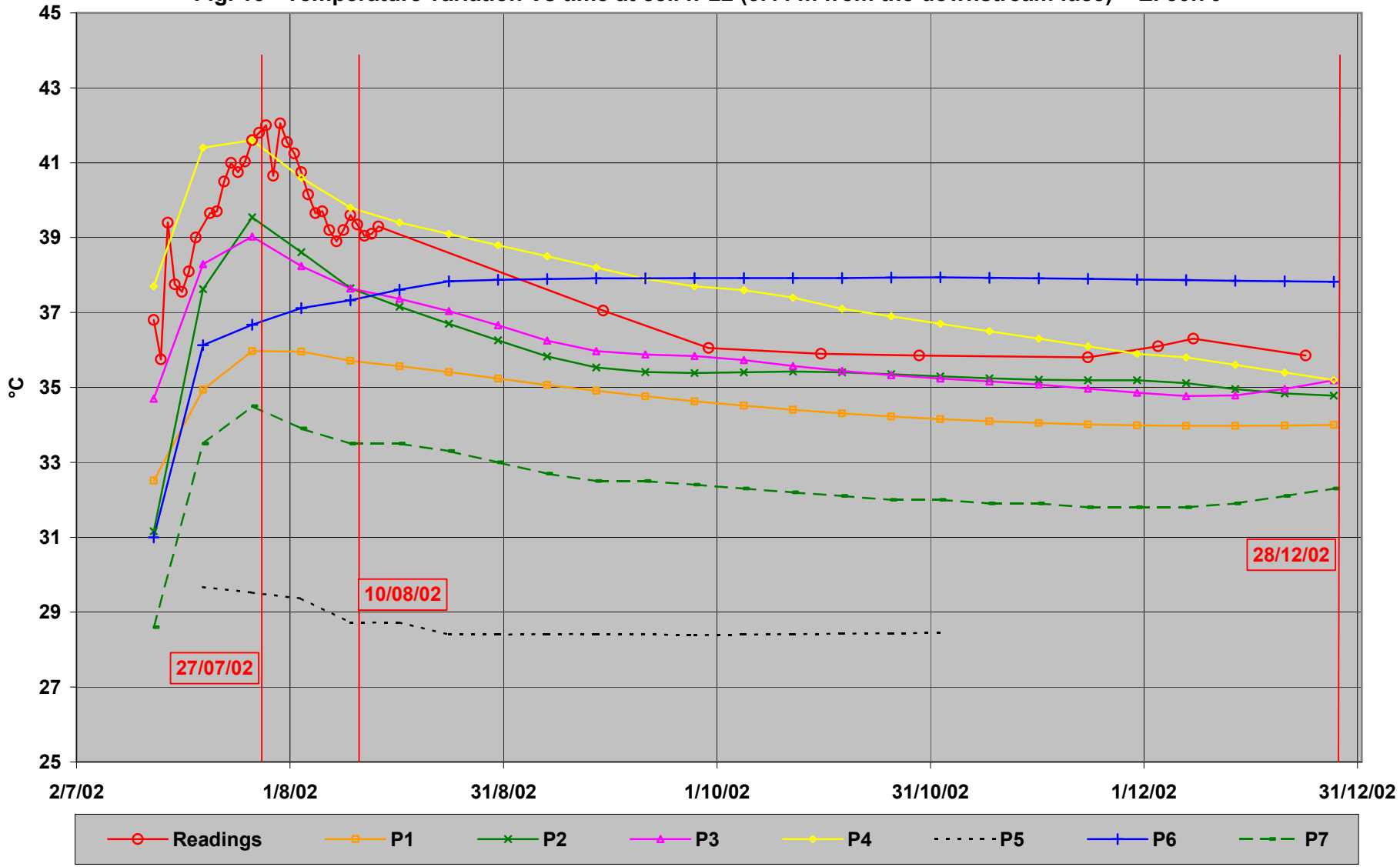

Fig. 16 - Temperature variation Vs elevation at 2 metre from the upstream face – 27/07/2002

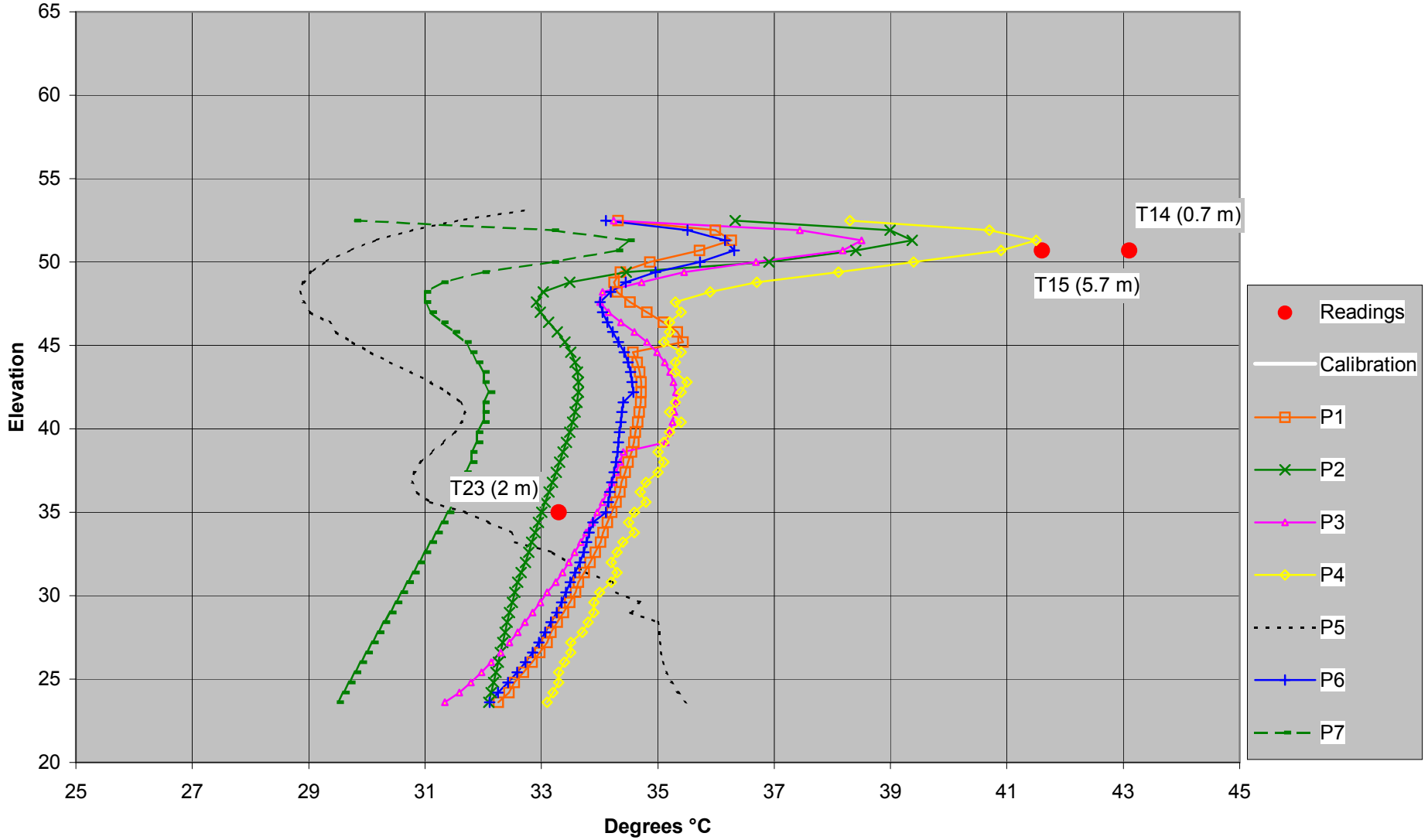

Fig. 17 - Temperature variation Vs elevation at 2 metre from the downstream face – 10/08/2002

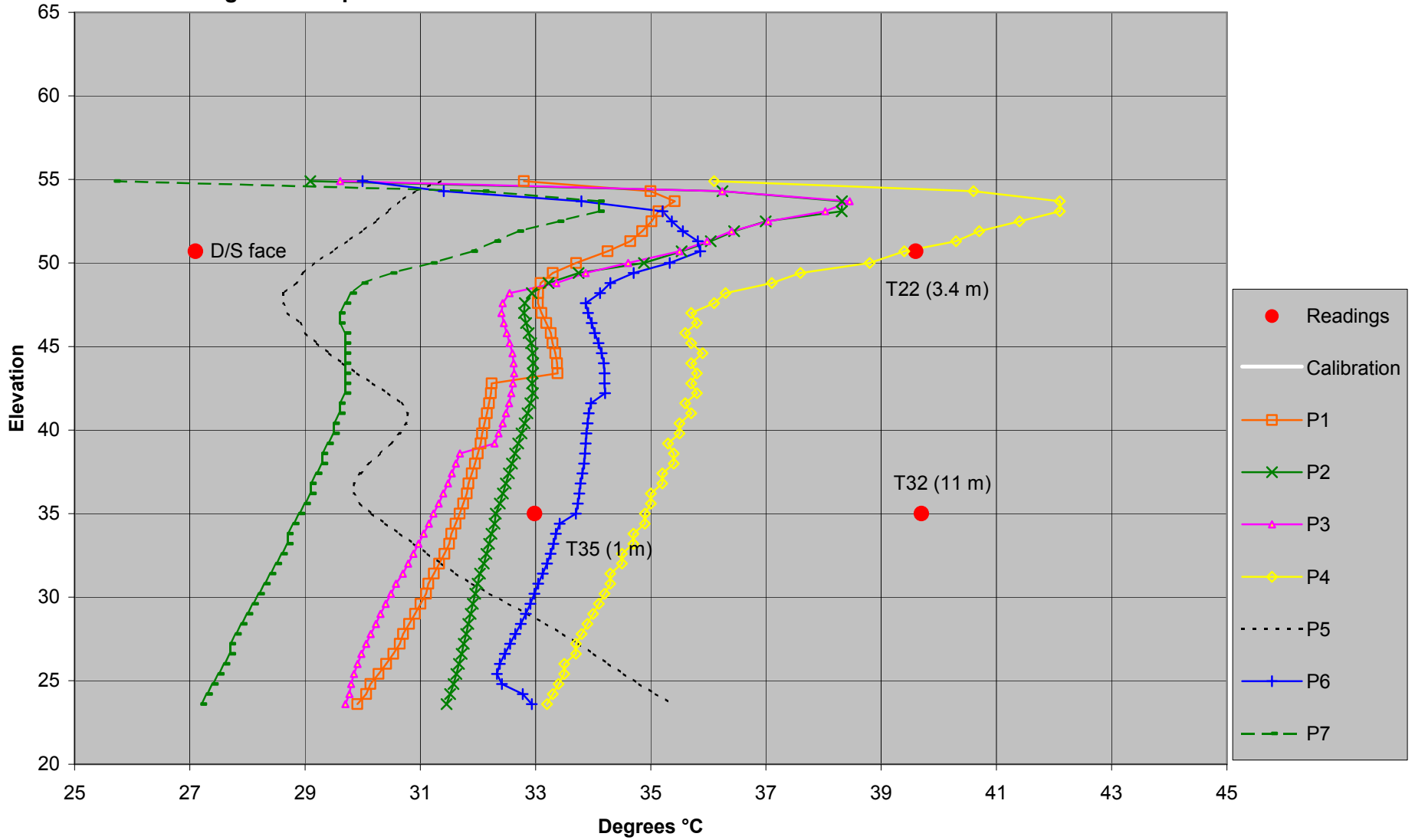

Fig. 18 - Temperature variation Vs elevation at 4 metre from the downstream face – 28/12/2002

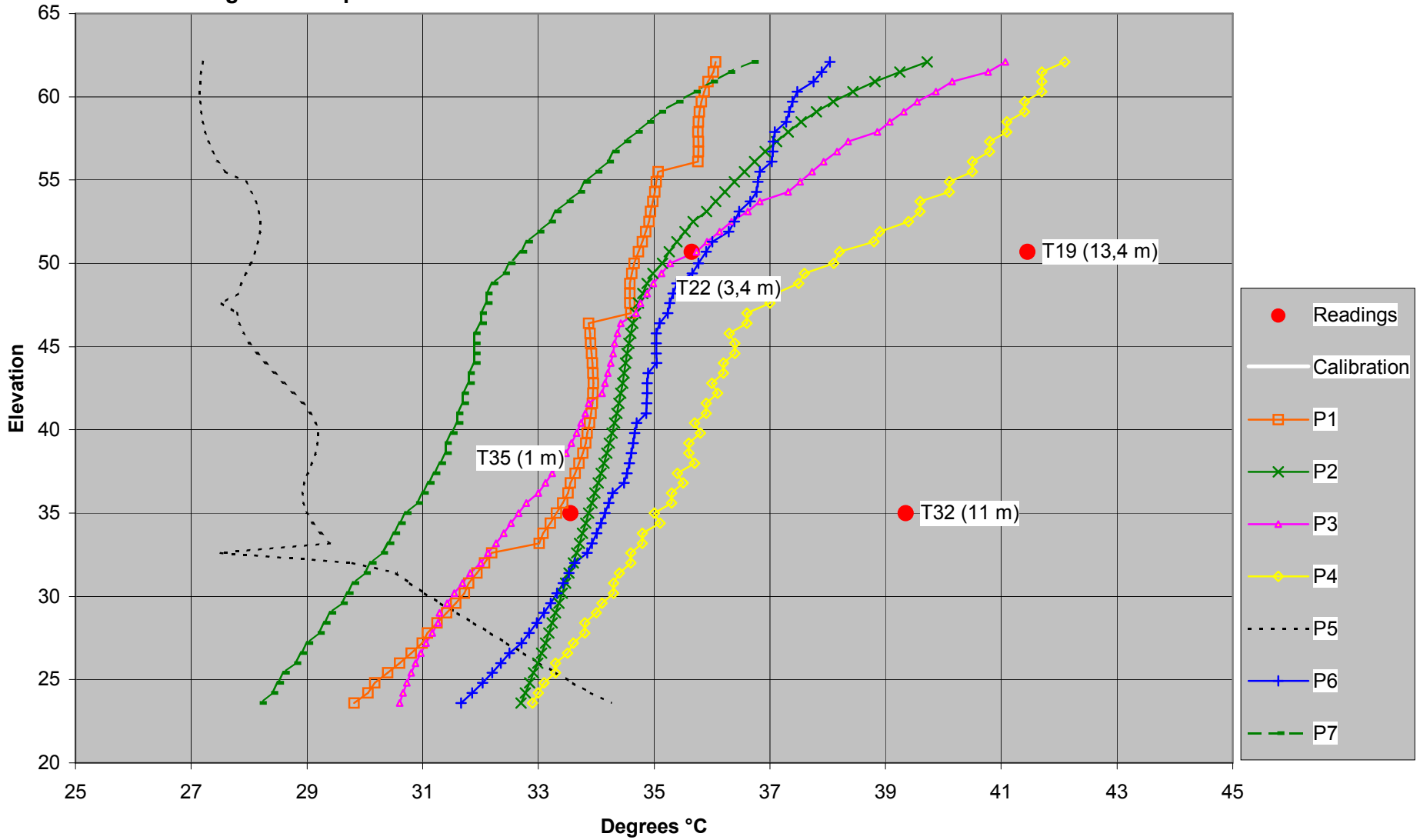

Fig. 19 – Temperature horizontal distribution on 27/07/2002

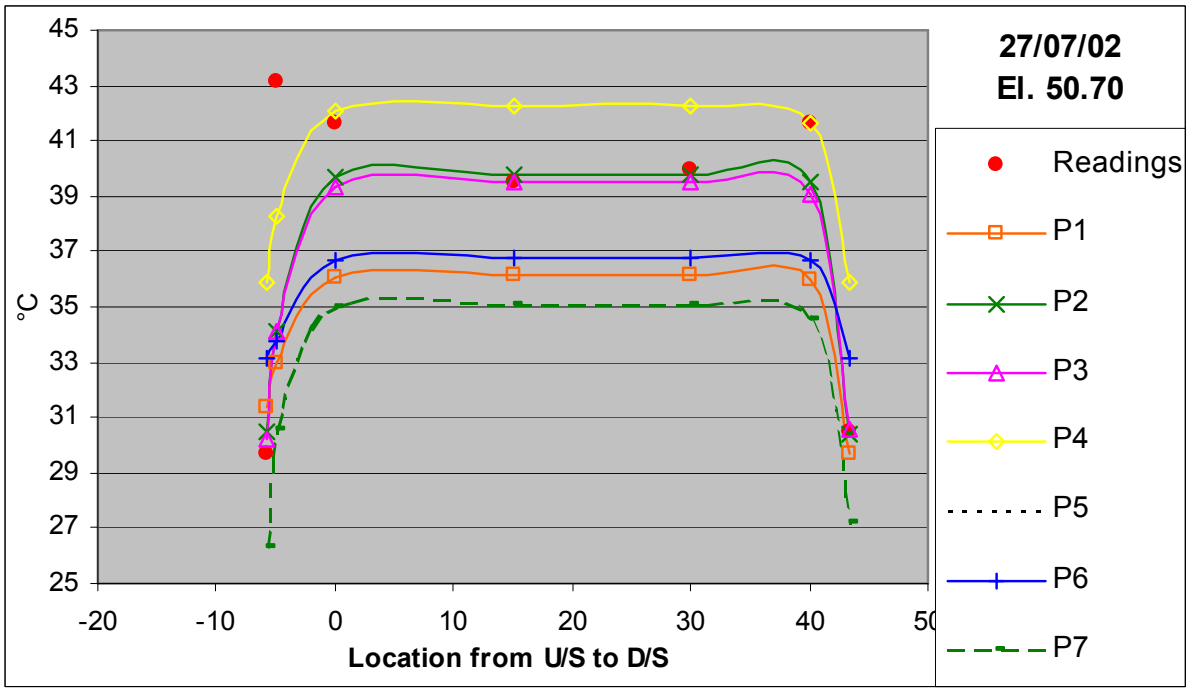

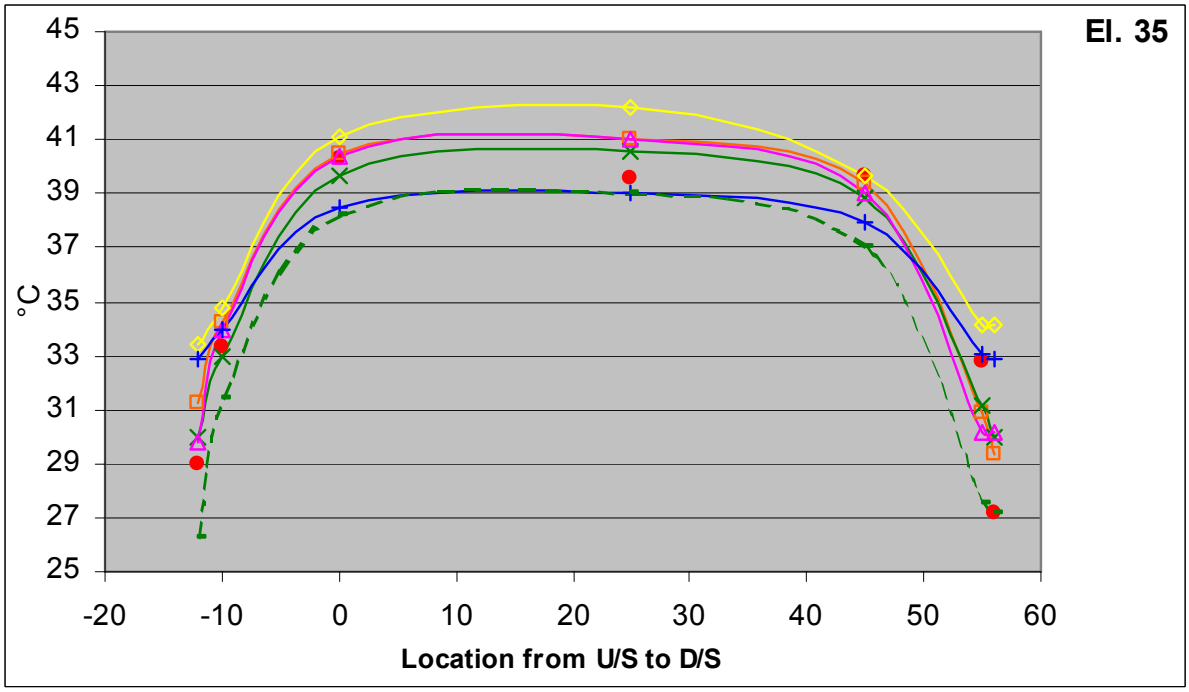

Fig. 20 – Temperature horizontal distribution on 08/08/2002

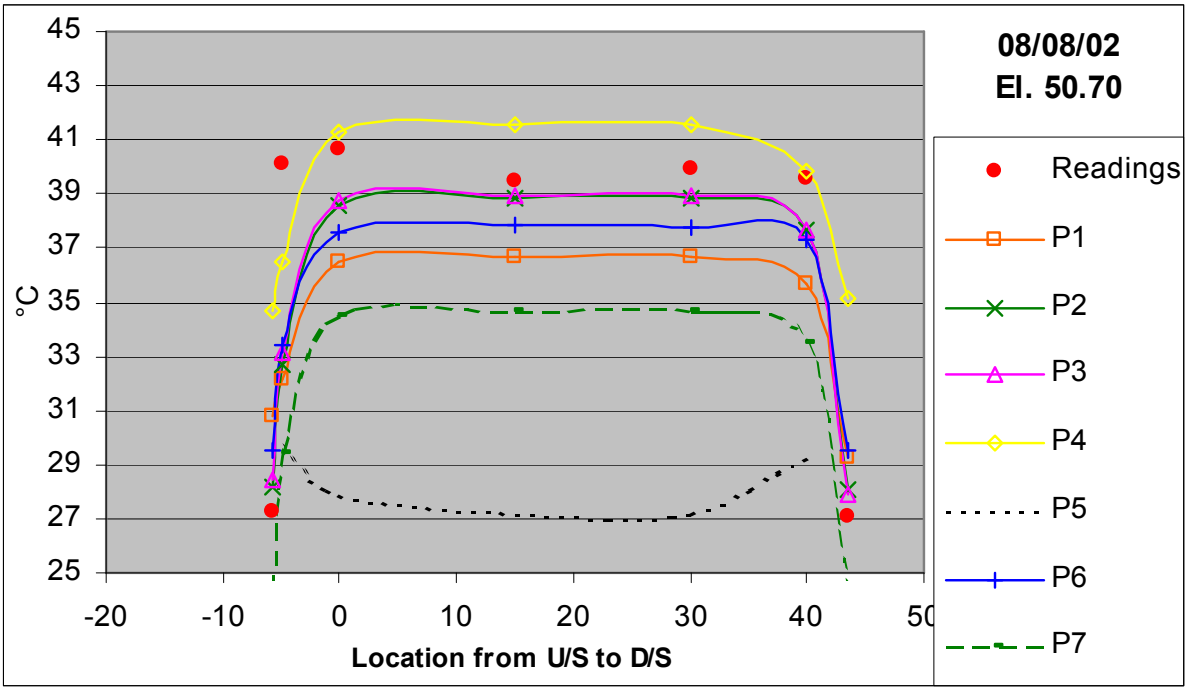

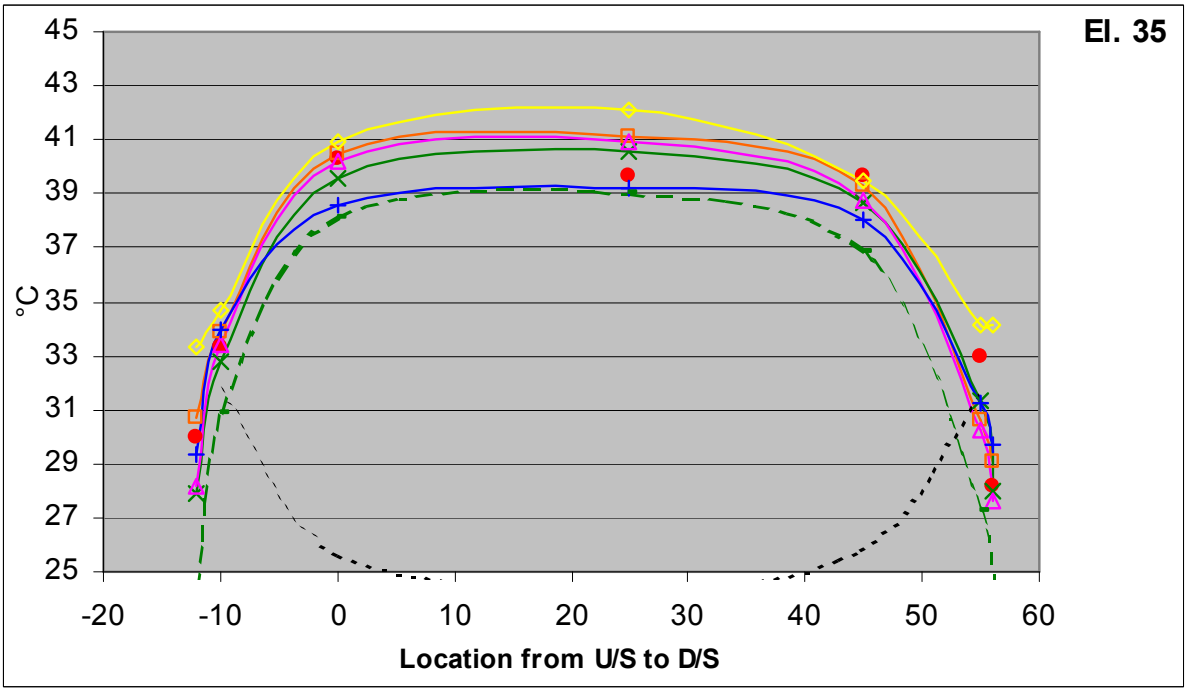

Fig. 21 – Temperature horizontal distribution on 28/12/2002

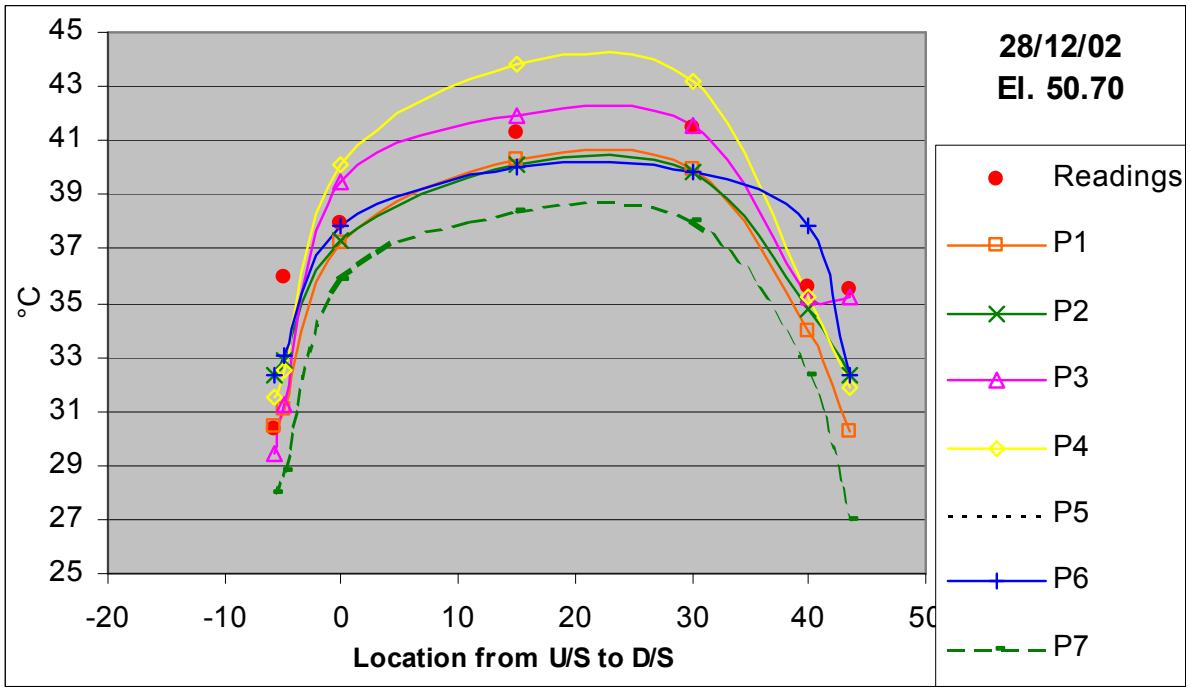

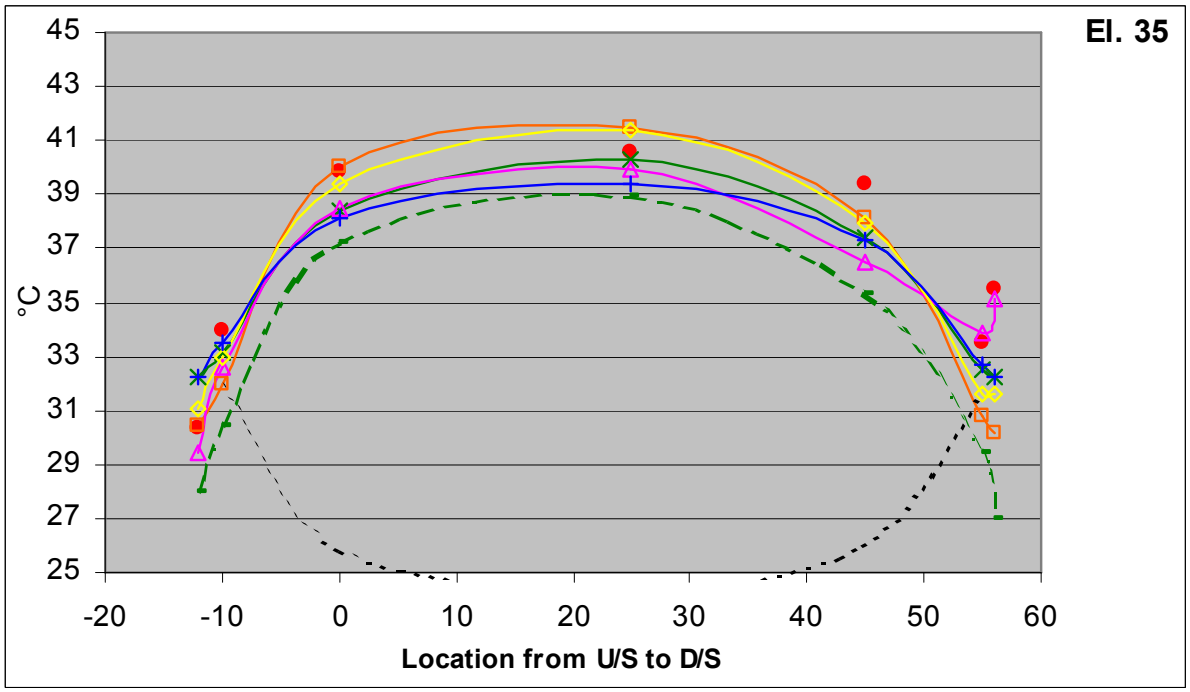

THERMAL ANALYSIS OF A RCC DAM DURING CONSTRUCTION *

Francesco Amberg
Lombardi Engineering Ltd., SWITZERLAND

SUMMARY: The paper presents a study carried out to evaluate the thermal behavior of a 92 m high RCC dam during construction. This calculation exercise was proposed in the frame of the 7th Benchmark Workshop on Numerical Analysis of Dams organized by the ICOLD, with the aim to provide a critical examination of the computational methods used for dam analyses.
The simulation considers in a very detailed manner the conditions on a dam site, as the concreting schedule, the curing and protection of the surfaces, the development of the hydration heat; this obviously in relation to the environmental conditions, i.e. the air and water temperature, the solar radiation and the reservoir level. The analysis was carried out in a 2-D section of the dam body using a software developed by Lombardi Ltd. to analyze this type of problems. The software, based on the explicit Finite Difference Method, has already been used in a number of thermal analyses [see 1] with the purpose to define and optimize the cooling process for dams or to evaluate the thermally induced stresses and deformations.

RÉSUMÉ: L'article présente une vérification du comportement thermique d'un barrage-poids en BCR de 92 m de hauteur. L'exercice de calcul a été proposé dans le cadre du 7ème *Benchmark Workshop* en Analyse Numérique des Barrages organisé par la CIGB, dont le but est la comparaison et l'évaluation des méthodes numériques utilisées pour l'analyse des barrages.
Toutes les conditions qui peuvent se présenter au cours de la vie du barrage sont prises en compte dans l'analyse: ainsi le programme de bétonnage, le curage et la protection des surfaces, le développement de la chaleur d'hydratation, etc. tout en considérant naturellement les conditions de l'environnement, c'est-à-dire la température de l'air et de l'eau, l'ensoleillement et le niveau du réservoir. L'analyse a été conduite en une section bi-dimensionnelle du barrage en utilisant un logiciel développé spécifiquement par le bureau d'études Lombardi SA pour ce type d'analyses. Le logiciel, basé sur la méthode de calcul des différences finies explicites, a été employé pour l'analyse thermique de plusieurs barrages [voir 1], en particulier dans le but de définir et

* Analyse thermique d'un barrage BCR pendant la construction.

d'optimiser les systèmes de refroidissement artificiel du béton et d'évaluer les contraintes et déformations d'origine thermique.

1. INTRODUCTION

The 7th Benchmark Workshop on Numerical Analysis of Dams deals with the analysis of the thermal behavior of a RCC dam during construction. The 92 m high dam, which name and location hasn't been disclosed by the formulator of the problem, is apparently one of the largest RCC gravity dams presently under construction, with a total volume of several millions of cubic meters. The dam is located in a region with tropical climate.
The exercise consists in the prediction of the temperatures at different points. The calculated values will finally be compared with measurements done in the dam in order to evaluate the accuracy of the results and thus that of the computational methods used.

At the time of the problem formulation the construction of the dam had already reached a little more than half of the total height. Thus the real back analysis is limited to this first period. For that purpose, a 2-D or a 1-D analysis could be carried out, considering that in the short time most of the hydratation heat will flow vertically to the upper dam surface. The analyses presented perform also a long term prediction, for which a 2-D analysis is clearly required. The first part of the construction program given corresponds exactly to the reality while the second part is a prospective schedule to complete the construction of the dam.

2. THEORETICAL BACKGROUND

2.1 BASIC EQUATIONS FOR HEAT TRANSFER WITHIN THE DAM BODY

The heat transmission in a body is taken into account by a linear function of the temperature gradient according to the well-known Fourier's Law:

$$q_x = -\lambda \cdot \frac{\partial T}{\partial x} \tag{1}$$

q_x being the heat flow in x direction and λ the thermal conductivity. At any time step the temperature changes are obtained from the heat balance considering the heat generated inside the concrete and the heat flow exchanged with the nearby elements:

$$\gamma \cdot c \cdot \frac{\partial T}{\partial t} = E_{Idrat} - \frac{\partial q_x}{\partial x} - \frac{\partial q_y}{\partial y} - \frac{\partial q_z}{\partial z} \tag{2}$$

where the rate of hydration heat E_{Idrat} is given in W/m^3 and represents the deve-lopment of energy inside the concrete body; γ being the density and c the specific heat.

2.2 HEAT TRANSMISSION AT SURFACES

2.2.1 *Convection and thermal radiation*

At the surfaces, the transmission of heat to the environment is given by the following linear relationship:

$$q_{Air} = \frac{1}{R} \cdot (T - T_{Air}) \tag{3}$$

in which T and T_{Air} are the surface and the air temperature respectively while R is the thermal resistance, defined for general conditions as follows:

$$R = \sum \frac{1}{\alpha} + \sum \frac{d}{\lambda} \tag{4}$$

with α = interface transmission coefficient

λ, d = thermal conductivity and thickness of the formwork or an insulating layer.

If a direct contact between concrete and air does occur, the convection coefficient may vary between 15 and 45 W/°C/m^2 depending primarily on the wind velocity. The direct contact between concrete and water corresponds instead to a very high convectivity, so that the surface temperature can be assumed at any time to equal the one of the water.

For thick dams, if no insulation is considered, the thermal resistance at the surface is of secondary importance, due to the fact that the thermal resistance would correspond roughly to an *over thickness* of concrete of only 5-10 cm.

2.2.2 *Solar radiation*

The solar radiation must be taken into account as it represents a significant amount of energy. The energy flow absorbed by the surface can be defined in the following form:

$$q_{Sun} = E_{Rad} \cdot c_{Abs} \cdot \cos\beta \tag{5}$$

where, E_{Rad} = actual radiation intensity at the dam face, calculated as the basic radiation of 1 kW/m^2 reduced according to the atmospheric conditions

c_{Abs} = absorbivity of the concrete surface (0.50-0.65)

β = angle between the sun and the outward normal of the face.

The energy flow is updated at every calculation step according to the actual position of the sun.

The solar radiation can be also taken into account in a simplified way in assuming an equivalent increase of the air temperature variable between 2 and 4°C (sometimes until 6°) depending of the site and the orientation of the surface.

2.2.3 *Evaporation of water on surfaces*

The computational code used takes into account also the effect of the curing of both the upper surface and the lateral faces. The specific energy flow q_{Evap} due to the evaporation of water on the surfaces depends directly from the rate of water evaporated w and is defined by the following linear relationship:

$$q_{Evap} = c_{Evap} \cdot w \tag{6}$$

where c_{Evap} is the specific evaporation heat, which was assumed to be 2'255 kJ/kg. The rate w of evaporating water in kg/h/m^2 can be estimated by: [see 2]:

$$w = (25 + 19 \cdot v) \cdot (x'' - x) \tag{7}$$

in which v is the wind velocity in m/s, x the absolute humidity of the air in kg/kg and x" the saturation humidity at the temperature T, in °C, of the concrete face. Said saturation humidity is defined by the following equation:

$$x'' = (4.2 + 0.25 \cdot T + 0.0125 \cdot T^2 + 0.00028 \cdot T^3) \cdot 10^{-3} \tag{8}$$

The curing can play a very important role in the energy balance. Assuming a temperature of 30°C for the air and the concrete surface, a relative humidity of 70% and a wind velocity of 1 m/s, the specific energy flow corresponds to about 250 W/m^2 by an evaporating water mass of 0.4 l/h/m^2. The total energy dissipation by evaporation corresponds thus to 21.8 MJ/m^2 per day (24 h), which is nearly the double of the total hydration heat produced during the first day by a 1 m^3 of RCC concrete.

2.3 COMPUTATIONAL METHOD USED

The transient heat balance in the dam body was simulated using a specific software developed by Lombardi Ltd., which performs pseudo-three-dimensional thermal analyses. The effective calculation of temperatures, deformations and stresses is carried out in a two-dimensional model, which takes into account the heat losses or gains of the lateral faces when the block under calculation has a higher elevation as the adjacent ones. Indeed, the software was especially developed to analyze and optimize the artificial post-cooling for usual concrete dams. This procedure is simulated in a very accurate way by taking into account many of the factors and parameters affecting the cooling. This aspect is no further discussed in the present paper because it is not included in the analysis presented hereafter.

The computation is based on the explicit Finite Difference Method. By this numerical technique, every derivative in the set of equations is directly replaced by an algebraic expression written at discrete points in space. This procedure first invokes the Fourier's equation (1) to obtain the heat flows from the known temperatures, and then the new temperatures using equation (2). During this second step the heat flows remain unchanged, thus the calculated temperatures do not affect them. This assumption is justified if the time step is small enough, i.e. smaller then a critical value taking care of

the requirements for numerical stability. The accuracy of the numerical solution is checked at each time step in comparing the balance of the internal energy with the heat transferred to the boundaries. The well known explicit method, perhaps the oldest numerical technique, is still very efficient in modeling nonlinear systems like the temperature development in setting concrete.

To model the heat transfer at the boundaries one-dimensional elements without any thermal inertia are used. This allows an adequate accuracy of the results quite independently from the dimension of the mesh used. As an example a comparison of two calculations is shown in **Figure 1**.

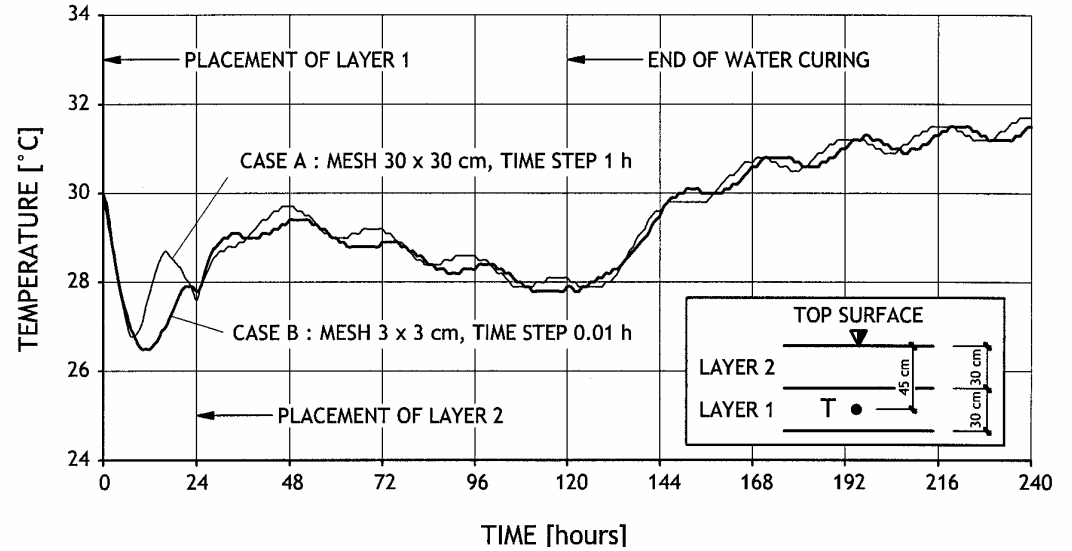

Fig. 1. Comparison of calculations with different mesh sizes (30 cm vs. 3 cm) Only a short time lag can be observed.

Case A was performed with a mesh of 30x30 cm and a time step of 1 h while Case B was performed with a mesh of 3x3 cm and a time step of 0.01 h. The figure shows the temperature development at the center of the first placed layer after placing two 0.3 m thick RCC layers, i.e. at 45 cm below the upper surface (at 15 cm during the first 24 h) by taking into account the hydration heat, the solar radiation, the water evaporation as well as the convection with a daily variation of the air temperature. A small difference, less then 1°C, is shown for short times, but the long term development is quite well simulated.

For the actual 2-D analysis a discretisation of 30 cm in the vertical and 33 cm in the horizontal direction was used. A time step of 1 h was chosen for updating the solar radiation even if the numerical stability could accept a longer one. The total number of calculation elements was 19'100 for the foundation rock and 35'700 for the concrete body.

3. BASIC DATA

3.1 CALCULATION MODEL

3.1.1 *Dam geometry*

The geometry of the block and the different concrete types are shown in **Figure 2**.

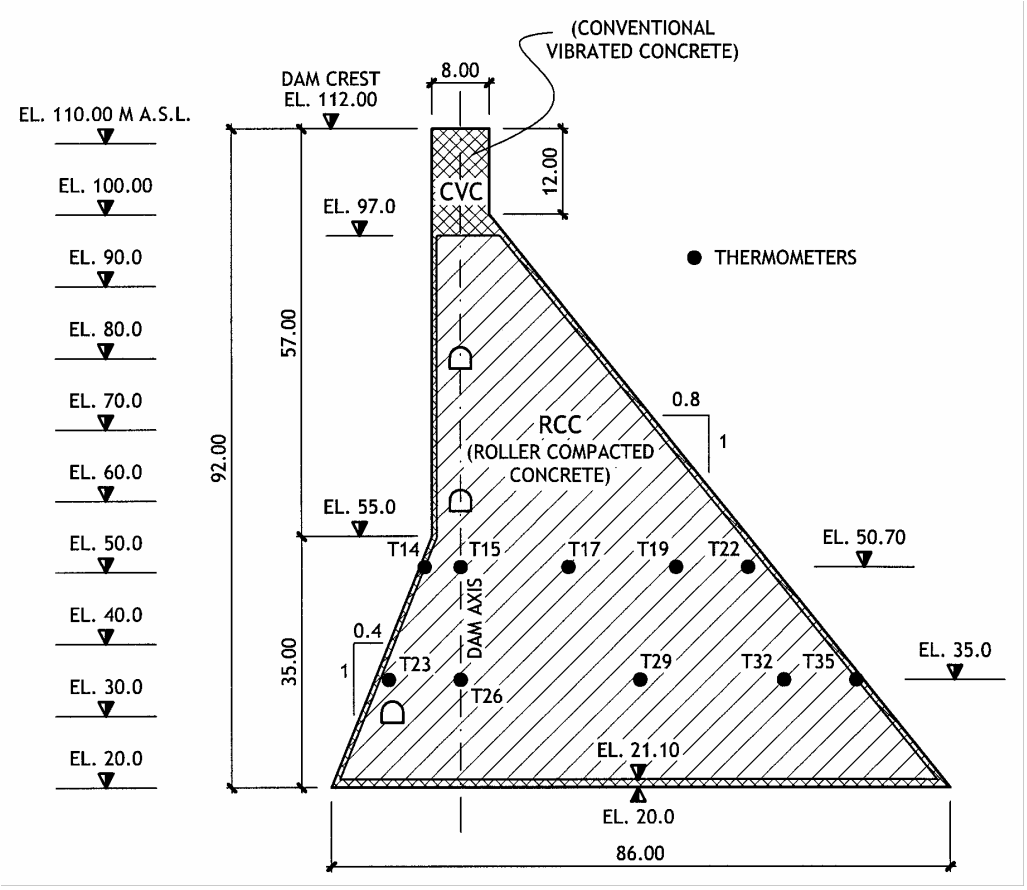

Fig. 2. Dam cross section and distribution of different concrete types.

The dam is mainly composed of RCC while both faces are made of conventional vibrated concrete CVC. The boundary surface between CVC at the dam faces and the RCC has the typical shape as a Christmas tree due to the placement method. In the simulation the thickness of the downstream as well as of the upstream face concrete was taken uniformly as 66 cm. The first layer on the rock as well as the crest section are made of CVC. For the CVC in the upper part no data were given by the formulator. For simulation purpose of the final dam some assumptions concerning the CVC had thus to be done, which may not correspond exactly to the real values.

Three inspection galleries are spared out at elevation 30, 60 and 80 m a.s.l. respectively. The temperatures of the RCC were measured during the construction at elevation 35.0 and 50.7 m a.s.l. by a total of 10 thermometers in order to allow a comparison of the measured and the computed temperatures.

The dam is placed on the foundation rock, which is modeled with a thickness of about 20 m. At the bottom and the sides of this bloc adiabatic conditions were assumed.

3.1.2 *Construction procedure*

The RCC is placed in 0.30 m thick layers. The top elevation of the placed lifts vs time is shown on **Figure 3**.

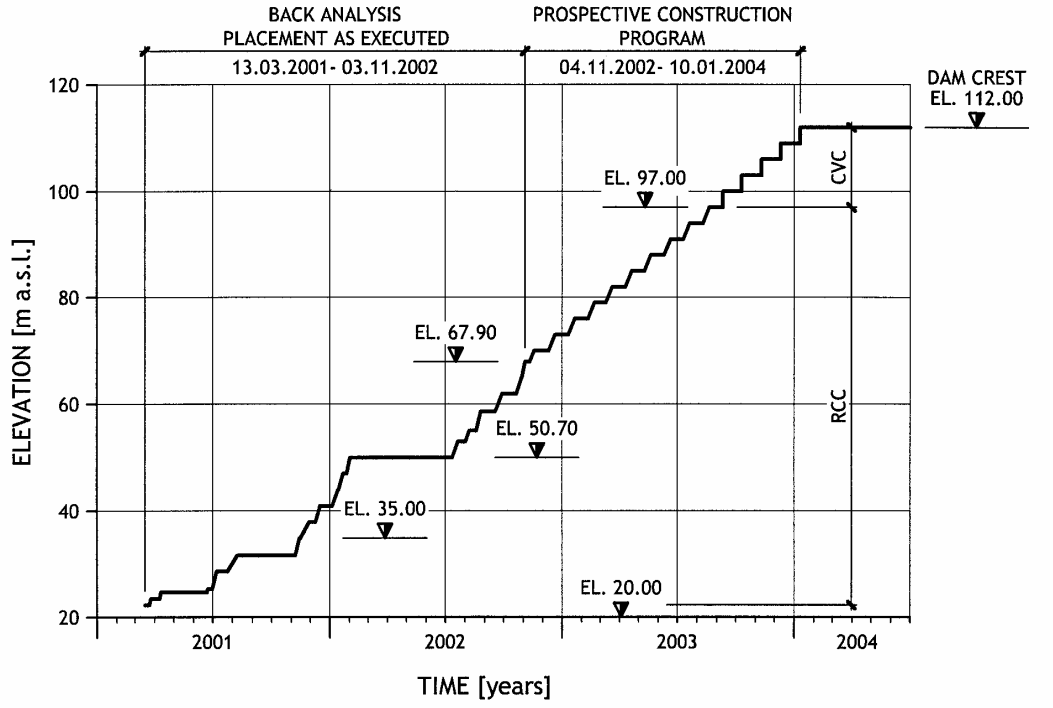

Fig. 3. Construction schedule.

Typically 10 layers are placed at a rate of about 1 layer per day, then a stoppage takes place during which the concrete is poured in other sections. The first part of the construction was simulated as to respect the actual placement date of each single lift until 3rd of September 2002. The second part of Figure 3 is a prospective construction program set up to simulate the completion of the 92 m high dam. The placement rate of the 30 cm thick layers corresponds to the steepest segments of the plot shown in this figure. The CVC at the top of dam is placed in 3 m thick layers.

3.2 CALCULATION PARAMETERS

3.2.1 *Material properties*

The parameters required to define the thermal behavior of the materials are summarized in **Table 1**.

Variable	Symbol	Unit	Rock	RCC	CVC
Unit weight	γ	kg/m^3	2'700	2'380	2'450
Specific heat	c	kJ/kg/°C	0.92	1.00	1.00
Conductivity	λ	W/m/°C	3.38	2.79	3.08

Tab. 1.Propreties of the materials considered.

The cementitious material incorporated into the RCC is a mix of 100 kg Portland cement (STC) and 90 kg pouzzolanic fly ashes (PFA) per cubic meter of RCC. The hydration heat development of the mix was determined experimentally for the first week. The total heat generated corresponds to 265 J per gram cementitious material.

The CVC contains 350 kg/m^3 of Portland cement. The hydration heat curve of the Portland cement was assumed to correspond to the one of the RCC binders multiplied by a factor of 1.25 since no direct measurements were available.

For both materials considered, the adiabatic temperature rise due to the cement hydratation heat and its development with time is shown in **Figure 4**.

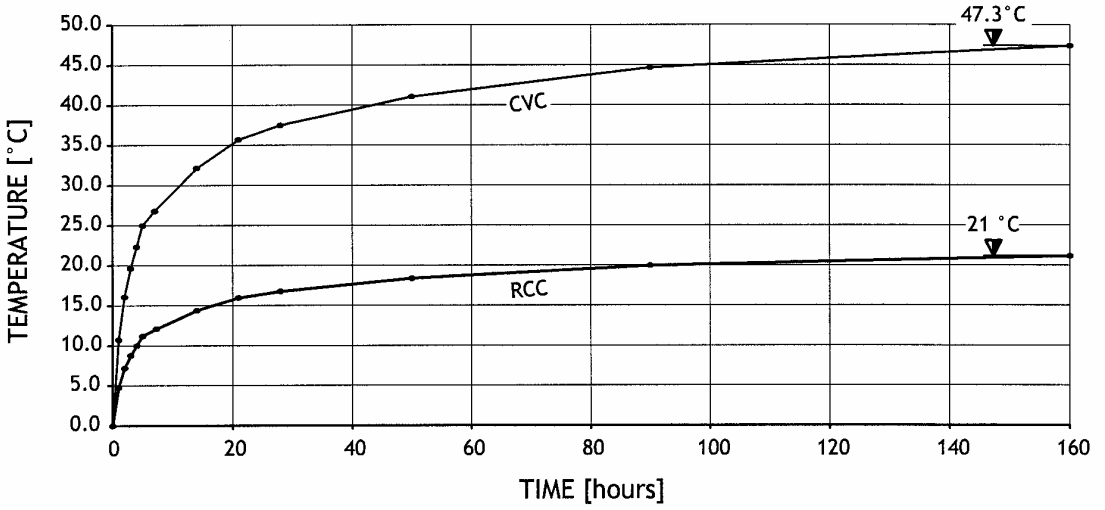

Fig. 4. Adiabatic temperature rise due to hydration heat.

3.2.2 *Initial and boundary conditions*

The ambient temperature at the site was measured close to both dam faces at irregular dates. The average value of the 88 readings made during a period of total about 13 month corresponds to 30°C. During two periods of a month a daily reading of the temperature was made: up to middle of November 2001, with an average temperature of 29°C, and up to middle of July 2002, with an average temperature of about 30°C. The annual variation of the air temperature is very small due to the location of the dam in a tropical country. It must however be pointed out that the influence of the solar radiation on the measurements is not clearly defined and that a single measurement per day does not procure any information about the daily variation. Therefore, since no further information is available, an arbitrary assumption had to be made. The air temperature follows thus a seasonal oscillation and a daily sinusoidal variation with a minimum at 6:00 AM and a maximum at 6:00 PM. **Table 2** summarizes the average temperatures assumed at mid-month, the daily variations as well as the average relative humidity. The tropical climate is characterized by typical springtime-summer monsoons, while the winter is dryer and slightly colder.

Month	Air temperatures [°C]		Relative humidity [%]
	Monthly average	Daily amplitude	
January	28.5	± 4.0	55
February	28.5	± 4.0	65
March	29.0	± 3.5	75
April	29.5	± 3.0	85
Mai	30.0	± 2.5	90
Juni	30.5	± 2.5	95
July	31.0	± 2.5	90
August	31.0	± 2.5	85
September	30.5	± 3.0	75
October	30.0	± 3.5	65
November	29.5	± 4.0	55
December	29.0	± 4.0	50

Tab. 2. Air temperature and relative humidity.

The following boundary conditions were assumed:

- The convection surface coefficient between concrete and air is α=35 W/m^2/°C.
- The reservoir water is not included in the present analysis.
- The maximal duration of the water curing on the upper surface is 5 days.
- The average wind speed is 1 m/s.
- For a height of 1.5 m below the lift top an insulation is placed on the lateral faces. The heat transfer of the insulated formwork is λ/d=17 W/m^2/°C.
- The solar radiation is computed with the parameters listed below:
  - Geographical latitude of the dam (north hemisphere) 15 degrees
  - Orientation of the outward normal of the u/s face (north to east) 90 degrees
  - Average height of screen by mountains 5 degrees
  - Absorbivity of solar radiation by the concrete 0.60
  - Reduction factor for general nebulosity 0.65
  - Reduction factor for transmittance near horizon 0.60

In order to estimate the initial RCC temperatures, measurements have been carried out with the fresh concrete at the batching plant; additionally few (4) initial temperatures have been measured at the time of placement. These data seem to indicate that the temperature of the fresh RCC at this time is substantially higher than the one measured at the batching plant. The RCC temperature seems to correspond quite well to the temperature of the air at the same time. It was therefore decided to use the air temperature as initial RCC temperature. The layers at elevations 35.0 and 50.7 m a.s.l., which are equipped with thermometers to compare the measured and the computed temperatures, were thus supposed to having been placed at 30°C and 32°C respectively.

Finally, the temperature of the foundation rock at pouring the first concrete layer was computed along a previous period of 8 months, assuming an initial temperature of 30°C.

3. MAIN RESULTS

Figure 5 shows the temperature development at elevation 35.0 m a.s.l. after placing the layer, for different assumptions on the water curing of the upper surface. The air temperature and the adiabatic temperature development are also shown to ease the interpretation. The effect of both solar radiation and increasing temperature during the day can cause a temperature rise, which may exceed the adiabatic one. The figure illustrates as well the time of placing the next RCC layers and the increasing elevation of their top.

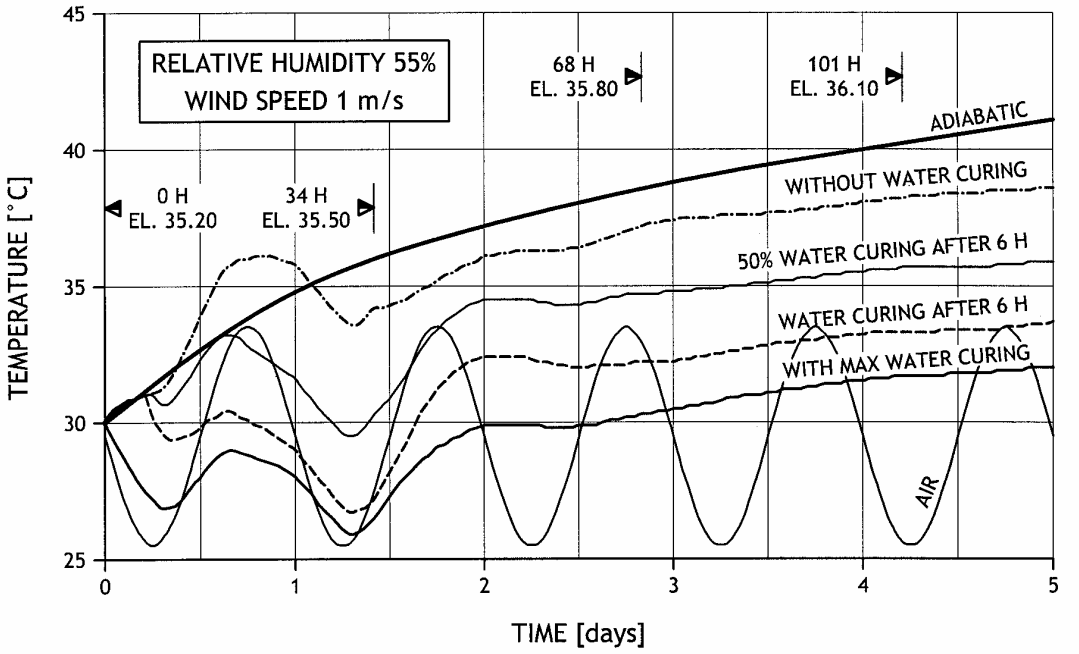

Fig. 5. Concrete temperature at elevation 35.0 m a.s.l. during setting at 55% relative humidity. (Month of November)

The water curing until placing the next layer (after 34 h) is of great importance. It can reduce the temperature by about 6-7°C from the case without water curing. This potentially maximal cooling is obtained when the curing starts immediately after placing the lift. In this case the amount of water sprayed must be measured very carefully, in order to avoid an excessive humidification of the concrete and a possible loss of strength. As a more practical case it was assumed that the water curing starts only 6 h after placing the RCC. At this time of maturity, the concrete should have reached a sufficient strength. In this case the reduction of the temperature is about 5°C.

By traditional concrete dams the effect of the curing is of less importance due to the fact that the concrete is placed in thick layers, while the effect of the water curing is limited to the top surface. Due to the low thickness of the RCC layers, most of the hydration heat, which develops during the first days, can be led away by the evaporation of water. Placing the concrete in thin layers allows to reduce the temperatures of each single lift and thus all along the entire dam height, while for conventional dams most of the concrete can't be reached by this positive effect.

During the construction of the dam the water curing might not occur systematically. So the last case shown on Figure 5 assumes that the water curing is only 50% effective, i.a. that at any time the evaporating water mass is only half of the potential one. This case is considered to be the most representative for the actual conditions at the site.

Logically, the effect of a water curing is reduced if the relative air humidity increases. **Figure 6** presents the temperature development at elevation 50.7 m a.s.l. for a relative air humidity of 90%. The difference between the cases with and without curing is reduced to 2°C at the best.

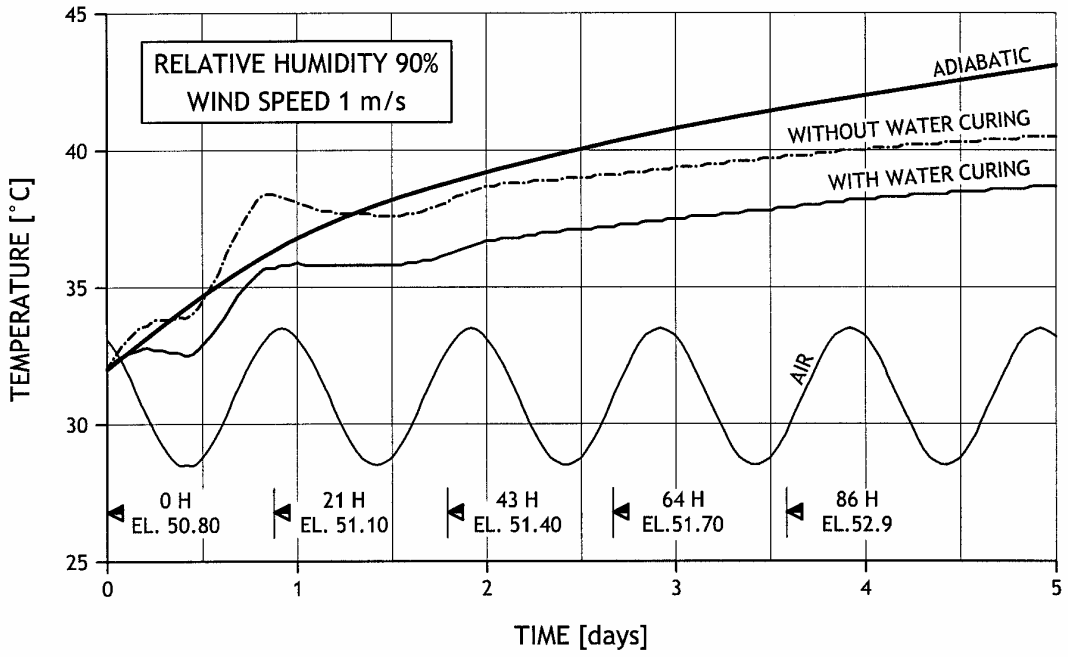

Fig. 6. Concrete temperature at elevation 50.7 m a.s.l. during setting at 90% relative humidity. (Month of July)

Figures 7 to 12 show the section of the dam during construction with the temperature field represented by isothermal lines at different dates and for the case of water curing activated at 50%.

Figure 7 refers to the temperature of the foundation rock before placing the first concrete layer. This initial condition is already the result of a preliminary calculation.

The thermal states of the dam during construction are presented in the Figures 8 to 11. The influence of a long stoppage in placing concrete can be observed as a local decrease in temperature vs elevation. So the temperature on 14.11.2001 (**Figure 8**) is influenced by the stoppage of 3 month at elevation 31.6 m a.s.l., while the temperature field on 10.08.2002 (**Figure 9**) is influenced by the stoppage of 5.5 month at elevation 49.9 m a.s.l.

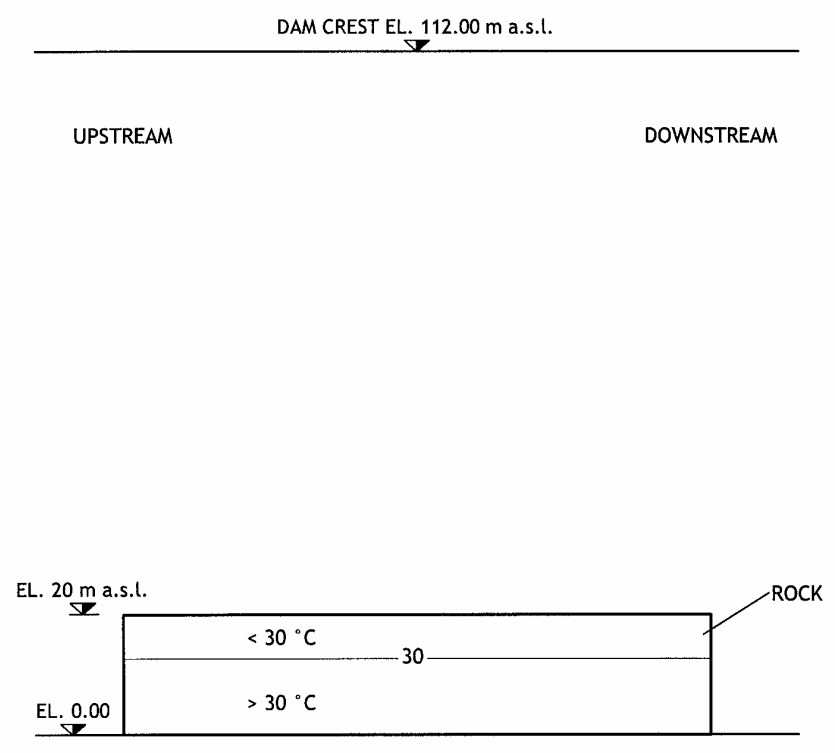

Fig. 7. Temperature in the foundation rock on 08.02.2001, before starting the construction of the dam.

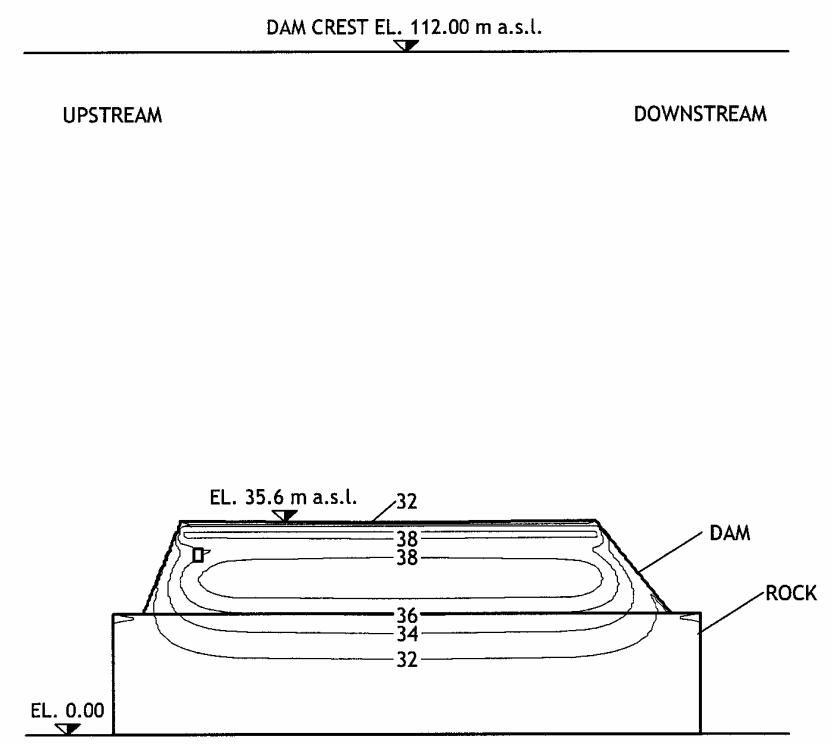

Fig. 8. Temperature in °C during construction on 14.11.2001 .

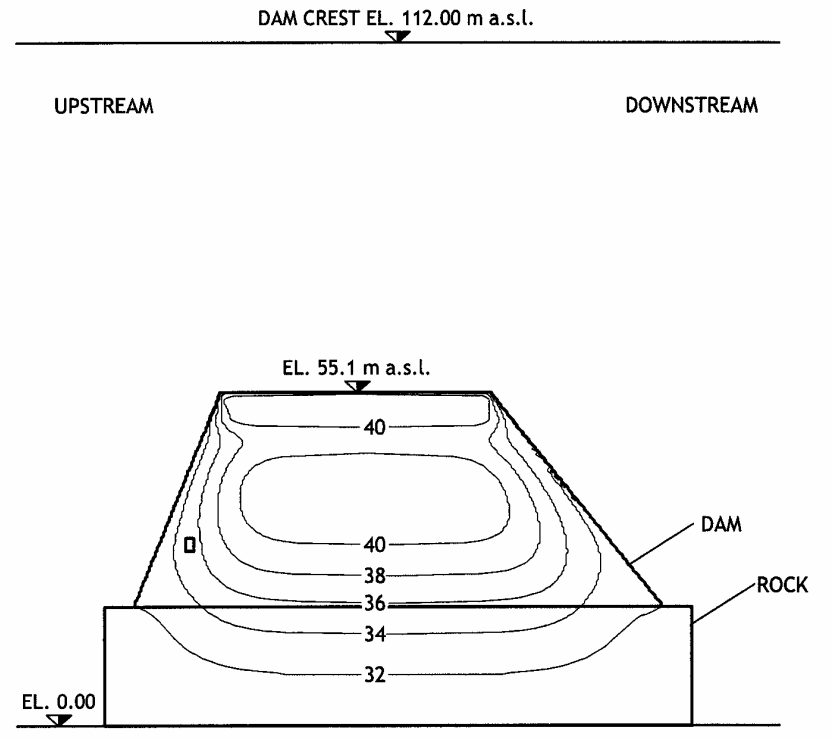

Fig. 9. Temperature in °C during construction on 10.08.2002 .

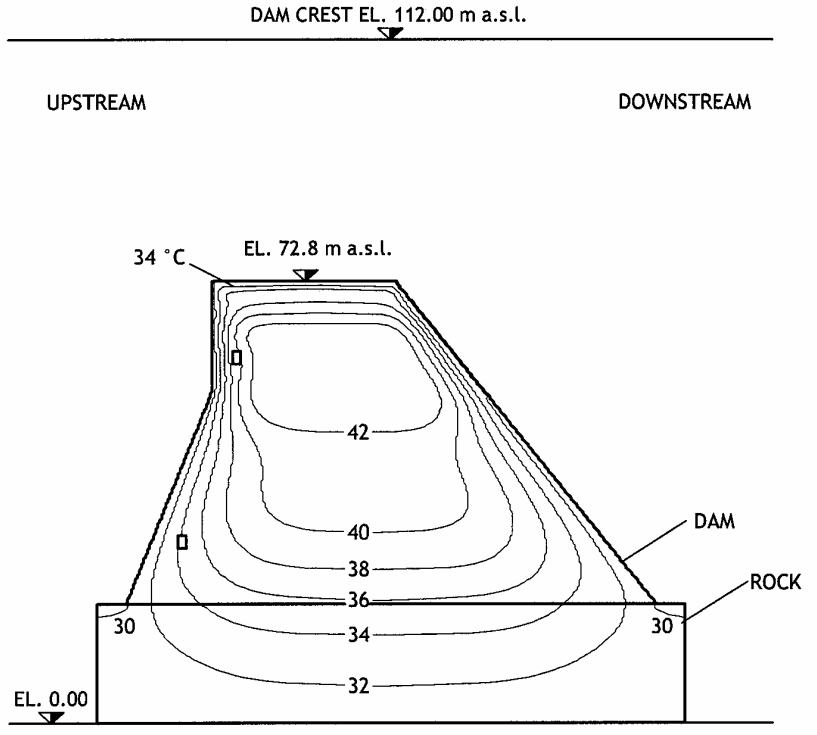

Fig. 10. Temperature in °C during construction on 28.12.2002 .

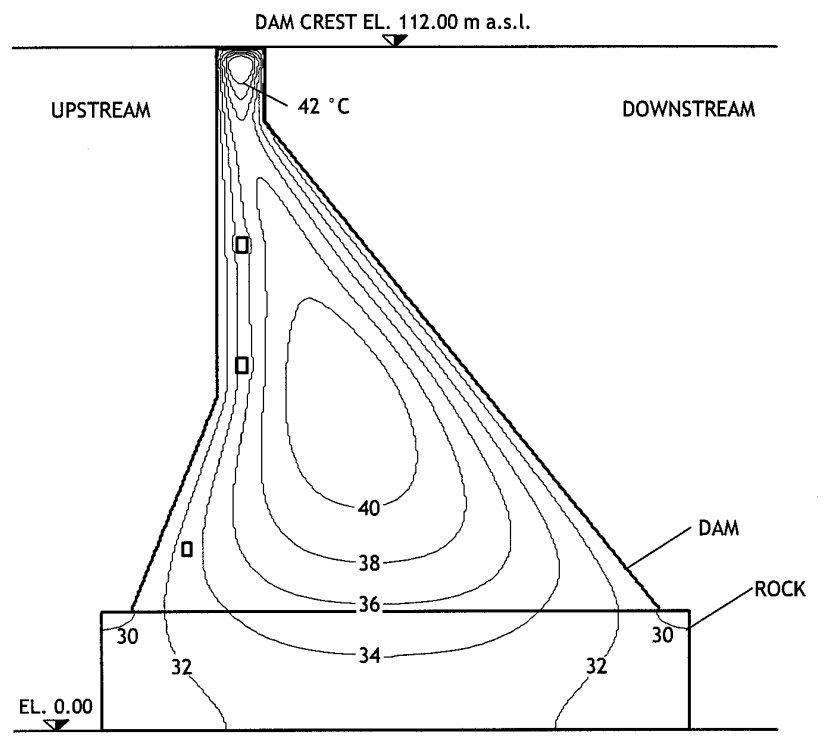

Fig. 11. Temperature in °C for the completed dam on 15.01.2004 .

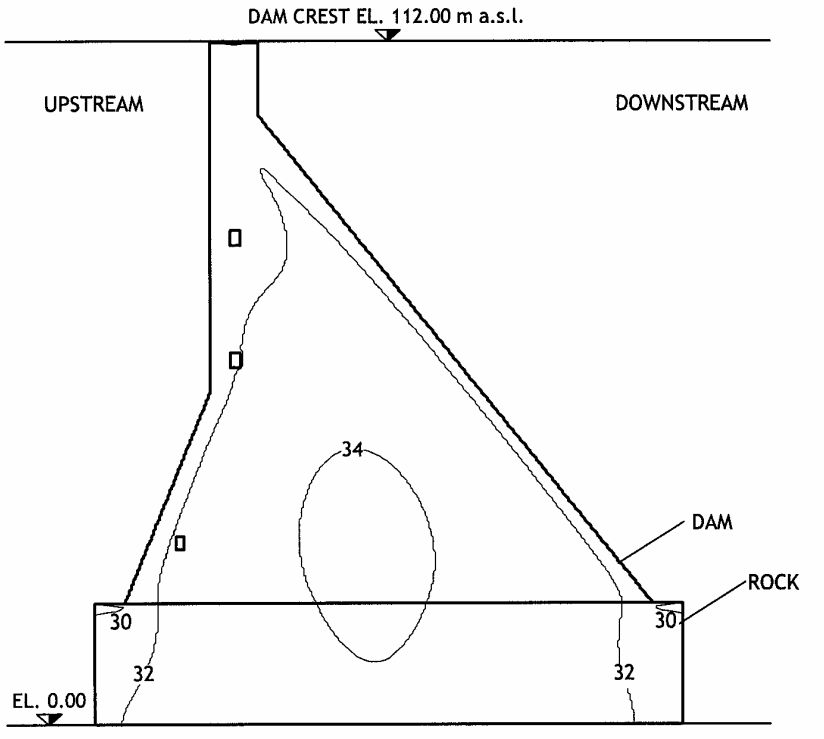

Fig. 12. Temperature in °C after several years (06.12.2010) .

Figure 10 shows the temperature field on 28.12.2002. Between elevations 50 and 65 a maximal temperature in the RCC is observed, which fact is due to the high average placing rate of about 1.75 days per layer during the warm and humid season of the year. A high temperature is reached also at the top of the dam as shown in **Figure 11**, were only CVC was used.

Figure 12 shows the temperature after approximately 7 years after completion. A residual hot zone is observed in the central part of the dam body. The raising of the pound level could not be considered, due to lacking information on the water management.

Figure 13 presents the long term history of the temperature in the center of the dam at four different elevations as well as the air temperature.

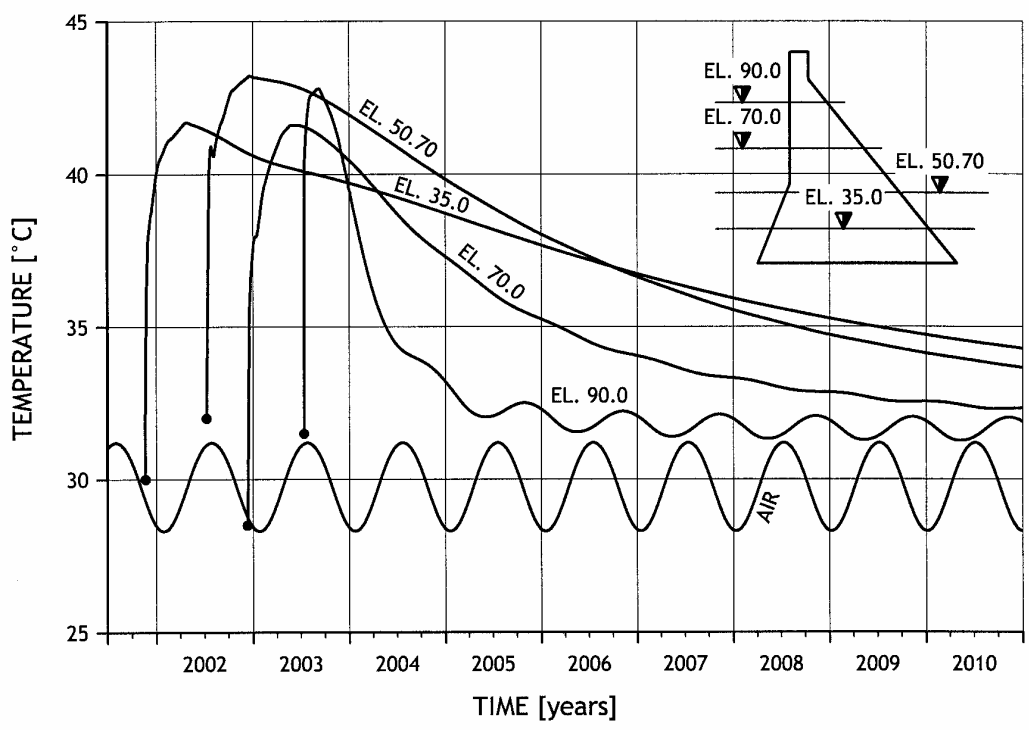

Fig. 13. History of the temperature at the center point of 4 elevation .

The temperature at elevation 90.0 m a.s.l. reaches already after 4 years a final equilibrium, while at the other elevations the hydration heat needs more then 9 years to be almost completely led away. It may be noticed that the final average temperature at elevation 90.0 m a.s.l. is still 1.9-2.0°C higher then the air temperature because of the solar radiation. At elevation 35.0 m a.s.l. a residual of the temperature rise of about 2.5°C at the central point may still be observed 9 year after placing the lift. The maximal temperature of 43°C is reached at elevation 50.7 m a.s.l., which corresponds to a temperature increase of 11°C due to the hydration heat. It must be pointed out that an adiabatic temperature would have reached a temperature peak of 53°C.

The maximal difference between the internal and the air temperature is about 15°C. This value can be considered acceptable for RCC dams in matters of thermal cracking. For conventional dams a maximal value of 20°C is generally considered as a

limit for practical reasons since the calculation of the stresses in the concrete during hardening is very uncertain.

4. CONCLUSIONS

The present paper reports on a thermal study of a 92 m high RCC dam during and after construction. The following conclusions may be stated:

- For RCC dams the temperature of each thin layer after its placement can be significantly reduced by the water evaporating on the upper face. For conventional dams, this phenomenon is of lesser importance due to the greater thickness of the layers and because of the limited extension in space of its influence. The final result for RCC dams is comparable to a pre-cooling of the fresh concrete.
- RCC dams are hardly subjected to thermal cracking if the external temperature is more or less constant, as in tropical climate, and the initial concrete temperature is not very different of that of the air.
- Obviously, by significant seasonal variations, cracks may appear at the faces of a thick RCC gravity dam during the following winter if the placing occurred at summer time. The cracking is caused by the temperature increase in the interior of the dam combined with the fast cooling of the surface in winter. For this reason a post-cooling with pipes was proposed for the Three Gorges Dam [3].
- The temperature of the core of a thick gravity dam requires a long time to drop to the final equilibrium state (more then 9 years in this case).

To conclude, it may be stated that the main difficulty of the presented exercise - and in general of thermal calculations- consists in the correct determination of the parameters to be used. The thermal behavior during setting is a very complicated process, which involves many uncertainties in both material properties and environmental conditions. An error of 20-30% can thus be considered as an excellent accuracy for the analysis of practical problems [4]. The main source of errors are due rather to the input data than to the modeling or computation techniques, because many key parameters and material properties vary in quite wide ranges.

.

REFERENCES

[1] Mondada, A. – Adaptation au cours des travaux du projet du système de refroidissement au barrage de Zimapán, CNSGB Symposium de Crans-Montana, Septembre 1995

[2] Recknagel, H., Sprenger, E. – Taschenbuch für Heizung und Klimatechnik, R. Oldenbourg Verlag München, 61. Auflage 1981

[3] Bofang, Z., Ping, Xu – Thermal Stresses in Roller Compacted Gravity Dams, Dam Engineering, Vol. VI, Issue 3, 1995

[4] Wang, Ch., Dilger, W.H. – Prediction of temperature distribution in hardening concrete, International RILEM Symposium of Munich, October 1994

THERMAL ANALYSIS OF A RCC DAM DURING CONSTRUCTION USING FLAC*

António Tavares de Castro
National Laboratory for Civil Engineering (LNEC), Lisbon, PORTUGAL

Teresa Santana
New University of Lisbon, Lisbon, PORTUGAL

Noemí Schclar Leitão
National Laboratory for Civil Engineering (LNEC), Lisbon, PORTUGAL

SUMMARY: In RCC dams construction, the high rate of concrete placement reduces to a minimum the loss of hydration heat, which can cause important thermal cracking.

This paper describes a methodology for predicting the thermal state of a RCC dam using a two dimensional model. The calculations are carried out using numerical analysis performed with the two-dimensional finite difference code FLAC (Fast Lagrangian Analysis of Continua), developed by Itasca, and the proposed data. Results referring to the time evolution of the temperatures observed in the thermometers and to temperature profiles in several instants will be presented and discussed.

RÉSUMÉ: Le très court temps de construction des barrages en BCR limite la dissipation de la chaleur d'hydratation, pouvant causer la fissuration du béton.

Ce travaille présente une méthodologie pour prévoir l'état thermique d'un barrage en BCR en utilisant un modèle 2-D. Le calcul numérique effectué utilise le logiciel FLAC (Fast Lagrangian Analysis of Continua), élaboré par Itasca, et les donnés proposés. Résultats de l'évolution de la température avec le temps et des températures en différents instants sont présentés.

* Analyse thermique d'un barrage en BCR pendant la construction utilisant FLAC

1 INTRODUCTION

One of the main features of RCC dams is the speed and continuity of concrete placement, making it possible to construct this type of dams in short periods of time. This reduces to a minimum the time of concrete exposure, creating an almost adiabatic behaviour inside the dam, as there is not enough time to dissipate the heat generated, before placing the next layer.

The prediction of the thermal state, as a basis of a structural analysis, is essential in the design of this type of dams, because thermal stresses may exceed the tensile resistance of the concrete, leading to cracking phenomena.

In this paper it is described a methodology, based on a 2-D analysis, which correspond to consider that most of the hydration heat developed during construction will migrate through the RCC only vertically and upstream-downstream.

After some considerations about the main features of RCC dams, the principal characteristics of the model are referred. Finally, the main results of the analysis carried out are presented and discussed.

2 RCC DAMS

Roller compacted concrete (RCC) is a concrete that, in its unhardened state, can support a roller while being compacted [1]. It is a material placed like embankment materials but that exhibits structural properties of concrete. RCC construction techniques can present an economically alternative to conventional concrete dams due to savings in material costs and in construction time.

In large RCC projects the unit cost of concrete range from 25% to 50% less than conventionally placed concrete and the construction time, when compared with conventional concrete dams, can be reduced by several months to several years [2], reducing or deleting diversion facilities. Like conventional concrete dams, RCC dams have the possibility of integrate spillways and appurtenant works.

The external compaction with heavy equipment allows the use of concrete with low water and low cement content, which is economically and technically favourable in structures, like gravity dams, where the concrete strength isn't an important structural requisite.

Nevertheless, the high placement rates of RCC presents technical problems related to the hydration heat of large concrete volumes. These problems can be minimized through the use of mixtures with low heat generation and the adoption of adequate construction procedures. RCC mixtures usually have low cementitious contents and non-heat generating materials, like fly ashes, substitute, as possible, the cement, which is responsible for the heat generation. The construction programme is adjusted in order to allow the loss of most of the heat generated by the lifts that are already constructed, before the placement of another lift.

Therefore, a realistic evaluation of the concrete temperature evolution during the construction period is essential to prevent the thermal cracking associated to temperature decrease due to hydration heat dissipation. This evaluation shall be supported by results of thermal analyses considering the real properties of the concrete and the actual construction schedule. These analyses can be updated during the construction, supporting decisions of eventual changes in the RCC placement rate or in the concrete composition.

3 THERMAL ANALYSIS MODEL

In this paper, a mathematical model for thermal analyses of RCC dams construction was developed using FLAC (Fast Lagrangian Analysis of Continua) code [3]. In the next paragraphs a brief reference to the theoretical background of this code is presented.

Consider, in a general x_i (i,j=1,2) two dimensional coordinates system [m], a body with mass density ρ [kg.m^{-3}], specific heat C [J.kg^{-1}.°C^{-1}] and thermal conductibility k [W/m^{-1}.ºC^{-1}], subjected to a heat source Q [W.m^{-3}]. The temperature T (ºC) distribution is governed by the general Fourier equation, which may be solved for particular geometries and properties, given specific boundary and initial conditions:

$$k\frac{\partial^2 T}{\partial x_i^2} + Q - \rho C\frac{\partial T}{\partial t} = 0 \tag{1}$$

This equation result of both the energy balance (2) and the transport law (3) equations

$$-\frac{\partial q_i}{\partial x_i} + Q = \rho C\frac{\partial T}{\partial t} \tag{2}$$

$$q_i = -k_{ij}\frac{\partial T}{\partial x_j} \tag{3}$$

where q_i represents the heat flux vector component [W.m^{-2}].

The solution of equation (1) requires the definition of initial conditions and of boundary conditions. Initial conditions correspond to a given temperature field and boundary conditions are generally expressed in terms of temperature or the component of the heat-flux vector normal to the boundary. Five types of boundary conditions can be considered: i) given temperature; ii) given component of the flux normal to the boundary; iii) convective boundaries; iv) radiative boundaries; and v) insulated (adiabatic) boundaries.

A convective boundary condition has the form

$$q_n = h(T - T_e) \tag{4}$$

where q_n is the component of the flux normal to the boundary in the direction of the exterior normal, h [W.m^{-2}.ºC^{-1}] is the convective heat-transfer coefficient, T [ºC] is the temperature of the boundary surface, and T_e [ºC] is the temperature of the surrounding fluid. Radiative and adiabatic boundaries are handled in a similar fashion.

The above equations are solved in *FLAC* using a finite-difference approach based on a medium discretization into zones, defined by four corner nodes, composed of two overlays of constant heat-flux triangles. In each triangle a linear temperature variation is assumed, the temperature gradient being expressed in terms of the nodal values of temperature by the following expression:

$$\frac{\partial T}{\partial x_j} = -\frac{1}{2A}\sum_{n=1}^{3} T^{(n)} n_j^{(n)} L^{(n)} \tag{5}$$

where $n_j^{(n)}$ is the unit vector normal to edge n (which is opposite to node n), A is the triangle area and $L^{(n)}$ is the length of the triangle edge n.

The numerical scheme rests on a nodal formulation of the energy-balance equation, which requires that, at each global node, the sum of the equivalent nodal heat from all triangles meeting at the node and nodal contribution of applied boundary fluxes and sources is zero. The nodal form of the energy-balance equation at node n is

$$\frac{dT^{(n)}}{dt} = -\frac{1}{\sum\left[\frac{\rho A C}{3}\right]^{(n)}}\left[Q_T^{(n)} + \sum Q_{app}^{(n)}\right] \tag{6}$$

where

$$\left[Q_T^{(n)} + \sum Q_{app}^{(n)}\right] \tag{7}$$

is the "out-of-balance heat". In this expression, $Q_T^{(n)}$ is a function of the nodal temperatures and

$$\sum Q_{app}^{n} = -\sum\left[\frac{q_v A}{3} + Q_w\right]^{(n)} \tag{8}$$

correspond to the sum of the applied volume sources, q_v, and boundary fluxes, Q_w.

Together with the transport law equation (3), the nodal energy-balance equations (6) at all the nodes involved in the discretization form a system of ordinary differential equations that is solved in FLAC using both explicit and implicit finite-difference schemes. In the explicit finite-difference scheme, used in this work, the temperature at a node is assumed to vary linearly over a time interval Δt. The derivative in the left-hand side of equation (6) is expressed using forward finite differences, and the out-of-balance heat (7) is evaluated at time t. Starting with an initial temperature field, nodal temperatures at incremental time values are updated, provided the temperature is not fixed. Numerical stability can be achieved if the timestep remains below a limit value,

function of the dimension of the elements and of the material thermal properties. The thermal calculation will be performed until the ratio of the change in temperature at a gridpoint, divided by the temperature at the gridpoint, falls below a given value (in general 10^{-3}) for all nodes in the model.

4 RCC DAM CONSTRUCTION THERMAL MODEL

4.1 GEOMETRY, BOUNDARY AND INITIAL CONDITIONS

The proposed case study is a high RCC dam (Fig. 1), with a height of about 100 m, under construction in a country with a tropical climate. The dam is mainly composed of RCC, placed in 0.3 metre thick layers. Both dam faces are made of conventional vibrated concrete. The dam disposes of several thermometers to follow the concrete temperature evolution.

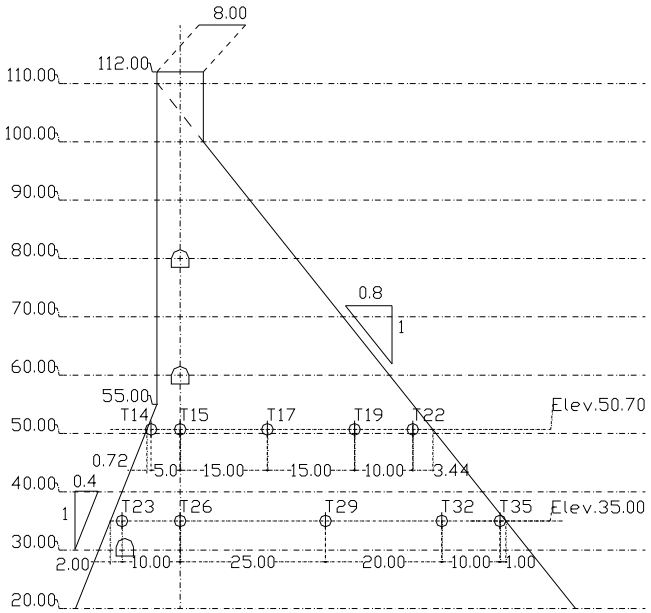

Fig. 1 – Geometrical definition of the dam and localization of the thermometers

As the construction programme ends when the RCC reaches elevation 68 m, in November 2002, the dam was discretized only until this elevation (Fig. 2). In the dam body the model considers 0.3 m height elements to represent all the RCC layers. Along the thickness of the dam there are 50 elements, with minor dimensions near the faces, where there are more important temperature gradients. The elements near the dam faces correspond to the conventional concrete zone. The model considers also 10 m depth of the foundation rock mass, including zones upstream and downstream of the dam.

The boundary conditions considered were null heat flux in the upstream and in the downstream boundary of the foundation and convective boundaries in the top of the foundation and in the dam faces, considering temperature variations with annual period cycles which were adjusted with the measured air temperatures (Fig. 3). The initial temperature of each layer was taken equal to the average air temperature calculated for the placement date.

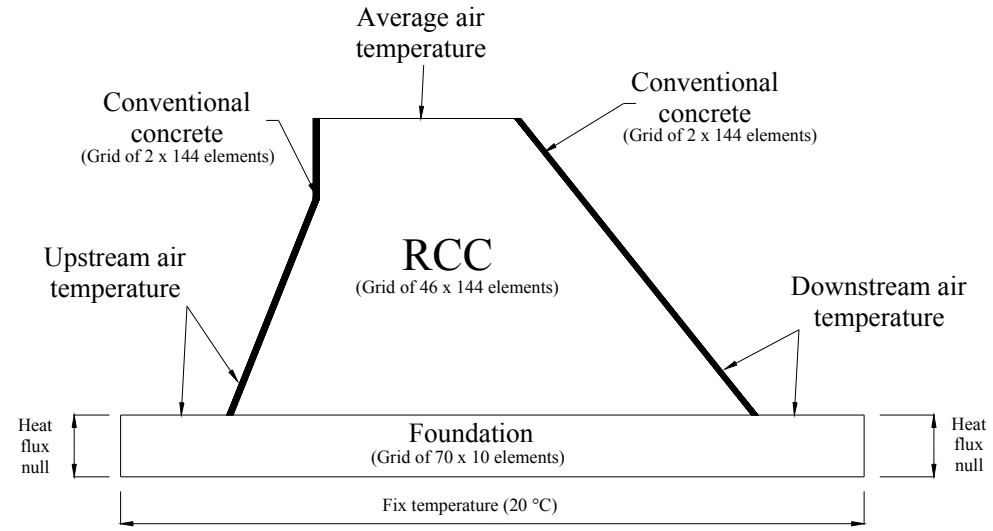

Fig. 2 – FLAC model

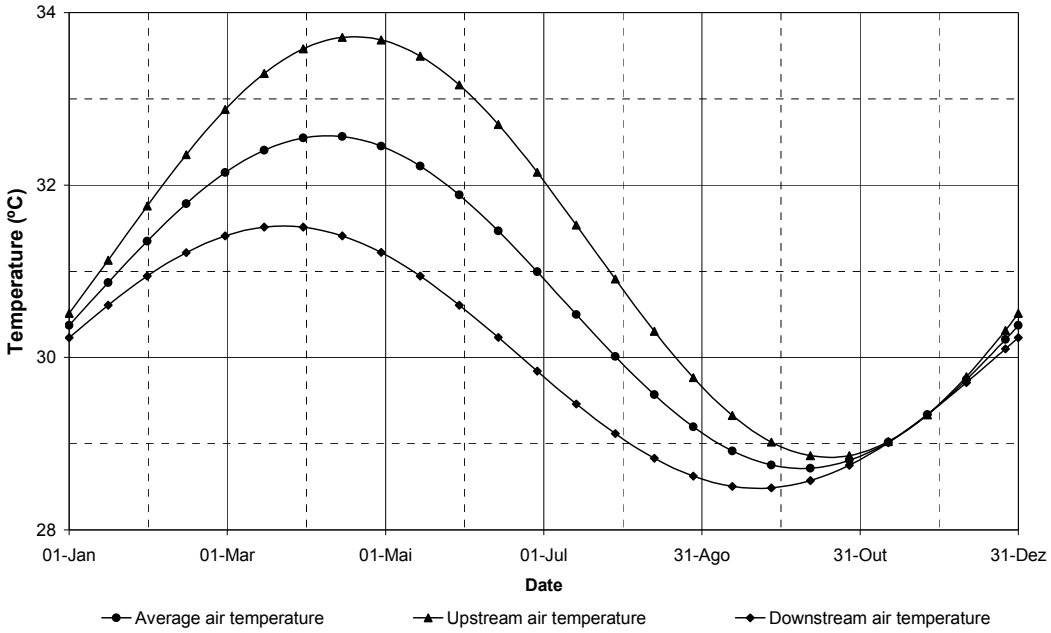

Fig. 3 – Annual periodic cycles of the air temperature

4.2 MATERIAL PROPERTIES

The concrete thermal properties are given in table 1 below.

Table 1: RCC thermal properties

Property	Value	Unit
Unit weight (ρ)	2380	$kg.m^{-3}$
Specific heat (C)	1.0	$kJ.kg^{-1}.°C^{-1}$
Conductivity (λ)	10.0	$kJ.m^{-1}.h^{-1}.°C^{-1}$

For the rock mass foundation, the same thermal properties were considered.

In order to have a continuous representation of the hydration heat for the RCC cementitious materials, a function of the form

$$Q(t-t_0) = Q_0\left(1-\left(t-t_0+1\right)^a\right), \text{ [J.g}^{-1}\text{]} \quad (9)$$

was used, where Q_0 and a are coefficients adjusted with the known values, t is the actual time and t_0 is the time correspondent to the placement of the RCC layer. The calculated curves and the known values are represented in figure 4 and the correspondent coefficients are given in table 2 below.

Table 2: Hydration function parameters

Coefficient	$t - t_0 < 7$ days	$t - t_0 > 7$ days
Q_0	9929.623	9955.307
a	2.688×10^{-3}	3.266×10^{-3}

In each timestep, the hydration heat generated in each element was calculated through the expression of the derivative of the equation (9), taking into account that there are 190 kg of cementitious material per cubic metre of RCC. The hydration heat curves of the Portland cement used in the conventional concrete were obtained multiplying by a factor of 1.25 the previous values and taking into account that there are 350 kg of Portland cement per cubic metre of concrete.

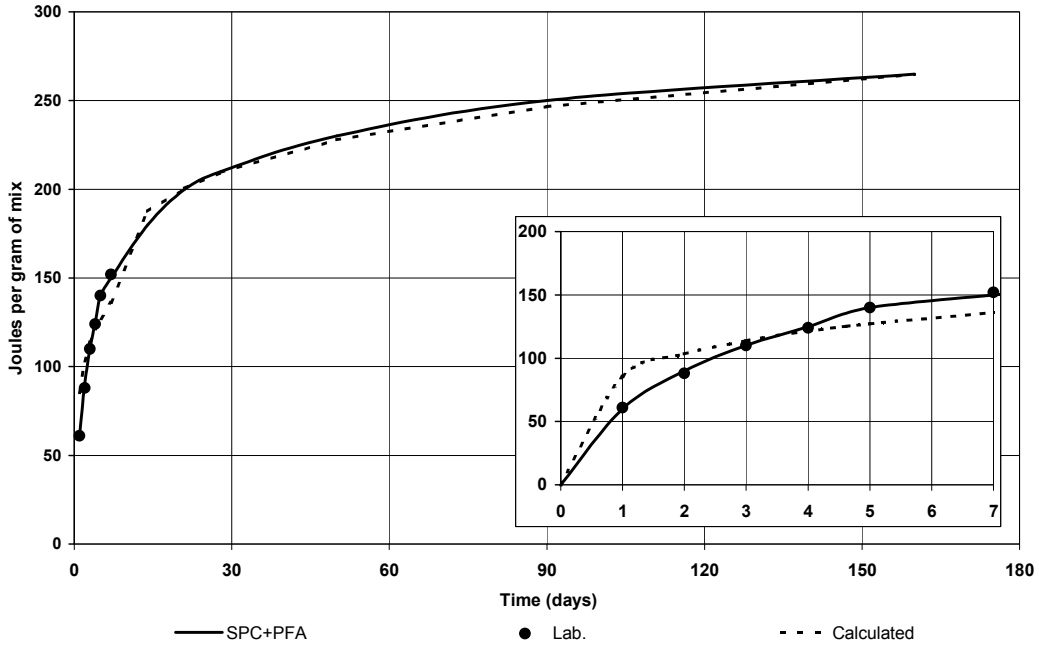

Fig. 4 – Hydration heat for RCC cementitious materials

The time interval considered by FLAC for the thermal analysis during the RCC placement was about 45 minutes.

4.3 THERMAL ANALYSIS

Before the start of the RCC placement, in 13 March 2001, a thermal analysis of the foundation mass subjected to the annual average air temperature was executed. Three boundary conditions were considered in this previous calculus: i) fix temperature at 10 m depth (20 ºC); ii) null flux a few metres upstream and downstream of the base of the dam; and iii) a convective boundary at the top of the foundation, considering the air temperature equal to the values of the average air temperature. An initial uniform temperature of 20 ºC was considered in all the foundation. The analysis executed corresponds to a period of about 14 months (beginning in 1 January 2000). The final temperature distribution (Fig. 5) was considered as an initial condition for the thermal analysis of the dam.

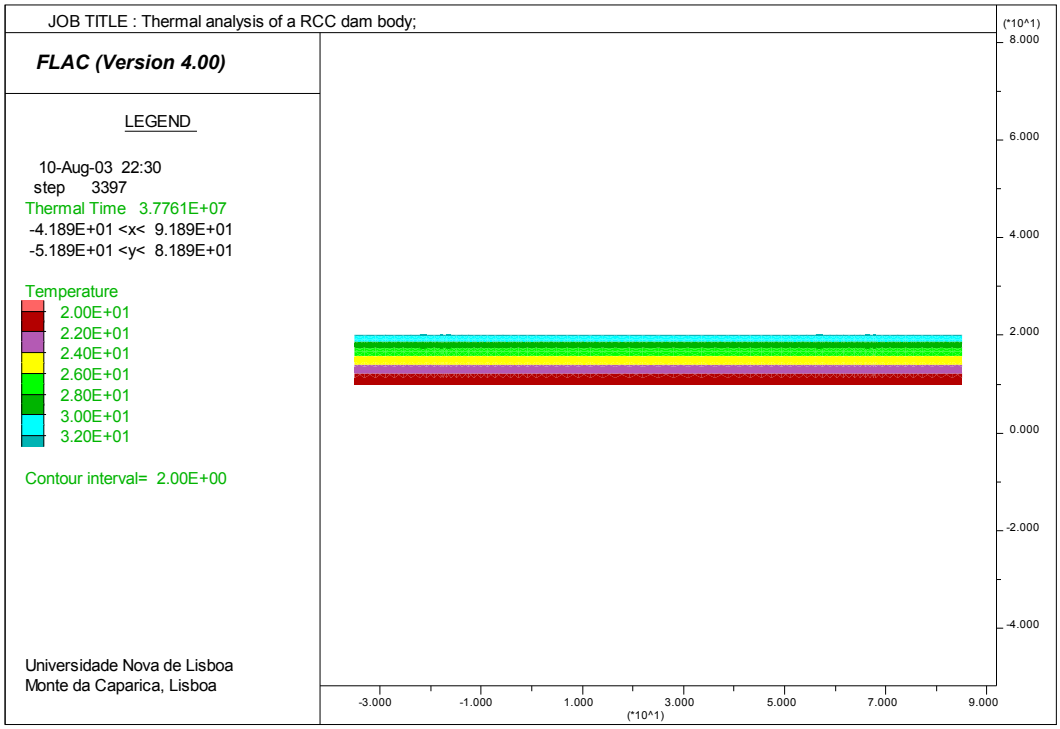

Fig. 5 – Temperature distribution in the foundation when the placement of the RCC has started

The placement of RCC has begun in 13 March 2001 and, in November 2002, has reached the elevation of 68 m. The construction programme was adapted, considering that between every pair of dates there was a continuous placement of RCC layers with a constant rate (Fig. 6).

Every time a new layer was placed, the following procedures were taken: i) removal of the convective boundary condition correspondent to the top of the last layer; ii) thermal activation of the correspondent elements, considering an initial temperature equal to the calculated average air temperature for that date; iii) activation of three convective boundary conditions in the new layer, namely the average air temperature in the top, the upstream air temperature in the upstream face and the downstream air temperature in the downstream face. It was considered that the conventional concrete

and the RCC were instantaneously and simultaneously placed. In figure 6 are also plotted the dates at which the thermal state of the dam was object of analysis.

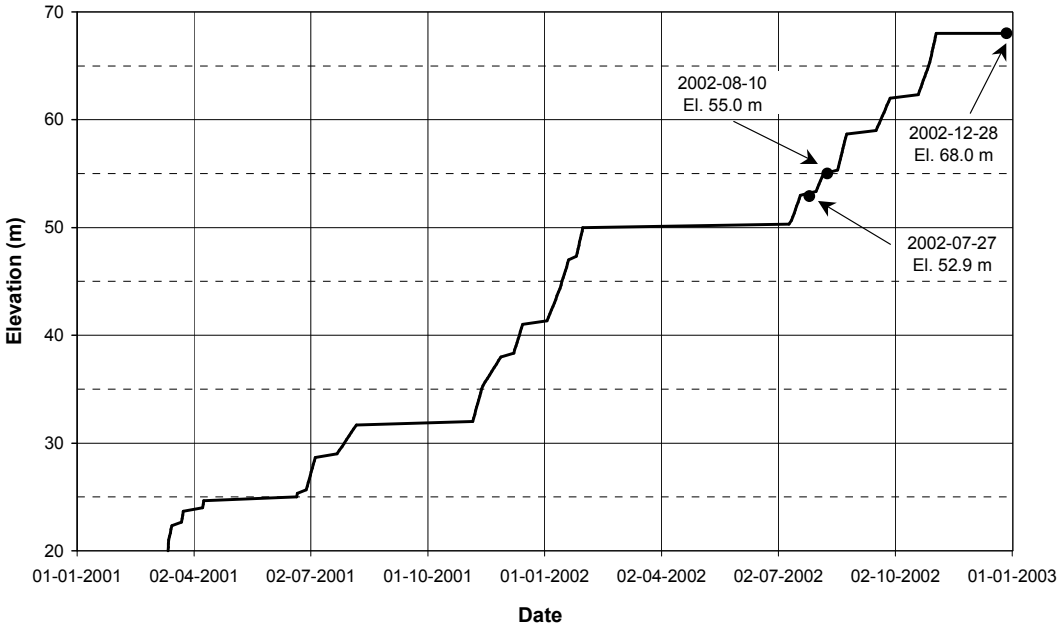

Fig. 6 – Adopted construction programme

5 ANALYSIS OF THE RESULTS

5.1 THERMAL STATE OF THE RCC DAM BODY

The thermal analysis of the dam body at three different dates (2002-07-27, 2002-08-10 and 2002-12-28) is presented in the next paragraphs. The results calculated at the three dates are summarised in the next figures, namely: i) temperature isolines (figures 7, 8 and 9); ii) horizontal profiles at elevations 35.0 m and 50.7 m (figures 10 and 11); iii) vertical profiles at the centre of the dam and at 2 m from each face (Fig. 12); iv) time evolution of the temperatures calculated in the locations where the thermometers are installed (figures 13 and 14).

At 2002-07-27 the temperature of the concrete in the interior of the dam is about 41 ºC at elevation 35.0 m (Fig. 10) and about 36 ºC at elevation 50.7 m (Fig. 11). At the dam faces the temperature of the concrete is similar to the air temperature (about 31 ºC near the upstream face and about 30 ºC near the downstream face), as imposed by the convective boundary conditions. The difference of temperature between the centre and the faces of the dam at elevation 35.0 m is of 10 ºC and occurs in about 12 m (8.3 ºC.m^{-1}); at elevation 50.7 m this difference is of 5 ºC and occurs in about 3.7 m (1.4 ºC.m^{-1}). The temperature drop that is observable in the temperature isolines (Fig. 7) and in the vertical profiles (Fig. 12) near elevation 48 m is due to the long period without concrete placement that occurred between March and July when the concrete was at elevation 54 m. At the top of the dam there was an important temperature decline due to the influence of the air temperature.

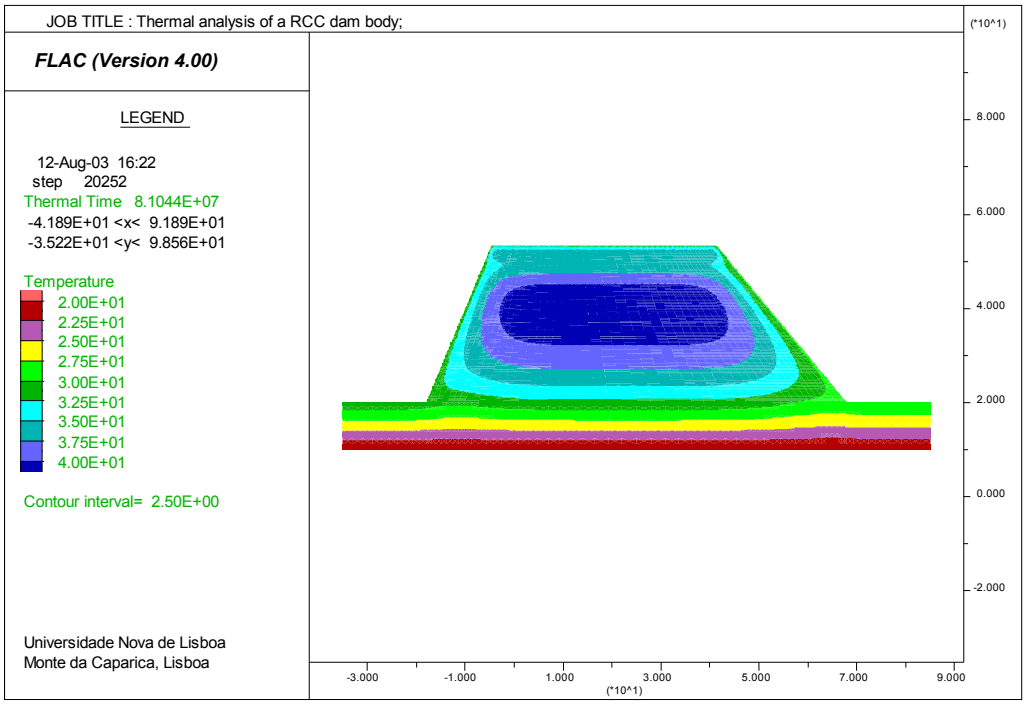

Fig. 7 – Thermal state of the dam at 2002-07-27

There are no significant changes between the thermal sate in 2002-07-27 and 2002-08-10. The analysis of the figures shows only a temperature increase at the elevations where the concrete was placed (between elevations 53.9 m and 55.0 m). At the centre of the dam, the influence of the long period without concrete placement is less important than in July.

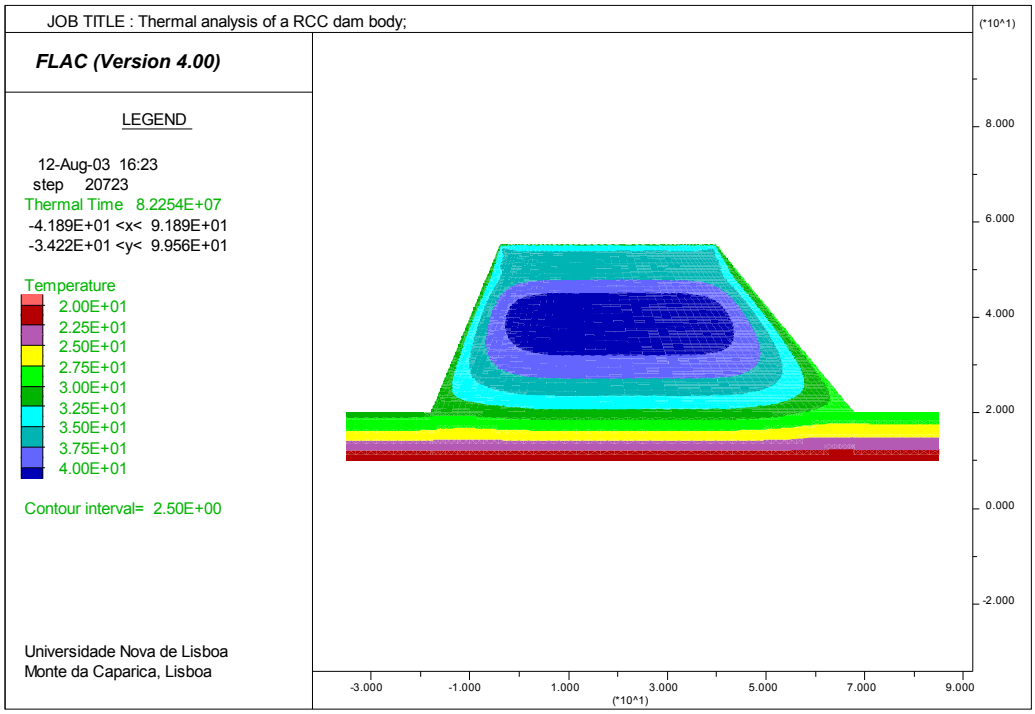

Fig. 8– Thermal state in 2002-08-10

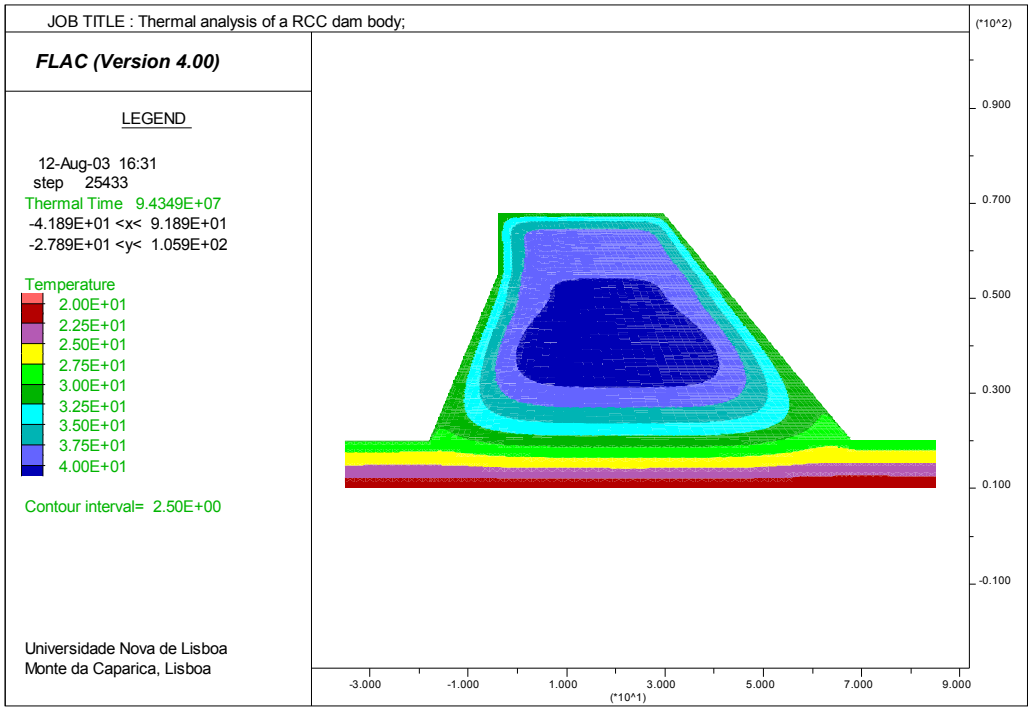

Fig. 9 – Thermal state in 2002-12-28

The placement of the concrete layers between elevations 55.0 m and 68.0 m has not introduced important temperature variations at elevation 35.0 m (Fig. 10), but at elevation 50.7 m there was important temperature variations in the centre of the dam (Fig. 11). At this elevation, the temperature increased about 5 ºC at the centre of the dam, reaching 40.3 ºC, but the temperature gradient near the dam faces has diminished, (1.2 ºC.m^{-1}).

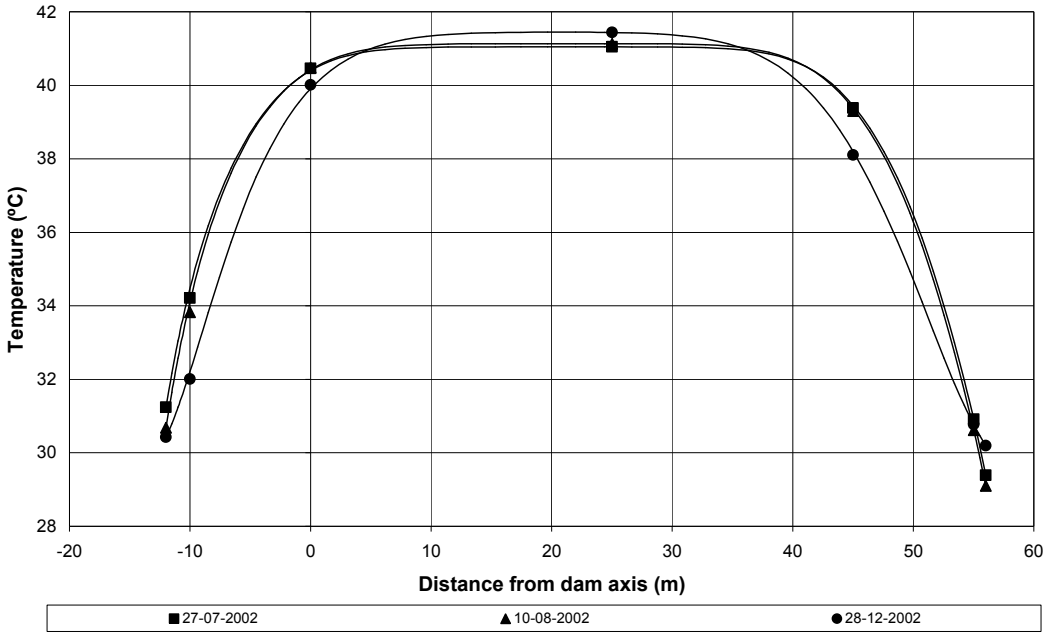

Fig. 10 – Horizontal temperature profiles at elevation 35 m

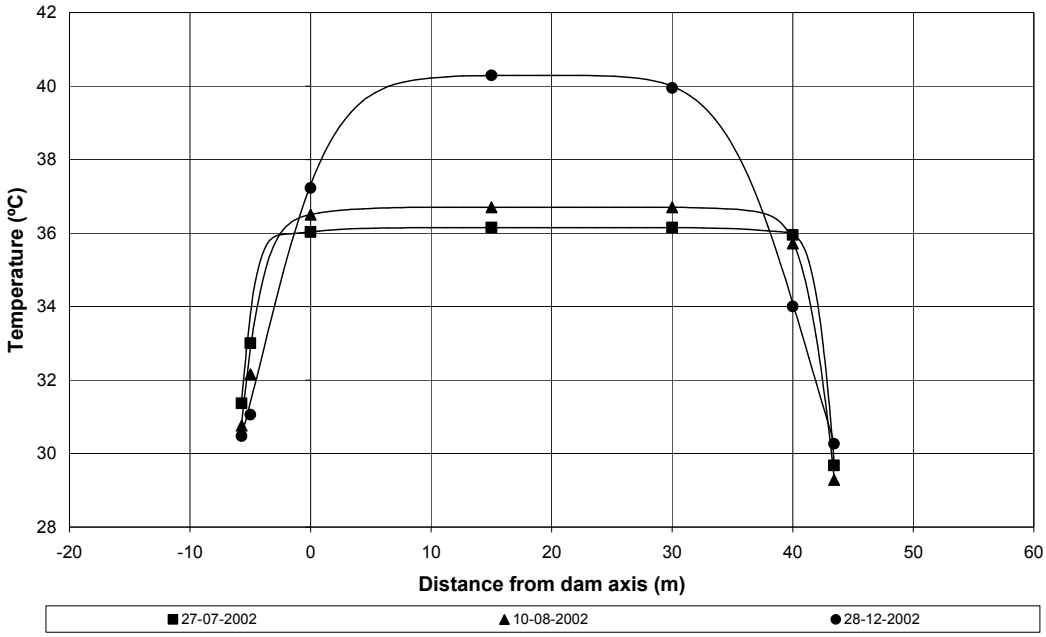

Fig. 11 – Horizontal temperature profiles at elevation 50.7 m

The temperatures at elevation 50.7 m developed at a time rate greater than at elevation 35.0 m (figures 13 and 14), because the speed of the concrete placement increased after August and affected more the temperatures at higher elevations. The time evolution of the temperatures calculated where were installed the thermometers show that the temperature increase is more important in the central locations, because the other ones are influenced by the air temperature at the dam faces. At elevation 50.7 m a temperature of 40 ºC was reached in a small period of time than at elevation 35.0 m.

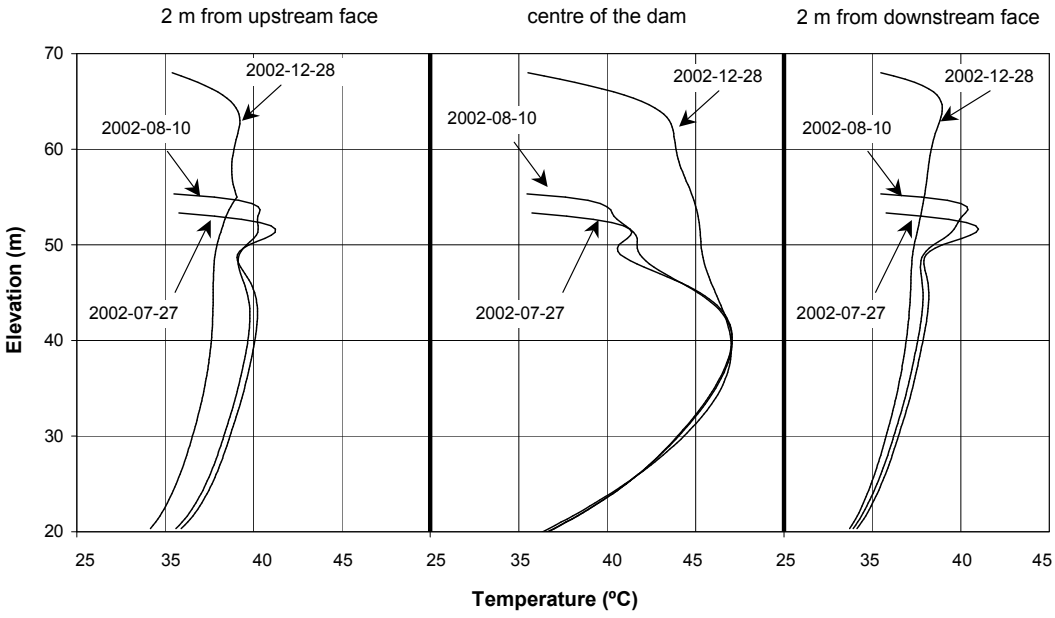

Fig. 12 – Vertical temperature profiles

In figure 16 the maximum temperatures reached in the entire dam body are represented through the use of isolines. The maximum temperatures reached were between 40 ºC and 42.5 ºC in a zone near the centre of the dam at an intermediate elevation. This zone is limited due to the existence of periods without concrete placement, which shows the importance of the concrete placement rate in the maximum temperature reached. On the other hand, the consideration of the conventional concrete near the dam faces is not important, as showed by the analysis of the figures.

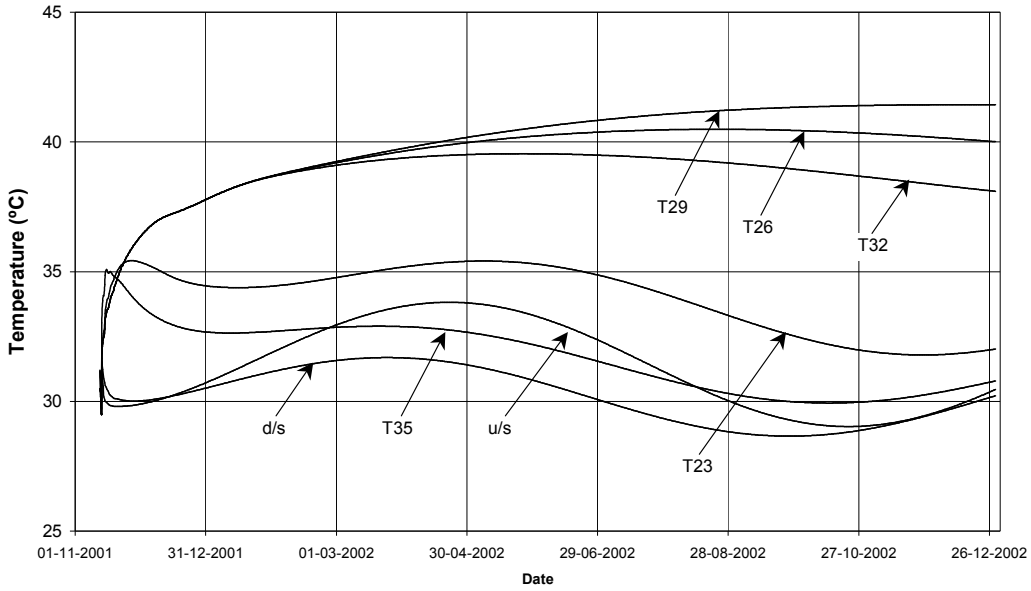

Fig. 13 – Time evolution of the temperatures in the thermometers at elevation 35.0 m

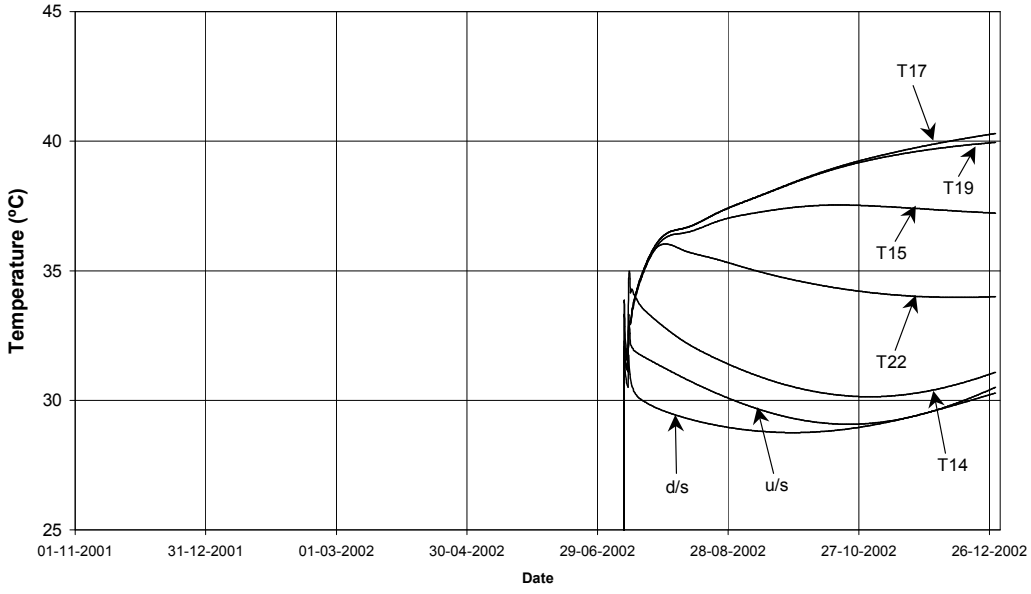

Fig. 14 – Time evolution of the temperatures in the thermometers at elevation 50.7 m

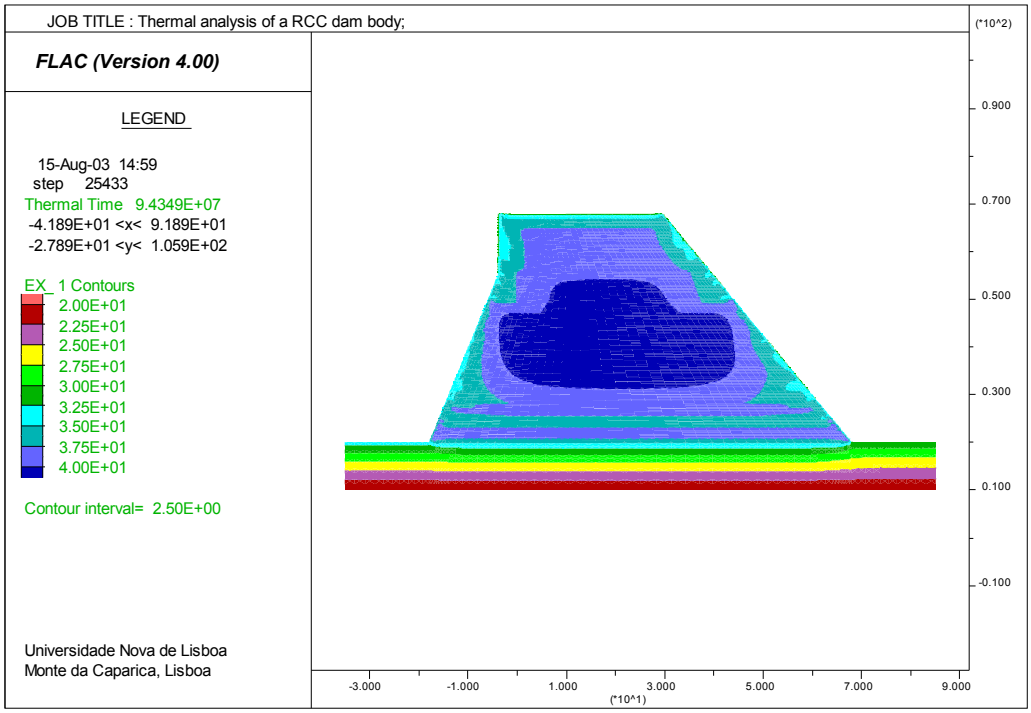

Fig. 15 – Maximum temperatures reached in the dam body

6 FINAL CONSIDERATIONS

The use of RCC allows the construction of concrete dams in short periods of time, through the use of heavy equipment for the placement and the vibration of the concrete. Generally, it corresponds to high volumes of concrete placed in short periods of time, producing important quantities of hydration heat, whose dissipation can originate cracking of the concrete. For this reason, RCC dams projects require detailed thermal analysis during the construction to support decisions about the use of cementitious mixes with low heat generation and adequate construction rhythms.

In this paper, a thermal analysis of a high RCC dam construction, built in a region with a tropical climate, was presented. It was developed a mathematical model using FLAC, a commercial programme from Itasca Consulting Group [3], which allows the simulation of the placement of 0.3 m thickness layers of RCC, according to the proposed schedule construction programme. The model considers the existence of two conventional concrete 1 m strips, one near the upstream face and the other near the downstream face, which present more important heat generation. The hydration heat of each concrete layer is calculated as a function of its age, whose parameters were determined from results of in situ and laboratory tests.

The model includes a zone of the foundation with the same thermal properties of the RCC. The thermal state of this zone in the beginning of the RCC placement was calculated considering two boundaries with null heat flux upstream and downstream of the dam, a boundary with a fix 20 ºC temperature at 10 m depth, and a convective boundary at the top, considering the influence of the average air temperature during fourteen months. Each concrete layer has three convective boundaries – the upstream

face, the top of the layer and the downstream face – each one with its own temperatures. It was considered that the initial temperature of each concrete layer was the calculated air temperature.

The results show the importance of the time rate of the concrete placement and of the existence of periods without concrete placement that increase the hydration heat dissipation. On the other hand, the consideration of the conventional concrete strips near the dam faces, which produce more hydration heat, is not relevant for the thermal analysis. Nevertheless, this results depends on the input data, namely of insufficient data about the air temperature, which influence the initial temperature of the concrete layers and the convective boundary conditions. In fact, the calculated air temperature corresponds to annual periodic cycles with small amplitudes, typical in tropical climates. The consideration of temperature variations with daily cycles, not considered due to insufficient data, could produce more severe results.

Thermal analyses shall be developed coupled with mechanical analysis that considers the time evolution of the concrete properties, namely its deformability [4]. The consideration of the time variation of concrete properties is important because, at early ages, the concrete presents higher deformability (which means that thermal variations produces lower stresses) and higher creep rates (which means higher thermal stresses relaxation), but these properties have important variations in small periods of time. These kind of coupled studies are complex, because each concrete layer must be considered with its own deformability and its own hydration heat, since these characteristics are function of the concrete age. Besides, they require laboratorial tests to characterize the time evolution of the deformability and of the thermal properties of the concrete, including the hydration heat of the cementitious mix.

REFERENCES

[1] American Concrete Institute (ACI) – Manual of Concrete Practice. Cement and Concrete Terminology. ACI 116R, Detroit.

[2] US Army Corps of Engineers – Roller-Compacted Concrete. Engineer Manual EM 1110-2-2006, 2000.

[3] ITASCA – FLAC User's Guide, Itasca Consulting Group, Minneapolis, 2002.

[4] US Army Corps of Engineers – Engineering and design. Thermal studies of mass concrete structures. Engineer Technical Letter ETL 1110-2-542, 1997.

7th Benchmark Workshop on Numerical Analysis of Dams

Theme B: Thermal Analysis of a RCC Dam Body during Construction

Mojtaba Farrokh*, Gholamreza Khoshrang
Structural Division of Dam Department
Mahab Ghodss Consulting Engineers; Tehran, Iran

SUMMARY: This paper presents the computational results obtained for a RCC dam concerning participation on theme B of 7th benchmark workshop on numerical analysis of a dam. Thermal analysis is performed using a finite element program named "ANSYS". The geometry of dam and initial information are similar to suggested with some modification. The results are presented as suggested tables and also in the form of contour lines.

1. BASIC EQUATION FROM HEAT TRANSFER

The concept and fundamentals equation of the three basic heat transfer modes: conduction, convection and radiation are summarized. For an isotropic solid with temperature-independent thermal conductivity the law of conservation of energy with Fourier's law yields the thermal energy equation. The law of conservation of energy is;

$$\frac{\partial^2 T}{\partial x^2}+\frac{\partial^2 T}{\partial y^2}+\frac{\partial^2 T}{\partial z^2}+\frac{Q}{k}=\frac{1}{\alpha}\frac{\partial T}{\partial t} \tag{1}$$

Where T(x,y,z,t) is the temperature, Q is the internal heat generation rate per unit volume, ρ is the density, c is the specific heat, t is time and α is thermal diffusivity defined by

$$\alpha=\frac{k}{\rho c} \tag{2}$$

Convection is the transfer of thermal energy through a fluid due to motion of fluid. In this study we use specified convection surface over surfaces of dam which are adjacent to air.

The heat conduction equation (1) is solved subject to an initial conduction and appropriate boundary conditions. The initial condition consists of specifying the temperature throughout the solid at initial time. The boundary conditions encountered in finite element formulations are the followings:

Prescribed Temperature

The surface temperature of a boundary is specified to be constant or a function of a boundary coordinates and/or time.

* Ph.D. student of Sharif University of Technology ,Tehran , Iran

Prescribed Heat Flow

The rate of heat flow across a boundary is specified to be a constant or a function of a boundary coordinate and/or time. For an isotropic solid, Fourier's law expresses surface heat flow as

$$-k\frac{\partial T}{\partial n} = q_s \tag{3}$$

Where n is normal to boundary, and q_s is the rate of surface heat flow per area. It is possible to apply adiabatic boundary condition when the rate of flow across a boundary is zero.

Convective Heat Exchange

When the rate of heat flow across a boundary is proportional to the different between the surface temperature Ts and a convective exchange temperature Te of adjacent fluid, from Fourier's the convective boundary condition is

$$-k\frac{\partial T}{\partial n} = h(T_s - T_e) \tag{4}$$

Where h is a convection heat transfer coefficient (film coefficient).
A convection coefficient may be temperature dependent. The convective exchange temperature Te may be a function of a boundary coordinate and/or time.

Radiation heat exchange

In this case the rate of heat flow across a boundary is specified in terms of the emitted energy from the surface and the incident radiant thermal energy, emitted and reflected from other solids and/or fluids. The boundary condition is

$$-k\frac{\partial T}{\partial n} = \sigma\varepsilon T_s^4 - \beta q_r \tag{5}$$

Where σ is the Stefan- Boltzman constant, ε is the surface emissive and Ts is the surface temperature. The coefficient β is the surface absorptive and q_r is the incident radiant thermal energy.

The boundary condition previously described covers many cases of practical interest. Other boundary condition is beyond the scope of this study.

2. FINITE ELEMENT FORMULATION

Consider transient heat transfer in a three-dimensional isotropic solid Ω bounded by a surface Γ. The problem is governed by equation (1). The heat conduction equation is solved subject to an initial condition and boundary conditions on all portions of the surface Γ. The initial condition specifies the temperature distribution at time zero,

$$T(x, y, x, 0) = T_0(x, y, z) \tag{6}$$

As mentioned before, heat conduction boundary conditions take several forms which consist of specified surface temperature, specified surface heat flow, convective heat exchange, and radiation heat exchange. These boundary conditions are

$$T_s = T_1(x, y, z, t) \qquad on \quad S_1$$

$$(7a)\ k\left(\frac{\partial T}{\partial x}n_x + \frac{\partial T}{\partial y}n_y + \frac{\partial T}{\partial z}n_z\right) = q_s \quad on \quad S_2 \tag{7b}$$

$$k\left(\frac{\partial T}{\partial x}n_x + \frac{\partial T}{\partial y}n_y + \frac{\partial T}{\partial z}n_z\right) = h(T_e - T_s) \quad on \quad S_3 \tag{7c}$$

$$k\left(\frac{\partial T}{\partial x}n_x + \frac{\partial T}{\partial y}n_y + \frac{\partial T}{\partial z}n_z\right) = \beta q_r - \sigma\varepsilon T_s^4 \quad on \quad S_4 \tag{7d}$$

where T_1 is the specified surface temperature, which may vary with position and time, n_x, n_y, and n_z are direction cosines of outward normal to the surface. By defining

$$\{L\}^T = \left\{\frac{\partial}{\partial x} \quad \frac{\partial}{\partial y} \quad \frac{\partial}{\partial z}\right\} \tag{8}$$

$$\{n\}^T = \{n_x \quad n_x \quad n_z\} \tag{9}$$

$$[D] = \begin{bmatrix} k & 0 & 0 \\ 0 & k & 0 \\ 0 & 0 & k \end{bmatrix} \tag{10}$$

Equations (1) and (7) can be written in matrices form a

$$\{L\}^T [D]\{L\}T + Q = \rho c \frac{\partial T}{\partial t} \tag{11}$$

$$\{n\}^T [D]\{L\}T = q_s \qquad on \quad S_2 \tag{12a}$$

$$\{n\}^T [D]\{L\}T = h(T_e - T_s) \qquad on \quad S_3 \tag{12b}$$

$$\{n\}^T [D]\{L\}T = \beta q_r - \sigma\varepsilon T_s^4 \qquad on \quad S_4 \tag{12c}$$

As stated before, the variable T was allowed to vary in both space and time. This dependency is separated as

$$T = \{N\}^T \{T^e\} \tag{13}$$

Where

$$\{N\} = \{N(x, y, z)\} = element\ shap\ function$$
$$\{T^e\} = \{T^e(t)\} = nodal\ temperature\ vector$$

Thus the time derivative of equation (13) may be written as

$$\dot{T} = \frac{\partial T}{\partial t} = \{N\}^T \{\dot{T}^e\} \tag{14}$$

The combination {L} T is written as

$$\{L\}T = [B]\{T^e\} \tag{15}$$

Where

$$[B] = \{L\}\{N\}^T$$

The method of weighted residuals can be used to derive the element equations. By using Gauss's theorem and boundary conditions after some manipulation the result element equation become

$$[C]\{\dot{T}^e\} + ([K_c] + [K_h])\{T^e\} = \{R_Q\} + \{R_q\} + \{R_h\} + \{R_\sigma\} + \{R_r\} \tag{16}$$

Where

$$[C] = \int_{\Omega^e} \rho c \{N\}\{N\}^T d\Omega$$

$$[K_c] = \int_{\Omega^e} [B]^T [D][B] d\Omega$$

$$[K_h] = \int_{S_3} h \{N\}\{N\}^T d\Gamma$$

$$\{R_Q\} = \int_{\Omega^e} Q \{N\} d\Omega$$

$$\{R_q\} = \int_{S_2} q_s \{N\} d\Gamma$$

$$\{R_h\} = \int_{S_3} h T_e \{N\} d\Gamma$$

$$\{R_\sigma\} = -\int_{S4} \sigma \varepsilon T_s^4 \{N\} d\Gamma$$

$$\{R_r\} = \int_{S4} \beta q_r \{N\} d\Gamma$$

The coefficient matrix [C] of the time derivative of the nodal temperatures is the element capacitance matrix. The coefficient matrix $[K_c]$ and $[K_h]$ are element conductance matrices and relate to conduction and convection only for elements with surface convection. The vectors $\{R_Q\}$, $\{R_q\}$, and $\{R_h\}$ are heat load vectors arising from internal heat generation, specified surface heating, and surface convection, respectively. The vectors $\{R_\sigma\}$ and $\{R_r\}$ arise from surface radiation.

Criteria for heat transmission in solid material, boundary condition and the finite element method for solving heat equation were discussed in the above lines. In order to control crack which is from cement and water content, thermal studies for predicting temperature and stress should be performed for RCC dam. The most complicated thing in thermal analysis for a RCC dam is the rapid method of construction. The concrete lifts, which are placed at different time, have different thermal and mechanical properties as well as different boundary condition. In order to appropriately calculate the temperature and thermal stress, the spatially and temporally changing material properties, boundary conditions and geometry should be considered as realistically as possible and reasonable. For this purpose 'ANSYS' program which is able to birth and death elements, solving most various physical problems as well as heat flow, was chosen.

According to the size and thickness of a RCC dam, most heat flux only in the vertical direction and presumes that the concrete mass in the two horizontal dimensions is infinite. This method is appropriate to determine the temperature of points which are located far enough from the dam faces. However, the temperatures distribution is a two dimensional problem in RCC dams. Because the construction method eliminates the lateral faces of the blocks and one can consider that there is no heat flux along the dam and then it is sufficient to consider to transverse section. Only in the cases where the chord-height rate is low there is an influence of the heat transmission in the longitudinal direction towards the foundation ground. For these reason two dimensional analyses is chosen. The details are as follows:

3. DAM GEOMETRY

General information of dam geometry is shown in figure (1) and is the same as the author's proposal. Dam shape between elevations 21.1m and 67.9m is only considered in finite element model.

4. PROPERTIES OF RCC MATERIAL

The properties of RCC material are given in table (1).

Table (1).Properties of RCC material

Variable	Symbol	Value	Unit
Unite weight	ρ	2380	kg/m^3
Specific heat	c	1.0	kJ/kg/°C
Conductivity	k	10	kJ/m/h/°C
Diffusivity	α	0.0042	m^2/h

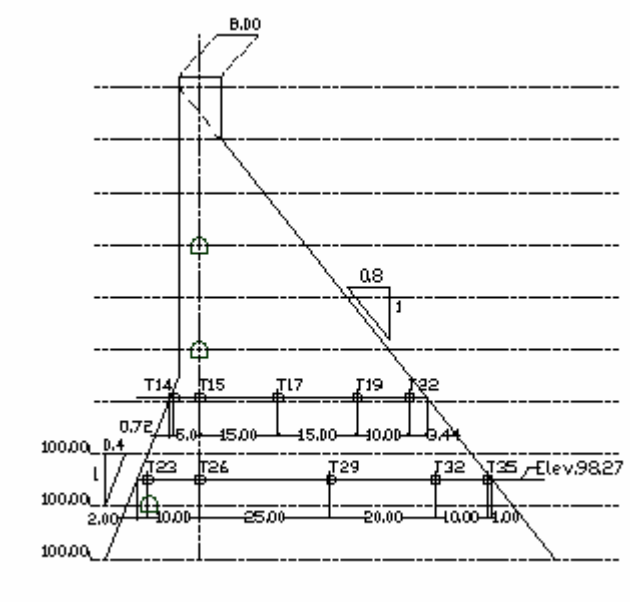

Figure (1): Dam geometry and sensor placement

The cementitious material incorporated into RCC is a mix of Portland cement (STC) and pouzzolanic fly ashes (PFA), with 100 kg and 90kg of PFA per cubic meter. The hydration heat of the STC+PFA mix is given in figure (2).

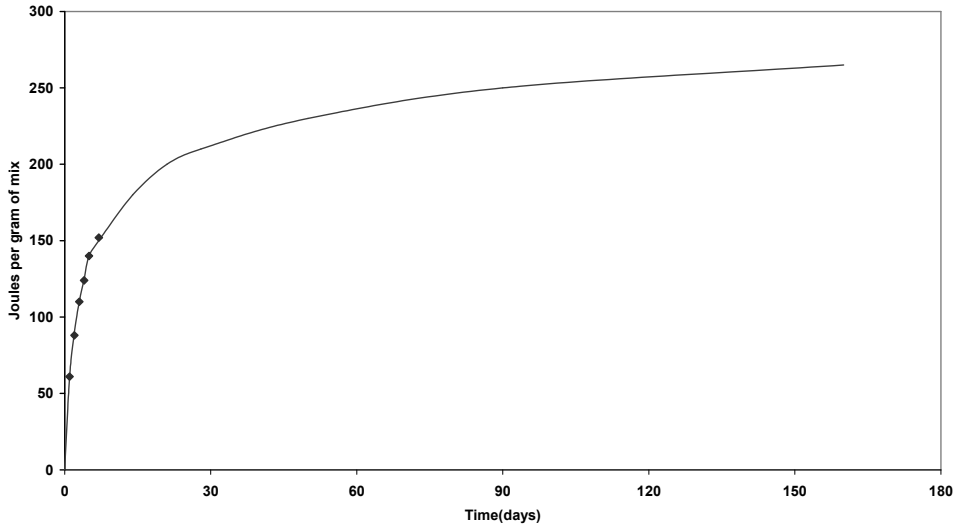

Figure (2): Hydration Heat of Cementitious Material

With above information, the heat generation rate and adiabatic temperature of RCC material can be estimated. By multiplying the hydration heat of STC+PFA mix in 190 and differentiating it with respect to time the heat generation rate per unit of volume will be calculated. The heat generation rate of RCC material which is used in finite element method is shown in figure (3).

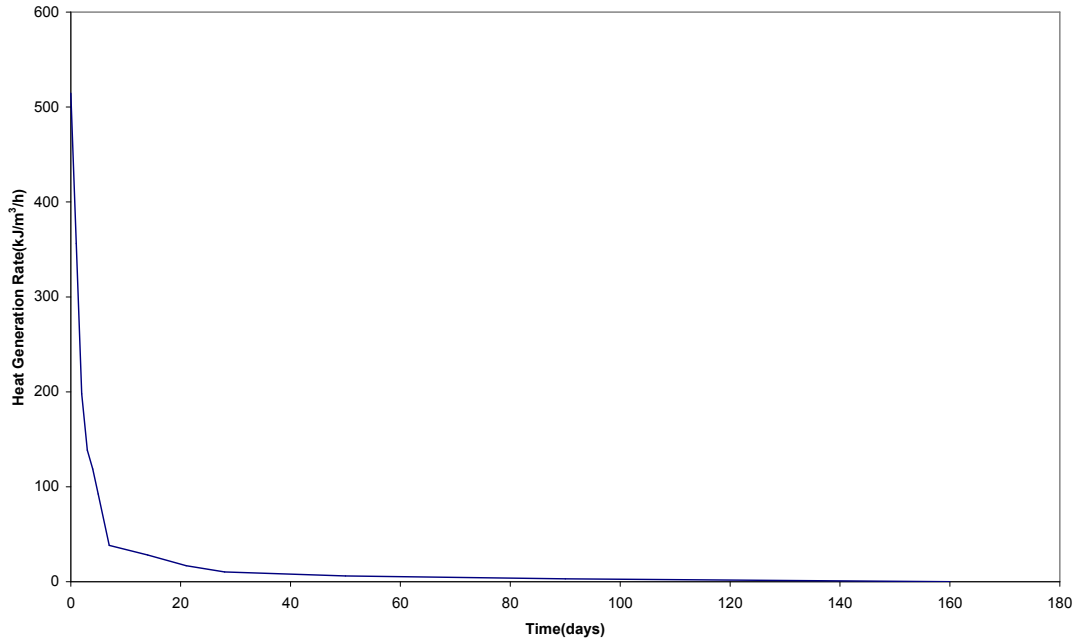

Figure (3): Heat Generation Rate of RCC Material

The adiabatic temperature is also estimated by equation (17) and is shown in figure (4).

$$Q = mc\Delta\theta \tag{17}$$

Where Q is heat energy, m is mass; c is specific heat and $\Delta\theta$ is adiabatic rise temperature.

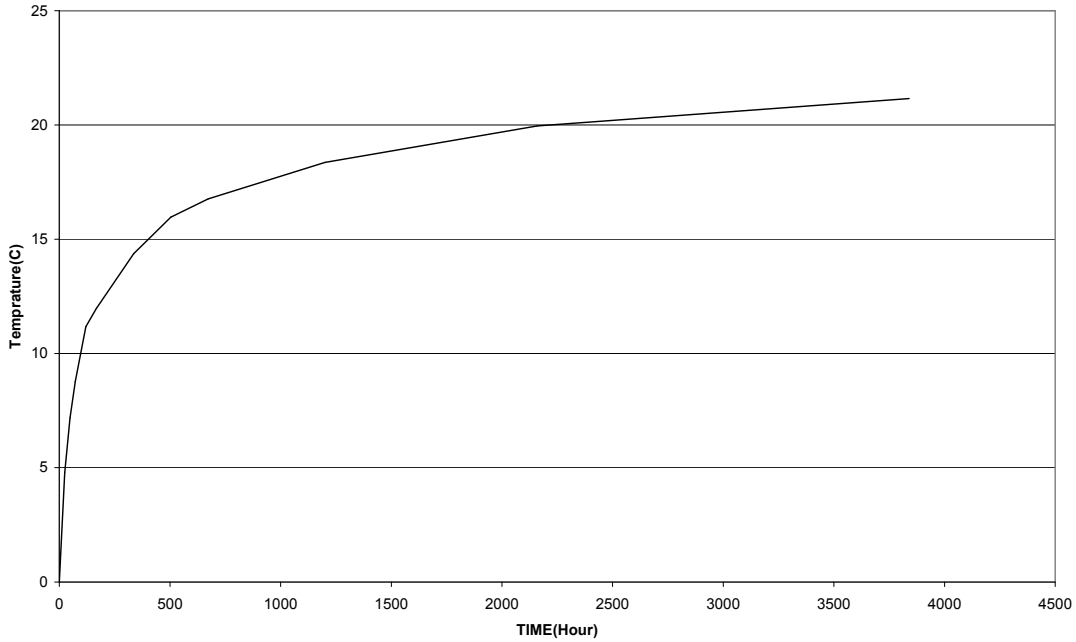

Figure (4): Adiabatic Temperature of RCC Material

5. AMBIENT TEMPERATURE OF AIR

Ambient temperature at the side is given from 14 November 2001 up to 24 December 2002, but duration of construction of dam is from 13 March up to 3 November 2002. For this reason the ambient temperature is repeated from next year.

6. INITIAL TEMPERATURE

Initial temperature of concrete those are not given, are assumed the same as the ambient temperature.

7. BOUNDARY CONDITIONS

Boundary conditions for thermal analysis of the RCC dam are as follows:
Initial temperature of each layer is calculated except those are given. Because of no information for foundation, prescribed temperature on boundary between dam and foundation is assumed to be equal of annual ambient temperature. (Say 30^{o}C)

To perform convective heat exchange in finite element model, the film coefficient is considered. In this study for radiation and convection effects, the film coefficient is equal to h=100kJ/m^2/h/^{o}C. According to the h value, boundary condition for radiation effect is simplified.

Concrete temperature in vicinity of air changes in respect to time and assumed that temperature for upper surface of concrete is the average of U/S & D/S temperature on that time

8. FINITE ELEMENT AND CONSTRUCTION MODEL PROCCESS

Finite element mesh for thermal analysis in ANSYS program includes 44304 elements and 44759 nodes. Every 30cm concrete layer has two element rows. The model is only considered between elevation 21.1m and 67.9m.

In order to consider construction method in model, total elements are built at first, and all nodes of elements will be reached to initial temperature by using a steady state analysis. Then according to the rate and period of construction, the time when the element should be activated, is calculated. After activating of the elements for each layer, the boundary condition related to convective heat exchange will be changed appropriately. And finally, transient analysis with time step integration of 6 hours will be performed.

9. RESULTS

Thermal analysis of the RCC dam has been done for period of 21 months and the requested results for two dimensional models are shown in tables (2) & (3). The tables are included of temperature in specific points and profile of temperature in different elevation of dam body as well as. Furthermore the results of temperature for different time are given as follows;
In figure (5) temperature distribution on dam body after 8 months when the dam builds up to elevation (34.9) is shown.

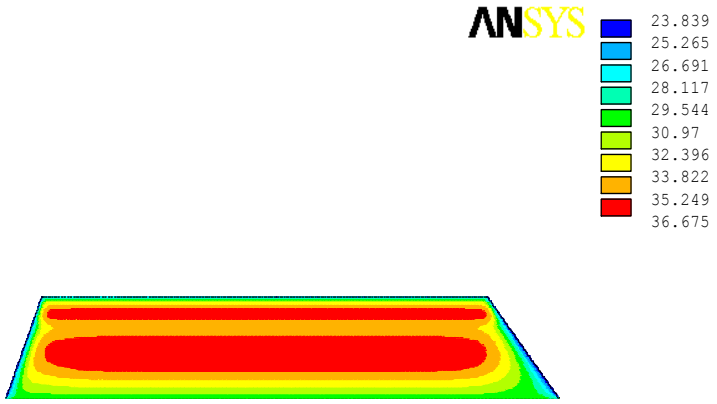

Figure (5): Temperature Distribution of RCC Dam on 14 November 2001

In figure (6) temperature distribution on dam body after one year when the dam builds up to elevation (46.9) is shown.

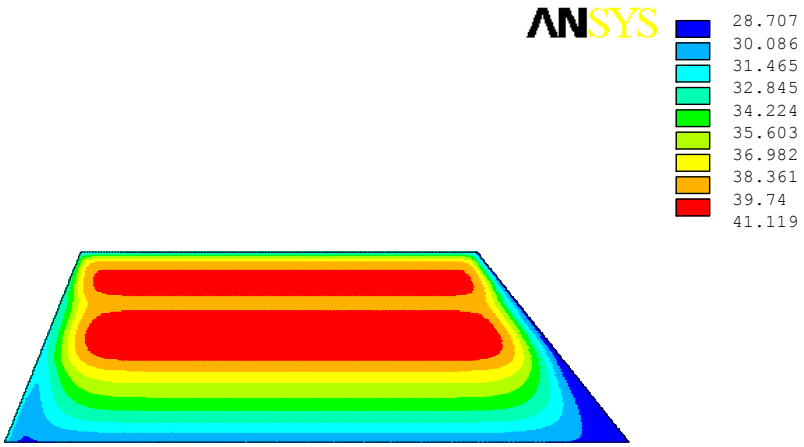

Figure (6): Temperature Distribution of RCC Dam on 11 July 2002

In figure (7) temperature distribution on dam body at the end of analysis is shown.

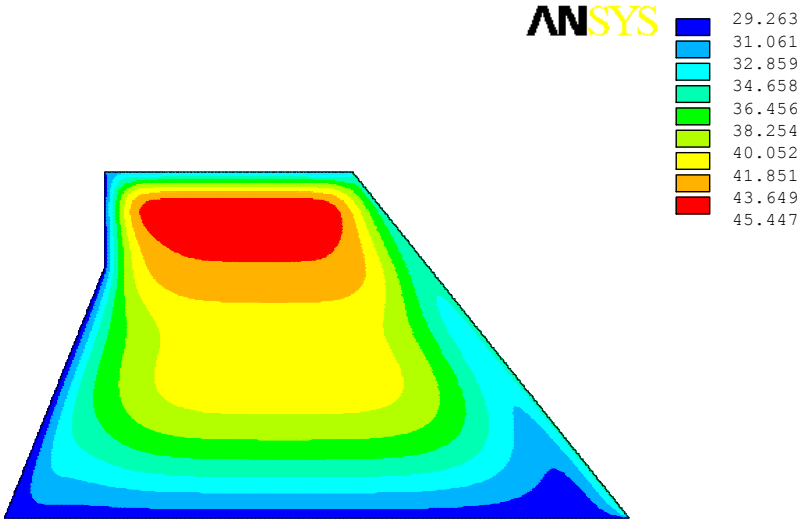

Figure (7): Temperature Distribution of RCC Dam on 28 December 2002

Table (2): Results at Center of Horizontal Sections

Center - Results Vs time			
Date	Value at center at el 35.00 participant	Date	Value at center at el. 50.70 participant
2001/11/14	24.9	**2002/07/13**	34.71
2001/11/17	31.3	2002/07/20	38.43
2001/11/24	36.0	2002/07/27	39.49
2001/12/01	38.2	2002/08/03	39.18
2001/12/08	39.2	2002/08/10	38.97
2001/12/15	39.41	2002/08/17	39.35
2001/12/22	39.68	2002/08/24	39.71
2001/12/29	40.07	2002/08/31	39.91
2002/01/05	40.44	2002/09/07	40.08
2002/01/12	40.74	2002/09/14	40.29
2002/01/19	41.0	2002/09/21	40.5
2002/01/26	41.1	2002/09/28	40.7
2002/02/02	41.2	2002/10/05	41.0
2002/02/09	41.3	2002/10/12	41.1
2002/02/16	41.4	2002/10/19	41.3
2002/02/23	41.4	2002/10/26	41.4
2002/03/02	41.5	2002/11/02	41.5
2002/03/09	41.5	2002/11/09	41.6
2002/03/16	41.6	2002/11/16	41.7
2002/03/23	41.6	2002/11/23	41.8
2002/03/30	41.6	2002/11/30	41.8
2002/04/06	41.6	2002/12/07	41.9
2002/04/13	41.6	2002/12/14	41.9
2002/04/20	41.6	2002/12/21	42.0
2002/04/27	41.5	2002/12/28	42.0
2002/05/04	41.5		
2002/05/11	41.5		
2002/05/18	41.4		
2002/05/25	41.4		
2002/06/01	41.4		
2002/06/08	41.3		
2002/06/15	41.3		
2002/06/22	41.3		
2002/06/29	41.2		
2002/07/06	41.2		
2002/07/13	41.2		
2002/07/20	41.1		
2002/07/27	41.1		
2002/08/03	41.1		
2002/08/10	41.0		
2002/08/17	41.0		
2002/08/24	40.9		
2002/08/31	40.9		
2002/09/07	40.9		
2002/09/14	40.8		
2002/09/21	40.8		
2002/09/28	40.7		
2002/10/05	40.7		
2002/10/12	40.6		
2002/10/19	40.6		
2002/10/26	40.5		
2002/11/02	40.4		
2002/11/09	40.4		
2002/11/16	40.3		
2002/11/23	40.3		
2002/11/30	40.2		
2002/12/07	40.2		
2002/12/14	40.1		
2002/12/21	40.1		
2002/12/28	40.0		

Center - Results Vs elevation			
Elevation	Value at center on 27/07/02 participant	Value at center on 10/08/02 participant	Value at center on 28/12/02 participant
62.10			45.43
61.50			45.31
60.90			45.13
60.30			44.92
59.70			44.71
59.10			44.49
58.50			44.29
57.90			44.11
57.30			43.96
56.70			43.83
56.10			43.7
55.50			43.56
54.90		31.76	43.4
54.30		37.37	43.23
53.70		39.22	43.04
53.10		39.27	42.84
52.50	34.49	38.81	42.62
51.90	38.05	38.69	42.4
51.30	39.5	38.85	42.18
50.70	39.49	38.97	41.97
50.00	38.61	38.85	41.77
49.40	37.5	38.5	41.58
48.80	36.9	38.23	41.42
48.20	36.83	38.13	41.28
47.60	37.2	38.24	41.17
47.00	37.88	38.54	41.09
46.40	38.7	39.01	41.04
45.80	39.56	39.58	41.01
45.20	40.38	40.18	41
44.60	41.1	40.78	41.02
44.00	41.71	41.32	41.04
43.40	42.19	41.79	41.07
42.80	42.56	42.17	41.11
42.20	42.83	42.46	41.14
41.60	42.99	42.66	41.16
41.00	43.08	42.78	41.18
40.40	43.08	42.82	41.17
39.80	43.03	42.8	41.15
39.20	42.91	42.72	41.1
38.60	42.75	42.58	41.02
38.00	42.55	42.41	40.93
37.40	42.31	42.19	40.8
36.80	42.05	41.94	40.64
36.20	41.75	41.66	40.46
35.60	41.44	41.35	40.25
35.00	41.1	41.03	40.01
34.40	40.75	40.68	39.75
33.80	40.37	40.31	39.46
33.20	39.99	39.93	39.15
32.60	39.58	39.53	38.82
32.00	39.16	39.11	38.46
31.40	38.73	38.68	38.09
30.80	38.29	38.24	37.7
30.20	37.83	37.79	37.3
29.60	37.37	37.33	36.88
29.00	36.89	36.85	36.45
28.40	36.4	36.37	36
27.80	35.91	35.88	35.55
27.20	35.41	35.38	35.08
26.60	34.9	34.87	34.61
26.00	34.38	34.36	34.13
25.40	33.86	33.85	33.64
24.80	33.34	33.32	33.15
24.20	32.81	32.8	32.66
23.60	32.28	32.27	32.16

Table (3): 2-D Results

2-D results Vs time			
Date	Value at T23 sensor (u/s, el 35.00)	Date	Value at T22 sensor (d/s, el. 50.70)
2001/11/14	24.9	**2002/07/13**	34.7
2001/11/17	31.2	2002/07/20	38.29
2001/11/24	35.4	2002/07/27	39.03
2001/12/01	36.6	2002/08/03	38.24
2001/12/08	36.74	2002/08/10	37.64
2001/12/15	36.13	2002/08/17	37.37
2001/12/22	35.58	2002/08/24	37.04
2001/12/29	35.24	2002/08/31	36.66
2002/01/05	35.01	2002/09/07	36.25
2002/01/12	34.82	2002/09/14	35.97
2002/01/19	34.7	2002/09/21	35.9
2002/01/26	34.9	2002/09/28	35.8
2002/02/02	35.3	2002/10/05	35.7
2002/02/09	35.7	2002/10/12	35.6
2002/02/16	35.8	2002/10/19	35.4
2002/02/23	35.9	2002/10/26	35.3
2002/03/02	35.9	2002/11/02	35.2
2002/03/09	36.1	2002/11/09	35.2
2002/03/16	36.7	2002/11/16	35.1
2002/03/23	37.4	2002/11/23	35.0
2002/03/30	37.9	2002/11/30	34.9
2002/04/06	38.0	2002/12/07	34.8
2002/04/13	37.7	2002/12/14	34.8
2002/04/20	37.0	2002/12/21	35.0
2002/04/27	36.4	2002/12/28	35.2
2002/05/04	36.6		
2002/05/11	36.5		
2002/05/18	35.7		
2002/05/25	34.9		
2002/06/01	34.6		
2002/06/08	34.4		
2002/06/15	34.2		
2002/06/22	34.1		
2002/06/29	34.1		
2002/07/06	34.1		
2002/07/13	34.3		
2002/07/20	34.3		
2002/07/27	34.0		
2002/08/03	33.4		
2002/08/10	33.4		
2002/08/17	33.2		
2002/08/24	33.0		
2002/08/31	32.9		
2002/09/07	32.9		
2002/09/14	33.0		
2002/09/21	33.2		
2002/09/28	33.7		
2002/10/05	34.3		
2002/10/12	34.6		
2002/10/19	34.7		
2002/10/26	34.7		
2002/11/02	34.6		
2002/11/09	34.6		
2002/11/16	34.7		
2002/11/23	34.9		
2002/11/30	35.0		
2002/12/07	34.5		
2002/12/14	33.6		
2002/12/21	33.0		
2002/12/28	32.6		

2-D results Vs elevation			
Elevation	Value at 2 m from u/s face on 27/07/02	Value at 2 m from d/s face on 10/08/02	Value at 4 m from d/s face on 28/12/02
62.10			41.07
61.50			40.77
60.90			40.15
60.30			39.87
59.70			39.55
59.10			39.31
58.50			39.07
57.90			38.86
57.30			38.35
56.70			38.16
56.10			37.93
55.50			37.73
54.90		31.76	37.52
54.30		37.37	37.32
53.70		39.22	36.83
53.10		39.27	36.62
52.50	34.24	38.81	36.34
51.90	37.44	38.69	36.13
51.30	38.5	38.85	35.92
50.70	38.18	38.97	35.73
50.00	36.69	38.85	35.28
49.40	35.45	38.5	35.13
48.80	34.72	38.23	34.99
48.20	34.05	38.13	34.88
47.60	34.01	38.24	34.76
47.00	34.15	38.54	34.69
46.40	34.37	39.01	34.42
45.80	34.6	39.58	34.37
45.20	34.81	40.18	34.32
44.60	34.99	40.78	34.29
44.00	35.12	41.32	34.25
43.40	35.21	41.79	34.2
42.80	35.27	42.17	34.15
42.20	35.31	42.46	34.1
41.60	35.31	42.66	33.87
41.00	35.29	42.78	33.81
40.40	35.25	42.82	33.74
39.80	35.2	42.8	33.66
39.20	35.14	42.72	33.57
38.60	34.41	42.58	33.48
38.00	34.35	42.41	33.35
37.40	34.28	42.19	33.24
36.80	34.21	41.94	33.12
36.20	34.13	41.66	33
35.60	34.05	41.35	32.79
35.00	33.96	41.03	32.66
34.40	33.87	40.68	32.53
33.80	33.77	40.31	32.4
33.20	33.68	39.93	32.27
32.60	33.57	39.53	32.13
32.00	33.47	39.11	32
31.40	33.36	38.68	31.82
30.80	33.25	38.24	31.69
30.20	33.1	37.79	31.55
29.60	32.98	37.33	31.42
29.00	32.85	36.85	31.29
28.40	32.72	36.37	31.27
27.80	32.59	35.88	31.17
27.20	32.45	35.38	31.06
26.60	32.3	34.87	30.97
26.00	32.14	34.36	30.88
25.40	31.97	33.85	30.8
24.80	31.79	33.32	30.73
24.20	31.59	32.8	30.66
23.60	31.34	32.27	30.6

Horizontal profiles				
Cell	X=	2002/07/27	2002/08/10	2002/12/28
u/s	-5.72	30.21	28.41	29.47
T14	-5.00	34.14	33.13	31.23
T15	0.00	39.38	38.74	39.45
T17	15.00	39.49	38.97	41.96
T19	30.00	39.49	38.97	41.55
T22	40.00	39.03	37.64	35.19
d/s	43.44	30.58	27.89	35.21

Elevation 35.00				
Cell	X=	2002/07/27	2002/08/10	2002/12/28
u/s	-12.00	29.81	28.21	29.39
T23	-10.00	33.96	33.43	32.63
T26	0.00	40.36	40.2	38.44
T29	25.00	41.01	40.94	39.94
T32	45.00	39.05	38.79	36.46
T35	55.00	30.17	30.23	33.89
d/s	56.00	30.12	27.61	35.12

REFERENCES

[1] ANSYS Manuals (Theory manual, User's guide Element manual), 1998. V5.5.1

[2] Huebner, K.H., Dewhirst, D.L., Smith, D.E., Byrom, T.G. –The finite element method for engineers. Fourth edition, John Wiley & Sons, Inc.

[3] Giesecke, J., Qin, M., Marx, W. - Realistic and computational efficient evaluation of temperature and stress development in large RCC dam. German Dam Research and Technology

PARAMETER IDENTIFICATION IN MATHEMATIC MODELS OF TEMPERATURE REGIME OF ROLLED CONCRETE DAMS DURING CONSTRUCTION

Sofia Ginsburg, Tatyana Rukavishnikova, Nicolae Sheinker,
Alexander Yudelevich
The B.E. Vedeneev All-Russian Research Institute Of Hydraulic Engineering (VNIIG), Inc., Russia

SUMMARY: Presented are the basic provisions of parameter identification of mathematic models of temperature regime of RCC massifs during construction. A suggested procedure is based on simulation models formed from results of numerical solution of heat conductivity problems with the use of experiment planning methods. Example is given of its application for more exact determination of values of specific heat hydration in concrete.

RÉSUMÉ: On propose la méthode de l'identification des paramètres du régime de température de béton compacté au rouleau «BCR» en train de la construction.
La méthode est basée sur l'utilisation des modèles d'imitation construits sur les résultats de la décision numérique de la tâche de la conductibilité de la chaleur avec l'application des méthodes de la planification de l'expérience. On amène l'exemple de son utilisation pour la précision des significations spécifique chaleur dans le béton

1. INTRODUCTION

In recent years rolled concrete gravity dams are finding widespread use. Though hydration heat of rolled concrete is rather limited, temperature cracking of concrete cannot be completely avoided in this case. Therefore, prediction of temperature fields and temperature stresses during construction of rolled concrete dams is not less important than for cases of vibrated concrete dams.

Due to specific material properties, determination of thermal physical parameters of rolled concrete presents a serious problem, mainly due to complexity of laboratory modeling of rolled concrete. In the present publication we suggest to determine the thermal physical parameters of concrete on the basis of observations of concrete temperature regime by identification procedures.

The identification problem is solved by forming a target function of inverse problem

$$\varphi = \sum_{j=1}^{M} p_j (z_j - Z_j)^2 , \qquad (1)$$

where $z_j, j = 1,...,M$ - computational realizations of observation parameters which should be compared with in-situ observation data

$$z_j = T_j(u_1, u_2, ..., u_N) \qquad (2)$$

$u_1,...u_N$ - governing parameters, i.e. unknown parameters of the computation scheme; $p_j > 0$ – weight factors intended for control of contributions of various parameters; $Z_j = T^{изм}$ - prescribed values of observation parameters (in-situ observation data).

Functional (1) shall be minimized during satisfaction of additional conditions

$$\overline{u}_i \le u_i \le \hat{u}_i, i = 1,..., N \qquad (3)$$

where $\overline{u}_i$ и $\hat{u}_i$ are boundaries of possible variation of parameters u_i.

Thus, the identification problem is written as minimization problem of target function

$$\varphi(u_1,...,u_N) \to min \quad \text{при} \quad u_i \in U_i, i = 1,..., N \qquad (4)$$

In this case the sense of identification problem lies in the fact that, basing on in-situ observation data, we determine the acting (effective) parameters of computation models most corresponding to parameters of actual structures.

It is assumed that we know the solution of relevant heat conductivity problem (for definiteness, one-dimensional problem is considered) as well as in-situ temperature observation data in characteristic points of concrete massif in definite time moments $Z = T^{изм}(x_n, t_m)$ ($n=1, 2,..., N; m=1, 2, ..., M$). Problem of identification of thermal physical parameters may be solved by analytical or numerical solutions of heat conductivity problem for specific computational schemes (e.g. concrete block resting on rock or old concrete foundation). Due to complexity of the problem, numerical solutions are used in most cases, however, analytical solutions may be also used in some convenient cases.

2. IDENTIFICATION OF THERMAL PHYSICAL PARAMETERS FOR NUMERICAL SOLUTION OF HEAT CONDUCTIVITY PROBLEMS

We suggest to solve identification problems of thermal physical parameters, using auxiliary simulation models formed from the results of numerical solution of heat conductivity problems.

The auxiliary simulation models are formed on the basis of theory of planning an experiment [1, 2] applied to computation analysis of temperature regime of concrete massif during construction. Here the response functions are the temperature values in points of the computation domain at various time moments, and the factors are the identification parameters and the spatial and temporal coordinates. For computation purposes, one should choose a plan of experiment and form a planning matrix with prescribed levels of factors.

For convenience of processing the experimental results and interpretation of mathematic models during the formation of experimental plan, the values of the factors are commonly represented as some conventional values and not as natural ones. These values are assumed according to normalized scale of variation of variables. Let some factor X in a natural scale vary in a range from $X_{\min}$ to $X_{\max}$. Then the transition from conventional value of factor *x* may be made from the expression

$$x = \frac{X - X_0}{\Delta X},$$

where $X_0 = \frac{X_{\max} + X_{\min}}{2}$ – the center of experiment for a given factor,

$\Delta X = \frac{X_{\max} - X_{\min}}{2}$ – variation interval for this factor.

Evidently, with $X = X_{\min}$ $x = -1,$ on the lower level, $X = X_0$ $x = 0,$ in the center of the experiment and $X = X_{\max}$ $x = +1.$ on the upper level.

The shape of a model (response function) is prescribed on the basis of a priori information, and in most cases it may be taken as a second degree polynomial of the factors assumed.

The coefficients of the polynomial are determined by a least squares procedure.

Various approaches may be used for solving identification problems of thermal physical parameters by simulation models.

The models may be obtained from various initial data. In a most general case, identification parameters, coordinates of points of concrete massif and time moments may be assumed as factors.

We select *N* points over coordinate and *M* points over time (of course, those points are selected, for which there exists data from in-situ temperature observations).For selected time moments auxiliary simulation temperature models are constructed as functions of coordinate, heat exchange and heat conductivity coefficients (as polynomials of second degree).

3. TWO PARAMETER IDENTIFICATIONS

For this case simulation model will assume the following form

$$T(x,t) = a_0 + a_1 x + a_2 x^2 + a_3 t + a_4 t^2 + a_5 \beta + a_6 \beta^2 + a_7 \lambda + a_8 \lambda^2 \qquad (5)$$

β and λ- parameters to be identified.

The desired parameters which give minimum value to functional (5) are determined by iteration process formed by first order sensitivity function procedure [3].

The derivatives of target function (6) from parameters β and λ may be equated to zero

$$\begin{aligned} \frac{\partial \varphi}{\partial \beta} &= 2\sum_{j=1}^{M}(T_j - Z_j)\frac{\partial T_j}{\partial \beta} = 0, \\ \frac{\partial \varphi}{\partial \lambda} &= 2\sum_{j=}^{M}(T_J - Z_j)\frac{\partial T_j}{\partial \lambda} = 0. \end{aligned} \qquad (6)$$

Let be known some approximate values of parameters $\beta^{(s)}$ u $\lambda^{(s)}$ (s – iteration number). To determine the next approximation $\beta^{(S+1)}$ u $\lambda^{(s+1)}$, we decompose the function $T_j(\beta^{(s+1)}, \lambda^{(s+1)})$ into Taylor series in close vicinity of values $\beta^{(s)}$ u $\lambda^{(s)}$ and limit ourselves by linear members

$$\begin{aligned} T_j(\beta^{(s+1)}, \lambda^{(s+1)}) &= T_j(\beta^{(s)}, \lambda^{(s)}) + \frac{\partial T_j(\beta^{(s)}, \lambda^{(s)})}{\partial \beta}(\beta^{(s+1)} - \beta^{(s)}) + \\ &+ \frac{\partial T_j(\beta^{(s)}, \lambda^{(s)})}{\partial \lambda}(\lambda^{(s+1)} - \lambda^{(s)}). \end{aligned} \qquad (7)$$

After substitution of (6) into (7) and appropriate transformations, receive a set of two equations with two unknowns

$$\left.\begin{aligned} a_{11}^{(s)}\beta^{(s+1)} + a_{12}^{(s)}\lambda^{(s+1)} &= d_1^{(s)} \\ a_{21}^{(s)}\beta^{(s+1)} + a_{22}^{(s+1)}\lambda^{(s+1)} &= d_2^{(s)} \end{aligned}\right\}. \qquad (8)$$

where:

$$a_{11} = \sum_{n}^{N}\sum_{m}^{M}\left[W_\beta^{(s)}\right]^2; \quad a_{22}^{(s)} = \sum_{n}^{N}\sum_{m}^{M}\left[W_\lambda^{(s)}\right]^2; \; a_{12}^{(s)} = \sum_{n}^{N}\sum_{m}^{M}\left(W_\beta^{(s)}\right)\left(W_\lambda^{(s)}\right)$$

$$d_1^{(s)} = \sum_{n}^{N}\sum_{m}^{M} b_{nm}^{(s)}\left(W_\beta^{(s)}\right); \qquad d_2^{(s)} = \sum_{n}^{N}\sum_{m}^{M} b_{nm}^{(s)}\left(W_\lambda^{(s)}\right);$$

$$b_{nm}^{(s)} = W_\beta^{(s)}\beta^{(s)} + W_\lambda^{(s)}\lambda^{(S)} + T_{nm} - T_{nm}^{изм}.$$

T_{nm} - computed temperature value in n –th point at m-th time moment;

$T_{nm}^{изм}$ - measured temperature value in n –th point at m-th time moment.

Using Kramer's expressions for solving (7) we receive the recurrent relationships for obtaining successive approximation

$$\beta^{(s+1)} = \frac{d_1^{(s)} a_{22}^{(s)} - d_2^{(s)} a_{12}^{(s)}}{a_{11}^{(s)} a_{22}^{(s)} - a_{12}^{(s)} a_{21}^{(s)}}; \qquad \lambda^{(s+1)} = \frac{d_2^{(s)} a_{11}^{(s)} - d_1^{(s)} a_{21}^{(s)}}{a_{11}^{(s)} a_{22}^{(s)} - a_{12}^{(s)} a_{21}^{(s)}} \qquad (9)$$

In this case sensitivity functions are equal to

$$W_\beta = \frac{\partial T}{\partial \beta} = a_5 + 2a_6\beta;; \qquad W_\lambda = \frac{\partial T}{\partial \lambda} = a_7 + 2a_8\lambda;$$

The analysis of convergence of identification iteration process is made by solving test problems, i.e. identification problems when solutions of direct problems are taken as «measured» values.

Below we present an example of test problem in which it is required to determine the values of heat conductivity coefficient λ and coefficient of heat transfer of thermal insulation β.

The computations indicated that in many cases it is reasonable to form models in the function of coordinates and identified parameters at various time moments.

M points are selected with respect to time. At the selected time moments constructed are simulation temperature models in the function of coordinate, heat exchange and heat transfer coefficients.

$$T_m = a_0^{(m)} + a_1^{(m)} x + a_2^{(m)} x^2 + a_3^{(m)} \beta + a_4^{(m)} \beta^2 + a_5^{(m)} \lambda + a_6^{(m)} \lambda^2,$$

where $a_i^{(m)}$ - model coefficients (i = 1, 2, …,6), determined by least squares procedure.

T_m – computed temperature at *m*-th time moment.

As an example, let us consider identification of heat transfer coefficient of concrete and coefficient of heat exchange between the surface of concrete and the ambient air.

The solution of heat conductivity problem resulted in the formation of mathematic models based on the following factors:

-heat transfer coefficient β,

-heat conductivity coefficient of concrete λ,

- coordinates of points in concrete, equipped with thermometers.

The following factor (level) variation boundaries are assumed

$$\beta - 10 < \beta < 20 \text{ (kcal/m}^2\cdot\text{h}\cdot^\circ\text{C)}$$
$$\lambda - 1.5 < \lambda < 2.1 \text{ (kcal/m}\cdot\text{h}\cdot^\circ\text{C)};$$
$$0.5 < x < 2.5 \text{ (m)}.$$

The models were constructed on the basis of full factor experiment for three levels of three factors (27 computed versions).

The values of temperature for 60 days and 90 days periods were assumed as response functions.

The models received are of the following form:

$T_{60} = 18.13 + 4.56x - 0.43x^2 - 0.26\beta + 0.13\beta^2 - 0.50\lambda + 0.05\lambda^2$;

$T_{90} = 16.67 + 3.87x - 0.27x^2 - 0.23\beta + 0.11\beta^2 - 0.48\lambda + 0.05\lambda^2$.

The multiple correlation coefficient characterizing the models accuracy is 0.998.

The obtained models were used for computation of temperature values of heat exchange coefficient β = 20 kcla/m^2·h·$^\circ$C and heat transfer coefficient λ = 1.8

kcal/m·h·°*C* and the values of factor x from -1 to +1 (from 0 to 2.5 m). Those values were assumed as «measured» values.

The computations indicated that the selection of initial approximations β_0 and λ_0 does not influence the convergence rate. Figures 1, 2 represent the pathway of iteration process. Practically, for all initial approximation values the number of iterations for achieving the prescribed result was equal to four.

4. ONE PARAMETER IDENTIFICATION

In case of one parameter identification (e.g. heat transfer coefficient or coefficient of heat transfer of heat insulation), the simulation model assumes the following form

$$T(x,t) = a_0 + a_1 x + a_2 x^2 + a_3 t + a_4 t^2 + a_5 \beta + a_6 \beta^2 \qquad (10)$$

where $T(x, t)$ –computed temperature values;

a_i – coefficients of polynomial, determined by least squares procedure;

β - identified parameter.

For the solution of identification problem we also used sensitivity function procedure [4].

In this case, on the basis of (10), the sensitivity function is

$$W = \frac{\partial T}{\partial \beta} = a_5 + 2a_6 \beta \qquad (11)$$

The desired parameter is determined by iteration process from expression

$$\beta^{(s+1)} = \beta^{(s)} + \frac{\sum_{n=1}^{N}\sum_{m=1}^{M} W_{nm}^{(s)}\left[T_{nm}^{изм} - T_{nm}^{(s)}\right]}{\sum_{n=1}^{N}\sum_{m=1}^{M}\left[W_{nm}^{(s)}\right]^2} \qquad (12)$$

where

β - identified parameter;

s- iteration number;

$T_{nm}^{изм}$ – measured temperature values (in-situ observation data) in n-th point at m-th time moment;

$T_{nm}^{(s)}$ - temperature values computed from the model.

The models were constructed using complete experiment for three levels of two factors.

Consider the identification of heat exchange coefficient β. The following factor levels are assumed:

$10 < \beta < 30$ (kcal/m^2·h·°C),
$0.5 < x < 2.5$ (m).

On the basis of performed computation experiments there were formed mathematic temperature models for 60 and 90 day periods. The models are of the following form

$$T_{60} = 17.62 + 4.28x - 0.35x^2 - 0.29\beta + 0.14\beta^2,$$

$$T_{90} = 16.13 + 3.54x - 0.27x^2 + 0.25\beta + 0.23\beta^2.$$

Multiple correlation coefficient R=0.998.

The solution of test problems indicated that the selection of initial approximations does not influence the convergence of iteration. «Measured» values were assumed from the solution of direct problem for β = 20 kcal/m^2·h·°C. The desired result was achieved by four iterations (Figure 3).

5. IDENTIFICATION OF SPECIFIC HEAT HYDRATION (Q)

One of basic parameters characterizing temperature fissure resistance of concrete masonry is heat hydration in concrete. The heat hydration is mostly dependent on type of cement. As a rule, during construction of high concrete dams various type of cement is used. To a certain extent, the prediction of temperature regime and the selection of relevant temperature control arrangements depend on the accuracy of assessment of heat hydration in concrete. Conventionally this assessment is made on the basis of laboratory studies requiring special equipment. Here we present a procedure of heat hydration assessment using in-situ observations of temperature regime of concrete blocks during construction. Temperature regime control is an obligatory component of diagnostics of concrete structures during construction.

For heat hydration identification it is also reasonable to use simulation mathematical models of temperature. One of the factors should be a value characterizing heat hydration, e.g. specific heat hydration in concrete placed at a certain time moment. The models should be formed on the basis of temperature regime evaluations for at least two or more characteristic periods, e.g. 3 days, 7 days, etc. in the points where temperature measurements are made.

An example of identification of specific heat hydration is given below.

The following parameters are assumed as factors:

X_1 – concrete mix temperature, $T_{б.см.}$ (°C);

X_2 – specific heat hydration, (q) kcal/kg;

X_3 – cement content, (C) kg/m^3;

X_4 – height of concrete block, (h) m;

The models were received using Hartley plan for three levels of four factors.

On the basis of temperature evaluations there were received mathematic simulation models T_3, T_5, T_7 for time moments t = 3, 5 and 7 days in points of concrete block where temperature measurements were made. The models have the following form

$$T_3 = 39.47 + 2.62x_1 + 1.94x_2 + 10.33x_3 + 1.77x_4 -$$
$$- 0.004x_1^2 - 0.11x_1x_2 + 0.02x_1x_3 + 0.35x_1x_4 - 0.02x_2^2 +$$
$$+ 0.81x_2x_3 + 0.11x_2x_4 + 0.04x_3^2 + 1.40x_3x_4 - 1.83x_4^2$$

$$T_5 = 40.06 + 2.31x_1 + 1.97x_2 + 10.52x_3 + 3.89x_4 + 0.05x_1^2 -$$
$$- 0.062x_1x_2 + 0.58x_1x_4 - 0.01x_2^2 +$$
$$+ 0.84x_2x_3 + 0.26x_2x_4 + 0.05x_3^2 + 0.60x_3x_4 - 1.25x_4^2$$

$$T_7 = 38.95 + 2.03x_1 + 1.92x_2 + 10.13x_3 + 5.31x_4 +$$
$$+ 0.05x_1^2 - 0.04x_1x_2 + 0.01x_1x_3 + 0.71x_1x_4 -$$
$$- 0.08x_2^2 + 0.84x_2x_3 + 0.36x_2x_4 + 0.05x_3^2 + 1.95x_3x_4 - 1.85x_4^2$$

Identification was made using equation (12).

The solution of test problems indicated that the process converges to initial values already during the second iteration.

Next we made identification of specific heat hydration on the basis of measured temperature in concrete blocks of Bureiskaya HPP.

The computations indicated the value of specific heat hydration q = 69.5 kcal/kg, already at 4th iteration $\varepsilon = \left| q^{(4)} - q^{(3)} \right| < 2 \cdot 10^{-5}$.

Figure 4 presents the pathway of iteration processed for various initial approximations.

6. CONCLUSION

The paper presents basic provisions for identification of concrete thermal physical parameters during construction based on the data of temperature control of concrete masonry. The suggested procedure uses mathematic simulation models formed by solving heat conductivity problem of concrete massif built by blocks.

References

1. Kozdoba L.A., Krukovsky P.G. - Procedures for solving heat transfer inverse problems., Kiev, 1982..
2. Ginsburg S.M., Sh.N.Pliat - Mathematic model for assessment of thermal fissure resistance of concrete massif during construction. Izvestiya B.E.Vedeneev VNIIG, 1978, v.121.
3. Ginzburg S.M., Ye.Ye.Zazerskaya, N.Ya.Sheinker - Some problems of optimizing the parameters of temperature regime and thermal stress state of concrete hydraulic structures. Izvestiya B.E.Vedeneev VNIIG, 1983, v.163.
4. Ivashintsov D.A., Sokolov A.S., Shulman S.G., Yudelevich A.M. - Parameter identification of design models of hydraulic structures. St. Petersburg, 2001.

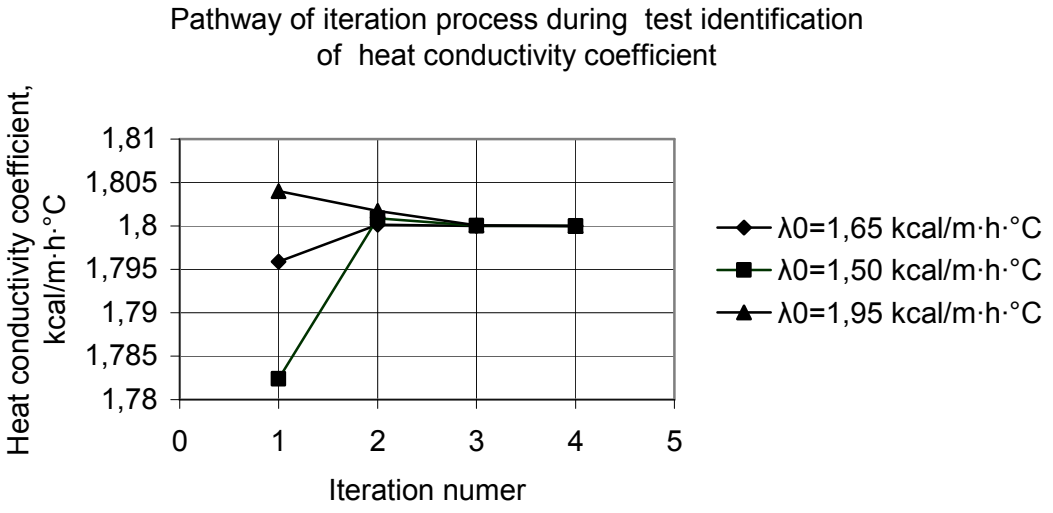

Figure 1

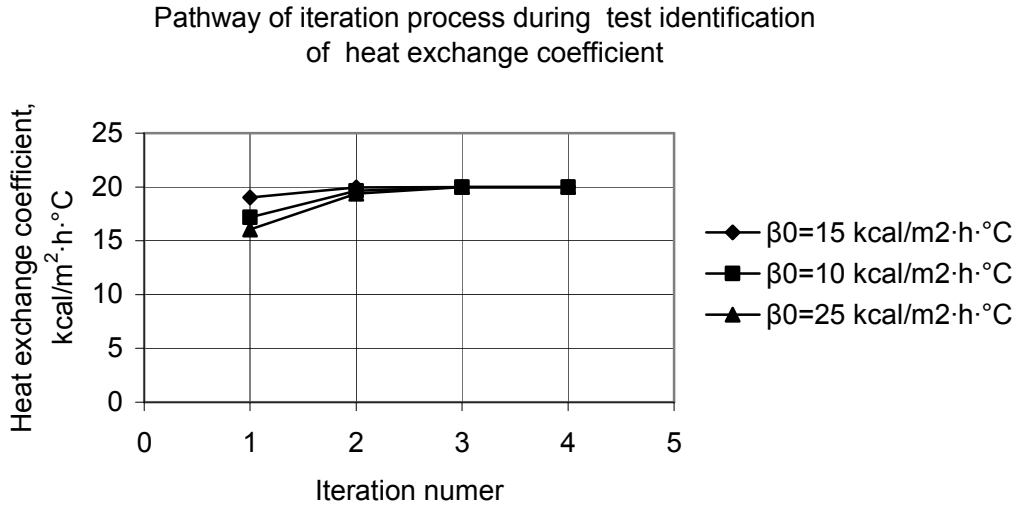

Figure 2

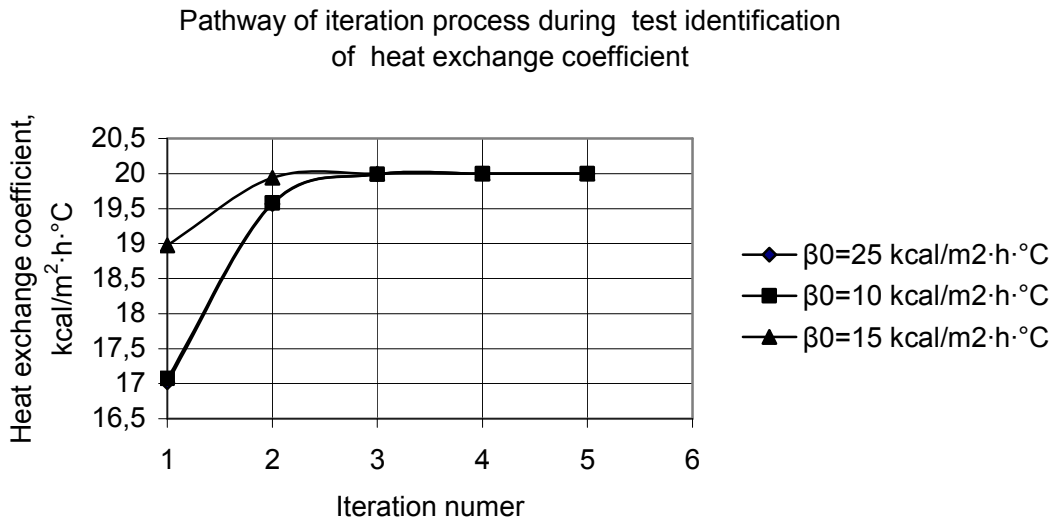

Figure 3

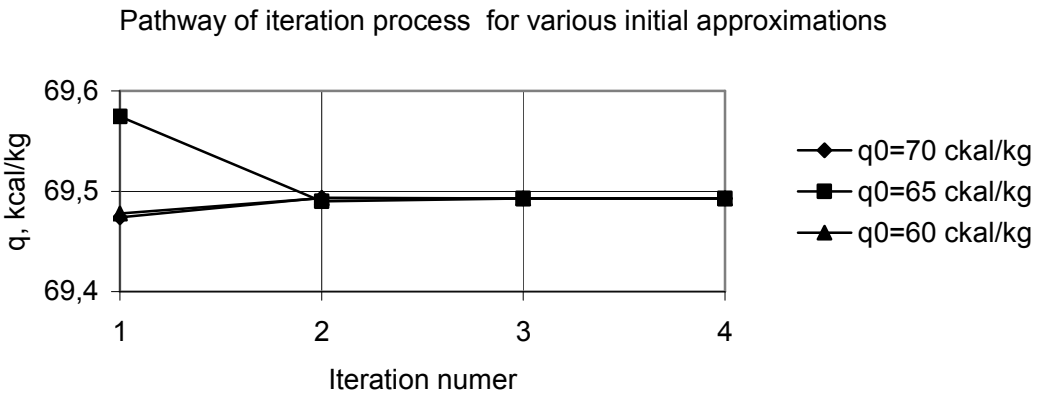

Figure 4

BIDIMENSIONAL THERMAL ANALYSIS OF A RCC DAM DURING CONSTRUCTION*

Lucian Ilie
Labora Consulting – Paris, FRANCE
Adrian Popovici, Altan Abdulamit, Radu Sârghiuță, Cornel Ilinca
Technical University of Civil Engineering of Bucharest, ROMANIA

SUMMARY:

The results of the thermal analysis of a large RCC gravity dam during construction are presented. The analysis is performed with ANSYS computer code using a two dimensional model. The erection of the dam in a representative cross section was simulated by birth and death of the finite elements according to real construction of the THA DAN dam in Thailand. The initial temperature of a new placed RCC layer was the average ambient temperature at the time of the RCC pouring. The foundation of the dam was not included in the finite element mesh. The results of the analysis are presented as temperature contours in the dam profile for different time moments and temperature time variations in different points or sections in profile

RÉSUMÉ:

L'article présente les résultats du calcul thermique d'un grand barrage-poids BCR pendant la construction. L'analyse a été fait au moyen du logiciel ANSYS, sur un modèle bi-dimensionnel. La construction du barrage dans une coupe transversale représentative a été simulé à l'aide de technique de "naissance et mort" des éléments finis. L'analyse a respecté le programme réel de bétonnage du barrage THA DAN en Thaïlande. Comme température initiale d'un nouveau couche de béton on a consideré la température moyenne de l'environnement au moment du bétonnage. Le maillage en éléments finis n'a pas modélé le terrain de fondation. Comme résultats de l'analyse on a présenté les températures dans la coupe transversale selectionnée pour les analyses pour des differents moments et les variations temporelles des températures dans quelques points de controle.

* Analyse thermique bi-dimensionnelle d'un barrage BCR pendant la construction

1. INTRODUCTION

RCC (Roller Compacted Concrete) dams construction may be characterized by continous and high rate of the concrete pouring. Because of the high rate of the dam erection in successive layers there is not sufficient time to allow that an important part of the hydration heat developed during construction to be dissipated on vertical direction through the free surface of a current layer before the pouring of the next layer. Consequently, an important quantity of the hydration heat is initially accumulated in the dam body, the process of its dissipation through the dam surface, exposed to air or to the water reservoir being a very long process of a number of years.

The prediction of the thermal state, especially of the thermal stresses state, is very important for RCC dams in order to avoid excessive thermal tensile stresses or to take constructive measures to control the risk of the thermal cracks in the dam body.

In this paper are presented and commented the results performed with ANSYS computer code [1], in the thermal analysis of a large RCC dam, located in a country with a tropical climate, now under construction. The paper is carried out in compliance with the requirements of the problem formulated by Coyne et Bellier, Bureau d'Ingénieurs Conseil for Theme B of the 7th ICOLD Benchmark Workshop on Numerical Analysis of Dams [2].

2. THERMAL ANALYSIS MODEL

The temperature distribution in the dam body is evaluated solving the thermal-conductivity equation in which is taken into account the heat developed by cement hydration [3]:

$$\frac{\partial \theta}{\partial t} = a \nabla^2 \theta + \frac{1}{c \rho_c} \frac{\partial Q}{\partial t} \tag{1}$$

where θ is the temperature in the dam body, a – coefficient of diffusivity, $\nabla^2 = \frac{\partial}{\partial x^2} + \frac{\partial}{\partial y^2}$ – differential operator of second order (Laplace operator), c – concrete specific heat, ρ_c – concrete mass density, and Q – the heat quantity developed at the time considered on unit volume of concrete due to cement hydration.

The coefficient of diffusivity (a) can be computed with the formula:

$$a = \frac{\lambda}{c \rho_b} \tag{2}$$

where λ is the coefficient of thermal conductivity.

For more than 30...40 days from the last concrete pouring, the parameter Q can be neglected and equation (1) becomes a standard Fourier equation, as follows:

$$\frac{\partial \theta}{\partial t} = a \ \nabla^2 \ \theta \tag{3}$$

The solution of equations (1) or (3) requires to specify the initial and boundary conditions. The initial conditions correspond to the dam body temperatures at the initial time (t=0). The boundary conditions can be formulated according to the following four types:
– on the dam surface the temperatures are specified at every time moment;
– on the dam surface are specified the input/output of the heat flow;
– on the dam surface is valid the exchange heat law as follows:

$$-\lambda \frac{\partial \theta}{\partial n} = \alpha_t \ (\theta_s - \theta_a) \tag{4}$$

where n is the normal direction to dam surface, α_t – coefficient of heat transfer, θ_s – dam surface temperature and θ_a – ambient (air) temperature.
– on the contact boundary between two solids exists an intimately thermal contact, expressed by the relations:

$$\theta_1 = \theta_2 \qquad \lambda_1 \frac{\partial \theta_1}{\partial n} = \lambda_2 \ \frac{\partial \theta_2}{\partial n} \tag{5}$$

where θ_1, θ_2 are the temperatures of the two solids in contact and λ_1, λ_2 – their coefficients of thermal conductivity.

The input data used in the present thermal analysis were provided by the formulator [1].

The cross section of the dam considered in analysis including the locations of the thermometers is presented in figure 1. The profile is closely inspired from THA DAN dam in Thailand, now under construction. This dam was designed by Coyne et Bellier for the Royal Irrigation Department from Thailand. It is a RCC gravity dam, with a crest length of 2600 m and a maximum height of 92 m.

The analysis was performed with ANSYS software. The finite element mesh used in analysis is shown in figure 2. It consists of 36064 nodes and 35680 quadrilateral elements. The vertical size of each element is 30 cm, similar to the thicknesses of RCC successive layers during erection of the dam. The whole dam body was considered as being made of RCC, accepting the thermal properties of the conventional vibrated concrete (CVC) thin shells from the dam upstream and downstream faces as being similar to those of the roller compacted concrete (RCC).

Some properties of RCC are presented in Table 1. They were provided by the formulator of the problem.

Table 1

Property	Symbol	Value	Unit
Unit weight	ρ	2380	Kg/m^3
Specific heat	*c*	1.0	$KJ/Kg/^0C$
Conductivity	λ	10.0	$kJ/m/h/^0C$
Diffusivity	*a*	0.0042	m^2/h

The convection + radiation surface coefficient was taken as α = 100 $kJ/m^2/h/^0C$.

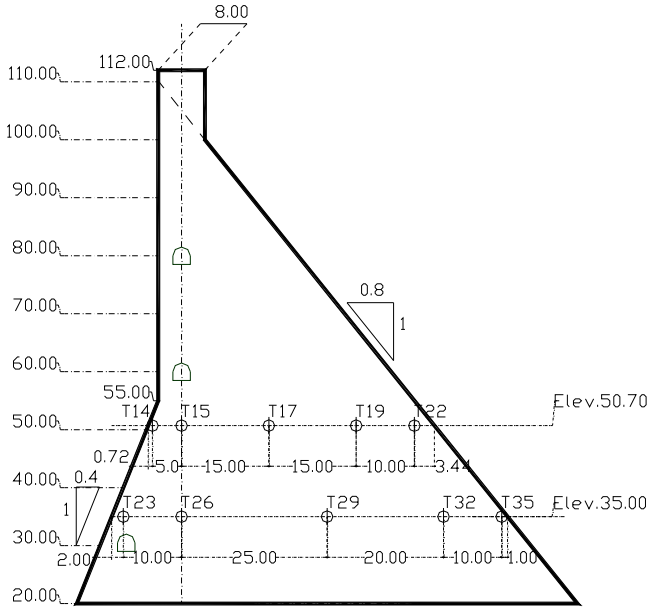

Figure 1. Dam cross section and location of thermometers

The heat generation rate of RCC was adopted in compliance with some information provided from literature [4]. The set of values considered in analysis are presented in Table 2.

Table 2

Heat generation rate ($J/m^3/s$)	Age of RCC (days)
130 ... 140	0
35 ... 40	3
8 ... 11	7
3 ... 5	28
1 ... 2	160

The initial temperature of each RCC layer placed during dam erection was the average ambient temperature at the time of placement. The time history integration scheme used a time step of 1 day.

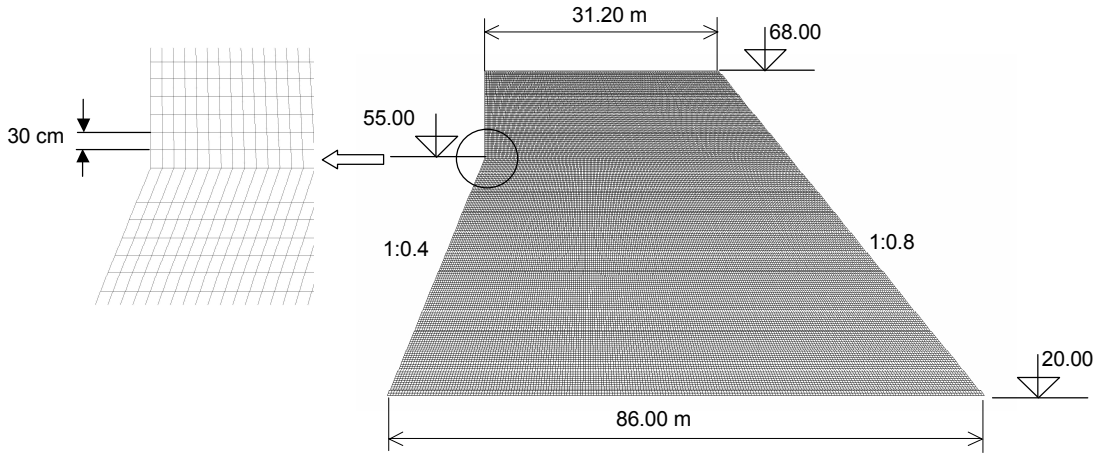

Figure 2. Finite element mesh used in analysis and detail of the mesh

The boundary conditions during dam erection are presented in the figure 3. As can be remarked from figure 3, on the dam – foundation contact the temperature was constant and equal to multiyear average air temperature (31^0C). The dam foundation was not included in the finite element mesh in order to simplify the mesh and to keep the computer time in reasonable limit.

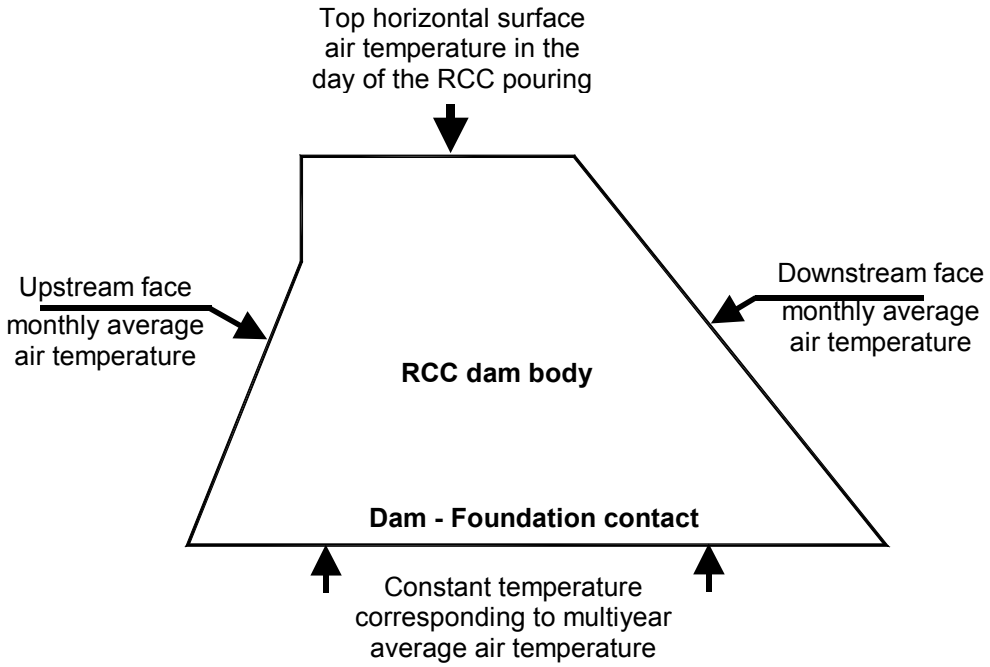

Figure 3. Boundary conditions during dam erection

The dam erection was simulated by birth and death of elements according to ANSYS implemented procedure. The construction schedule for the dam section considered in the present analysis corresponds to the real scheme of erection of the THA DAN dam and it can be seen in the figure 4. The pouring of RCC started on 13th March

2001 and has continued in sequences until 1st November 2002 when the dam reached the elevation of 68 m in the analysed cross section.

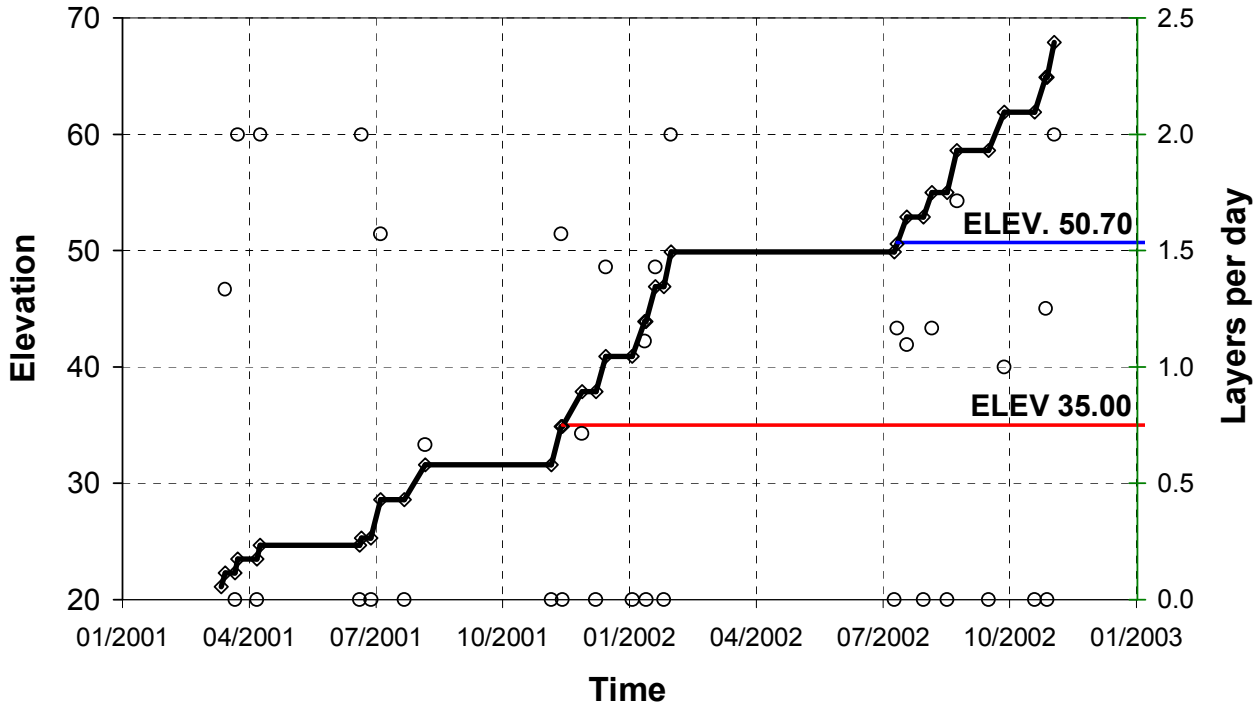

Figure 4. Construction schedule for the dam section

Some results obtained in analysis are illustrated in figures 5...13.

The contours of the dam body temperatures for different moments during dam erection are presented in figures 5...8. It can be remarked the maximum temperature in the dam body reached 41^0C at the end of the period of prediction (December, 2002).

The dissipation of the cement hydration heat developed during construction is very important on vertical direction versus upstream and downstream dam faces at least on short term. As was expected, the thermal gradients are much bigger to the free (air) faces of the dam and very small in the centre of the dam body.

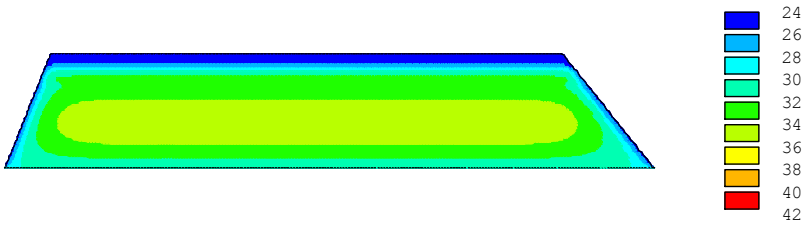

Figure 5. Contours of the dam body temperatures on 11/14/2001

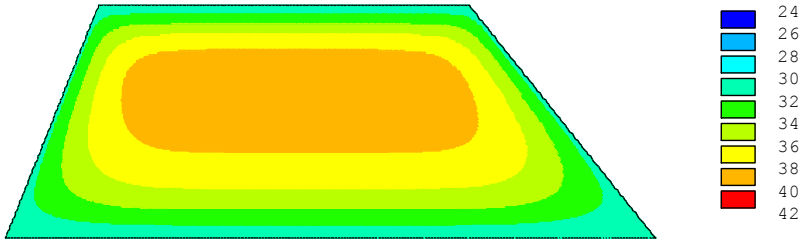

Figure 6. Contours of the dam body temperatures on 7/13/2002

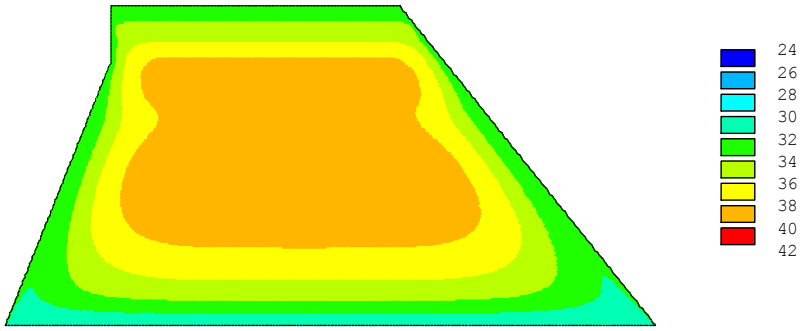

Figure 7. Contours of the dam body temperatures on 9/28/2002

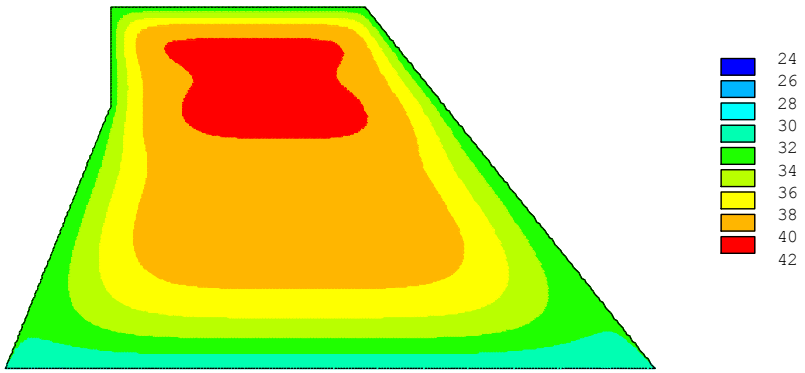

Figure 8. Contours of the dam body temperatures on 12/28/2002

The time evolution of the temperatures in the thermometers installed at elevation 35.00 m and, respectively 50.70 m are illustrated in figures 9 and 10. It can be remarked a rapid increase of the RCC temperatures in the next 10...12 days after pouring.

After this period the dissipation rate of the heat is very low in the central part of the dam body and more intensive to the upstream and downstream face zones where the effect of the air temperature is important. The results are in compliance with the set of values adopted for the heat generation rate of RCC (see Table 2).

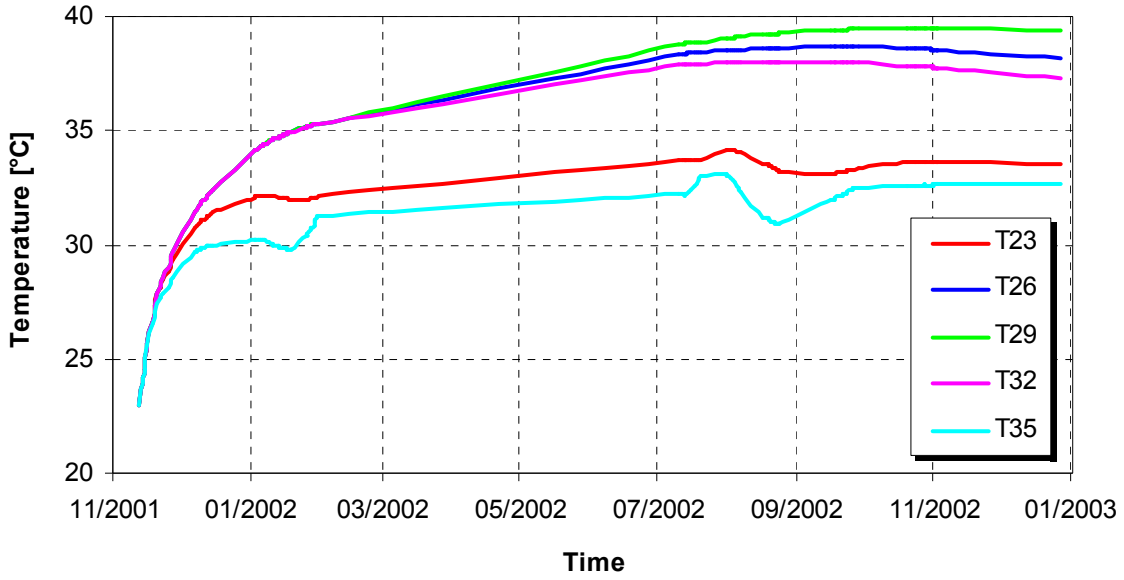

Figure 9. Time evolution of the temperatures in the thermometers at elevation 35.00 m

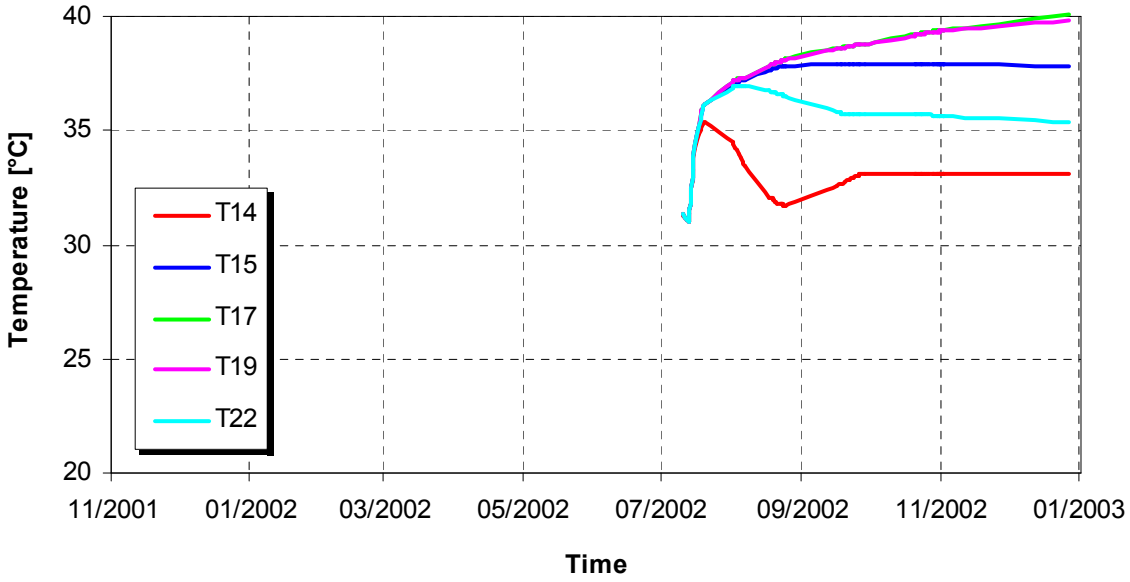

Figure 10. Time evolution of the temperatures in the thermometers at elevation 50.70 m

The same conclusions can be pointed out from figure 11 in which are illustrated the temperature variation in dam elevation at 2 m from upstream face, dam center and respectively 2 m from downstream face for three different time moments (27.07.02, 10.08.02 and 28.12.02). The temperatures in the center of the dam are higher than their correspondents to upstream and downstream face zones.

The distributions of the temperatures on horizontal sections at the elevations 35.00 m and 50.70 m for the same time moments (figures 12 and 13) emphasize the influence of the air temperatures on the dam temperatures from its faces vicinity and

very low rate of the heat dissipation in the central zones of the profile. The maximum temperature (41^0C) reached in the center of the section at the elevation 50.70 m, higher than maximum temperature (39^0C) reached in the section at the elevation 35.00 m, may be explained by higher comparative rate of the profile erection after reaching the elevation 50.70 m (see figure 4).

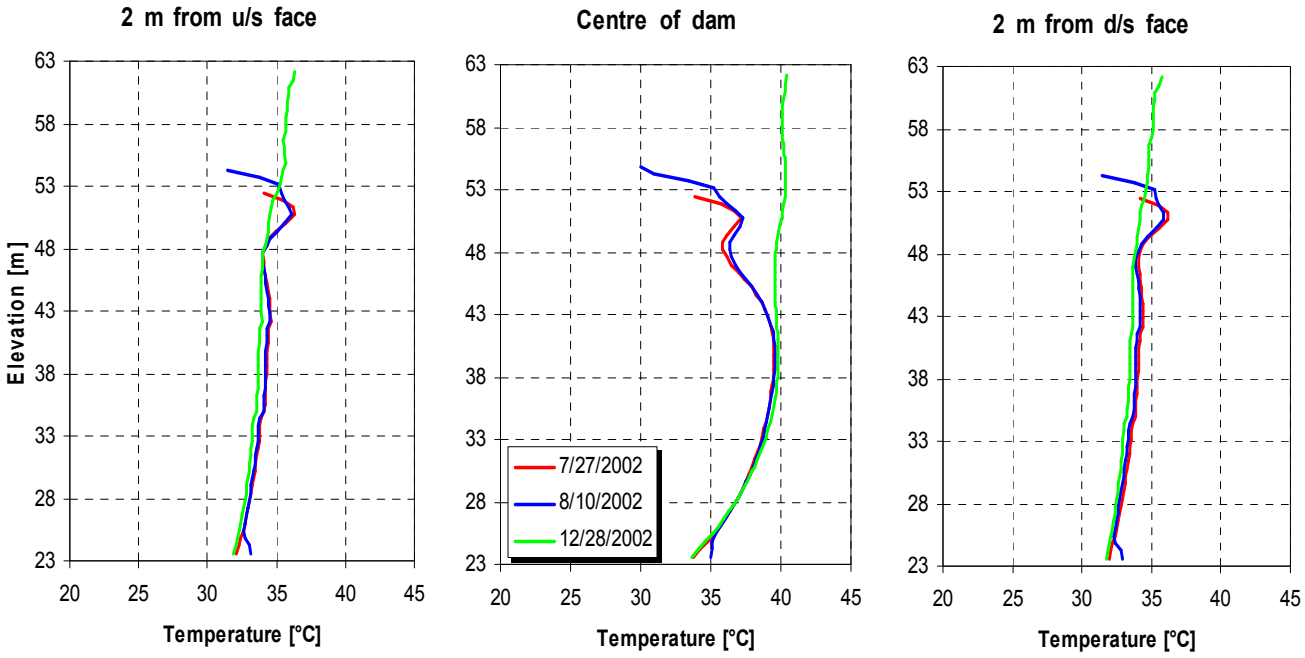

Figure 11. Temperature variation vs elevation at 2 m from upstream face, centre and 2 m from downstream face at different time moments

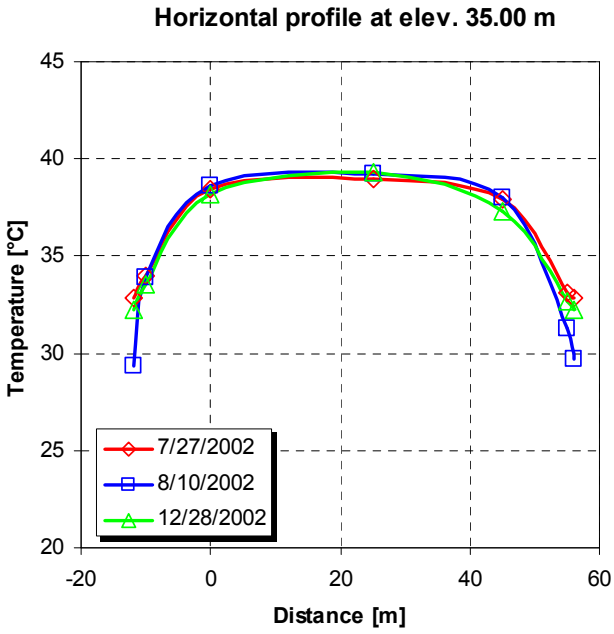

Figure 12. Temperature horizontal distribution at elevation 35.00 m for different time moments

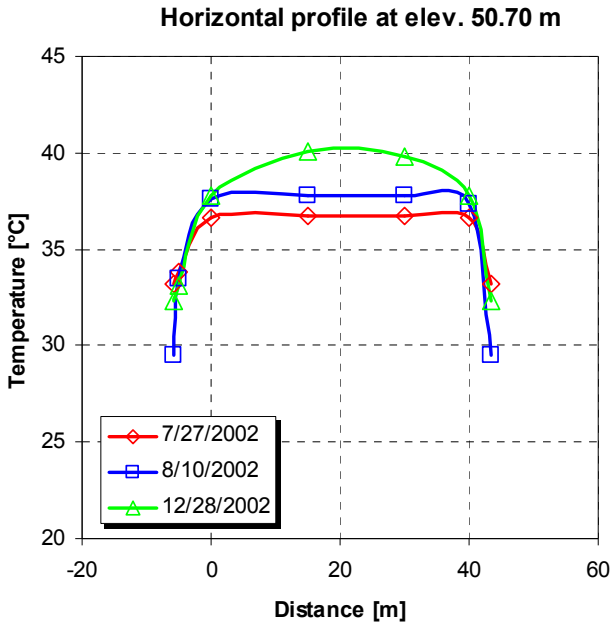

Figure 13. Temperature horizontal distribution at elevation 50.70 m for different time moments

4. CONCLUDING REMARKS

The thermal analysis in the cross section of a RCC dam during construction was performed using ANSYS software. The foundation of the dam was not included in the finite element mesh. On the contact dam – foundation was considered a constant temperature equal to the multiyear average air temperature.

The construction schedule of the dam profile considered in analysis was in compliance with the real scheme of construction of the THA DAN dam from Thailand. The maximum temperature in the dam profile predicted by the analysis was 41^0C. It is located in the central zone, at about 70% of the current height of the profile during construction.

The rate of the increase of temperatures is very high in the first 10...12 days after RCC pouring and it will succesively decrease in the following period.

The rate of the heat dissipation in the center of the profile is very low. On the contrary, this rate is higher in the adjacent zones to the dam upstream and downstream face, where the influence of the air temperatures is significant.

However, an important heat quantity seems to be dissipated on vertical direction in the first days after RCC layer placement. This remark may support the opinion that unidimensional thermal analysis for the dam construction period would perform satisfactory results as accuracy for engineering purpose. The bidimensional model applied in the dam cross section is compulsory for the study of the dam body thermal evolution after the end of the construction.

REFERENCES

[1] ANSYS computer code. Guide Manual. SAS, Inc., Houston, 1998.

[2] Carrere, A.J. - Coyne et Bellier, Bureau d'Ingénieurs Conseils. Thermal Analysis of a RCC Dam Body During Construction. Theme B – 7th ICOLD Benchmark Workshop on Numerical Analysis of Dams. Bucharest, September, 2003.

[3] Popovici, A., Popescu, C. Dams for Water Storage, Vol. 1 (in Romanian). Editura Tehnica, Bucharest, 1992.

[4] Pencescu, R. Study concerning RCC dams behaviour (in Romanian). Ph.D. Thesis, Technical University of Civil Engineering of Bucharest, 1998.

STRESS AND STRAIN STATE 2D MODELING BY THE FINITE ELEMENT METHOD IN AN RCC DAM ACTED BY THE CEMENT HYDRATION HEAT DURING THE CONSTRUCTION PERIOD

Gheorghe LAZAR, ass.prof.dr.eng.,
Serban-Vlad NICOARA, lect.dr.eng., Albert Titus CONSTANTIN, lect.eng.
"Politehnica" University of Timisoara, ROMANIA

SUMMARY: The paper presents an estimation of the temperature field and the stress and strain state by the 2D numerical modeling of an RCC dam at several construction stages. For the different sequential elevations, the largest block is modeled as loaded by the cement hydration heat. There is used the finite element method, applied through the ANSYS Programs package. The analysis is performed by considering a thermal-structural 2D finite element (Plane13) able to model the bidimensional thermal conduction and the stress and strain state in the solid material. By considering this Thermal-Solid option for the finite element meshing, it is possible to model the coupled situation of thermal transfer in transitory mode and stress and strain state.

The numerical modeling follows the boundary conditions given by the construction works and the RCC hydration heat variation. Based on the numerical modeling, an estimation of the temperature field and stress variation is reached for different moments along the dam construction period.

1. GENERAL CONSIDERATIONS

According to the subject proposed by theme B [1], the temperature field in a massif RCC dam has to be estimated. The development of a temperature field along the dam erecting stage influences the general stress and strain state. The thermal analysis refers to the cement hydration heat dissipation when the concrete is molded in lamellas of 10 layers. The analysis has to follow the boundary conditions determined by the specific working technology and the cement hydration heat for the two concrete types (RCC and CVC).

The 2D numerical modeling comprises a sequential estimation of the temperature field and stress state along the dam erecting period (from the elevation level of 20.00 m – December 3rd, 2001, to 67.90 m – October 31st, 2002). For this analysis, a coupled finite element PLANE 13 (type Thermic-Solid) is employed.

2. RUNNING DATA; DAM GEOMETRY AND WORKING SCHEDULE DEFINING

The analyzed structure corresponds to the concrete dam central block, with its inside part accomplished from RCC molded in layers of 0.30 m thickness. The structure geometry is presented by the figure 1 [1].

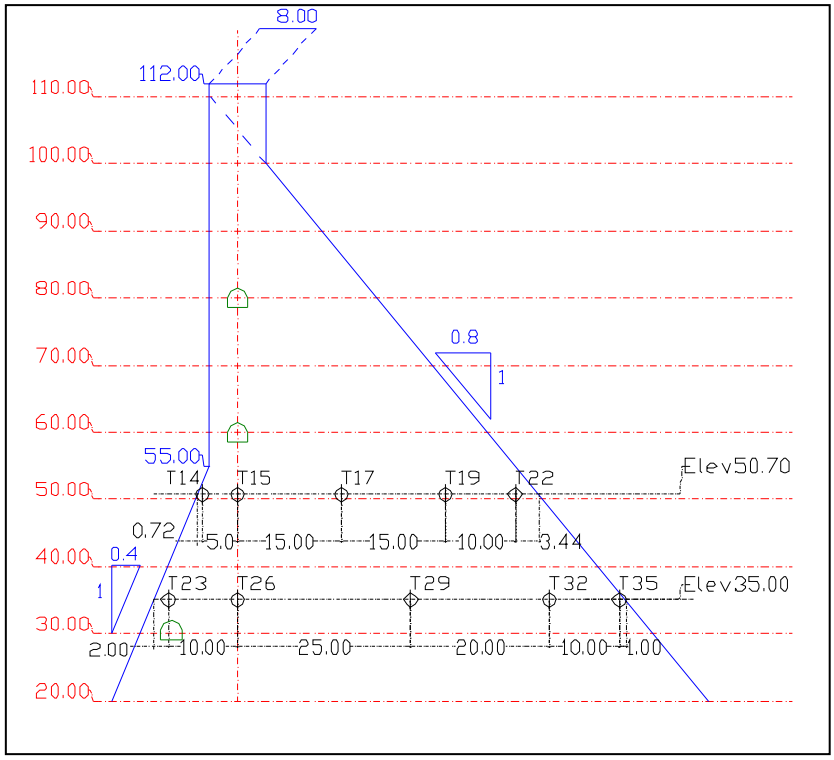

Figure 1 Dam cross section, indicating the monitoring devices location

The dam upstream and downstream faces are accomplished from conventional vibrated concrete (CVC), molded according to the details presented by the figure 2.

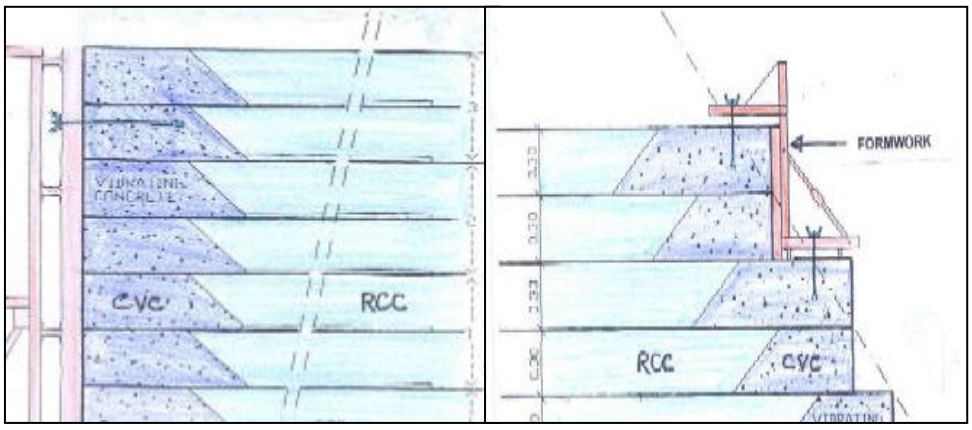

Figure 2 Concrete dam upstream and downstream faces working detail

The accomplishing method of a 0.30 m thickness layer in a common lamella keeps to the following working stages: the faces concrete (CVC) is molded, then the inside concrete (RCC) is molded, and finally the faces concrete is vibrated.

2.1 CONCRETE DAM MESHING AND WORKING PROCEDURE MODELING

A four nodes finite element PLANE 13, provided by the ANSYS Package of programs [4, 5], was employed in order to accomplish the 2D numerical modeling of the massif concrete dam. The considered element is of Thermal-Solid type, by the mean of which the bidimensional thermal conduction and the general stress and strain state can be modeled in a 2D solid domain, following the boundary conditions briefly mentioned.

Characteristic to the ANSYS Package of programs, geometric surfaces generating the analyzed model are associated to the finite elements. Thus, in order to follow the working technology specific to the studied structure, all the surfaces required for the successive meshing of the 0.30 m thickness layers were previously generated. For each common layer, there are at least three well-defined surfaces (maximum four at the layers containing the monitoring galleries holes) having attached the specific finite elements, according to the two material types (RCC and CVC). All these defined surfaces, related to the concrete type, are presented by the figure 3

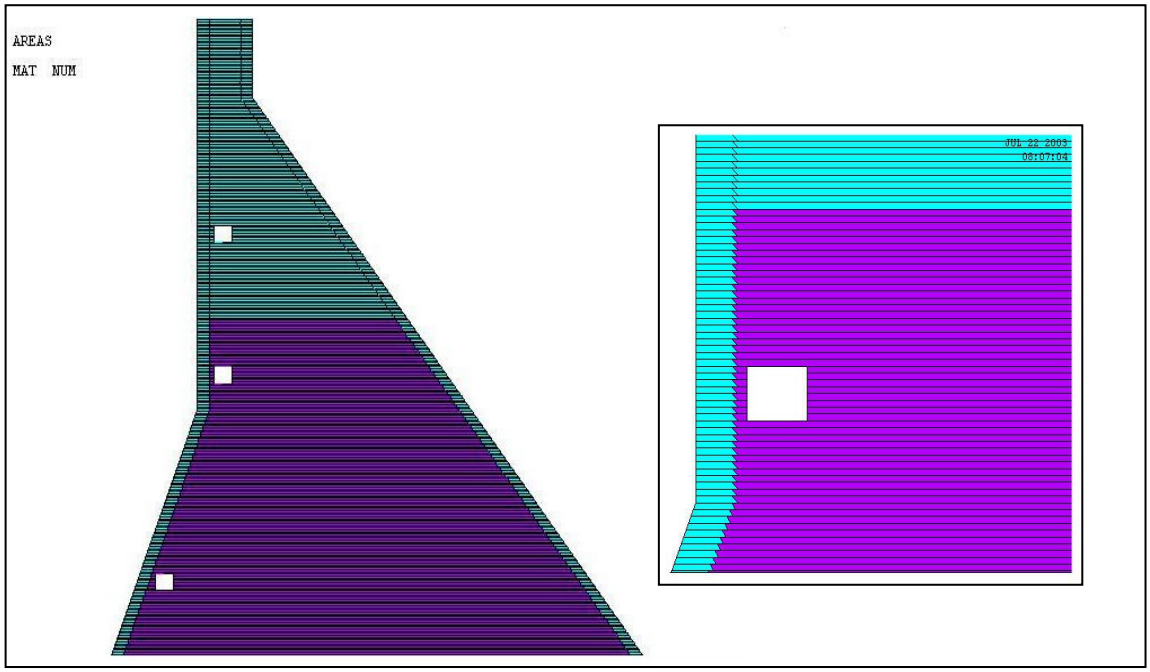

Figure 3 Finite elements attached surfaces; detail at the elevation of 67.90 m

It is noticed the accomplished high on October 31st, 2002, reaches the elevation level of 67.90 m, fulfilling the maximum high asked by the theme B notifications [1].

The successive finite elements meshing of the attached surfaces, was developed by an automatic successive generation (with the cycle step of one day, the number of layers 1 or 2 /day) that follows the lamellas working technology (10 layers per lamella).

Technically, the cyclic generation requires in ANSYS the issue of an entrance data file containing successive sequences of macro-commands (e.g. cycling commands - *DO … *ENDDO, testing commands - *IF … *ENDIF, setting commands - *SET, etc), by the help of which the three surfaces attached to each of the layers (1 minimum or 2 maximum) accomplished in a time step of one day shall be successively meshed.

Along a common cycle, once that the technological layer was meshed, the boundary and start conditions are to be considered for the beginning of the time interval. These conditions, given by [2, 3], are as follows:

- a required (known) temperature on the separation surface between two entities, specifically the concrete – air interface: upstream face, layer top surface, and downstream face;
- a heat exchange by convection, with given transition parameters at the separation surface, specifically at the three previously mentioned surfaces;
- the flow of the internal known heat sources (constant or time dependent), specifically the hydration heat for the interior and faces concrete types;
- a temporary temperature distribution, known at the process beginning, specifically the molding temperature for the fresh concrete.

The boundary and start conditions are associated to the general system of thermal and structural equations, which is then solved in order to obtain the unknown quantities in all the accumulated nodes of the mesh. The parameters values in the transitory analysis at the end of a time interval become start conditions for the following interval. The procedure is repeated, meaning that the next technological layer is meshed, changing the general system of the accumulated equations for the mesh accomplished until then. The new boundary and start conditions are associated to the new analyzing model (comprising all the previous finite elements to which the new elements are added). Some of the boundary condition need to be changed (those regarding the top of the last previous layer are to be canceled) and other new conditions need to be enforced.

The new general equation system is solved obtaining a new row of unknown quantities in all the mesh nodes accumulated until the moment. The described sequences are successively repeated until the total (final) analysis time is reached.

The successive changing of the general system of equations leads to a major inconvenience in the further results presentation, the in-between results being lost. In order to pass this disadvantage the authors propose two solutions.

First solution: testing sequences for the analyze moment are generated in the start data file. If the analyze moment is a specific one, there follows a sequence of macro-commands for reading the results from the data base file and their copy in distinctive external files specified by the user. The second solution: the generated structure is several times analyzed until the specified final time moments are reached. The results are post-processed at each final time moment, and so obtaining for the structure the temperature field variation, the thermal flow variation, the internal heat flows, and consequently the displacements and stresses variations.

The first solution led to the results presented by the table 2 (according to [1] - ThB_ResXXXX.xls for the T_{23} and T_{22} at the final distinct moment October 31st, 2002). The second solution was used in order to obtain the results for the three distinctive time moments: July 27th (502 days, 75 layers), August 10th (516 days, 83 layers), and October 31st, 2002 (598 days, 113 layers).

2.2 MATERIALS PROPERTIES; MONITORING DEVICES

The physical and mechanical characteristics of the facings (CVC) and inside (RCC) types of concrete, from which the massif dam is accomplished, are presented by the table 1.

Table 1

Material Type	E [N/m^2]	μ	α_x [m/m]	ρ [kg /m^3]	C [J /kg/°C]	λ [J/m/day/°C]	α [J/m^2/day/°C]
CVC	2.40E+10	0.17	9.9E-6	2380	1000	240000	2400000
RCC	2.38E+10	0.17	9.9E-6	2400	1000	240000	2400000

The cement used to produce the inside concrete (RCC) is a mixture of Portland cement (STC) and puzzolanic flying ash (PFA), 100-90 kg PFA / 1 cm of RCC. The facings concrete (CVC) comprises 350 kg of Portland cement per cubic meter of CVC. The hydration heat values, for the STC – PFA mixture and for the Portland cement at the faces, are presented by the figure 4 [1].

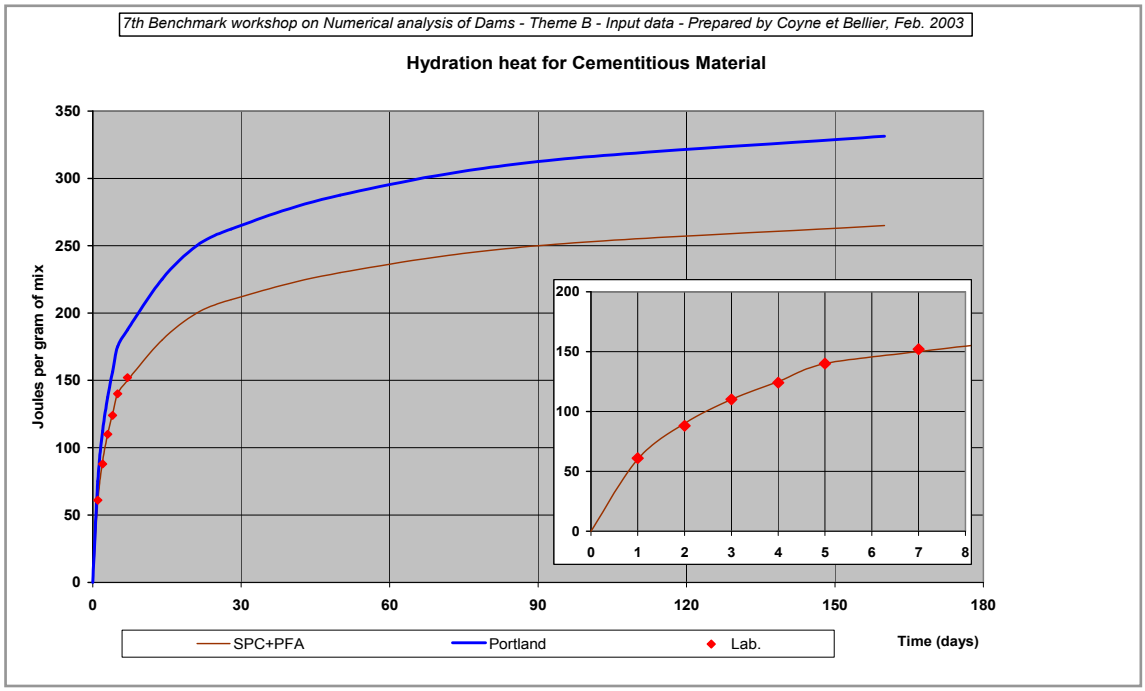

Figure 4 Hydration heat developments by time

Several electric thermocouples were placed at different levels and distances in order to monitor the temperature development (figure 1). Other temperature measuring devices are located around the dam structure, they monitoring the environment temperature.

2.3 BOUNDARY AND START CONDITIONS

The cycling adding of the concrete layers (at a one-day step) in the successive meshing of the attached surfaces, determines some difficulty in generating and updating the boundary and start conditions. Thus, the authors chose to consider five index variables for the boundary conditions in the incoming data file. There are two variables for the time variation of the faces temperatures (fig.5): T_AM_L1(i,1) and T_AV_L1(i,1), and one variable for the layer top temperature (fig.6) T_AO_L1(i,1), where i = 1, 2, …, n, and the maximum analysis time is a period of *n* days (specifically *n* = 598 days).

There are *k* index variables for the thermal flow determined by the cement hydration in the case of the faces concrete (CVC): T_HGE_LkC(i,1) (fig.7), where i = 1, 2, …, n, and k = 1, 2, …, m (m representing the total number of layers at the final analysis moment). For the example presented by the figure 7, the layer no. 10 determines m = 10 and the time interval i = 598 days.

It is noticed that the thermal flow variation for the Portland cement hydration at the faces of the layer no. 10 has the maximum value of 76875 J/kg during the first day,

at molding (day 110 at June 30th,2001), value that was declared 110 days before the actual molding.

The index variable for the thermal flow determined by the STC - PFA mixture hydration, in case of the inside concrete (RCC), T_HGEN_Lk(i,1), where k = 1, 2, …, m, is presented by the figure 8.

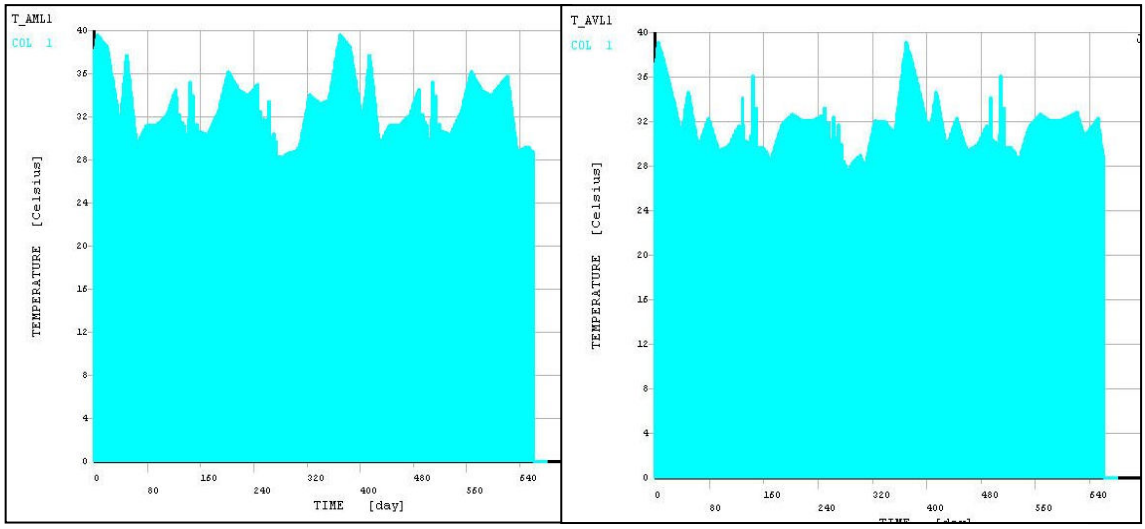

Figure 5 Faces temperature variation along the 598 days interval

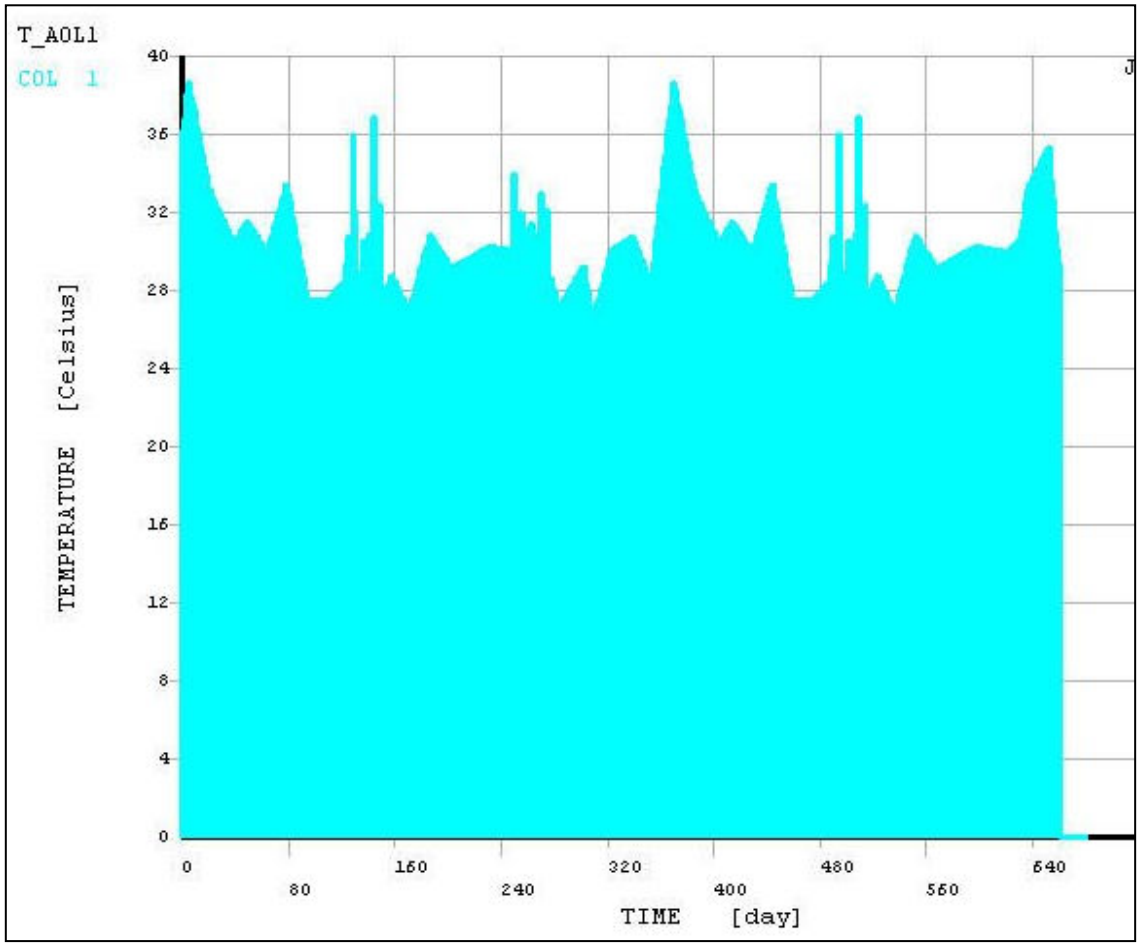

Figure 6 Fresh layer top temperature variation along the maximum interval of 598 days

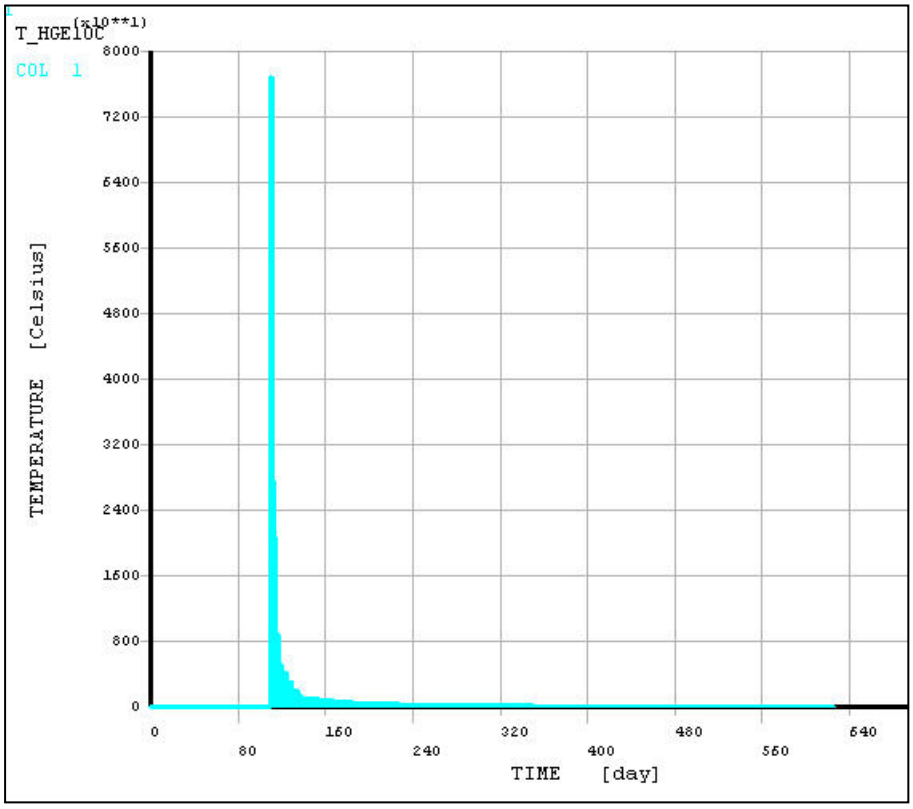

Figure 7 Variation of the thermal flow determined by the concrete hydration at layer no. 10

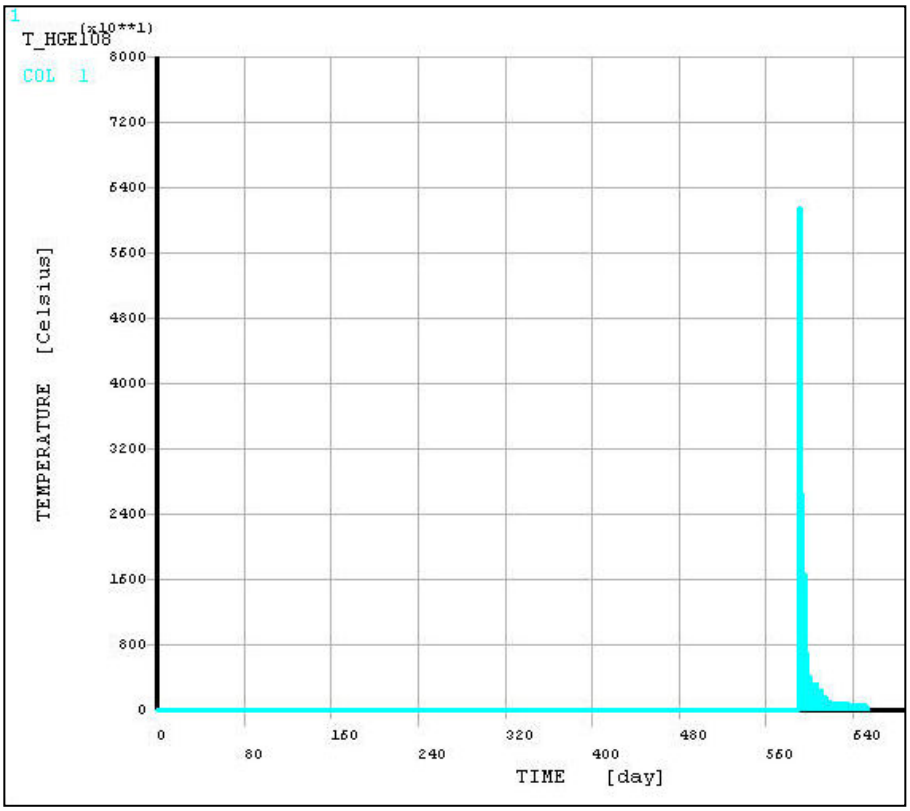

Figure 8 Variation of the thermal flow generated by the STC – PFA mixture hydration, layer m = 108

The thermal flow variation for the STC – PFA mixture hydration for the layer no. 108 has the maximum value of 61500 J/kg during the first day, at molding (day 593 at October 26th,2002), this value being so pre-declared with 593 days before the actual molding. The initial temperatures in the fresh inside concrete (RCC) and the fresh faces concrete (CVC), following to the notifications of the theme subject [1], were considered as presented by the figure 9.

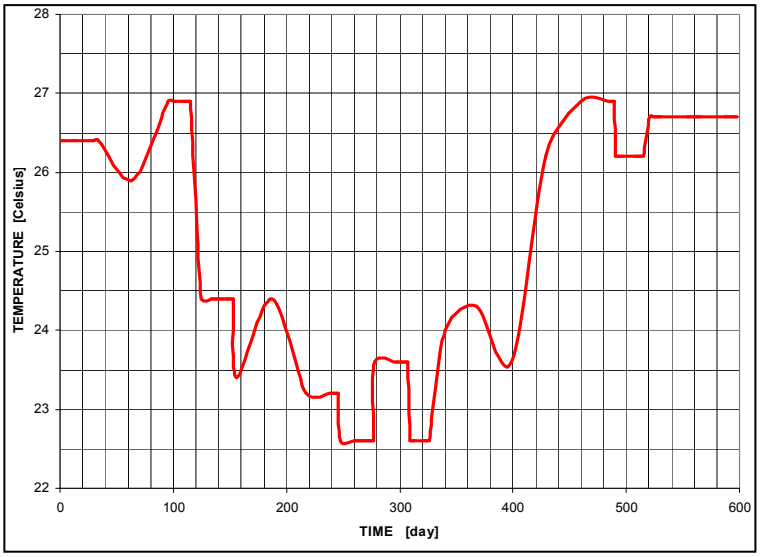

Figure 9 Initial temperature for the fresh RCC and CVC

3. RESULTS PRESENTATION

The analyzed model was cyclic loaded in three specific stages, a cycle being equivalent to a one-day step time. For a cycle a transitory numerical simulation with a time step Δt = 24 hours was considered, this requiring the use of thermal parameters according to the table 1.

During *the first stage*, there was modeled the transitory thermal conduction, consequently obtaining the stress and strain state in transitory development, for the 598 days time interval (December 3rd, 2001 – October 31st, 2002). The in-between results requested by the theme B specifications were selected from the external generated files, and were filled in a file as presented by the table 2. The selected values were graphically processed and so the temperature time developments were obtained at the location point of the T_{23} and T_{22} sensors (fig.10 and 11).

Based on the post-processing operations performed upon the determined parameters in the accumulated nodes of the mesh, the temperature distribution at the final analysis moment of the 598-day (October 31st, 2002) was obtained, as the figure 12 presents. It is noticed that a middle area with a minimum reached temperature of 24.23 °C is formed, a value closed to the mean temperature at lamellas molding. This leads to low levels of the stresses determined by the cement hydration heat and seasonal temperature variations. The maximum reached value, 39.60 °C, occurred at the faces bottom side.

By processing the obtained results in all the accumulated mesh nodes of the structure, the stresses developments were estimated. The figure 13 presents the horizontal stress σ_{xx} development at the final moment of analysis (the 598-day). It can

be noticed that the σ_{xx} stress reaches a tension (maximum) value of 91.94 N/cm^2 and a compression (minimum) value of 150.00 N/cm^2 (in the monitoring gallery area).

The vertical stress σ_{yy} development at the final moment of analysis, 598-day, is presented by the figure 14. The maximum tension value reached by the σ_{yy} stress is 85.72 N/cm^2, in the area where the structural boundary conditions were imposed (blocked uy displacements), and the minimum compression value is 317.00 N/cm^2, in the monitoring gallery area.

Table 2

2-D results Vs time					
Date	Value at T23 sensor (u/s, el 35.00)	Date	Value at T23 sensor (d/s, el 35.00)	Date	Value at T22 sensor (d/s, el 50.70)
14.11.2001	31.56377	15.06.2002	31.60825	20.07.2002	29.6675
17.11.2001	31.54979	22.06.2002	31.62515	27.07.2002	29.52129
24.11.2001	31.55492	29.06.2002	31.64167	03.08.2002	29.36061
01.12.2001	31.27388	06.07.2002	31.65775	10.08.2002	28.71822
08.12.2001	31.03347	13.07.2002	31.67253	17.08.2002	28.72582
15.12.2001	30.98326	20.07.2002	31.68574	24.08.2002	28.39707
22.12.2001	31.01175	27.07.2002	31.70025	31.08.2002	28.39792
29.12.2001	31.04071	03.08.2002	31.71430	07.09.2002	28.40939
05.01.2002	31.06800	10.08.2002	31.72521	14.09.2002	28.42076
12.01.2002	31.14826	17.08.2002	31.73935	28.09.2002	28.38983
19.01.2002	31.15246	24.08.2002	31.75001	05.10.2002	28.40064
26.01.2002	31.17509	31.08.2002	31.76344	12.10.2002	28.41303
02.02.2002	31.19811	07.09.2002	31.77653	19.10.2002	28.42520
09.02.2002	31.22521	14.09.2002	31.78951	26.10.2002	28.43512
16.02.2002	31.25158	28.09.2002	31.81391	31.10.2002	28.44245
23.02.2002	31.27678	05.10.2002	31.82612		
02.03.2002	31.30205	12.10.2002	31.83818		
09.03.2002	31.32595	19.10.2002	31.85004		
16.03.2002	31.34942	26.10.2002	31.86158		
23.03.2002	31.37253	31.10.2002	31.86969		
30.03.2002	31.39480				
06.04.2002	31.41667				
13.04.2002	31.43810				
20.04.2002	31.45903				
04.05.2002	31.49934				
11.05.2002	31.5182				
18.05.2002	31.53716				
25.05.2002	31.55568				
01.06.2002	3157345				
08.06.2002	31.59099				

The figure 15 presents the σ_{xy} shear stress development at the final moment of analysis, 598-day. The extreme levels are reached on the two directions of the faces: the maximum value of 62.40 N/cm^2, at the dam downstream face, and the minimum value of -72.60 N/cm^2, at the upstream face.

The maximum reached displacements (DMX) occur at the structure top with the value of 4.694 mm.

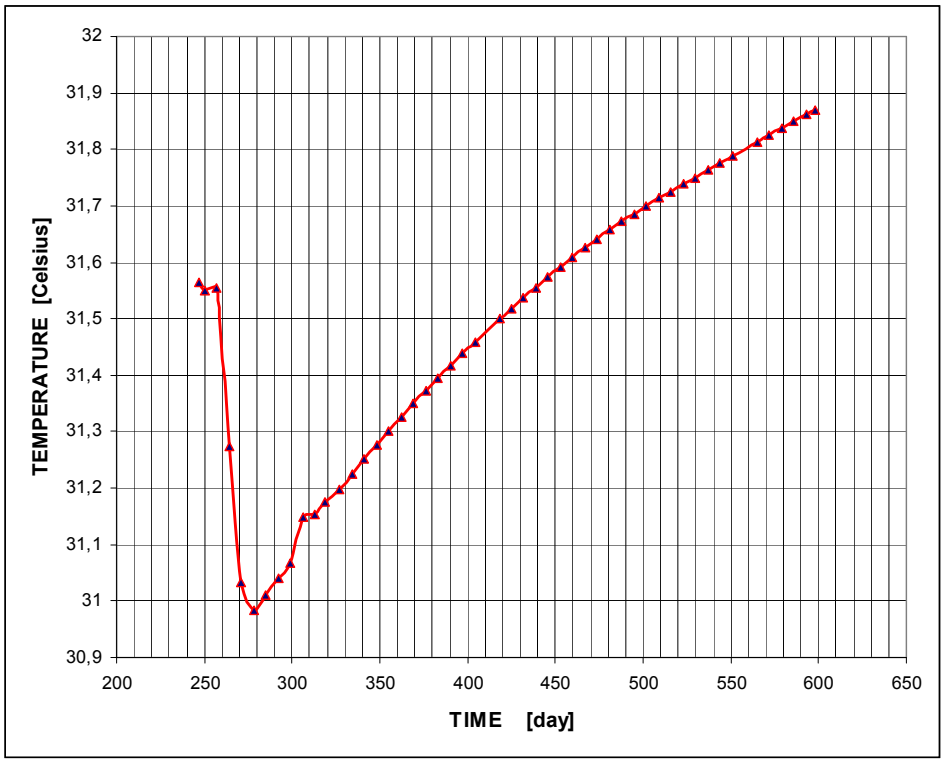

Figure 10 Temperature time development at the T_{23} sensor location

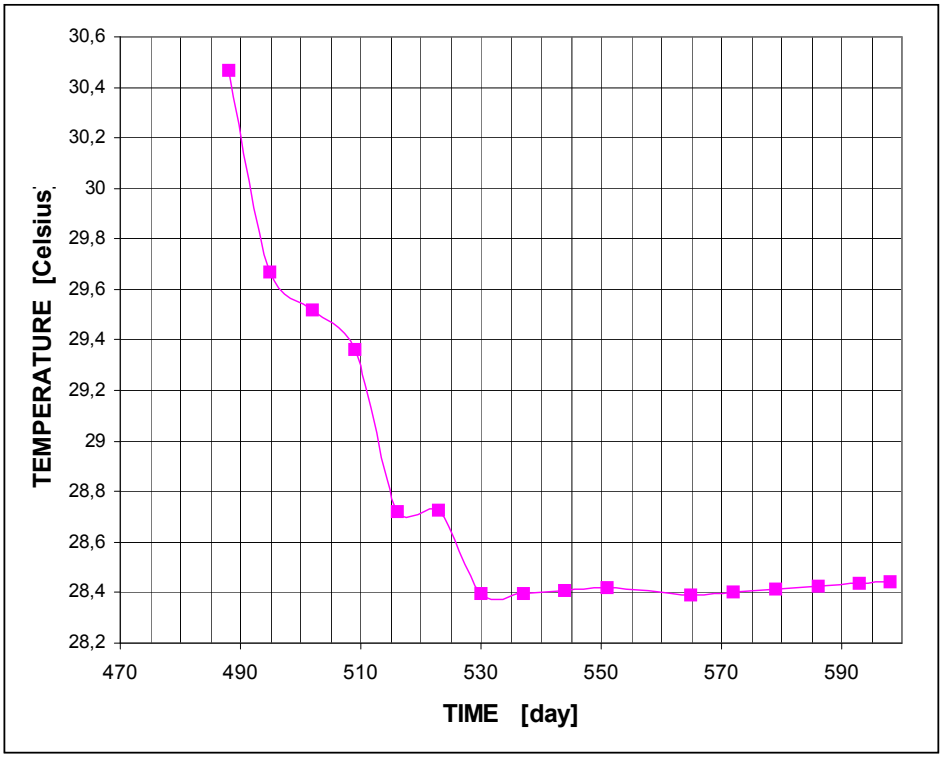

Figure 11 Temperature time development at the T_{22} sensor location

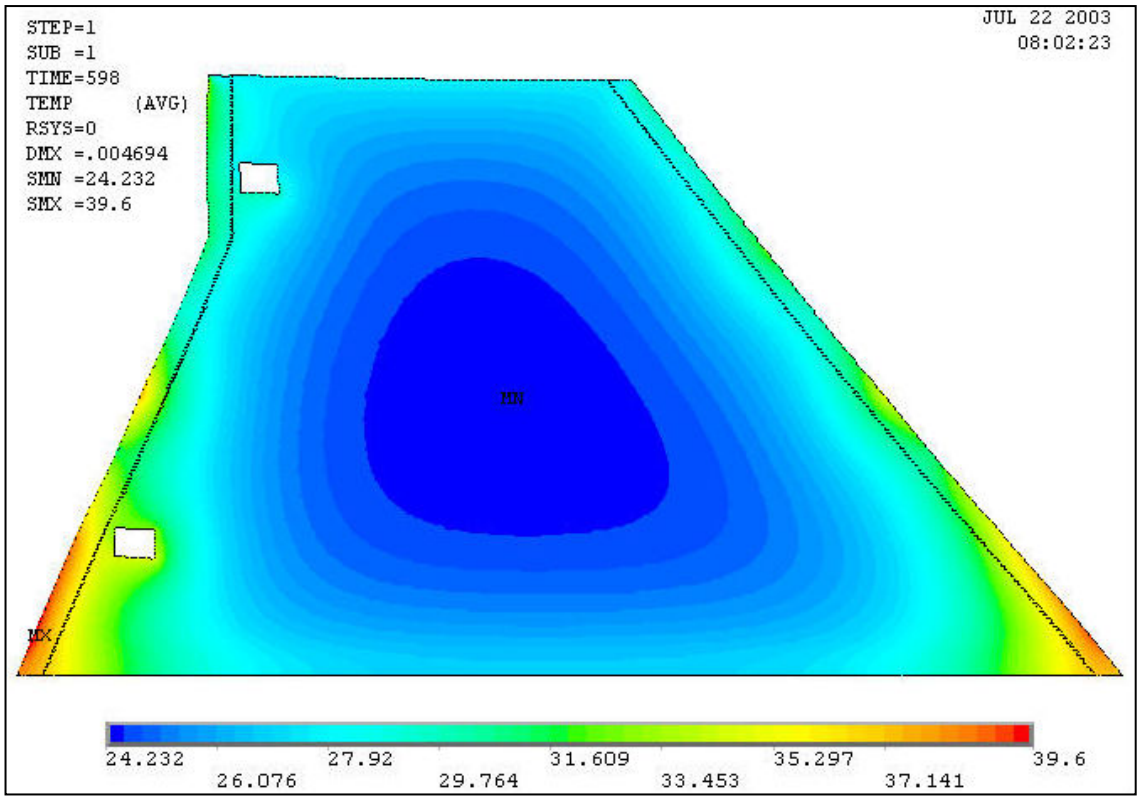

Figure 12 Temperature spectrum at the final moment of analysis, 598-day

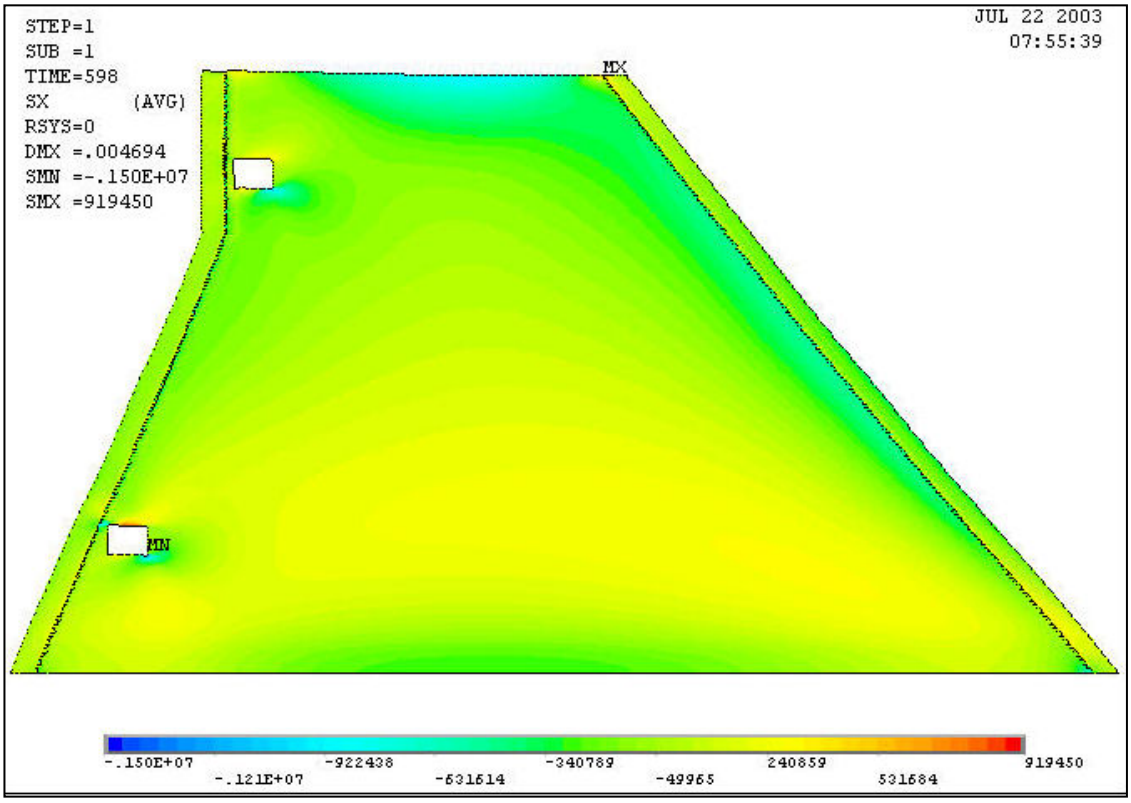

Figure 13 Horizontal stress σ_{xx} spectrum at the final moment of analysis, 598-day

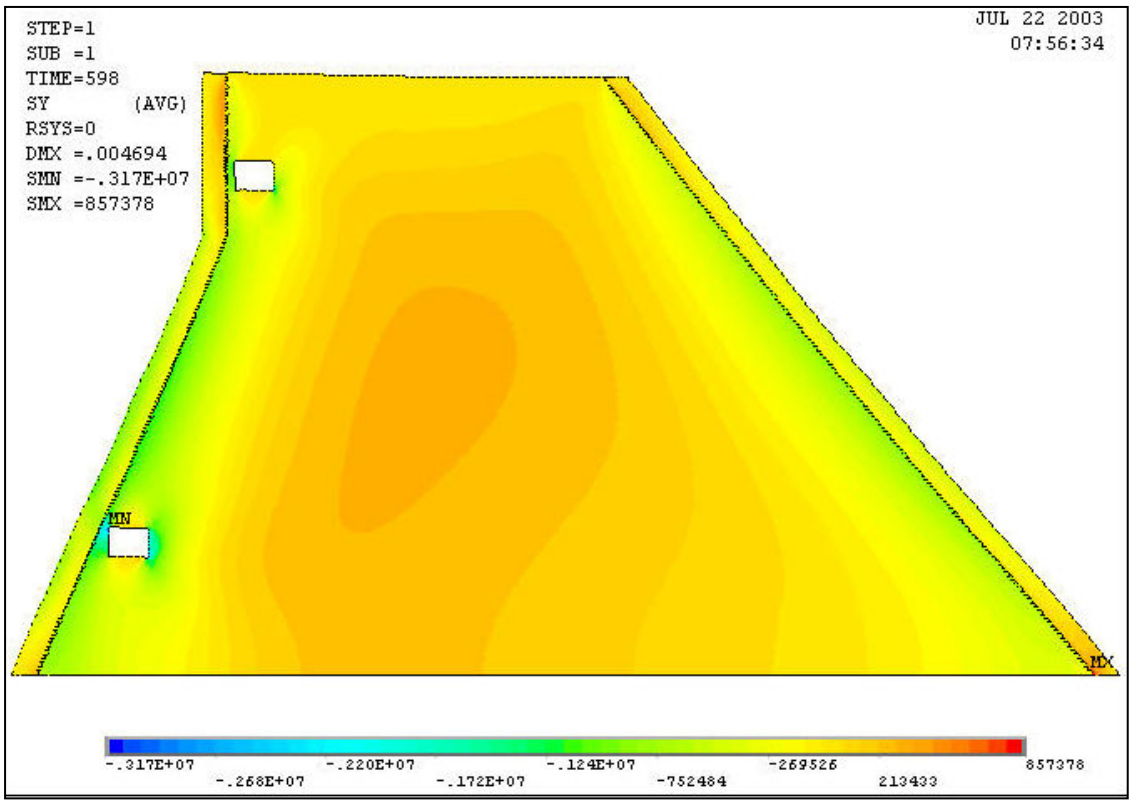

Figure 14 Vertical stress σ_{yy} spectrum at the final moment of analysis, 598-day

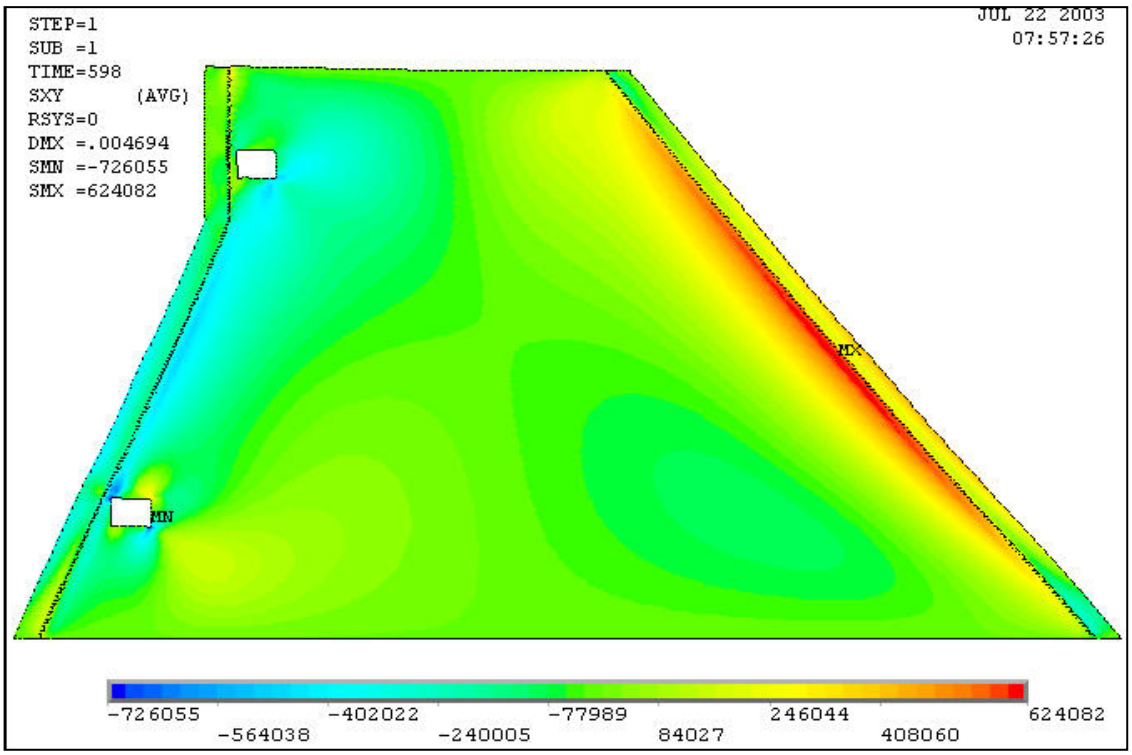

Figure 15 Shear stress σ_{xy} spectrum at the final moment of analysis, 598-day

During *the second stage*, the transitory thermal conduction, and consequently the stress and strain state in transitory development, was modeled for a 502 days time interval (December 3rd, 2001 – July 27th, 2002). A new nodes selection was performed [4] in order to obtain the results according to the B theme specifications [1]. These results were placed in a specified external file, as the table 3 presents.

Table 3

2-D results vs. elevation				**2-D results vs. elevation**			
Elevation	**Value at 2 m from u/s face on 27/07/02**	**Value at 2 m from d/s face on 10/08/02**	**Value at 4 m from d/s face on 31/10/02**	**Elevation**	**Value at 2 m from u/s face on 27/07/02**	**Value at 2 m from d/s face on 10/08/02**	**Value at 4 m from d/s face on 31/10/02**
62,10			27.2020	42,20	31.402	30.4480	28.7590
61,50			27.1690	41,60	31.612	30.6690	28.9300
60,90			27.1530	41,00	31.690	30.7840	29.0600
60,30			27.1470	40,40	31.640	30.7630	29.1520
59,70			27.1510	39,80	31.499	30.6460	29.1930
59,10			27.1680	39,20	31.312	30.4820	29.1850
58,50			27.2000	38,60	31.114	30.3000	29.1540
57,90			27.2340	38,00	30.934	30.1190	29.0880
57,30			27.2960	37,40	30.807	29.9580	29.0170
56,70			27.3700	36,80	30.774	29.8490	28.9560
56,10			27.4490	36,20	30.869	29.8420	28.9210
55,50			27.5970	35,60	31.089	29.9560	28.9350
54,90		31.3530	27.9540	35,00	31.700	30.1560	28.9900
54,30		30.9100	28.0320	34,40	32.092	30.3980	29.0920
53,70		30.6360	28.1180	33,80	32.488	30.6490	29.2340
53,10	32.700	30.4390	28.1700	33,20	32.549	30.8910	29.4010
52,50	31.559	30.2250	28.1980	32,60	33.198	31.1280	27.5110
51,90	30.789	29.9810	28.1940	32,00	33.470	31.3680	29.7910
51,30	30.143	29.7240	28.1590	31,40	33.780	31.6210	30.5440
50,70	29.711	29.4730	28.1100	30,80	34.219	31.9000	30.7840
50,00	29.275	29.1600	28.0300	30,20	34.288	32.2080	31.0410
49,40	29.041	28.9710	27.9470	29,60	34.696	32.5350	31.3160
48,80	28.902	28.8390	27.8700	29,00	34.528	32.8640	31.6030
48,20	28.856	28.6260	27.8120	28,40	35.000	33.1810	31.8900
47,60	28.904	28.6230	27.5300	27,80	35.025	33.4780	32.1780
47,00	29.036	28.6990	27.7910	27,20	35.034	33.7510	32.4600
46,40	29.350	28.9190	27.8280	26,60	35.051	34.0110	32.7500
45,80	29.477	29.0090	27.9010	26,00	35.086	34.2710	33.0270
45,20	29.759	29.2060	28.0030	25,40	35.144	34.5340	33.3100
44,60	30.070	29.4220	28.1400	24,80	35.229	34.8050	33.6040
44,00	30.404	29.6540	28.2820	24,20	35.342	35.0880	33.9140
43,40	30.754	29.9060	28.4360	23,60	35.484	35.3900	34.2570
42,80	31.100	30.1790	28.5970				

As it was performed in the first stage, the results of the second stage were graphically processed. The horizontal stress σ_{xx} reaches a maximum tension value of 83.87 N/cm^2, and a minimum compression value of 207.00 N/cm^2 (at the monitoring

gallery area and in the top lamella). The vertical stress σ_{yy} reaches a maximum tension value of 80.28 N/cm^2, and a minimum compression value of 346.00 N/cm^2.

Along the third stage, the previous stages sequences were reconsidered for a final analysis moment corresponding to the 516 days interval (August 10th, 2002). The selected results, saved in a specified file, are presented by the table 4.

Table 4

Horizontal profiles					**Horizontal profiles**				
Elevation 50.70					**Elevation 35.00**				
Cell	X=	node	10.08.2002	31/10.02	Cell	X=	node	10/08/02	31/10/02
u/s	-5,72				u/s	-12,00			
T14	-5,00	13487	29.593	29,511	T23	-10,00	7323	31.725	31,870
T15	0,00	13472	27.860	26,728	T26	0,00	7302	25.650	25,849
T17	15,00	13430	27.133	24,561	T29	25,00	7392	24.360	24,348
T19	30,00	13421	27.207	25,052	T32	45,00	7359	25.781	26,017
T22	40,00	13402	29.243	29,129	T35	55,00	7338	31.540	31,627
d/s	43,44				D/s	56,00			

The results were graphically processed. The horizontal stress σ_{xx} reaches a maximum tension value of 88.57 N/cm^2, and a minimum compression value of 154.00 N/cm^2 (at the monitoring gallery area and in the top lamella). The vertical stress σ_{yy} reaches a maximum tension value of 84.63 N/cm^2, and a minimum compression value of 316.00 N/cm^2. The shear stress σ_{xy} reaches a maximum value of 61.60 N/cm^2, and a minimum value of -73.17 N/cm^2.

In conclusion, it can be considered that the technology of successively molding the concrete in layers of about 0.30 m thickness for a massif dam, allows a favorable dissipation of the thermal flow determined by the employed cement types hydration (Portland cement and puzzolanic flying ash - Portland cement mixture). Seasonal temperature variations do not influence in a decisive way the structure's stress and strain state.

It is mentioned that the maximum tension stress values may overpass the admitted values for the simple concrete. But since these extremes occur in the technical cavities areas, which are commonly reinforced, it can be considered that the adopted working technology satisfies all the technical requirements enforced at a massif concrete dam accomplishment.

REFERENCES

[1] Coyne et Bellier – "Thermal analysis of a RCC dam body during construction", 7th Benchmark Workshop on Numerical Analzsis of Dams, September 24-26, 2003 - Bucharest, ROMANIA.

[2] Dan GARBEA – "Analiză cu elemente finite", Ed. Tehnică, Bucureşti, 1990

[3] Gheorghe LAZAR – "Optimizarea exploatării sistemelor geotermale prin simulare hidraulică şi termică cuplată", Teză de doctorat, Universitatea Politehnica Timişoara, Facultatea de Hidrotehnică, Timişoara, 1997.

[4] **** - "ANSYS User's Manual, COMMANDS", vol II Commands, Copyright 1971, 1978, 1982, 1985, 1987, 1989, 1992-1996 by SAS IP - ISO 9001- 1994.

[5] **** - "ANSYS/ED" - Student Edition, Release 5.3, Copyright 1971, 1978, 1982, 1985, 1987, 1989, 1992-1996 by SAS IP - ISO 9001- 1994.

THERMAL ANALYSIS OF AN RCC GRAVITY DAM DURING CONSTRUCTION : BI-DIMENSIONAL SOLUTION PROPOSED BY STUCKY – COMSA [1]

Jean-Luc Sarf
ComSA Consulting Engineering, SWITZERLAND

Alexandre Wohnlich
STUCKY Consulting Engineers Ltd, SWITZERLAND

SUMMARY : With the help of a 2D Finite Elements software, the assessment of the dam body behaviour due to the concrete heat emission has been performed. The concrete temperatures at several locations of the dam body have been computed, in particular at the exact position of the thermometers at levels 35.0 masl and 50.7 masl. The maximal temperature reached in the centre of the dam body is around 41°C. The significant effect of the air temperature acting on the top of the dam and on the upstream and downstream faces has been observed with temperatures along the faces closely linked to the air temperature. As well, the thermal stresses within the concrete triggered by the heat emission have been assessed. A maximal tensile stress value ranging between 0.7 MPa and 1.0 MPa develops in the vicinity of both faces.

RÉSUMÉ : Au moyen d'un programme bi-dimensionnel d'Eléments Finis, le comportement du barrage dû au dégagement de chaleur du béton durant la construction a été estimé. La température du béton en plusieurs points particuliers du barrage a été calculée, en particulier à l'emplacement des thermomètres aux niveaux 35.0 msm et 50.7 msm. La température maximale atteinte vaut environ 41°C au centre du barrage. L'effet important de la température de l'air a été constaté à proximité des parements amont et aval du barrage, avec des températures de béton réagissant fortement aux conditions ambiantes. Egalement, les contraintes thermiques dans le béton engendrées par le dégagement de chaleur du béton lors de sa prise ont été calculées. La valeur maximale de la contrainte de traction est relevée à proximité des parements et varie entre 0.7 MPa et 1.0 MPa.

[1] Analyse thermique d'un barrage-poids BCR durant sa construction : solution bidimensionnelle proposée par STUCKY – ComSA

1. INTRODUCTION

In the framework of the 7th Benchmark Workshop on Numerical Analysis of Dams held in Bucharest in September 2003, the study of the thermal behaviour of an RCC gravity dam during construction is proposed to the participants.

As requested, emphasis is put in this paper on the temperature development within the dam body. But the computation of stresses due to temperature has also been performed and is shortly presented at the end of the study[2].

The method used in this analysis relies on a bi-dimensional Finite Elements modelling of the dam and the successive construction steps by means of the software Z_SOIL. This versatile software allows to take into account the influence of all determinant parameters playing a role in the long-term temperature and stress fields inside the concrete dam body.

Section 2 recalls the main data of the problem, whereas Section 3 introduces briefly the characteristics of the software used to solve the problem. Then Section 4 describes the main assumptions made for the purpose of the computation, leading to Section 5 addressing the results of the problem in terms of temperature and stresses. Finally Section 6 summarises in a conclusion the main results and lessons learned with this exercise.

2. MAIN DATA

Only the main features of the project are mentioned below. The reader interested in the complete data of the problem, in particular the common cross-section of the dam, the construction schedule and the tables/curves with the properties of the RCC material and the temperatures monitored on site will refer to the information of the problem provided by the formulator.

The gravity dam to be studied is 92 m high (between elevation 20.0 and 112.0 masl), with a 8 m large crest, a vertical upstream face and a 0.8:1.0 downstream face. The lower part of the upstream face between elevations 20.0 and 55.0 masl is inclined with a 0.4:1.0 slope.

The dam is essentially composed of RCC, which is placed in 0.30 m thick layers with a rate of placement of approximately 1 lift per day. Typically 10 layers are placed at this rate and then a standby is observed locally, during which RCC is placed in other sections.

Both dam faces are made up of conventional vibrated concrete (CVC) which is placed against the formwork and carefully vibrated in order to ensure the best possible bond with the RCC.

[2] With the quantity of information available for the case study, it was decided from the beginning to stick to a maximum of 60 hours of work. The results presented could actually be obtained within that time frame.

The cementitious content of RCC is composed of 100 kg/m^3 of Portland cement and 90 kg/m^3 of pouzzolanic fly ashes (PFA). On the other hand the CVC used along the faces is made of 350 kg/m^3 of Portland cement.

3. DESCRIPTION OF THE SOFTWARE

Z_SOIL software provides an attractive alternative to traditional approaches to geotechnical and structural problems. It uses recent advances in non linear finite element techniques and plastic modelling of soils and rocks to solve stability, load carrying capacity, deformation and creep issues, including consolidation of two-phase media and transient flow, with excavation/construction sequences, in an unified, cost-effective way. Thermal effects and moisture migration are also included in the software. Z_SOIL exists in 2D and 3D versions.

In the framework of this present study, the 2D version has been used (Z_SOIL V.6.11; for further details, see the web site : www.zace.com). As the problem raised is mainly a thermal issue, the modules of the software linked to rock and soil mechanics have not been used. For the purpose of this study, mainly the possibilities of modelling taking into account the time and construction sequences as well as the thermal effects developing within the concrete mass have been used.

4. MAIN ASSUMPTIONS

4.1 DAM GEOMETRICAL DEFINITION

The model of the gravity dam reflects the exact dimensions and geometry as given in the general information of the problem. Figure 1 shows the model, which is composed of 5’784 nodes and 5’577 elements.

For the sake of simplicity, both CVC strips along the upstream and downstream faces have been discarded.

The use of a 2D Finite Elements model to assess the temperature development within the dam body implies that no heat transmission takes place in the third dimension. This assumption is particularly sensible as the method of RCC placement in successive layers makes the problem essentially bi-dimensional.

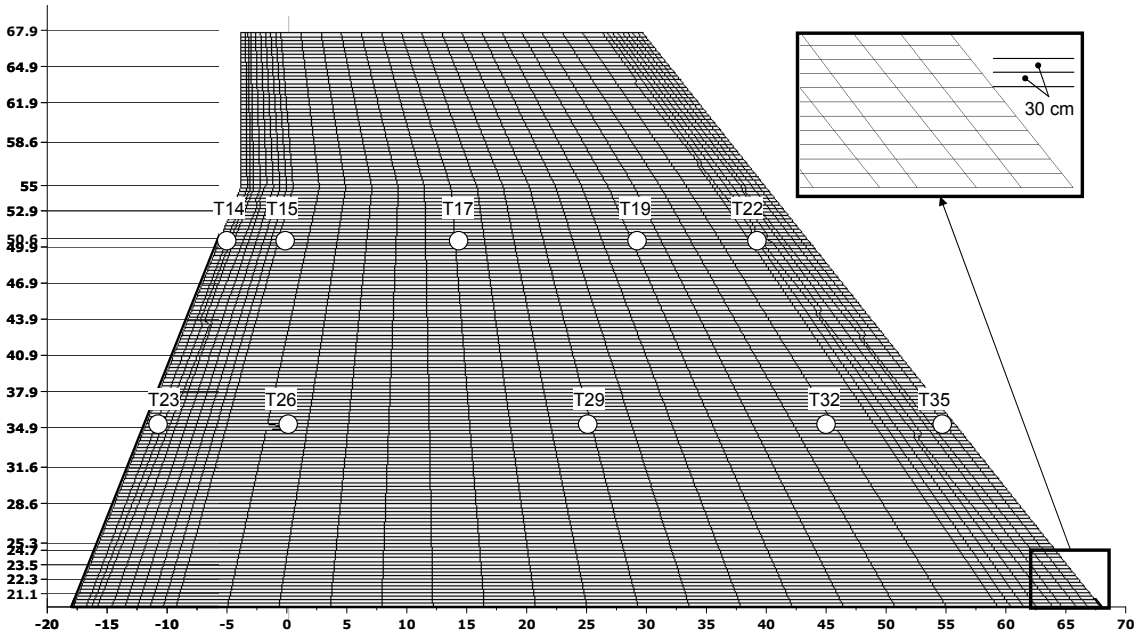

Figure 1 : General View of the 2D FE Model

4.2 CONSTRUCTION PROCEDURES AND SCHEDULE

The schedule of RCC placement as given by the instruction of the formulator has been carefully followed. In particular, every 30 cm thick RCC layer has been introduced in the model and placed successively according to the schedule.

The upstream and downstream formworks have been maintained in position during three days after the RCC placement. Then the formwork is released and installed at its new, higher position. The concrete starts diffusing heat 5 hours after placing (dormant period). From 5 hours to 72 hours, the diffusion occurs through the formwork, whereas from 72 hours onwards, the formwork is removed and the diffusion takes place in the air.

The computation has been run with a selected time step of 12 hours.

4.3 CHARACTERISTICS OF MATERIALS

All properties of RCC material given in the directive have been used for the computation. To model the heat emission of RCC, the "Shrinkage Core Model" developed by Bazant has been used. Of particular interest is the formulation of the heat source H as a function of the maturity M :

$$H(t,T)=H_{\infty}\frac{aM}{1+aM} \qquad (1)$$

The maturity M is a function of the absolute temperature T and time t :

$$M(t,T)=\int_{td}^{t}\exp\left[\frac{Q}{R}\left(\frac{1}{T_1}-\frac{1}{T}\right)dt\right] \qquad (2)$$

Where : H_∞ Total value of concrete hydration heat per unit volume [kJ/m^3]
a Heat source parameter [1/day]
Q/R Activation energy / universal gas constant [°K]
T_1 Reference temperature, normally 20°C = 293 °K
t_d Dormant period [day]

For this exercise the values adopted are the following :

H_∞ 265 kJ/kg x 190 kg/m^3 = 50'350 kJ/m^3
a 0.125 1/day
Q/R 4'000 °K
T_1 20°C = 293°K
t_d 5 hours = 0.2083 day

This set of parameters (in particular the parameter a) has been selected according to the own experience of the authors and in order to fit in an acceptable way the hydration heat curve given by the formulator.

4.4 INITIAL AND BOUNDARY CONDITIONS

The ambient temperature at site has been chosen equal on both upstream and downstream faces as well as on the upper face of the dam. Even though it might be considered somewhat rough, the average temperature given by the formulator has been selected for the case study. As the average temperature data provided cover approximately 12 months and the problem extends on 22 months, the data have been assumed equivalent cyclically from one year to the next.

Furthermore, the RCC temperature at placement has been assumed constant throughout the year at the value of 24°C. Given that this temperature ranges during the year from 23°C up to 27°C, this assumption is deemed acceptable.

The convection & radiation surface coefficient has been selected as α=100 kJ/m^2/h/°C, as suggested in the directive. During the first three days after RCC placement (when the formwork is still in position), this coefficient has been selected at the value of α=28.8 kJ/m^2/h/°C (=8 W/m^2/°K). No correction of both parameters has been made owing to the sunshine effect.

Finally the rock foundation of the dam has been selected as providing adiabatic thermal conditions, that is, no heat dissipation of concrete occurs through the foundation.

5. RESULTS

5.1 TEMPERATURE

5.1.1 Temperature Versus Time

The temperature development at levels 35.0 masl and 50.7 masl is shown in Figures 2 (Level 35.0 masl) and 3 (Level 50.7 masl).

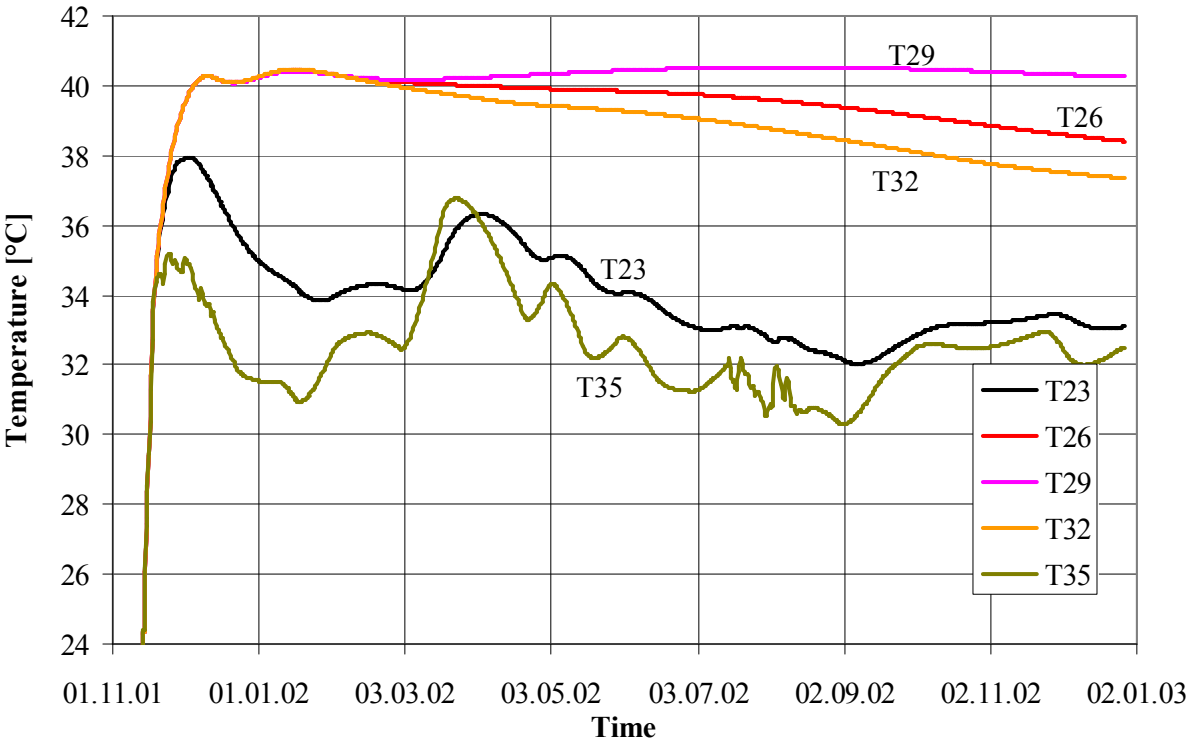

Figure 2 : Elevation 35.0 masl, Temperature Vs. Time

At level 35.0 masl, the temperature at the core of the dam is stable around 40.5°C. Thermometer T29 is located at the centre of the dam, whereas thermometers T26 and T32 are at 12 m and 11 m respectively from the upstream and downstream faces. That is the reason why the temperature at those two points drops faster than in the very centre (T29).

When coming closer to the dam faces, the variations of temperature become similar to the average air temperature. It is interesting to see that thermometer T23, located 2 m behind the upstream face, is less sensitive to air temperature moves than thermometer T35, which is located only 1 m behind the downstream face. The curves for these two thermometers seem somewhat chaotic, because the rough average air temperature curve has been used for boundary conditions. Making that curve smoother by considering seasonal trends rather than daily average air temperature values would have resulted in smoother concrete temperature curves close to the faces (T23 & T35).

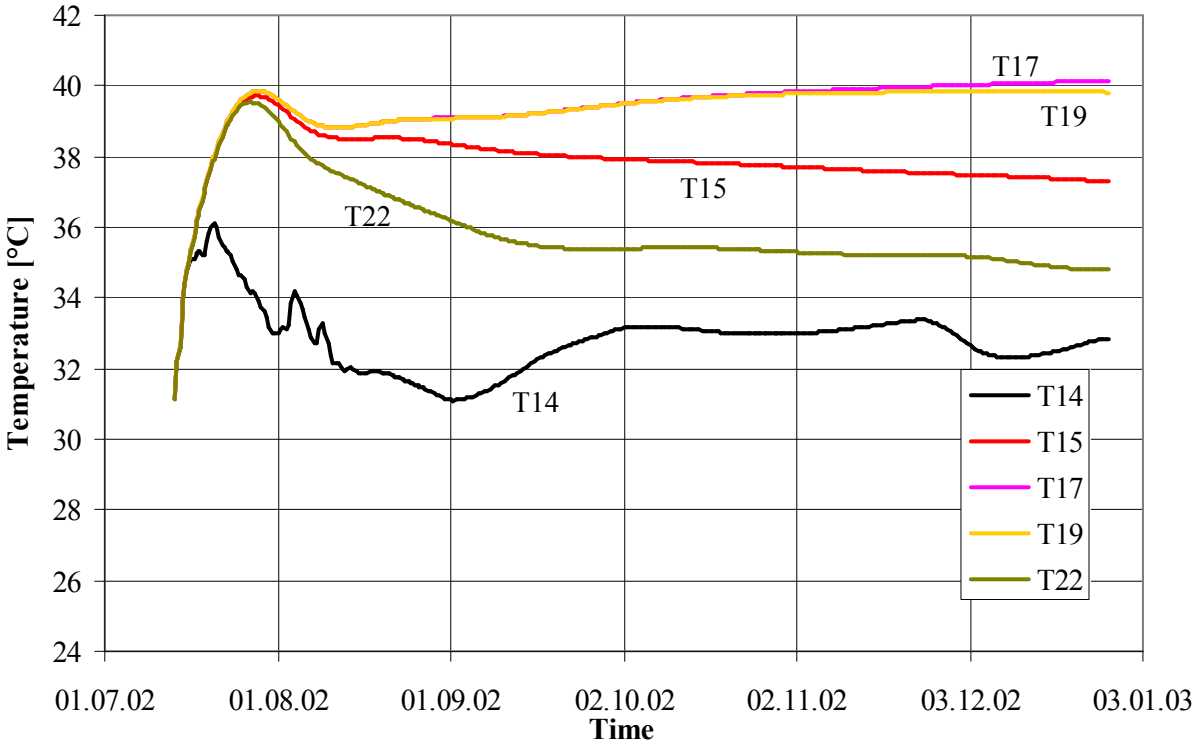

Figure 3 : Elevation 50.7 masl, Temperature Vs. Time

The temperature behaviour described for the elevation 35.0 masl also applies to elevation 50.7 masl (Figure 3). The temperature at the centre of the dam stabilises around 40°C.

Thermometer T14 is the most sensitive to average air temperature for it is located only 72 cm behind the upstream face. Thermometer T22, 3.44 m behind the downstream face, is already far less influenced by the air temperature.

With regard to both Figures 2 and 3 above, it can be seen that the main temperature gradient takes place in the first 3 to 5 m behind the dam faces.

5.1.2 Elevation Versus Temperature

For three given dates, Figure 4 shows the evolution of temperature within the concrete mass at different locations and elevations of the dam. For each specific date, two curves are provided that show the temperature in the centre of the dam (bold line) and in the vicinity of the dam face (thin line).

It is to notice that the distance from the face of the curves showing the temperature close to the face is variable with the three different dates : on July 27, 2002 the curve shows the temperature at 2 m from the upstream face, on August 10, 2002 the temperature is monitored at 2 m from the downstream face and on December 28, 2002 the temperature is shown at 4 m from the downstream face. This difference reflects in the curves, with the temperature measured 4 m behind the downstream face (December 28, 2002) clearly with higher temperature than the other two curves measured closer to the face (2 m distance) and thus more sensitive to the air temperature.

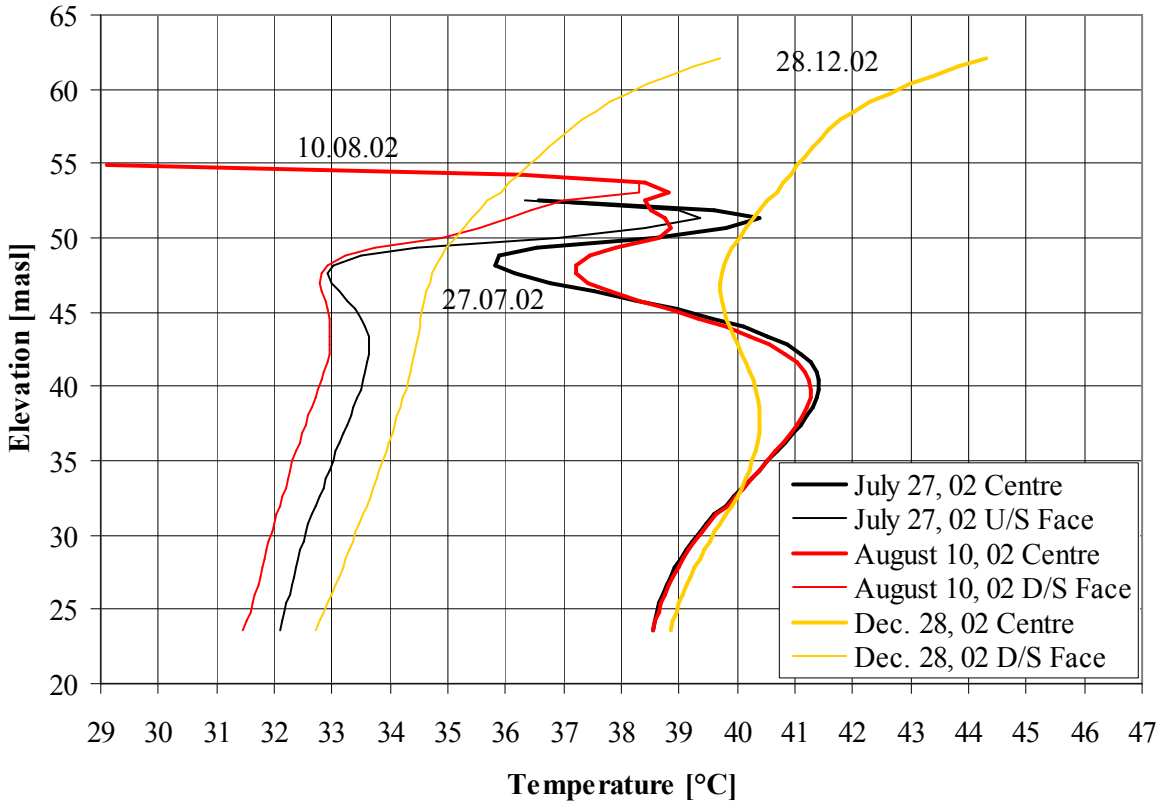

Figure 4 : Elevation Vs. Temperature at Given Dates

In addition it is to note that the temperature value ranging from 39°C to 41°C and prevailing in the core of the dam is clearly visible in Figure 4. When going up and coming closer to the upper, more recently placed RCC layers, the effect of the heat emission and air temperature builds up and becomes increasingly noticeable.

5.1.3 Horizontal Profiles

Figures 5 and 6 show the horizontal temperature profiles at level 35.0 masl and 50.7 masl respectively.

The temperature profile seen at level 35.0 masl is more constant and regular than at level 50.7 masl. This is explained by the distance from the level of measures (35.0 masl and 50.7 masl) up to the level of RCC placement at the date considered : the closer to the upper surface, the closer to the high, ongoing temperature emission and to the effect of air temperature acting of the upper surface. This is clearly noticeable on Figure 6 (level 50.7 masl), where on July 27, 2002 the temperature reaches more than 40°C whereas it has notably started cooling down to approximately 39°C on August 10, 2002.

The strong influence of the air temperature is also remarkable along the dam faces. In particular the very end of the temperature curve is not very relevant and significative, as it is directly influenced by the average air temperature, which has not been smoothed for the purpose of this case study.

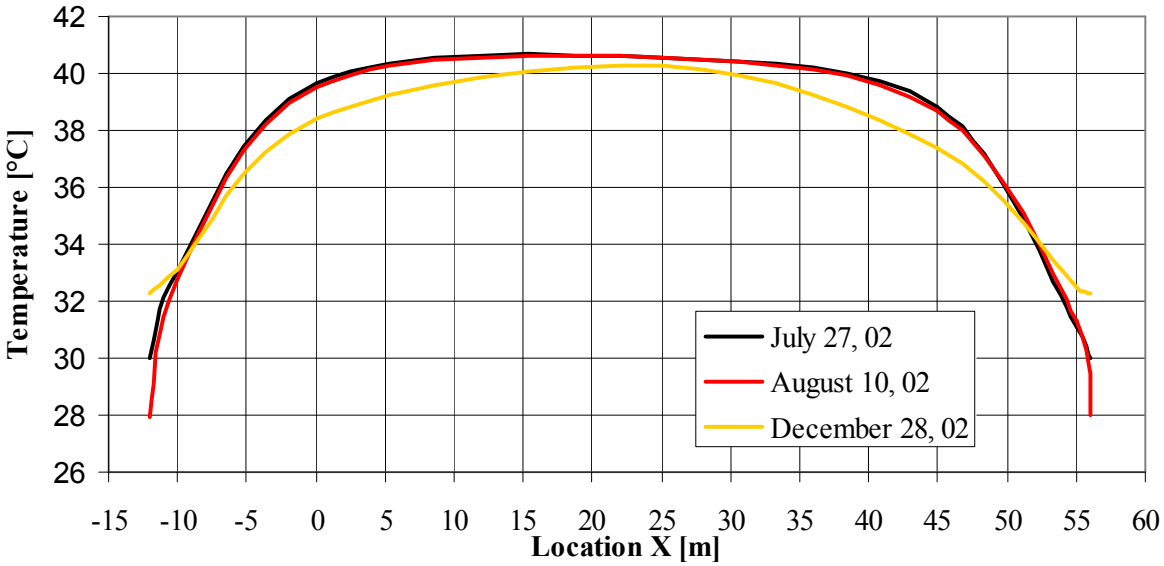

Figure 5 : Horizontal Temperature Profile at Level 35.0 masl

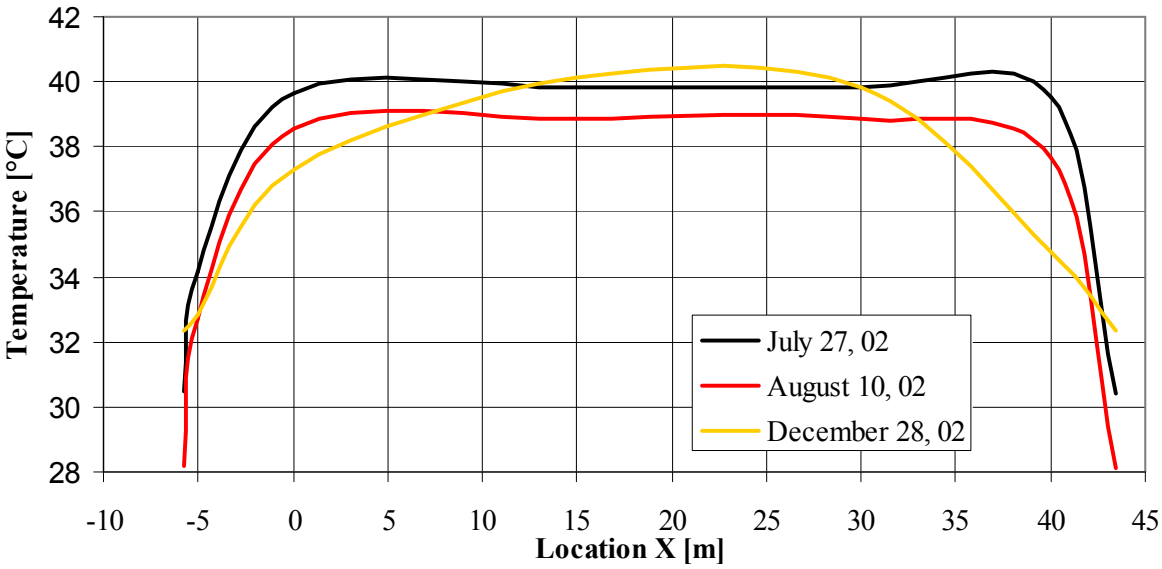

Figure 6 : Horizontal Temperature Profile at Level 50.7 masl

Finally it is interesting to note that the effect of heat dissipation through the dam faces becomes more and more visible in the long-run (see the curves for December 28, 2002); the cooling of the central portion of the dam has not started yet at that date, mainly due to the progress of works (addition of new RCC layers on the top of the dam).

5.1.4 Graphic Outputs

Some 2D graphic outputs are given below (Figures 7 to 10), that show by means of isotherm lines the temperature distribution in the dam body at the date considered.

Two pairs of dates have been selected : (1) August 7, 2001 and November 6, 2001, period during which the concrete works were stopped at level 31.6 masl, and (2) January 31, 2002 and July 11, 2002, when the concrete works were stopped at level 49.9 masl.

Although with black and white pictures only, the process of heat emission and concrete cooling is clearly noticeable in both cases. As well, the adiabatic boundary condition of the foundation is particularly obvious on those figures.

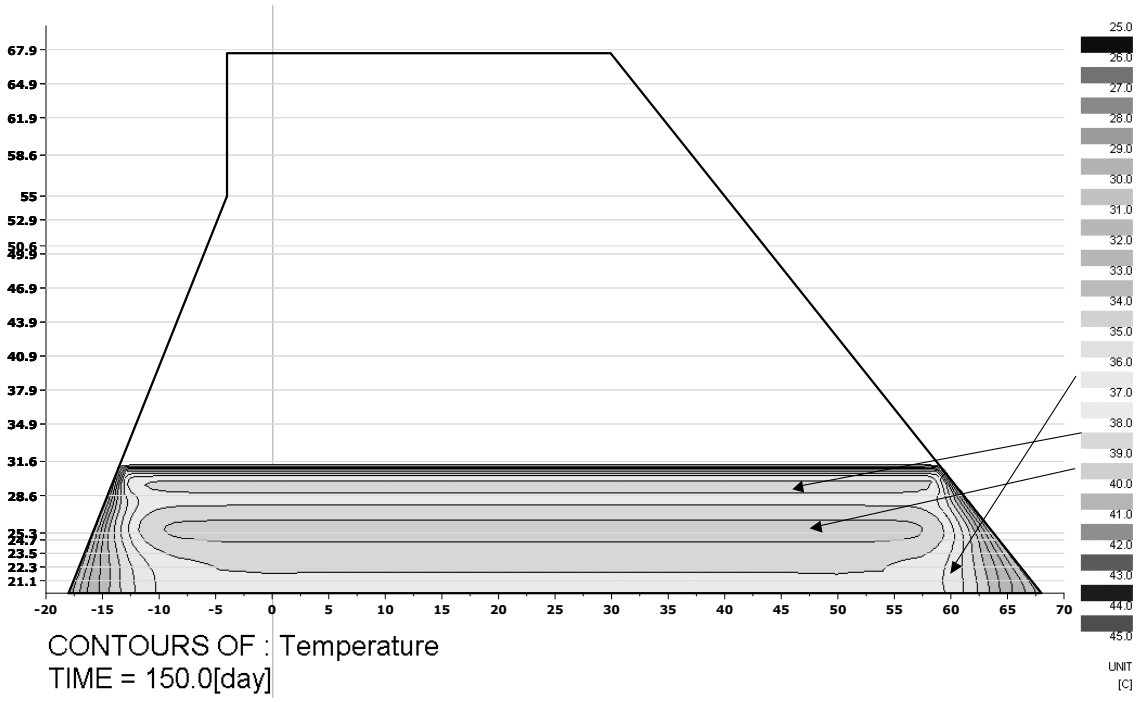

Figure 7 : Temperature Distribution in the Dam Body on August 7, 2001

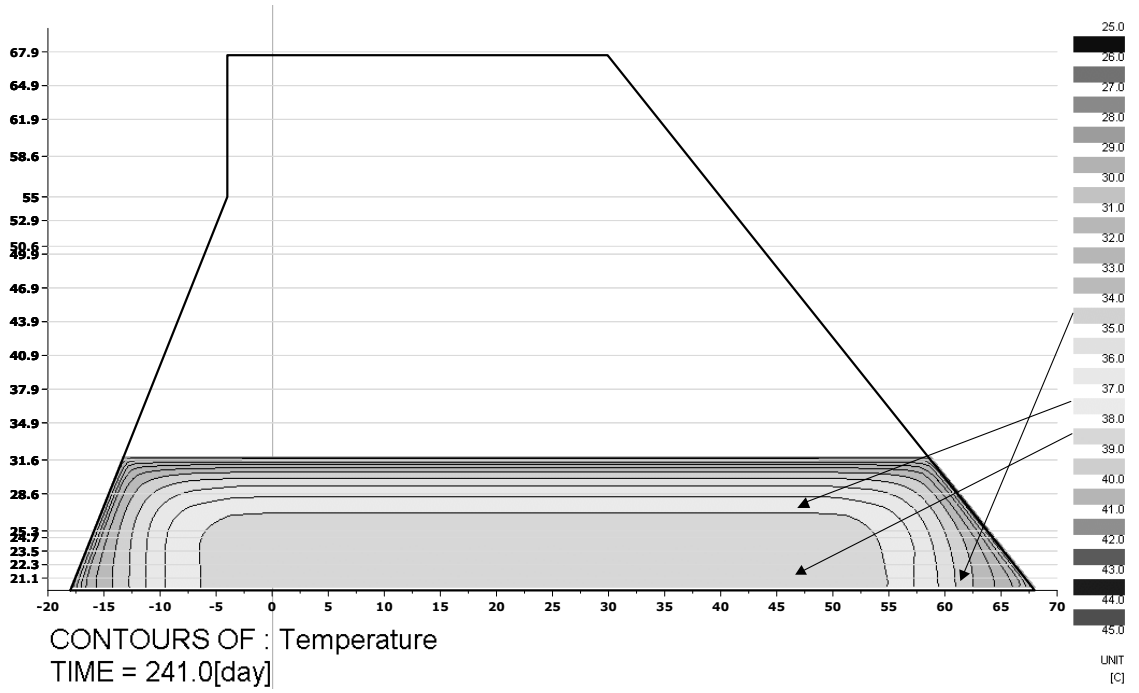

Figure 8 : Temperature Distribution in the Dam Body on November 6, 2001

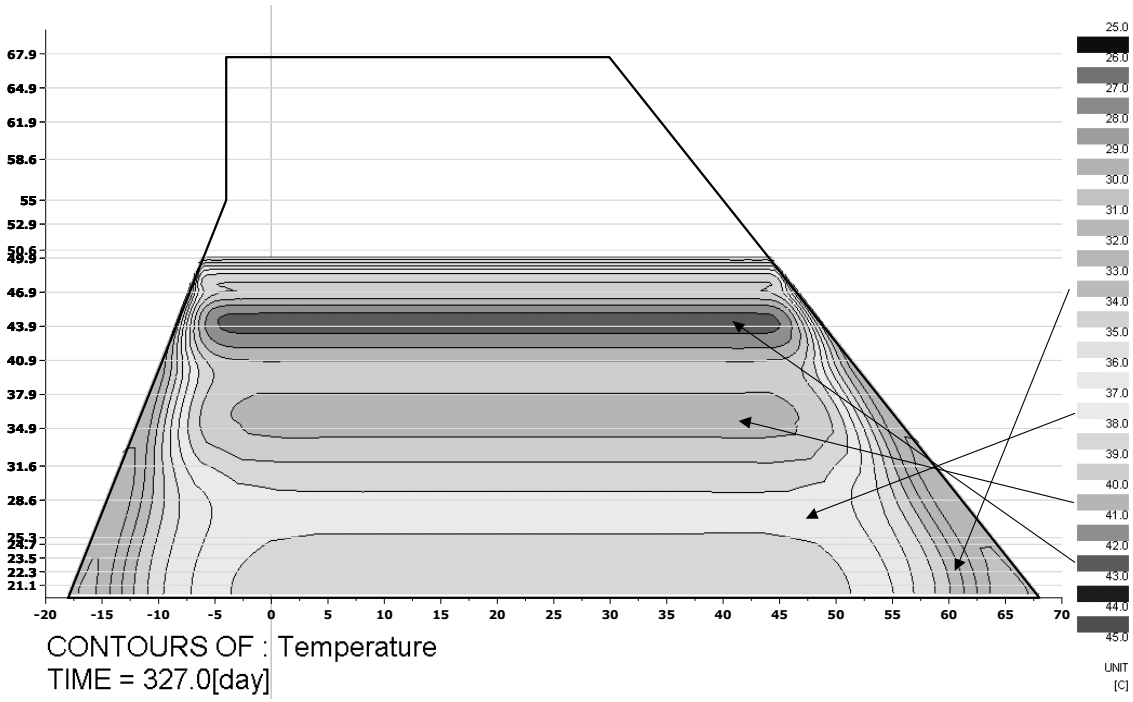

Figure 9 : Temperature Distribution in the Dam Body on January 31, 2002

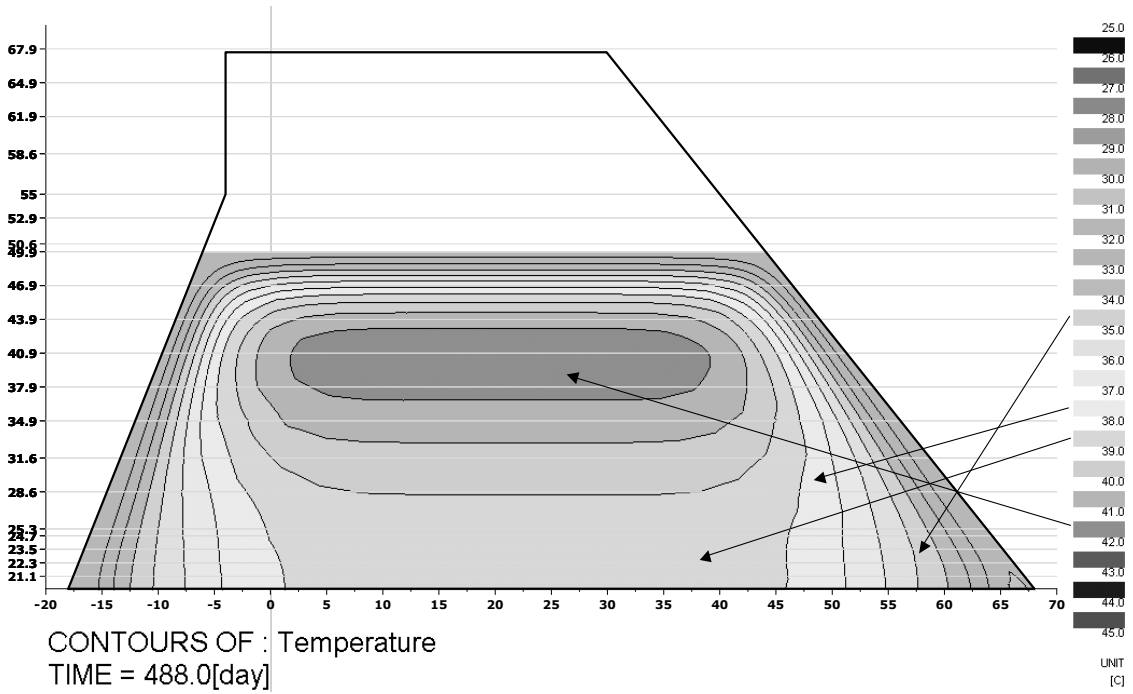

Figure 10 : Temperature Distribution in the Dam Body on July 11, 2002

5.2 STRESSES

The temperature developing within the concrete body induces thermal stresses. More attention is to be paid to tensile stresses, as they may trigger cracks in the concrete mass. Below are given some general considerations about the stress field due to the thermal conditions discussed above (concrete heat emission and air temperature). A more detailed and thorough study on the issue of thermal stresses would require more time and is anyway irrelevant in the context of the current case study.

The computation has been run in elastic conditions. A conventional Elasticity Modulus vs. Time law has been introduced in the model in order to enable the software to compute stresses in the concrete.

The tensile stress field is shown in Figures 11 and 12 for two dates : January 31, 2002 and July 11, 2002. Interestingly these two pictures can be linked to Figures 9 and 10 presenting the temperature field at the same time. Between these two dates no additional RCC layer is placed (the upper surface remains unchanged at elevation 49.9 masl), meaning that the evolution of the temperature and stress fields is only caused by the air temperature changes and the cooling through the upper surface and both upstream and downstream faces of the dam.

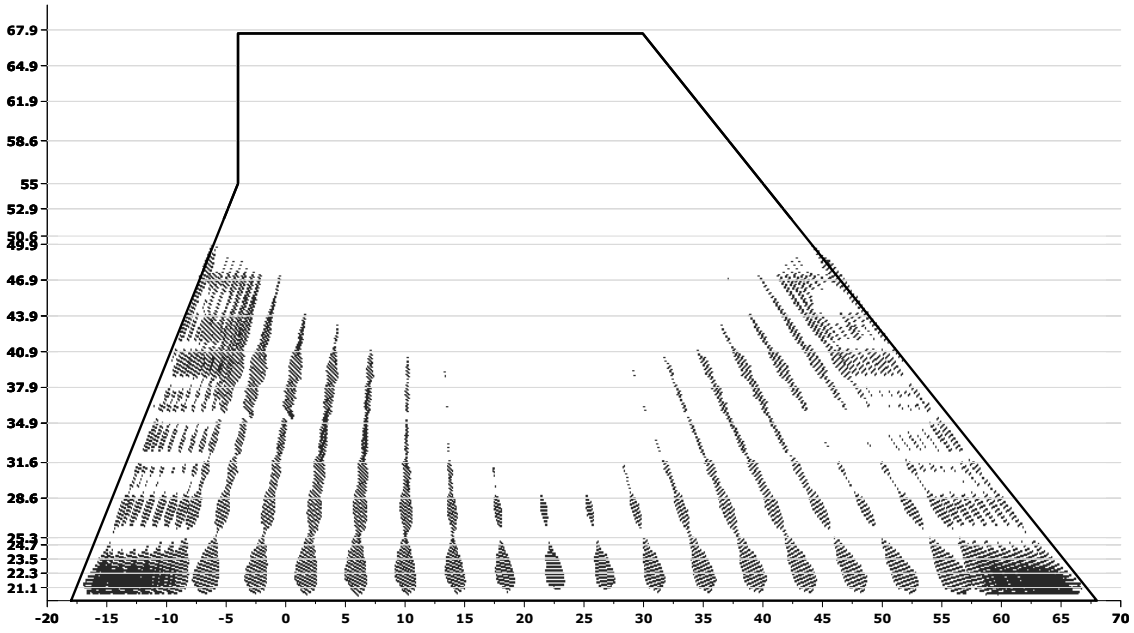

Figure 11 : Tensile Stresses Distribution in the Dam Body on January 31, 2002

It is to notice that both Figures 11 and 12 do not show stresses due to temperature effect only. As the dead weight of the concrete is inseparable from any other load case, it has been included in the computation and is therefore taken into account in the graphic outputs.

Not surprisingly the tensile stresses are the highest close to both faces and reach values ranging between 0.7 MPa and 1.0 MPa, depending on which time is considered. They occur mostly perpendicular to the faces, where the temperature gradient is the highest.

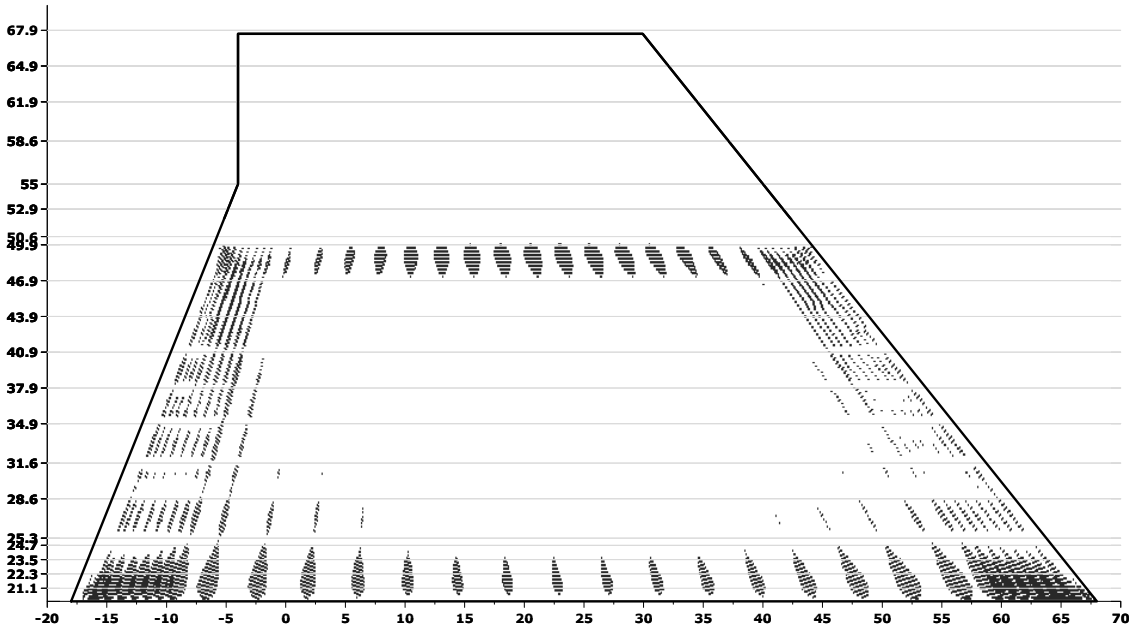

Figure 12 : Tensile Stresses Distribution in the Dam Body on July 11, 2002

When comparing Figures 11 and 12 carefully, it is clearly noticeable that with time going by and the temperature field moving to a more steady state (see Figures 9 and 10), the stress field accordingly moves toward less tensile stresses. The large area without tensile stresses located in the centre of the dam body on Figure 12 illustrates that slow and gradual change.

Finally the effect of the foundation is clearly visible. The tensile stresses prevailing there are due to the FE modelling : the boundary conditions for the foundation have been selected as rigid, thus not allowing any movement of the foundation. This assumption is too pessimistic and explains why the highest tensile stresses are observed in the vicinity of the foundation.

6. CONCLUSION

The analysis of the thermal behaviour of an RCC gravity dam during construction has been presented in this article. Beside the data provided by the formulator of the problem, the study has called for further assumptions. The most crucial ones are the following :

(1) The model is two-dimensional.
(2) The CVC strips located on both the upstream and downstream faces of the dam have not been considered.
(3) The air temperature accounted for in the study is not a smooth annual curve, but the average temperature provided in the instruction of the case.

Assumption (1) can be considered as acceptable, because the RCC placement method is mostly continuous in the third dimension, that is along the dam longitudinal axis (across the valley). On the other hand, assumptions (2) and (3) are more subject to discussion and might well have played a role in the results presented here. However, it

has been assumed that both assumptions affect the temperature field developing in the dam body only locally in the vicinity of both dam faces and in an reasonable way for the major portion of the dam.

The temperature field has been presented. The temperature developing in the centre of the dam body reaches approximately 41°C and is very slow to decrease. Conversely the concrete temperature in the first metres behind the upstream and downstream faces is strongly influenced by the air temperature prevailing on the job site. In addition to the various temperature curves asked by the formulator in the context of the case study, some graphic outputs have been given that allow a different outlook onto the temperature development within the dam body.

Finally, some considerations, results and graphic outputs have been provided about the thermal stresses triggered by the concrete heat emission. Those thermal stresses develop mainly along the dam faces, where the temperature gradient is the highest. The maximal stress observed seems to range between 0.7 MPa and 1.0 MPa.

THEME C

SEEPAGE THROUGH AN EARTHFILL DAM – FOUNDATION SYSTEM AND PIEZOMETRIC LEVEL VARIATION.

INTERNAL EROSION IN EMBANKMENT DAMS. CASE HISTORIES AND STATE OF THE ART IN THE MATHEMATICAL MODELING.

Prof. Adrian Popovici
Technical University of Civil Engineering of Bucharest

1.INTRODUCTION

Internal erosion is one of the most common causes of the deterioration and failure of embankment dams. However the processes involved in internal erosion are not completely understood as for instance, the mechanisms associated with slope stability. The statistics of failure of embankment dams by piping, one of the mechanisms of internal erosion, have shown the piping account for 43% of all embankment dam failures, respectively, 54% for dams constructed after 1950.

Internal erosion involves the removal of solid material, usually in suspension, from within an embankment or its foundation by the flow of water. The various mechanisms of internal erosion may be associated with construction defects and weaknesses or with the deformations and stress conditions within the embankment. Internal erosion may cause increased leakage and some form of surface settlement, possible in the form of a sinkhole (Charles, 2000).

There are several forms of internal erosion. Charles (2001) made a distinction between localised and mass internal erosion.

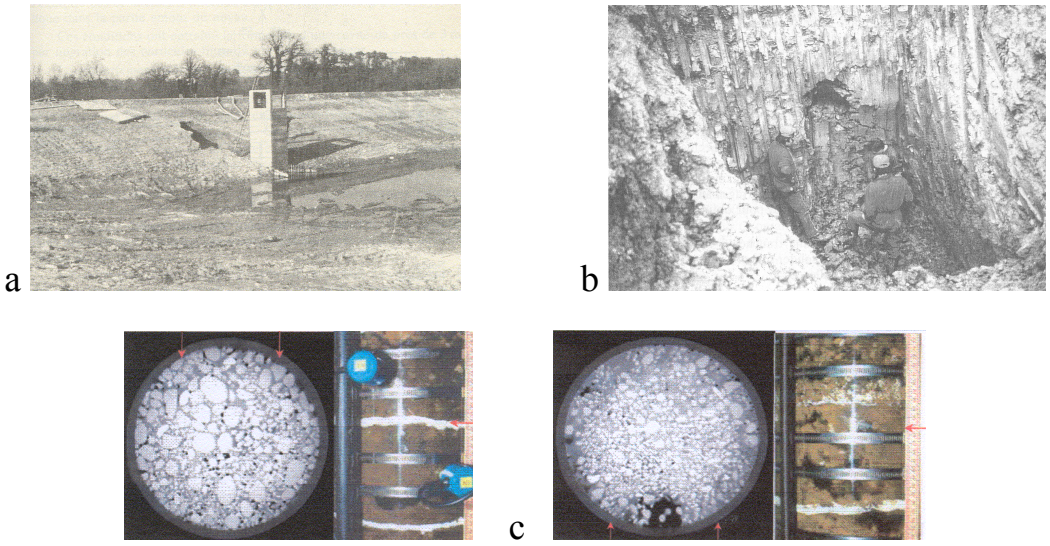

Fig. 1. Exemplifications of internal erosion processes
a – Saint-Julien-de-Landes dam (France): contact internal erosion around the outlet and upstream face sinkhole; b – Buget dam (France) – piping at downstream face; c – laboratory tests showing effects of suffosion in gap graded cores and filters.

The localised internal erosion may be related to some local defect or may be associated with piping or hydraulic fracture. The term piping is usually applied to a process starting at the exit point of seepage and in which a continuous passage or pipe is developed in the soil by backward erosion. Cohesionless soils, particularly fine sands and silts, are most susceptible. The hydraulic gradient at the point where the water flows out of the ground is critical but is difficult to predict as it depends on localised weaknesses in the fill.

In a cohesive soil, which is capable of sustaining an open crack, concentrated leaks may occur with erosion of soil particles along the walls of the cracks. Hydraulic fracture of the core by the reservoir water pressure may occur where the internal stresses in the upstream core zone are less than adjacent hydrostatic pressures and some favorable factors, such as an existing crack or more permeable layer in connection with the reservoir are existing.

In contrast with above mentioned localised forms of erosion, the type of mass erosion known as suffosion can occur by seepage flow in soils which are internally unstable. Fines are transported by seepage flow through the embankment fill or foundation soil and the process may lead either to an accumulation of fines in some part of the fill or to fines being taken entirely out of the embankment. The term of suffosion is used also to the process where infills in bedrock bedding planes and joints are washed out under the pressure of seepage (subsurface erosion) (Garner, Sobkowicz, 2002). Suffosion, therefore, could be considered as permanently damaging and potentially unsafe behavior within a core or filter of a dam.

Soils inadequately compacted at low moisture contents may be susceptible to collapse compression on saturation. Layers of better-compacted material may arch over the collapsing soil resulting in the formation of loose, erodible, wet seams.

Certain clay soils disperse or deflocculate in the presence of relatively pure water and are therefore highly susceptible to internal erosion. The tendency for dispersive erosion depends on the mineralogy and chemistry of the clay, and dissolved salts in the pore water and the eroding water.

Internal erosion is often associated with the presence of structures such as outlet conduits and culverts, which pass through an embankment. The contact between the embankment fill and the structure can be a potential zone of weakness as the fill may have inadequately compacted, making suffosion and piping more probably. Leakage into a culvert may cause internal erosion and, where an unprotected outlet pipe has been placed in the embankment fill (Charles, 2001).

This invited lecture opening the works for Theme C of the 7th ICOLD Benchmark Workshop is focused on comments about case histories of internal erosion including remedial works, investigation on internal erosion processes and state of the art in the mathematical modeling of the seepage and internal erosion in embankment dams including a number of representative analyses.

2. CASE HISTORIES OF INTERNAL EROSION

The report of European Working Group chaired by J.A. Charles on Internal Erosion in Embankment Dams contains an excellent synthesis about case histories of internal erosion in European embankment dams (Charles, 2001). The data presented in the followings were taken from this report.

In the Table 1 has been summarized a selected group of 47 dams which have suffered internal erosion processes. They are classified under four headings, as follows:

A. Severity of problem or incident
B. Cause of problem or incident
C. Symptoms of problem or incident
D. Remedial works

The categories for each of the above mentioned headings are presented after the Table 1.

Table 1

Dam	**Country**	**Date built**	**Watertight element**	**Problem or incident**			
				A	B	C	D
1	2	3	4	5	6	7	8
Arbon	Spain	1967	Central gravel and silty sand core	2b	6	1,3	1
Balderhead	United Kingdom	1965	Central rolled clay core	2b	6,7	1,2,3	1
Buget	France	1980	Homogeneous clayey earth fill embankment	2a	2	2,4	4
Caspe	Spain	1988	Clay core	2b	9	1,2	2
Elbe-Seitenkanal	Germany	1976	Upstream asphaltic membrane	1	1	4	11
Fonte Longa	Portugal	1988	Homogeneous earth fill	3	1,3	5	4
Gostei	Portugal	1993	Homogeneous earth fill	3	1	5	4
Gourdon	France	1983	Upstream geomembrane, clay blanket on foundation	2b	5	4,6,7	6
Greenbooth	United Kingdom	1961	Central puddle clay core	2b	6	1	2
Grossee	Austria	1980	Upstream asphaltic membrane	3	4	2	5
Grundsjoarna	Sweden	1972	Central moraine core	2b	7	1,7	11
Haliby	Sweden	1970	Central moraine core	2b	10	1,2	2
Hyttejuvet	Norway	1965	Central moraine core	2b	6	1,2	2
Ibra	Germany	1975	Upstream geomembrane	1	1,4	4,7	5
Jukla	Norway	1974	Central moraine core	2b	6,7	2	2
Juktan	Sweden	1978	Central moraine core	2b	6,7	2	1
La Prade	France	1982	Wide central clay core	2b	2	4	2
Lavaud-Gelade	France	1943	Homogeneous sand fill embankment	3	8	4	10
Lluest Wen	United Kingdom	1896	Central puddle clay core	2b	3	1	1
Lovon	Sweden	1973	Upstream sloping moraine core	2b	6,7	1	2
Main-Donau-Kanal	Germany	1978	Upstream asphaltic membrane	1	1	4	11
Martin Gonzalo	Spain	1987	Upstream geomembrane	2a	4	1,2	5
Moravka	Czech Republic	1965	Upstream asphaltic membrane	2a	4	1,2	5
Motru	Romania	1984	Central clayey core	3	10	2	1
Mysevatn	Norway	1973	Moraine core	2b	6	1,2	2
Nepes	France	1945	Reinforced concrete core wall	2b	10	2,3,6	2
Nyrsko	Czech Republic	1970	Upstream reinforced concrete facing	2b	4	2	5

1	2	3	4	5	6	7	8
Porjus	Sweden	1980	Central moraine core	2b	6,7	1	2
Rengard	Sweden	1970	Moraine core	2b	6,7	1,2,3	2
Saint Aignan	France	1965	Homogeneous earth fill embankment	1	8	4	11
St Julien des Landes	France	1969	Homogeneous earth fill embankment	2a	1	5	4
Saint Pardoux	France	1975	Homogeneous earth fill embankment	2b	8	4,7	1
Sapins	France	1978	Homogeneous earth fill embankment	2a		4,9	1
Seitevare	Sweden	1967	Central moraine core	2b	10	4	2
Songa	Norway	1962	Central moraine core	4	6,7	2,3	12
Sorpe	Germany	1935	Central moraine core wall	2a	12	1,2	2
Stenkullafors	Sweden	1983	Central moraine core	2b	1,6	1	10
Suorva	Sweden	1972	Central moraine core	2b	6,7	1,2,3	2
Sylvenstein	Germany	1958	Central vertical soil-cement core	3	7	2,7	2
Taibilla	Spain	1973	Upstream sloping clay core	2a	9	8	11
Torcy Vieux	France	1800	Homogeneous earth fill embankment	2b	11	4,7	9
Uljua	Finland	1970	Central moraine core	2a	10	1,2,3	1
Viddalsvatn	Norway	1971	Central moraine core	2b	7	1,2,3	2
Warmwithens	United Kingdom	1870	Central puddle clay core	1	1		12
Winscar	United Kingdom	1975	Upstream asphaltic concrete membrane	3	4	2	5
Withens Clough	United Kingdom	1894	Central puddle clay core	3	6	2	1

Notations in Table 1:

A **Severity of problem or incident**
- A1 Failure
- A2 Serious incident involving emergency action or drawdown
  - 2a) Without emergency action, a breach was likely
  - 2b) Little danger of immediate breach
- A3 Incident causing concern, major investigation and remedial works
- A4 Symptoms causing concern

B **Cause of problem or incident**
- B1 Erosion at contact with pipe or structure
- B2 Outlet pipe failure
- B3 Erosion into the pipe or culvert
- B4 Upstream membrane failure
- B5 Fracture of clay foundation blanket
- B6 Fracture of core
- B7 Inadequate filter
- B8 Absence of internal drain/filter
- B9 Foundation solubility
- B10 Inadequate foundation treatment
- B11 Rotting tree roots

B12 Military action

C **Symptoms of problem or incident**

C1 Sinkhole
C2 Excessive or increasing seepage and leakage
C3 Turbid seepage and leakage
C4 Wet areas or seepage and leakage on downstream slope
C5 Leakage into or around culvert
C6 Piping
C7 Excessive or increasing pore pressures
C8 Vortex in reservoir
C9 Slip

D **Remedial works**

D1 Diaphragm wall
D2 Grouting
D3 Jet grouting
D4 Pipe or culvert repair
D5 Upstream membrane repair
D6 Clay blanket repair
D7 Drainage gallery
D8 Relief wells
D9 Filters
D10 Slope flattening or addition of berm
D11 Partial or total reconstruction
D12 None

In compliance with the data presented in the Table 1, the followings concluding remarks can be pointed out.

From the total of 47 case histories analyzed, a number of 14 (30%) have been classified as A1 (failure) or A2a (serious incidents involving emergency action or drawdown where, without emergency action, a breach was likely). In eight of these cases the problem occurred during, or immediately following first filling of the reservoir. For others six dams the events have taken place many years after their commissioning.

Generally, the internal erosion processes are not restricted to one particular type of fill. For instance of the 14 dams above mentioned in the A1 and A2 severity categories, four are homogeneous earth fill embankments, five have upstream membrane, four have earth fill core and one has a central concrete wall.

In five cases, erosion at the contact between the embankment and a structure or pipe passing through the embankment (B1) was a major factor in the incident.

In three cases, the failure of the upstream membrane (B4) was critical. The hydraulic gradient across such a membrane is very high and flow can be very great at a localised defect.

Concerning the symptoms of the internal erosion process, in the 20 cases from the total of the 47 cases analyzed, the internal erosion manifested itself in the form of sinkholes (C1). In one case, a vortex (C8) was observed in the reservoir. In the majority of the case histories analyzed, seepage and leakage have been warning signals. They could be in the form of excessive or increasing flow (C2), turbid flow (C3), wet areas on the dam downstream slope (C4) or leakage into or around a culvert (C5).

Remedial works consisted in grouting (D2) in about half of the 47 case histories. In ten cases diaphragm walls (D1) were installed. In about on third of the cases, remedial works included earthmoving operation in the form of slope flattening, berm construction and reconstruction of the embankment.

In the following will be described a number of typical internal erosion processes which have caused failure or sever damage of the dam.

Saint Aignon dam (H=8 m, France) was a homogeneous earth fill which failed catastrophically almost 20 years after construction (1965). The embankment was constructed of variable fills and had not internal drainage. It was believed that suffosion had eventually turned into piping. No alarm was given prior failure, but the downstream slope had shown signs of saturations. Failure was attributed to variable permeability in the fill inducing high seepage rates, the lack of an internal drain, and the absence of monitoring and maintenance.

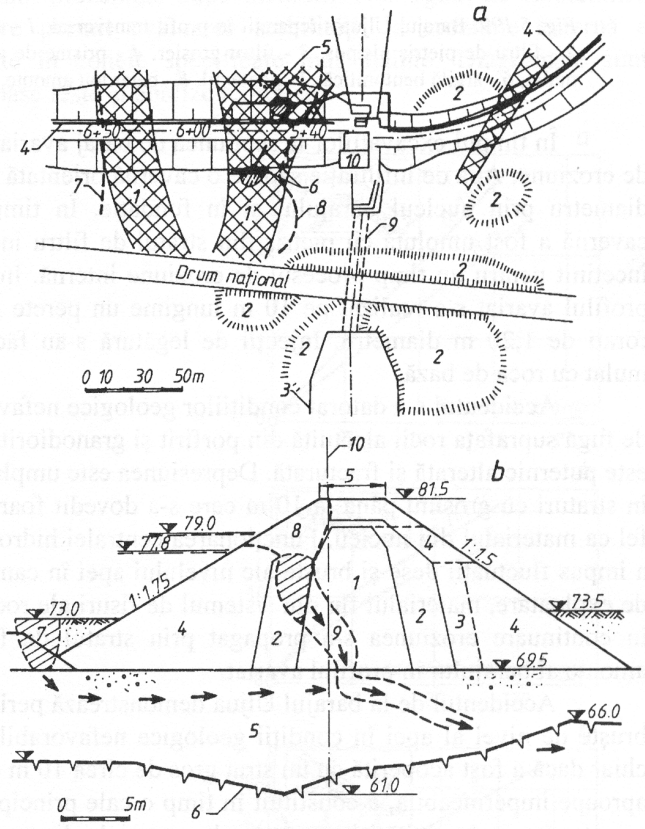

Fig. 2. Uljua dam (Finland) – Incident by internal erosion
a – layout of the damaged zone: 1 – fractured rocks zone, 2 – rock outcrops, 3 – leakage, 4,5,6 – grout curtains, 7,8 – limits of the sinkhole, 9 – tairace gallery, 10 – hydropower station; b – damage in a dam cross section: 1 – core of glacial till, 2,3 - filters, 4 – rockfill, 5 – glacial till, 6 – weathered bedrock, 7 – crater, 8 – sinkhole, 9 – gravel tube, 10 – drillings for grouting.

Uljua dam (Finland, 1970 year of commissioning). On 29 May 1990, twenty years after construction, a major incident occurred in which a sinkhole appeared in the upstream slope near the crest. The upstream slope dropped 3m over a length of 7m and the rate of leakage increased to 100 l/s. Rapid remedial measures saved the dam from total collapse. An erosion channel 1m in diameter across the dam core was found during the repair works.

Sapins dam (H=16 m, France, 1978 year of commissioning) is a homogeneous sand fill embankment. In 1988, ten years after first filling, flows of water and a shallow

slip occurred in the lower part of the downstream slope of the dam. The situation rapidly worsened, and the reservoir was emptied. The homogeneous embankment was composed of the sand fill with a chimney drain, which stopped 2 m below the maximum water level. The incident was attributed to suffosion within the embankment.

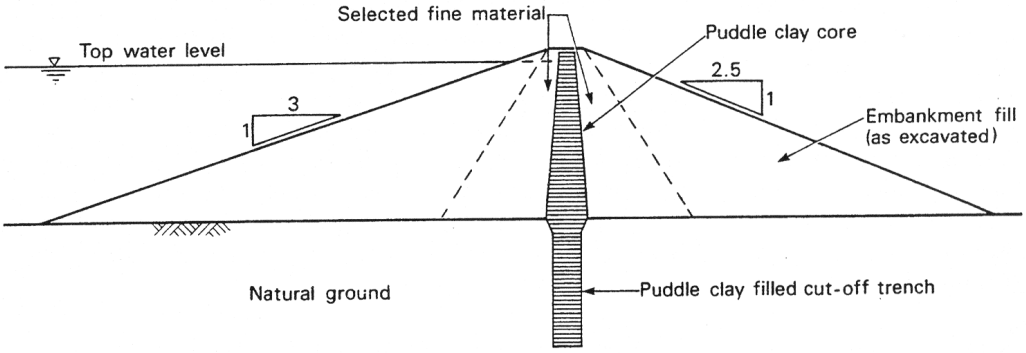

Fig. 3. Typical old British embankment dam.

Warmwithens dam (H=10 m, United Kingdom, 1870 year of commissioning). This dam with central puddle clay core failed just over 100 years old as a result of internal erosion on 24 November 1970. A 1.5 m diameter tunnel lined with concrete segments had been driven through the embankment to certain new outlet pipes during rehabilitation works carried out between 1964 and 1966. On 24 November 1970 after rapid increase of the water flow through embankment, the dam failed. A breach, 20m wide at crest level, extended down to the tunnel, which was washed out, large sections of the concrete segments being deposited downstream.

The above given examples and many other similaires point out the significant risk that internal erosion processes can have on embankment dams integrity. Internal erosion is a hidden phenomenon and until some feature such as a sinkhole appears at the surface of the soil, it is difficult to identify and investigate.

3. INTERNAL EROSION PROCESSES – IDENTIFICATION AND INVESTIGATION

Internal erosion processes are mechanically very complex phenomena, depending on internal hydraulic gradients, soil gradation, settlement fracturing, filter and drain performance, etc.

Otherwise, internal erosion is one of the major reasons for embankment dams failure or severe damage. The identification and investigation of internal erosion processes are essential activities for embankment dams safety. They consist of field monitoring and investigations, laboratory testings and mathematical model analyses. Of course, the analyses with mathematical models use input data provided from field and laboratory.

Seepage monitoring through embankment dams including their foundation and abutments is one of the main measures for internal erosion control. Generally, internal erosion causes an increased seepage flow due to loss of fines. Many existing seepage monitoring systems are not however sensitive enough to detect small changes in the seepage flow.

The geophysical methods of determining seepage and erosion in embankment dams are the most used. Many different techniques can be mentioned in this category as

measurements of temperature, electrical resistivity, self potential, seismic wave velocity, ground penetrating radar.

- Temperature measurements. Temperature can normally be easily measured in existing standpipes. The temperature in an embankment dam depends mainly on the temperature in the air and the water temperature in the upstream reservoir. These two temperatures vary seasonally and create temperature waves propagating through the dam. The seepage rate, and its change with time, can be evaluated from measurements repeated at regular intervals. The sensivity of the method depends mainly on the distance between the dam crest and the measurement point, the size of the dam, the location of the standpipes and the temperature variation in the reservoir at the inflow level. The method gives reasonable information concerning the condition of the dam. Zones with anomalous seepage rates have been located and seepage flow rates have been quantified. Changes in the seepage flow rate as well as the seepage pathway have been observed (Johanson, 1997).
- Electrical sensitivity measurements. Resistivity measurements are more complicated; they require a computer-based monitoring system and minor technical installations on the dam. The electrical sensitivity of an embankment is changed by concentrated seepage and erosion of fine material. In addition to the changed electrical properties of the soil, the high seepage frequently introduces water into the eroded zone which is a different temperature and has different conductivity than the surrounding water. Laboratory and analytic study were carried out to separate the effects of the various changed soil and water properties on resistivity measurements taken from the crest of the dam.
- Ground penetrating radar and borehole radar methods are based on the measurement of the material dependent properties. These are less sensitive to seepage changes than flow dependent parameters. The relatively high accuracy obtained by borehole radar measurements compensates however for their lower sensitivity to porosity changes. Borehole radar based on tomographic analysis can be a valuable method for mapping areas with increased and anomalous porosity formed as a consequence of increased seepage and internal erosion.
- Self potential (or Streaming potential) measurements. When water flows through soil, electrons get scraped off. This generates a voltage. The voltage is small and the interpretation of all the seepage through a dam from voltage measurements along a dam crest is difficult. Laboratory tests of the cross-coupling coefficient (voltage/flow) for various soil were carried out and computer programs were developed that define the electric field for any seepage pattern.
- Seismic wave velocity measurements. A network of seismic paths between two boreholes on each side of a sinkhole has been successfully used in a tomographic analysis to visualize a sinkhole. Shear waves were used as the shear wave velocity in the sinkhole vecinity is only about one third of the shear wave velocity in the undamaged portion of the dam.

Laboratory tests are used to determine some soil parameters having influence on internal erosion (graded curves, mechanical parameters, permeability etc.) or to simulate internal erosion mechanism for different soils or combination of soils in laboratory controlled conditions.

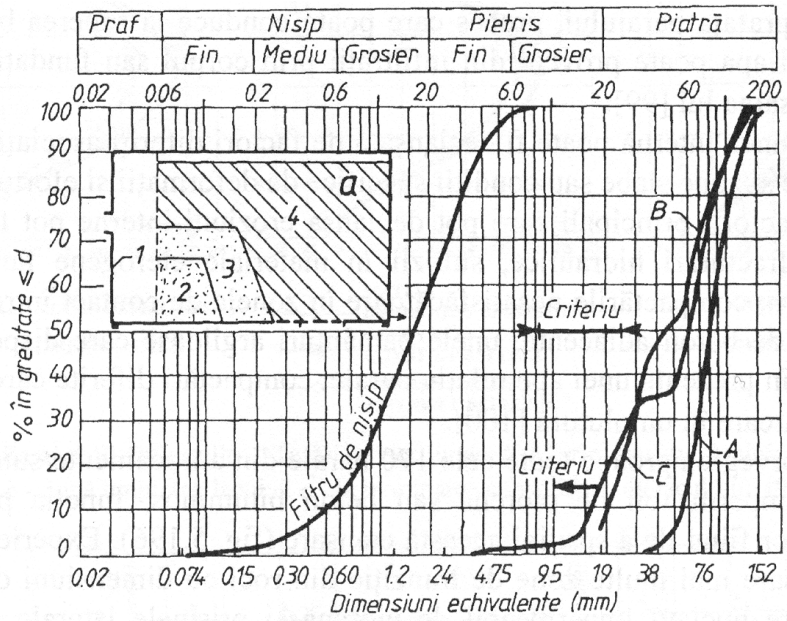

Fig. 4. Laboratory investigations on internal erosion risk: a – device scheme: 1 – reservoir with a glass wall, 2 – moraine core, 3 – sand filter, 4 – tranzition material; b – graded curves of the sand filter and others three tested tranzition materials (A, B, C).

The device presented in Figure 4 were used to investigate in the case of Norway rockfill dams whether internal erosion of the sand filter can occur where the filter specifications between the sand filter and the transitional zone have not been meet, or when the sand filter has been overtopped.

As it can see, the upper edge of the sand filter on the air side of the dam was carried out together with the transitional material into a channel 2 m high, 1 m wide and 3 m long. There was a small reservoir behind the dam where the water level and the water flow could be altered, to cause overtopping of the sand filter. One side of the channel was made of glass so that any erosion could easily be observed. (Skoglund, Solvik, 1995).

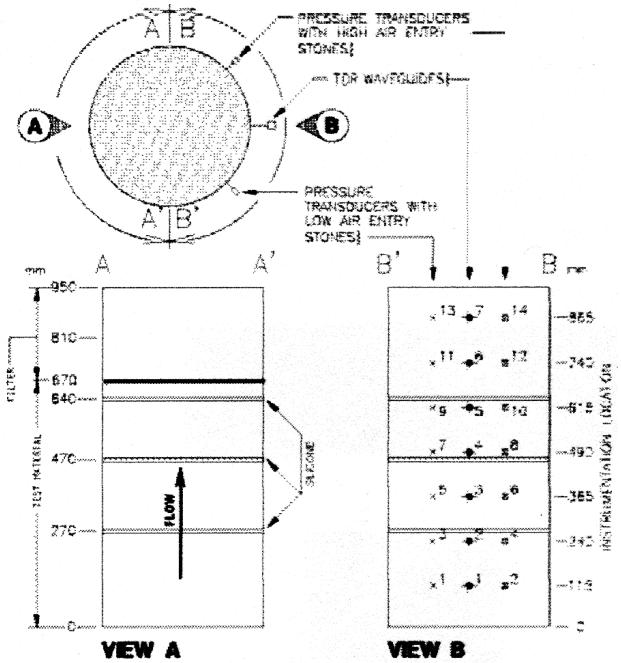

Fig. 5. The scheme of the permeameter

The scheme of a permeameter setup used to investigate internal instability in gap-graded cores and filters is shown on Figure 5. The permeameter was constructed from a 1 m long, 30.48 cm cast acrylic (Lucite) tube. The aluminum bottom-cap had a central hole and perforations for inflow of water, and both circular and radial grooves to transmit water over its entire surface. The top-cap was also grooved and fitted with a baffle plate, in a similar manner to the bottom-cap. It held an O-ring that sealed the top-cap but allowed it to move vertically within the tube. Water from an aeration/de-aeration tank entered through the bottom-cap and was discharged through the top-cap.

The permeameter assembly was mounted in a reaction frame so that a seating load of 600 kPa could be continuously applied and monitored through a proving ring. Flow rates and pressures were controlled by a series of valves and accumulators. Data from the piezometers, TDR probes, LVDT' s and load cells were collected through a multiplexer and stored in data loggers. (Garner, Sobkowicz, 2002).

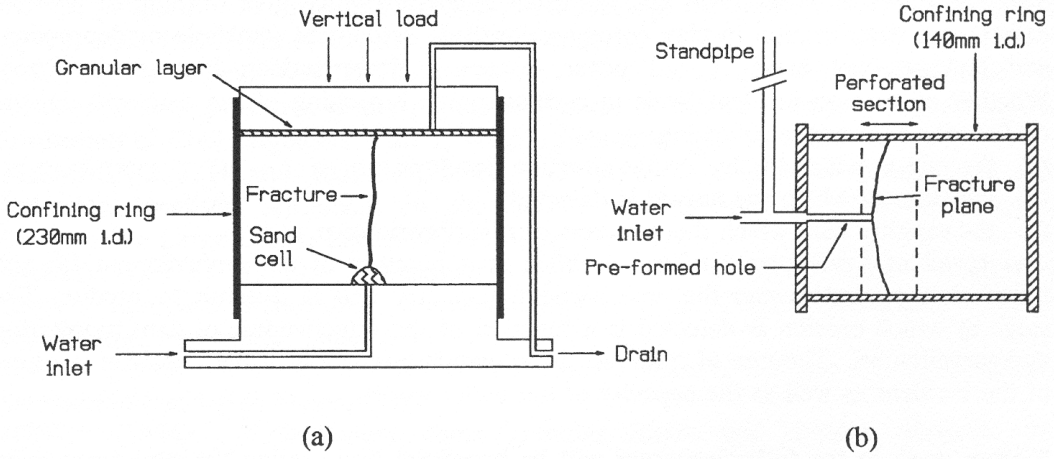

Fig. 6. Laboratory apparatus for internal erosion studies.

The scheme of a laboratory apparatus built for internal erosion investigations especially the erosion of the puddle clay typically to British old embankment dams is presented in Figure 6. The apparatus was developed for specimens 150 mm in diameter and 250 mm high in which a fracture is formed in the general direction of the layering. During a test the apparatus was laid on its side (Fig. 6.b) and placed in a tray to collect the eroded material. The tests pointed out that hydraulic fracture was followed by internal erosion, with the rate of erosion decreasing with time. There are indications that the rate of erosion was related to the head loss and velocity of flow along the fracture.

The mathematical models were developed in order to give answers to tasks as: flow net with flow and equipotential lines providing information on seepage quantity, velocity flow, uplift pressure, risk of piping and internal erosion etc.

Generally, the mathematical models for seepage analysis were developed in the hypothesis of saturated soils under steady-state conditions. Additionally, the soil particles, soil structure, and water are assumed incompressible and flow obeys Darcy's law. Thus transient conditions such as a wetting front or other movement of water in unsaturated soil, consolidation and subsidence are not usually considered for analysis. The Laplace equation is the mathematical bases for several models or methods used in seepage analysis.

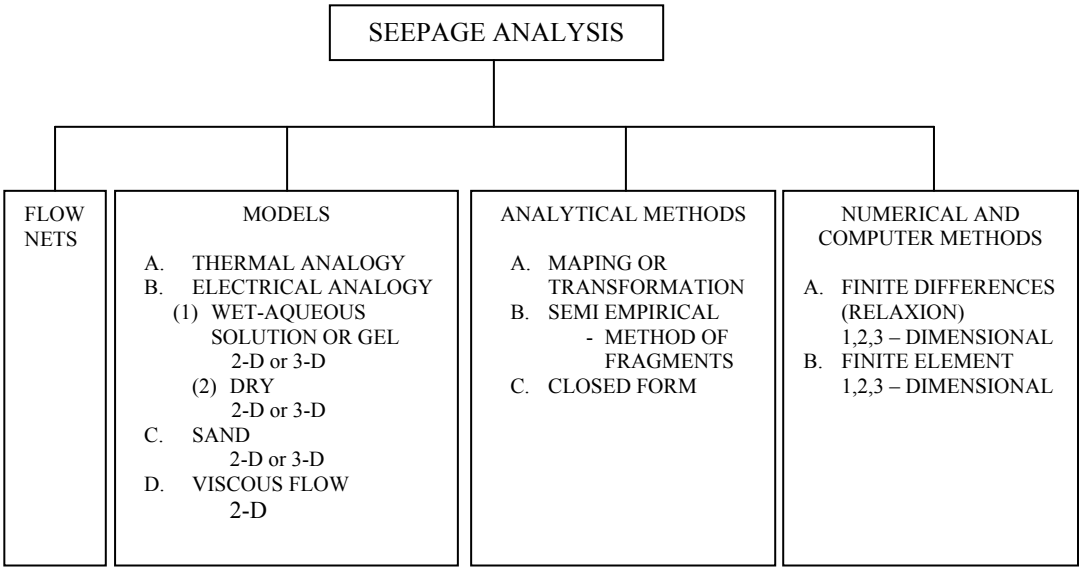

Fig. 7. Seepage analysismethods (from Radthakrishnann).

Figure 7 presents a synthesis of the seepage analysis after Radthakrishnann (USACE, 1986). More information on seepage analysis methods are given in the next paragraph.

4. SEEPAGE ANALYSIS METHODS. SOFTWARE.

The Laplace equation is the mathematical basis for several models or methods used in seepage analysis. In the two dimensional orthogonal system xoz Laplace equation has the form:

$$\frac{\delta^2\Phi}{\delta x^2}+\frac{\delta^2\Phi}{\delta z^2}=-Q$$

where Φ is velocity potential function and Q flow rate per unit area.

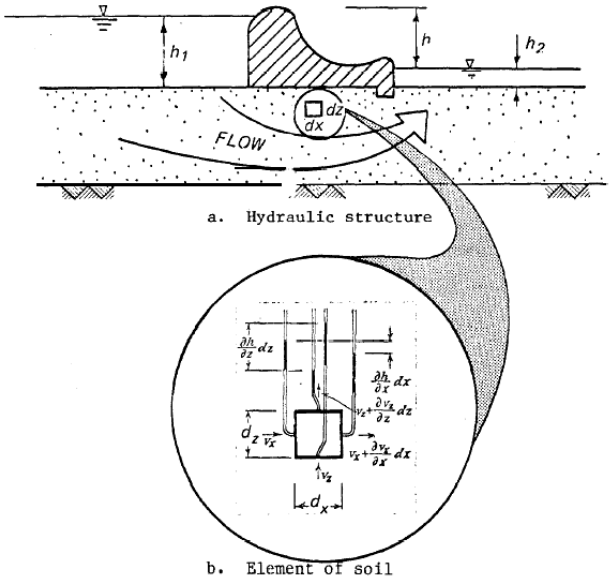

Fig. 8. Flow of water through saturated pervious soil beneath a hydraulic structure.

Development of Laplace's equation depends on six assumptions as follows (fig.8).

- heads h_1 and h_2 are constant and thus flow is steady state;
- water is incompressible;
- volume of voids does not change – soil is incompressible;
- flow is laminar – Darcy's law applies;
- the flow is two-dimensional (no flow takes place perpendicular to the plane of the figure 8, xoz);
- the saturated pervious soil stratum is homogeneous.

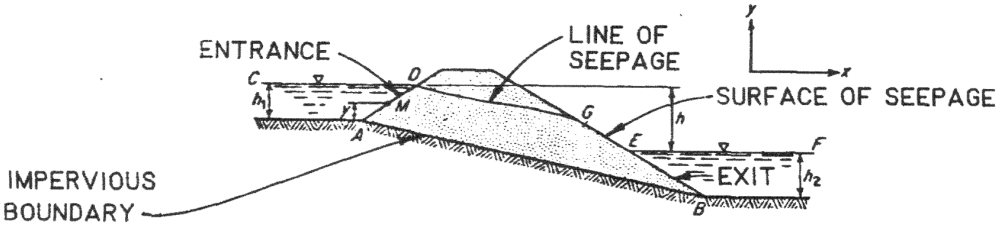

Fig. 9. Exemplification of boundary conditions.

The saturated soil which is considered for analysis must be defined by boundaries, permeability of the soil, and heads imposed upon the water. Generally, seepage analysis problems associated with dams involve four possible types of boundaries (fig. 9): impervious boundaries, entrances and exits, surface of seepage, line of seepage. There are two cases of seepage: confined and unconfined flow. Confined flow exists in a saturated pervious soil mass which does not have a line of seepage boundary. Unconfined flow, exists when the pervious soil mass has a line of seepage. For embankment dams, the unconfined flow is characteristic.

Solution to steady-state, laminar flow, seepage problems must solve Laplace's equation. The same equation governs electrical field and heat transfer. Consequently, some softwares use this analogy in solving the seepage problems.

Because of the complicated geometry and of the density of materials which are usually met in the seepage problems from the dams field, the solution of Laplace's equation is generally given by numerical and computer methods: finite element and finite differences.

The finite diference method solves the Laplace equations by approximating them with a set of linear algebraic equations. The flow region is divided into a discrete rectangular grid with nodal points which are assigned values of head (known head values along fixed head boundaries as points, estimated heads for nodal points that do not have initially known head values). Using Darcy's law and the assumption that the head at a given node is the average of the surrounding nodes, a set of N linear algebraic equations with N unknown values of head are developed (N equals number of nodes). A wide range of finite difference solutions suited to the digital computer has been developed. For simple problems, the finite difference method is usually more economical than the finite element method.

In the finite element method the flow region is subdivided into a number of elements and permeabilities are specified for each element. Boundary conditions are specified in terms of heads and flow rates and a system of equations is solved to compute gradients and velocities in each element or heads at nodes and flows in the elements. A lot of two and three dimensional finite element computer programs for both confined and unconfined flow problem have been developed. Steady state and transient problems (that can be treated as a series of steady-state problems) can be solved.

Interactive graphics preprocessors are available to generate the finite element mesh. It is possible to compute the stream function and potential and contours of the values to obtain the flow net. Also, several interactive graphics postprocessors are available to assist in the analysis of the finite element results.

As advantages can be mentioned, the finite element method is well suited to complex geometry, including sloping layers and packets of material of varying permeability. By varying the size of the elements, zones when seepage gradient or velocity is high can be accurately modelled. As disadvantages, the finite element method is usually more costly than the finite difference method for simple problems.

The finite element method has been intensively used in several cases to provide solutions to seepage problems.

Coming back to the results in seepage analysis it may point out that flow net is a picture of seepage conditions under given geometry and boundary conditions. It explains how pressures are distributed and where flow is being directed. Completed with the knowledge of head imposed on and the permeability of the porous media, the flow net can supply important information as seepage quantities escape and critical gradients which are in direct relation with piping and internal erosion mechanisms, heave, seepage forces, uplift pressures.

The escape or exit gradient, i_e, is the rate of dissipation of head per unit of length in the area where seepage is exiting porous media. Escape gradients for flow through embankments may be studied by choosing squares from the area of interest in the flow net (usually at or near the exit face and downstream toe) and calculating gradients. If the gradient is too great where seepage is exiting, soil particles may be removed from this area. This phenomenon, called flotation, can cause piping with all its negative effects (undermining and loss of structure). The gradient at which flotation of particles begins is termed the critical gradient, i_{cr}. Critical gradient is determined by the in-place unit weight of the soil and is the gradient at which upward drag forces on the soil particles equal the submerged weight of the soil particles. The critical gradient is dependent on the specific gravity and density of the soil particles and can be defined in terms of specific gravity of solids G_s, void ratio, e, and porosity, n:

$$i_{cr} = \frac{\gamma'_m}{\gamma_w} = \frac{G_s(1-n)\gamma_w + n\gamma_w - \gamma_w}{\gamma_w} = (G_s - 1)(1-n)$$

If typical values of G_s, e and n for sand are used in the above equation, i_{cr} will be approximately 1…1.2.

Critical gradients, observed in field for horizontal areas were between 0,5…0,8 because the flow line are not perfect vertically, but easily inclined versus the normal to surface.

Generally, the regulations in different countries recommend ranges for factor of safety for escape gradient FS=$\frac{i_{cr}}{i_e}$ from 2,5…3 depending on knowledge of soil and possible seepage conditions.

In other cases the mass of soil may be lifted initially, followed by piping. This phenomenon is called heave and occurs when the upward seepage force due to differential head equals the overlying buoyant weight of soil. Heave occurs under conditions of critical hydraulic gradient.

Is it possible to evaluate internal erosion process based on mathematical analysis results? The studies concluded that initiation of internal erosion process requires two conditions:

- hydraulic criteria, respectively critical gradients i_{cr} evaluated by mathematical analysis
- geometric criteria, respectively some granule size and ratio taken materials graded curves.

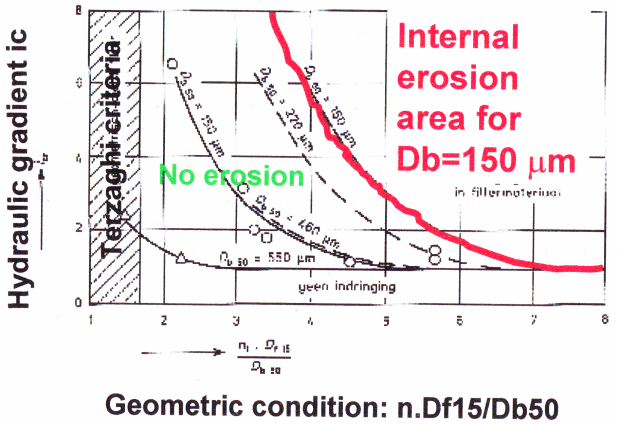

Fig. 10. Diagram for evaluating the internal erosion risk.

In the Figure 10 is shown a diagram with internal erosion area for Db=150 μm (Fry, 2001).

As already was mentioned, a lot of computer programs based especially on finite element method have been developed along the year to solve seepage problems, respectively internal erosion risk analysis. Some codes are dedicated exclusively to seepage analysis problems, others are general FEM codes solving seepage problems by thermal (electrical) analogy.

In the categories of the general FEM codes that can be applied for solving seepage problems may be mentioned: ABAQUS, ANSYS, NASTRAN, ADYNA and many others.

It is hoped, the contributors for Theme C of the present Benchmark Workshop will offer useful information in order to select the most performant computer programs for seepage respectively internal erosion analysis.

5. EXEMPLIFICATIONS WITH SEEPAGE AND INTERNAL EROSION ANALYSIS

A number of specific seepage problems solved by FEM methods will be commented in the following in order to emphasize the performances of the method in this field.

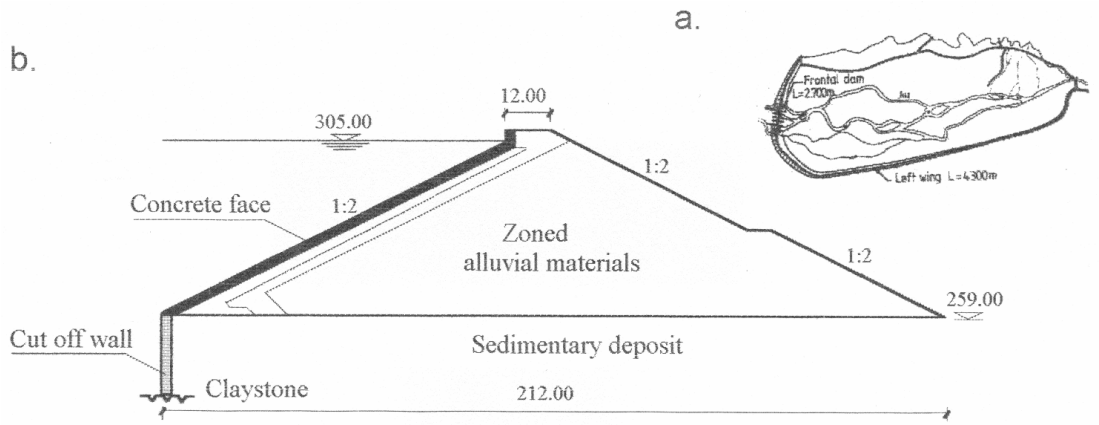

Fig. 11. Valea Sadului dam: a – general view; b – dam typical cross section..

- The concrete faced earthfill dam Valea Sadului, now under construction in Romania (fig. 11) is founded on thick layers of permeable soils. These foundation conditions increase significantly the technical problems in providing a satisfactory watertightness in the zone of upstream toe of the dam in order to avoid excessive seepage and internal erosion process.

The special geological conditions for the frontal zone of the dam required a sealing up to depth of 45…50 m in heterogeneous alluvial layers, with gravels and boulders inclusion. A number of alternative sealing solutions were taken into account, in the design stage, as follows (fig. 12):

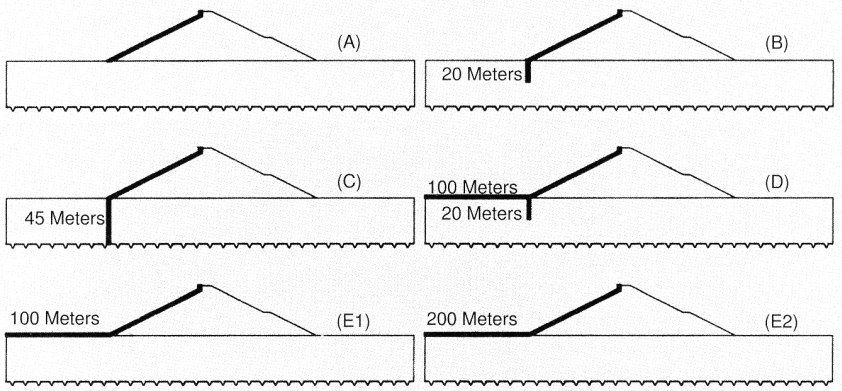

Fig. 12. Alternative solutions for watertightening the dam foundation.

A - "witness solution" – dam without any watertightening solution;
B - cut off wall of 20 m depth;
C - cut off wall (or grout curtain) of 45 m depth;
D - cut off wall of 20 m depth combined with impervious blanket of 100 m length;
E1 - upstream impervious blanket of 100 m length;
E2 - upstream impervious blanket of 100 m length;

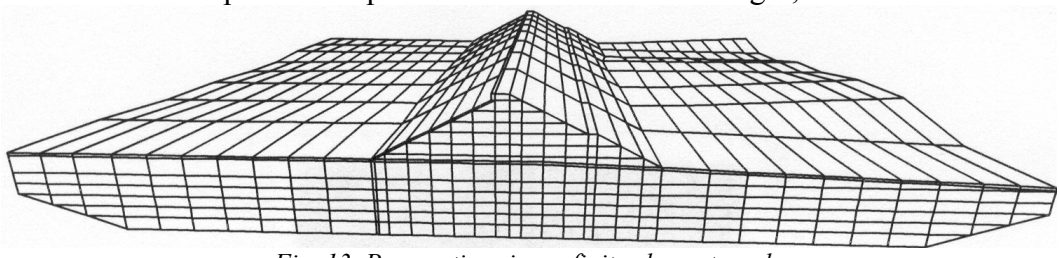

Fig. 13. Perspective view – finite element mesh.

The comparative analysis for selecting the sealing solution was based on FEM, using ANSYS computer code. For the analysis it was accepted the hypothesis of a stationary flow through a three dimensional, orthotropic porous media. The perspective view of the finite element mesh is shown in Figure 13.

Computed rates of seepage for a central profile in the dam are listed in Table 2. Alternatives E1 and E2, consisting of horizontal impervious blankets of different length, permitted an unsatisfactory high rate of seepage, which can be attributed to a high-permeability shallow soil layer. Alternative D, a combination of a cutoff wall and a seepage blanket, did not perform significantly better than the same cutoff wall without the horizontal blanket (alternative B). Therefore, all except alternatives B and C were eliminated based on the computed specific seepage rates.

Table 2

Variant code	Specific seepages in profile 5	
	L/sxm	%
A	119	100
B	1.16	0.97
C	0.84	0.70
D	1.10	0.92
E1	25.6	21.51
E2	15.9	13.36

An examination of hydraulic gradients and the spatial distribution of flow velocities provided additional information for selecting the best option. In alternative B, in which the cutoff wall extended only partway to bedrock, the model predicted very high hydraulic gradients at the bottom of the wall. In this situation, internal erosion is likely to occur at the base of the wall, weakening the dam foundation.

Erosion also is an important consideration at the downstream toe of the dam, when the computed seepage flow velocity typically were among the highest in all the model domain. Alternative C (a complete vertical seal extending to bedrock) showed a marked advantage over alternative B in this regard, with maximum flow velocities at the toe being well within recommended design limit (Abdulamit, A. ,2000).

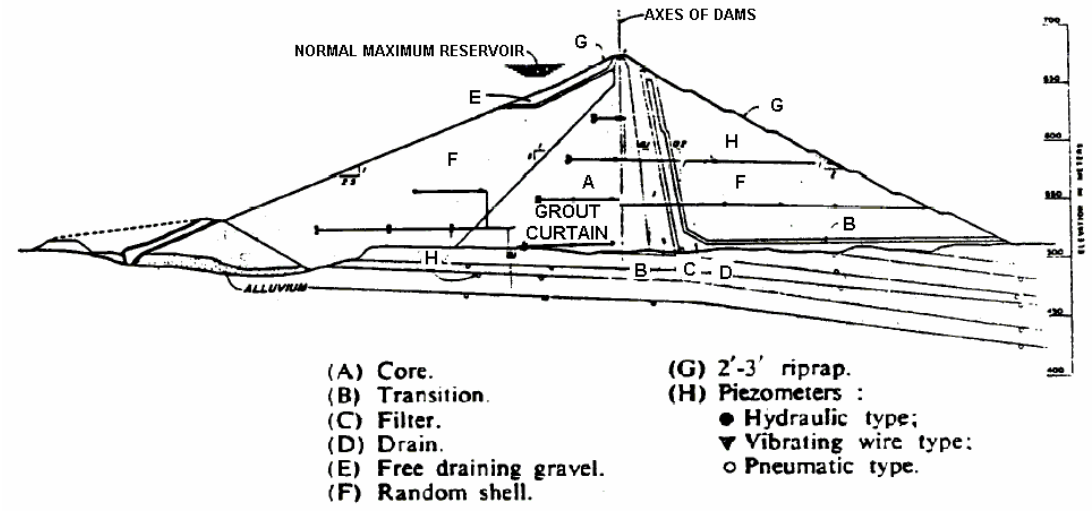

Fig. 14. W.A.C. Bennett Dam – Typical cross section.

- W.A.C. Bennett Dam (H=192 m) is an earth dam with clay core from British Columbia-Canada (Fig. 14). The finite element method was used to asses the potential seepage flows and uplift pressures in the foundation rock of the dam. The analysis was carried out assuming the following conditions:
  - with an effective grout curtain;
  - without an effective grout curtain;
  - with a drainage system;
  - without a drainage system;
  - with various rock permeabilities.

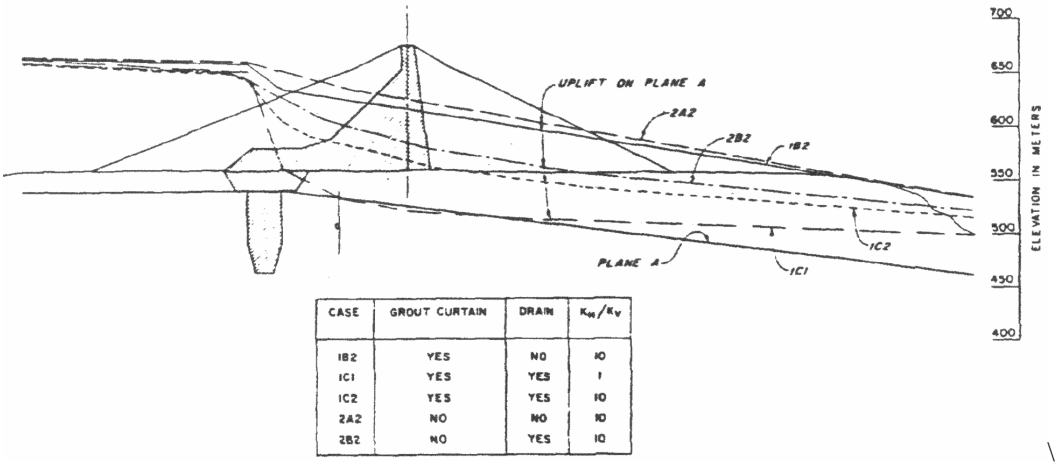

CASE	GROUT CURTAIN	DRAIN	K_H/K_V
1B2	YES	NO	10
IC1	YES	YES	1
IC2	YES	YES	10
2A2	NO	NO	10
2B2	NO	YES	10

Fig. 15. W.A.C. Bennett Dam – Uplift pressure under various conditions.

The results of the finite element analysis, shown in Figure 15 indicate the greatest reduction in seepage flow and hydrostatic pressure could be accomplished by an effective grout curtain and downstream-drainage system.

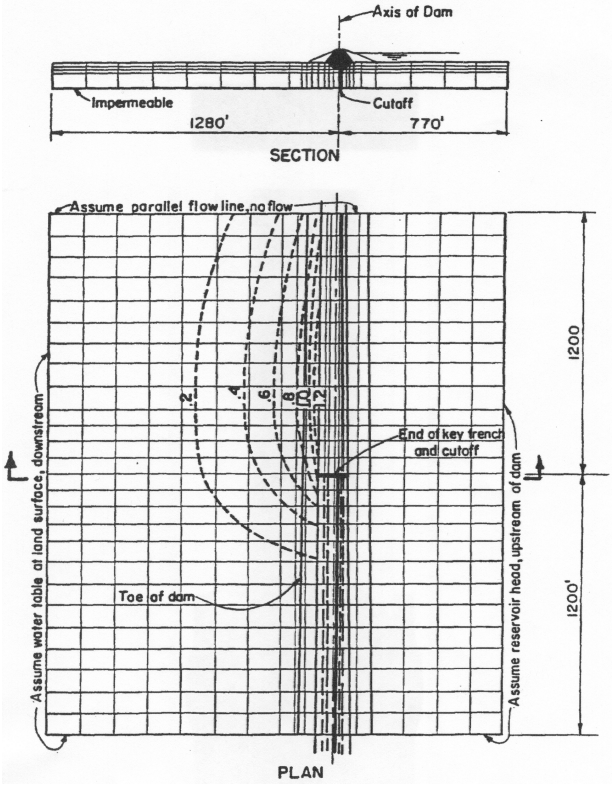

Fig. 16. Contours of exit gradient from three dimensional finite element model study of Narrows Dam, Colorado.

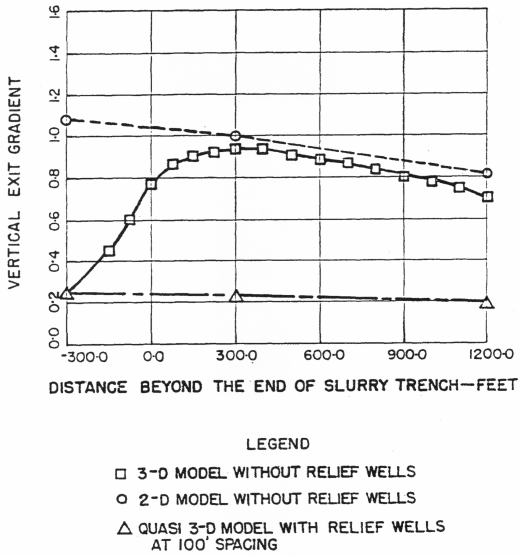

Fig. 17. Vertical gradients from three-dimensional finite element model study of Narrows Dam, Colorado.

Narrows Dam is an earth dam on pervious foundation on South Plate River, Colorado county – USA. The two and three dimensional finite element models were used to study the seepage through dam-foundation system at the feasibility stage. Because of a pervious foundation, the planners called for a positive vertical cutoff by constructing a slurry wall down to the underlying shale. However near the right abutment the shale drops away to depth too great for economical slurry wall construction. A three-dimensional finite element model was used to determine the vertical exit gradients at the downstream toe of the dam. The finite element method was used to study the effect of a toe drain, partial depth slurry trench, partially and fully penetrating relief wells (Fig 16, 17).

Of course many other similar exemplifications can be presented. The finite element method has proved its ability in giving useful information for engineering decisions in very complex problems from embankment dams field including seepage and internal erosion risk.

It is expected, the contributors for Theme C of the Benchmark Workshop to point out the performances of the new software in solving complex problems of seepage and internal erosion, as is the Motru Dam case.

REFRENCES

Abdulamit, A., Sarghiuta, R., Popovici, A. (2000). Using a computer model to design a seepage cutoff wall. Hydro Review Worldwide, Vol 8, No.1.

Abdulamit, A., Sarghiuta, R., Popovici, A., Teodorescu, C. (1998). Special solution for a cutoff wall of a large earthfill dam. Proceedings Hydro-Vision'98, USA.

Charles, J.A., Tedd, P., and Holton, I.R. (1995). Internal erosion in clay core of British dams. Proceedings European Symposium on Research and Developments in the Dams field, Crans-Montana.

Charles, J.A. (2001) Internal erosion in European embankment dams. European Working Group Report, Geiranger.

Dobrescu, D., Teodorescu, C., Popovici, A., Sargiuta R. (1999). Problems related to water tightness of a dam foundation consisting of a thick alluvial layer. ICOLD International Symposium Dam foundation Problems and Solutions, Antalya.

Fell, R., Bowles, D., Anderson, L., Bell, G. (2000). The status of methods for estimating of the probability of failure of dams for use in quantitative risk assessment. Q76. Proceedings 20th International Congress in Large Dams, Beijing.

Fenton, G.A., Griffits, D.V. (1997). Extreme hydraulic gradients statistics in a stochastic earth dam. Journal of Geotehnical and Geoenviornamental Engineering, ASCE, Vol 123, No 2.

Fry, J.J. (1995) Développements concernant les risques d'érosion interne et de séismes relatifs aux remblais. Proceedings European Symposium in Research and Developments in the Dams Field, Crans-Montana.

Fry, J.J. (1997). Typologie de l'érosion interne et détection. Proceedings XIX-th International Congress on Large Dams, Vol 2, Florence.

Fry, J.J. (2001) Risk Analysis and Data Bases. European Working Group Report, Geiranger.

Garner, S.J., Sobkowicz, J.C. (2002). Internal instability in gap-graded cores and filters. Proceedings 2002 Annual Conference Canadian Dam Association, Victoria B.C.

Johanson, S. (1997). Seepage monitoring in embankment dams PhD Thesis, Royal Institute of Technology, Stockholm.

Kuusiniemi, R., Pöllä, J. and Rathmayer, H. (1992). Internal erosion at the Uljua earth dam. International Journal on Hydropower & Dams, Vol 44, No 3, U.K.

Popovici A., Sarghiuta R., Abdulamit A., Teodorescu C. (1998). Study concerning the excessive leakage from a large reservoir. Symposium Rehabilitation of Dams, New Delhi.

Skoglund, M., Solvic, O. (1995).External and internal erosion in rockfill dams. International Journal on Hydropower & Dams, Vol 2, No 3, U.K.

***(1986). Engineering and Design - Seepage analysis and control for dams. EM 1110-2-1901 US Army Corps of Engineers Publications.

***(2001) ANSYS - User's Manual. Ansys Inc., U.S.A.

7th INTERNATIONAL BENCHMARK WORKSHOP
ON NUMERICAL ANALYSIS OF DAMS
SEPTEMBER 24-26, 2002, Bucharest-Romania

ICOLD
Ad-Hoc Committee on Computational Aspects of Analysis and Design of Dams

Theme C – Embankment dams

SEEPAGE THROUGH AN EARTHFILL DAM - FOUNDATION SYSTEM AND PIEZOMETRIC LEVEL VARIATION DOWNSTREAM OF THE DAM

Formulators: A. Popovici, A. Abdulamit and C. Ilinca
TECHNICAL UNIVERSITY OF CIVIL ENGINEERING
OF BUCHAREST

1. INTRODUCTION

1.1 Objective of the theme C

The objective of the theme C is to apply the statistical, neural networks and/or finite element methods for prognosis of the seepage through an earthfill dam – foundation system and piezometric level variation in a selected well located downstream of the dam. The necessary data to solve this problem were obtained from monitoring system of the Motru dam (H = 48 m, Romania), which was commissioned in 1983.

The input data, provided by the formulator are the followings:

• Time histories of reservoir water level, snowfall, rainfall, air temperature, water level in some piezometric wells downstream of the dam for the period between 1990 and 2002.

• Time histories of the total seepage through the dam right wing – foundation system and piezometric level in the selected well downstream of the dam for the period between 1990 and 2001.

• Finite Element mesh of the dam right wing – foundation system including material characteristics, seepage measurement point and selected well location.

The required results are as follows:

• The prognosis of the total seepage flow through the dam right bank – foundation system for the period from 01.01.2002 to 31.12.2002.

• The prognosis of the piezometric level in the selected well for the period from 01.01.2002 to 31.12.2002.

Optionally, the participants are invited to make considerations about the internal erosion phenomenon in the Motru dam right wing – foundation system and its long term effects and, also to propose eventually remedial solutions.

The analysis may be performed by statistical, neural networks and/or finite element methods.

1.2 General information about Motru dam

1.2.1. Description of the dam

Motru dam is a clay core earthfill dam with 48 m maximum height and 377 m crest length. The dam water reservoir having 4 x 10^6 m^3 total volume is used for hydropower generation. (fig.1)

The dam foundation consists of cristaline rock (granite, gneisse) in central zone (profiles 1...10, fig. 2) and of sedimentary deposits at the right wing (profiles 10...17, fig. 2). The foundation variation imposed some adaptations in cross sections of the dam which can be seen in figure 2 b,c.

In the central zone the cross section of the dam (fig. 2.b) consists of a thick clay core, protected by filter zones of sandy gravel. A horizontal gravel drain placed in the downstream shell to the dam base discharges the vertical filter to the dam toe. The shells consist of alluvium clay but the upstream shell corresponding as levels to seasonal water level variations consists of gravel with good permeability. The upstream face of this part of the upstream shell is protected against wave erosion by rip rap layer.

Figure 1. General view of the Motru dam from upstream

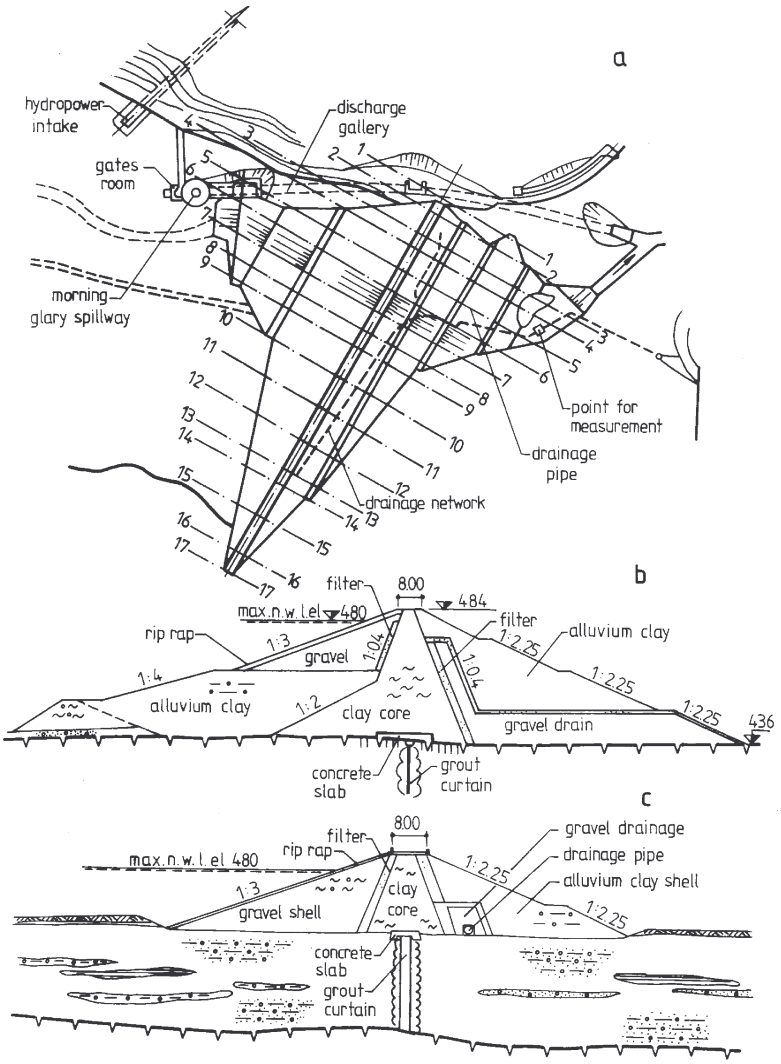

Figure 2. Motru dam: a - layout, b - typical cross section in central zone (profiles 1...10), c - typical cross section in right wing (profiles 10...17).

On the right bank (fig. 2.c) the drainage of the profile is carried out by a pipe network which discharges at the dam downstream toe in the central zone.

A concrete slab is placed at the base of the clay core in the dam axis. It was the platform for the equipments used to carry out the dam grout curtain. It may be remarked, the solution with grout curtain was used for sealing also the sedimentary deposit from the dam right wing, instead of classical solution with cut off wall.

Concerning the dam site, it can be remarked the existence of two dejection cones at the river right bank. They forced Motru river to change its course versus left bank which was strongly eroded and became very steep. As a consequence, the packets of schist layers from bed rock were taken out at surface on the left bank, instead the right bank remained covered by a sedimentary deposit of over 20 m thickness (fig. 3).

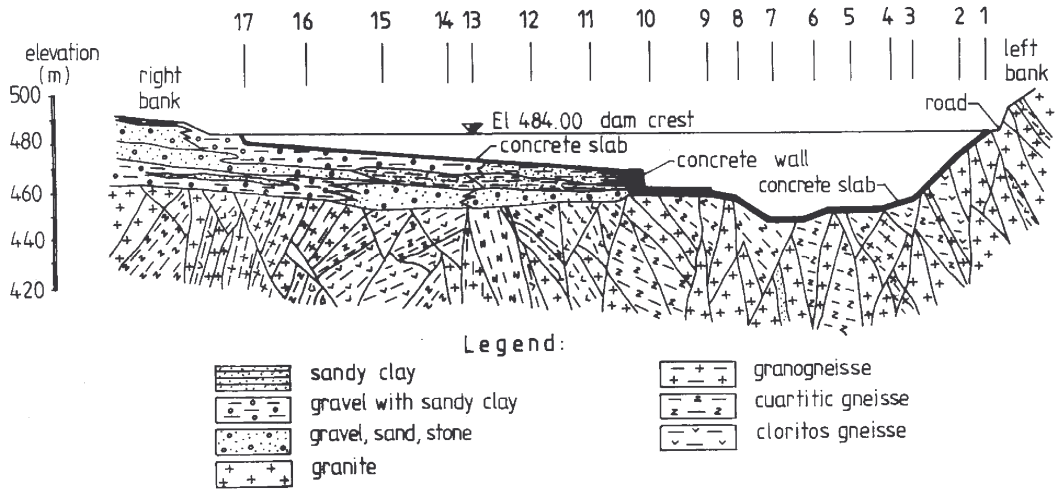

Figure 3. Geologic longitudinal section through the dam axis

The sedimentary deposit consists of different material as sand clay, gravels with sand clay, boulders and gravels included in clay matrix.

The sealing by grout curtain of the sedimentary deposit put special technological problems. First there were performed experimental tests in order to find the spacing of the drillings and grout prescription. The drillings were spaced 2 m upstream – downstream and 1.5 m along the dam. The grouting material was cement with bentonite addition. However, the efficiency of this work was only a partial one, as it will be presented in the followings.

The dam was commissioned in 1983 and, short time after the reservoir first filling the seepage at the dam downstream toe reached 40...50 l/s.

1.2.2. Comments about dam behaviour during operation

The dam – foundation system was well equipped with monitoring devices. Figure 4 shows the locations of some piezometric wells on Motru right bank. Recordings of the dam displacements (settlements), pore pressure evolution in clay

core, piezometric level variation in the dam downstream wells, seepage through dam – foundation system by monitoring devices as well as periodical visual inspections and geodetic measurements have offered sufficient data in order to know on line the safety state of the dam.

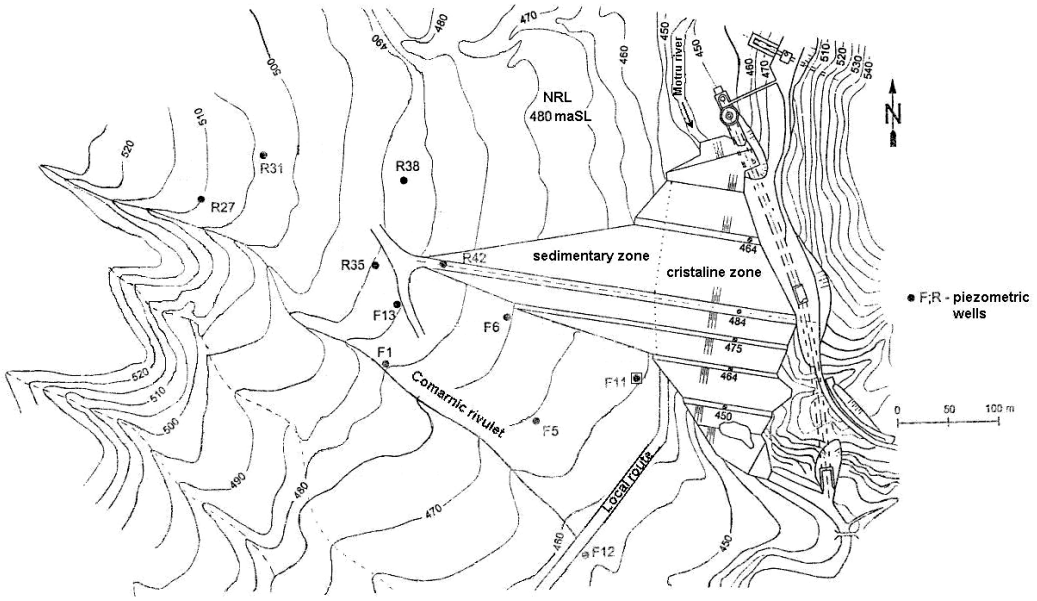

Figure 4. Motru dam – Locations of some piezometric wells

In figure 5 there are illustrated the settlements of some marks installed on dam crest. It may be remarked that crest settlements of the dam right wing are significantly larger than the corresponding dam central zone ones. The same remark can be made about the settlement rate. After 18 years dam operation the crest settlements at the right wing have not tendency to stop. These results can be a warning signal concerning the develompment of the internal erosion in the sedimentary deposit from right wing foundation. This phenomenon could be correlated with time history of the seepage water recorded in some points from right wing downstream toe as well as measurements of the solid material transported by seepage water.

The time histories of the total leakage water measured at the dam right wing downstream toe versus reservoir water level and of the water elevation in the selected piezometric well is shown in Figure 6. Generally, there is a good correlation between seepage flow and reservoir water level. The maximum flow of 45 l/s was measured in 1990 when the reservoir was at the maximum water elevation.

The granulometry of the sediments from seepage water contained grossier fractions and was different from reservoir sediment granulometry. This fact is also an indicator about the existence of an internal erosion process in the sedimentary deposit.

Some tests with radioactive tracers carried out in 1998 (fig. 7) put in evidence some caves in the right bank in both dam wing and reservoir foundation, where the velocity of the seepage water was so high that tracers were rapidly washed. The seepage spectrum (fig. 7) emphasizes that the main route of the seepage is through sedimentary deposit existent under dam right bank. The tests have shown, also, the important drainage effects of the two walleys downstream of the dam.

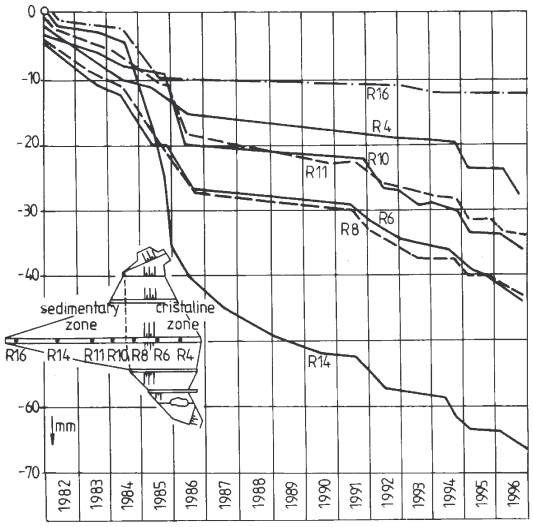

Figure 5. Time histories of the dam crest settlements in different points

Some coarse analysis, based on specific solid quantity measured peridically in the seepage water pointed out that each year, starting from the first filling in 1983, about 5...15 tons solid material from dam right bank sedimentary deposit were transported downstream by seepage water.

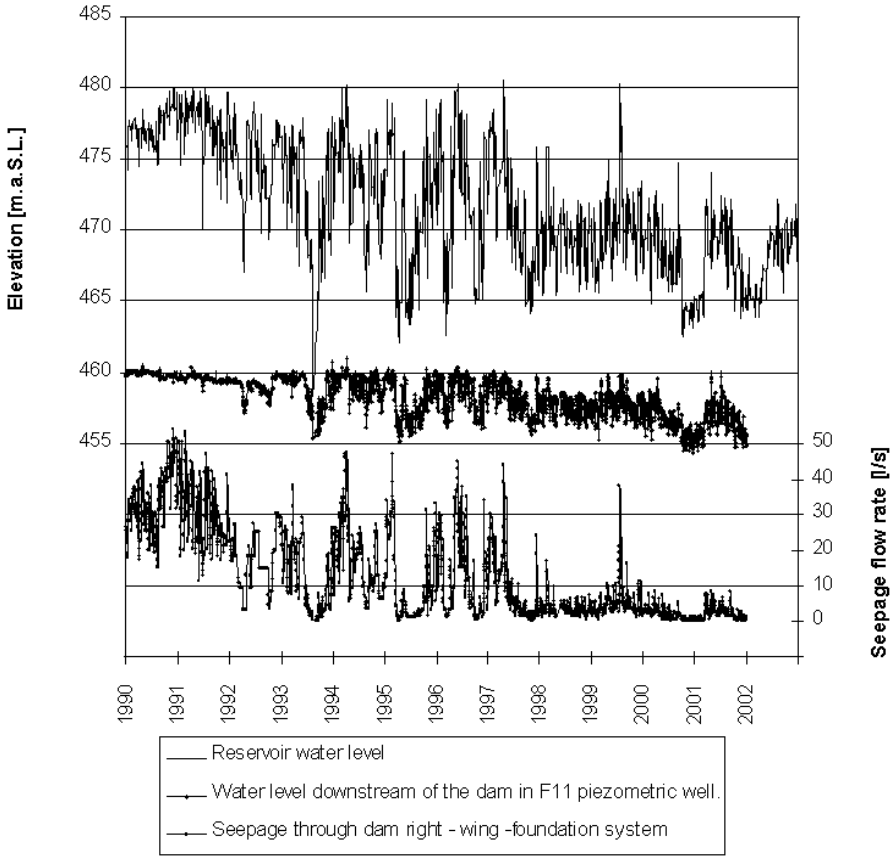

Figure 6. Time histories of the reservoir water level, water level variation in F11 piezometric well and seepage through dam right wing – foundation system.

In order to reduce the rate of the internal erosion, in 1996 the owner of the dam (Hidroelectrica S.A.) took the decision to decrease the maximum level alowed during reservoir operation with 10 m under normal elevation (470 maSL). Concomitently, some studies for rehabilitation solution were started.

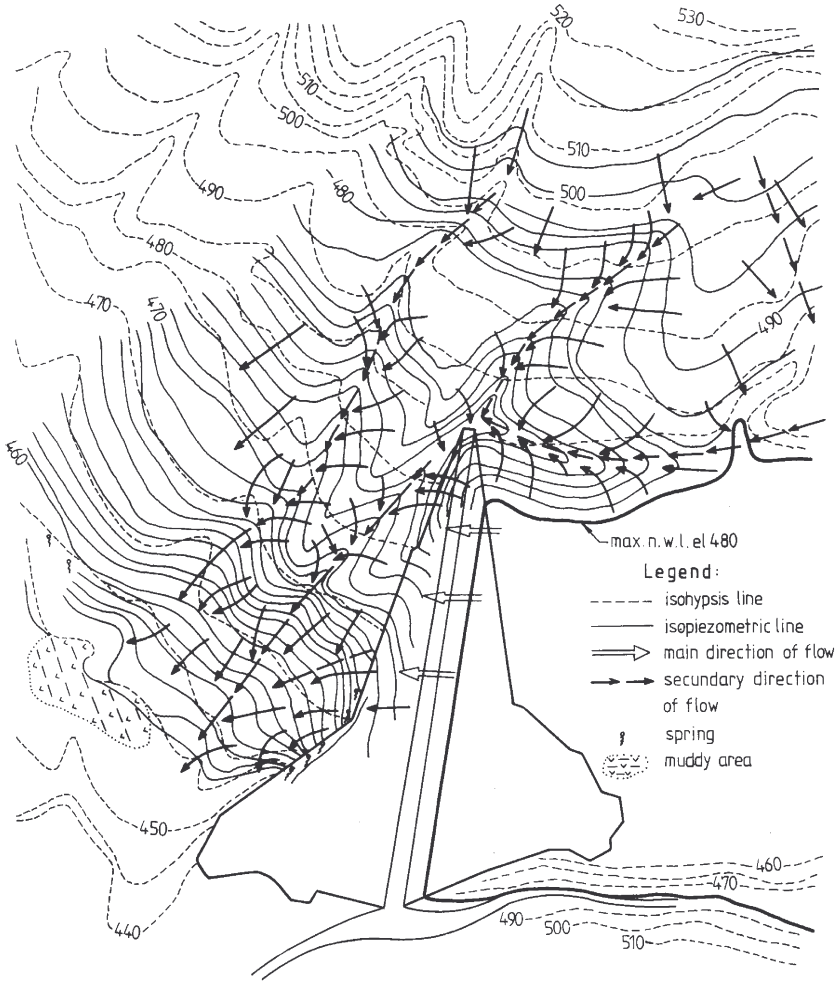

Figure 7. Seepage spectrum through dam right bank corresponding to full reservoir evaluated with radioactive tracers

2. INPUT DATA

2.1 Introductory remarks

The input data, needing to solve the problem, are collected in the following files:

MONIT.TXT and MONIT.DBF	measured data	(see section 2.2)
NODES.TXT	nodes, x, y, z coordinates	(see section 2.3)
ELEMENTS.TXT	brick elements (8 nodes)	(see section 2.3)
MATERIALS.TXT	material parameters	(see section 2.3)
CONTROL POINTS.TXT	location of piezometric well	

2.2 Monitoring Data

The monitoring data are provided in files 'MONIT.TXT' or 'MONIT.DBF'. The files represents a table with columns and 4249 data lines plus one heading line. The table is sorted by date. Data records start at 01/01/1990 and end at 31/12/2002. The recordings of downstream seepage level-measurements and of piezometric levels in F11 well are removed from the dataset from 01/01/2002 until 31/12/2002 (These values should be prognosticated).

Description of Columns in 'MONIT.TXT' or 'MONIT.DBF'

Column 1 (COUNT)
The value represents a counter, starting with "1" in the first line. It increments by 1 each day.

Column 2 (DATE)
In this column are written the dates of monitoring in the format DD.MM.YYYY (f.e. 31.12.2001 means 31/December/2001).

Column 3 (W_LEVEL)
In this column are written daily mean values for the water level in meters above sea level (m.a.S.L.).

Column 4 (RAIN)
In this column are written daily sum values for the rainfall or equivalent snow in mm.

Column 5 (T_AIR)
In this column are written daily mean values for the air temperature in ^{o}C.

Column 6 (F1)
The water piezometric level in piezometer F1, measured in m.a.s.l.

Column 7 (F5)
The water piezometric level in piezometer F5, measured in m.a.s.l.

Column 8 (F6)
The water piezometric level in piezometer F6, measured in m.a.s.l.

Column 9 (F12)
The water piezometric level in piezometer F12, measured in m.a.s.l.

Column 10 (F13)
The water piezometric level in piezometer F13, measured in m.a.s.l.

Column 11 (R27)
The water piezometric level in piezometer R27, measured in m.a.s.l.

Column 12 (R31)
The water piezometric level in piezometer R31, measured in m.a.s.l.

Column 13 (R35)
The water piezometric level in piezometer R35, measured in m.a.s.l.

Column 14 (R38)
The water piezometric level in piezometer R38, measured in m.a.s.l.

Column 15 (R42)
The water piezometric level in piezometer R42, measured in m.a.s.l.

Column 16 (F11)
The water piezometric level in piezometer F11, measured in m.a.s.l. This values are provided until 31/12/2001 only.

Column 17 (FLOW)
The recordings of downstream seepage flow, measured in l/s. This values are provided until 31/12/2001 only.

2.3 FE Model (optional)

It is the choice of each participant to perform a FE analysis for the prediction of the required output values or to perform a statistical analysis using the available data set or to do both FE and statistical analysis.

If it is decided to perform a FE analysis the necessary data for the model can be found in the following section.

2.3.1 Description of the FE Model

Basic data

The mesh contains 774 nodes resulting into 774 degrees of freedom. The nodes can be found in the file named 'NODES.TXT' (node numbers, x, y, z coordinates).

Table 1. Basic data of the FE Mesh

	Nodes	Elements
Dam	142	86
Rock	700	607

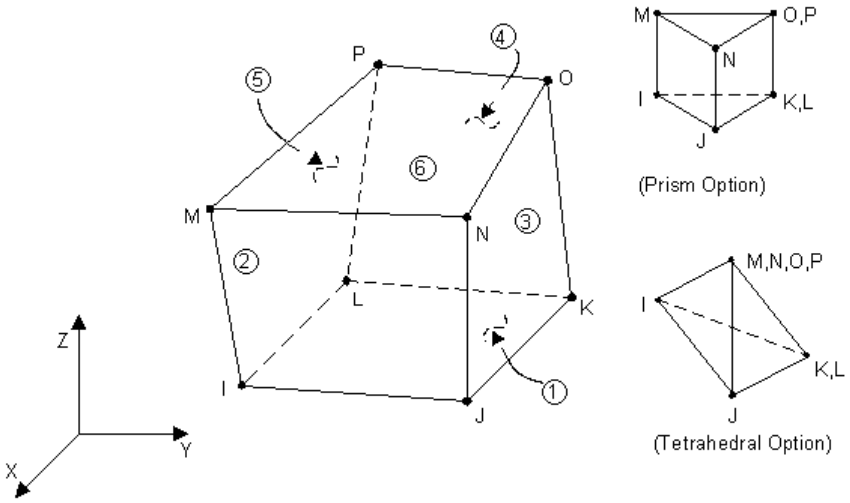

Figure 8. 3-D Thermal Solid element description

The elements of the FE mesh have three-dimensional thermal conduction capability. Each element has eight nodes with a single degree of freedom, temperature, at each node. The element is applicable to a three-dimensional, steady-state or transient thermal analysis. An option exists that allows the element to model nonlinear steady-state fluid flow through a porous medium. With this option, the thermal parameters are interpreted as analogous fluid flow parameters. For example, the temperature degree of freedom becomes equivalent to a pressure degree of freedom. The geometry, node locations, and the coordinate system for this element are shown in figure 8. The element is defined by eight nodes and the orthotropic material

properties. Orthotropic material directions correspond to the element coordinate directions.

The FE mesh is presented in figure 9.

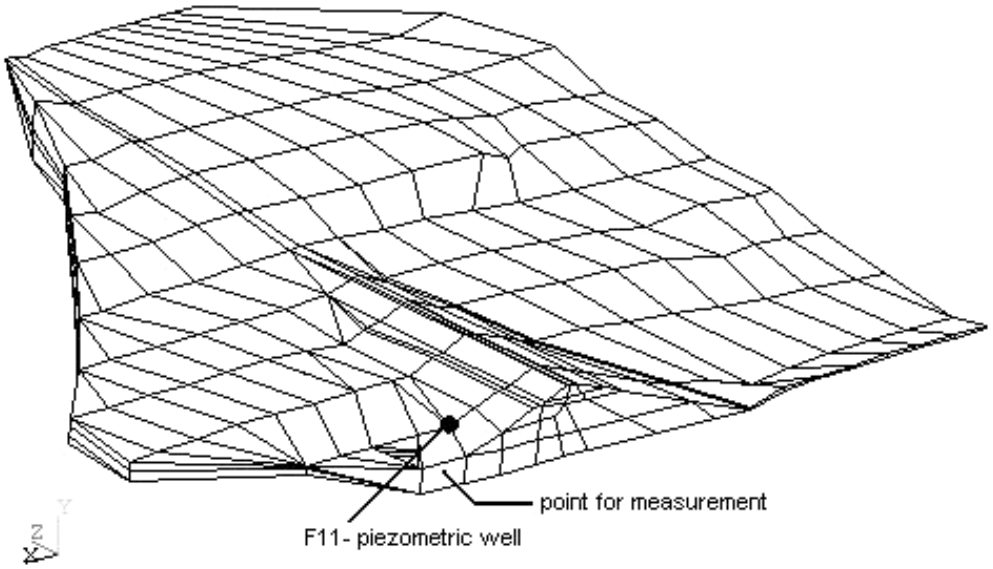

Figure 9. Axonometric view of the Motru dam – foundation three dimensional finite element mesh proposed for seepage analysis

Representative cross sections through the FE mesh and the longitudinal section through the dam axis are presented in figures 10 – 13.

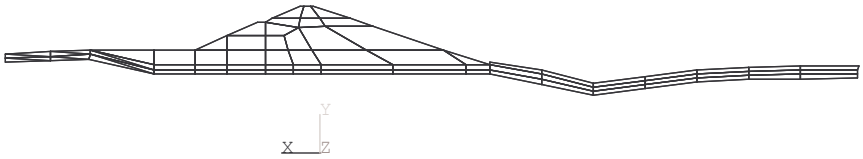

Figure 10. Cross section through the FE mesh corresponding to Z = 34.00 m

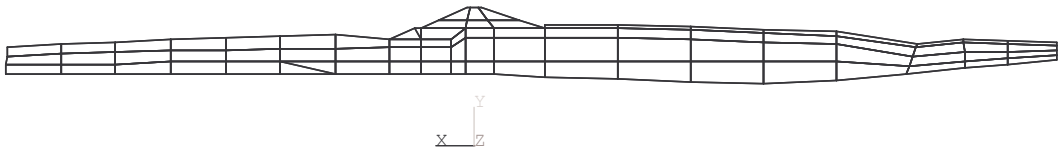

Figure 11. Cross section through the FE mesh corresponding to Z = 156.00 m

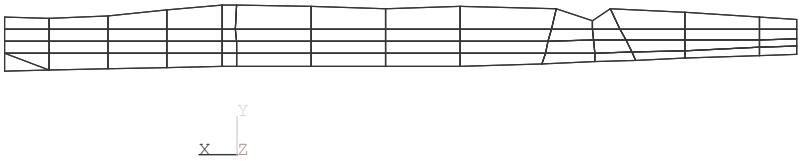

Figure 12. Cross section through the FE mesh corresponding to Z = 310.00 m

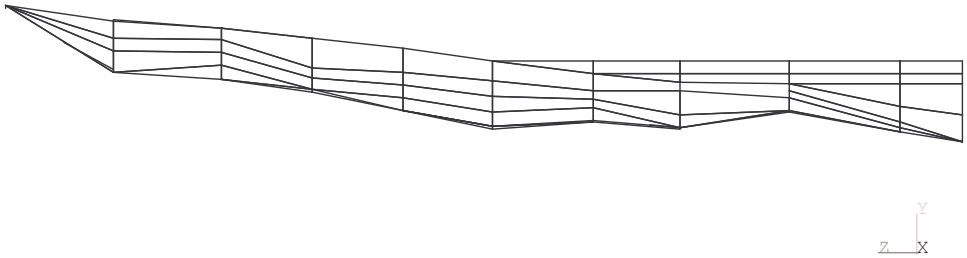

Figure 13. Longitudinal section through the dam axis

The elements can be found in the file named 'ELEMENTS.TXT'.
Note that the proposed FE mesh is optional, the participant are free to use the proposed FE mesh or to improve it.

In the file 'CONTROL POINTS.TXT' are written the coordinates of the selected piezometric wells.

Material parameters

All the materials are considered as isotropic from the point of view of the permeabilities. The different materials are presented in Table 2.

Table 2. Material parameters for the FE Model

Code number	Type of material	Permeability coefficient Kx = Ky = Kz [m/s]
1	Clayey alluvium	5×10^{-4}
2	Gravels and boulders	2.5×10^{-3}
3	Grout curtain in alluvium	10^{-5}
4	Dam earthfill	3.47×10^{-4}
5	Dam clay core	10^{-8}

The material parameters can be found in the file named 'MATERIALS.TXT'.

Loading

The loadings to be considered are due to the reservoir level change at different time moments. For the given reservoir level values the corresponding total heads are provided for different piezometric wells located downstream the dam and the total flow is also a calibration parameter measured at a point located at the dam downstream toe.

The boundary conditions for the FE mesh models a current surface. For the calibration purpose some computations for the given reservoir levels, the corresponding total head values in the downstream piezometric wells and the total flow collected at dam's downstream toe are required, thus determining the position of the seepage free surface through the dam body.

The loading conditions (reservoir levels at several given time moments, the corresponding total head values in selected piezometric wells downstream the dam and the total flow collected in a location near dam's downstream toe) are provided in the file named 'MONIT.TXT' or 'MONIT.DBF'.

3. RESULTS

3.1 Required output

The required results, as was already presented in introduction are the followings:

• The prognosis of the total seepage flow through the dam right bank-foundation system for the period from 01.01.2002 to 31.12.2002. A separation concerning contribution of the different ambiental factors (reservoir elevation, rainfall) at the total seepage flow is recommended; also, a synthetic diagram of the total seepage flow versus reservoir elevation.

• The prognosis of the piezometric level in the selected piezometric well [F11] for the period from 01.01.2002 to 31.12.2002.

The prognosticated values of the total seepage flow and of piezometric level for 2002 year should be provided in the same format as the corresponding values given for the period 1990...2001.

Optionally, the participants are invited to make considerations about internal erosion phenomenon in the Motru dam right wing foundation including long-term effects and to propose rehabilitation solutions.

The analysis may be performed by statistical, neural networks and/or finite element methods.

The results of the analyses are to be provided in a file named 'RESULTS.TXT' or 'RESULTS.DBF'.

7th INTERNATIONAL BENCHMARK WORKSHOP
ON NUMERICAL ANALYSIS OF DAMS
SEPTEMBER 24-26, 2002, Bucharest-ROMANIA

ICOLD Ad-Hoc Committee on Computational Aspects
of Analysis and Design of Dams

Theme C – Embankment dams

SEEPAGE THROUGH AN EARTHFILL DAM - FOUNDATION SYSTEM AND PIEZOMETRIC LEVEL VARIATION DOWNSTREAM OF THE DAM

SYNTHESIS REPORT

Prepared by

Altan Abdulamit
Technical University of Civil Engineering Bucharest

1. INTRODUCTION

The 6th Benchmark Workshop from Salzburg (2001) proposed to the participants, for the first time in the workshop history, to solve a problem concerning the prediction of displacements from a concrete dam applying the finite element method and/or statistical methods. Based on this experience, the 7th Benchmark Workshop from Bucharest proposed a similar approach for solving one of the problems, this time in the case of an embankment dam.

The objective of the Theme C was to use the statistical and/or finite element method for the prediction of the seepage through an earthfill dam – foundation system and piezometric level variation in a selected well located downstream of the dam. The required data to solve this problem were obtained from the monitoring system of the Motru dam (H = 48 m, Romania), which was commissioned in 1983.

The input data, provided by the formulator were the followings:

- The time histories of the reservoir water level, snowfall, rainfall, air temperature, water level downstream of the dam for the period between 1983 and 2002.

- The time histories of the total seepage through the dam right wing – foundation system and of the piezometric level in a selected well downstream of the dam for the period between 1983 and 2001.

- The finite element mesh of the dam right wing – foundation system including the material characteristics, seepage measurement point and selected well location.

The required results were as follows:

- The prognosis of the total seepage flow through the dam right bank – foundation system for the period from 01.01.2002 to 31.12.2002.

- The prognosis of the piezometric level in the selected well for the period from 01.01.2002 to 31.12.2002.

Optionally, the participants were invited to make considerations about the internal erosion phenomenon in the Motru dam right wing foundation and its long term effects, eventually to propose remedial solutions.

It was required to perform the analysis by either or both the statistical and finite element method.

The locations of the control section for the seepage flow computation and of the control point representing the F11 piezometric well are shown in Figure 1.

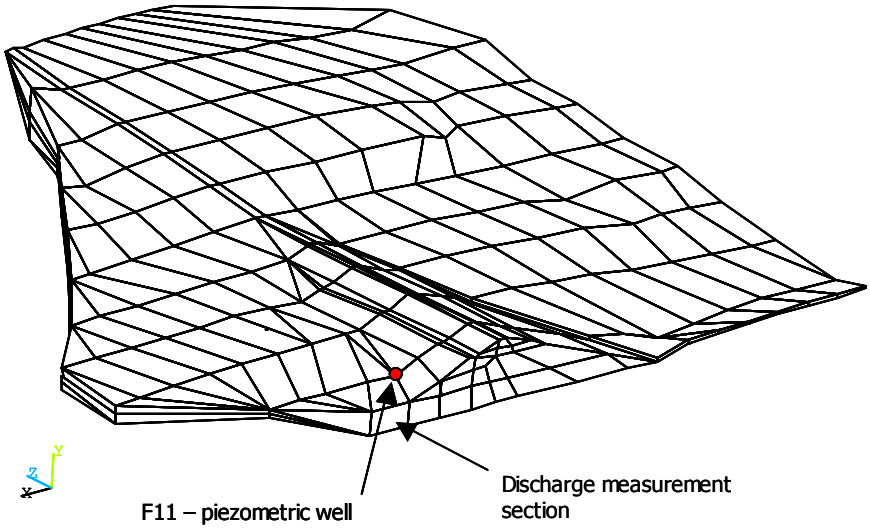

Figure 1. Axonometric view of the FE Mesh of the Motru Dam – foundation system with the location of the control section and F11 piezometric well

2. LIST OF PARTICIPANTS

A number of six participants provided results for the proposed benchmark. Brief information upon the contributors to the Theme C are given in Table 1.

Table 1

Participant	Authors and Title	Country	Analysis Method
1	V. GLAGOVSKY, T. MATROSHILINA, V. PROKOPOVICH, G. STARODUBTSEVA Statistical and Finite Element Analysis of Motru Dam Seepage	RUSSIA	MLR FE
2	C. NORET-DUCHENE, A. CARRERE Prediction of Seepage and Piezometry at Motru Dam With Statistical Models	FRANCE	MLR
3	B. TOUILEB Evolution of Seepage at Motru Dam	CANADA	MLR
4	G. LAZAR, S-V. NICOARA Numerical Modeling of an Unsteady Water Flow Through a Rockfill Dam and Its Foundation Rock	ROMANIA	FE
5	D. STEMATIU, C. ILINCA, D. BOBOCU Prediction of Seepage and Piezometry at Motru Dam with Statistical Models	ROMANIA	MLR
6	O. MATEESCU, C. ILINCA, G. SANDA Prediction of Seepage and Piezometry at Motru Dam Using Neural Networks	ROMANIA	NN

Legend: MLR – multiple linear regression
FE – finite element method
NN – neural networks

3. COMMENTS UPON THE RESULTS PROVIDED BY THE PARTICIPANTS

The submitted results are compared to the on-site measurements. Furthermore, each computed result is plotted vs the corresponding measurement. For each participant the following statistical data have been used as indicators:

R – the correlation coefficient between the computed values and the measured ones;

σ – the standard deviation of the residuals;

μ – the mean value of the residuals.

Brief comments are given, in the next sections, referring to each participant's contribution.

3.1 PARTICIPANT 1

V. GLAGOVSKY, T. MATROSHILINA,
V. PROKOPOVICH, STARODUBTSEVA
B.E. Vedeneev Research Institute (VNIIG), St. Petersburg, RUSSIA
Statistical and Finite Element Analysis of Motru Dam Seepage

Participant 1 solved the proposed problem using both statistical and finite element methods, as follows:

a. Statistical model:

For the statistical model the multiple linear regression with additional variables (F1, F5, F6, F12, F13, R35) was used.

The model was calibrated for the period 1997 – 2001, using the LSM (Least Squares Method).

b. F.E. Model:

2 FE Models were developed (a coarse mesh and a fine one) using ABAQUS rev. 6.3. At the time of the Workshop the FE computations did not produce satisfactory results.

c. The statistical indicators of the results are: (see also Table 2)

For the piezometric levels in F11 well:
$R = 0.777$; $\sigma = 0.689$; $\mu = -0.219$.

For the seepage flow in the downstream section of the dam:
$R = 0.727$; $\sigma = 0.948$; $\mu = -0.373$.

3.2 PARTICIPANT 2

C. NORET-DUCHÊNE, A. CARRÈRE
Coyne et Bellier, Bureau d'Ingénieurs Conseils, Gennevilliers, FRANCE
Prediction of Seepage and Piezometry at Motru Dam With Statistical Models

Participant 2 used 3 different statistical models for solving the problem.

a. Statistical models:

#1. CONDOR – HST Multiple linear regressive model.
Model calibration made for the whole time domain using LSM.

#2. Multiple linear regressive model with additional variables (F6, F12, F13, R35, R42).
Model calibrated for the period 1998 – 2001, using the LSM.

#3. Same as #2, but refined, considering the nonlinear hydrostatic effect and additional variables.

b. The statistical indicators of the results are: (Table 2)

For the piezometric levels in F11 well:
$R = 0.734$; $\sigma = 0.758$; $\mu = 0.172$.

For the seepage flow in the downstream section of the dam:
$R = 0.808$; $\sigma = 0.824$; $\mu = 0.244$.

3.3 PARTICIPANT 3

B. TOUILEB
Hydro – Québec, Montréal, Québec, CANADA
Evolution of Seepage at Motru Dam

Participant 3 submitted results by statistical analyses. He was the only participant who made considerations on the internal erosion phenomenon from Motru dam – foundation system and suggested a number of remedial measures.

a. Statistical model:

Multiple linear regression with delay effect for the reservoir water level (RWL).
Autoregressive component for the flow.
Model calibration made for the whole time domain using LSM.

b. The statistical indicators of the results are: (Table 2)

For the piezometric levels in F11 well:
$R = 0.826$; $\sigma = 0.651$; $\mu = -0.021$.

For the seepage flow in the downstream section of the dam:
$R = 0.750$; $\sigma = 0.905$; $\mu = -0.219$.

c. Remedial measures

Participant 3 proposed a number of alternative solutions to control the seepage through the dam-foundation system thus increasing the dam stability. These are presented in section 4 of the synthesis

3.4 PARTICIPANT 4

G. LAZAR, S-V. NICOARA
"Politehnica" University of Timisoara, ROMANIA
Numerical Modeling of an Unsteady Water Flow Through a Rockfill Dam and Its Foundation Rock

Participant 4 provided results obtained by analysing the problem using the finite element method.

a. F.E. Model

A 3-D FE model was used derived from the 3-D mesh proposed by the formulator of the problem.

For the FE computations the ANSYS program was used. The seepage problem was treated using a thermal analogy, this allowing the participant to solve a non-linear unsteady water flow through the porous solid domain.

b. The statistical indicators of the results are: (Table 2)

For the piezometric levels in F11 well:
$R = 0.342$; $\sigma = 1.250$; $\mu = -0.732$.

For the seepage flow in the downstream section of the dam:
$R = 0.728$; $\sigma = 1.038$; $\mu = -2.189$.

3.5 PARTICIPANT 5

D. STEMATIU, C. ILINCA, D. BOBOCU
Technical University of Civil Engineering Bucharest, ROMANIA
Prediction of Seepage and Piezometry at Motru Dam with Statistical Models

Participant 5 used 2 statistical models for predicting the required results.

a. Statistical models:

#1. CONDOR – HST Multiple linear regressive model.
Model calibration made for the whole time domain using LSM.

#2. Multiple linear regressive with additional variables (F1, F6, F13, R35) with delay effect for RWL

Model calibrated for the period 1990 – 2001, using the LSM.

b. The statistical indicators of the results are: (Table 2)

For the piezometric levels in F11 well:
$R = 0.838$; $\sigma = 0.586$; $\mu = -0.053$.

For the seepage flow in the downstream section of the dam:
$R = 0.778$; $\sigma = 1.222$; $\mu = -0.606$.

3.6 PARTICIPANT 6

O. MATEESCU*, C. ILINCA, G. SANDA****
*** Hidroelectrica S.A., ** Technical University of Civil Engineering**
Bucharest ROMANIA
Prediction of Seepage and Piezometry at Motru Dam Using Neural Networks

Participant 6 used the neural networks method for his predictions.

a. Neural networks

Neural networks model fully connected (with 2 layers – 1 hidden).
INPUT: time, RWL, temperature, precipitations.
OUTPUT: F11 and flow discharge.
Model calibration made for the whole time domain using the gradient method.

b. The statistical indicators of the results are: (Table 2)

For the piezometric levels in F11 well:
$R = 0.760$; $\sigma = 0.712$; $\mu = -0.015$.

For the seepage flow in the downstream section of the dam:
$R = 0.701$; $\sigma = 0.987$; $\mu = 0.348$.

4. REMEDIAL MEASURES TO CONTROL THE SEEPAGE

Participant 3 proposed some alternative solutions to increase the dam stability taking into account the long term effects of the seepage process, respectively of the internal erosion process through the right wing of the dam foundation.

"It is suggested to install a number of staged and sealed piezometers in the area located between the downstream toe of the clay core and the downstream toe of the dam in order to validate the presence of an artesian condition. Based on these values, the stability of the downstream slope must recalculated.

Three different remedial measures are suggested knowing that the dam is located in a seismic area and that it needs a certain margin of safety at normal loading conditions. The following solutions ranged from the less to the most expensive are presented hereafter :

Solution # 1 : Despite the noticeable absence of an upstream blanket - that would have been an efficient second line defence against any lower performance of the cut-off, one could suggest that an appropriate number of relief wells could improve substantially the control of seepage and the stability. This is the less expensive solution.

Solution # 2 : If the first and most economical solution would be not sufficient, then it would be necessary to built an upstream impervious blanket (approximately 200 m long and 2 m thick) that is connected to a new impervious core (clay or membrane) located along the actual upstream face of the dam. Some relief wells could also be added downstream of the dam. Such a remedial measure has been successfully applied to the case of Lac Sainte-Anne dam (Quebec) in 2001.

Solution # 3 : A jet grouted cut-off is added to the last solution. However, the cost of this solution could be too high."

5. CONCLUSIONS

The problem proposed for Theme C of the 7th Benchmark may be considered a successful one, taking into account the number of participants and the accuracy of the solutions.

A number of 6 participants solved the the proposed problem and submitted their results. Some participants used more than one model for their analyses. The solutions were generally satisfactorily and most of the predictions were of acceptable quality to be used in further evaluations.

The following models were used by the participants:

- MLR – multiple linear regression
- FE – finite element
- NN – neural networks

The proposed problem was a complex 3-D seepage phenomenon through a dam – foundation system. The complexity of the phenomena governing the seepage process through the dam – foundation system and the lack of information concerning the boundary conditions made very difficult to build a reliable FE deterministic model. Consequently, the results provided by the statistical analyses were much closer to the monitoring data than the results provided by the finite element analyses.

The great number of monitoring points and the quality of the data base provided by the monitoring system allowed to successfully use the neural networks model for making predictions upon the seepage flow and upon the piezometric level variations within the dam – foundation system. Neural network models may be considered in the future as reliable alternatives for the statistical models.

Most of the approaches were statistical, of the MLR type, using quite different number of parameters – more than 10 for some participants.

Although the benchmark was meant to compare different methods of solving a complex 3-D seepage problem, the practical aspect was not forgotten. Participant 3 proposed a number of remedial solutions for the problems associated to the development of seepage phenomena through the dam – foundation system.

Table 2

Statistical indicators of the predictions made by all the participants

		PARTICIPANT 1	PARTICIPANT 2	PARTICIPANT 3	PARTICIPANT 4	PARTICIPANT 5	PARTICIPANT 6
F11	R	0.777	0.734	0.826	0.342	0.838	0.760
	σ	0.689	0.758	0.651	1.250	0.586	0.712
	μ	-0.219	0.172	-0.021	-0.732	-0.053	-0.015
FLOW	R	0.727	0.808	0.750	0.728	0.778	0.701
	σ	0.948	0.824	0.950	1.038	1.222	0.987
	μ	-0.373	0.244	-0.219	-2.189	-0.606	0.348

Figures A1…A14 present the graphs used for comparring the results provided by the participants.

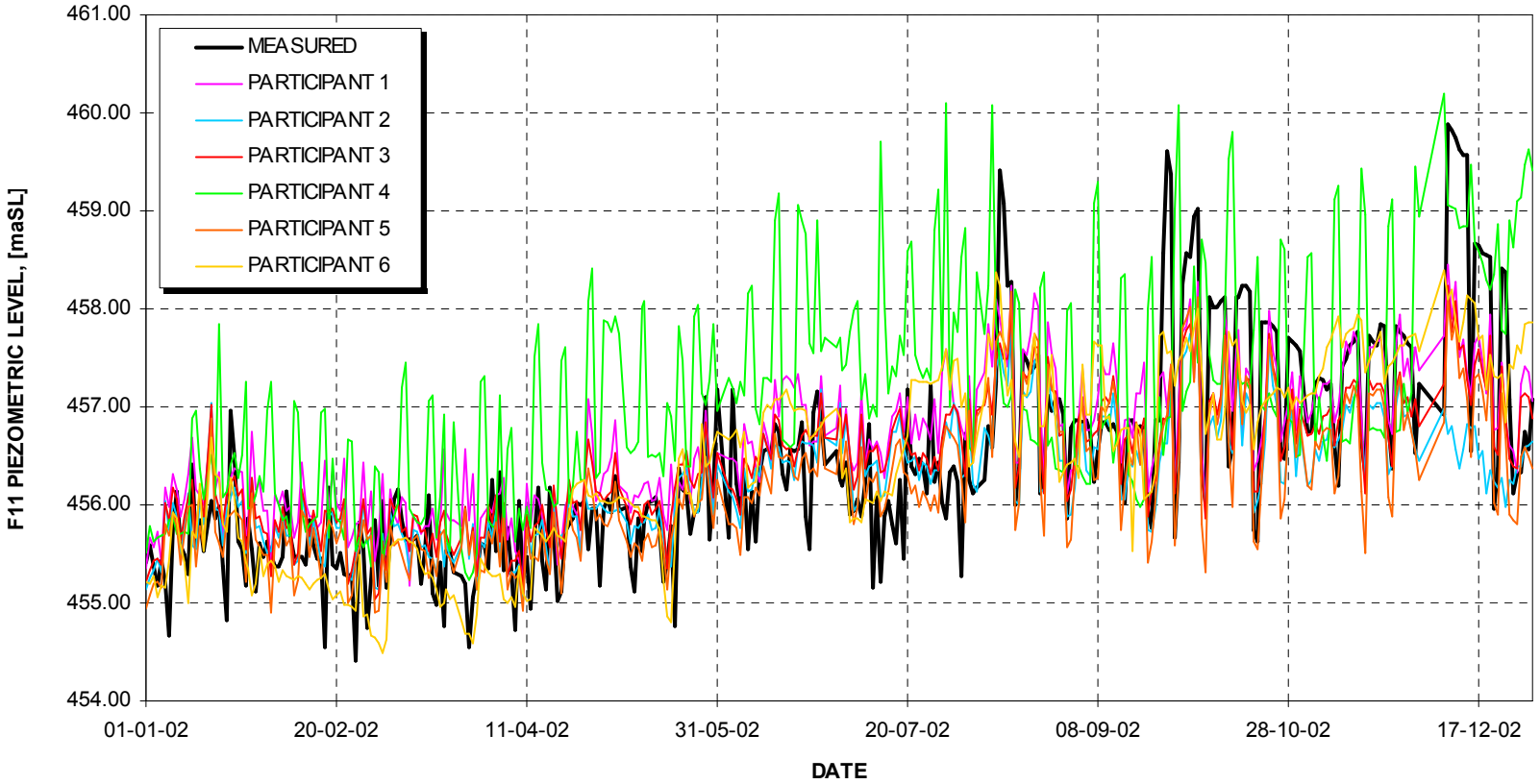

Figure A1. Piezometric level time history in the F11 well for all participants

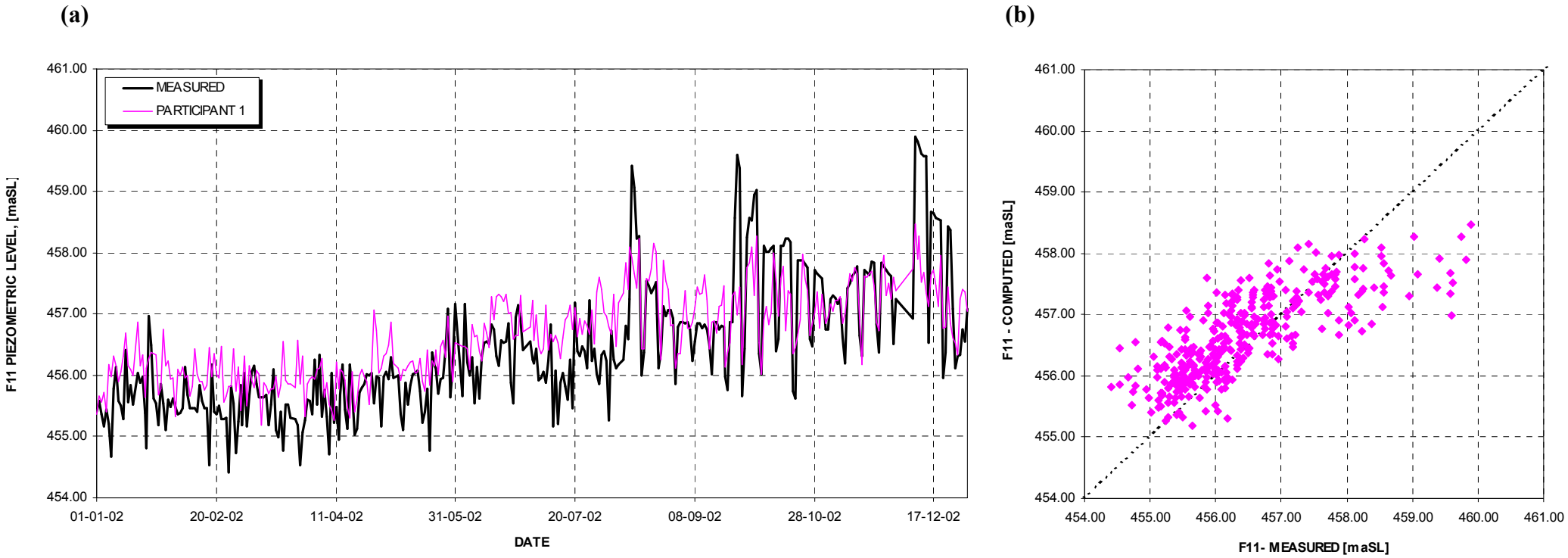

Figure A2. *(a) Piezometric level time history in the F11 well for participant 1*
(b) Measured vs computed piezometric levels in the F11 well for participant 1

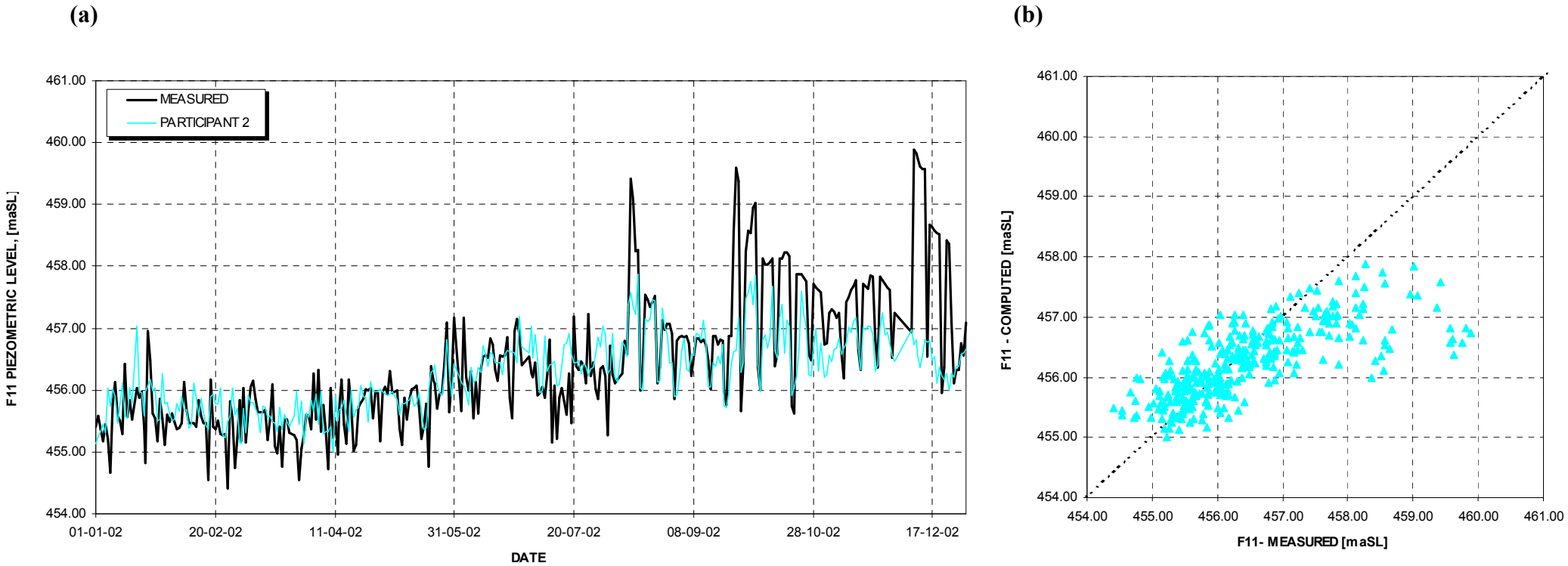

Figure A3. *(a) Piezometric level time history in the F11 well for participant 2*
(b) Measured vs computed piezometric levels in the F11 well for participant 2

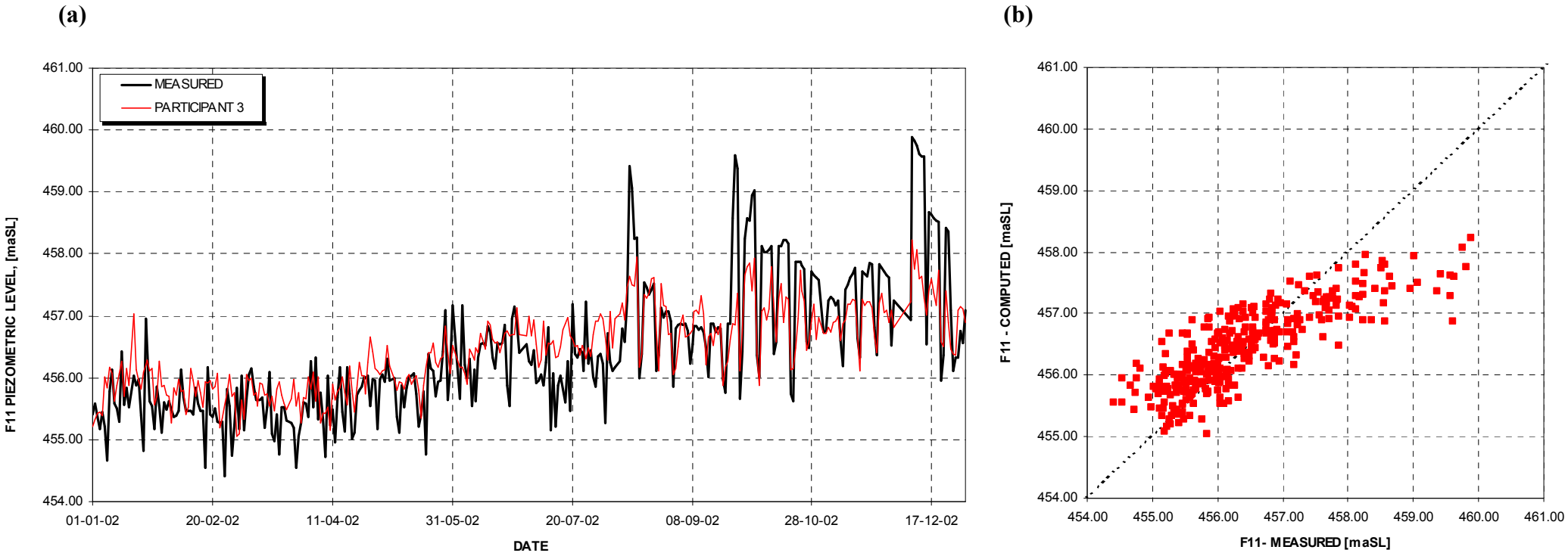

Figure A4. *(a) Piezometric level time history in the F11 well for participant 3*
(b) Measured vs computed piezometric levels in the F11 well for participant 3

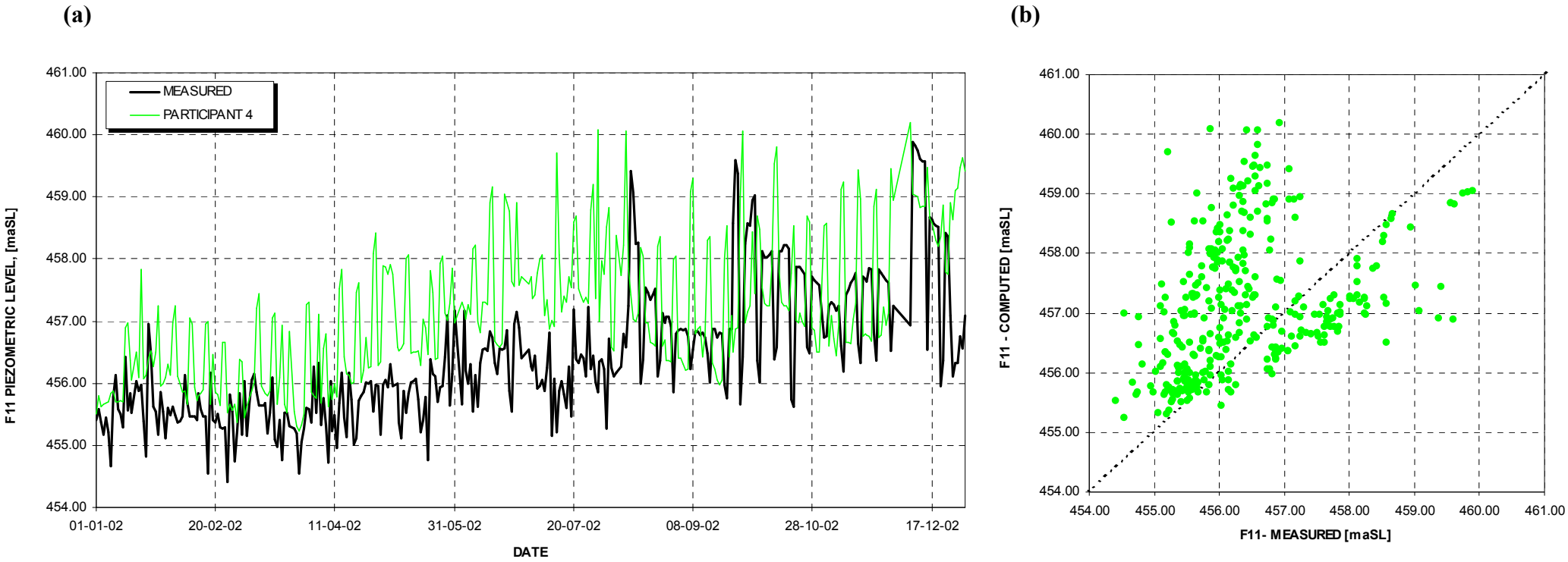

Figure A5. *(a) Piezometric level time history in the F11 well for participant 4*
(b) Measured vs computed piezometric levels in the F11 well for participant 4

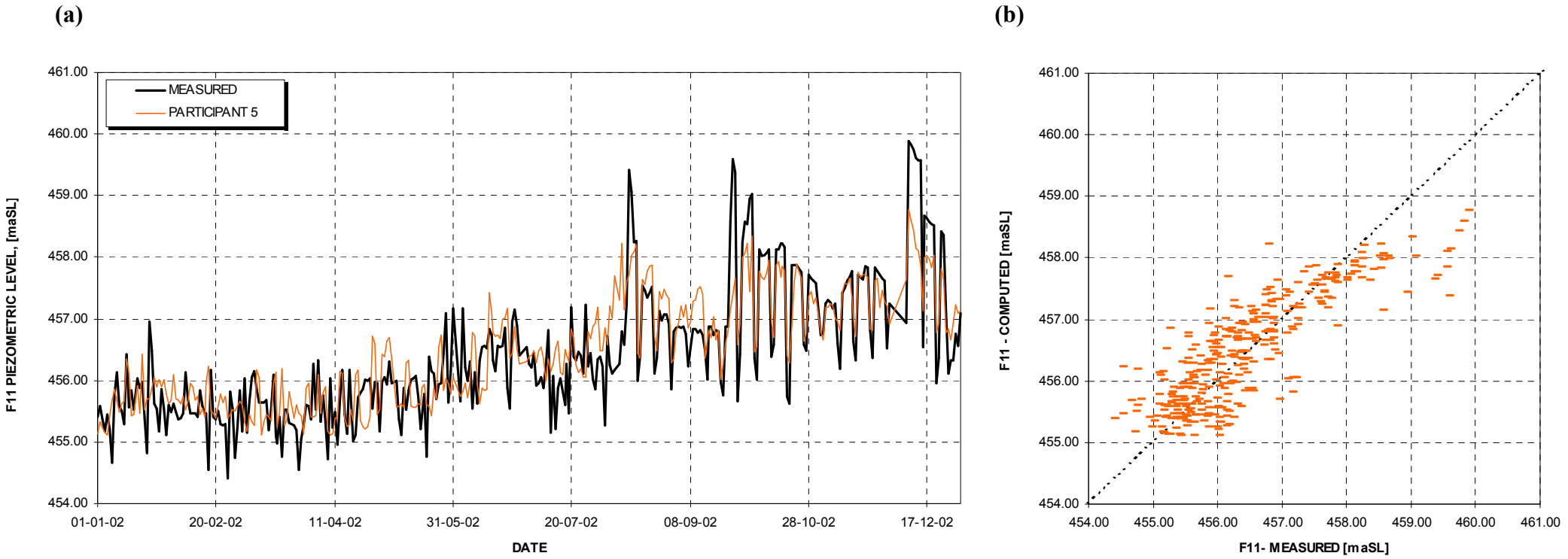

Figure A6. *(a) Piezometric level time history in the F11 well for participant 5*
(b) Measured vs computed piezometric levels in the F11 well for participant 5

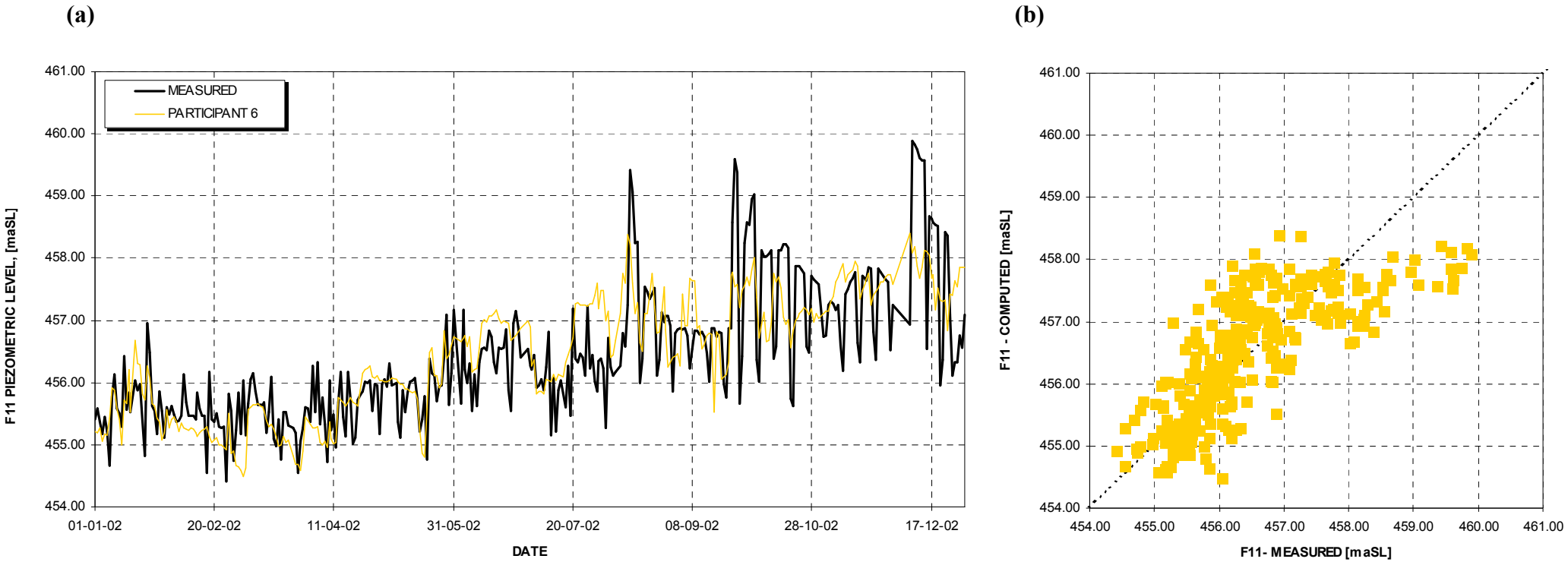

Figure A7. *(a) Piezometric level time history in the F11 well for participant 6*
(b) Measured vs computed piezometric levels in the F11 well for participant 6

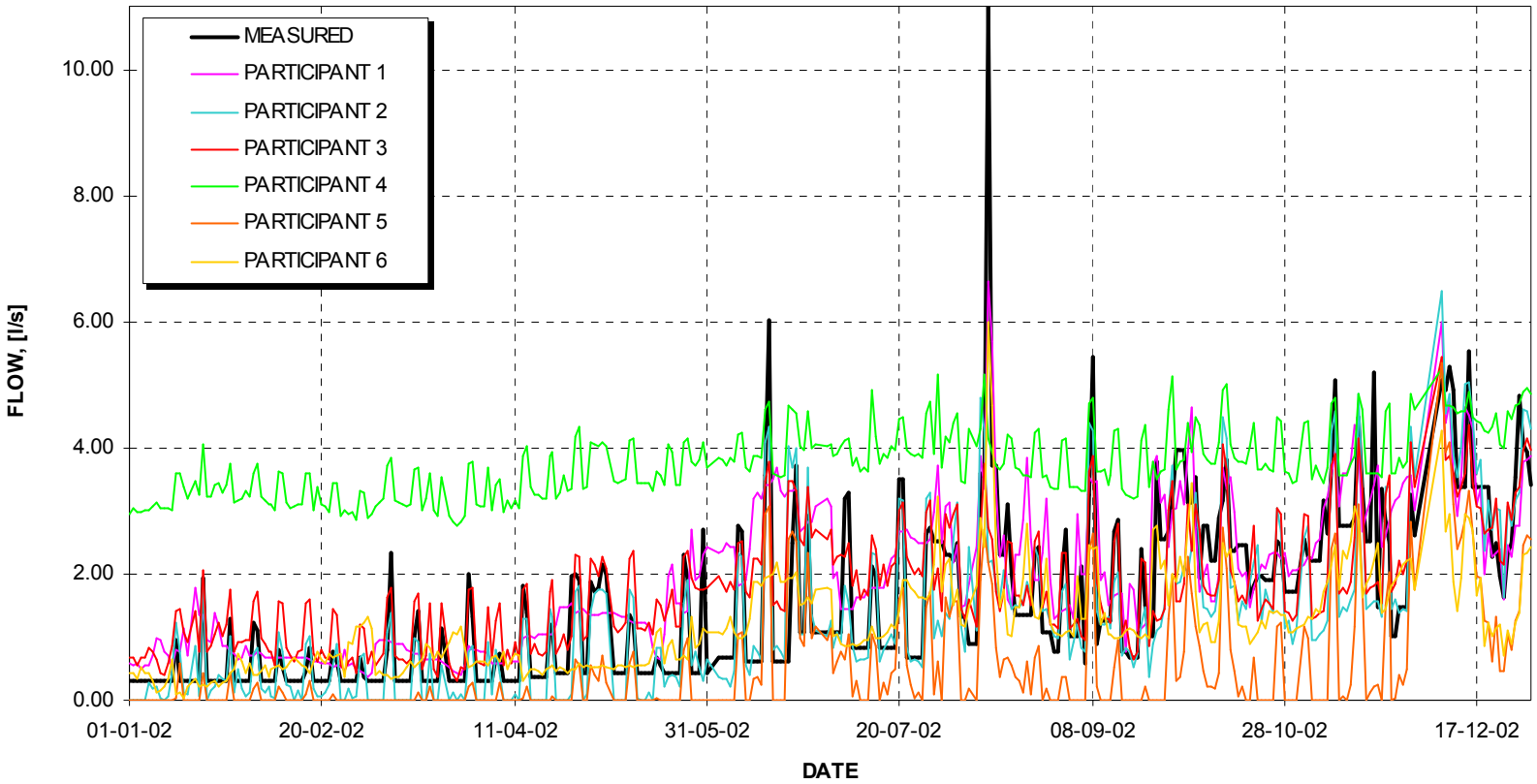

Figure A8. Seepage flow time history in the downstream section for all participants

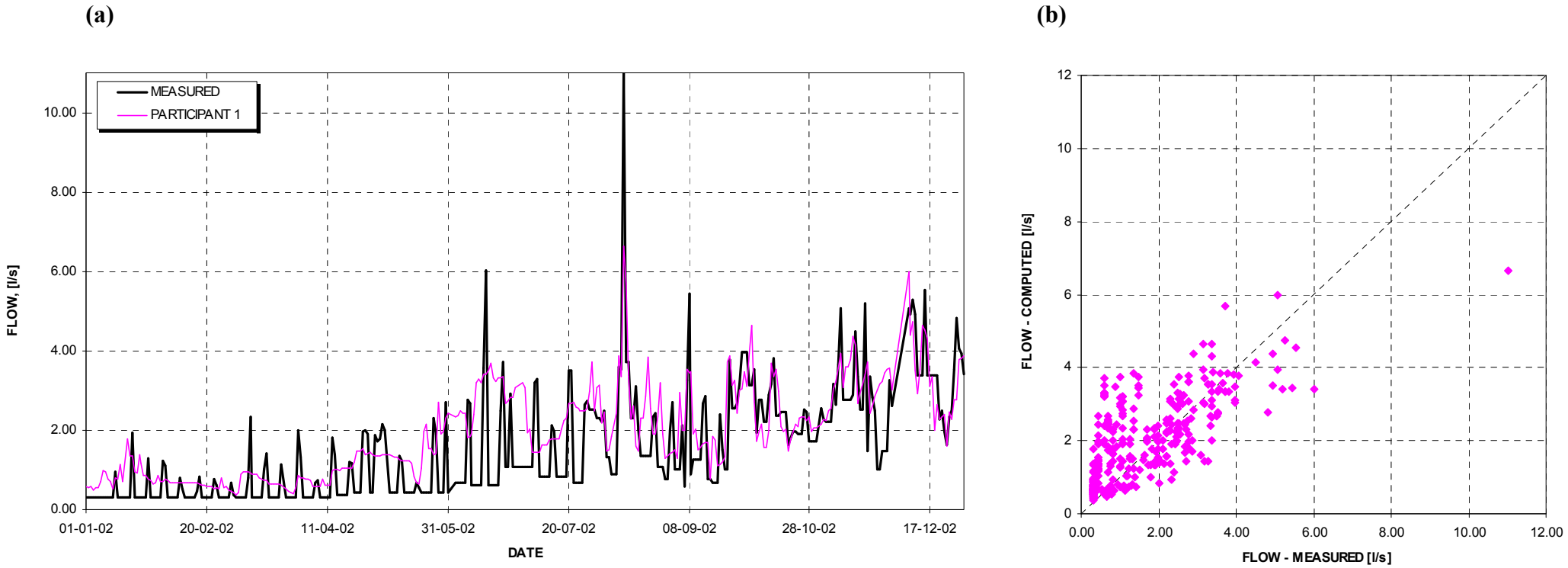

Figure A9. *(a) Seepage flow time history in the downstream section for participant 1*
(b) Measured vs computed seepage flow in the downstream section for participant 1

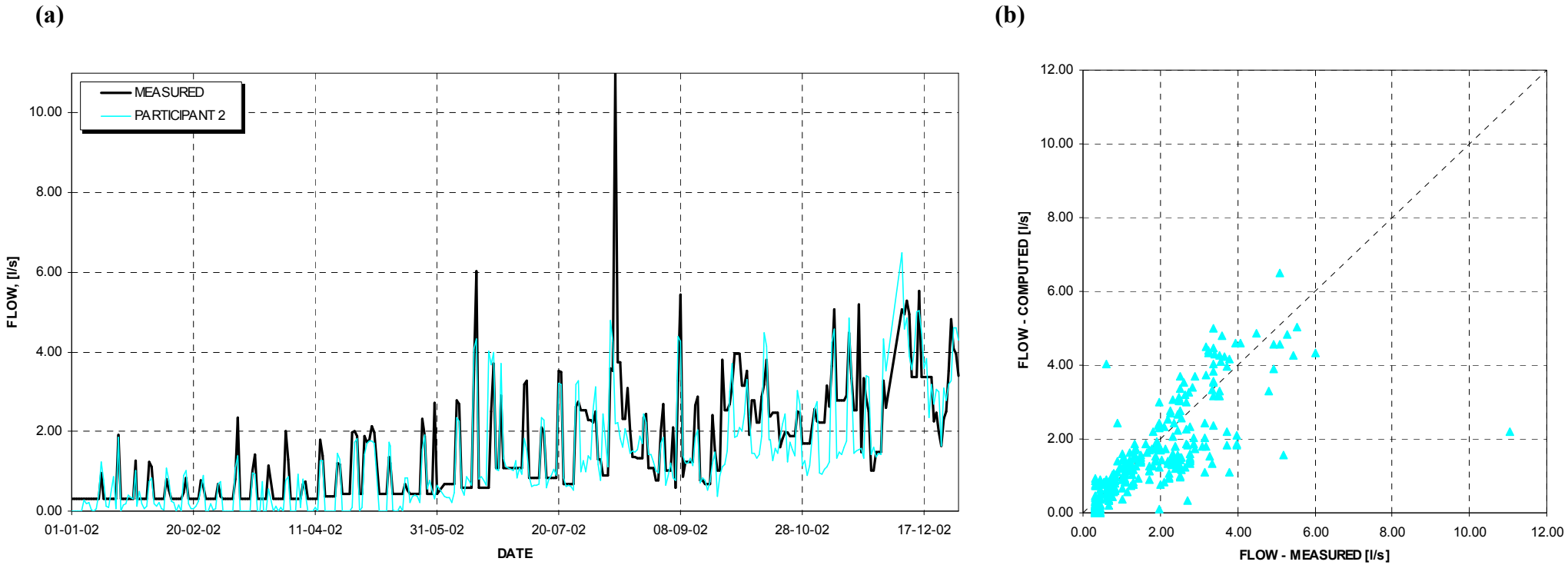

Figure A10. *(a) Seepage flow time history in the downstream section for participant 2*
(b) Measured vs computed seepage flow in the downstream section for participant 2

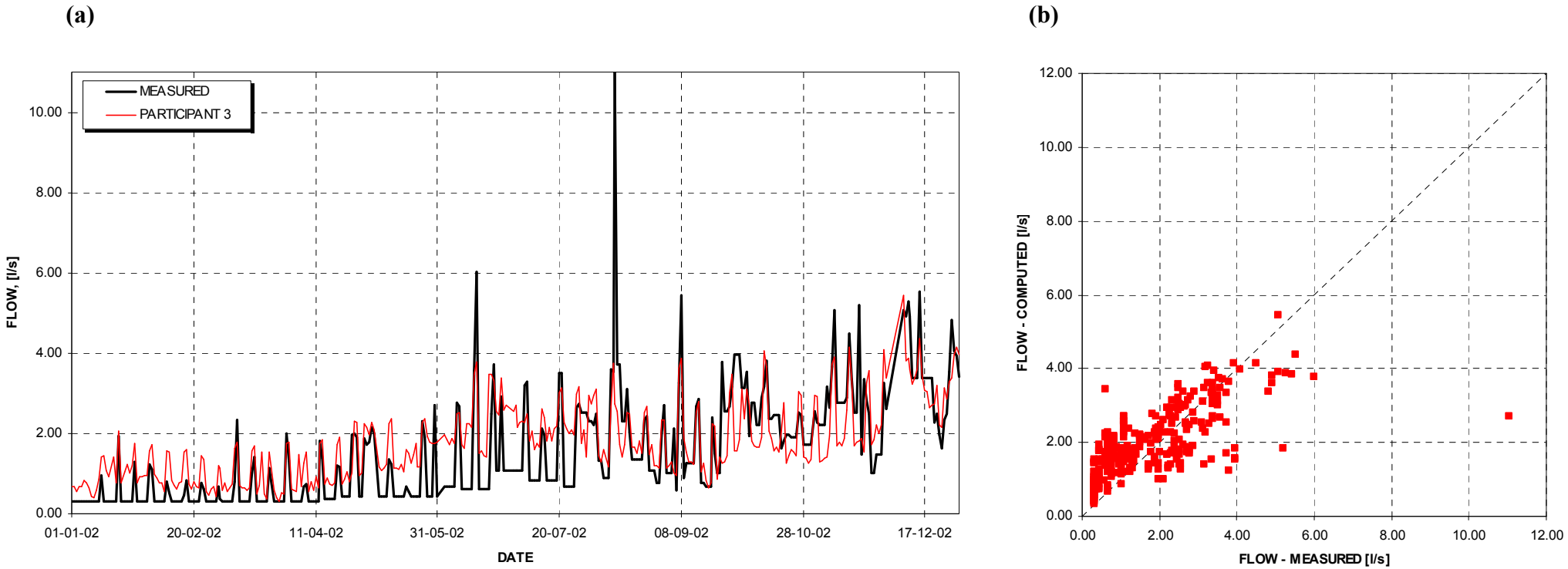

Figure A11. *(a) Seepage flow time history in the downstream section for participant 3*
(b) Measured vs computed seepage flow in the downstream section for participant 3

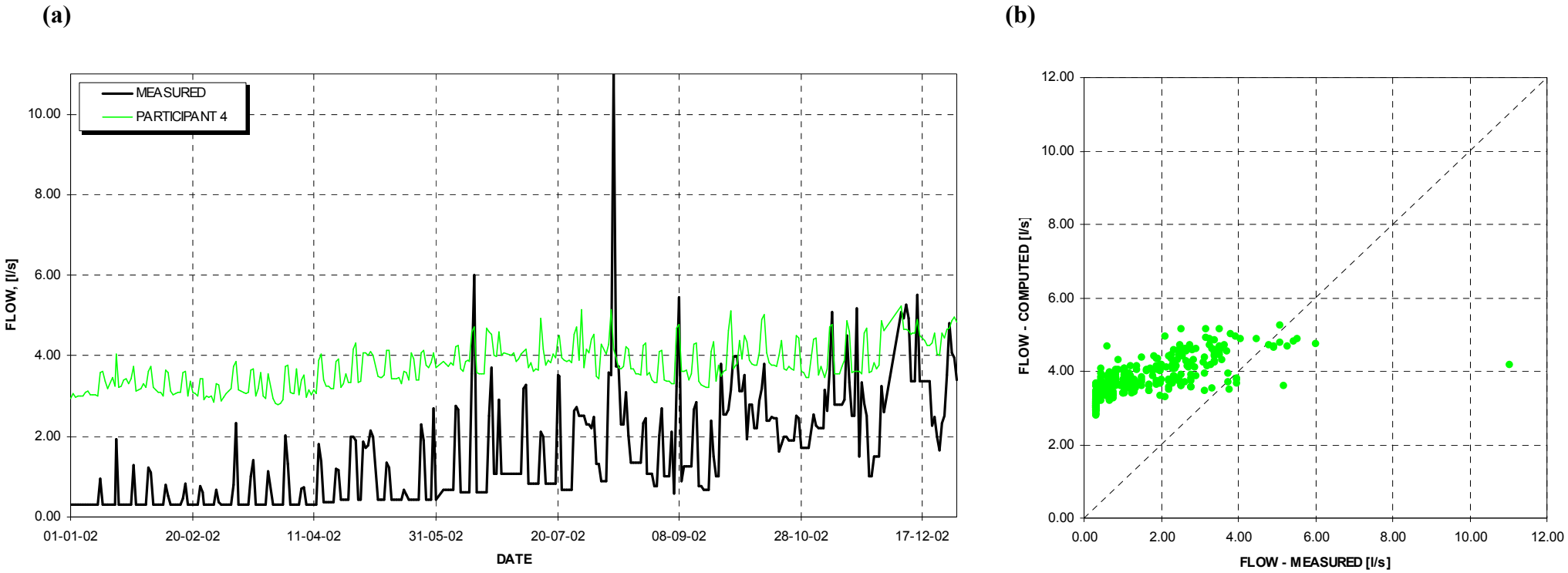

Figure A12. (a) Seepage flow time history in the downstream section for participant 4
(b) Measured vs computed seepage flow in the downstream section for participant 4

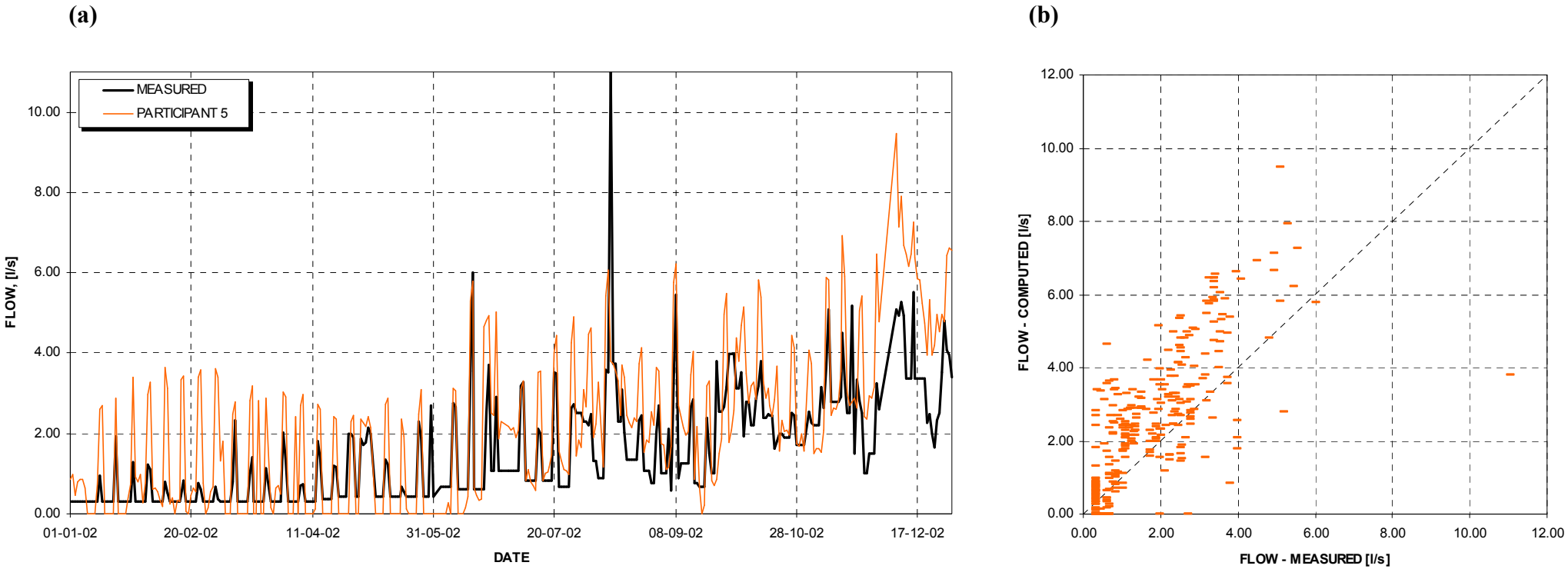

Figure A13. *(a) Seepage flow time history in the downstream section for participant 5*
(b) Measured vs computed seepage flow in the downstream section for participant 5

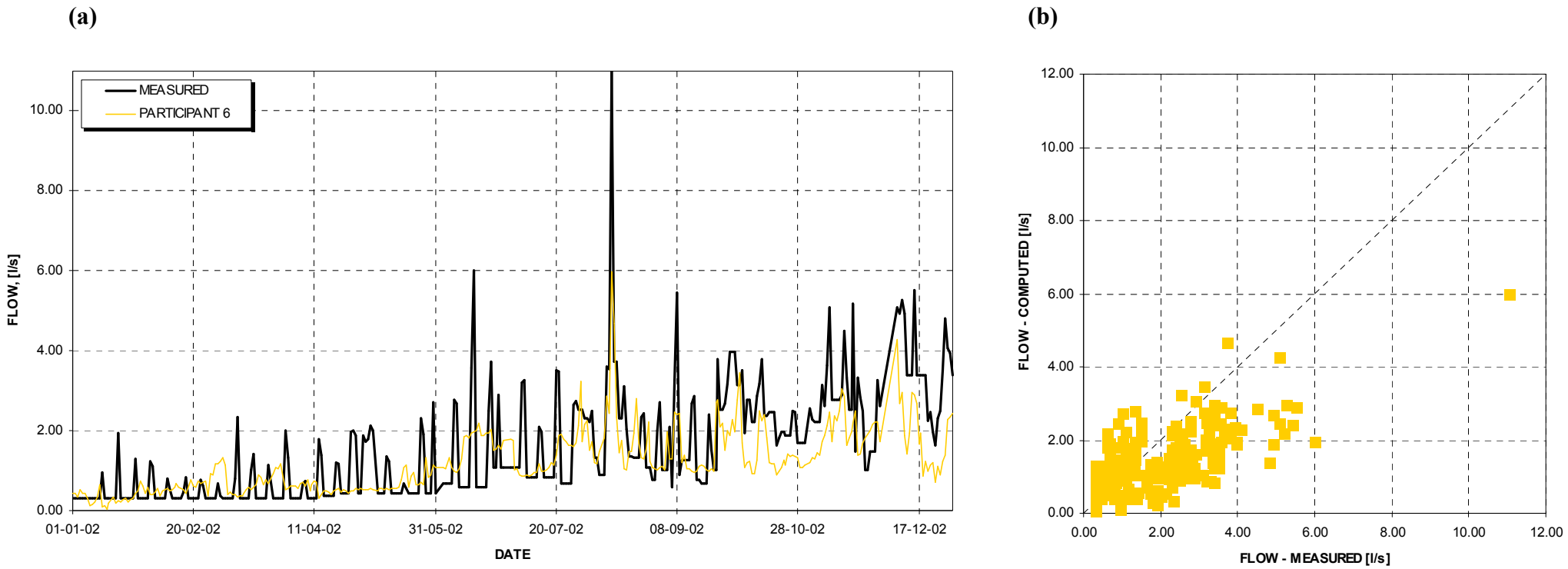

Figure A14. *(a) Seepage flow time history in the downstream section for participant 6*
(b) Measured vs computed seepage flow in the downstream section for participant 6

PREDICTION OF SEEPAGE AND PIEZOMETRY AT MOTRU DAM WITH STATISTICAL MODELS *

Christine Noret-Duchêne, Alain Carrère
Coyne et Bellier, Bureau d'Ingénieurs Conseils, Gennevilliers, FRANCE

SUMMARY:

The statistical approach has been preferred for the prediction of two instrument readings at MOTRU dam over the year 2002, because the hydrological behaviour of the dam foundation is affected by many parameters and all boundary conditions are not well known. The high variability of operation conditions with time led to limit the calibration period to the last four years. Two families of readings have been identified, which seem to be mainly depending on the day of the week, with some exceptions. This feature imposed to analyse separately readings from each family. The HST models have been built first, using the CONDOR software. They clearly show that internal erosion suspected to affect the dam foundation does not result in increasing leakages. Good correlations between several instrument readings allowed the development of efficient multilinear regressive models, which were used to predict the requested readings for the year 2002. The expected accuracy of the prediction is ±50 cm for F11 and ±1 l/s for FLOW, unless wrong classification of the 2002 readings between readings families.

RÉSUMÉ:

C'est l'approche statistique qui a été choisie pour prédire les mesures de deux instruments du barrage de MOTRU sur l'année 2002, car le régime hydrologique de la fondation du barrage dépend de nombreux paramètres et les conditions limites sont imparfaitement connues. La grande variabilité des conditions d'exploitation a conduit à limiter la période de référence aux seules quatre dernières années. Deux familles distinctes de mesures ont été identifiées, qui semblent dépendre du jour de la semaine, à quelques exceptions près. Il a donc fallu analyser séparément les mesures des deux familles. Les modèles HST, établis avec le logiciel CONDOR, démontrent que l'érosion interne suspectée dans la fondation du barrage ne se traduit pas par une augmentation des débits. Les corrélations entre plusieurs grandeurs ont permis d'établir des modèles multilinéaires efficaces, qui ont été utilisés pour prédire les mesures demandées sur 2002. La précision de la prédiction devrait être de ±50 cm pour F11 et de ±1 l/s pour FLOW, à moins de classification erronée des mesures 2002 entre les deux familles.

* Prédiction des fuites et de la piézométrie au barrage de Motru par modèles statistiques

1. INTRODUCTION

The objective of the present exercise is to predict the seepage and the piezometry at the downstream right toe of MOTRU embankment dam during the year 2002, starting from observations accumulated during the previous period 1990-2001. Two main families of methods are generally applied to solve such problems:

i) the so-called 'deterministic' methods, in which a numerical model of the problem is built with a representation of the geometry, materials and loadings as close as possible to the prototype; unknown parameters are determined by adjustment to monitoring readings accumulated in the past;
ii) the statistical approach, where correlations between readings and trends are identified, irrespective of their physical causes.

When physical mechanisms involved in the behaviour of the structure are complex, the building of a deterministic numerical model requires a number of assumptions to be done, for which a preliminary statistical analysis of the data is helpful. For example, the correlation curve of a leak flow as a function of the water level gives an indication of the elevation of the main leak. Building a seepage model without such preliminary analysis would be meaningless, and the combination of both statistical and deterministic analyses is recommendable (Carrère [1], [2]). Only very straightforward problems (e.g. the deflection of a concrete dam under hydrostatic and thermal loads) can omit the first statistical step without prejudice (Verbunplan [3]).

MOTRU dam and its foundation represent a complex 3-D seepage problem in which the boundary conditions are not well known. Moreover the flow net is suspected to concentrate in a few layers of the foundation mass, whose location is unknown. For these reasons, the Authors decided to base their contribution mainly on statistical analyses. Three different types of models can be used:

- standard HST models, built with functions of water level, season and time (Willm [4]),
- models with delayed effects of the physically explicative variables, i.e. in the present case the reservoir level, rain and maybe other boundary conditions such as the tailwater level,
- multilinear models with functions of all readings well correlated with the unknown, with or without delayed terms.

In the present case, our limited knowledge of the boundary conditions made the use of the second category uneasy. Consequently, it has been decided that prediction for F11 and FLOW would be tentatively based first on HST models (Section 3), then that multilinear regressive models would be built (Section 4).

2. PRELIMINARY ANALYSIS OF THE DATABASE

The database provided by the Formulator in the file MONIT.DBF has been carefully examined before starting with analyses. The monitoring readings appear to be quite heterogeneous with time. The attention has been called upon three special aspects, which are discussed below.

2.1 RESERVOIR OPERATION

Since 1990, three periods may be distinguished in the operation of the reservoir, as shown on Figure 1 below:

- 1990-1991: the lake level is kept around El. 477 with only small variations,
- 1992-1997: very important and rapid variations of the lake level are observed, with an average value of 472.50,
- 1998-2002: the water level is kept below El. 473 with an average of 468.60 and variations of about ± 5 m, with few exceptions e.g. in July 1999, where the water level raises up to El. 480.30.

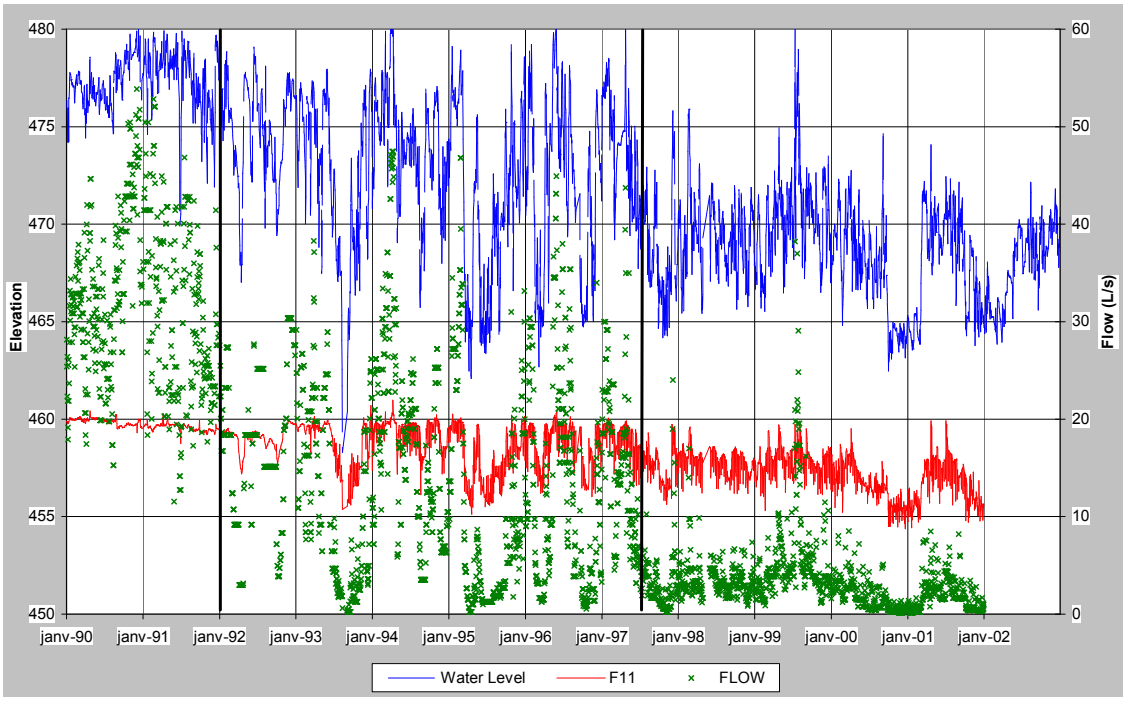

Figure 1: Variations of the water level, piezometer F11 and seepage flow Vs time

Period		1990-91	1992-97	1998-2001	2002
First count		1	507	2481	3900
Last count		506	2480	3899	4249
W_LEV					
	Average	477.3	472.5	468.8	467.8
	Std. Deviation	1.5	4.0	2.6	1.9
	Autocorrel. Coef.	0.84	0.96	0.93	0.94
Flow					
	Average	32.0	12.8	3.1	
	Std. Deviation	8.7	10.2	3.1	
	Autocorrel. Coef.	0.79	0.96	0.82	
F11	Average	459.7	458.6	457.3	
R42	Average	474.2	468.8	465.0	463.6
F6	Average	466.2	462.8	459.2	457.7
F13	Average	474.2	470.7	468.3	468.9

Table 1: Statistics on main monitored variables

In the same time the responses of piezometers and leakage are quite different from one period to another. For example, the seepage flow has decreased by a factor of 10 between 1990-92 and 1998-2001, as shown on Table 1. The same observation is applicable, to a lesser extent, to most of piezometers. It is therefore suspected that different hydrogeologic regimes might have prevailed during these different periods. On the opposite, it is clear also from Table 1 that the 2002 period for which predictions are requested is quite similar to the 1998-2001 period. It is therefore reasonable to base analyses to be carried out mainly on readings accumulated during the years 1998-2001.

2.2 HETEROGENEITY OF SERIES OF READINGS

The attention has been called upon many sudden variations of readings for several instruments. Piezometer F1 is the best example. These variations first appear to be random, but they are not really. Figure 2 presents readings made during week days and during week-end days. Both series are rather regular, but they do not match each other. The phenomenon is still more obvious on Figure 3 which focuses on the recent period 2000-2001: For F1, two families of points appear clearly: readings made during week-ends are very close to the reservoir level, while those done during week days seem to keep along a bottom line, nearly 4 metre below ! The same remark is applicable to nearly all instruments, including the variables F11 and FLOW to be predicted.

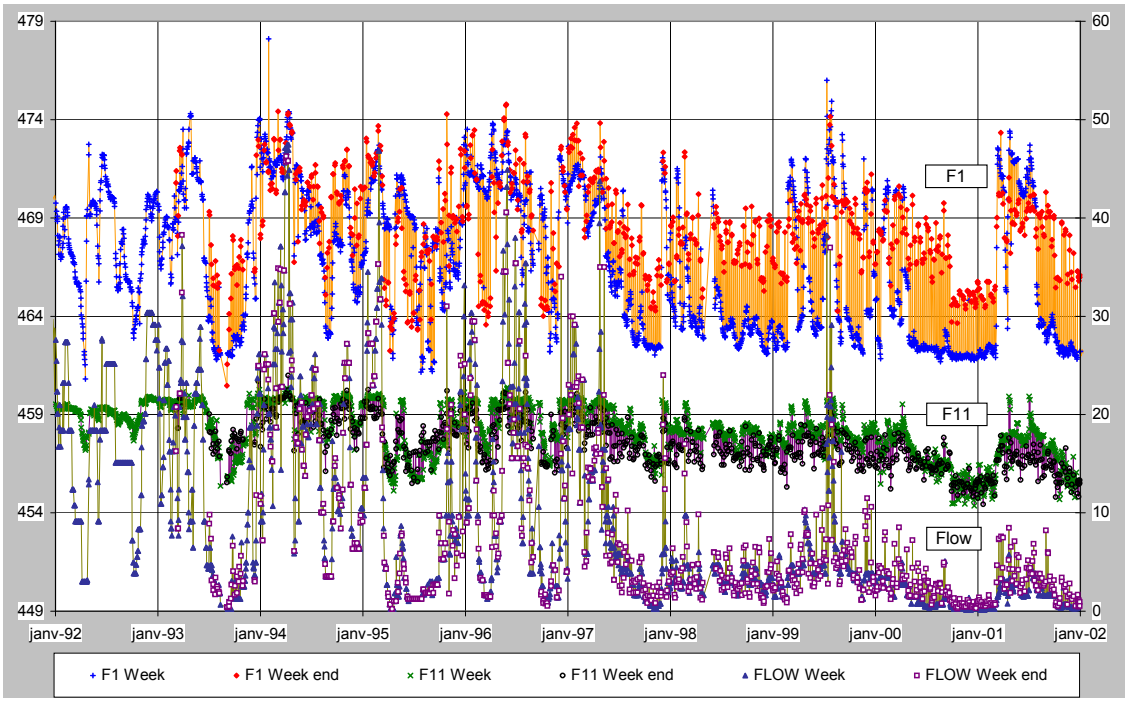

Figure 2: Identification of heterogeneity in readings for F1, F11 and FLOW

The reason for such variability of readings with the day of the week is not clear, and there are many possible explanations:

- differences of operational rules of the dam (bottom outlet, close hydropower plant ?) affecting the tailwater level during week-ends,
- readings made by different teams,
- readings made at different hours or with different methods,
- systematic mistakes on instrument names,

- systematic mixes in writing or reading recorded values,
- etc.

Since it was not possible to identify the origin of the phenomenon, it has been decided to make the distinction between readings made during weeks and those made during week-ends, and to apply the following process:

- first, classify all readings in two families: S1 corresponding to week days (Monday-Friday), and S2 corresponding to week-ends (Saturday-Sunday),
- refine the classification by examining the variations of readings for each family and each instrument, in order to get the best possible continuity of each family,
- build a statistical model for each family S1 and S2 and for each instrument,
- make the prediction for the year 2002 with the model of the family corresponding to each particular date.

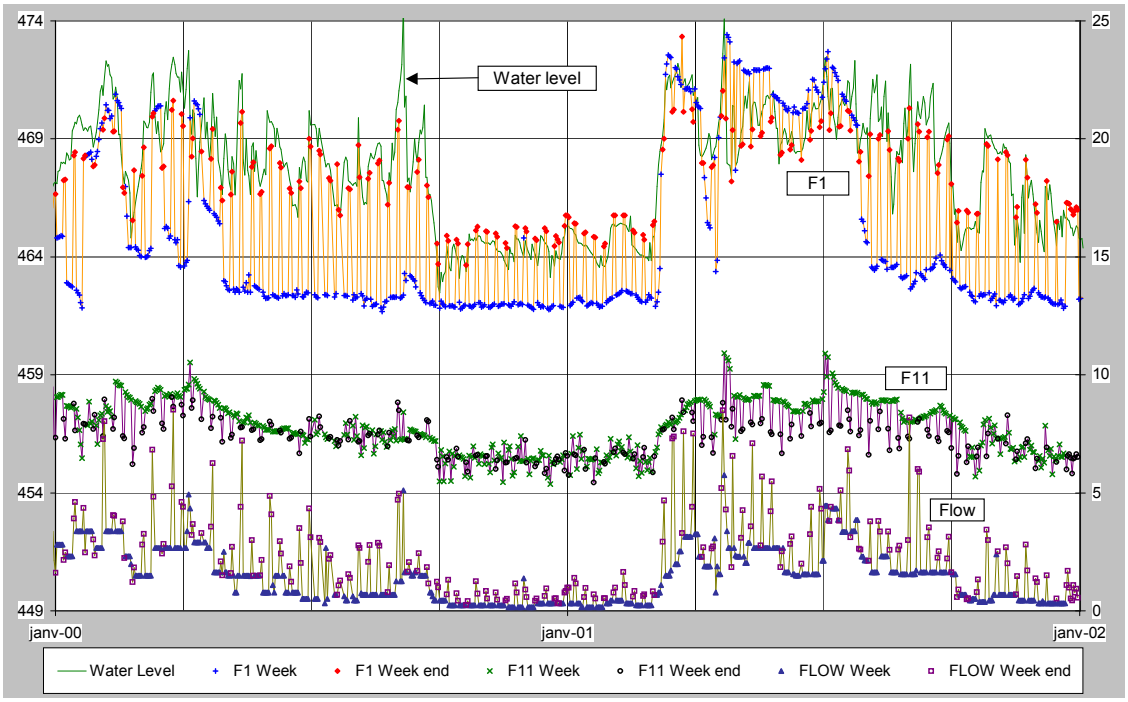

Figure 3: Heterogeneity of readings for F1, F11 and FLOW – Period 2000-2001

2.3 CORRELATIONS BETWEEN READINGS

A strong correlation does exist between the water level, the leakage flow, piezometer F11, and 6 others piezometers. Table 2 shows the correlation coefficients between readings for the 1990-2001 period (both families S1 and S2 put together), with instruments classified according to their correlation coefficient with F11 and FLOW.

F11 has a correlation coefficient higher than 0.75 with water level and 5 piezometers: R42, F6, R35, F13, F12. FLOW has a correlation coefficient higher than 0.75 with water level and the same 5 piezometers: R42, F6, R35, F13, F12, plus piezometer F5. Correlation coefficients with the air temperature, rain records and other piezometers are low. This particular feature of the database opens the possibility to create statistical models based on correlations not only with the reservoir level and other explicative variables, but also with other different instruments. Consequently, it has been decided that multilinear regressive models would be built for F11 and FLOW,

based on readings of the water level, piezometers R42, F6, R35, F13, F12, plus F5 in the case of FLOW. The detail of calculations is given in Section 4.

	F11	FLOW	Water Level	R42	F6	F13	R35	F12	F5	F1	R27	R31	R38
F11	1,00	0,75	0,85	0,86	0,87	0,79	0,83	0,84	0,65	0,64	0,59	0,51	0,42
FLOW		1,00	0,87	0,85	0,82	0,83	0,79	0,76	0,75	0,63	0,55	0,60	0,46
W_LEV			1,00	0,96	0,92	0,94	0,90	0,88	0,84	0,68	0,62	0,66	0,51
R42				1,00	0,92	0,92	0,92	0,88	0,82	0,67	0,62	0,63	0,51
F6					1,00	0,90	0,86	0,83	0,82	0,78	0,61	0,60	0,48
F13						1,00	0,87	0,82	0,84	0,68	0,60	0,64	0,48
R35							1,00	0,82	0,78	0,70	0,59	0,63	0,56
F12								1,00	0,69	0,61	0,58	0,59	0,45
F5									1,00	0,70	0,52	0,67	0,52
F1										1,00	0,47	0,54	0,46
R27											1,00	0,37	0,27
R31												1,00	0,57
R38													1,00

Table 2: Correlation coefficients between readings

3. HYDROSTATIC-SEASONAL-TIME (HST) MODELS

HST models have been built for F11 and FLOW, using the last version of the CONDOR software (Carrère [5]). Different tests have been done, with calibration periods of 1990-2001 and 1998-2001, for all readings, those of Family S1 only and those of Family S2 only. Altogether 6 models have been built for each instrument.

Results have been evaluated on the basis of the residual variation coefficient, which quantifies the average difference between the prediction and the measure over the calibration period. Models are not very efficient as a general rule, since residual variation coefficients range between 0.62 and 0.90 for F11, and between 0.77 and 0.89 for FLOW. The residuals are between 37 and 67 cm for F11 and from 1.1 to 4.2 l/s for FLOW.

Such relatively poor performance is probably due to sudden variations of the boundary hydraulic conditions, which cannot be properly represented by the sinusoïdal "S" functions of HST models. Multilinear regression models are therefore to be preferred to carry out prediction over the year 2002.

However, all HST models provide a very important result, which is a clear trend to a decrease with time on the long term, whatever the calibration period and the family of readings used as reference. Figure 4 shows the corrected values given by CONDOR for F11, i.e. values which would be obtained at constant water level. Such decreasing trend of the piezometric level in F11 could be physically due to a slow change in the river regime downstream, which we do not know. But the same trend is also observed for FLOW, as shown on Figure 5. This clearly indicates that the phenomenon of internal erosion, which is suspected to affect the dam foundation, does not result in an increased flow on the long term.

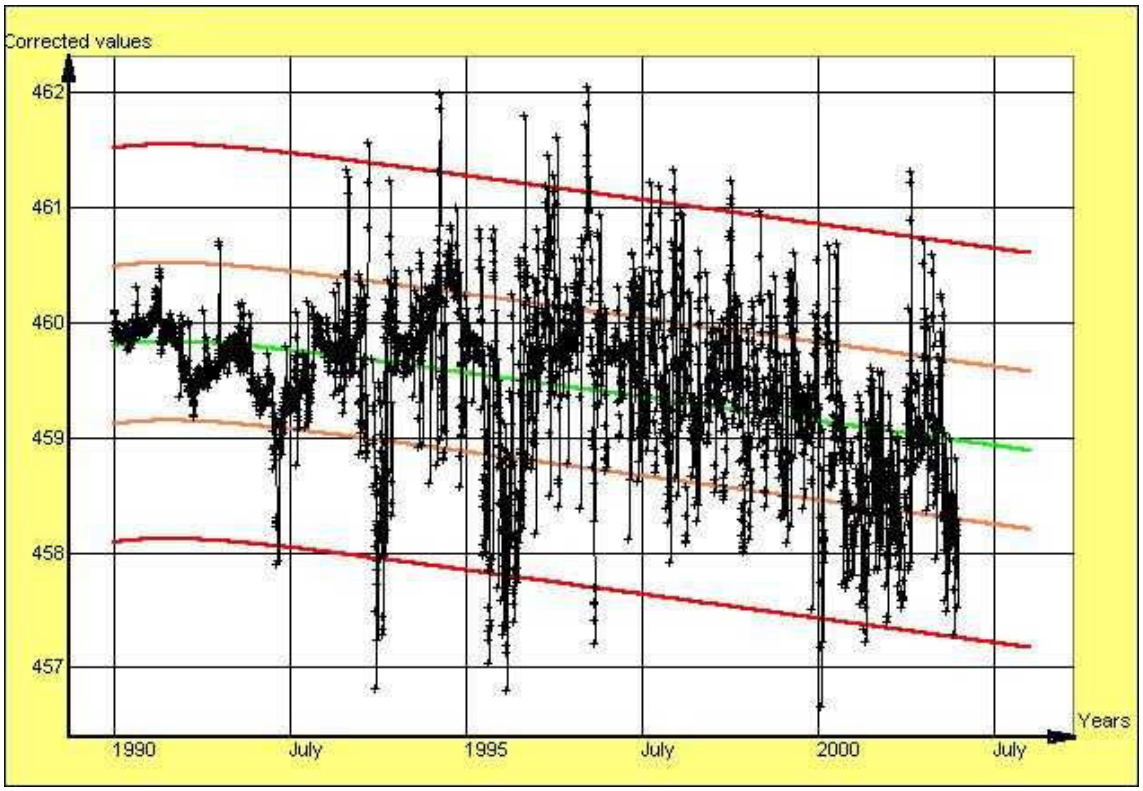

Figure 4: HST model for F11 – Family S1 – Calibration period 1990-2001

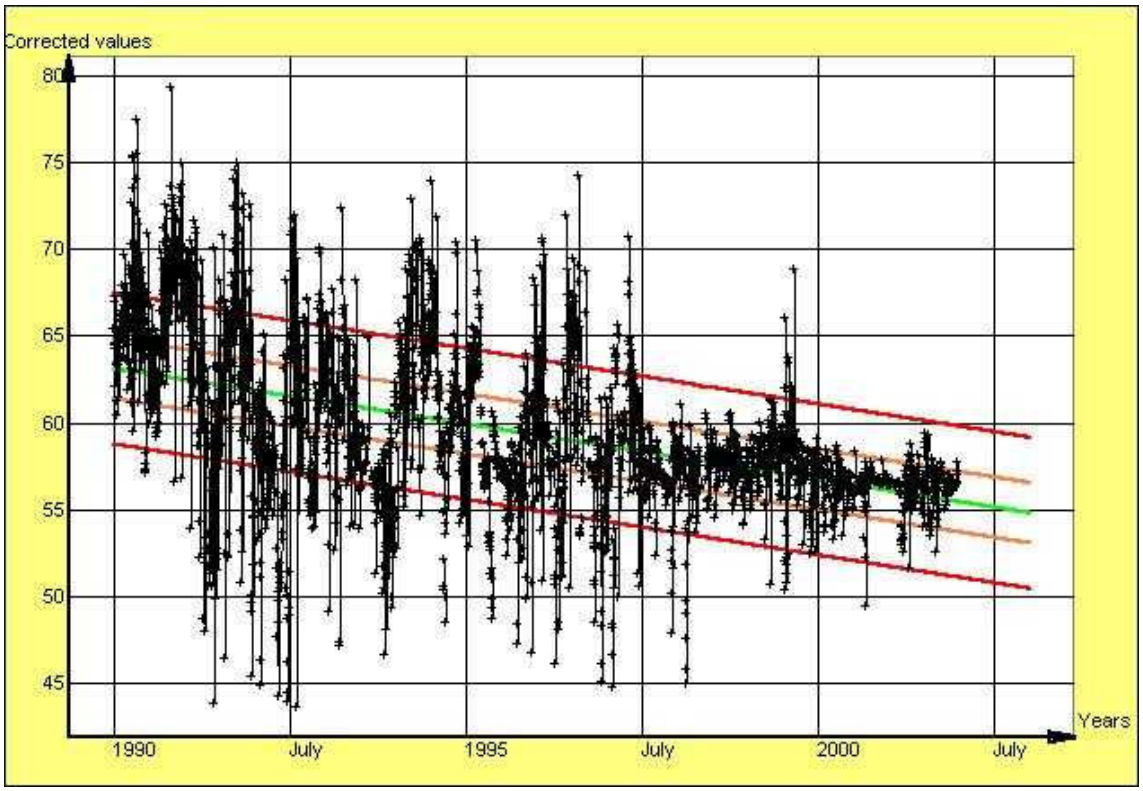

Figure 5: HST model for FLOW – Family S1 – Calibration period 1990-2001

4. MULTILINEAR REGRESSIVE MODELS

4.1 MULTILINEAR MODELS FOR F11

Several models have been prepared successively, until reaching a prediction considered optimal. Their characteristics and performances are shown in Table 3 below. Results have been evaluated on the basis of the residual variation coefficient R^2, which quantifies the average difference between the prediction and the measure over the calibration period.

Model		**Initial**	**N°2**	**N°3**	**Best**
Linear functions with variables : WL – R42 – F6 – R35 – F13 – F12		+	+	+	+
Additional functions	Time (linear)				+
	WL^2			+	
Calibration period	1998-2001	+		+	+
	2000-2001		+		
Results for Family S1 (weekdays)	Residual (m)	0.39	0.45	0.38	0.38
	R^2	0.88	0.84	0.88	0.88
	Drift (m/yr)				-0.10
Results for Family S2 (weekends)	Residual (m)	0.38	0.39	0.38	0.37
	R^2	0.80	0.77	0.80	0.82
	Drift (m/yr)				-0.18

Table 3: Characteristics of statistical models for F11

4.1.1 *Initial models over the period 1998-2001*

The first models are built with linear functions of the 6 following variables: Water level, R42, F6, R35, F13 and F12. The calibration period extends from 1/1/1998 to 31/12/2001. It includes 997 readings for Family S1 (week days) and 422 for Family S2 (week-end days). The residual standard deviations are 39 cm for Family S1 and 38 cm for Family S2, with regression factors R^2 of 0.88 and 0.80 respectively.

4.1.2 *Tentative calibration over a reduced period 2000-2001*

Model n°2 is formally identical to the initial one but the calibration period is reduced to 2000-2001, with only 502 readings for Family S1 (weekdays) and 218 for Family S2 (weekend days). The residual standard deviations are slightly increased (45 cm for Family S1 and 39 cm for Family S2), while regression factors R^2 decrease down to 0.84 and 0.77 respectively. The calibration period from 1998 to 2001 is therefore preferred for the following of the optimisation.

4.1.3 *Non-linear effect of the reservoir level*

Model n°3 incorporates the square function of the water level, which may represent possible non-linear effects of the reservoir level. Its results are not better than those of the initial model. This function is therefore not kept in the following of the model optimisation.

4.1.4 *Model with time-drift function*

The previous models are completed with a linear function of time. The residual standard deviation for the weekend model is reduced to 36 cm and the R^2 coefficient increases to 0.88. The residual standard deviation and the R^2 coefficient for the weekdays model are nearly unchanged. The time drift is a reduction of about 18 cm per year for the weekends model and about 10 cm per year for the weekdays model, which confirms the conclusions taken from HST models. Figures 6a and 6b present readings and model values over the 1998-2002 and the residual difference, for families S1 and S2 respectively.

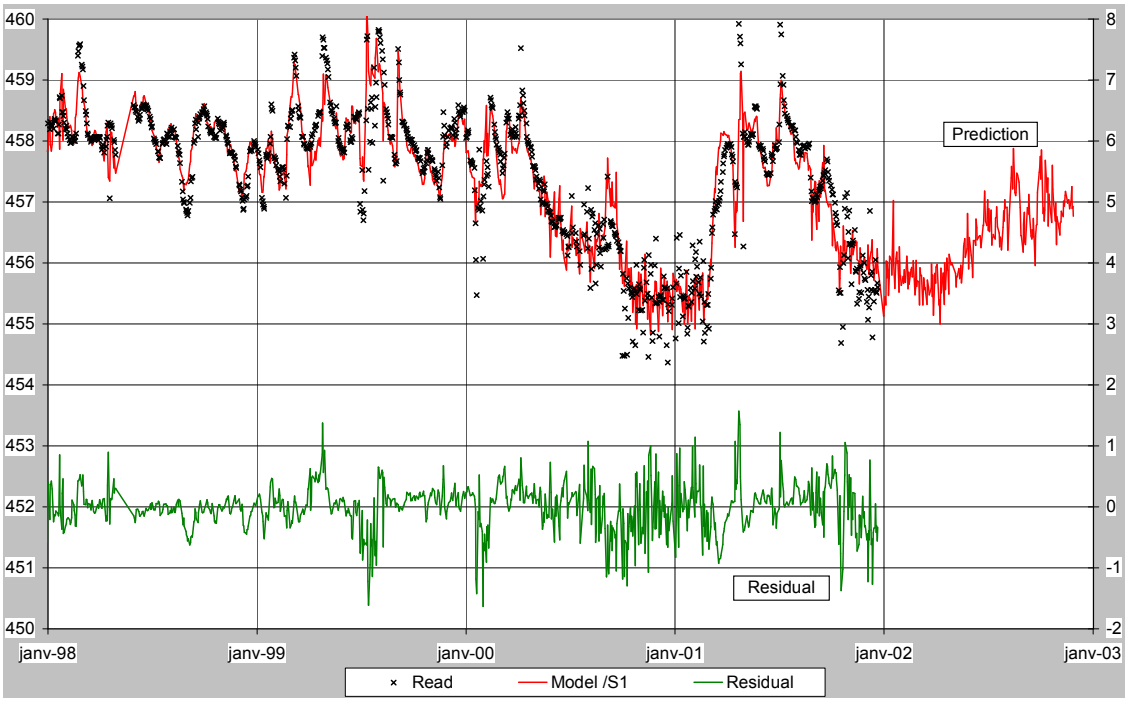

Figure 6a: Best model for F11 – Family S1 (weekdays)

4.1.5 *Conclusion and discussion on F11 models*

Any further attempt to obtain better adjustments over the 1998-2001 period have failed, which means that the models described above are the optimal one. It has therefore been decided use them to carry out the prediction over the year 2002.

It is to be noticed that the residual remains permanently above a value of about 40 cm which seems to be a physical minimum. It is true that the analyses did not incorporate delayed effects, but the quick and well synchronised variations between different instrument readings indicate that there is virtually no delayed effect on piezometer F11. It can therefore be concluded that the accuracy of the readings on F11 is in the order of magnitude of 40 cm. This is not much surprising, if one considers that this instrument is placed at a depth of 369 m according to the information provided. Moreover it is not indicated which type of piezometer is F11 (open piezometer, electric or pneumatic cell, or other) nor whether this instrument is a local piezometer (i.e. with a small pressure chamber) or a global open well.

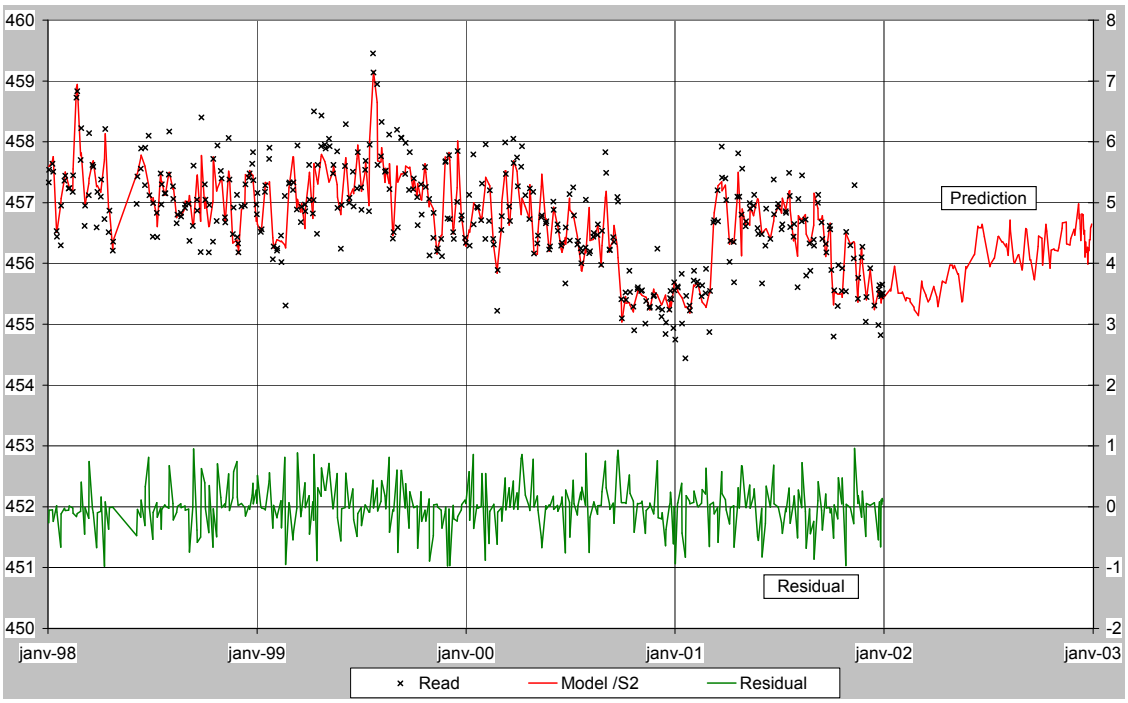

Figure 6b: Best model for F11 – Family S2 (Weekends)

4.2 MULTILINEAR MODELS FOR FLOW

In the same way as for F11, several models have been prepared successively for FLOW, until reaching a prediction considered optimal. Results have been evaluated on the basis of the residual variation coefficient over the calibration period. Their characteristics and performances are shown in Table 4 below.

Model		**Initial**	**N°2**	**N°3**	**N°4**	**Best**
Linear functions with variables : WL – R42 – F6 – R35 – F13 – F12 – F5		+	+	+	+	+
Additional functions	Time (linear)			+		+
	WL^2				+	+
Calibration period	1998-2001	+				
	2000-2001		+	+	+	+
Results for Family S1 (weekdays)	Residual (l/s)	1.81	0.53	0.51	0.50	**0.47**
	R^2	0.65	0.78	0.80	0.81	0.83
	Drift (l/s/yr)					-0.35
Results for Family S2 (weekends)	Residual (l/s)	1.88	0.88	0.88	0.72	**0.72**
	R^2	0.66	0.79	0.79	0.86	0.86
	Drift (l/s/yr)					+0.03

Table 4: Characteristics of statistical models for FLOW

4.2.1 *Initial models over the period 1998-2001*

The first models are built with linear functions of the 7 following variables: Water level, R42, F6, R35, F13, F12, plus F5. The calibration period extends from 1/1/1998 to 31/12/2001. It includes 997 readings for Family S1 (week days) and 422 for Family S2 (week-end days). Negative values of flow are converted automatically to zero. The residual standard deviations are 1.81 l/s for Family S1 and 1.88 l/s for Family S2, with regression factors R^2 of 0.65 and 0.66 respectively.

4.2.2 *Restriction of the calibration period to 2000-2001*

Model n°2 is formally identical to the initial one but the calibration period is reduced to 2000-2001, with only 502 readings for Family S1 (weekdays) and 218 for Family S2 (weekend days). Results become much better, with residual standard deviations dramatically decreased to 0.53 l/s for Family S1 and 0.88 l/s for Family S2, while regression factors R^2 increase to 0.78 and 0.79 respectively.

The improvement of the adjustment when reducing the calibration period to 2000-2001 can be understood if one considers the quite different aspect of the curve before and after January 2000 : the measured flow seems to be smaller and more regular after this date than before. This could be the consequence of a change in the flow regime or catchment system. In any case the calibration period limited from 2000 to 2001 is preferred for the following of the optimisation.

4.2.3 *Model with time-drift function*

Models n°3 incorporate a linear function of time which hardly improves global results. Incorporation of this function for the following of the optimisation is debatable.

4.2.4 *Non-linear effect of the reservoir level*

Models n°4 incorporate the square function of the water level. It improves slightly the model performance especially for Family S2. This function is therefore to be kept for the following of the optimisation.

4.2.5 *Best models for FLOW*

The last models incorporate both additional functions previously tested: the linear function of time, and the square function of the water level. The residual standard deviation for the weekend model is reduced to 0.72 l/s and the R^2 coefficient increases to 0.86. For the weekdays model the residual standard deviation is also reduced to 0.47 l/s and the R^2 coefficient increases to 0.83. The time drift is a decrease of about 0.35 l/s per year for the weekdays model, which again is conform to results of HST models already discussed. The drift is virtually 0 for the weekends. Figures 7a and 7b present readings and model values over the 1998-2002 and the residual difference, for families S1 and S2 respectively.

Any attempt to obtain better adjustment of the model on readings over the 2000-2001 period have failed, which means that the model described above is the optimal one although the R^2 coefficients are not very good on an absolute scale. It has therefore been selected to carry out the prediction over the year 2002.

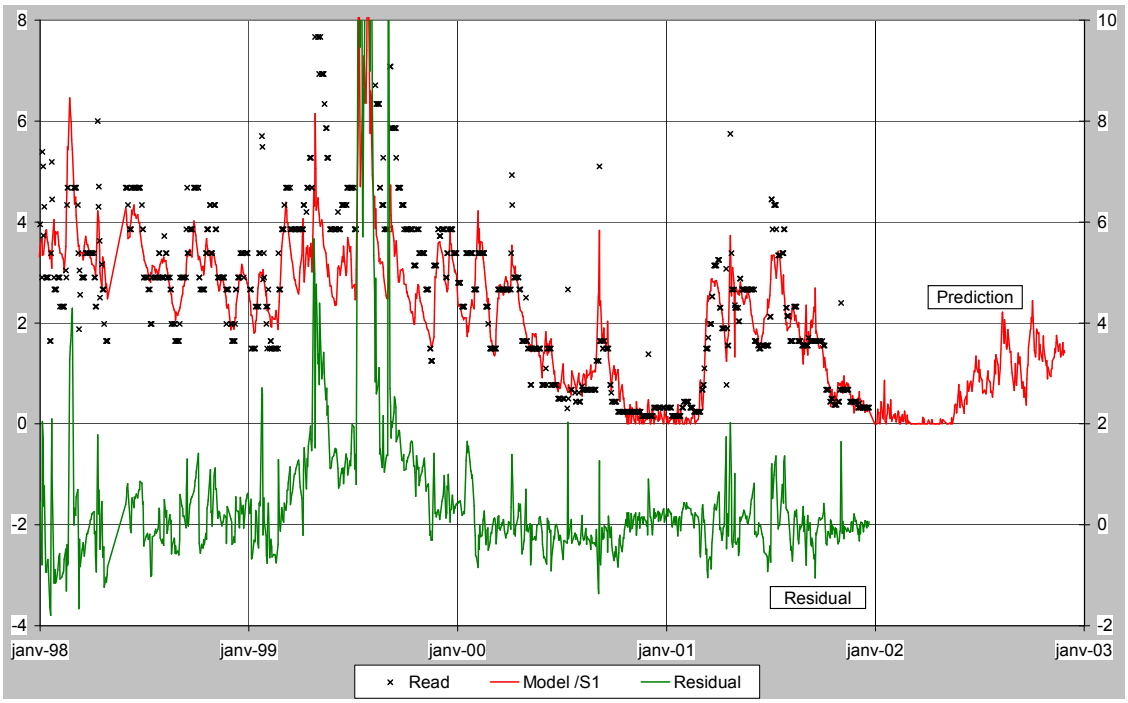

Figure 7a: Best model for FLOW – Family S1 (weekdays)

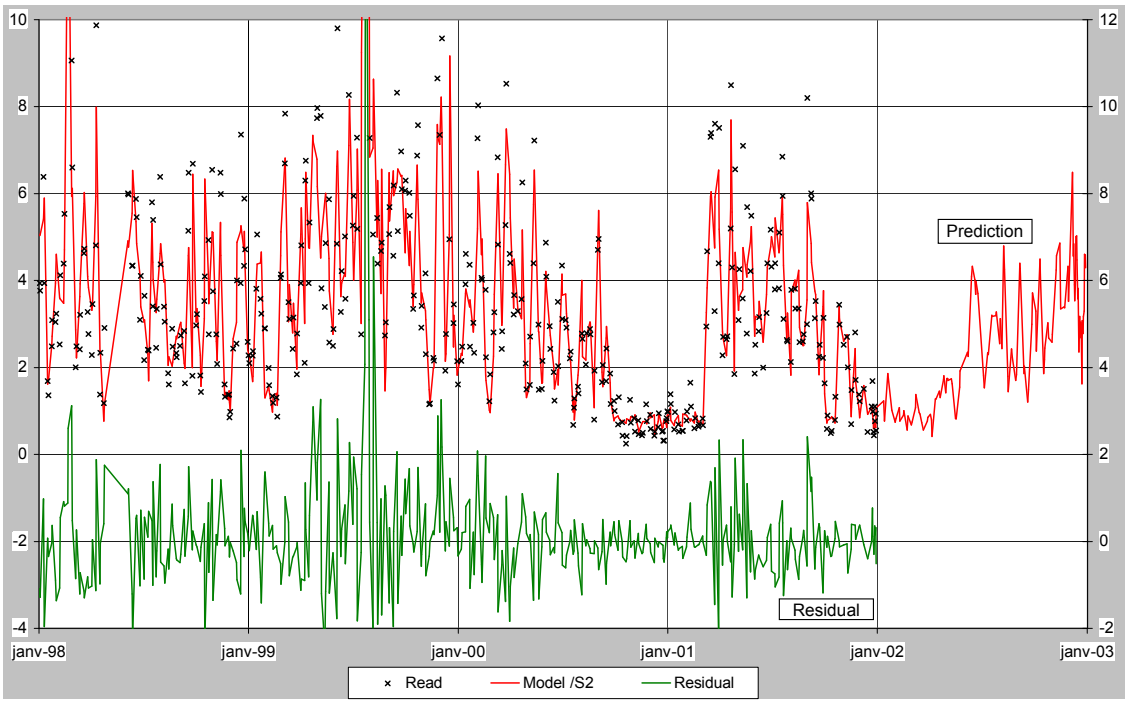

Figure 7b: Best model for FLOW – Family S2 (weekends)

5. RESULTS

Results required by the Formulators have been calculated with the best statistical models obtained for F11 and FLOW, both for Families S1 and S2. The formal expression of these models is given in Tables 5 and 6 below.

Formulation of models for F11	Family S1 Weekdays	Family S2 Weekend	Function
Prediction (m) =	94.3541824	322.904417	Constant
+	-0.02093095	0.25341982	x Water level (WL)
+	0.1110347	0.00815778	x R42
+	0.01805548	-0.03946576	x F6
+	-0.01771141	0.0445204	x F13
+	0.0922632	-0.00205996	x R35
+	0.60773901	0.02162917	x F12
+	-0.09693831	-0.18243372	x Time (*)

** Time function with T in years from 01/01/1998*

Table 5: Formulation of the statistical model for the piezometer F11

Formulation of models for FLOW	Family S1 Weekdays	Family S2 Weekend	Function
Prediction (m) =	6757.6104	20388.407	Constant
+	-30.11991	-87.57807	x Water level (WL)
+	0.1069432	-0.053259	x R42
+	0.1136808	0.2050409	x F6
+	0.0468584	-0.283392	x F13
+	0.0781397	-0.046357	x R35
+	0.3112804	0.0238967	x F12
+	-0.00705	-0.069089	x F5
+	0.0321501	0.0945384	x WL*WL
+	-0.347494	0.0328908	x Time (*)

** Time function with T in years from 01/01/1998*

Table 6: Formulation of the statistical model for the seepage flow

Based on the residual variation coefficient of 38 cm obtained during the 1998-2001 observation period for F11, the predictions given below are expected to have an average accuracy of ±50 cm within each family of readings. For the FLOW readings, predictions could be supposed to have an average accuracy of ±1 l/s, based on the residual variation coefficient of 0,70 l/s obtained during the 2000-2001 observation period.

The definition of the family to which one particular reading belongs has been done as indicated previously, i.e. considering the weekday or weekend day of any given date. It is however to be noticed that the differentiation between families is not as obvious as during previous years, especially during October and December 2002 where variations are very uneven. Additional differences might therefore appear, due to mixes between families during these periods.

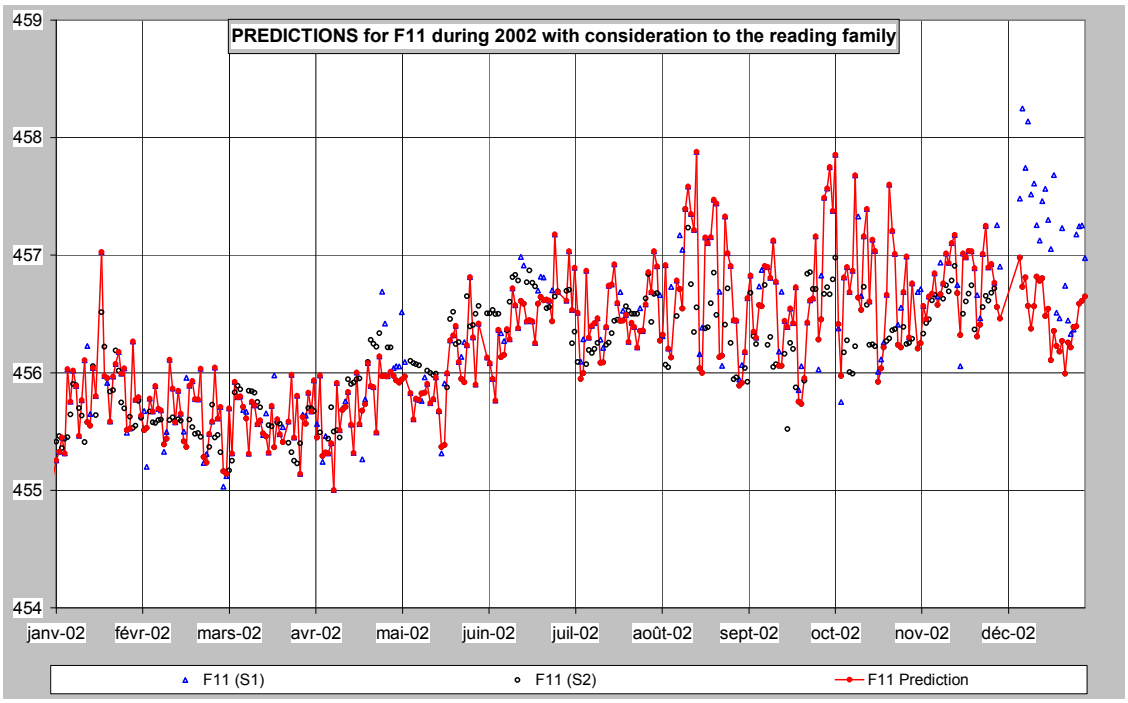

Figure 8: Prediction for F11 readings during 2002

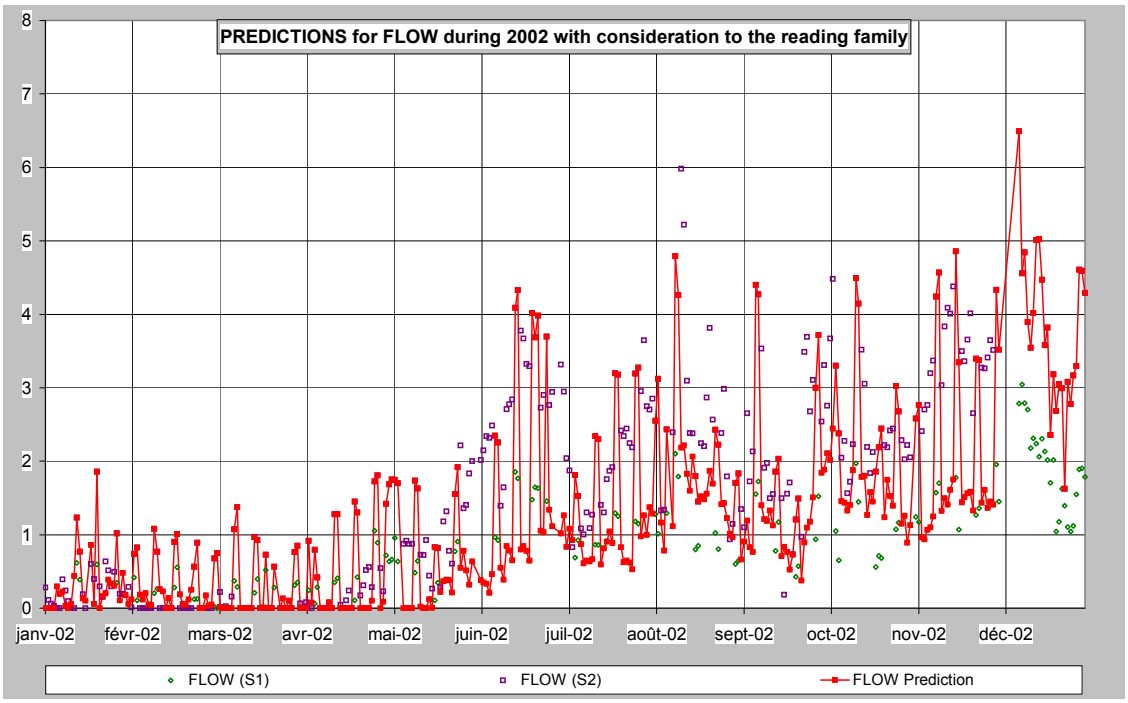

Figure 9: Prediction for FLOW readings during 2002

Numerical predicted values for F11 and the seepage flow for the year 2002 are included into the BW7C_Cob.XLS and BW7C_Cob.TXT files. Figures 8 and 9, which present predicted variations of F11 and FLOW respectively, have been extracted from the BW7C_Cob.XLS file.

5. CONCLUSIONS

The conditions of operation of MOTRU dam during the period of monitoring have been quite variable and it has therefore been necessary to reduce the calibration period to the last four years.

Two families of readings have been identified, which seem to be mainly depending on the day of the week, with exceptions. This feature imposed to separate all data in two families, S1 (mainly weekdays) and S2 (mainly weekend days), and to develop distinct models for each family.

The HST models have been built first, using the CONDOR software. Their adjustment is not very good, because the physical variables which physically control the seepage through the foundation do not follow the sinusoïdal 'S' functions of these models. However the HST model leads to the very important conclusion, that the long term trend for the seepage flow is a slow decrease at constant hydrostatic loading. This contradicts the initial assumption that internal erosion could be responsible for increasing leakages.

Good correlations between the flow measurement, piezometer F11, the water level and 6 other piezometers allowed the development of efficient multilinear regressive models, which were used to predict the F11 and FLOW readings for the year 2002. The expected accuracy of the prediction is ±50 cm for F11 and ±1 l/s for FLOW, maybe more if the 2002 readings have been wrongly classified between families S1 and S2.

REFERENCES

[1] A. Carrère, M. Colson, B. Goguel, C. Noret, "modelling: a means of assisting interpretation of readings" *("La modélisation : outil d'aide à l'interprétation des mesures")*, Q78 R63, 20th ICOLD Congress, Beijing 2000. (Vol. II, pp 1005-1037, and Vol. V, pp 355-362).

[2] A. Carrère, L. Mei, M. Hoonakker, E. Bourdarot, "Combined use of monitoring and modelling for the dam behaviour analysis" *("Apports combinés de l'auscultation et de la modélisation pour l'analyse et la compréhension du comportement des barrages")*, Q78 R64, 20th ICOLD Congress, Beijing 2000. (Vol. II, pp 1039-1061)

[3] Verbundplan "Interpretation of measurement results", Theme C, 6th International Workshop on Numerical Analysis of Dams, Salzburg, Austria, Oct. 2001.

[4] G. Willm "Les méthodes de surveillance des barrages au service de la production hydraulique d'Electricité de France", Q34 R30, 9th ICOLD Congress, Istambul 1967.

[5] A. Carrère, C. Noret "Interpretation of an arch dam behaviour using enhanced statistical models" Theme C, 6th International Workshop on Numerical Analysis of Dams, Salzburg, Austria, Oct. 2001.

STATISTICAL AND FINITE ELEMENT ANALYSIS OF MOTRU DAM SEEPAGE *

Vyacheslav Glagovsky, Tatiana Matroshilina, Vladimir Prokopovich, Galina Starodubtseva
B.E. Vedeneev Research Institute (VNIIG), St.-Petersburg, RUSSIA

SUMMARY: The results of the analysis of the seepage through an earthfill dam – foundation system of the Motru dam are stated. The model analysis has been performed by statistical and finite element methods. The calculations by finite element method were carried out with use of the program complex ABAQUS, Version 6.3. The data from monitoring system of the Motru dam for the period between 1997 and 2001 were used for modelling. The forecast of the total seepage flow through the dam right bank – foundation system and piezometric level in the selected well for the period of one year is given.

RÉSUMÉ: On présente les résultats de l'analyse de la filtration à travers le système "barrage de terre - fondations du barrage Motru". L'analyse du model a été effectué par la méthode statistique et celle des éléments finis. Le calcul par la méthode des éléments finis a été exécuté en utilisant le complex des programmes ABAQUS, version 6.3. Les données du monitoring sur la barrage Motru entre 1997 et 2001 ont été utilisées pour la modélisation. On donne le pronostic du flux total de filtration à travers le système " barrage de le rive droite – fondations" et celui du niveau piézométrique dans le puits sélectionné.

1. INTRODUCTION

An earthfill dam with clay core is located in the Motru river valley. The dam central and left bank foundation is composed by crystalline rock (granite, gneiss). In the dam right bank foundation the bed rock is covered with soft sedimentary deposits; sand clay, gravel and sandy gravel with 20-30 m thickness.

* L'analyse de la filtration du barrage Motru par la méthode statistique et celle des éléments finis

The dam crest length is 377 m; crest width 8 m; maximum height 48 m. The rate of slope**:** upstream 1:3; 1:4; downstream 1:2,25. Grout curtain at the dam foundation is used as a filter protection element.

The following monitoring devices have been installed to control the dam safety state:

- sedimentary geodetic marks at the dam crest;

- piezometric wells located at the right river bank (R27, R31, R38, R35, R42), at the dam right wing downstream toe (F13, F6, F11) and at the streamlet at a distance of 100-150 m from the downstream slope (F1, F5, F12);

- a water rate measurement device intended to measure the water seepage through the dam right wing and foundation.

Air temperatures, snow and rainfall, upstream and piezometric water levels have been monitored on the daily level beginning from 1990. Seepage flows in the dam right bank sedimentary deposit have been identified by means of radioactive indicators.

Monitoring of seepage water turbidity has detected internal erosion processes at the dam foundation.

A considerable amount of data obtained in full-scale monitoring at the Motru dam has been provided for analysis. However, it is necessary to state that the materials provided lack data on the full-scale monitoring which would allow to control seepage strength of the dam body and seepage protection devices as a piezometric network in the dam core and at the foundation is absent.

In order to detect possible directions of concentrated seepage (piping) in the dam body and foundation it is advisable to carry out monitoring of the seepage flow temperatures in piezometric wells (along the bottom-to-surface height) in addition to measurements of the earthfill suspension particles content (turbidity). In parallel with seepage flow temperature measurements it is advisable to monitor water temperatures at the water boundary (reservoir) and at drainage facilities and seepage locations. It is also advisable to measure water temperatures in the reservoir at the raid verticals at depth from the bottom to the surface taken in several test points.

2. PROGNOSIS BY MEANS OF STATISTICAL METHODS

The value of seepage through the dam body is determined mainly by water head (down and upstream water levels). It also depends on the amount of rainfalls, air temperatures and other factors. An impact of different external factors varies in time lag values. For example, a seepage rate at the same upstream level depends on the time related level of change; results at water elevation and reservoir draw down can differ [1].

The data of piezometric monitoring are analysed both for each individual piezometric level and for measurement ranges as well as for the dam and foundation in total.

Time related level change curves, depression surface, equal pressure lines in the dam body, foundation and bank abutment drawn based on the full-scale monitoring data. The curves of piezometric water level in relation to the upstream level are drawn on the basis of data of full-scale monitoring in the established dam operation mode. A confidence interval zone is singled out then, measurement errors and time lag values are taken into account. Surpass of the measurement points beyond the confidence interval indicates changes in the seepage process or instability in the device operation.

The statistical method of full-scale data analysis is based on defining an empirical relation between the diagnostic parameters and factors modifying them. The sought empirical relation can often be presented as a total of individual factor functions. These functions should possibly represent the character of a factor impact. Such a statistical model contains coefficients of factor variables which values are found in a manner that the model should meet the results of full-scale monitoring in the most efficient way, that is with minimum error value (normally as a mean square deviation value).

A polynomial relation is often used for the function showing the impact of the head of water upon the parameter under consideration. In many cases one or two terms are sufficient. The impact of temperature is usually approximated by a periodical time function. However, the ambient air temperatures are not factored in calculating the flow rate value for the earthfill core dams.

A function showing the facility operation time impact is sometimes introduced.

After unknown coefficients are defined by the least square method a significance value for the coefficients obtained is estimated with using the available full-scale data. The terms with negligible coefficients are ruled out and coefficients of the model corrected are defined.

From the point of technical diagnostics of an earthfill dam it is important to reveal an irreversible constituent basing on the full-scale data processing. The constituent describes the time related seepage changes. The presence of this constituent testifies changes in the seepage process during operation. An increase in seepage rate can be found during the internal erosion process, and a decrease at mudding.

A difference between the water levels in drainage and nearest piezometric level can be used as the criterion in estimating seepage in the dam body. Any time related change in the difference attests to some processes taking place in the dam, either internal erosion or silting of reverted filters.

In order to describe such parameters as the seepage rate and change of the piezometric level in the selected downstream well, the statistical model of seepage process of the Motru dam can be represented as a total of functions. This total shows an impact of the certain independent factors (the upstream level and rainfalls deemed as the most significant) upon the parameters researched.

Application of the available measurement data of the piezometric levels in several wells is possible for building up a statistical model of the piezometric level in

the selected well. These data have already taken into account the impact of independent factors. A combination of both approaches is also possible.

We have used the data of full-scale monitoring obtained in the period from 1997 till 2001 in building up the statistical model due to the fact that in 1996 the normal upstream level was lowered and the facility operation mode modified.

Different statistical models have been built up, estimation of individual constituents has been carried out for selection of the most efficient regression model by means of applying the backward elimination method or forward selection methods. Both mutual correlation between the piezometric levels data in individual wells and significance of the constituents have been verified with applying Student's t-distribution and F-criterion.

3. PROGNOSIS OF PIEZOMETRIC LEVEL BY MEANS OF STATISTICAL METHOD

One of the tasks set by the Formulator was to develop a prognosis of the water level in the piezometric well F11 for the period from 01.01.2002 till 31.12.2002.

The regression analysis methods are efficient in analysing the full-scale monitoring of the seepage mode. Setting up relationships between the defined parameters by means of approximation of the linear functions is reduced to obtaining a confidence interval for measurement of the value under consideration.

In fig. 1 a scheme of piezometers location in the dam right wing foundation is given.

In fig.2 the arrows indicate the direction of seepage flows obtained according to the results of monitoring by means of radioactive indicators.

In fig. 3 the surfaces of the level built up according to the piezometers data are shown, at the high (23.04.2001) and low (26.04.2001) upstream levels.

In considering the seepage flows direction one can assume that the water level in the F11 piezometer, besides the reservoir water level (RWL), is impacted by the by-pass seepage flows (R35, F13 and F6) and by the streamlet seepage flows (F5 and F12).

This assumption is proved by three-dimensional graphs of the depression surfaces (fig. 3) built up on different dates at high (474,08 m) and low marks (467,91 m) of RWL. The following cases have been considered:

at the high upstream level (mark 474,08 m) water level in piezometer R35 – low (mark 473,35 m);

- at the low upstream level (mark 467,91 m) water level in piezometer R35 – high (mark 476,45 m).

The water level marks in piezometers F1, F5, F6, F12, F13, R35, F11 and RWL on different dates were analysed and used for model development.

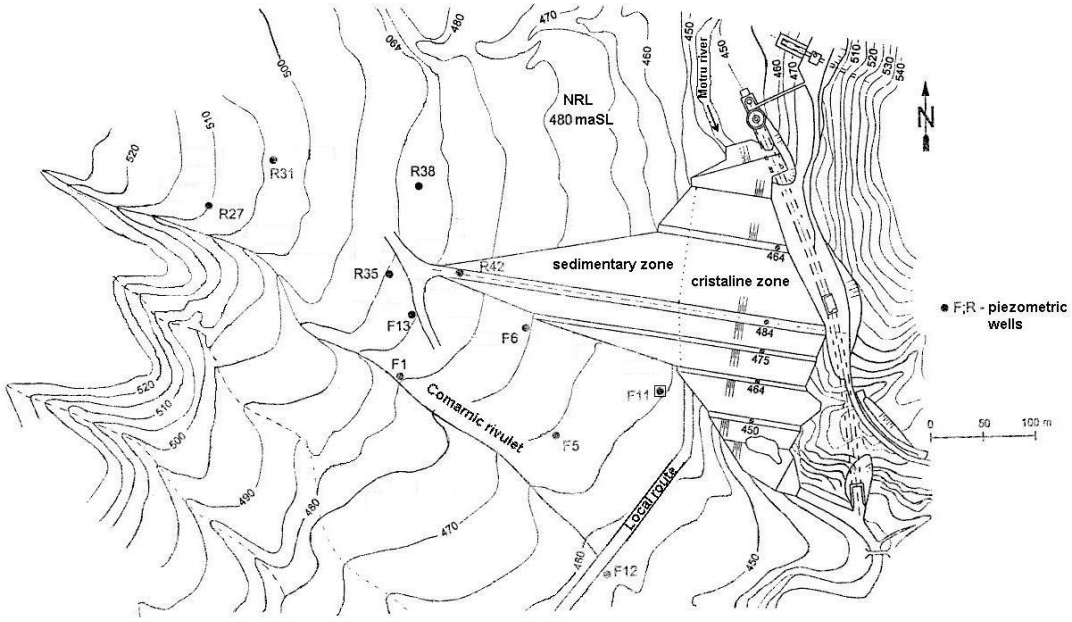

Fig. 1. Motru dam – Locations of some piezometric wells

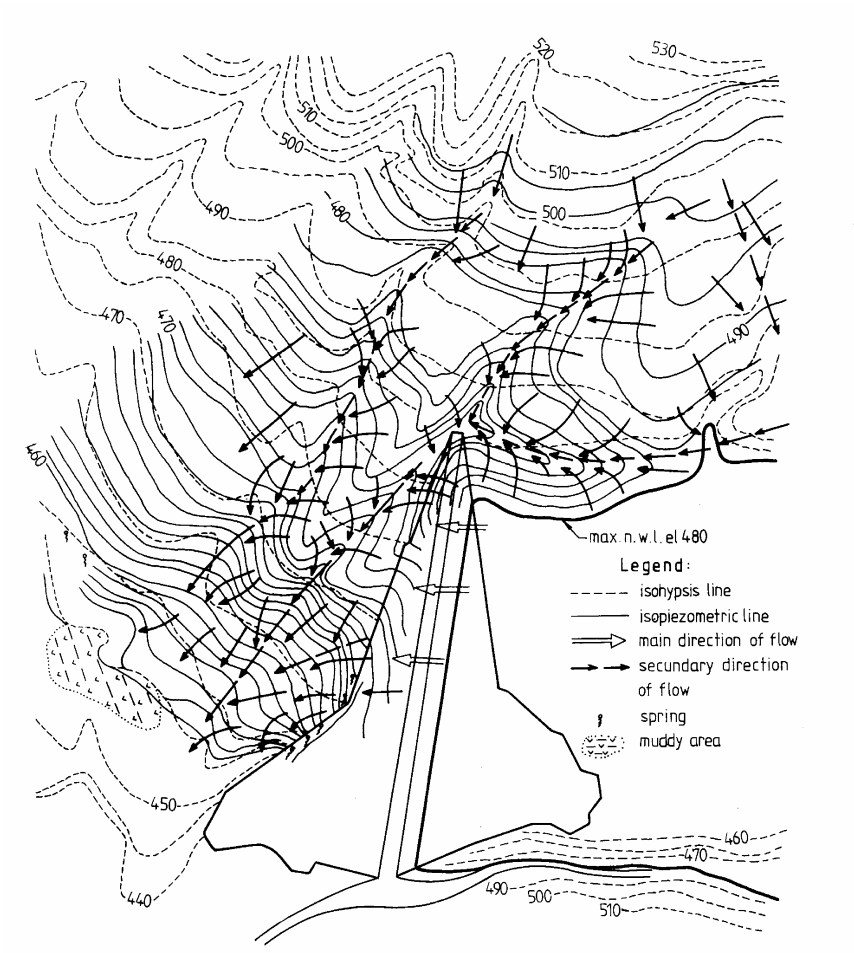

Fig. 2. Seepage spectrum through dam right bank corresponding to full reservoir evaluated with radioactive tracers

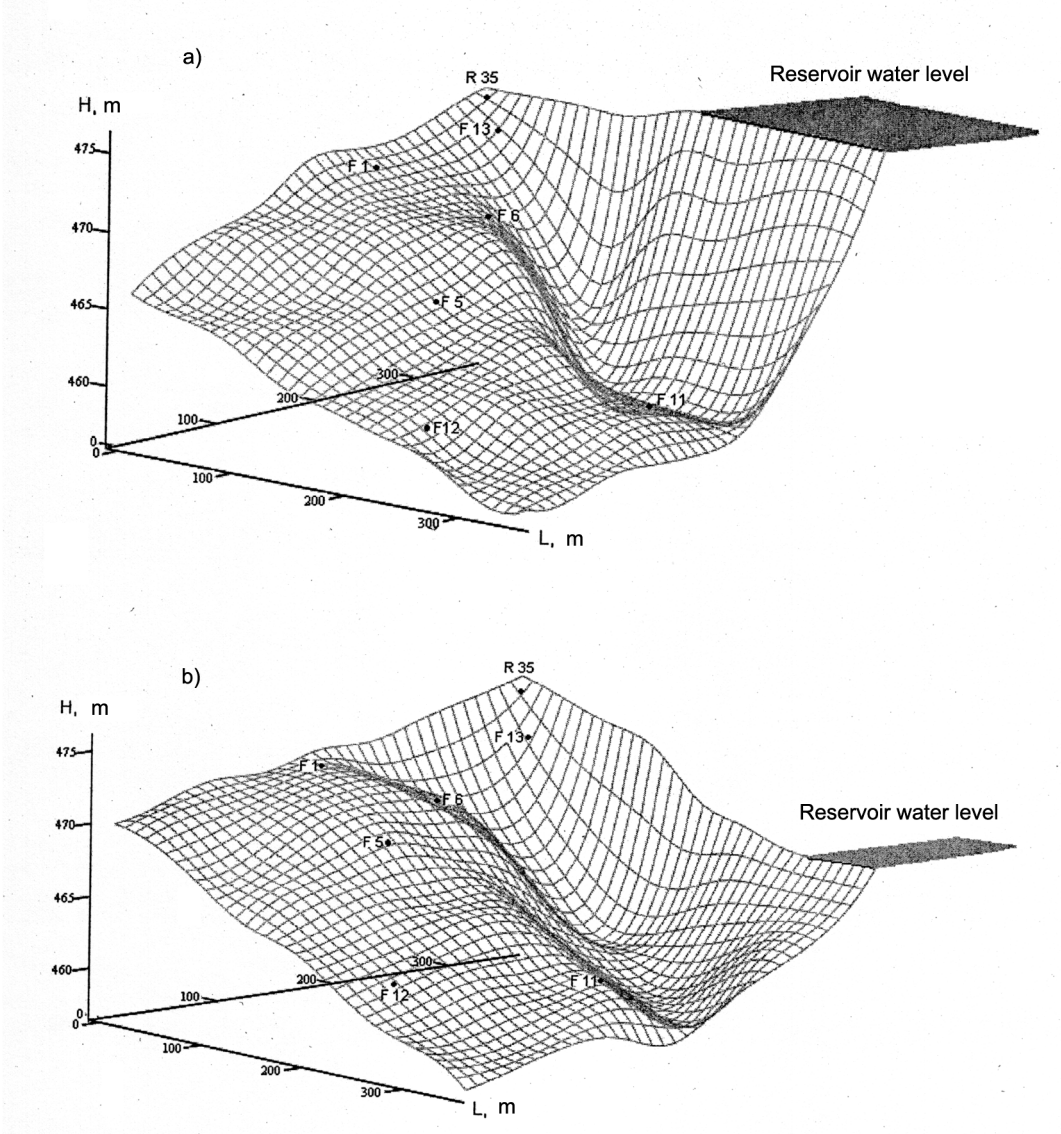

Fig. 3. Water level in piezometric wells at: a) 23.04.2001; b) 26.04.2001

In order to carry out a prognosis of the water level in piezometer F11 for the period from 01.01.2002 until 31.12.2002 a linear mathematical model can be applied as quite efficient. This model shows a relation between water levels in the F11 piezometer and the reservoir water levels and water levels in piezometers R35, F13, F6, F1, F5 and F12.

Empirical coefficients of the model were defined by the least-squares method.

The mathematical model allows forecasting the water level in the F11 piezometer, defining a mean quadratic deviation for the measurement results obtained from the estimated values and providing a numerical value for the results of a regular measurement procedure.

During the calculation procedure the full-scale monitoring data obtained in monitoring the water levels in the reservoir and in the piezometers for the period from 1997 until 2001 have been applied.

In fig. 4 a graph of the time related water levels measured in the F11 piezometer in 2001 is shown. Here also the water levels in the F11 piezometer are given which have been calculated according to an equation allowing for a relation of the F11 piezometer data to the reservoir water level only, and estimated according to the derived equation.

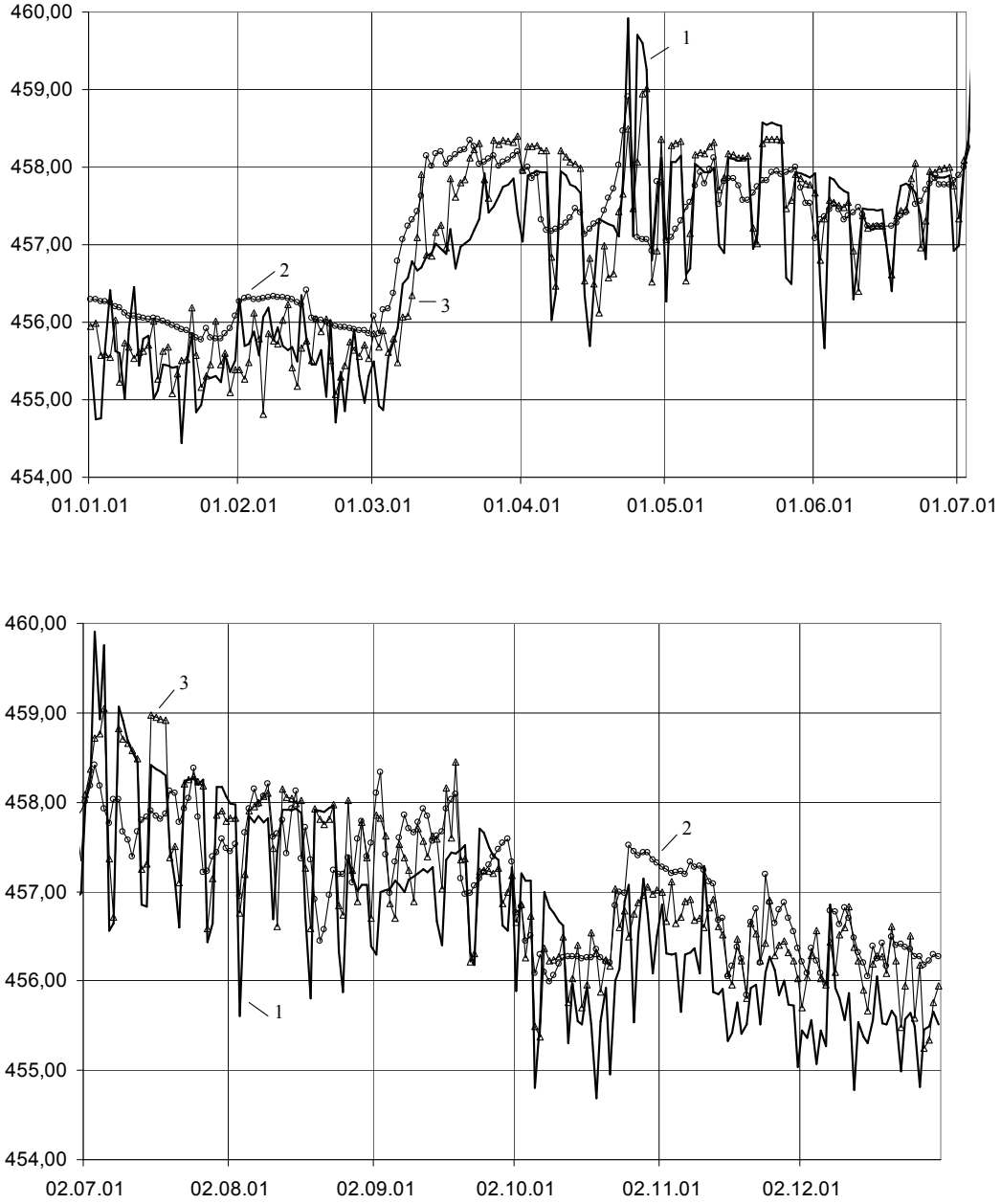

Fig. 4. Time histories of the water level variation in F11 piezometric well: 1 – measured; 2 – calculated as function of RWL; 3 – calculated according to the derived equation.

In fig. 5 a graph of the time related water levels forecast in the F11 piezometer is given for 2002.

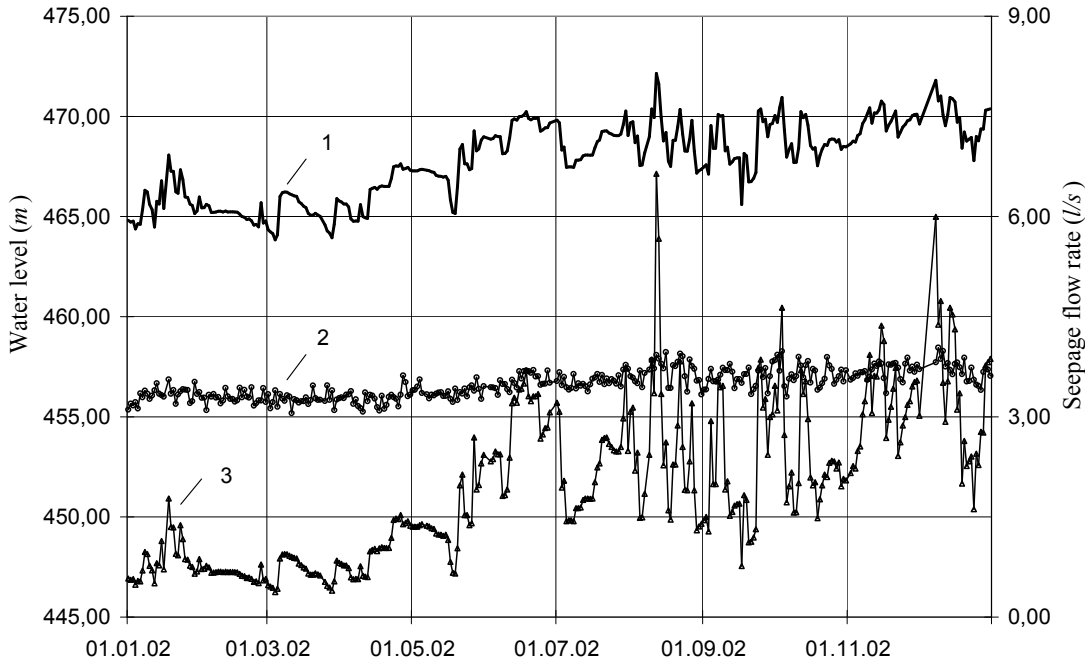

Fig.5. The prognosis of the piezometric level and seepage flow rate:
1 – reservoir water level; 2 – forecast piezometric level in F11 well; 3 – forecast seepage flow rate.

4. PROGNOSIS OF FLOW RATE BY MEANS OF STATISTICAL METHOD

The second task set was to forecast rates of water seepage through the right dam wing and foundation for the period from 01.01.2002 until 31.12.2002.

The value of seepage flow rate is a working and integral index of an earthfill dam and foundation state. A measurement range is available in the Motru dam intended to control the rate of seepage water through the dam right wing.

The value of rate depends mainly on the water head. The rate – head relation mathematical model can be presented at the simplest as a power function or polynomial approximation of the rate - head relation. Empirical coefficients of the model were defined by the least-squares method after processing the monitoring results (for as long as 5 years).

The mathematical model obtained allows prognosticating the seepage water rate measurement results in relation to the water head, defining a mean square deviation of the monitoring results from the estimated values.

In fig. 6 the seepage rate – head relation is given. The confidence interval zone allowing for the measurement error is selected in the graph. The result of each regular measurement procedure is plotted in the graph. If a point falls into the confidence interval it attests to seepage flow stability. Location of a point below the confidence interval attests to a decrease of seepage. Falling of a graph experimental point above the confidence interval attests to a increase of dam permeability (for example, as a result of internal erosion development or a crack in the dam body).

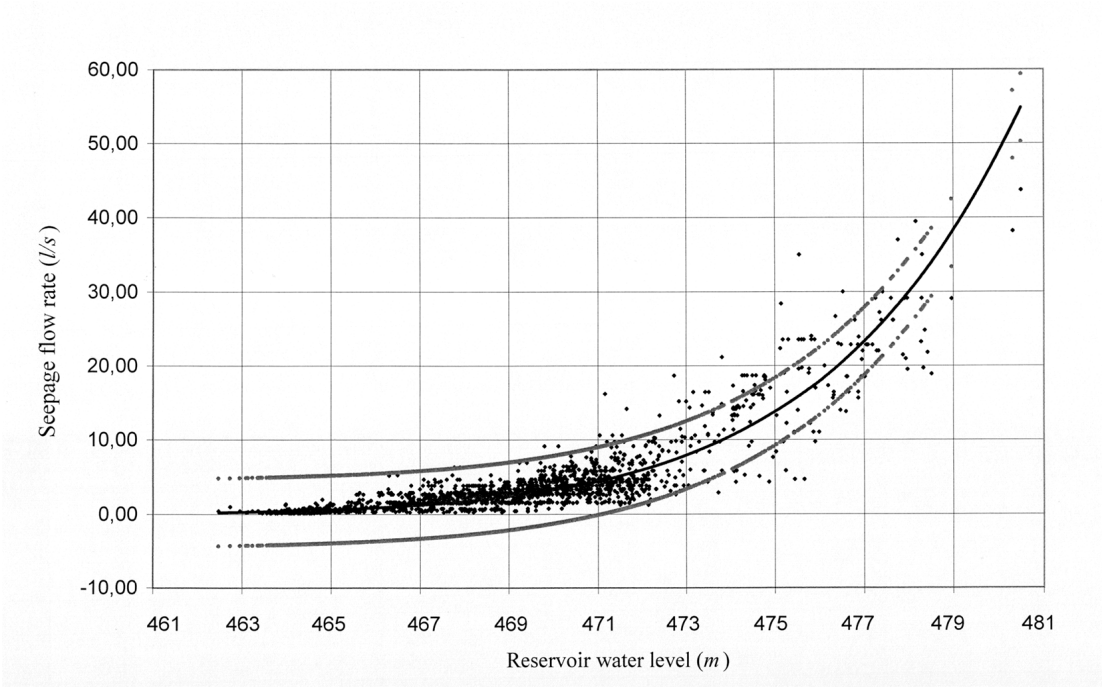

Fig. 6. Seepage flow rate – reservoir water level relation.

In fig. 7 a graph showing the reservoir water level and time related measured flow rate change is given (for the year 2001). Here are the rate values estimated according to the derived equation.

A graph showing time related flow rate forecast in the year 2002 is given in fig. 5.

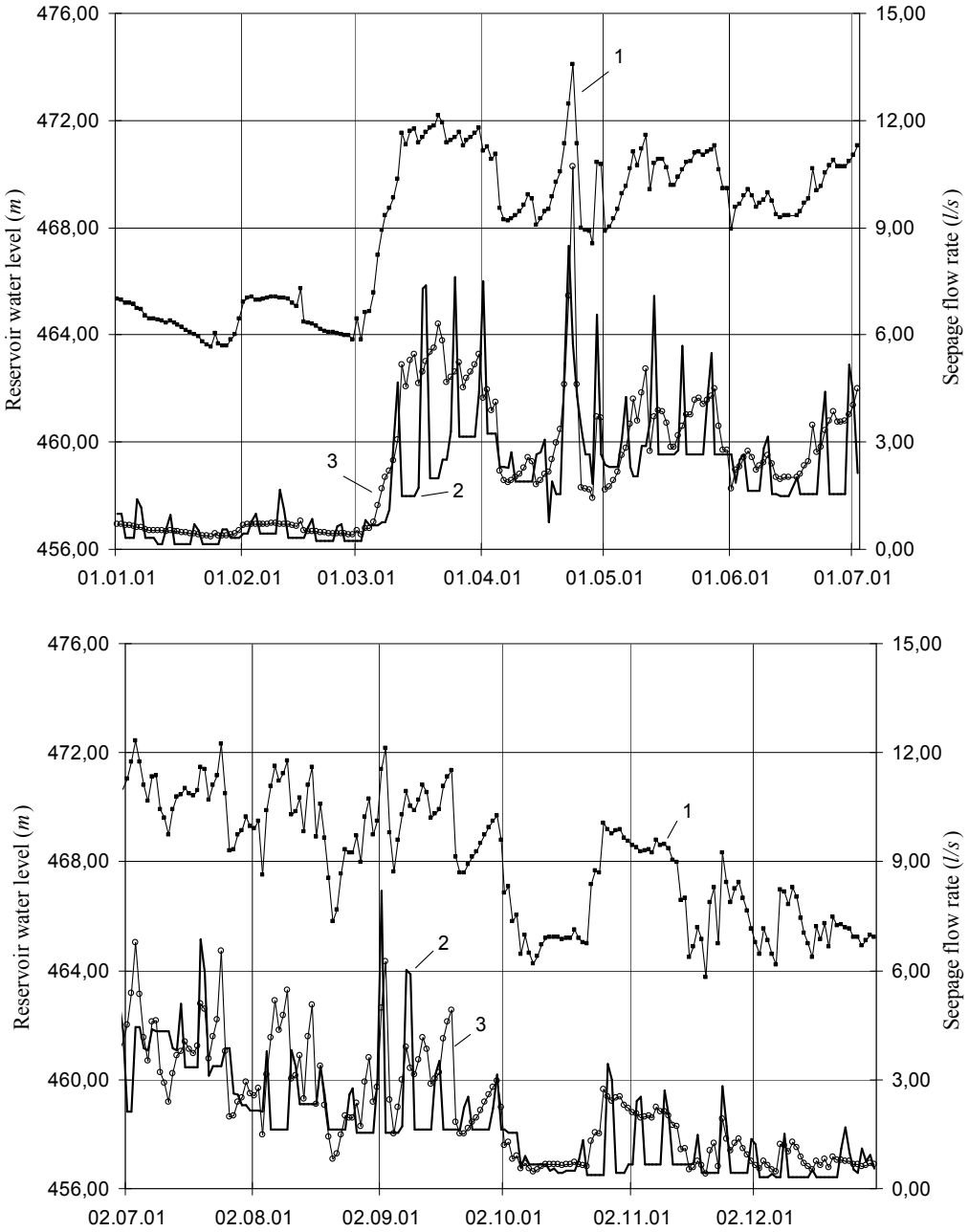

Fig. 7. Time histories of the seepage flow rate:
1 – reservoir water level; 2 – measured seepage flow rate;
3 – calculated according to the derived equation.

5. MATHEMATICAL MODELLING OF SEEPAGE BY THE FINITE ELEMENT METHOD

Estimations of the seepage mode in the dam - foundation system by the finite element method have been carried out with applying the ABAQUS software system, 6.3 version [2]. The system allows to locate a free seepage surface in the dam body and use

its advantages in making estimations with account of both fully and partially water saturated fields. The depression surface is located at the boundary of a fully saturated part of the field modelled. Thus, the flow rate is defined as a pore pressure function**.** This approach is conspicuous for its ability of defining capillary zones over the depression surface. The first, second and third types of conditions can be considered as the boundary conditions. Distributed flows and surface-based flows are available for elements with pore pressure degrees of freedom.

On the basis of calculations made with applying the primary mathematical model and full-scale monitoring data a specified model was supposed to be developed and model parameter calibration was supposed to be carried out. For the modelling procedure the Motru dam full-scale monitoring data obtained for the period from 1997 until 2001 were used. After model calibration the prognosis estimations were supposed to be carried out for defining a seepage rate and piezometric level in well F11 for the year 2002.

A porous medium is modelled approximately in ABAQUS system by attaching the finite element mesh to the solid phase, liquid can flow through this mesh. Darcy's law describes the liquid flow. For the liquid phase the continuity equation should be met which is attained in an approximate manner in the finite element model through applying an excess liquid pressure as the additional nodal variable interpolated over the elements. The equation is integrated in time with applying the Euler backward method.

In the ABAQUS software system a solution of fully coupled consolidation problems is provided for fully or partially water saturated porous media. In solving the seepage problem we take the liquid flow into consideration only. Skeleton deformation is neglected. Due to this all displacement degrees of freedom are prescribed to be zero. However, in the more general analysis stress and deformation in the soil mass should be considered.

A solution of a non-steady state problem of seepage is done by applying a step-by-step integration procedure in time. As the initial conditions either a steady state problem solution or some initial water head field specified in some nodes and interpolated onto the entire mesh can be used. For each time step the seepage characteristics are defined by the water head values obtained at a previous step.

For analysis of the Motru dam seepage a three-dimensional finite element model (model 1) containing 5862 nodes and 4 8882 elements was developed (total number of variables in the model - 23448). The C3D8P type elements were used – 8-node brick, trilinear displacement, trilinear pore pressure (fig. 8a). The finite element mesh for model 1 is given in fig. 9.

The estimations have shown that this finite element model does not allow to do the model calibration with sufficient precision applying the available well piezometric levels data.

Then a finite element model (model 2) was developed which contained 87436 nodes and 54815 elements (total number of variables in the model - 569004). The C3D10MP type elements were used – 10-node modified displacement and pore pressure tetrahedron, hourglass control, with three additional displacement variables and one

additional pore pressure variable (fig. 8b). The finite element mesh for the model 2 is represented in fig. 10. The mesh features considerable condensation in the downstream side area and at the dam downstream foundation.

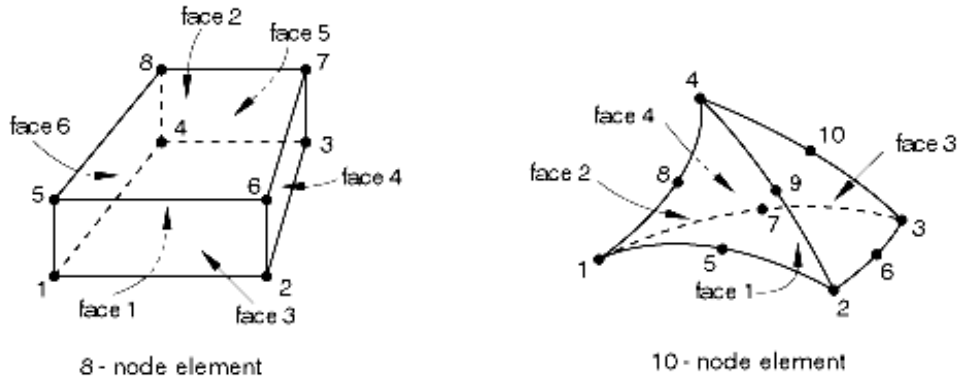

Fig. 8. Finite elements description

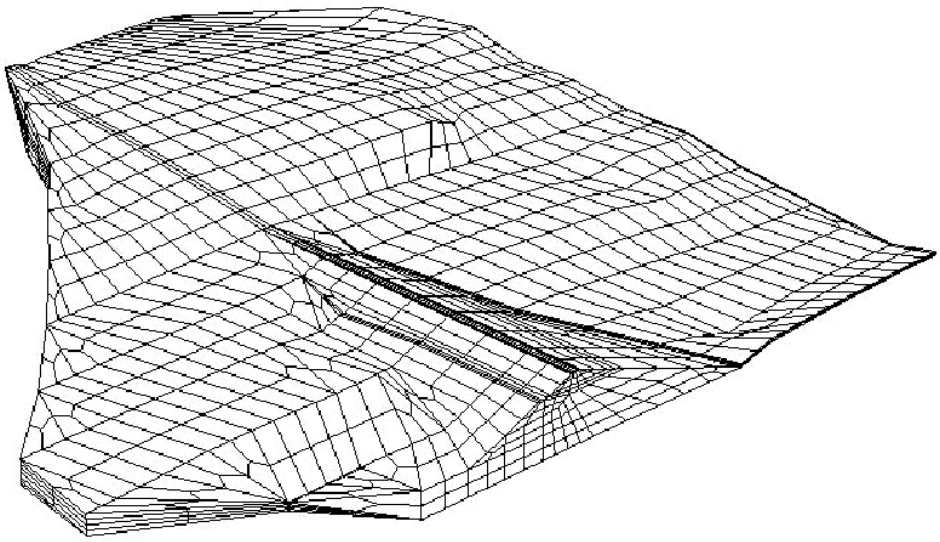

Fig. 9. Finite element mesh for model 1.

The model analysis has proved to be quite laborious and computer time consuming. Due to this fact the model calibration and prognosis estimations have not been completed up to now. But we hope to continue work and to present results of analysis at the Workshop.

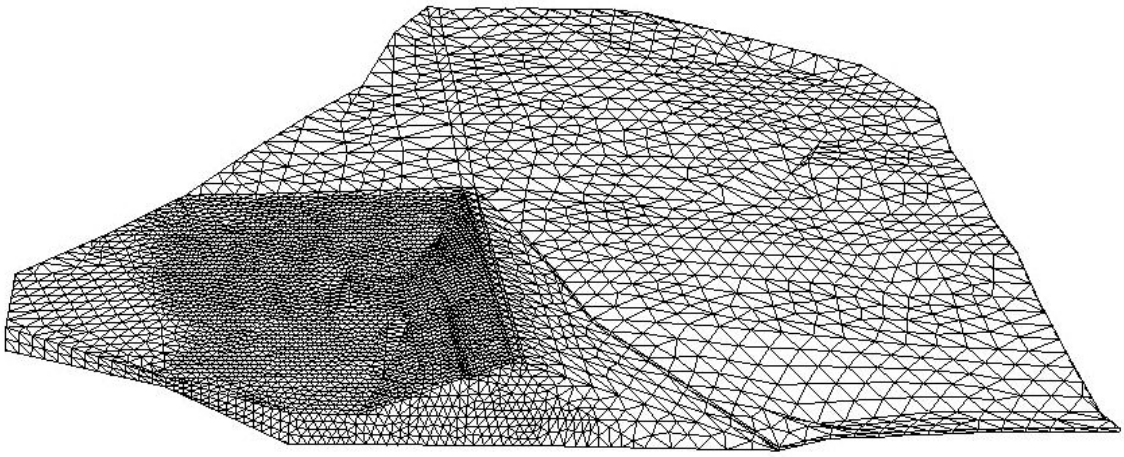

Fig. 10. Finite element mesh for model 2.

REFERENCES

[1] Malakhanov V.V. – Technical diagnostics of embankment dams. Energoatomizdat, Moscow, 1990 (in Russian).

[2] ABAQUS/Standard User's Manual, Version 6.3, Volumes I-III.

NUMERICAL MODELING OF AN UNSTEADY WATER FLOW THROUGH A ROCKFILL DAM AND ITS FOUNDATION ROCK

Gheorghe LAZAR, ass.prof.dr.eng., Serban-Vlad NICOARA, lect.dr.eng.
"Politehnica" University of Timisoara, ROMANIA

SUMMARY: The paper presents the numerical modeling of the unsteady water flow through a 3D permeable domain representing a rockfill dam with a clay core, together with its foundation soil and the mountain sides. There is considered the finite element method, in the ANSYS program package. In the finite element analysis a 3D element (SOLID 70 – Thermal) is considered, able to model the space thermal conductivity through a solid domain. By this option and considering the proper analogy, the thermal parameters are interpreted as the fluid flow parameters. The mentioned option for the finite element (Solid Thermal) alows a non-linear modeling of the unsteady water flow in the 3D porous space. Based on the developed numerical modeling the water flow and level variation forecast at the F_{11} well is obtained.

1. GENERAL CONSIDERATIONS

According to the subject proposed by the theme C [1], there is to be modeled the unsteady water flow through a porous spatial domain representing a rockfill dam with a clay core (the Motru Dam) placed on a soil consisting of crystallized rocks (granite, gneiss) in the central zone and sedimentary rocks at the mountainsides (as the profiles 1 to 12 from figure 1.a revealed). The figures 1.b and 1.c present the current dam cross section. A drainage system was performed downstream the clay core, the infiltrated water being evacuated by a pipe placed in the central zone. The following data are considered as known: the spatial geometry of the dam together with its foundation place and the right mountainside, the permeability ratios for the involved materials, and the boundary conditions.

As stated by the theme notifications, a forecast regarding the infiltrated water flow captured by the drainage pipe downstream the clay core, as well as the water levels in the F_{11} observation welling downstream of the dam is to be given along the specific period of time January 1st, 2002 – December 31st, 2002.

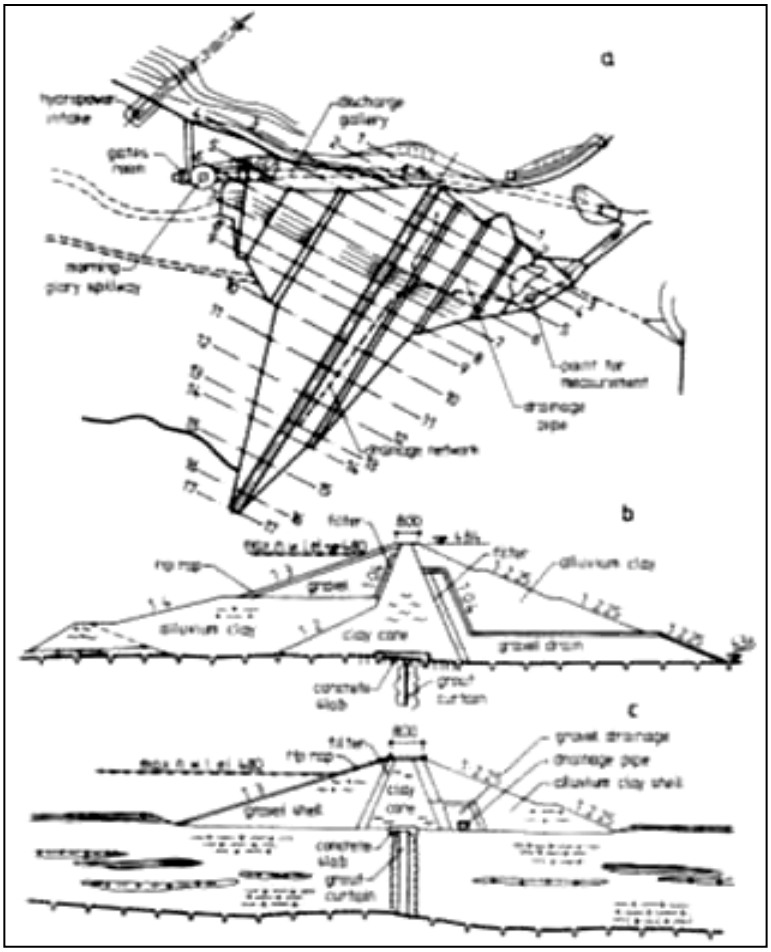

Figure 1 Motru Dam: a- layout, b- typical cross section in central zone, c- typical cross section in right wing

2. DOMAIN MESHING, BOUNDARY CONDITIONS

The study model proposed for the analysis [1] was given as follows: by the "nodes.txt" file - for the model's nodes defining; by the "elements.txt" file - for defining the model's elements, for connecting the nodes and assigning the material numbers; by the "material.txt" file - for assigning the material characteristics; by the "control points.txt" file – for specifying the coordinates of the checking points (wells); by the "monitor.txt" (or "monitor.dbf") file – showing the water levels variation, rainfalls monitoring, and variation of the water flow evacuated by the drainage pipe.

The entire meshed domain is showed in the figure 2, which presents an aerial view, a downstream side view and a detail from a longitudinal section at the dam middle in order to visualize the five types of material.

In order to develop a 3D model of the unsteady water flow through the given domain the ANSYS package of programs was employed. The finite element type considered by the authors for the proposed analysis is Brick Thermal – SOLID 70 [2]. Using this finite element type, the program is able to model a thermal conduction through a solid, which is similar to the required water flow analysis. By analogy [3], the thermal parameters are taken as parameters for a fluid flow through a porous

environment. The choice of the Solid Thermal type of element allows the modeling of a transitory water motion through a porous spatial domain, by following the specific boundary conditions:

- a daily water level variation in the reservoir along the period of time in between January 1st, 1990 and December 31st, 2002;
- a daily rain quantity variation falling on the modeled area;
- a daily water level variation at the given wells (F_1, F_5, F_6, F_{11}, F_{12}, F_{13}, F_{27}, F_{31}, F_{35}, F_{38}, F_{42}) along the mentioned period of time. (It is mentioned that the water level variation at the F_{11} welling is known only until December 31st, 2001.)

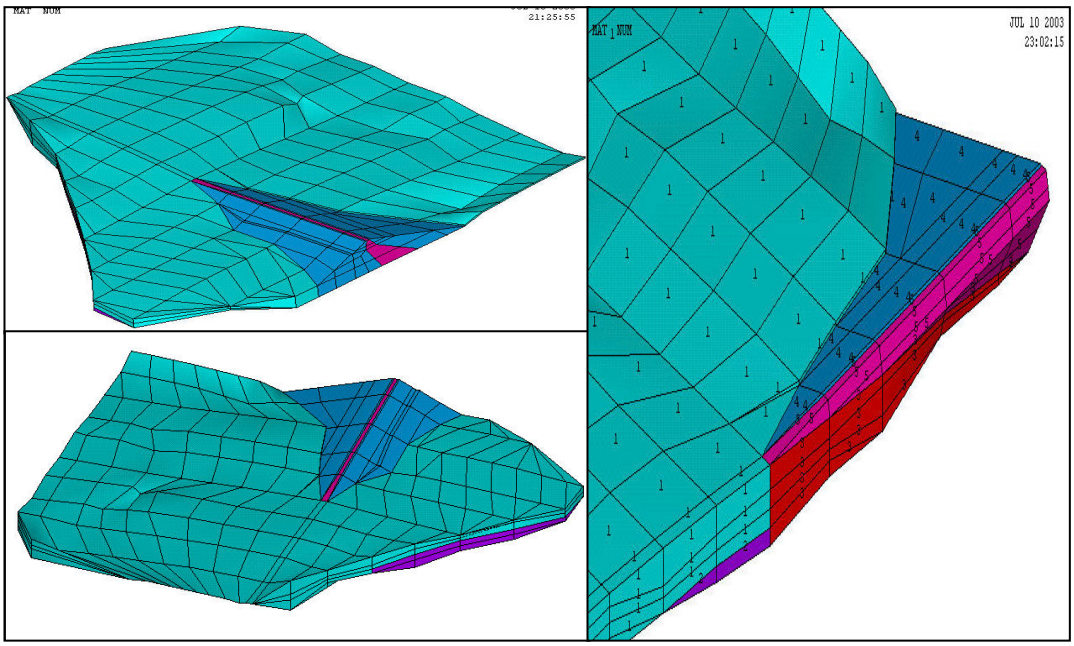

Figure 2 Views of the analysis meshed domain, and a detail showing the involved materials

The permeability coefficients characterizing the materials involved by the current study are presented in table 1.

Table 1

Element type	Material number	Material type	K_{xx} ,K_{xy} [m/s]
SOLID 70	1	Clayey alluvium	5.00E-04
	2	Gravels and boulders	2.50E-03
	3	Grout curtain in alluvium	1.00E-05
	4	Dam earthfill	3.47E-04
	5	Dam clay core	1.00E-08

The figure 3 presents the wells location on the right mountainside and downstream the Motru Dam.

The considered cyclic numerical modeling uses a one day time step, knowing the initial conditions for each interval start. By a transitory modeling of a time step Δt = 1/(2×day) the parameters values are obtained at the interval end, values becoming the initial conditions for the following interval.

Considering a current cycle, the figure 4 presents the typical boundary conditions (wells water levels, rainfall at the elements surface, water level at the

reservoir nodes), which will determine the initial conditions for the following transitory analysis interval.

Figure 3 Location of some piezometric wells at Motru dam

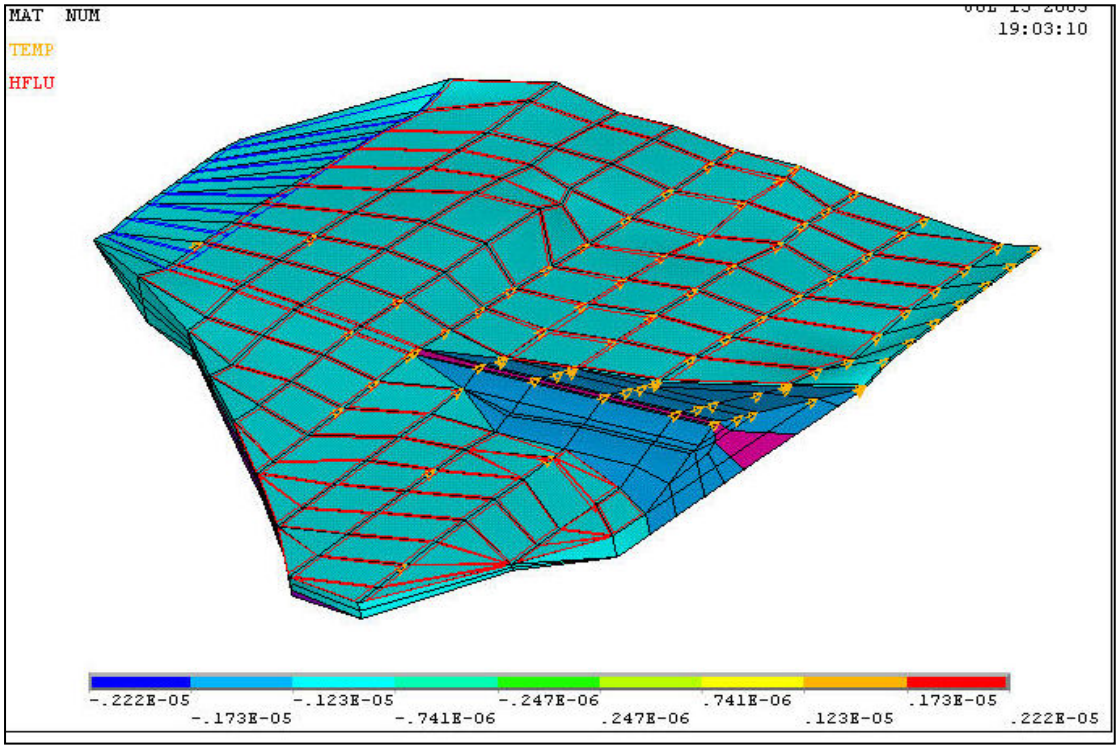

Figure 4 Analysis meshed domain and boundary conditions

The figure 5 presents the water levels variation for three representative nodes in the analyzed domain (reservoir – node 342, well F_6 – node 356, and well F_5 – node 459), along the period of time in between January 1st, 1990 and December 31st, 2001.

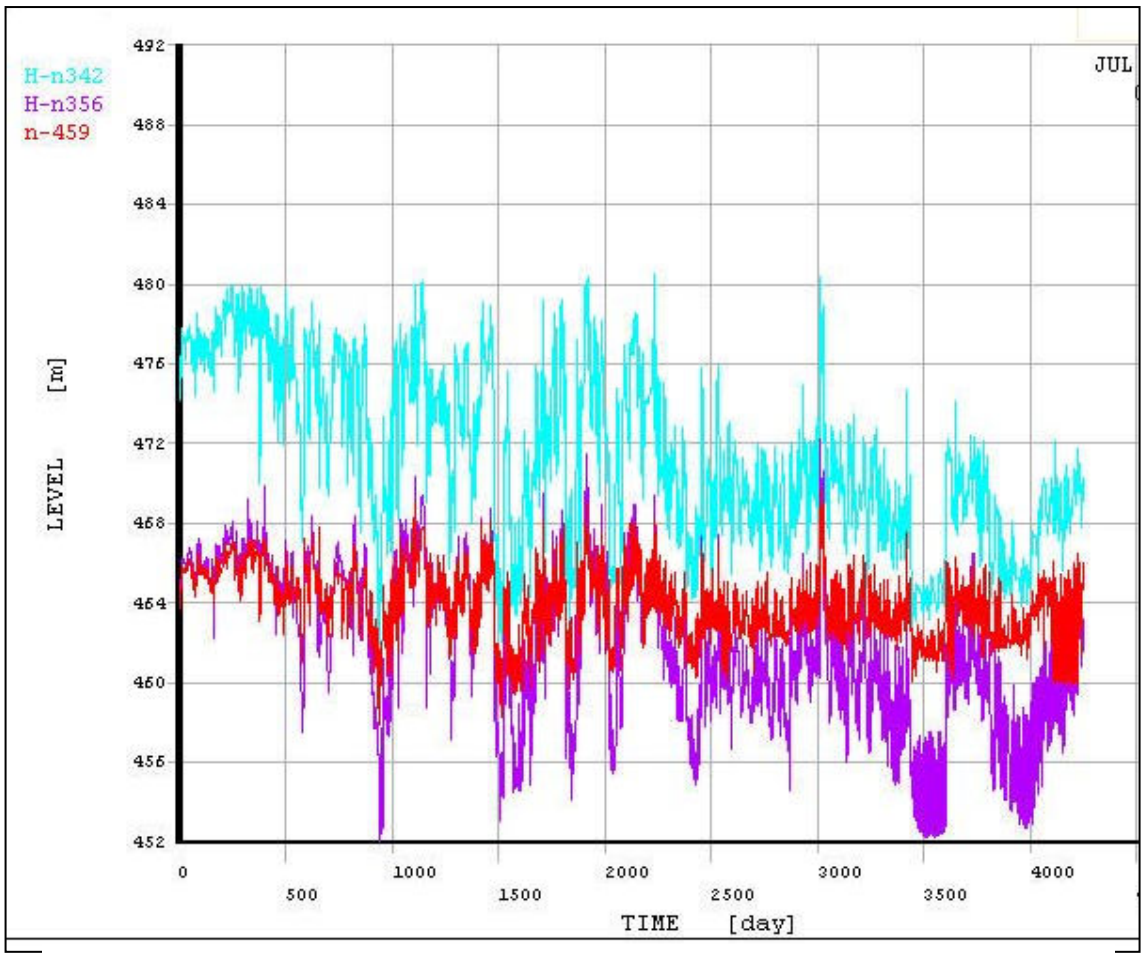

Figure 5 Water levels variation in between January 1st, 1990 and December 31st, 2001, node 342 – the reservoir. node 459 – the F_5 well. node 356 - the F_6 well

3. RESULTS PRESENTATION

The analyzed model was cyclic loaded by 4249 times, one cycle being equivalent with one day time step. Along each cycle a numerical simulation in transitory regimen was considered at a time step of $\Delta t = 1/(2\times\text{day})$, meaning in two steps.

In a I-st stage, the unsteady infiltration through the mountainside and the dam was modeled by following the mentioned boundary conditions, obtaining thus the water level variation at the F_{11} well along the time period in between January 1st, 2002 and December 31st, 2002 (the level variation in the well being known in between January 1st, 1990 and December 31st, 2001). From the figure 6, presenting this water level variation in the F_{11} well, it can be noticed that for a free working regimen (corresponding to the drainage system blocking) the water level rises about 7 m with respect to the situation along the previous three years.

In the II-nd stage of the analysis, the obtained level configuration at the F_{11} well (for the interval January 1st, 2002 - December 31st, 2002) was transferred down with a constant value of 7 m, being considered further on as a known forecast. The values and graphic processing was performed by the help of the EXCEL program, the outcome being presented by the figure 7.

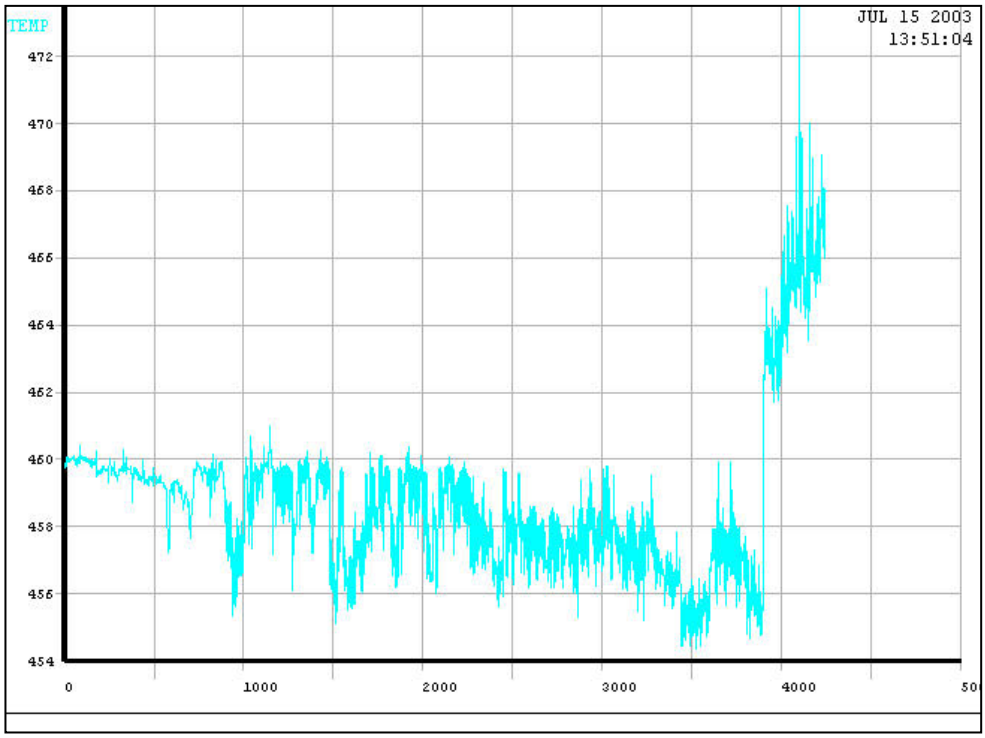

Figure 6 Water level variation at F_{11} well – node 729,
January 1st, 1990 - December 31st, 2001, given,
January 1st, 2002 - December 31st, 2002, estimated for specific working conditions

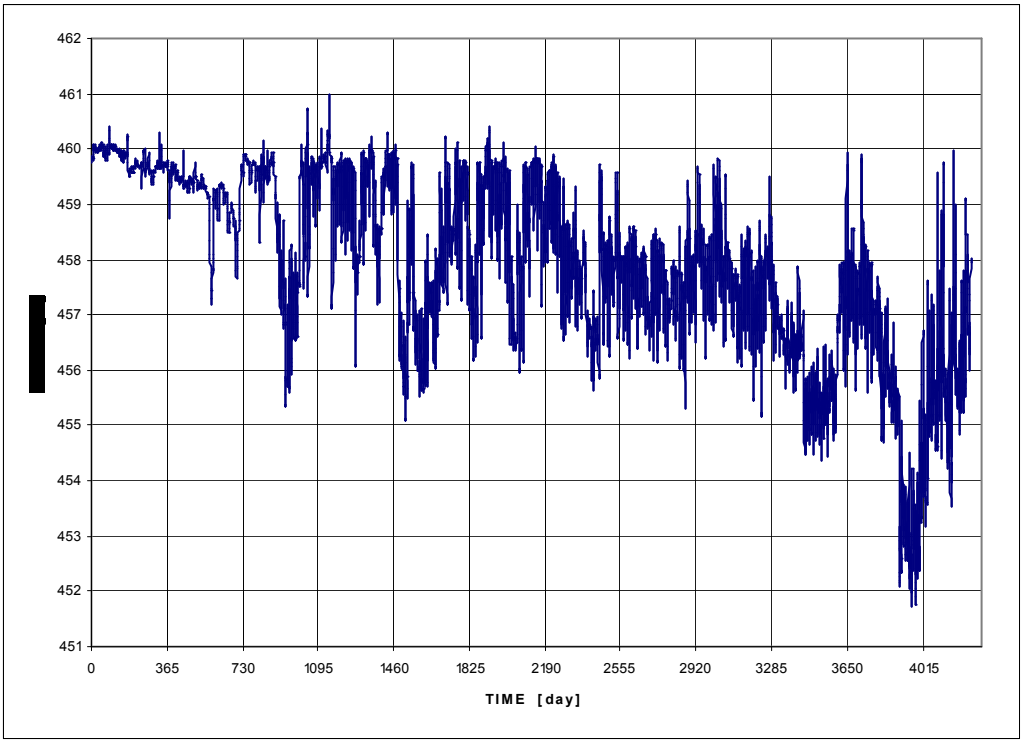

Figure 7 General considered water level variation at the F_{11} well – node 729

The selection of the cross section along the interception drainage and evacuating pipe (11 and 12 profiles from figure 1, meshing nodes from 497, 498 to 517, and 518) requested a calibration check of the model. For this purpose, the period of time in between January 1st, 1990 and December 31st, 1990 was considered. Knowing the pipe evacuated water flow, the water flow values at a 10 days time step were obtained by a numerical modeling. Both, the given and the obtained, variations of the water flow values are presented by the figure 8. The phase difference of the two numerical rows can be noticed.

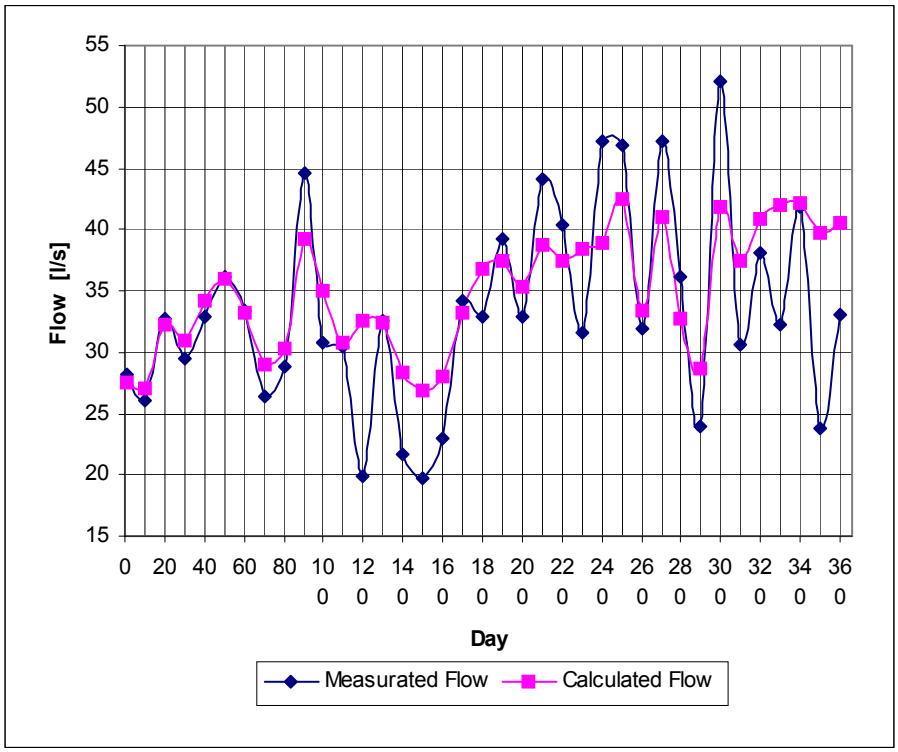

Figure 8 Calibration check regarding the pipe evacuated flow

In order to estimate the water flow captured by the drainage system and downstream evacuated by the interception pipe, a shorter modeling period of time was considered (January 1st, 2000 – December 31st, 2002). In this way a more detailed variation is to be obtained.

The graphical developments of the reservoir water level and the forecasted F11 well water level for the above mentioned period of time are presented by the figure 9.

The values for the hydraulic head and specific water flow at each time step along the period of time in between January 1st, 2001 and December 31st, 2002, were obtained by a numerical modeling, in all the meshing nodes. Following a contour graphic processing, the figure 10 presents the levels development and the figure 11 presents the specific water flow development at the end of the period of time (analyze moment 4249, meaning December 31st, 2002).

The specific water flow variations in all the nodes from the interception cross section were obtained by post processing operations along the transitory analysis. The figure 12 presents few typical water flow variations in the interception cross section.

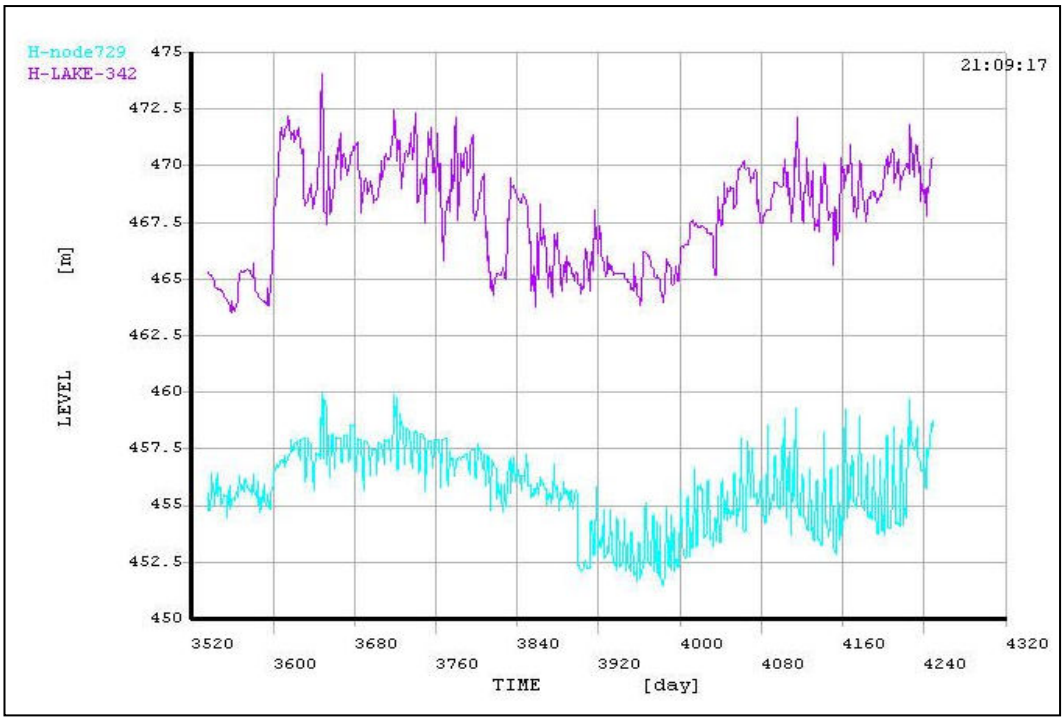

Figure 9 Reservoir (node 342) and F_{11} well water level variation, January 1st, 2001 - December 31st, 2002

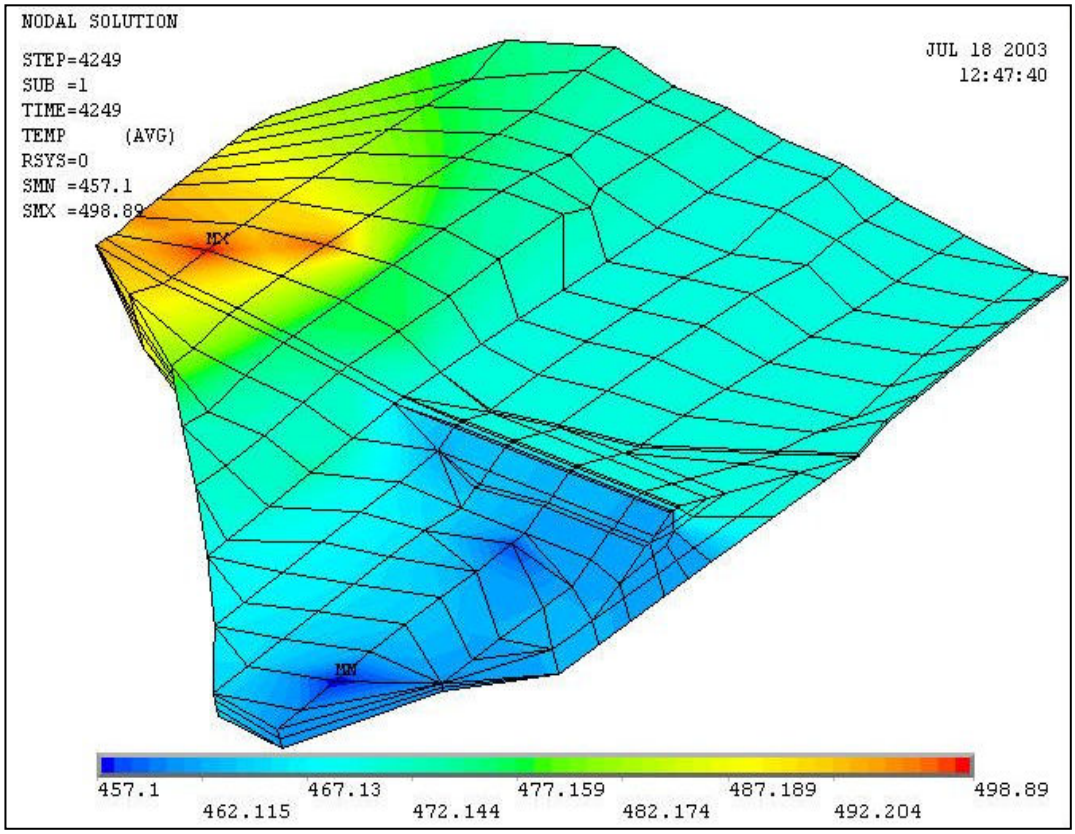

Figure 10 Water level development at December 31st, 2002 (4249 time moment)

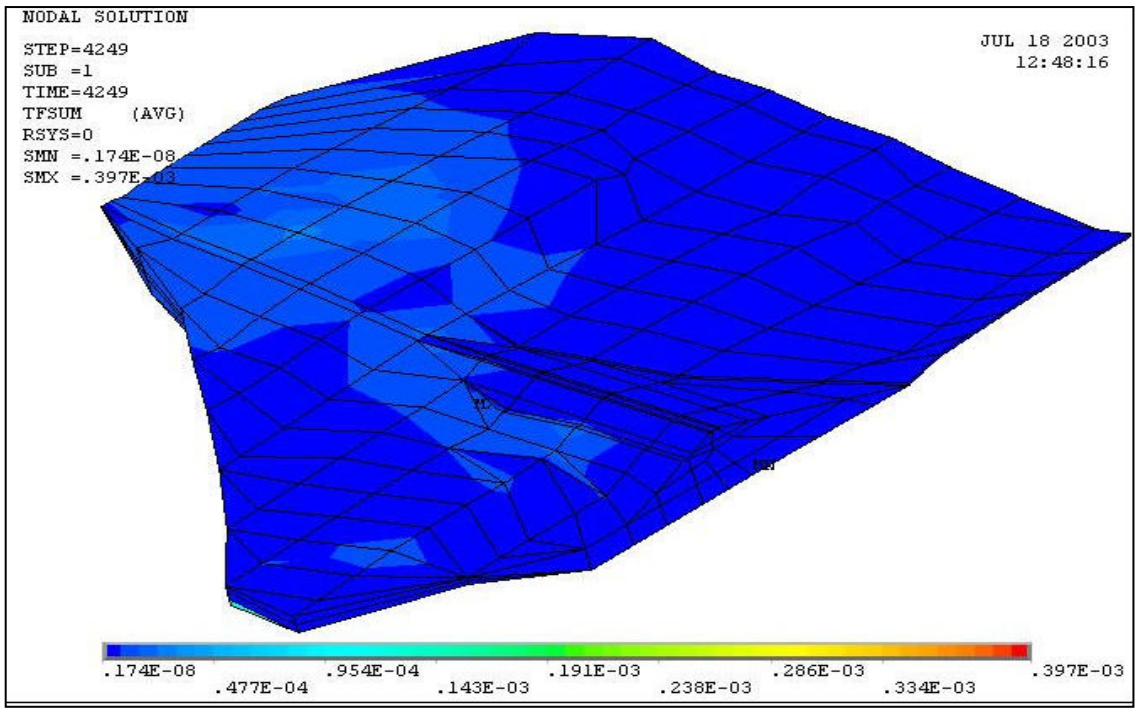

Figure 11 Specific water flow development at December 31st, 2002 (4249 time moment)

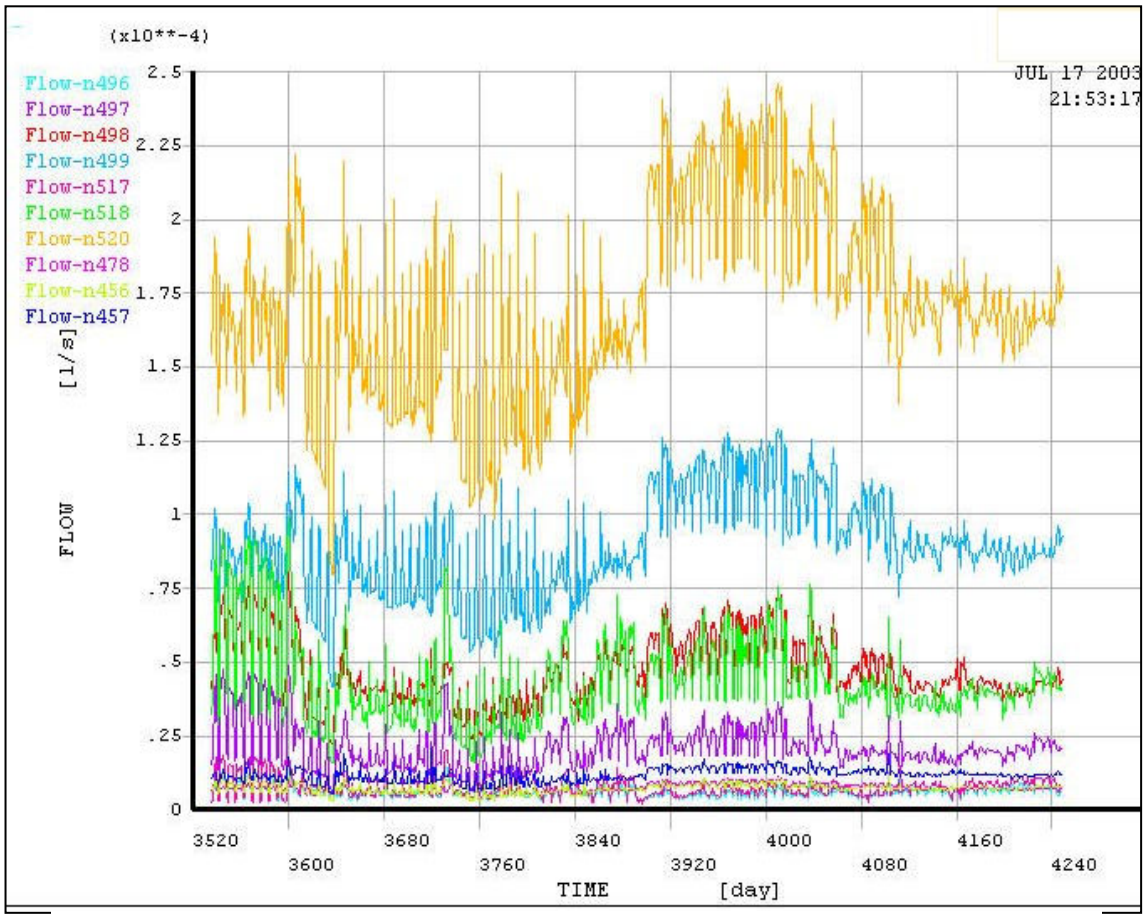

Figure 12 10 typical water flow variations in the interception cross section

The numerical values were transferred in a file and processed by associating the corresponding surfaces. By summation, the water flow transported by the interception pipe was obtained. The figure 13 presents this forecast of the evacuated water flow along the January 1st, 2001 - December 31st, 2002 period of time.

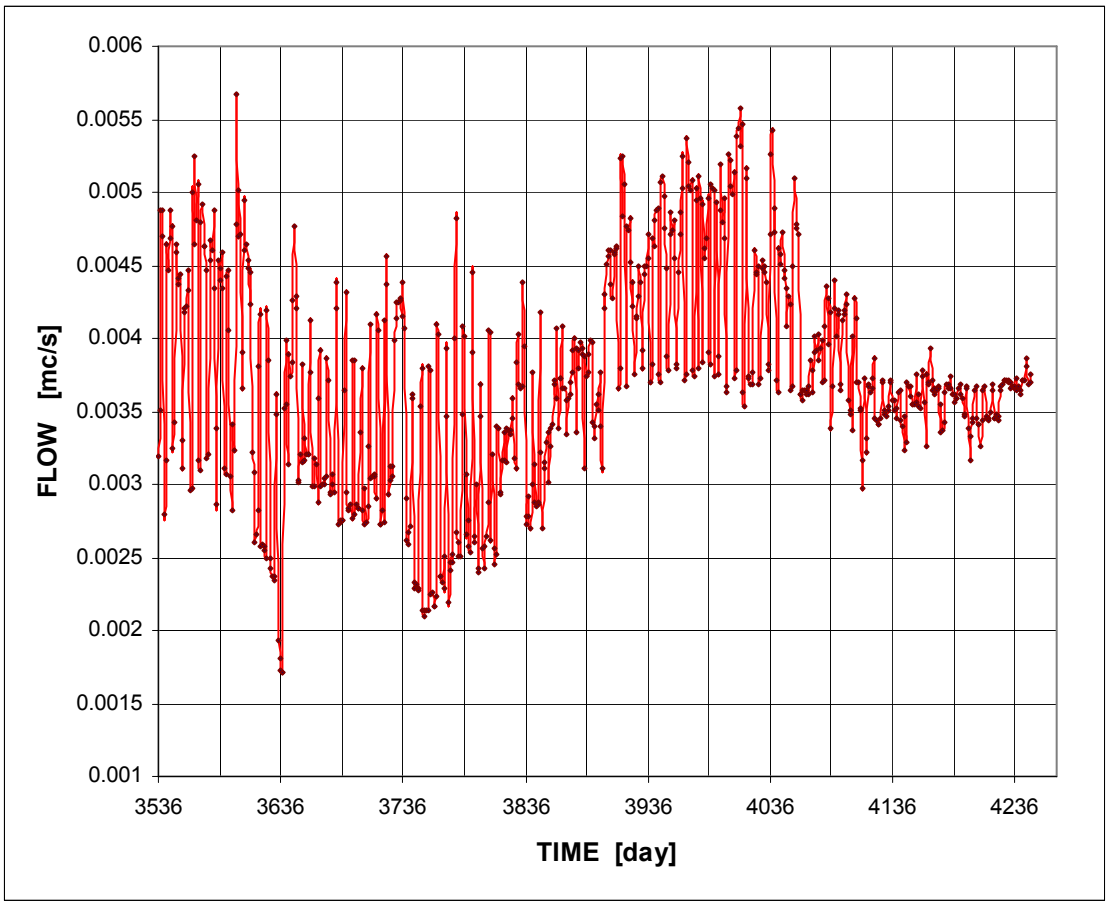

Figure 13 Pipe evacuated water flow forecast for the January 1st, 2001 - December 31st, 2002 period of time

In a III-rd approach, an equivalent drainage strip was modeled in the drainage system interception area (figure 14). The drainage model is considered characterized by a permeability ratio K_{xx} = 0.0003 m/s and a hydraulic head determined on the side surface – left bank at the elevation of 452.00 mSL (nodes N-773, N-774, N-689, N-690). The specified permeability ratio and hydraulic head were obtained by the general model calibration oppreations.

The forcasted levels developed at the F_{11} well for the mentioned conditions along the time interval January 1st, 2001 – December 31st, 2002 are presented in the figure 15.

By the postprocessing calculations the water flow development in the nodes of the interception strip side surface was obtained as presented in the figure 16. The values corresponding to the four nodes were imported in an EXCEL spreadsheet and, by summation, the forcasted water flow was established (figure 17).

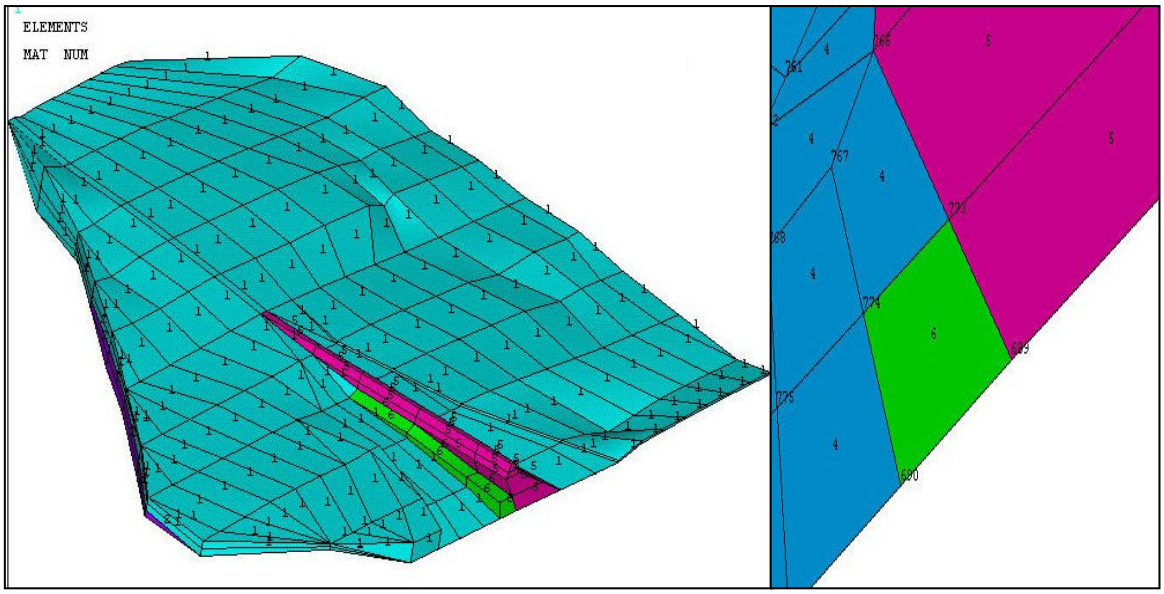

Figure 14 General view and detail for the draining strip

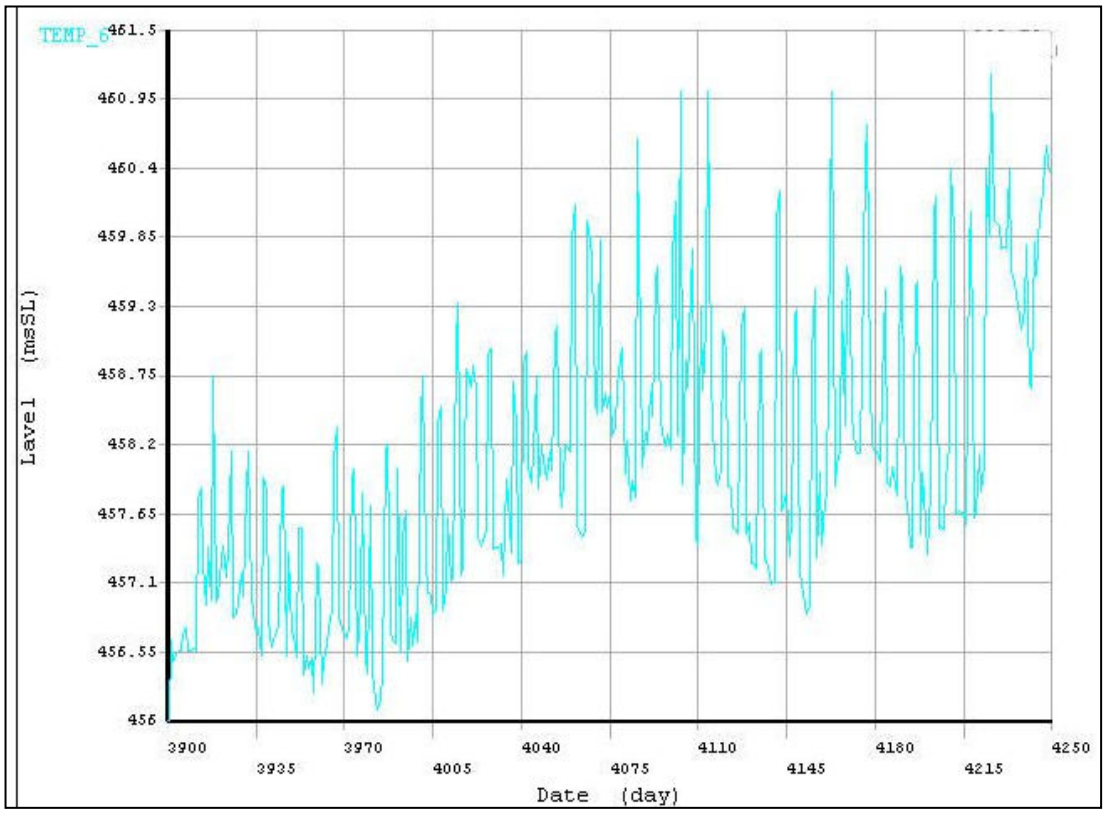

Figure 15 Final forcasted water level variation,
January 1st, 2001 - December 31st, 2002

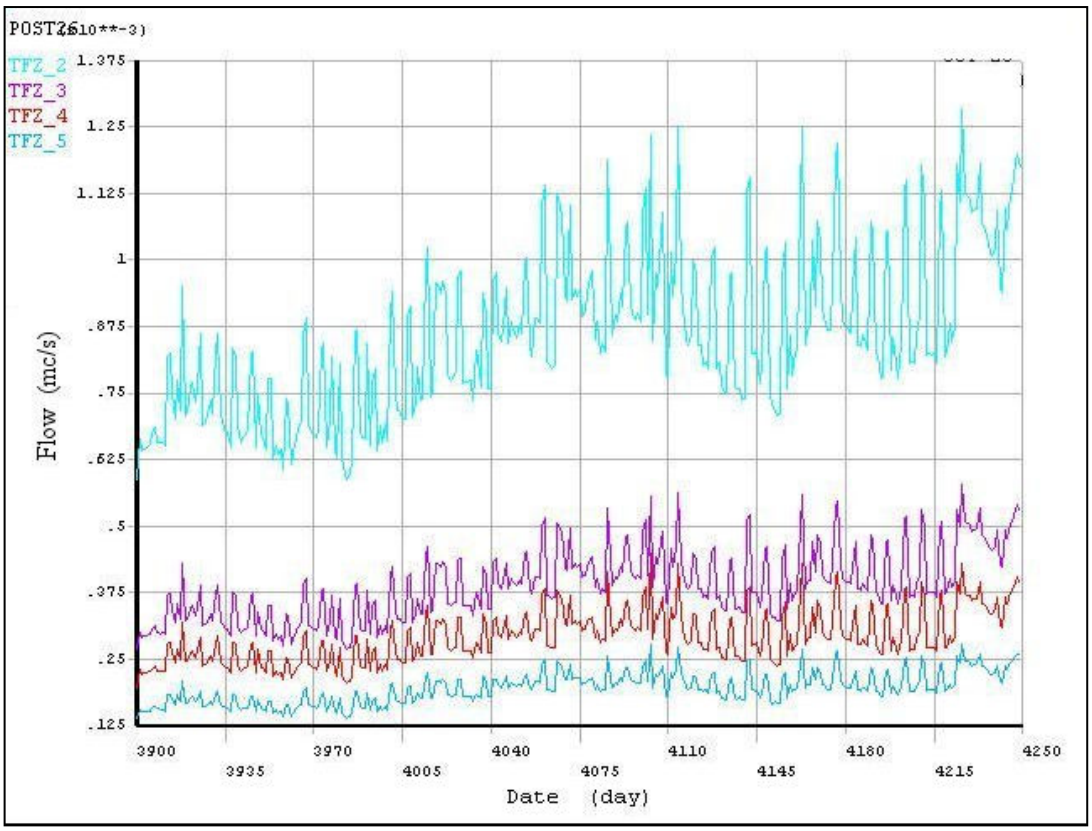

Figure 16 Water flow variation in the four nodes, side surface of the inteception strip

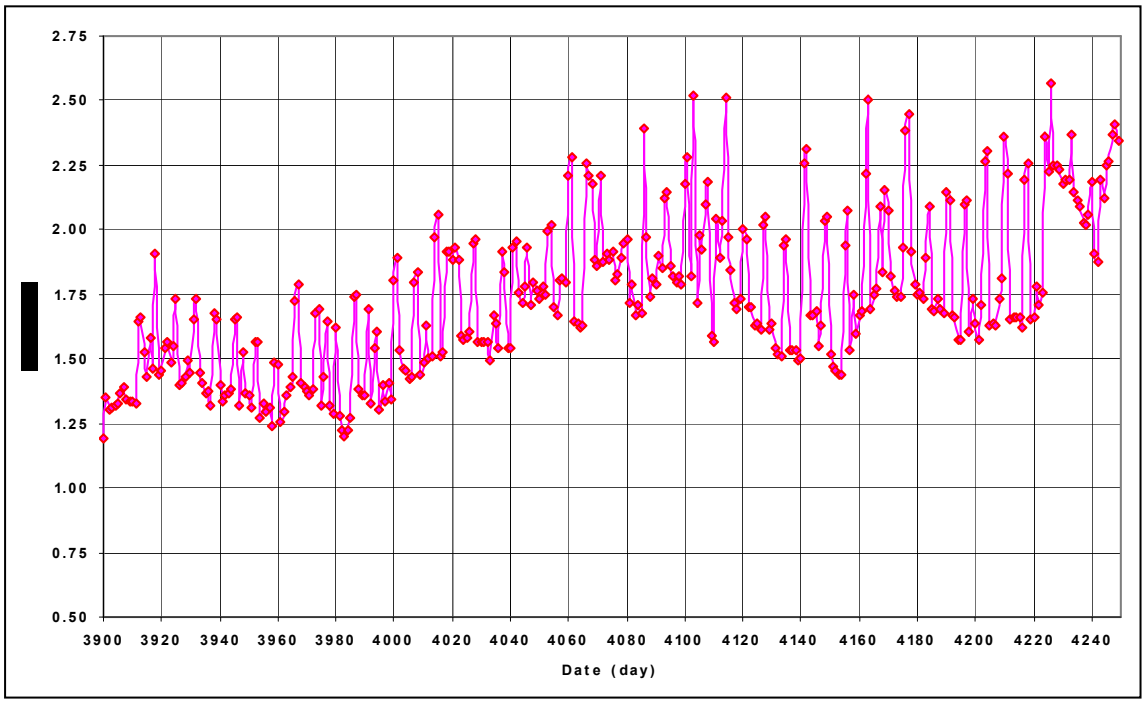

Figure 17 Total water flow forcast, January 1st, 2001 - December 31st, 2002

In conclusion, it is noticed that the forecasted pipe evacuated water flow has a development close to the given one, characterizing the previous year, with a slight increase of the minimum value to 1.19 l/s. The maximum flow ranges around the value of 2.60 l/s, and the mean flow around the value of 1.75 l/s.

REFERENCES

[1] G.Giuseppetti, & al – "Theme C: Seepage through a rockfill dam – foundation system and piezometric level variation downstream of the dam" 7th Benchmarck Workshop on Numerical Analysis of Dams, September 24-26, 2003 – Bucharest, ROMANIA

[2] **** - "ANSYS/ED" - Student Edition, Release 5.3, Copyright 1971, 1978, 1982, 1985, 1987, 1989, 1992-1996 by SAS IP - ISO 9001- 1994.

[3] Dan STEMATIU – "Calculul structurilor hidrotehnice prin metoda elementelor finite", Ed. Tehnică, Bucureşti 1988.

PREDICTION OF SEEPAGE AND PIEZOMETRY AT MOTRU DAM USING NEURAL NETWORK [1]

O. Mateescu[*], C. Ilinca[**] & S. Gheorghe[**]

[*]Hidroelectrica S.A., [**]Technical University of Civil Engineering Bucharest,ROMANIA

SUMMARY:

The paper presents the prediction of the total seepage flow through the right abutment of the Motru dam and the piezometric levels in a selected well located area in the downstream of the dam for the period 01.01.2002 to 31.12.2002. The predictions are based on neural network model, type McCullogh andPitts.

The model's calibration was made based on the recorded data in the dam monitoring system, corresponding to 1990 … 2003 period. An additional calibration was made for a shorter period (1998 … 2003) after a reservoir water level restriction imposed in 1997.

RÉSUMÉ:

Cette thèse présente la prédiction des fuites à travers le rive droit du barrage Motru et des niveaux piezométriques dans une zone sélectionnée localisée en aval du barrage pour la période entre 01.01.2002 et 31.12.2002. Les prédictions sont fondées sur un modèl de réseau neuronale de tipe McCullogh and Pitts.

Le calibrage du modèle a été faite en concordance avec les données enregistrés dans le système d'auscultation du barrage entre 1990 et 2003. Un calibrage supplémentaire a été fait pour une période plus courte (1998- 2003) après l'impôt d'une restriction du niveau de l'eau dans le réservoir.

1. INTRODUCTION

The theme C of the 7 [th] ICOLD Benchmark Workshop on Numerical Analysis of Dams is dedicated to prediction of the seepage flow and piezometric level variation developed on the right bank of the Motru dam in the year of 2002. The input data provided by the formulator consist of time histories of the reservoir water level, snowfall, rainfall, air temperature and water level in some piezometric wells for the

[1] Prédiction des fuites et de la piézométrie au barrage de Motru par modèles avec néuron artificiels

period 1990 … 2001. According to the theme requirements statistical, neural networks and / or finite element methods can be implied.

Motru dam is a clay core earthfill dam with 48 m maximum height and 377 m crest length (fig.1). The dam water reservoir volume is used for hydropower generation. The dam foundation consists of crystalline rock (granite, gneiss) in central zone (profile b, fig.1) and of sedimentary deposits (profile c, fig.1). The dam is founded on the bedrock on the left bank and on a sedimentary deposit of some 20 m thick on the right bank.

The foundation nonhomogenuity imposed some adaptation in cross sections of the dam, which can be noticed in Figure 1,b, and c. A concrete slab is placed at the base of the clay core in the dam axis. It was the platform for the equipment used to carry on the grout curtain. It may be remarked that the grout curtain solution was used for sealing also the sedimentary deposit underneath the right wing of the dam instead of the common solution with cut off wall.

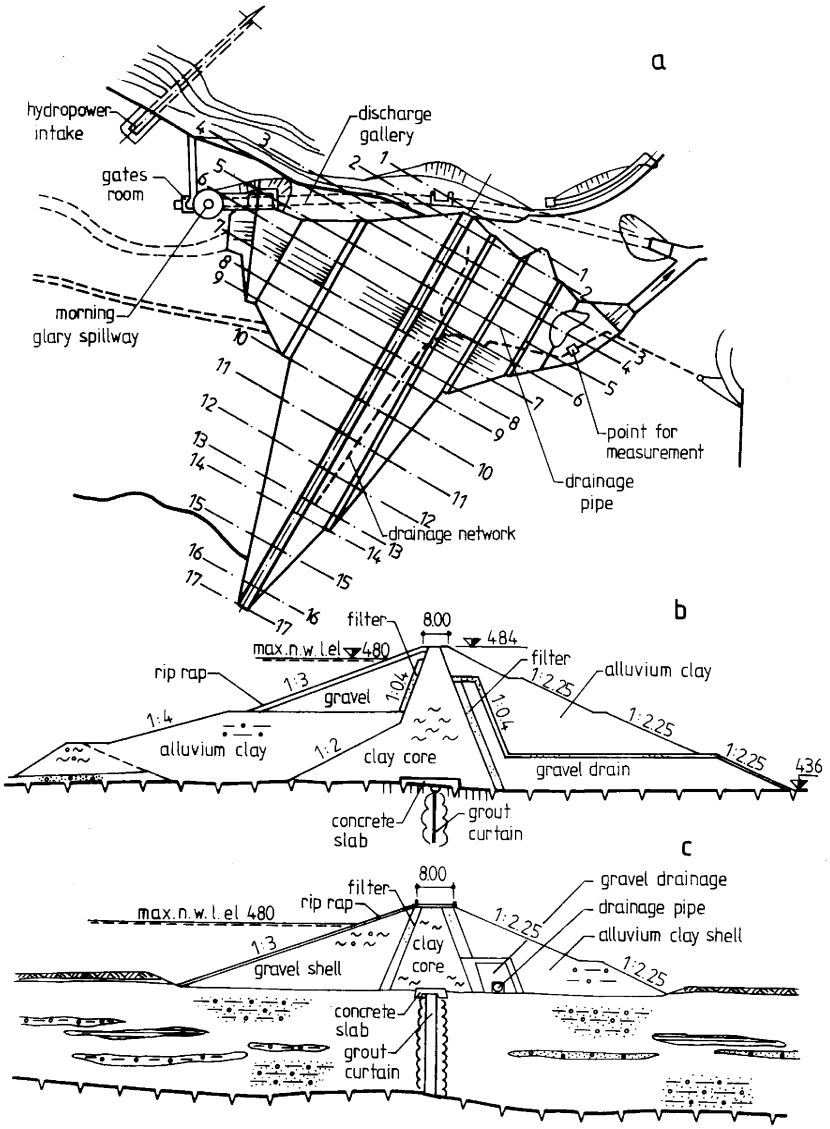

Fig. 1. Motru dam: a - layout, b - typical cross section in central zone (profiles 1...10), c - typical cross section in right wing (profiles 10...17)

The dam – foundation system was well equipped with monitoring devices. Figure 2 shows the locations of some piezometric wells corresponding to the right bank. Recordings of the dam displacements (settlements), pore pressure evolution in the clay core, piezometric level variation in the downstream wells, seepage through dam – foundation system were systematically obtained based on the monitoring devices. Their values as well as the periodical visual inspections have offered sufficient data in order to evaluate the safety state of the dam. [1]

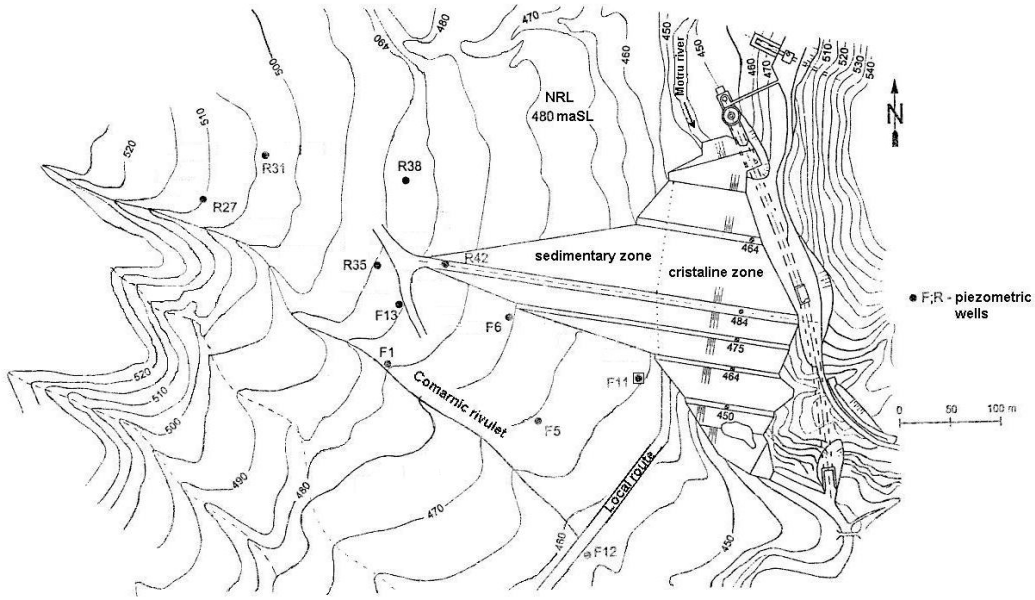

Fig. 2. Motru dam – Locations of some piezometric wells

The time histories of the total leakage measured at the downstream toe of the dam right wing versus reservoir water level elevation in the selected piezometers present a good correlation between seepage flow and the reservoir level. The maximum flow of 45 l/s was measured in 1990 when the reservoir was at its maximum elevation

The authors for the prediction of the seepage and piezometric levels have preferred the statistical approach. Two different calibration periods were selected. The first one covers the whole time interval 1990 … 2002 provided by the formulator. The second one corresponds to the last years (1998 … 2002) after a significant change in the reservoir operation that imposes a lowering by 10 m of the reservoir normal level.

The model were projected in QNet 2000.

The basis of the model, the calibration process and the prediction are presented in the following sections.

2. ARTIFICIAL NETWORKS OF NEURONES

2.1 Generals

In neural networks, the information is no longer memorised in well-established areas, as in the case of standard computers, instead it is memorised diffusely, in the entire network. The memorising is made through the establishment of corresponding values for the weight of the synaptic connections between the neurones of the network.

Another important element, which probably is the main responsible for the success of the connection models, is the ability of neural networks to learn from examples. In a traditional case, to solve a problem, one must elaborate a model of it (mathematically, logically, linguistically, etc). then, starting from this model, one must indicate a succession of operations representing the algorithm for the resolution of the problem. However, there are practical problems of great complexity for which the establishment of an algorithm, be it an approximate one, is difficult or even impossible.

In this case, the problem cannot be approached when using a traditional computer, no matter which are the resources of memory and the available calculation time.

It is characteristic for the neural networks that, starting from many examples, they are capable of synthesising implicitly a certain model of the problem. We might say that a neural network builds by itself the algorithm to solve a problem, if we provide a representative set of particular cases (examples of teaching).

The artificial neural networks are networks of models of neurones connected through some adjustable synapses. All the models of neural networks are based on the interconnection of some simple elements of calculation from a dense network of connections.

Each unit of the process is capable to execute only simple calculations, but the network, on the whole, can have remarkable qualities in the recognition of forms, the resolution of problems for which we do not have an algorithm, teaching from examples or from experience.

An artificial neurone has many entering ways, which correspond to the dendritical. The entering way ***i*** correspond in the neurone ***j*** to a real numerical value x_i, the equivalent of the electrical signal in the biological model of the neurone. Each size of entrance x_i is given the real numerical value $w_{j,i}$ the equivalent of the synaptic strength of the biological model of the neurone. The result of $x_i \cdot w_{j,i}$ represents the dendritical entering signal ***i*** in the artificial neurone ***j***.

The pondered sum:

$$I_j = \sum_{i=1}^{n} w_{j,i} \cdot x_i$$

represents the argument of a function, called activation function:

$$y_j = f\left(I_j + t\right) = f\left(\sum_{i=1}^{n}\left(w_{j,i} \cdot x_i + t\right)\right)$$

which will determine the exit axons value y_j of the neurone. The limit of excitability (bias) represents a signal of entrance in the neurone with the value 1 and weight *t*. The limit value can be removed from the argument of the activation function, in this case the axons exit y_j becomes:

$$y_j = f\left(\sum_{i=0}^{n}\left(w_{j,i} \cdot x_i\right)\right),$$

where $x_0 = 1, w_{0,i} = t$. [2]

This mathematical model of the artificial neurone, proposed for the first time by McCullogh and Pitts, although very simple, represents a very important unit of calculation.

The activation function depends on the chosen model of neural network and on the type of the problem to be solved, its choice is not restricted by no condition, except

eventually by the analogy with the biological model. The value obtained through the application of the activation function is spread through the exit ways, equivalent to the axons tree from the biological model.

The most used activation functions are (figure 3):

- the sigmoid function:

$$f: R \to (0,1), f(x) = \frac{1}{1+e^{-x}} \tag{1}$$

- the hyperbolical tangent function:

$$f: R \to (-1,1), f(x) = \tanh(x) = \frac{e^{x} - e^{-x}}{e^{x} + e^{-x}} \tag{2}$$

- the secant hyperbolic function:

$$f: R \to (0,1), f(x) = \operatorname{sech}(x) := \frac{1}{\cosh(x)} \tag{3}$$

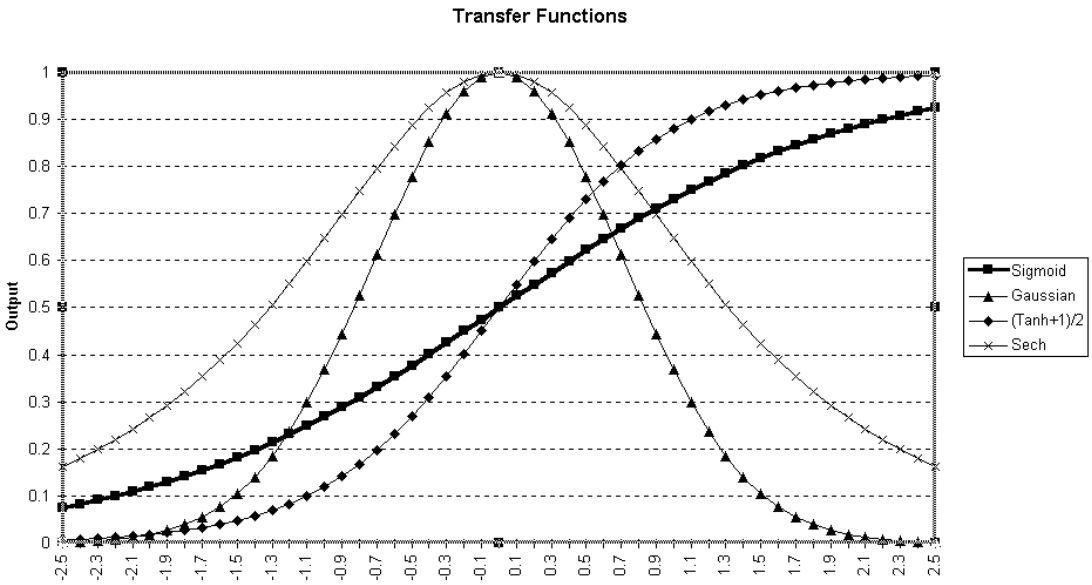

Fig. 3. Activation functions used by the program Qnet 2000

The neural artificial networks are built out of numerous artificial neurones interconnected with each other. The artificial neurone is schematically represented in figure 4.

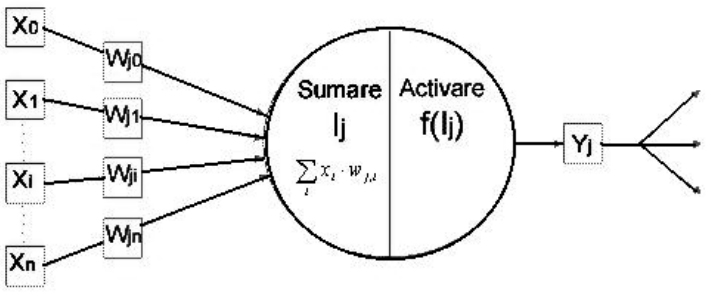

Fig. 4. Schematically representation of the artificial neurone

2.2. The neural network

The structural model of neural networks is defined by:

a. the geometry of the network;

The feedforward multilevel networks raise special problems in dimension because, except for the number of input units (entrance vectors) and output units (exit vectors), which are established in accordance with the way of representing the data, for the rest of the units (the hidden neurones) are hard to establish the dimension. The proper establishing of the number of units is extremely important because:

- if there are few hidden units, the network cannot teach itself (cannot generalise, because it has few connections on which it could make the representation of entrance and exit characteristics);
- if there are too many hidden units, the network, too, doesn't generalise correctly, trying to memorise too other characteristics except the ones, which are common to all, forms (so, of the essential characteristics).

b. the scheme of the interconnection of the units

It has been adopted the general solution of network totally connected, thus resulting the network from figure 5. The particular solution of locally connected network is efficient in the cases when the wanted result is the removal of some insignificant influences (for example the temperature multiplied by the level of accumulation). The entrances in the network are the calendar date in numerical format, the level of the reservoir, the daily rainfall and the average daily temperature. The exits from the network are formed of the piezometric level from F11 and the drained flow.

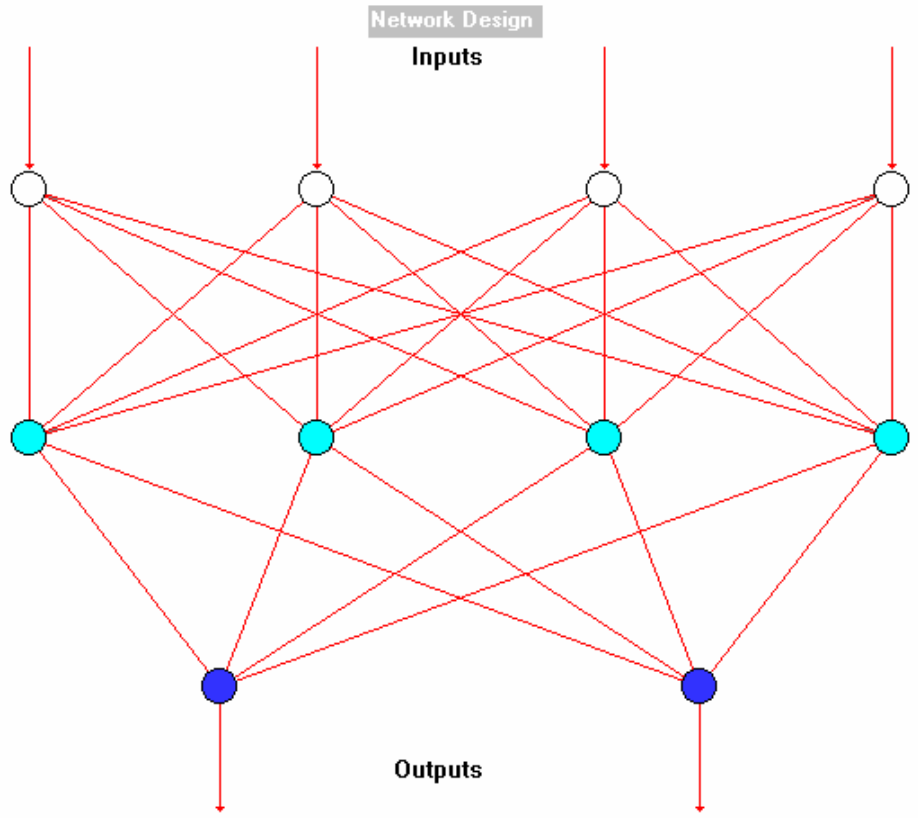

Fig. 5. Network design for Motru dam

The general model of a neural network represents the total of the characteristics of a neural network. All these characteristics are proposed and adjusted by the program Qnet, thus taking this charge from the duties of the designer of the application, which in the case of the program Mathcad was a difficult stage. These characteristics can be grouped into:

- local characteristics;
- global characteristics.

The local characteristics of a neural network are represented by the characteristics of the neurones:

- the bias (the limit of activation of the neurone);
- the function of combination of the entrances, g;
- the activation function, f ;
- the presence/ absence of the local reaction.

The global characteristics of a neural network are:

- static characteristics, represented through the topologicaland functional properties of the network (including the method of teaching of the network);
- dynamical characteristics, that characterise the evolution in time of the network.

The pre-processing of the data consists in the preparing of the entrance and exit data. The entrance and exit data are systematised in a table form (DBF format). For the entrances of the network the variables considered relevant are chosen. In certain cases, it is necessary to generate some supplementary vectors (columns) that contain data specific to the analysed phenomenon. In the case of the seepage it was chosen the calendar date converted into a numerical form, the level in the lake, the average daily air temperature.

The training/teaching of the network establishes the values of the neurones from the network. This operation can lead to wrong results, that's why it is recommended to permanently display the evolution of the error of the network (fig 6) or of the global rapport of correlation (fig 7). The values of the connection are calculated by the method of the descendent gradient.

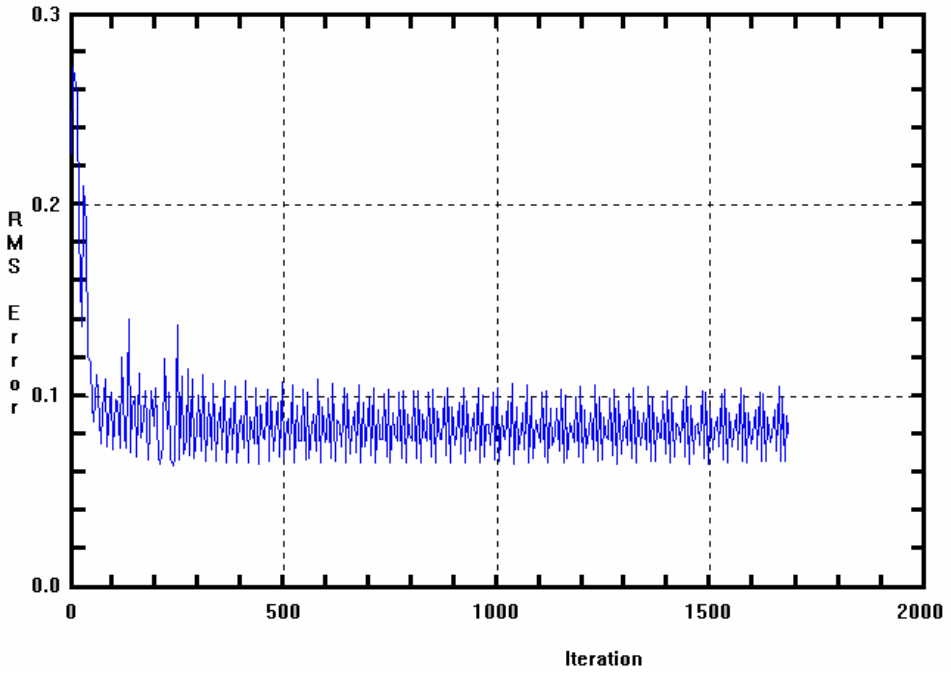

Fig. 6. The evolution of the Network

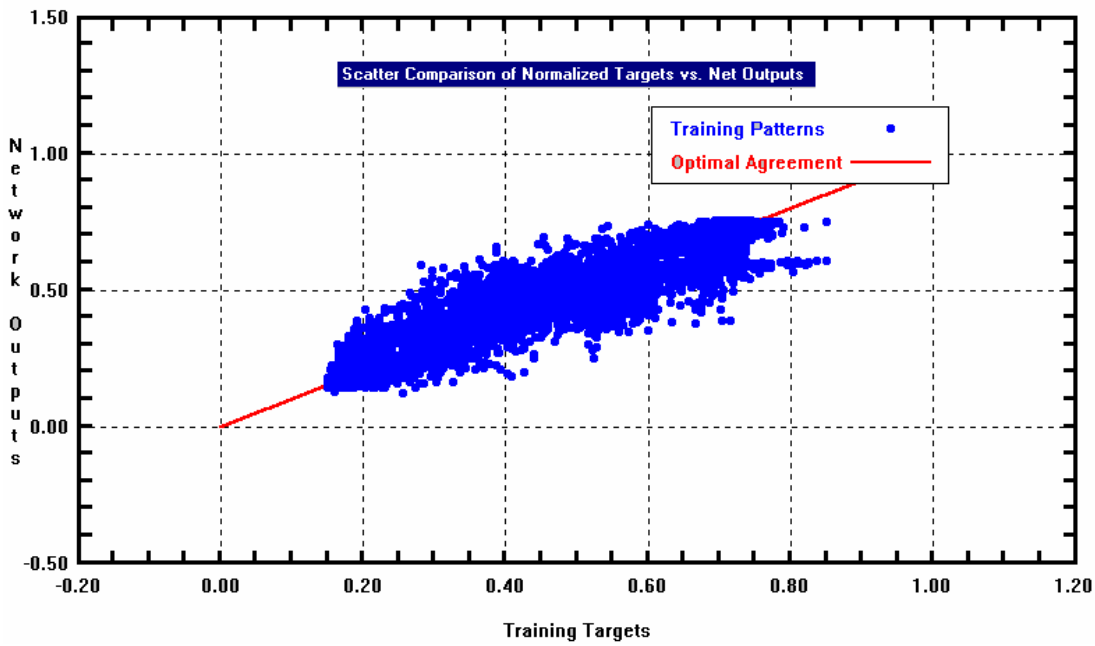

Fig. 7. The global correlation measured-calculated

2.3. The analysis of the seepage phenomenon using the designed network

Usually neural networks are considered models Black box. The statistical models, due to the efforts made by famous companies in the domain of hydrotechnics, (EdF, Coyne&Bellier,…) are nowadays unanimously accepted as being grey box models, those being the result of the interpretation of influence functions. For the neural networks there have existed two ways of interpretation. The first interpretation, finally abandoned, was the interpretation of the values of the connections, which is similar to the interpretation of the coefficients of the static models. The second one is represented by the realisation of diagrams of influence of the entrances over the exits, and is similar to the interpretation of the influence functions from the static models. Next we will analyse the phenomenon of seepage utilising the designed network.

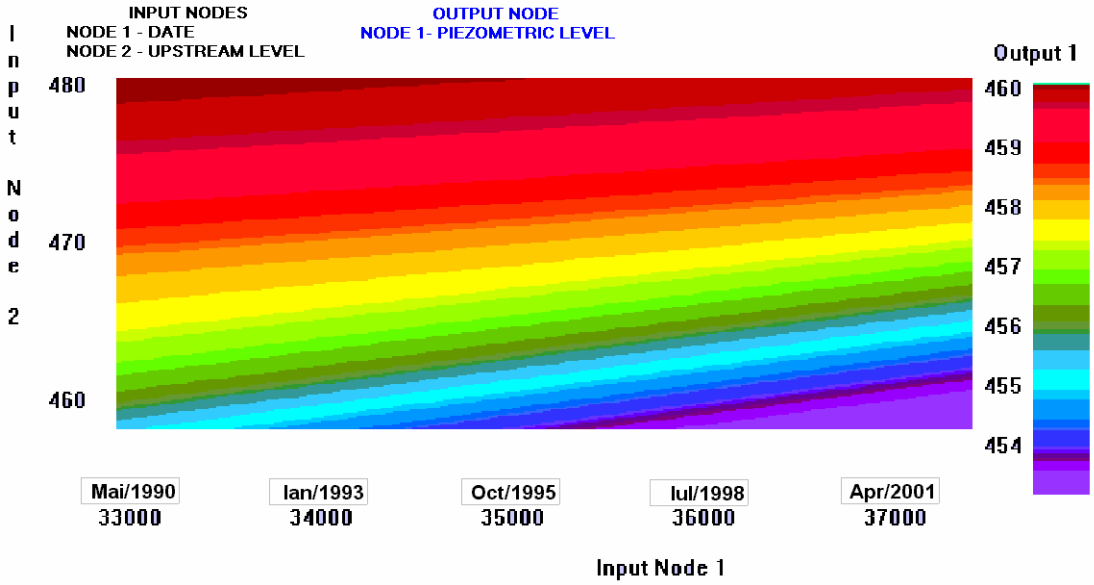

Fig. 8. The diagram of influence factors, F11 = ℱ(Time,Reservoir level) .

From the diagram of influence presented in figure 8, f(time, reservoir level) there can be noticed the fact that the piezometric level in the drilling F11 is substantially decreasing in time, approximately 0.50m. Similarly, in figure 9 there can be noticed the fact that the drained flow decreases in time with approximately 5.00m. Moreover, these diagrams reveal the evolution in time of the drained flow and of the piezometric level from the drilling F11.

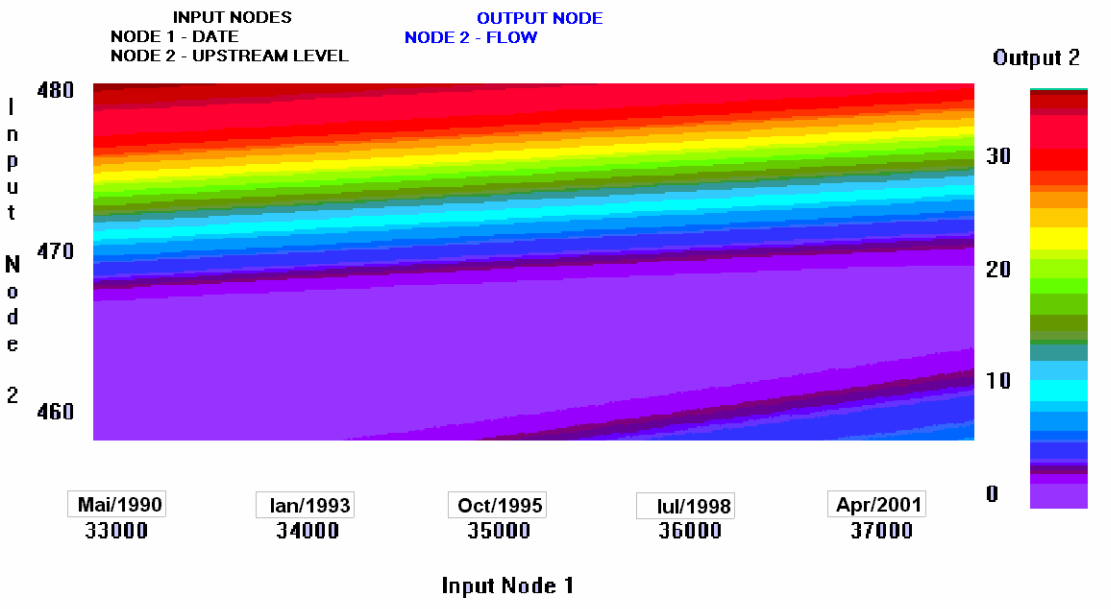

Fig. 9. Diagram of the influence functions , Q = f(Time,Reservoir level)

The influence of the rainfall over the piezometric level from the drilling F11 is very little, and can be considered insignificant.

From the influence diagram, presented in the figure 10 f(time, rain) it can be noticed that the drained flow decreases in time, from 1990 till 2001, from 28l/s to 20 l/s. It can also be noted that for a rainfall of 50l/m^2 the contribution of the drained flow is of approximately 1 l/s.

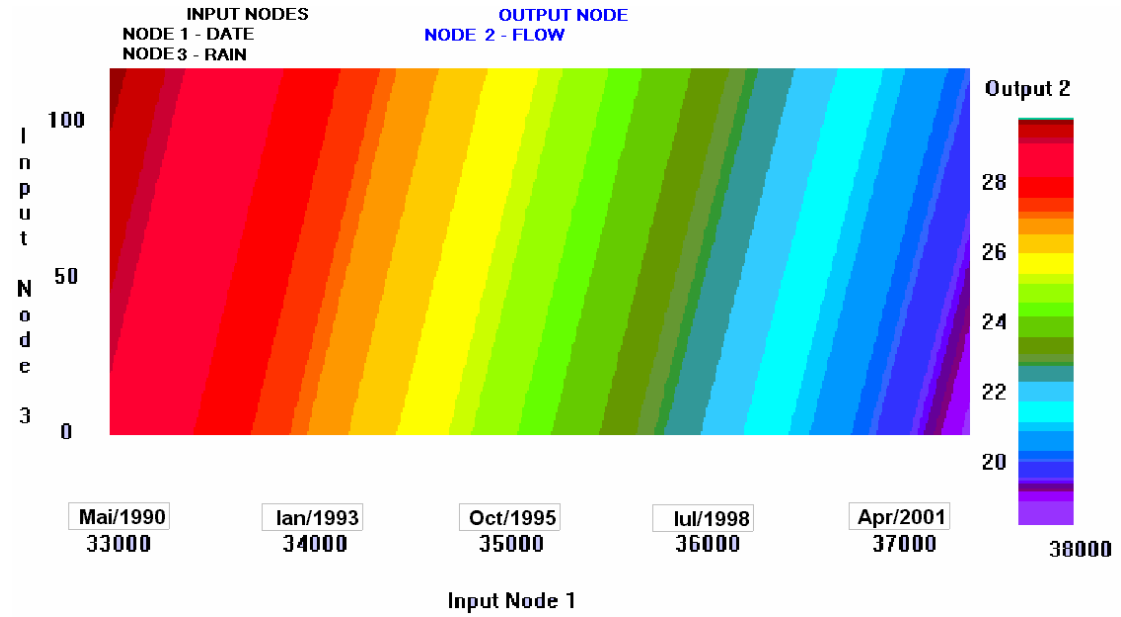

Fig. 10. Diagram of the influence functions , Q = f(Time,Rain)

Normally the influence of the average temperature of air over the seepage should be insignificant. From the diagram of influence presented in fig 11 f(time, temperature) there can be observed the fact that the drained flow increases with the temperature, this being explained by the melting of the snow. The contribution of the drained flow is of about 2 l/s.

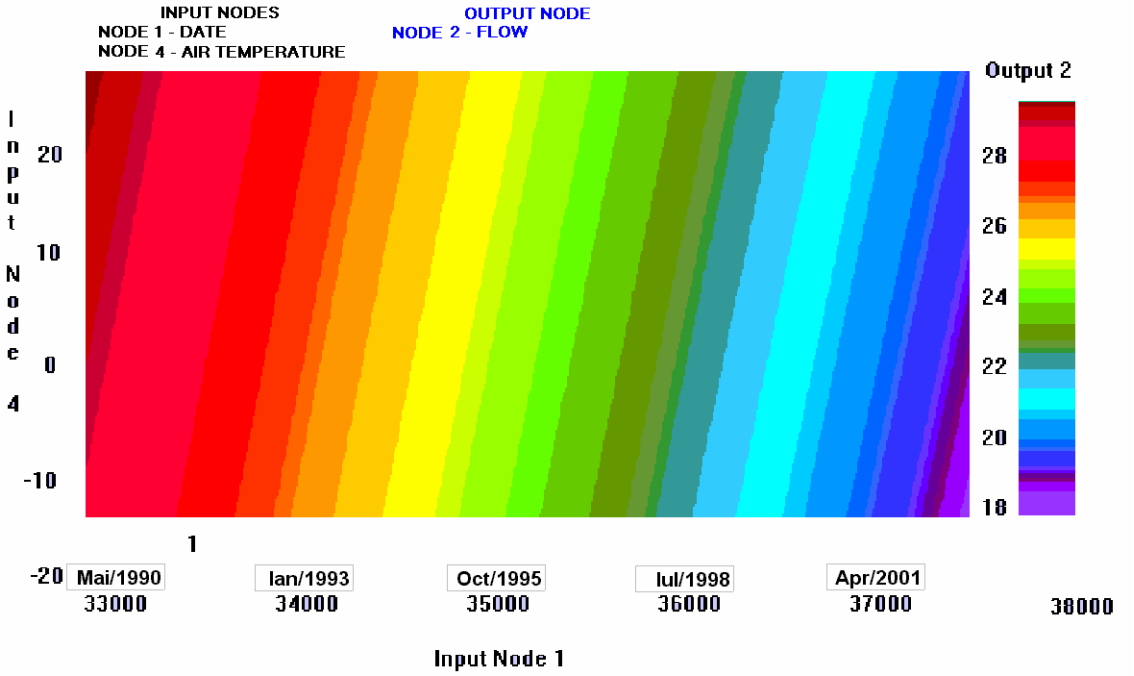

Fig. 11. Diagram of the influence functions, Q = 𝒻(Time,Temperature)

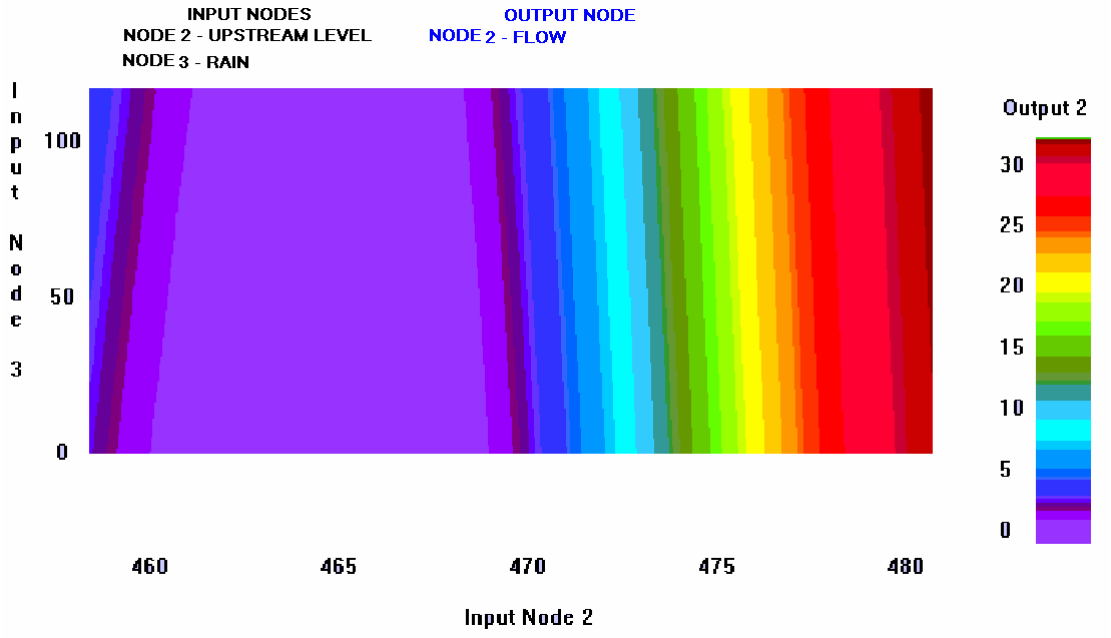

Fig. 12. Diagram of the influence functions, Q = 𝒻(Reservoir level, Rain)

Another influence analyzed was rain-reservoir level on the drained flow, as is presented in figure 12. For different reservoir levels in the presence of a rain fall the values of drained flow are increasing with 1 to 3 l/s in the domain of 470…477 m.a.S.L.

2.4 Results

The predicted water levels in the F11 piezometric well and flow are presented in the figures 12 and in a DBF file as required by the formulator.

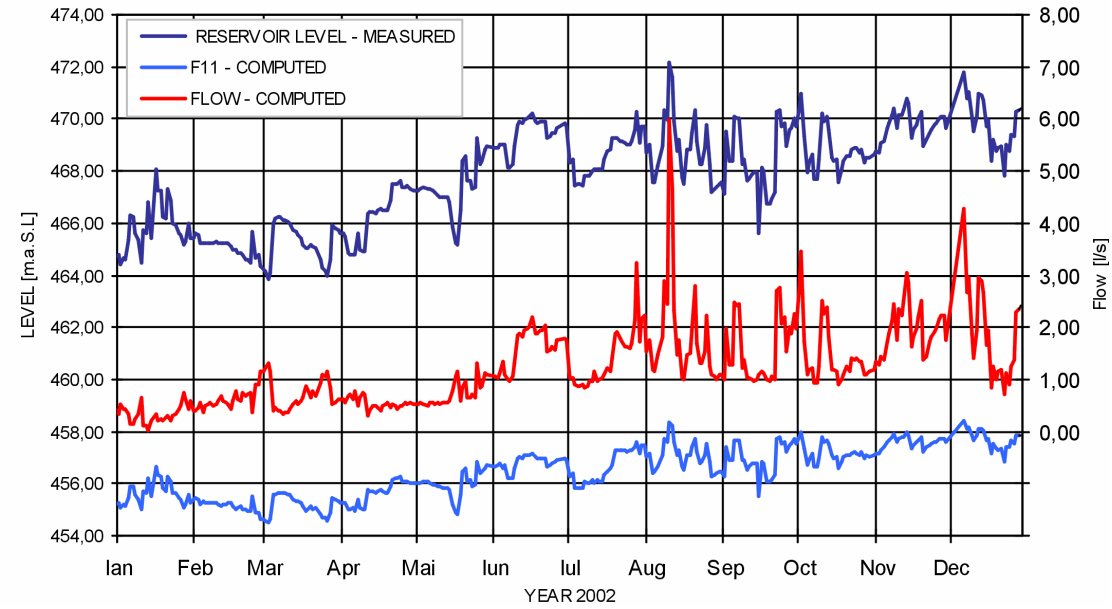

Fig. 13. Prediction for F11 and Flow readings during 2002

3. CONCLUDING REMARKS

The above-presented neural network is a network that can be applied with success to different phenomena noticed during the supervising of the behaviour of hydro-technical buildings.

We could have built a neural network that would contain as entries other additional variables, but its purpose would have only been a strict prediction in the context of this problem. This simple architecture was chosen in order to study the phenomenon of seepage in the Motru dam> it can be said that through the analysis from the paragraph 2.4 we managed to prove too the efficaciousness of the use of these neural networks in this field, and the fact that these can be used in the future as models of the grey-box type.

In the table 1 are presented the technical parameters of the model during the "training period" of neural network, using the data base gave by the formulator of the **Theme C**.

Table 1. Results for model training period (1990-2001)

Parameters	F11	Flow
Coefficient of correlation	0.874	0,931
Residual standard deviation	0,685	4,436
Shift	0.050	0.397

REFERENCES

[1] D. Stematiu, C. Ilinca & D. Bobocu prediction of seepage and piezometry at Motru dam with statistical models , BW7, Bucharest 2003.

[2] Al. P. Tacu, R. Vancea, Şt. Holban, A. Burciu – *Inteligența Artificială*, Ed. Economică, Bucureşti, 1998

PREDICTION OF SEEPAGE AND PIEZOMETRY AT MOTRU DAM WITH STATISTICAL MODELS *

D. Stematiu, C. Ilinca & D. Bobocu
Technical University of Civil Engineering Bucharest, ROMANIA

SUMMARY:

The paper presents the prediction of the total seepage flow through the right abutment of the Motru dam and of the piezometric levels in a selected well located downstream the dam for the period 01.01.2002 to 31.12.2002. The predictions are based on two statistical models, namely multiple linear regression with delay and multiple linear regression with additional response data. The model's calibration was made based on the recorded data in the dam monitoring system corresponding to 1990 … 2003 period. An additional calibration was made for a shorter period (1998 … 2003) after a reservoir water level restriction imposed in 1997.

RÉSUMÉ:

Cette thèse présente la prédiction des fuites à travers le versant droit du barrage Motru et des niveaux piezométriques dans un réservoir sélectionné localisé en aval du barrage pour la période entre 01.01.2002 et 31.12.2002. Les prédictions sont fondées sur deux modèles statistiques, voire la régression multiple linéaire avec délai et la régression multiple linéaire avec des données de correspondance additionnelles. Le calibrage du modèle a été faite en concordance avec les données enregistrés dans le système de monitorisation du barrage entre 1990 et 2003. Un calibrage supplémentaire a été fait pour une période plus courte (1998- 2003) après l'impôt d'une restriction du niveau de l'eau dans le réservoir.

1. INTRODUCTION

The theme C of the 7 th ICOLD Benchmark Workshop on Numerical Analysis of Dams is dedicated to prediction of the seepage flow and piezometric level variation developed on the right bank of the Motru dam in the year of 2002. The input data provided by the formulator consist of time histories of the reservoir water level, snowfall, rainfall, air temperature and water level in some piezometric wells for the

* Prédiction des fuites et de la piézométrie au barrage de Motru par modèles statistiques

period 1990 … 2001. According to the theme requirements statistical, neural networks and / or finite element methods can be implied.

Motru dam is a clay core earthfill dam with 48 m maximum height and 377 m crest length (fig.1). The dam water reservoir volume is used for hydropower generation. The dam foundation consists of crystalline rock (granite, gneiss) in central zone (profile b, fig.1) and of sedimentary deposits (profile c, fig.1). The dam is founded on the bedrock on the left bank and on a sedimentary deposit of some 20 m thick on the right bank.

The foundation nonhomogenuity imposed some adaptation in cross sections of the dam, which can be noticed in Figure 1,b, and c. A concrete slab is placed at the base of the clay core in the dam axis. It was the platform for the equipment used to carry on the grout curtain. It may be remarked that the grout curtain solution was used for sealing also the sedimentary deposit underneath the right wing of the dam instead of the common solution with cut off wall.

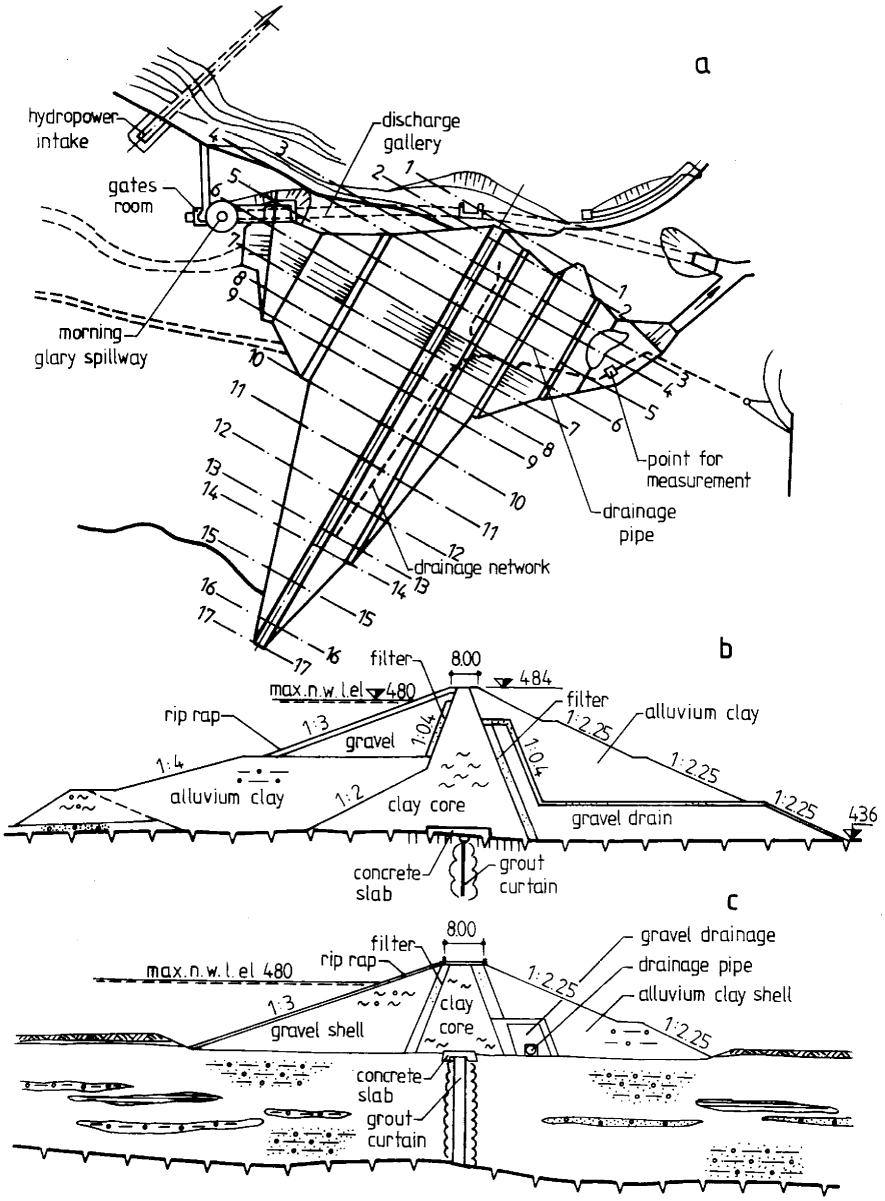

Fig. 1. Motru dam: a - layout, b - typical cross section in central zone (profiles 1...10), c - typical cross section in right wing (profiles 10...17).

The dam – foundation system was well equipped with monitoring devices. Figure 2 shows the locations of some piezometric wells corresponding to the right bank. Recordings of the dam displacements (settlements), pore pressure evolution in the clay core, piezometric level variation in the downstream wells, seepage through dam – foundation system were systematically obtained based on the monitoring devices. Their values as well as the periodical visual inspections have offered sufficient data in order to evaluate the safety state of the dam.

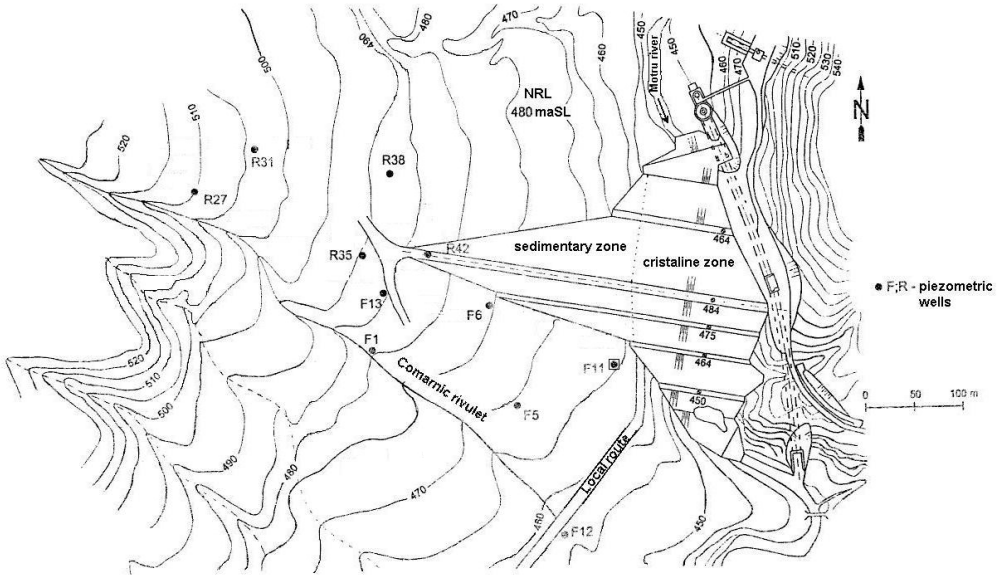

Fig. 2. Motru dam – Locations of some piezometric wells

The time histories of the total leakage measured at the downstream toe of the dam right wing versus reservoir water level elevation in the selected piezometers present a good correlation between seepage flow and the reservoir level. The maximum flow of 45 l/s was measured in 1990 when the reservoir was at its maximum elevation.

The authors for the prediction of the seepage and piezometric levels have preferred the statistical approach. Two different calibration periods were selected. The first one covers the whole time interval 1990 … 2002 provided by the formulator. The second one corresponds to the last years (1998 … 2002) after a significant change in the reservoir operation that imposes a lowering by 10 m of the reservoir normal level. Two different types of models were used.

- multiple linear regression with delay:
- multiple linear regression with additional response data.

The models were projected in MathCAD 11, due to the multiple facilities of writing and checking of the computerized applications.

The basis of the models, the calibration process and the prediction are presented in the following sections.

2. MULTIPLE LINEAR REGRESSION WITH DELAY MODEL

2.1 The model

The multiple linear regression with delay model is basically a hydrostatic-seasonal-time (HST) model where the influence function corresponding to the reservoir

water level includes not only the readings of the day but also the readings from the previous days. [1]

Consequently, the mathematical formulation of the model is:

$$y = a_0 + f_1(h) + f_2(s) + f_3(t) + FN + E \quad (1)$$

where:

- the influence of the hydrostatic pressure is expressed by a two-degree polynomial function in terms of the water levels:

$$f_1(h) = a_1 h_t + a_2 h_t^2 + a_3 h_{t+1} + a_4 h_{t+1}^2 + a_5 h_{t+2} + a_6 h_{t+2}^2 \quad (2)$$

and:

$$h_{t+j} = \frac{H_{t+j} - C_f}{H_b}$$

H_{t+j} - is the reservoir level measured with j days before the measurement of the predicted parameter y;
H_t - C_f - is relative water depth in the reservoir;
H_b - is the normal retention level.

- the seasonal influence induced mainly by the reservoir operation is modeled by a trigonometric function:

$$f_2(s) = b_1 \cos(s) + b_2 \sin(s) + b_3 \sin^2(s) + b_4 \sin(s)\cos(s) \quad (3)$$

where:

$$s = 2\pi \frac{D_i - D_0}{365.25} (rad)$$

D_0 is the reference day of the model;
D_i is the day of the measurement.

- a time polynomial function and an exponential one represent the long-term effects:

$$f_3(T) = c_1 T + c_2 T^2 + c_3 e^{-\beta T} \quad (4)$$

where T is the total time since reservoir commissioning;
β is the parameter of modification of the importance of the exponential term.
Additionally, FN represents neglected phenomena influence and E denotes the measurement errors of the response parameter.

2.2 Model calibration

2.2.1. Piezometric level in F_{11}. The model calibration for F_{11} was made for two calibration periods 1990 – 2001 and 1998 – 2001. Consequently, two models of the kind were build for the piezometric readings (see Figures 3 and 4). The accuracy of the calibration has been evaluated on the basis of the residual variation coefficient (shift), which quantifies the average difference between the prediction and the measure over the

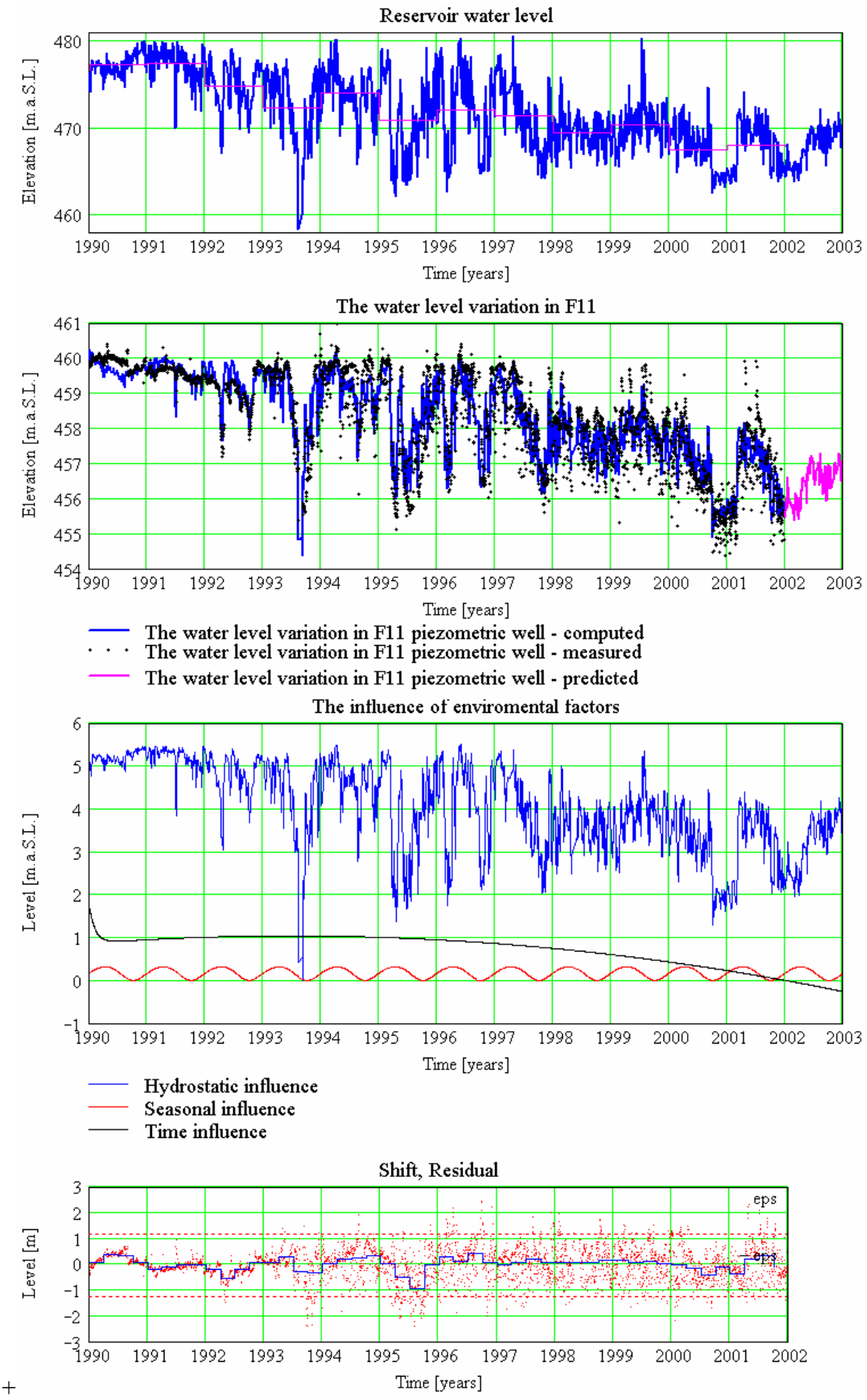

Fig. 3. Model multiple linear regression with delay for F11 (1990-2002; β=10)

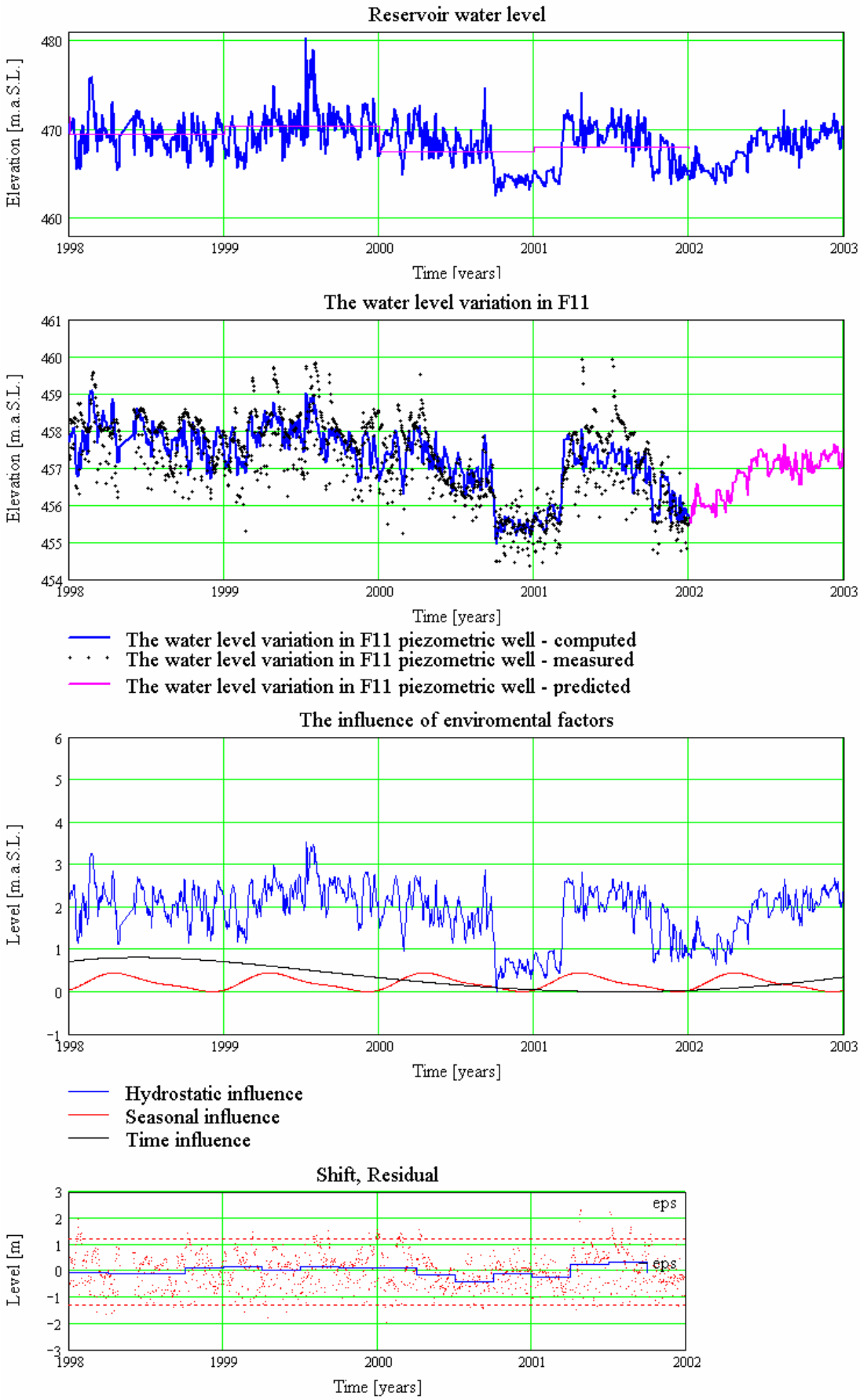

Fig.4. Model multiple linear regression with delay for F11 (1998-2002; β=1)

calibration period. The model corresponding to 1990 – 2001 (β=10) period is characterized by **0.625** residual variation coefficient with residuals between **-2.418** m and **2.453** m. The second model, calibrated for 1998 – 2001 (β=1) period is characterized by **0.641** residual variation coefficient and the residual values range between **-1.956** m and **2.318** m.

The influence of the environmental factors is shown in Figure 3, c and Figure 4,c for each model. The main contribution is due to reservoir water variation while the seasonal influence is negligible. There can be noticed a general trend of piezometric level decreasing, indicating that we are not facing an evolutive process.

2.2.2. Seepage flow. As for the piezometric levels, two different models have been developed, based on the two calibration periods, namely 1990 – 2001 and 1998 – 2001 respectively. The model corresponding to 1990 – 2001 (β=10) period has residual variation coefficients in the range of **3.817** and the residual values between **-21.24** l/s and **19.432** l/s. The second model, corresponding to 1998 – 2001 (β=1) period is characterized by **1.49** residual variation coefficients and by residual values in the range of **-8.38** l/s and **15.618** l/s.

The influence of the environment factors is shown in figures 5 and 6, c. Similarly with the case of the piezometric levels, the water level in the reservoir has the most significant contribution, the seasonal effects are negligible and the general trend renders evident a progressive reduction of the seepage flow.

2.3. Results

The predicted water levels in the F11 piezometric well are presented in the figures 3 … 6 and in a DBF file as required by the formulator.

3. MULTIPLE LINEAR REGRESION WITH ADDITIONAL RESPONSE DATA

3.1. The model

The multiple linear regression with additional response data model is, as a core, a hydrostatic-seasonal-time (HST) model similar with the one described in the previous section that includes the influence of some other available readings in the monitoring system. Consequently, the mathematical formulation of the model is:

$$y = a_0 + f_1(h) + f_2(s) + f_3(T) + \Sigma f(x) + FN + E \qquad (5)$$

where the additional term $\Sigma f(x)$ includes the water level readings in the neighbouring piezometric wells F1, F6, F13 and R35, as well as the precipitation. All the other terms in the relationship (5) are the same as in the relationship (1) and are described in the section 2.

3.2 Model calibration

3.2.1. Piezometric level in F_{11}. The model calibration for F_{11} was made for the same two calibration periods 1990 – 2001 and 1998 – 2001. Consequently, two new models were build for the piezometric readings (see Figures 7 and 8). The accuracy of the

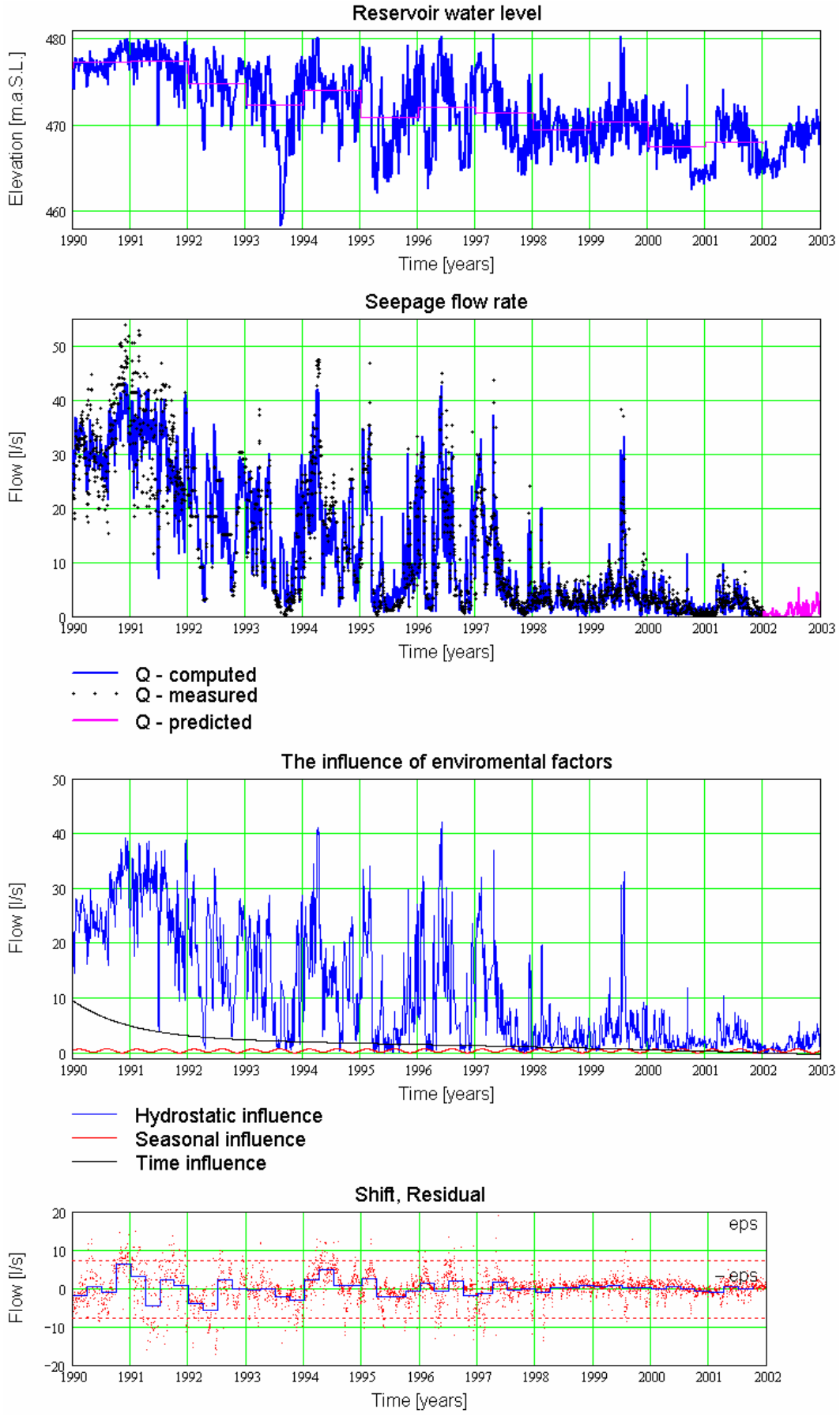

Fig. 5. Model multiple linear regression with delay for flow (1990-2002; β=10)

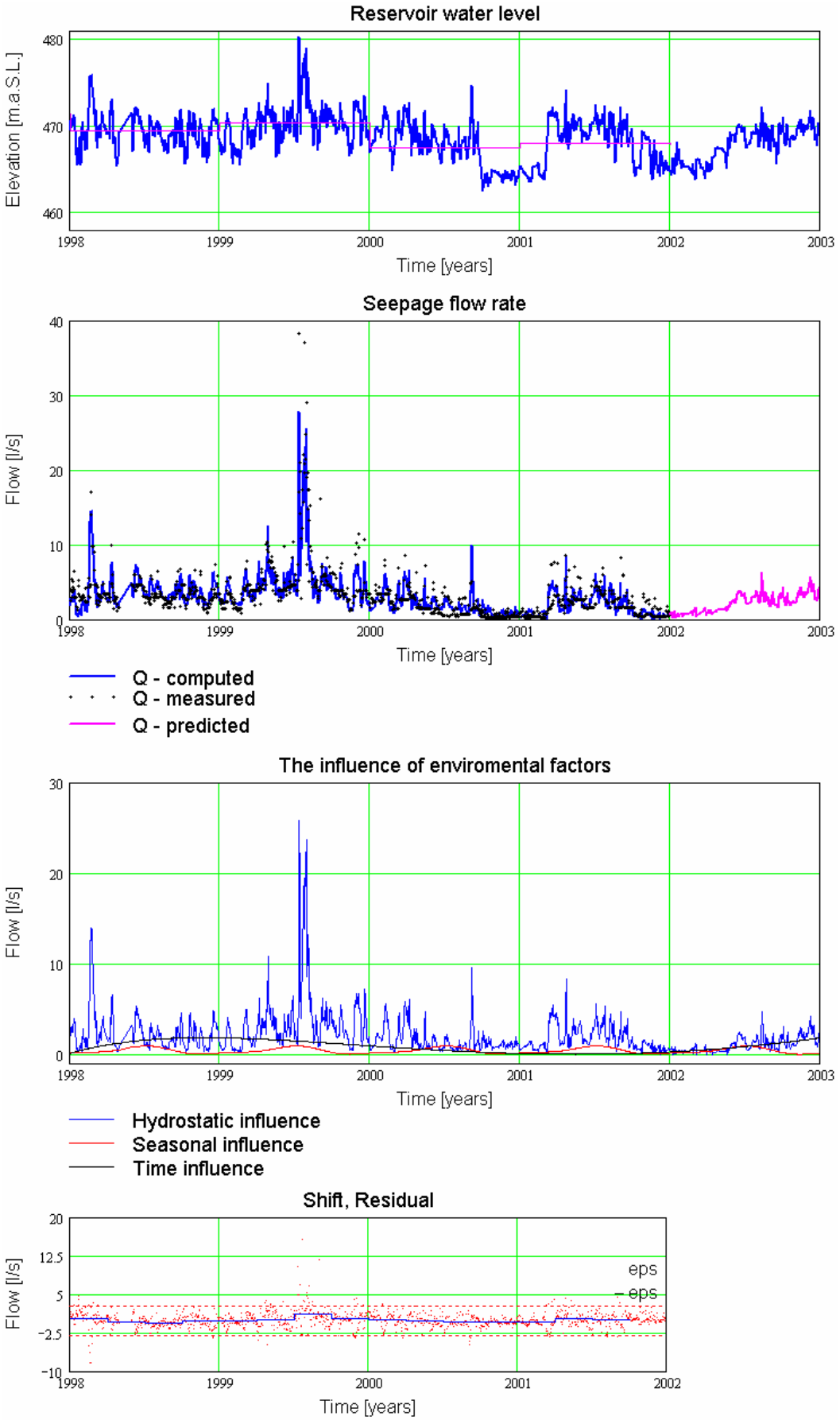

Fig. 6. Model multiple linear regression with delay for flow (1998-2002; β=1)

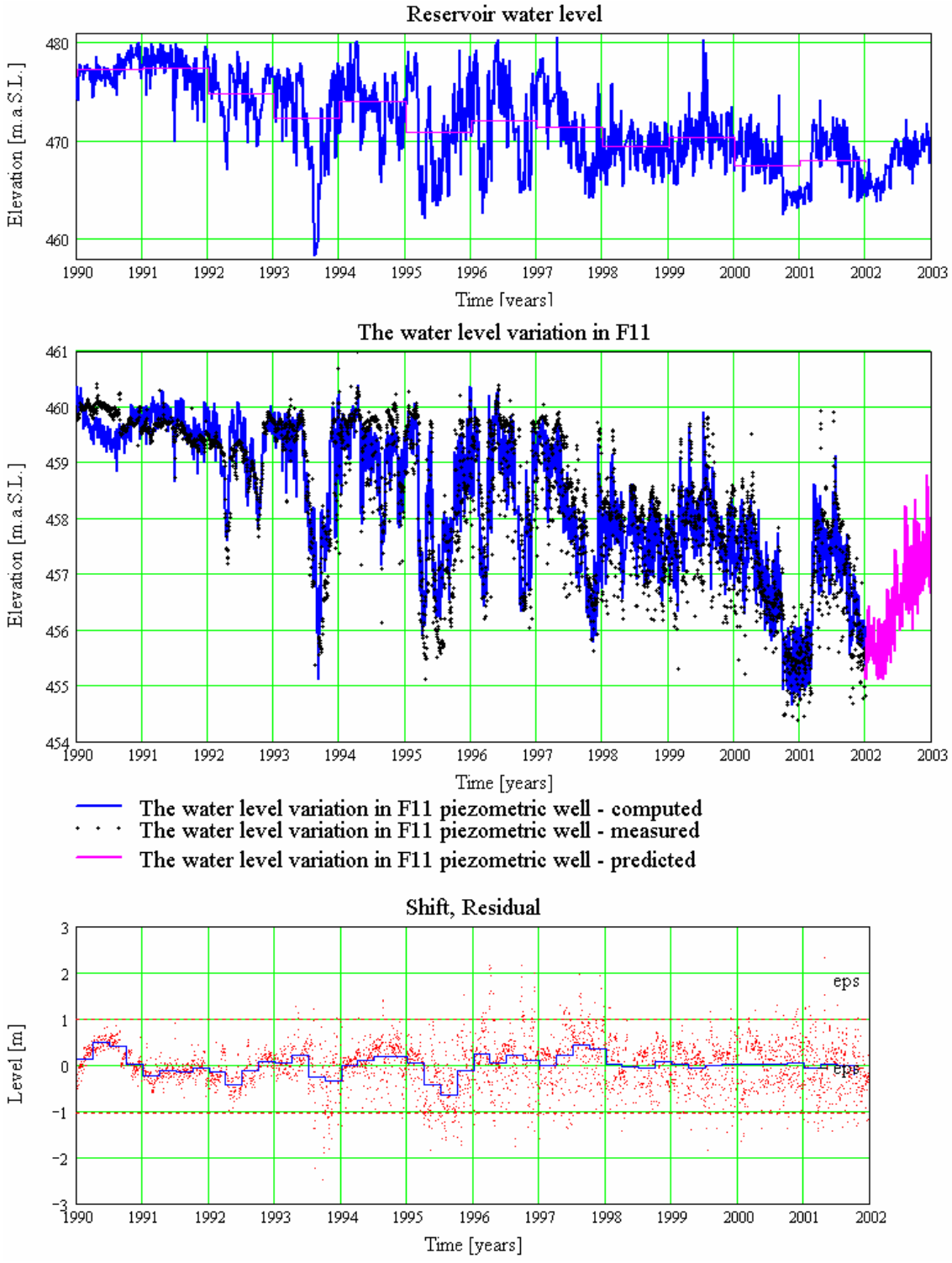

Fig.7. Model multiple linear regression with additional response data for F11 (1990-2002; β=10)

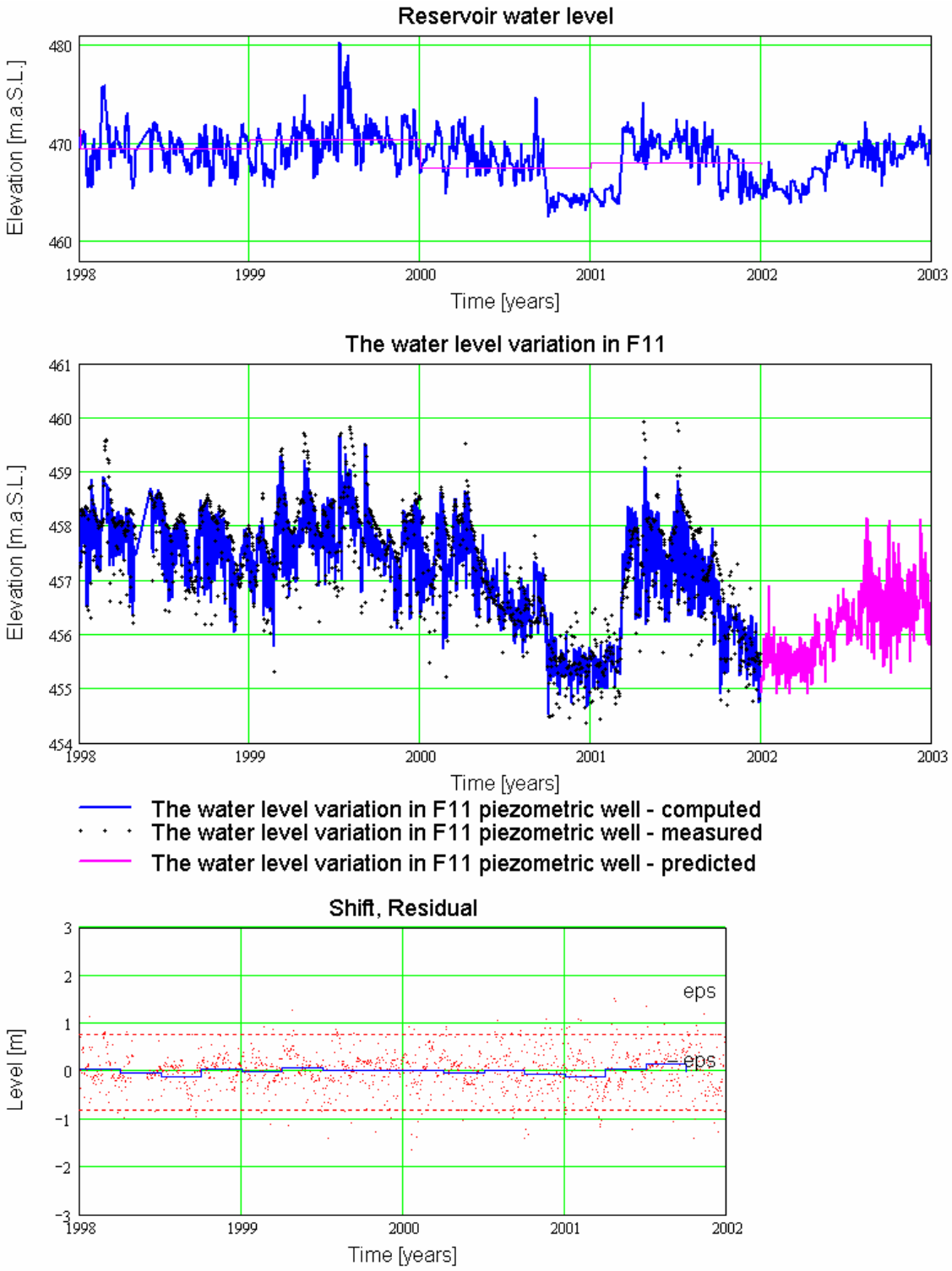

Fig.8. Model multiple linear regression with additional response data for F11 (1998-2002; β=1)

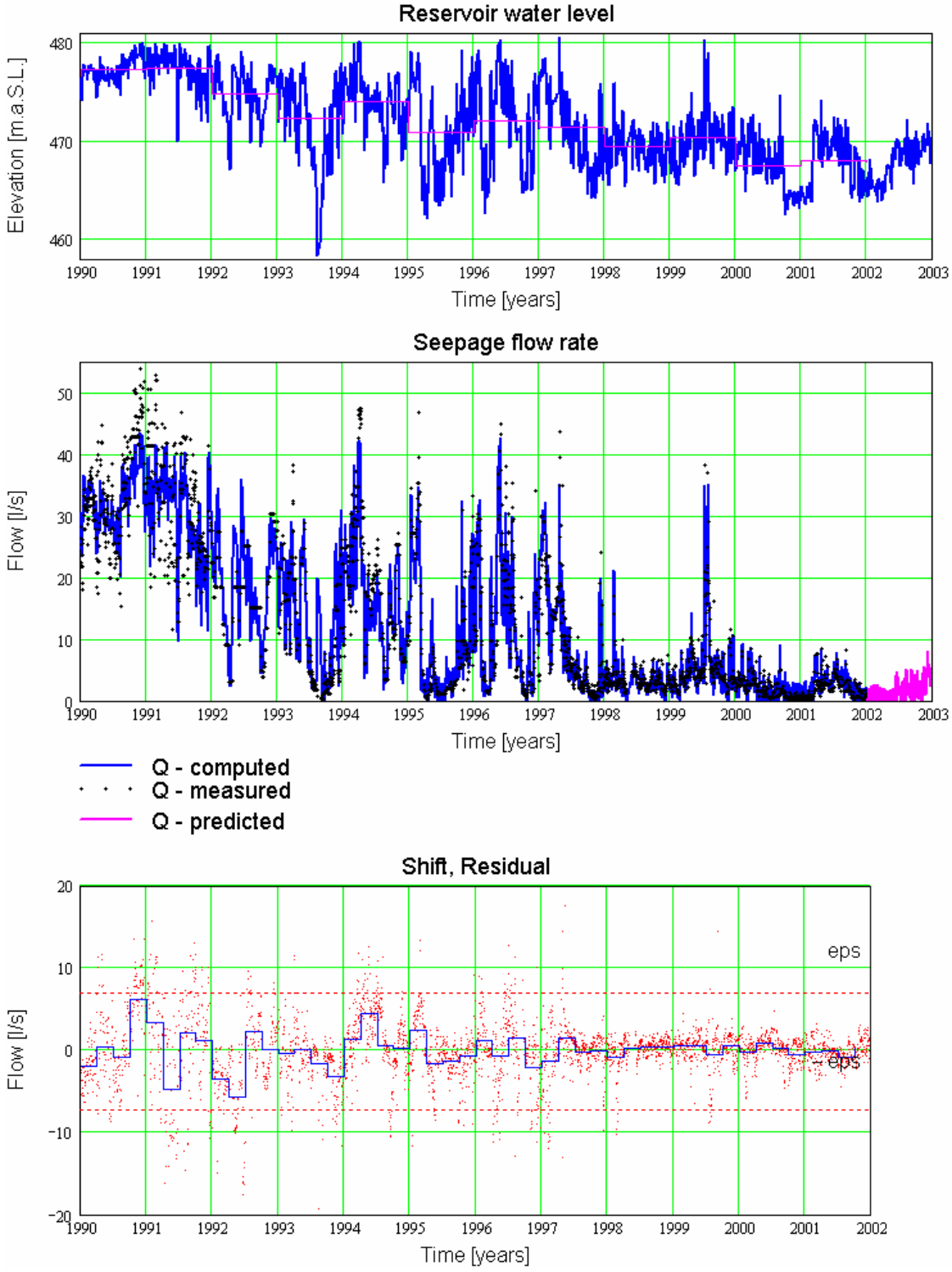

Fig.9. Model multiple linear regression with additional response data for flow (1990-2002; β=10)

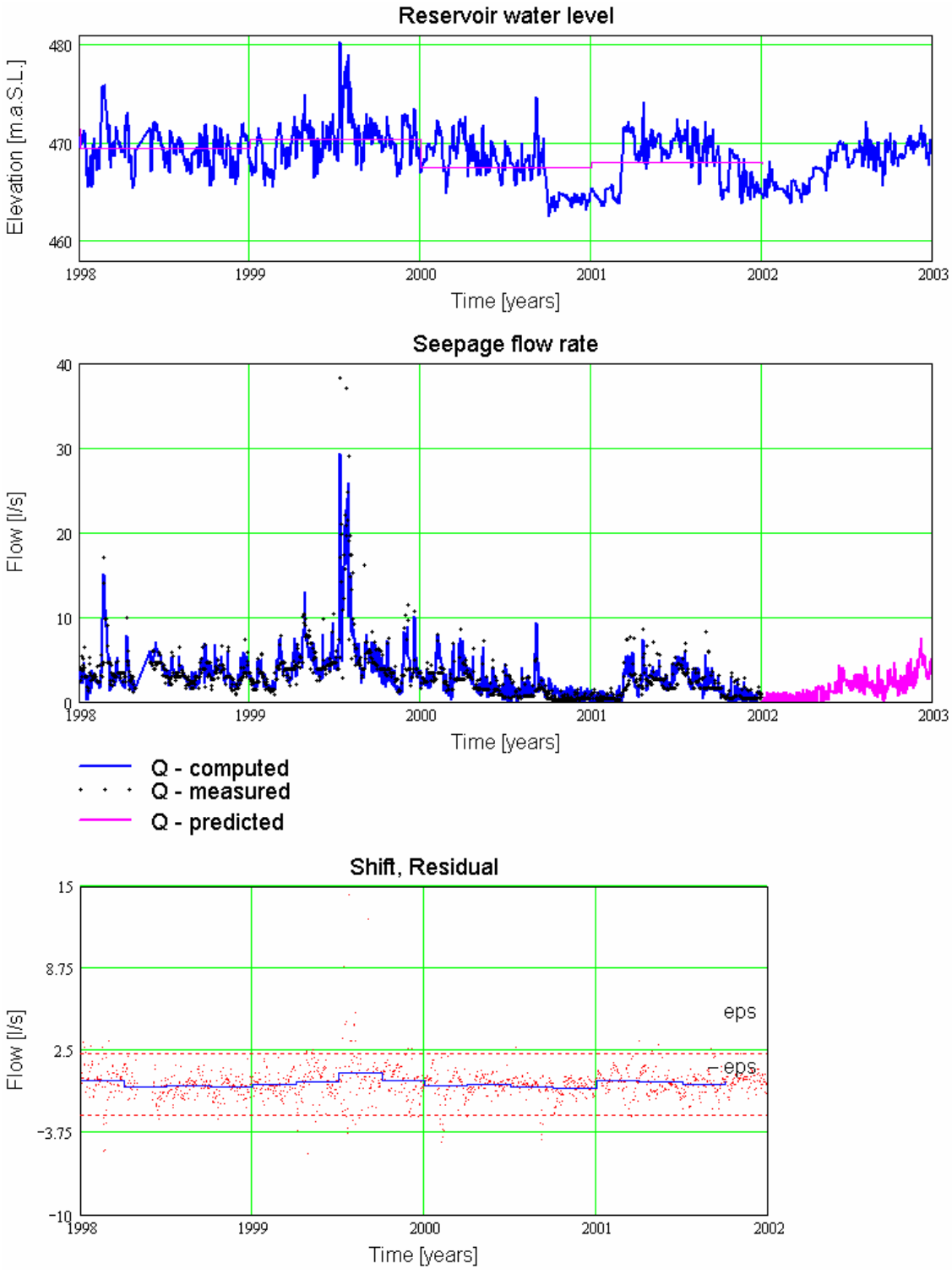

Fig. 10. Model multiple linear regression with additional response data for flow (1998-2002; β=1)

calibration have been evaluated on the basis of the residual variation coefficient (shift) which quantifies the average difference between the prediction and the measure over the calibration period. The model corresponding to 1990 – 2001 (β=1) period is characterized by **0.519** residual variation coefficient with residuals between **-2.49** m and **3.307** m. The second model, calibrated for 1998 – 2001 (β=1) period is characterized by **0.396** residual variation coefficient and the residual values range between **-1.639** m and **1.526** m.

3.2.2. Seepage flow. As for the piezometric levels, two different models have been developed based on the two calibration periods, namely 1990 – 2001 and 1998 – 2001 respectively. The model corresponding to 1990 – 2001 (β=10) period has residual variation coefficients in the range of **3.668** and the residual values between **-20.977** l/s and **17.976** l/s. The second model, corresponding to 1998 – 2001 (β=1) period is characterized by **1.185** residual variation coefficients and by residual values in the range of **-5.32** l/s and **14.374** l/s.

3.3. Results

The predicted water levels in the F11 piezometric well are presented in the figures 7… 10 and in a DBF file as required by the formulator.

4. CONCLUDING REMARKS

Good correlations between seepage flow, piezometer level in F11 and the reservoir level;

Efficient prediction by multiple regressive statistical models;

Best results were obtained when calibration period extends to the whole period of monitoring (1990 – 2002) as compared with the last operation period (1998 – 2002) with lowered level in the reservoir;

Multiple linear regression with additional data (other piezometers) model leads to better results as compared to the multiple linear regression with delay model;

Time influence rendered evident by HST models show a slow decrease of seepage at constant hydrostatic load;

Multiple linear regression with delay model is a more convenient tool for dam behavior monitoring.

REFERENCES

[1] Popovici, A. – Dams for water storage, Ed.Tehnică, Bucharest 1992.

A STATISTICAL MODEL FOR THE EVALUATION OF FLOW AND PIEZOMETRIC LEVELS AT MOTRU DAM

Bachir Touileb
Hydro-Québec, Montréal, Québec, Canada

INTRODUCTION

The evolution of seepage at Motru dam (Romania) is monitored by means of flow measurement devices and a large number of piezometers located downstream of the earth structure and in the right bank of the dam (figure 1 and 2). The present paper is aimed to develop a fairly accurate statistical model allowing for the prediction of future evolution of seepage based on a database of eleven years of daily field measurements of reservoir levels, daily rain accumulation and piezometric levels (figure 3).

An analytical relationship allowing for the estimation of total flow based on a set of available data such as the reservoir water level and the accumulation of rain is determined. The procedure that was used is mainly based on the calculation of a set of parameters by means of the minimisation of the error associated to the model compared to the field measurements. It is then followed by a tentative auto-regression model on the error itself in order to predict the range of the error corresponding to the calculated flow, and apply the appropriate correction..

GENERAL CONSIDERATIONS REGARDING EVOLUTION OF SEEPAGE

Preliminary analysis of different types of correlation among the available data, by means of the computation of the variance and the covariance, has shown a strong correlation between the actual flow and the actual water level of the reservoir. However, further investigation of the measured flow values revealed that some other variables are influencing the measured total seepage. Indeed, different daily flows were found to be associated to a single water level. Such a discrepancy was later explained by the fluctuation of the reservoir, in particular during a major drawdown or a major increase of the reservoir water level.

The incremental flow dQ, associated to an increment of time dt, downstream of a dam can be expressed as follows:

$$dQ = dQ_k + dQ_H + dQ_P$$

Where,
dQ_K = variation of flow due a change of permeability (K) of the materials of the dam,
dQ_H = variation of flow due a change of reservoir water level (H),
dQ_P = variation of flow due a change of precipitation such as rain or snow melt (P).

Each elemental increment entering into the summation leading to the total increment dQ could be expressed by the following partial differential equation :

$$dQ = \left| \partial Q/\partial K \right|_{C1} dK + \left| \partial Q/\partial H \right|_{C2} dH + \left| \partial Q/\partial P \right|_{C3} dP$$

where,
∂ refers to the partial differential operator,
C_1 = condition imposing H and P constant,
C_2 = condition imposing K and P constant,
C_3 = condition imposing H and K constant.

The evolution of seepage dQ_K due only to the change of permeability could be expressed as a function of time; that is without a specific introduction of the coefficient of permeability into the analytical relationship. Such a practical simplification aiming to the detection of change of flow that is specifically related to K can turn to be more useful than a more complex analysis of the flow such as by means of the finite element method as long as the device of flow measurement is reliable.

The evolution of seepage dQ_H due only to the change of reservoir water level was found to be mainly related to the actual water level. However, the consideration of water levels of the last two proved to increase substantially the accuracy.

The evolution of seepage dQ_P due only to a change of precipitation conditions such as rain could be determined by means of a linear combination of the accumulation of rain corresponding to the actual day, including the flow due to the rain corresponding to the last two days [1].

STATISTICAL ANALYSIS OF THE AVAILABLE DATA

Statistical analysis of the available data was perfomed by means of the determination of the coefficients of correlation between different instruments. Table 1 shows that both total seepage and the piezometric level at piezometer F11 are strongly related to the reservoir water level. Moreover, piezometers R42, F13, F6, R35, F12 and F5 are fairly well related to both seepage and piezometric level at F11.

The prediction of flow and piezometric levels in the case of Motru dam was found to be more suitable by means of the use of a statistical model. Most of the actual development was derived conformably to the available findings corresponding to the HST (Hydrostatic – Seasonal – Temperature) model [2]

Table 1 Coefficients of correlation for flow and piezometric level at F11

Measurement	Flow	Measurement	Piezometer F11
FLOW	1,000	**F11**	1,000
W_LEVEL	**0,869**	F6	**0,874**
R42	**0,853**	R42	**0,864**
F13	**0,830**	W_Level	**0,845**
F6	**0,821**	F12	**0,841**
R35	**0,791**	R35	**0,828**
F12	**0,763**	F13	**0,794**
F11	**0,755**	Flow	**0,755**
F5	**0,755**	F5	**0,647**
F1	0,631	F1	0,645
R31	0,595	R27	0,588
R27	0,550	R31	0,506
R38	0,455	R38	0,417
RAIN	0,024	RAIN	0,017
T_AIR	-0,076	T_AIR	-0,048

A STATISCAL MODEL FOR FLOW

The reproduction of measured flow at Motru dam was performed by means of a statistical model based on available data. The parameters of the model were determined by means of Newton's method for the minimisation of the sum of square differences between the calculated and measured flow values ($\Sigma\ (Q_{model} - Q_{measured})^2$). Such a procedure being available in the solver tool of the software Excel, it was used on the entire set of data and without any preliminary investigation of the quality of the data.

Several statistical analyses were performed including the consideration of the whole set of data. However, it is found that it is sufficient to built the statistical model only on the data corresponding to the years 2000 and 2001. The final relationship that is found to reproduce with sufficient accuracy the evolution of seepage Q is the following :

$$Q = A_1 + [\ \Sigma_{i=1,4}\ (B_i\ .\ Z^i)\ ] + [\ \Sigma_{i=1,6}\ (C_i\ .\ Y_i)\ ]$$

Where,
Z = Normalized water level = (H – Hmin) / (Hmax- Hmin),
H = Reservoir water level (m),
Y = Normalized piezometric level = (P – Pmin) / (Pmax- Pmin),
P = Piezometric level,
A_1 = Constant related to the units and the limits used for the problem,
B_1, B_2, B_3, and B_4 = Parameters related to the hydrostatic function or water level,
C_1, C_2, C_3, C_4, C_5 and C_6 = Parameters related to the piezometric levels in F5, F6, F12, F13, R35 and R42 respectively,

All the parameters of the model are shown in table 2.

Table 2 Parameters of the model of flow

Influence	**Parameters**			
Origin	**A_1**			
	0,198471			
Water level	**B_1**	**B_2**	**B_3**	**B_4**
	-5,414948	4,692656	0,199015	1,935295
Piezometers				
F5	**C_1**	1,907533		
F6	**C_2**	2,863423		
F12	**C_3**	0,332050		
F13	**C_4**	0,886502		
R35	**C_5**	0,086672		
R42	**C_6**	0,707902		

A STATISCAL MODEL FOR PIEZOMETRIC LEVEL AT F11

A statistical model equivalent to the one developed for the prediction of the flow was used. The piezometric level P_z at piezometer F_{11} is calculated as follows :

$$P_z = A_1 + [\ \Sigma_{i=1,4}\ (B_i\ .\ Z^i)\ ] + [\ \Sigma_{i=1,6}\ (C_i\ .\ Y_i)\ ]$$

Where,
Z = Normalized water level = (H – Hmin) / (Hmax- Hmin),
H = Reservoir water level (m),
Y = Normalized piezometric level = (P – Pmin) / (Pmax- Pmin),
P = Piezometric level,
A_1 = Constant related to the units and the limits used for the problem,
B_1, B_2, B_3, and B_4 = Parameters related to the hydrostatic function or water level,

C_1, C_2, C_3, C_4, C_5 and C_6 = Parameters related to the piezometric levels in F5, F6, F12, F13, R35 and R42 respectively,

All the parameters of the model are shown in table 3.

Table 3 Parameters of the model of the piezometric level at F11

Influence	**Parameters**			
Origin	**A_1**			
	454,340586			
Water level	**B_1**	**B_2**	**B_3**	**B_4**
	2,063771	-0,008406	-4,790931	3,651530
Piezometers				
F5	**C_1**	-0,270375		
F6	**C_2**	-0,002702		
F12	**C_3**	1,889698		
F13	**C_4**	-0,783392		
R35	**C_5**	1,416142		
R42	**C_6**	1,349326		

VALIDATION AND APPLICATION OF THE MODELS

Both models for flow and piezometric level at F11 were statistically evaluated with coefficients of correlation in the vicinity of 0,90 (see table 4).

Table 4 Statistical evaluation of the models

	Flow	**Piezometer F11**
Coefficient of Correlation	0,87	0,91
Standard deviation	1,34	1,01
Nash coefficient	0,743	0,827

Application of the models to the prediction of the flow and the piezometric level at piezometer F11 for the year 2002 lead to the results shown in figure 4 and figure 5 respectively. As it was stated during the workshop, a strong correlation is found between the highest discrepancies and the measurements corresponding to Saturdays and Sunday [3].

INVARIABILITY OF MAXIMUM SEEPAGE AND ACTIVE EROSION

Based on the analysis of the entire set of available data such as piezometric levels and differential amount of measured flow during major peaks, it is believed that the maximum value of seepage is rather stationary in the vicinity of about 50 l/s since the first reservoir impoundment [4]. No sudden increase of seepage was depicted following the early months or years following the reservoir filling period. In these circumstances, it is believed that there no evidence of continuous erosion or decrease of the permeability of the sealing components of the dam (clay core) or its foundation (grout curtain). Such a result was validated by means of the addition of a linear time function to the basic flow model described above. This component showed rather a decrease of few l/s over the entire period of time (1990 – 2001). The potential erosion of fine particles, that was noticed in situ, could be due to the artesian flow downstream of the grout curtain.

However, one could suspect the presence of medium to large windows in the grout curtain since the first use of the dam. Such a situation does not seem to have evolve during the last ten years. The potential existence of medium to large windows could give raise to an artesian flow condition below the downstream toe of the dam.

REMEDIAL MEASURES TO CONTROL STABILITY DUE TO SEEPAGE

Knowing that the dam was operated satisfactorily since the last 10 years, one could suggest to increase the stability of the dowstream slope of the dam by means of a better control of the artesian piezometric conditions. It is suggested to install a number of staged and sealed piezometers in the area located between the downstream toe of the clay core and the downstream toe of the dam in order to validate the presence of an artesian condition. Based on these values, the stability of the downstream slope must recalculated.

Three different remedial measures are suggested knowing that the dam is located in a seismic area and that it needs a certain margin of safety at normal loading conditions. The following solutions ranged from the less to the most expensive are presented hereafter :

Solution # 1 : Despite the noticeable absence of an upstream blanket - that would have been an efficient second line defence against any lower performance of the cut-off, one could suggest that an appropriate number of relief wells could improve substantially the control of seepage and the stability [5]. This is the less expensive solution.

Solution # 2 : If the first and most economical solution would be not sufficient, then it would be necessary to built an upstream impervious blanket (approximately 200 m long and 2 m thick) that is connected to a new impervious core (clay or membrane) located along the actual upstream face of the dam. Some relief wells could also be added downstream of the dam. Such a remedial measure has been successfully applied to the case of Lac Sainte-Anne dam (Quebec) in 2001.

Solution # 3 : A jet grouted cut-off is added to the last solution. However, the cost of this solution could be too high.

CONCLUSION

The variation of seepage at Motru dam was investigated by means of a statistical model based on the minimisation method of Newton. Such a model is also able to compute separately the flow due to the presence of the reservoir and the flow due to rain. A tentative determination of an error function allowing for the improvement of the accuracy was also performed. However, further investigation is needed in order to improve the later error function.

Regarding the remedial measures aiming for a better control of the seepage and an increase of the safety of the downstream slope of the dam especially against a major seismic loading, it is suggested to consider the installation of relief wells downstream of the dam (solution # 1) at first stage. Another solution consisting of a new upstream impervious blanket and a new core is suggested as the most robust one (solution # 2).

ACKNOWLDGEMENTS

The author is grateful to M. Jean-Yves Morency (Hydro-Québec) who shared some of his wide collection of pictures regarding the construction of Lac Sainte-Anne dam. The author is also grateful to M. Patrice Côté (Hydro-Québec – Manicouagan territorial direction) for providing some statistical developments regarding the HST (Hydrostatic – Seasonal – Temperature) model as it was previously applied to the prediction of displacements at Daniel-Johnson dam.

REFERENCES

[1] Gaume, E. – Hydrologie : cycle de l'eau et modélisation pluie-débit. École nationale des ponts et chaussées. Rapport technique. France. 2000.

[2] Comité Suisse des Barrages. Groupe de travail sur les methods numériques dans l'analyse du comportement des barrages. Méthodes de prédiction du comportement des barrages : Comparaison Mesuré – Calculé. 18 décembre 2000.

[3] Noret-Duchêne, C and Carrère A. – Prediction of seepage and piezometry at Motru dam with statistical models. 7th ICOLD Benchmark workshop on numerical analysis of dams. To be published.

[4] Popovici, A. – Technical university of civil engineering of Bucharest. 7th ICOLD Benchmark workshop on numerical analysis of dams. Theme C – Embankment dams. Seepage through an earthfill dam – foundation system and piezometric level variation downstream of the dam. Databook. Bucharest. 2003.

[5] American Society of Civil Engineering. Technical engineering and design guides as adapted from US army corps of engineers, No.3. – Design, construction, and maintenance of relief wells. Adapter from New York. 1993.

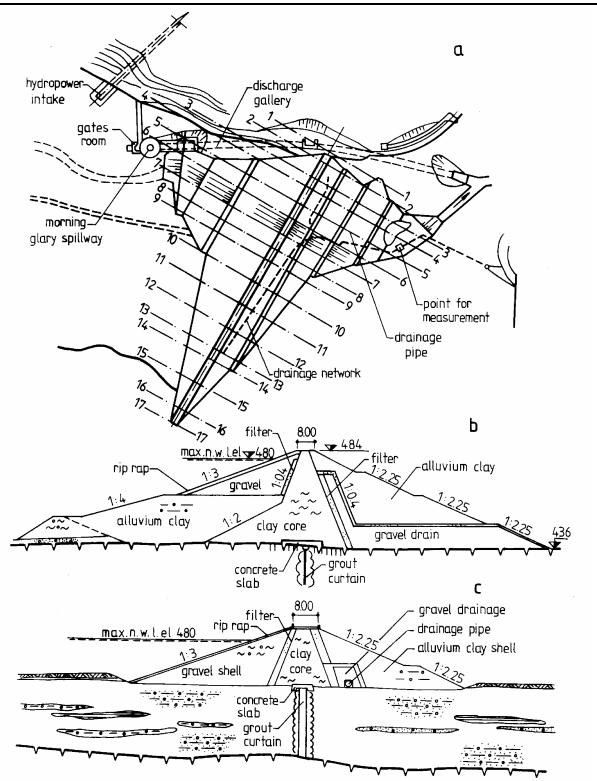

Fig. 1.Motru dam. Typical cross sections

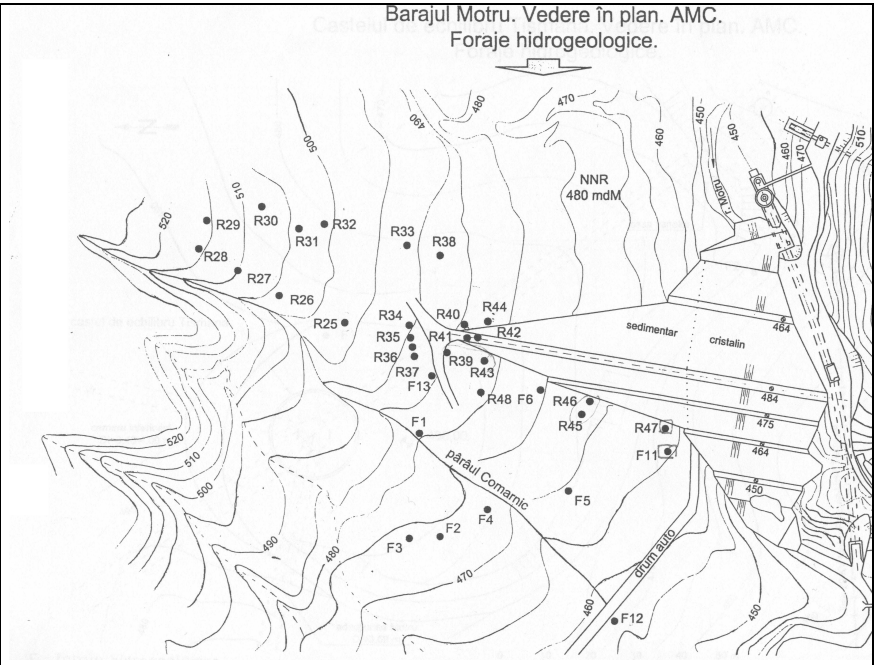

Fig. 2.Motru dam. Location of piezometers

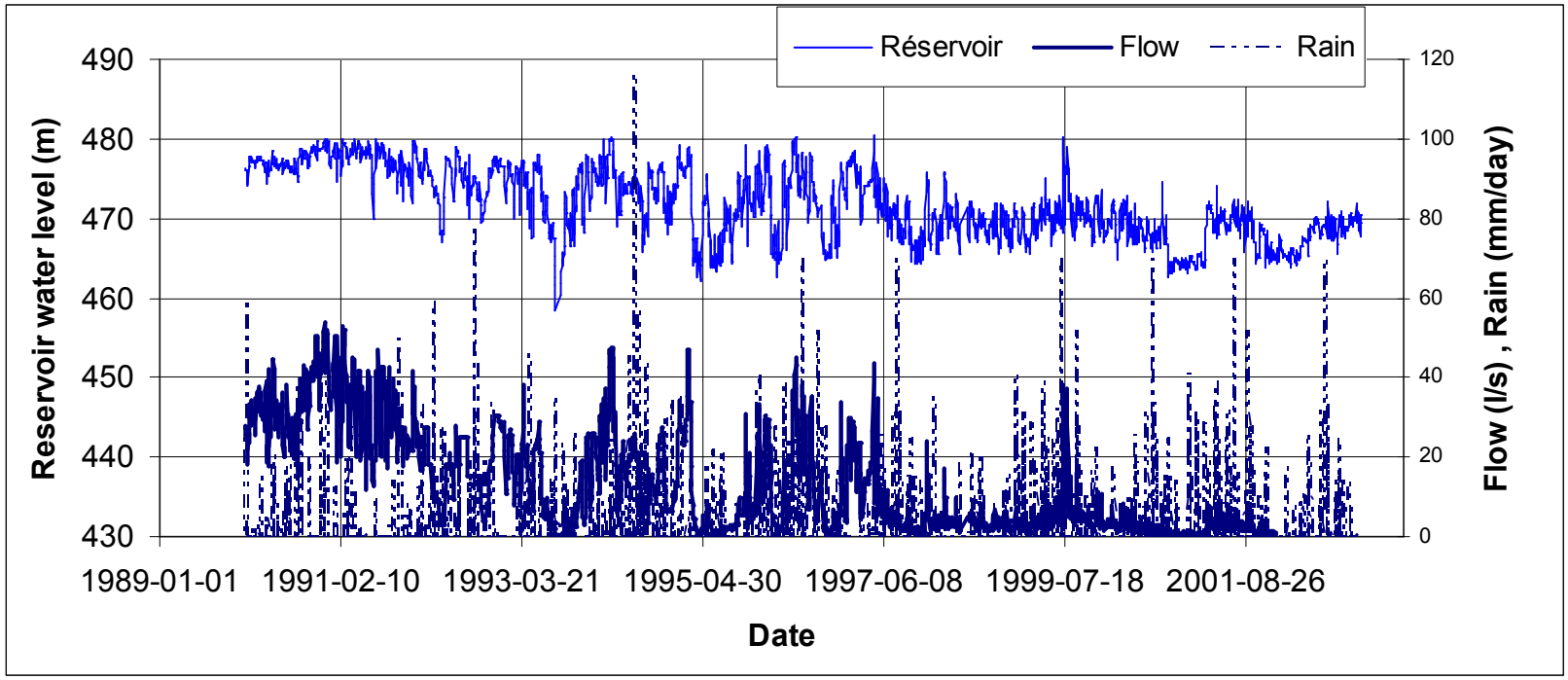

Fig.3Reservoir water level, rain accumulation and flow from field measurements

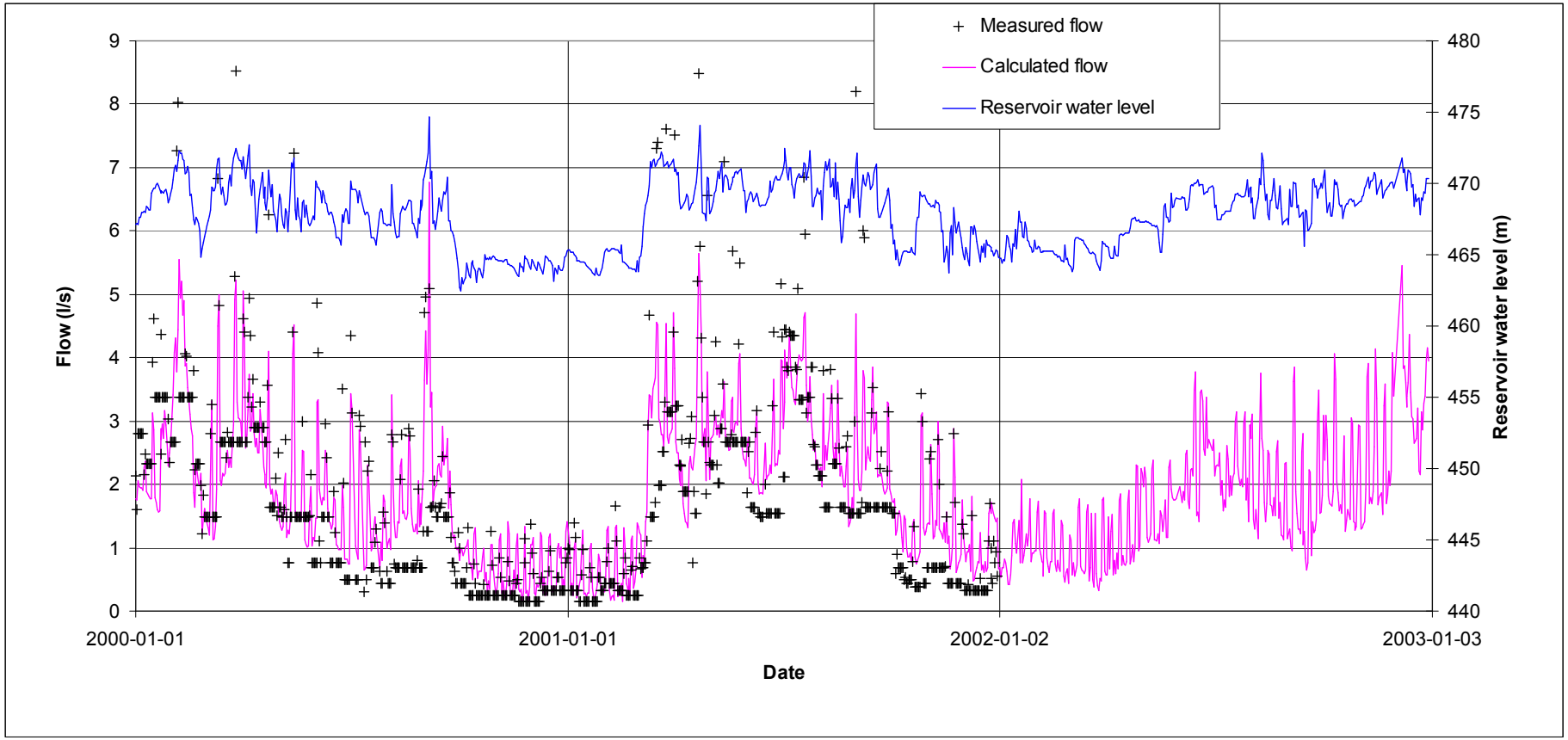

Fig. 4.Use of the model for the prediction of flow for the year 2002

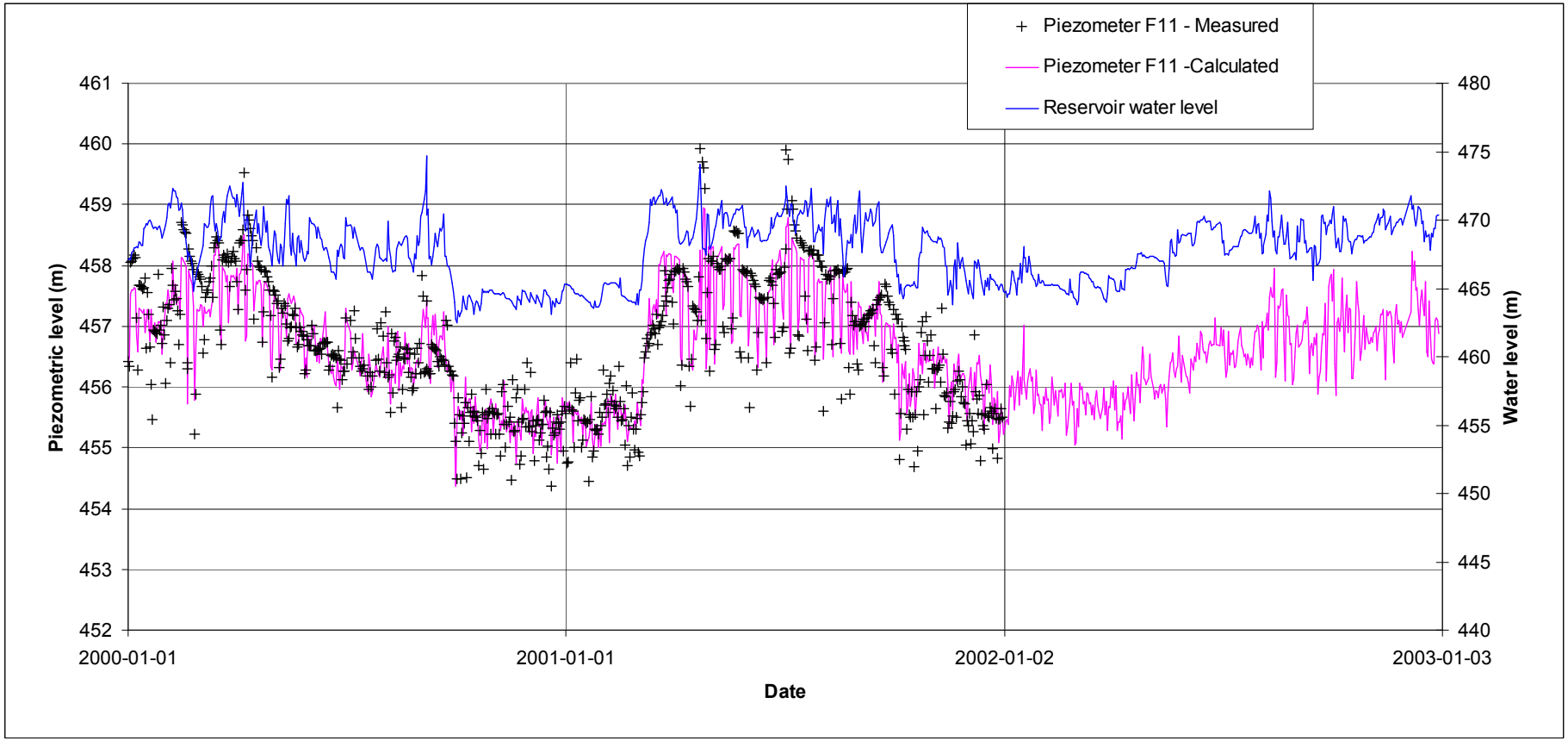

Fig. 5.Use of the model for the prediction of piezometric level at F11for the year 2002

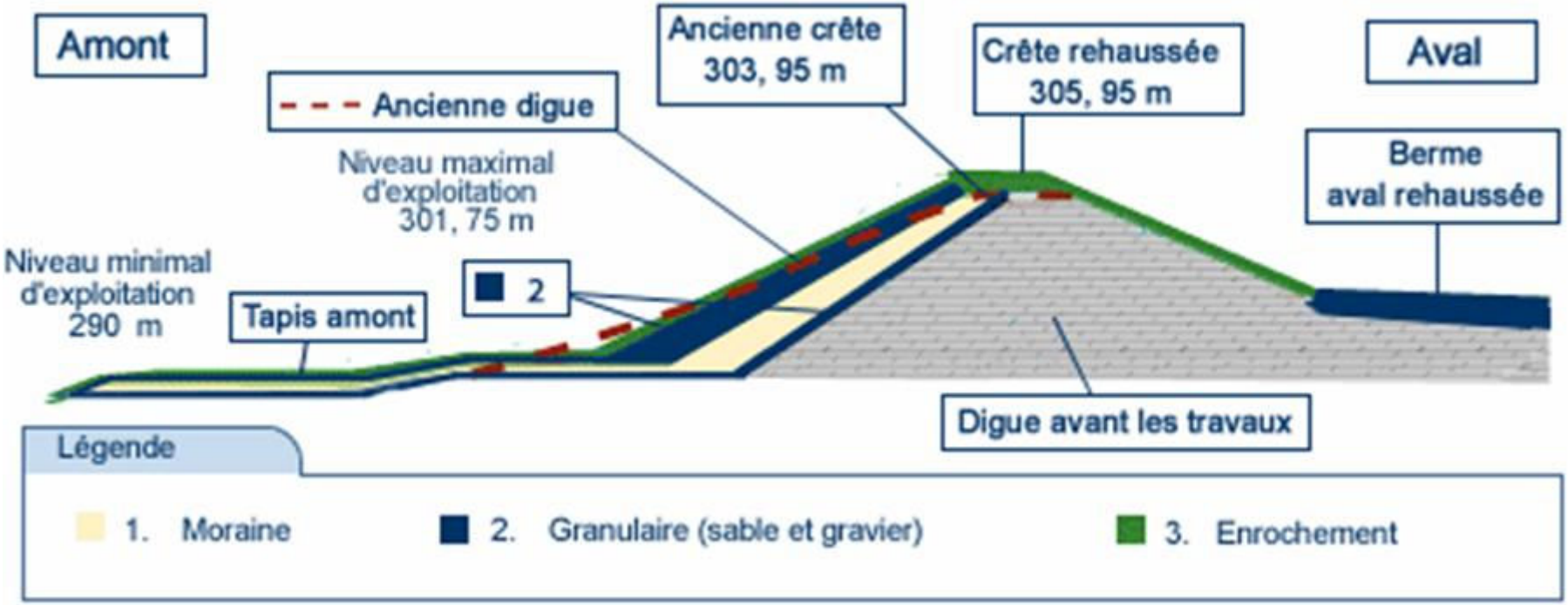

Fig. 6.Lac Sainte-Anne dam remedial works leading to the decrease of seepage and increase of the overall stability

POSTER SESSION

THE CALCULATION OF SEISMIC PRESSURE IN DAM CONDUITS AT OPERATING FLOW CONDITION AND ITS APPLICATION IN ASEISMIC DESIGN OF HYDRAULIC STRUCTURES & EQUIPMENT

Yousef Asadi-Khiavi

Electrical Engineering Services Co.(MOSHANIR), Tehran, Iran

ABSTRACT: The common practice for seismic pressure calculation is based on hydrostatic initial condition. This paper describes a new approach for computation of possible seismic pressure in dam conduits based on hydrodynamic initial condition and hydrodynamic loads on structure/equipment (like flap gate in fully opened position) subjected to Design Basis Earthquake (DBE) at maximum operating water level.

Résumé:La pratique ordinaire pour le calcul de pression sismique est basée sur la condition initiale hydrostatique. Cet article décrit une nouvelle approche pour le calcul de la pression sismique possible dans le conduit de barrage basé sur la condition initiale hydrodynamique et les forces de hydrodynamique sur les structures & équipement (e. g. la porte d'aileron en position entièrement ouverte) soumis au tremblement de terre de base de conception dans (DBE) l'opération maximum du niveau d'eau.

1. INTRODUCTION

1.1. GENERAL

It is clear that, huge masses of water enclosed in bottom outlet conduits will be set in motion by an earthquake and may cause great damage. The similar analyses to be performed for power outlets of hydropower plants. So, the analysis exemption at operating flow condition is not correct.

The theory of transient flow analysis, can be applied in two cases:

- The bottom outlet of dam during flow condition in various gate opening positions

- The power outlet (e.g. flap gate in draft tube) at operating flow condition

1.2. PROPOSED CALCULATION PROCEDURE

The new approach for calculation of seismic pressure consists following items:

1- Based on Earthquake Analysis Procedures For Dams(State of the Art-ICOLD), the transient seismic pressure function can be derived and can be applied as boundary condition at tailrace conduit outlet for set of Basic Equations for Unsteady Flow Through Conduit. It is applicable to both submerged bottom outlets and power outlets.

2- For Power outlets, the Hydraulic Turbine induced oscillating pressure function is available as turbine data to be applied as boundary condition at draft tube inlet for set of basic equations for Unsteady Flow Through Conduit. The exitation function can be approximated as sinusidal oscillation for francis turbines with resonable accuracy.

3- Pressure and velocity values at full load operating condition to be applied as initial conditions for set of basic equations for Unsteady Flow Through Power Outlets and Conduit at to be applied at.

The a/m basic equations and relevant coefficients and constants for steel lined conduit mentioned in particular hydraulic transient references can be applied.

In the last thirty years, the majority of research works that have been done in seismic pressure modeling correspond to hydrostatic initial conditions. Zienkiewicz [12] introduced the calculation procedure in its present form. In the new modified calculation procedure, a dynamic term is added to equations, to overcome this problem. The final form of the equations is given in the next section.

2. GOVERNING EQUATIONS

Mathematical model of the hydraulic transient hammer effect in a dam conduit under pressure is described by a set of two partical differential equations [8]

$$\frac{a^2}{g}\frac{\partial V}{\partial x} + V\frac{\partial H}{\partial x} + \frac{\partial H}{\partial t} + V\sin a = 0 \qquad (1)$$

$$g\frac{\partial H}{\partial x} + V\frac{\partial V}{\partial x} + \frac{\partial V}{\partial t} + \frac{\lambda |V| V}{2D} = 0 \qquad (2)$$

Where:
x-length co-ordinate,
t- time,
H- static pressure head,
V- flow velocity,
D- conduit equivalent hydraulic diameter
g- natural gravity,
a- increased pressure wave velocity,
α- inclination angle between conduit and horizontal line.
λ -friction factor

The first equation of continuity derived from the law of conservation of elastic fluid mass flowing in an elastic conduit. The second, is an amount of motion equation that descrbes dynamic equilibrium of fluid particles in a cross- section of the conduit. Equations (1) form a closed system of partical differential equations of hyperbolic type with unknown functions H(x,t) and V(x,t). The system can be solved numerically for adequate boundary conditions.

3. NUMERICAL SOLUTION

The characteristics method can solve this system of equations [8]. It enables transformation of the partical differential equations (1) into a system of diffeential equations, which in turn can be transformed into difference equations, i.e.:

$$\begin{aligned}
&\frac{\Delta x}{\Delta t} = V + a \\
&\frac{\Delta V}{\Delta t} + \frac{g\Delta H}{a\Delta t} + \frac{g}{a} V \sin a + \frac{\lambda |V| V}{2D} = 0 \\
&\frac{\Delta x}{\Delta t} = V - a \\
&\frac{\Delta V}{\Delta t} - \frac{g\Delta H}{a\Delta t} - \frac{g}{a} V \sin a + \frac{\lambda |V| V}{2D} = 0
\end{aligned} \tag{4}$$

Similar derivation is presented in work [9]. Calculations of unknown values of H(x,t), and V(x,t) are performed for a limited number of points (nodes) on (x,t) plane called the grid. This points are form nodes of the characteristic grid. Calculation process of unkown values of approximate solution of the equation system (1) in individual nodal points of the grid is based on adequate difference equations.

The relevent functional diagram have to include the following nodes of characteristic grid:

a) Internal nodes,

b) boundary node on the side of the upstream(e.g. turbine or gate,…).

c) boundary node next to the lower reservoir

d) boundary node at surge shaft, if any.

a) Equations for internal nodes.

In order to calculate values of functions HT(x,t), VT(x,t) in internal nodes of the grid, finite difference equations are as follows:

$$V_T = 0.5[V_R + V_S + (H_R - H_S)\frac{g}{a} - \frac{\lambda \Delta t}{2D}(V_R|V_R| + V_S|V_S|) - \frac{g}{a}\Delta t(V_R - V_S)\sin a] \quad (5)$$

$$H_T = 0.5[H_R + H_S + \frac{a}{g}(V_R - V_S) - \frac{a}{g}.\frac{\lambda \Delta t}{2D}(V_R|V_R| + V_S|V_S|) - \Delta t(V_R - V_S)\sin a] \quad (6)$$

where:

$$\begin{aligned} V_R &= V_O[1 - \Theta(V + a)_O] + V_M \Theta(V + a)_O, \\ V_S &= V_O[1 - \Theta(V - a)_O] - V_N \Theta(V - a)_O, \\ H_R &= H_O[1 - \Theta(V + a)_O] + H_M \Theta(V + a)_O, \\ H_S &= H_O[1 + \Theta(V - a)_O] - H_N \Theta(V - a)_O, \\ \Theta &= \frac{\Delta t}{\Delta x} \end{aligned} \quad (7)$$

indenxes M, N, O, T, R, S in the above equations are related to nodal points of the grid, and should abtion values interpolated from functions V and H.

4. RESULTS

A computer code is developed and tested with several simple flows to ensure that it works properly [8]. The code was first used to simulate one dimentional turbulent flow in one conduit and several different limiter and boundary conditions were used and stability and convergence of the numerical simulation were examined [8]. The results compared with Streeter [8] and Chaudry et al [9]. As a result, the maximum obtained pressure [12] in bottom outlet flow condition, which produced better results for the cases studied, were chosen and used throughout this paper. Finally the following three cases of turbulent flows were simulated and tested.

1- Bottom outlet flow condition in full opened position of gate.

2- Bottom outlet flow condition in partially opened position of gate

3- Power outlet flow condition in full load operation of turbine

The results of analysis based on a/m Calculation Procedure show that seismic pressure caused by DBE at operating flow condition is higher than seismic pressure calculated by conventional method with hydrostatic initial condition .

5. CONCLUSIONS

In this work, the numerical methos for solving the Allievi's equations are introduced. Then special boundary conditions for siesmic load cases were examined and compared by using conventional methods and relevant and phenomena.

The results are higher than values calculated based on conventional methods and worst case is when frequency of forced oscillations fits with one of the natural frequencies of the system so the presented new approach to be applied in aseismic design.

In the flow in draft tubes, the comparison of conventional and new results shows that this new method produce rather accurate and reasonable results.

REFERENCES

[1] Shul'man, S. G., Seismic Pressure of Water on Hydraulic Structure, Leningrad Section, Russian Translations Series, Publisher: BALKEMA, ISBN: 90 6191 480 9, 1987.

[2] USCOLD, Guidelines for Selecting Seismic Parameters for Dam Projects, United States Committee On Large Dams(USCOLD), October 1985.

[3] USCOLD, Observed Performance of Dams During Earthquake, United States Committee On Large Dams(USCOLD), July 1992.

[4] USBR, Design Standard No. 13-Embankment Dams-Chapter 13-Seismic Design and Analysis, United States Bureau of Reclamation(USBR), December 1989

[5] Asadi-Khiavi, Y., "Proposal for Revising the ISIRI 2800 Code and its Application in Aseismic Design of Power Piping Systems," The 13th. International Power System Conference(IPSC-98), EPRC, Tehran, Iran, November 1991.

[6] Jaeger C., Fuid Transients in Hydro-Electric Engineering Practice, Publisher: Blackie, ISBN: 0 216 90225 8, 1977.

[7] ICOLD, Earthquake Analysis Procedures For Dams-State of the Art, Bulletin 52, International Committee On Large Dams(ICOLD), 1986.

[8] Streeter, V. L., and Wylie, E. B., Hydraulic Transients, McGraw-Hill Book Company , 1967.

[9] Chaudry, M. H., Applied Hydraulic Transients, Van Nostrand Reinhold Company , 1987.

[10] Pejovic, S., Blody, A. P., and Obradovic, D., Guidelines to Hydraulic Transients Analysis, Gower Technical Press, 1987

[11] Pejovic, S., "Analysis of Earthquake Effects Upon Hydraulic Structures, " The 5th. International Conference on Pressure Surge, Hannover, Germany, September 1986

[12] Zienkiewicz, O. C., "Hydrodynamic Pressures Due to Earthquake, " The journal of Water Power, 1964

7TH BENCHMARK WORKSHOP ON NUMERICAL ANALYSIS OF DAMS

September 24 - 26, 2003, Bucharest, ROMANIA

STUDIES CONCERNING THE HEAT HYDRATION EFFECTS ON A MASSIVE CONCRETE DAM: – THE ISSUE OF TEMPERATURE CONTROL – THE ISSUE OF CRACK CONTROL

Roberto Menga - roberto.menga@enel.it - +39 035 5377 659
Rita Pellegrini - rita.pellegrini@enel.it - +39 035 5377 656

Enel.Hydro / Ismes Division – 24068 Seriate - Bergamo – Italy

ABSTRACT

The paper illustrates assessments that have been carried out at ISMES during the construction of a large concrete dam in the Sardinia island region (Italy).
The study was devoted to the prediction of temperature rise during construction, in order to avoid excessive temperature change in concrete, and thereby reduce the possibility of damage by cracking.
Analyses initially addressed mainly the dissipation of the cement hydration heat through conduction in the mass concrete material and different boundary environmental conditions; later the problem turned into thermo-mechanical and was devoted to the study of stress evolution.
The practical difficulty was the need to consider the frequent changes of the body geometry and boundary conditions, due to the sequence and rate of placement of successive concrete lifts.
The first part of the paper illustrates the thermal problem for temperature control and the second one shows the evolution of thermal stresses for crack control.

THE ISSUE OF TEMPERATURE CONTROL

1. DESCRIPTION OF THE DAM

The Cantoniera Dam is a concrete buttress dam, built in the period 1982-1996: the firsts casting begun in 1990. The dam body consists of 38 buttresses 15 m thick: the central (6) are provided of an overflow spillway. The buttresses have been designed to be joined each other at the outer sections (upstream and downstream expansions), while the internal section (the leg) has a hole to lighten the whole structure and enhance dissipation of hydration heat. Each internal leg is 11 m thick.
The dam is 100 m high, more than 500 m long and the concrete volume of the dam body is 870.000 m^3. The storage capacity is more than 790 hm^3, the area of reservoir is 28 km^2 and the catchment area is 2094 km^2. The dam is located on the Tirso river near the village of Cantoniera in the Busachi Municipality.

The foundation mass consists of metamorphic rocks (gneiss and micaceous schist), characterised by variable schistosity. Granite materials and, subordinately, porphyric and quartzose dykes abundantly inject such rocks. A lot of major, subvertical and winding discontinuities, intersect the rock mass; besides that there is a close net of secondary joints. The foundation rock has been consolidated by means of passive bolts.

Fig. 1 - The dam during the construction

The construction of the dam was over in 1996. The layout and the main sections of the dam are depicted in Fig.2.

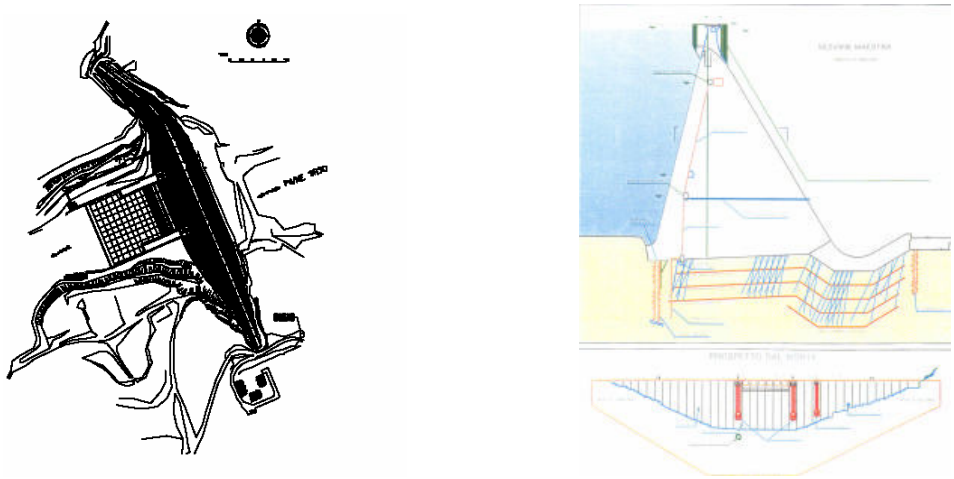

Fig. 2 - The layout and the main sections

2. THE CONSTRUCTION SEQUENCE

The dam body was cast with two concrete mixes and an overall amount of 260 kg/m^3 of reactive material: pozzolanic cement (200-220 kg/m^3) and fly ash (60-40 kg/m^3) for the legs and the expansions were used respectively. The aggregates were basaltic with a maximum diameter of 100 mm, very stiff. The dam construction programme started on December 1990. The buttresses of the dam were cast

according to a sequence of 3 metre thick layers (called the *blocks*), with sub-layers (called the *lifts*) 0,75 metre thick.
The resulting chronological schedule, for the central buttresses, is depicted in Fig. 3.
The casting time of each block was 2-4 days and the time between two successive blocks varied from 5 to 30 days.

Environmental conditions at the site are characterised by severe temperature seasonal change (+42°C, -2°C). The construction schedule in some cases (casting in summer – red blocks in figure 3) was considered potentially critical, since it might produce a comparatively unfavourable temperature drop within the concrete mass.

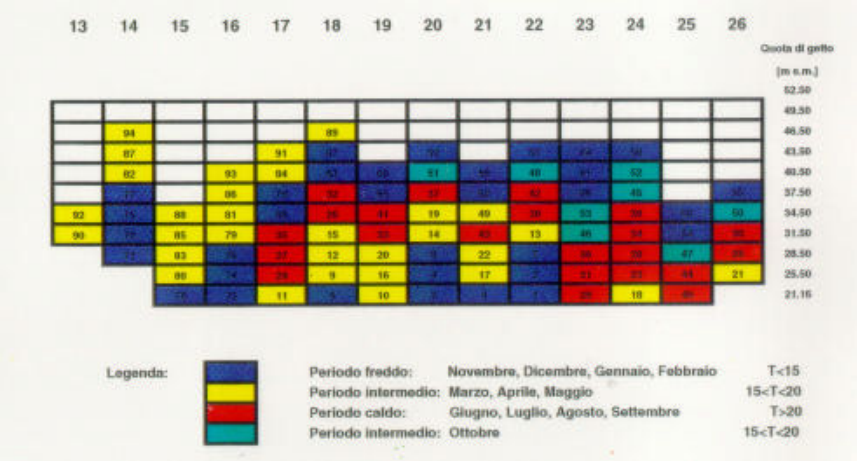

Fig. 3 - The chronological sequence of construction

3. THE OBJECTIVE

The Contractor decided to evaluate in detail casting prescriptions, in terms of allowed temperature change within the casting under the previously described situation. He asked to study possible options having impact on temperature control, as to safely proceed with the construction, and to analyse possible effects of the most unfavourable conditions in terms of cracks occurrence.

Some buttresses were selected for such studies, as representative in relation to the evolution of temperatures during the casting. Buttresses n. 22 and n. 26 were selected as the most representative of extreme casting and environmental conditions:

- n. 26 - casting in summer / cooling under decreasing external temperature;
- n. 22 - casting in winter / cooling under increasing external temperature.

4. THE THERMOMETER NETWORK

Electrical thermometers, in excess of two hundred, had been placed inside concrete layers at several elevations of the buttresses n. 15, 22 e 26. The figure 4 shows the typical locations of the instruments and the numbers of the thermometers for each elevation in buttress n. 26. Other thermometers were placed at different locations outside the dam to record the environmental temperature and the casting conditions. All the measurements were collected, in real time, by an automatic data logger.

The typical drawing of the measurements plotted by the MIDAS® software (Ref.1) is illustrated in figure 5.

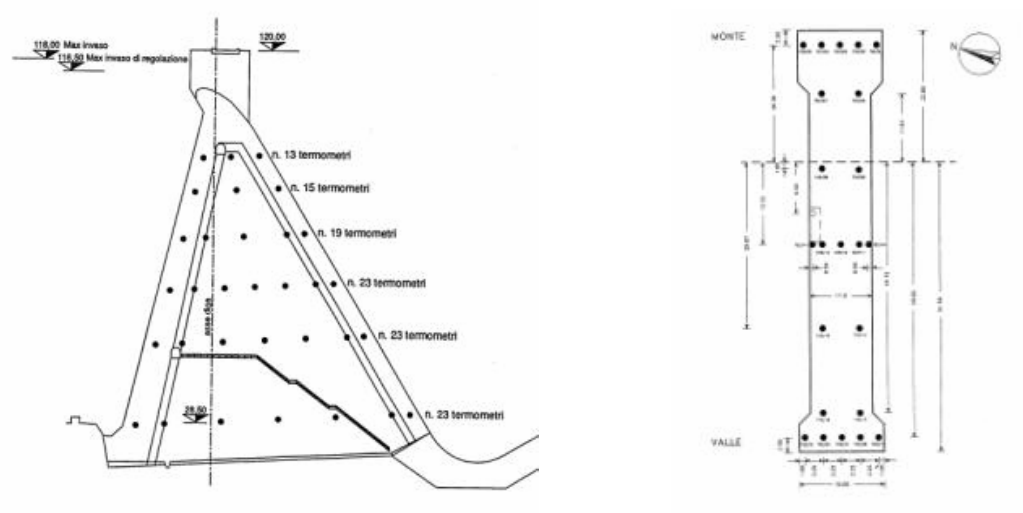

Fig. 4 – Buttress n. 26 - The thermometer network

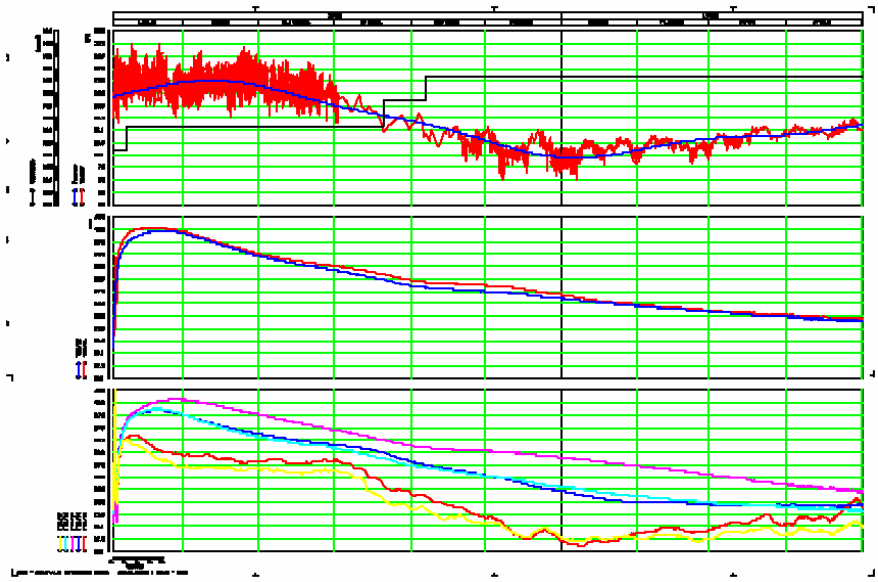

Fig. 5 – Chronological Measured Temperatures (MIDASâ software)

In buttress n. 26 the maximum temperature T(max) during hydration reached 42°C and the temperature drop (actual vs. maximum), **D**T, still amounted to 22 °C 270 days after.

5. MATERIAL CHARACTERISATION

Heat production properties were selected from tests on cement heat production averaged on actual cement content within the concrete. Heat conduction properties were taken, at first, by literature data on similar concretes. Later, a full set of experimental data were obtained by ENEL DSR Cris laboratories of Milan and Venice.
They regarded heat produced by concrete by semi-adiabatic tests and the thermal

properties of aggregates and concrete.
The thermal model used in the analyses for heat generation was based on the Reinhardt (1982) model coupled with diffusivity properties. The resulting temperature values and distributions confirmed the adequacy of the selected calibration. Figure 6 shows the comparison between actual temperatures value measured in the different elevation blocks of buttress 26 during construction and the predicted numerical value resulted from the FE analyses.

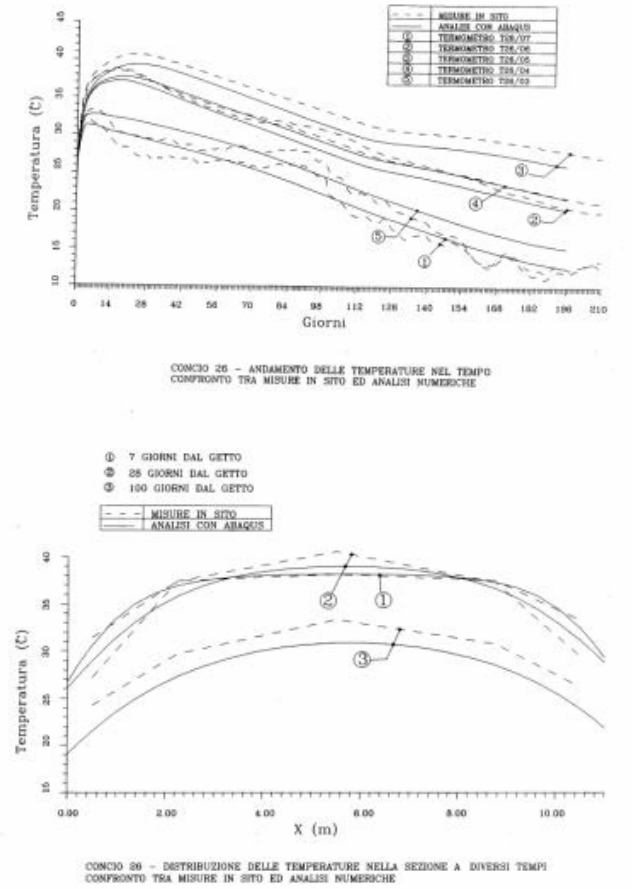

Fig. 6 – Comparision measured/theoretical vs. time and in the thickness of buttress 26
Analyses were run with the following FE codes:

- HKS / ABAQUS,
- TNO / DIANA.

6. THE THERMAL ANALYSES

The finite element model is a two-dimensional model prepared with iso-parametric elements, which reproduce the full section of a buttress (5 blocks). The solution took advantage of code capability of solving staged construction problems.

Boundary conditions were characterised by convection and free thermal flux (by assigning given temperatures). Environmental temperatures varied according to the actual measured values (described by Fourier series).

Several solutions to counteract the persistence of potentially critical temperatures differences between the block and the environmental conditions were analysed:

1. The actual sequence on site, for calibration purposes.
2. Reduced initial temperature of casting, obtained by the isolation of aggregate from solar radiation effects and addition of fresh water into the mix.
3. Curing with fresh flowing water taken by the tributary river.
4. Quicker rate of casting per day coupled with curing, as specified in 3.

Options for counteracting critical temperature drops were identified.

Solution 1 proved the adequacy of the calibration made in terms of resulting temperature absolute values, distribution and time dependency. Results regarding the temperature development in the middle of the blocks of buttress 26 are given in Fig. 7.

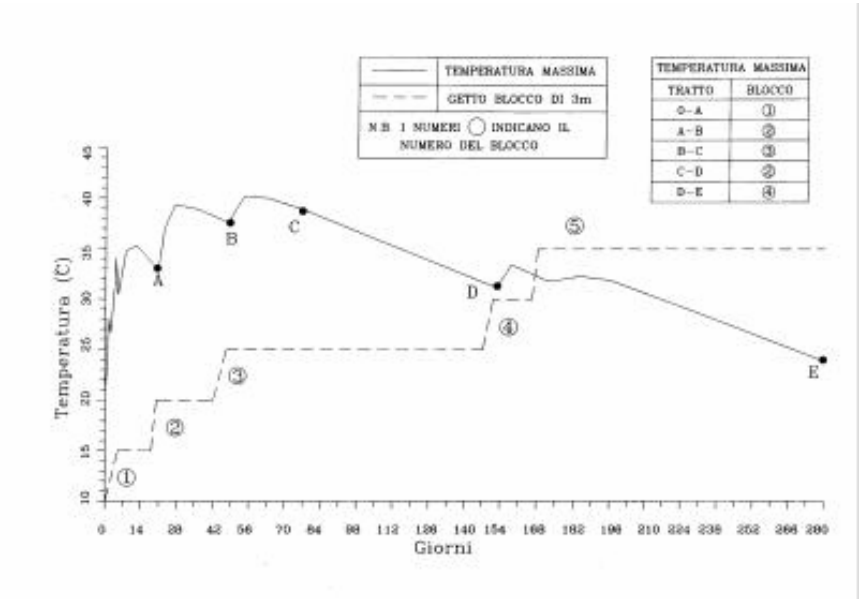

Fig. 7a - Time Histories of Predicted Max Temperatures for temperature mitigation solutions

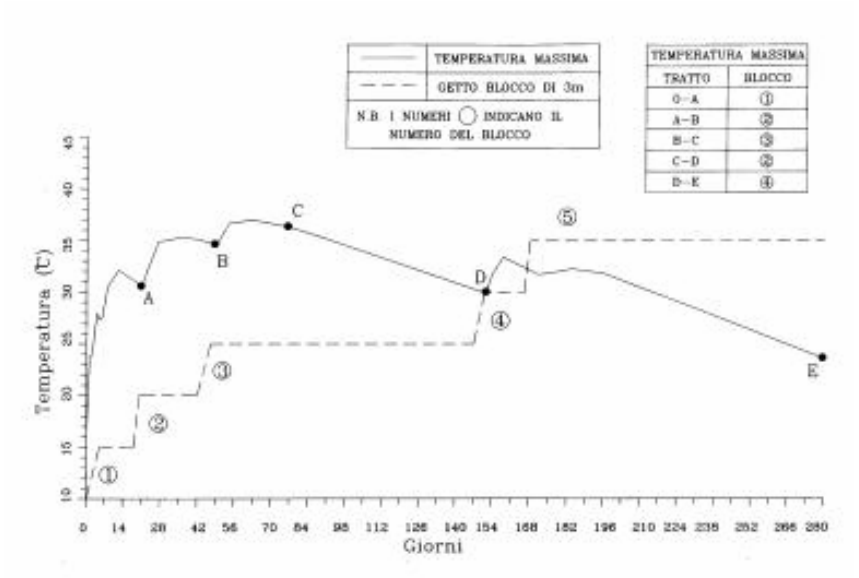

Fig. 7b – Time Histories of Predicted Max Temperatures for temperature mitigation solutions

7. GENERAL REMARKS

Based on the solutions analysed, it was concluded that pre-cooling of the cast with fluent fresh curing water, and the continuous casting of blocks , was the most effective way to obtain the most favourable temperature values for crack control.

THE ISSUE OF CRACK CONTROL

8. THE OBJECTIVE

Hydration heat generates stresses that turn from compressive to tensile few days after casting. At that age, concrete develops most of its tensile strength. Internal stress development is significantly mitigated by creep effects and by the initially low stiffness of the concrete mass. Stresses also depend on the restrain offered by the foundation and by adjacent castings. The stronger the restrain, the higher is the generation of tensile stresses at a given temperature change. Temperature drops during the cooling phase may still induce cracking of the concrete mass. Hydration stresses are destined to vanish in time, but even a moderate cracking may expose concrete to a more severe environmental attack. In this phase of the assessment, such conditions were studied in relation to the most unfavorable conditions identified in the thermal phase of the study. These refer to buttress n. 26. The study was therefore based on modeling actual casting conditions.

9. THE MATERIAL PROPERTIES

Ad hoc tests were carried out to calibrate the thermal and the thermomechanical viscoelastic model. The latter is associated to a non-linear fracture mechanics strength-based cracking criterion. Tests performed at ENEL-DSR-Cris laboratories in Milan and Venice provided the evidence for determination of material properties.

- Thermal properties:

- The ‘adiabatic curve’ of concrete by calorimetric tests
- Thermal diffusion proprieties of concrete and aggregates.

- Thermo-mechanical properties:

- Elastic modulus at different ages.
- Creep under compression tests at 3, 28 days.
- Traction uniaxial tests f_t at different ages.

A slab was cast (3,5x1,5x0,6 m approx) for the purpose to obtain representative specimens of concrete at different ages.

The Thermal and the Thermo-mechanical properties for the mature concretes are the
following (Fig. 8):

Variable	Value	Unit
Unit weight	2417	kg/m^3
Specific heat	1.067	kJ/kg/°C
Conductivity	5.024	kJ/m/h/°C
Diffusivity	0.00205	m^2/h
Poisson coefficient	0,20	
Thermal expansion coefficient (linear)	$6.0x10^{-6}$	$°C^{-1}$
Strength under direct traction	1,351	MPa
Fracture energy (90 days)	166.0	N/m
Stiffness are time dependent	According to the Bazant Panula model	

Fig. 8 – Thermal and Thermo-mechanical Properties of Concrete

Experimental values are given in the following figure 9 a,b,c together with model response.

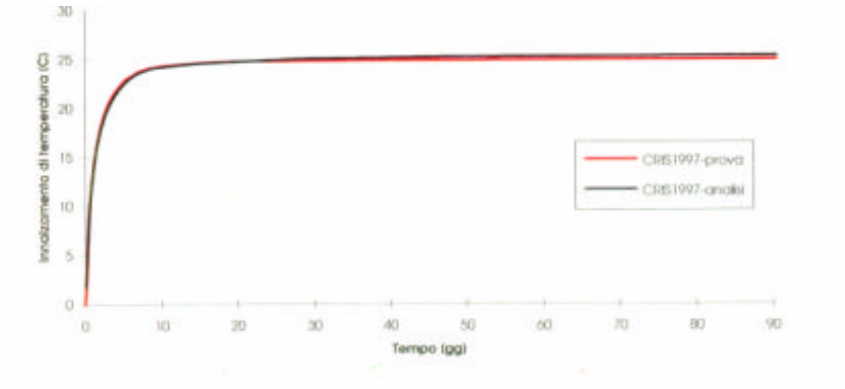

Fig. 9a

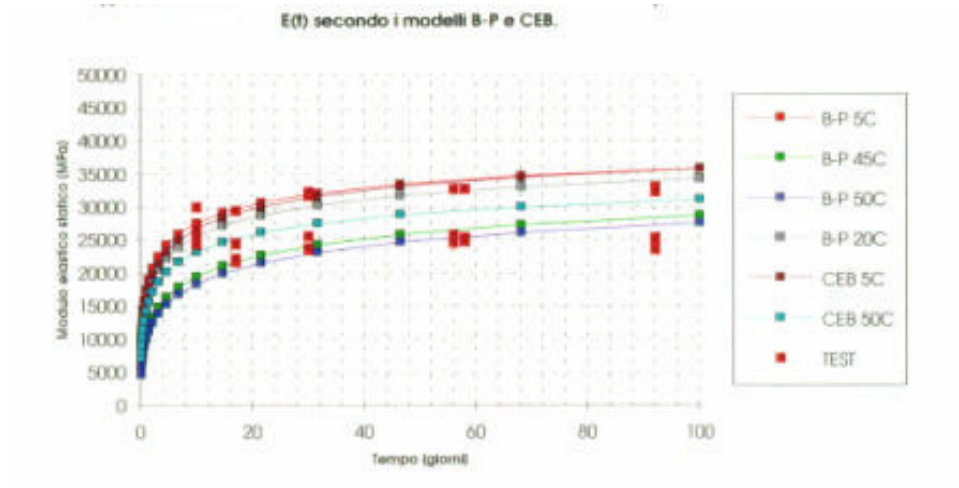

Fig. 9b

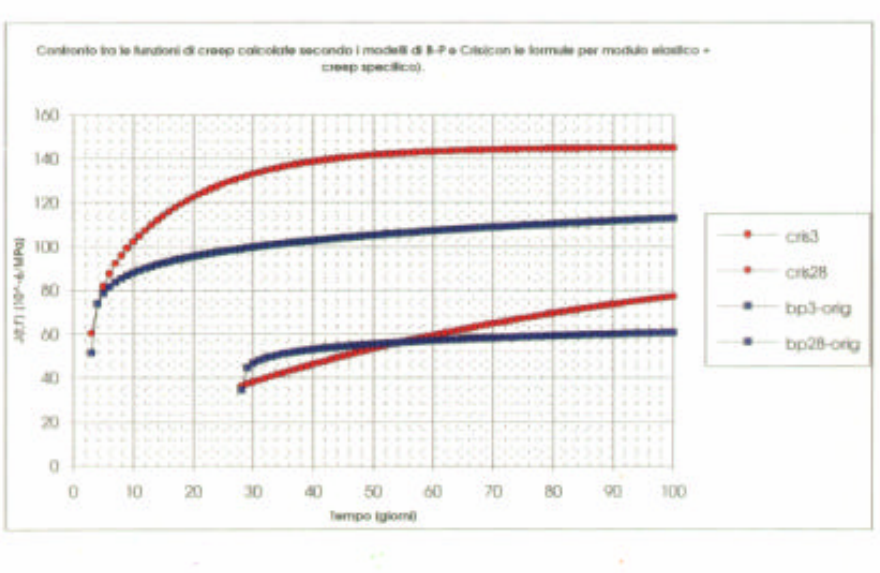

Fig. 9c

Fig. 9 a,b,c - Adiabatic temperature increase, time change of the elastic stiffness and tensile strength

10. THE MATERIAL MODEL

The Heat Conduction Model used was based on the Reinhardt [1982, Ref. 2] model for heat generation, coupled with diffusivity properties of concrete.

The Thermo-Mechanical Model used was based on the Bazant-Panula [1978, Ref. 3] viscoelastic model. This model incorporates age effects on stiffening (E) and creep properties. The Hordjik, Reinhardt, Cornellissen [1987, Ref. 4] model describes tensile softening. This model can be calibrated on mix design properties. Experience made at ISMES in several research programmes in cooperation with ENEL-DSR [Ref. 5] outlined the adequacy of such model, by checks with monitored prototype castings. A prototype thermo-mechanical stress-temperature apparatus was used to this scope and test results are used to demonstrate model adequacy (Fig. 10).

a)

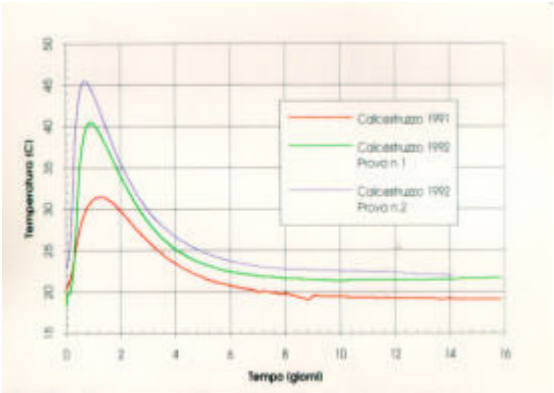

b)

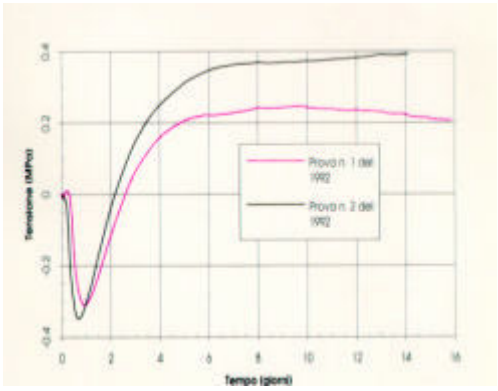

Fig. 10 a,b - TSTM (Thermal Stress Test Machine) typical results

11. THE FEM ANALYSES

Temperatures are assigned to the finite element stress model, which is made by isoparametric plane strain elements, reproducing the bottom portions of the dam buttress.

Evolutions of stresses at different times of the staged construction of buttress n.26 are observed. Looking the figures 11-12, horizontal stresses turn from compressive to tensile as time passes (from green to red) while temperatures first increase and then decrease.

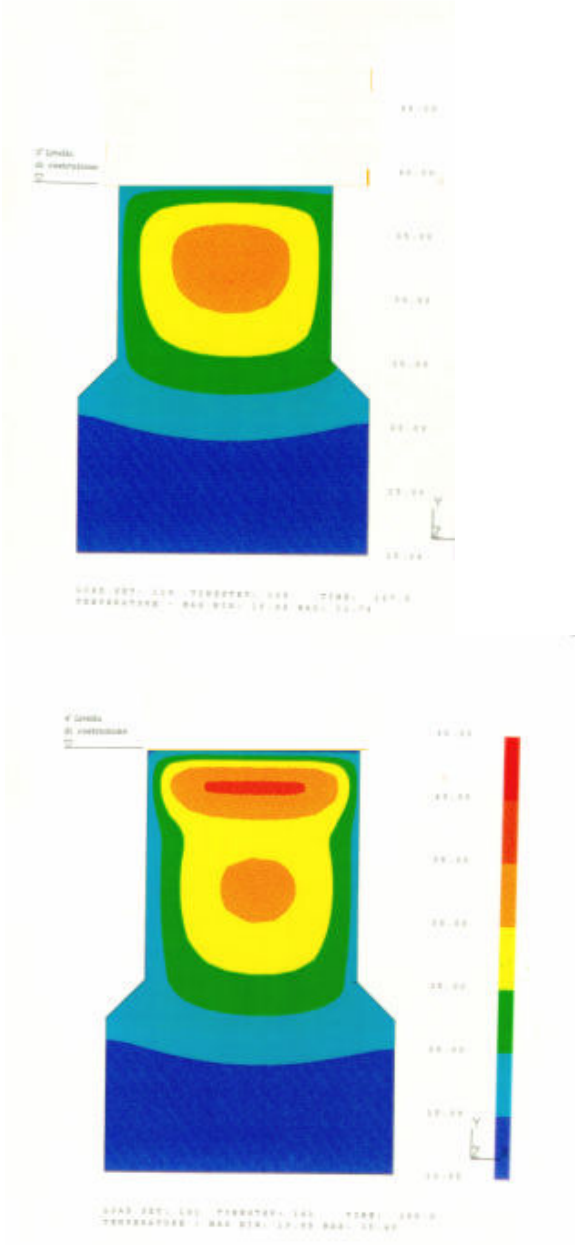

Fig. 11 – Temperature Distributions after 147 (left) and 166 (right) days [°C]

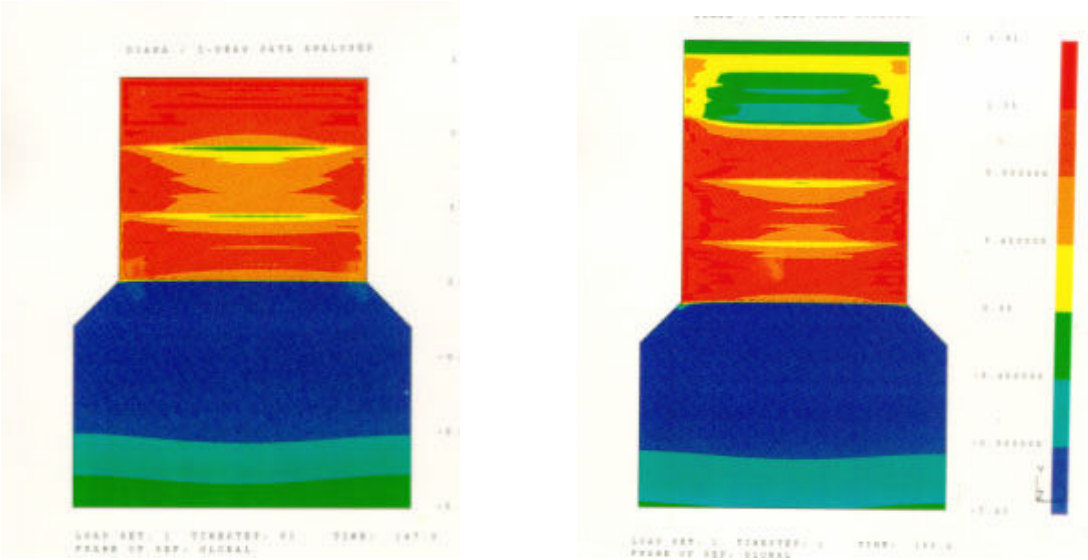

Fig. 12 – Horizontal L/R Stresses after 147 (left) and 166 (right) days [MPa]

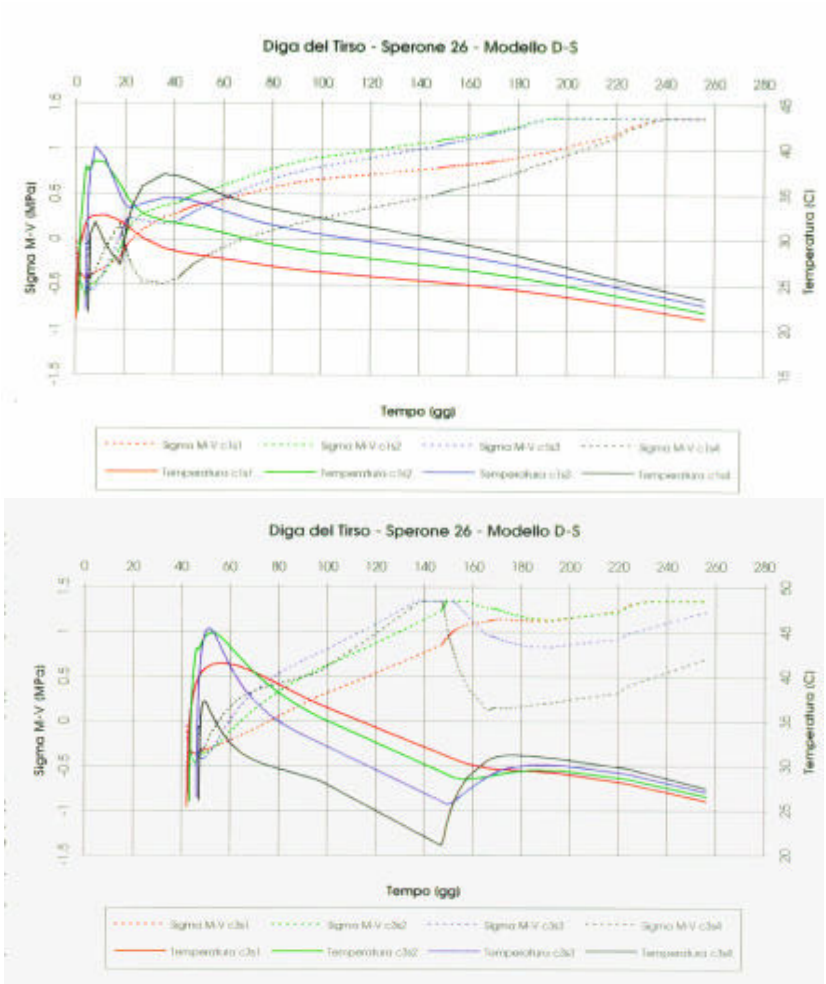

Fig. 13 a, b – Temperature and U/D-Stresses Histories in different block elevation

Concluding remarks

Through crack occurrence is predicted in the central part of the buttress at a ΔT as high as 20 °C. This temperature increase was found higher than that usually adopted for construction control (10 °C).

The assessment highlights however that criteria based on temperature control can be relaxed only if a careful evaluation based on modeling of actual concrete properties, of the sequence of casting and of environmental conditions.

Reference

[1] MIDAS Software – Management of Information for Dams Safety. Software for managing drawing and reference models. Enel.Hydro /Ismes Division.

[2] Reinhardt H, et al. –Temperature Development in Concrete Structures taking account of State Dependent Properties.- RILEM International Conference on Concrete at Early Ages. Paris, 1982

[3] Bazant Z.P., Panula L. – Dependent Deformation of Concrete.- Materials and Structures, Vol.11, n.65/69, 1978

[4] Hordijk D.A., Reinhardt H.W., Cornellisen H.A.W., - Fracture Mechanics Parameters of Concrete from Uniaxial Tests as Influenced by Specimen Length.
– Proc. SEM-RILEM Int. Conf. On Fracture of Concrete and Rock. S.P. Shah and S.E. Swartz eds., SEM, Bethel, 13,149, 1987

[5] Pellegrini R., Ferrara G., et al. – Physical and Mathematical Models for the Study of Crack Activation in Concrete Dams.- Bourdarot, Mazars and Saouma eds., Balkema, Rotterdam, 1994

CRITICAL CONDITIONS OF SEEPAGE UNDER RCC DAM ON PERMEABLE FOUNDATION
THE CASE OF THE DONA FRANCISCA DAM

José Antunes Sobrinho, Alexandre Marcon Fernandes, Sergio de Pauli Basso, Rafael Fernandes Pereira, Leonardo de Bem Silva, and Paulo Afonso Foes

Engevix Engenharia S/A., BRAZIL

SUMMARY: The Dona Francisca HPP on the Jacuí River, in the State of Rio Grande do Sul - Southern Region of Brazil - has a total installed capacity of 125 MW. The Gravity Dam is a 660 m long, 50 m high, built in roller compacted concrete. The dam foundation is constituted by basalt in the banks and by reddish sandstone, solid or with crossed stratification, with different grades of lithification in the river bed. The accurate estimate of seepage in the foundation dam was done with analyses carried out on a finite element method based model. A hydrogeological model of the bedrock was elaborated to subsidise the analyses. Results of flow gauges demonstrated an extremely good adherence to mathematical model results.

1. INTRODUCTION

Dona Francisca Hydroelectric Power Plant, with 40m of gross head for electrical power generation and a total installed capacity of 125 MW with two hydro-generator groups, is located on the Jacuí river, at the border of the municipalities of Agudo and Nova Palma, in the State of Rio Grande do Sul, in the Southern Region of Brazil. Geographic coordinates are 29°27' South and 53°16' West.

The river basin area at the Dona Francisca site is around 14,000 km^2 and the mean discharge is 281 m^3/s. The reservoir, with a surface area of about 8.0 km^2, with its normal operation level at elevation 94.50m, was formed after the execution of a RCC dam/spillway with a maximum height of 50.5 m, which required about 526,110 m^3 of RCC for its construction. The dam crest is set at El. 102.00m, with the top of the parapet wall at El. 102.50m. The downstream face slope is 0.75H:1.0V.

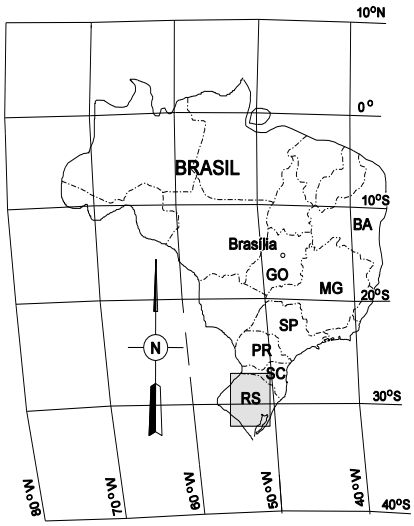

Figure 1 – Location Map

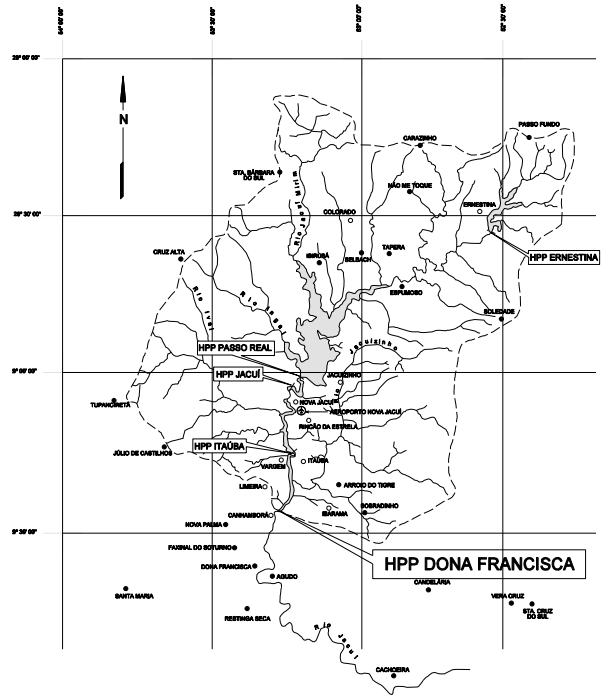

Figure 2 – Reservoir Plan of HPP Dona Francisca

2. LAYOUT

The project layout presents the following features:

- Dam/spillway in RCC, associated with the intake and the diversion structures, with a total length of 660 m and with the crest level at El. 102.00 m at the abutments, and a maximum height of approximately 50.5 m and a free overflow spillway, on the crest of the dam, at El. 94.50 m, with total length of 335 m and energy dissipation on the steps and stilling basin;
- 2nd Stage of river diversion through four galleries with 5.50 m x 11.00 m, complemented by three passages on the right side of the dam for high flow periods, with the following dimensions: 9.60 m x 5.50 m;
- Alleviated type power intake, excavated in rock, in a single block; two penstocks with 6.30 m of diameter and length of 80 m and an indoor powerhouse, with two Francis units of 62.5 MW each.

Structure	Type/Location
Dam	Gravity – RCC
Spillway	Free overflow over the dam
Headrace circuit	Right abutment, 2 Francis units
River Diversion 2nd stage	4 diversion galleries, b = 5.50 m and h = 11.00 m

Figure 3 – Summary of Main Structures

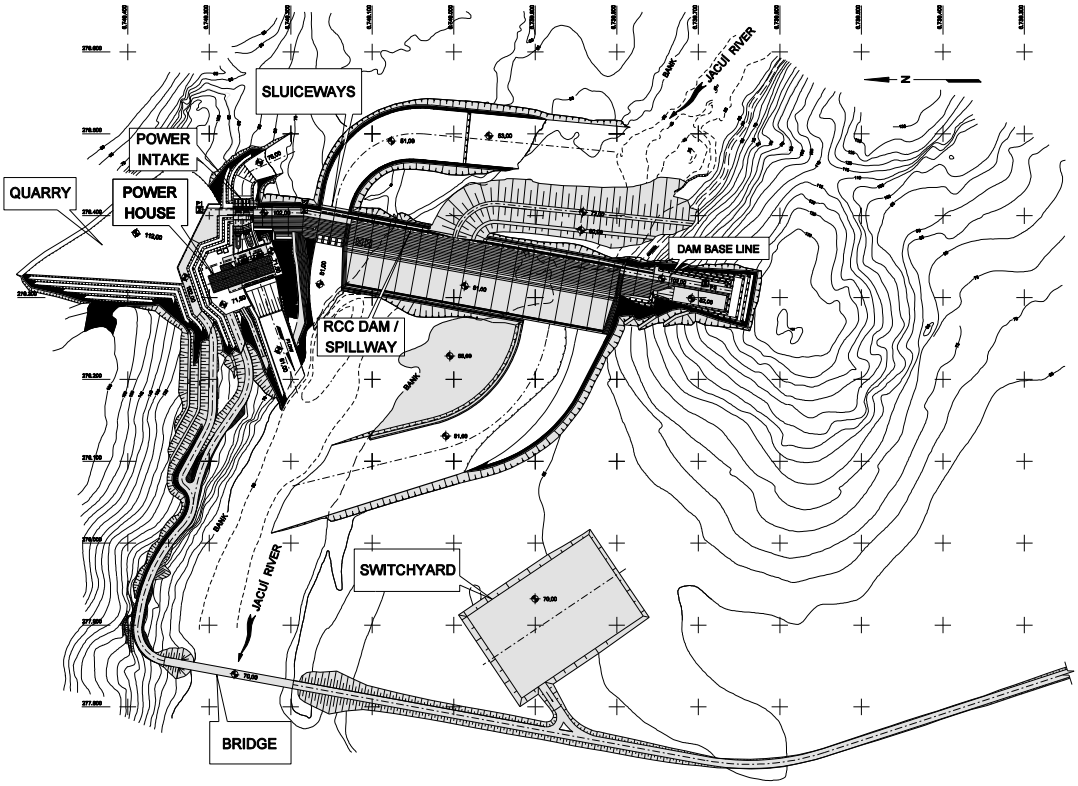

Figure 4 – HPP Dona Francisca General Layout

3. GEOLOGY AND HYDROGEOLOGICAL MODEL

The dam foundation is constituted by basalt in the banks and by sandstone in the river bed. In the right bank, the basalt was sound and sparsely jointed; in the left bank the basalt presented more fractured and it had been partially removed.

In the river bed, in the spillway section, the foundation is constituted by reddish sandstone, solid or with crossed stratification, with different degrees of lithification. Intercalated in the sandstone, occur sub-horizontal siltstone layers, claystone and intraformational breccia, centimeters thick and a set of ten meters extent. In these layers occur some clay horizons, millimeter to centimeter thick, sub-horizontal, with a set of ten meters extent, with passages of clay intercalated with rock fragments.

3.1 SANDSTONE HYDROGEOLOGICAL MODEL

The conception of the sandstone hydrogeological model was based in the hydraulic conductivity (CV) obtained in the water tests done in several sounding holes defined by geological cross sections project. The analysis of this data allowed the following interpretation:

- The average hydraulic conductivity (CV) of foundation rock above El. 35,00 is $1x10^{-4}$ cm/s;
- Between El. 35,00 and 30,00, a continuous zone of sandstone AV with a hydraulic conductivity (CV) of $1x10^{-3}$ cm/s was adopted;

- Below of El. 30,00, a hydraulic conductivity (CV) of $5x10^{-4}$ cm/s for the foundation rock was considered;
- For horizontal layers of siltstone and claystone, it was adopted a conservative hydraulic conductivity (CV) of $1x10^{-5}$ cm/s.

3.2 BASALT HYDROGEOLOGICAL MODEL

Basalt rock foundation present in both dam banks is characterized by pronounced sub-vertical and sub-horizontal cooling down fractures, associated with tectonic fractures, composing a discontinuous isotropic mesh responsible for the permeability of rock foundation. Evaluations of water tests in several sounding holes indicated an average hydraulic conductivity (CV) between $1x10^{-4}$ and $1x10^{-5}$ cm/s. For simulation in the hydrogeological model, a CV value of $5x10^{-4}$ cm/s for the hydraulic conductivity (CV) of rock foundation was adopted.

4. FINITE ELEMENT MODEL

The seepage studies in dam/spillway foundation was done with analyses carried out with the use of a finite element model aided by the software SEEP/W, elaborated and distributed by GEO-SLOPE International Ltd. The hydrogeological model previously described, subsidized the analyses. Figure 5 shows the cross section of dam and spillway in river bed.

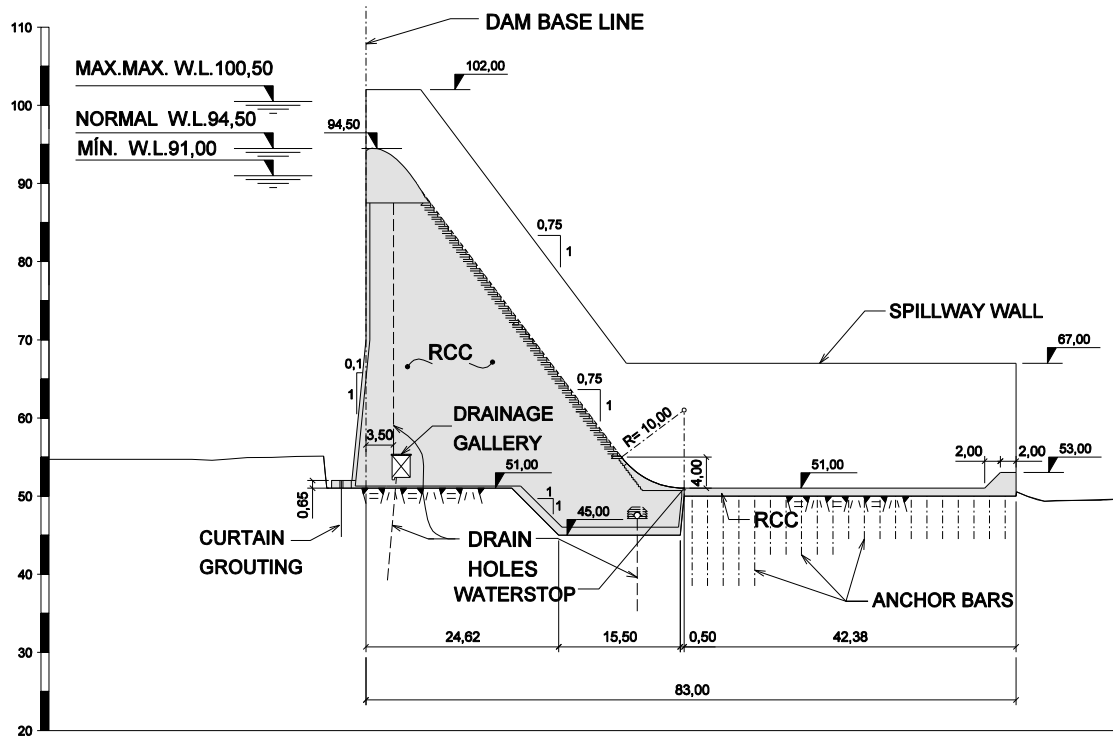

Figure 5 – Typical Dam/Spillway Section

The finite element model (FEM) was prepared based the criteria of unitary drilled drain hole. In the mesh corresponding to the foundation rock a group of elements in the influence area of drainage curtain was created. The permeability attributed to the drainage holes was $k_d = \lambda \times k$; where "λ" is the form factor of the curtain and "k" is the foundation permeability. Considering the foundation rock isotropic the formula of "λ"is:

$$\lambda = \frac{2 \times \pi}{a \times \ln\left(\frac{a}{\pi \times \phi}\right)};$$

where

a = distance between drilled drain hole;
ϕ = diameter of drilled drain hole

With the permeability of the influenced area of the drainage curtain, the permeability of the foundation rock and hydrostatic loads, the analyses on the finite element model were carried out as shown in Figure 6.

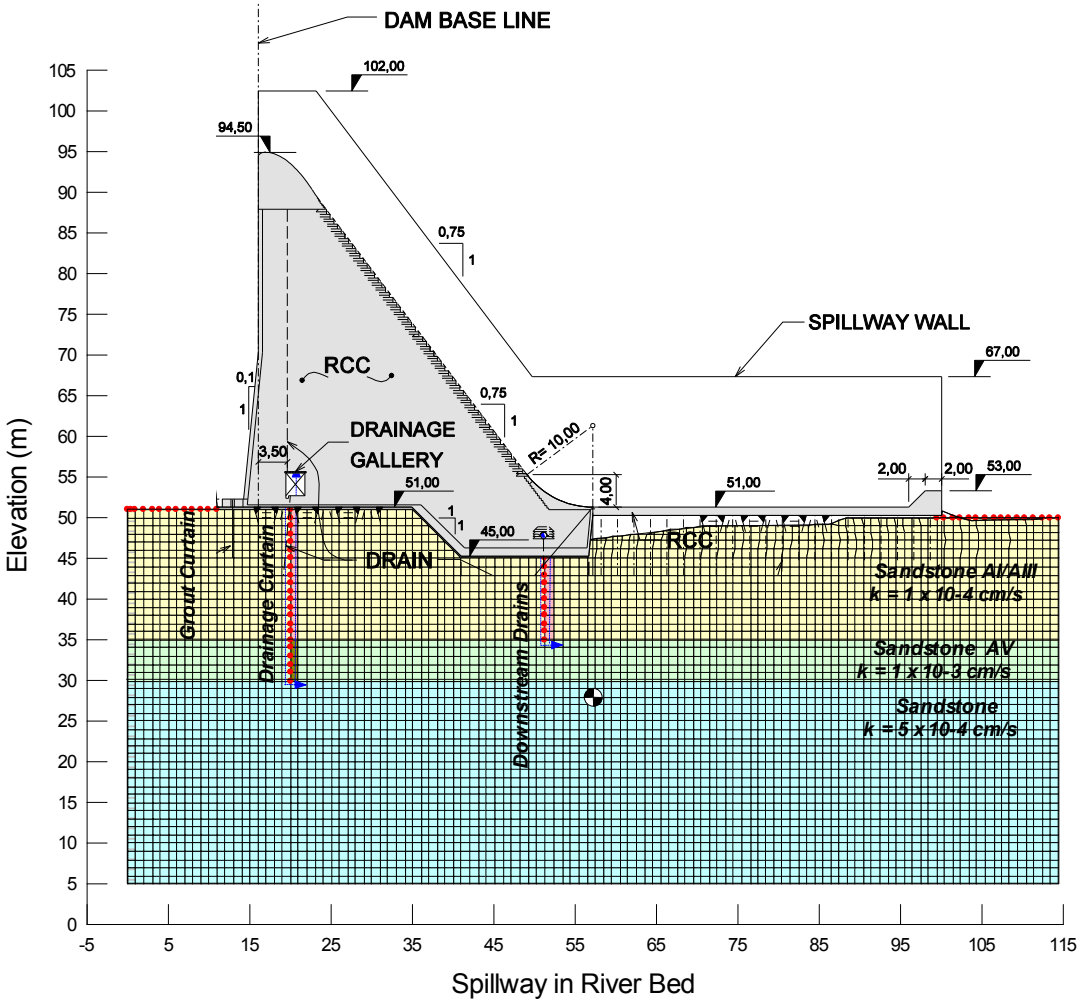

Figure 6 – Hydrogeological and FEM elaborated in SEEP/W

The results of finite element model are presented in Figure 7, showing pore-water pressures and unitary flows in drainage curtain.

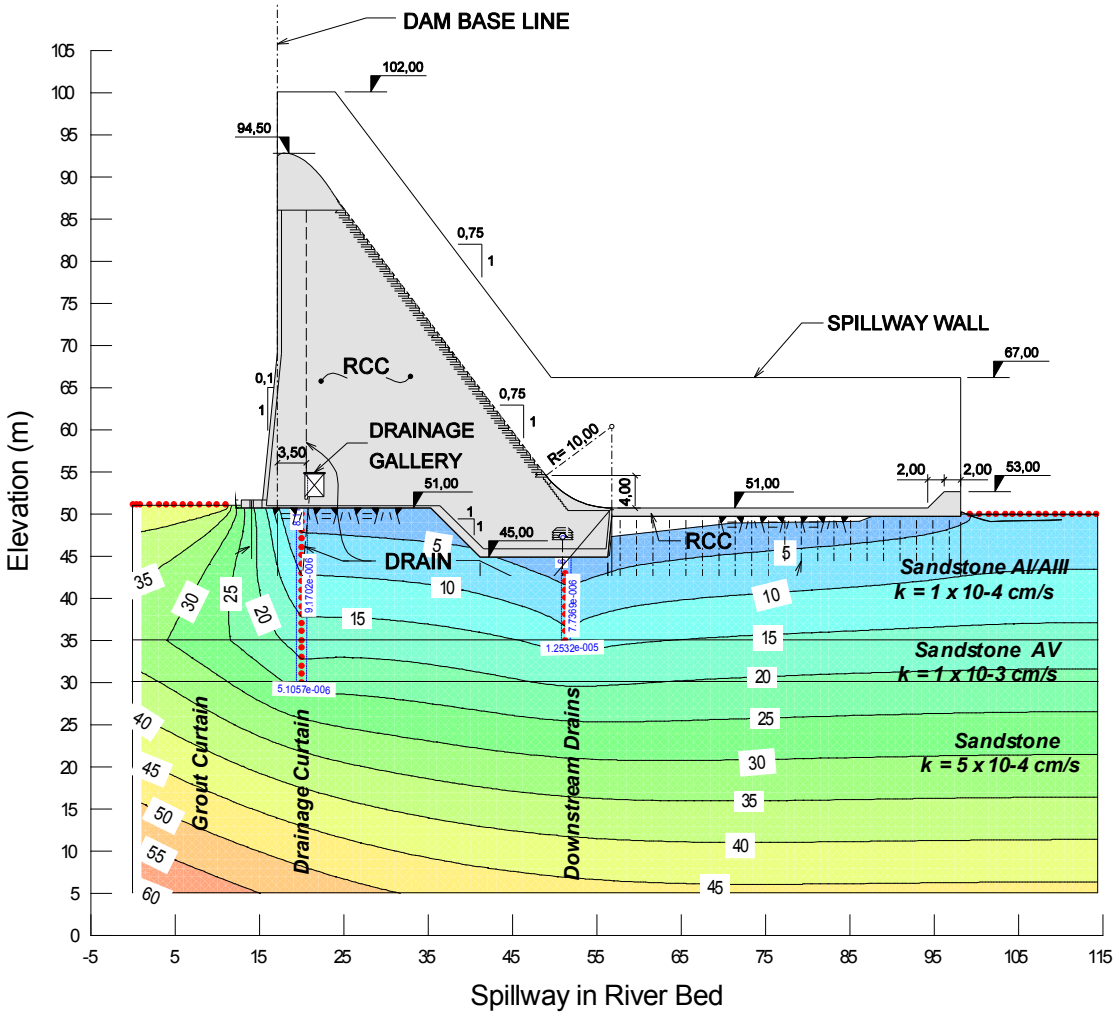

Figure 7 – Pore-water pressure and unitary flows in drainage system

5. ANALYSED SECTIONS

The distribution of the drainage curtain along the gallery, the execution of additional downstream drains and the differentiation of the hydrogeological models in banks and in the river bed, motivated the elaboration of 4 sections of analysis in FEM. The main characteristics of them in terms of drainage are described below:

- Section 1: Spillway – Blocks 17 to 27 – Upstream drainage curtain with drains each 1.5 meters. Downstream tilted drainage curtain from gallery drainage with drains each 2.0 meters. Toe downstream drains each 3.0 meters.

- Section 2: Spillway – Blocks 10 to 16 – Upstream drainage curtain with drains each 1.5 meters. Toe downstream drains each 3.0 meters.

- Section 3: Dam in Right Bank – Blocks 1 to 5 – Gallery drainage and tunnel drainage in Basalt rock. Upstream drainage curtain with drains each 3.0 meters. In tunnel drainage holes to up and down directions.

- Section 4: Dam– Blocks 6 to 9 (Right Bank) and 28 to 35 (Left Bank) – Upstream drainage curtain with drains each 3.0 meters.

6. SEEPAGE RESULTS

The analysed sections demonstrated the seepage in foundation rock conducted towards the two drainage wells, one in the right and the other in the left bank of dam.

6.1 ESTIMATION OF SEEPAGE IN THE RIGHT BANK DRAINAGE WELL

The contribution to the right bank drainage well is due to the drainage curtain of dam in right bank and spillway – Blocks 10 to 24. The seepage into this well was estimated as:

$$Q = (67{,}4 \times 8{,}1153 \times 10^{-5} + 93{,}6 \times 4{,}2321 \times 10^{-5} + 132{,}75 \times 9{,}5450 \times 10^{-5} + 150 \times 1{,}1213 \times 10^{-4})$$

$$Q = (0{,}00547 + 0{,}00396 + 0{,}01267 + 0{,}01682) \times 3600 = 140{,}12 m^3 / h$$

$Q_{Right\ Bank} = 140{,}12\ m^3/h$

6.2 ESTIMATIVE OF SEEPAGE IN THE LEFT BANK DRAINAGE WELL

The contribution to the right bank drainage well is due to the drainage curtain of dam in left bank and spillway – Blocks 24 to 27. The seepage into this well was estimated as:

$$Q = (63{,}45 \times 1{,}4151 \times 10^{-4} + 135{,}20 \times 4{,}2321 \times 10^{-5} + 150 \times 2{,}9384 \times 10^{-5} + 132{,}75 \times 2{,}6524 \times 10^{-5})$$

$$Q = (0{,}00898 + 0{,}00572 + 0{,}0044 + 0{,}00352) \times 3600 = 81{,}47 m^3 / h$$

$Q_{Left\ Bank} = 81{,}47\ m^3/h$

7. CONCLUSIONS

Analysing the data provided by the instrumentation of the dam during the period of reservoir impounding, and the total seepage flow in Pumping system – stable in 180 m³/h – we can conclude that the parameters adopted in the analysis were proper and consistent. The real seepage is about 81% of the total estimated by applying the described computational model.

ACKNOWLEDGEMENTS

The authors would like to express their gratitude to the project owner DFESA – Dona Francisca Energética S.A. - and the construction suppliers CONFRAN – Consórcio Fornecedor da UHE Dona Francisca – for allowing the publication of project data and references.

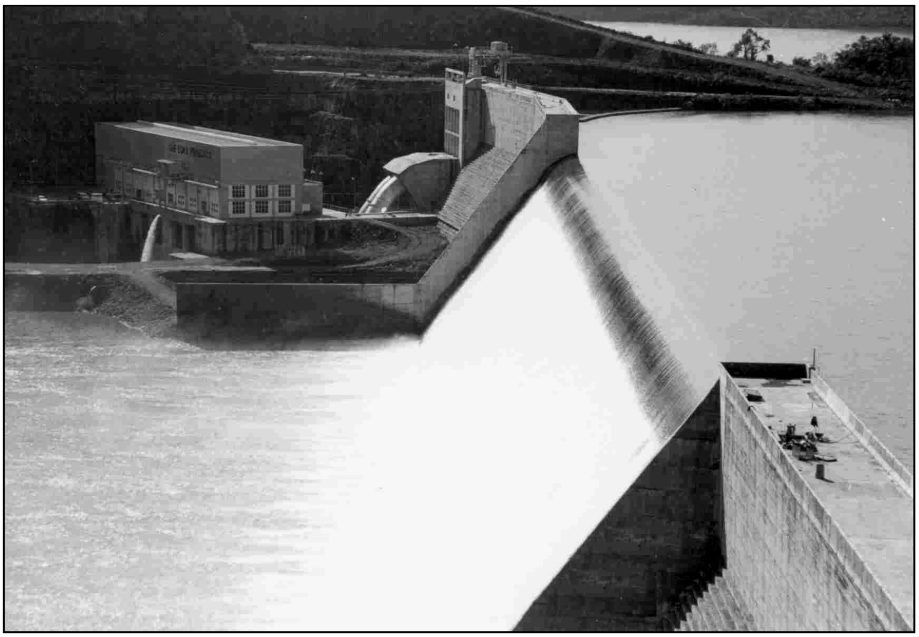

Figure 8 – Spillway in operation– W.L. ~ 95,00m (Head ~ 0,50 m)

REFERENCES

[1] Tajima, R. & Pereira, R.F. – Mapeamento, Injeção e Drenagem da Fundação da Barragem. Engevix Engenharia Ltda. Florianópolis, Brasil, 2001.

[2] UHE DONA FRANCISCA - TECHNICAL REPORT FOR THE BOARD OF CONSULTANTS – Board Meetings n^{os} 7, 8, 9, Curitiba, Brasil, 2000/2001.

[3] Andriolo, F.R.. THE USE OF ROLLER COMPACTED CONCRETE – São Paulo, Brasil, 1998

[4] Sobrinho, J. A. & Fernandes, A. M. & Foes, P. A. – DONA FRANCISCA HYDROPOWER PLANT – Engevix Engenharia Ltda., Florianópolis, Brasil.

EVALUATION OF THERMAL STRESSES IN A RCC DAM IN SUBTROPICAL REGION OF BRAZIL
THE CASE OF THE DONA FRANCISCA DAM

By José Antunes Sobrinho, Alexandre Marcon Fernandes, Sergio de Pauli Basso, Rafael Fernandes Pereira, Carlos Correa, Leonardo de Bem Silva and Paulo Afonso Foes

Engevix Engenharia S/A., BRAZIL

SUMMARY: The Dona Francisca HPP on the Jacuí River, in the State of Rio Grande do Sul - Southern Region of Brazil - has a total installed capacity of 125 MW. The Gravity Dam is a 660 m long, 50 m high and built with roller compacted concrete. The dam foundation is formed by basalt in the banks and by reddish sandstone, solid or with crossed stratification, with different grades of lithification in the river bed. One of the basic concerns during its design was the determination of the distance between the dam joints. The computational methods used for the analysis included the software SAP2000.

1. INTRODUCTION

Dona Francisca Hydroelectric Power Plant, with 40m of gross head for electrical power generation and a total installed capacity of 125 MW with two hydro-generator groups, is located on the Jacuí river, at the border of the municipalities of Agudo and Nova Palma, in the state of Rio Grande do Sul, in the southern region of Brazil. Geographic coordinates are 29°27' South and 53°16' West.

The river basin area at the Dona Francisca site is around 14,000 km^2 and the mean discharge is 281 m^3/s. The reservoir, with a surface area of about 8.0 km^2, with its normal operation level at elevation 94.50m, was formed after the execution of a RCC dam/spillway with a maximum height of 50.5 m, which required about 526,110 m^3 of RCC for its construction. The dam crest is set at El. 102.00m, with the top of the parapet wall at El. 102.50m. The downstream face slope is 0.75H:1.0V.

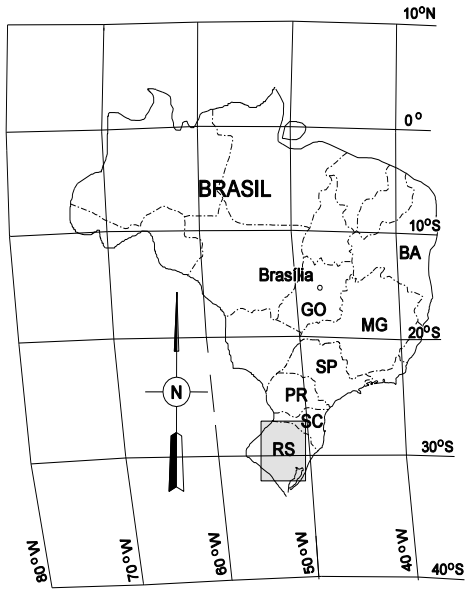

Figure 1 – Location Map

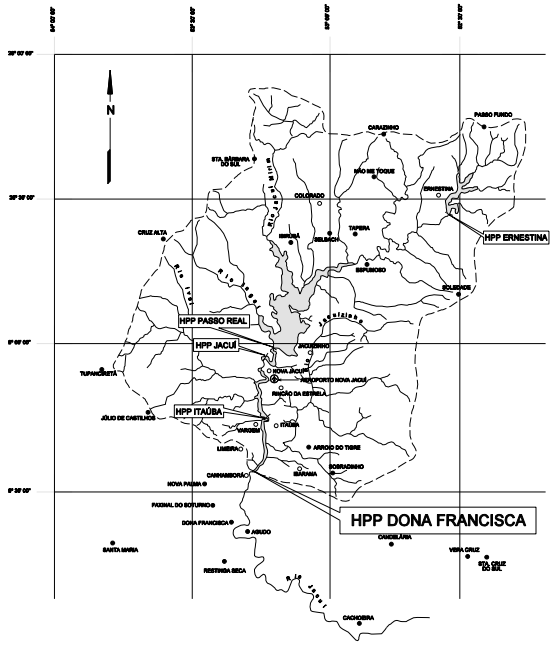

Figure 2 – Reservoir Plan of HPP Dona Francisca

2. LAYOUT

The project layout presents the following features:

- Dam/spillway in RCC, associated with the intake and the diversion structures, with a total length of 660 m and with the crest level at El. 102.00 m at the abutments, and a maximum height of approximately 50.5 m and a free overflow spillway, on the crest of the dam, at El. 94.50 m, with total length of 335 m and energy dissipation on the steps and stilling basin;
- 2nd Stage of river diversion through four galleries with 5.50 m x 11.00 m, complemented by three passages on the right side of the dam for high flow periods, with the following dimensions: 9.60 m x 5.50 m;
- Alleviated type power intake, excavated in rock, in a single block, two penstocks with 6.30 m of diameter and length of 80 m and an indoor powerhouse, with two Francis units of 62.5 MW each.

Structure	Type/Location
Dam	Gravity – RCC
Spillway	Free overflow over the dam
Headrace circuit	Right abutment, 2 Francis units
River Diversion 2nd stage	4 diversion galleries, b = 5.50 m and h = 11.00 m

Figure 3 – Summary of Main Structures

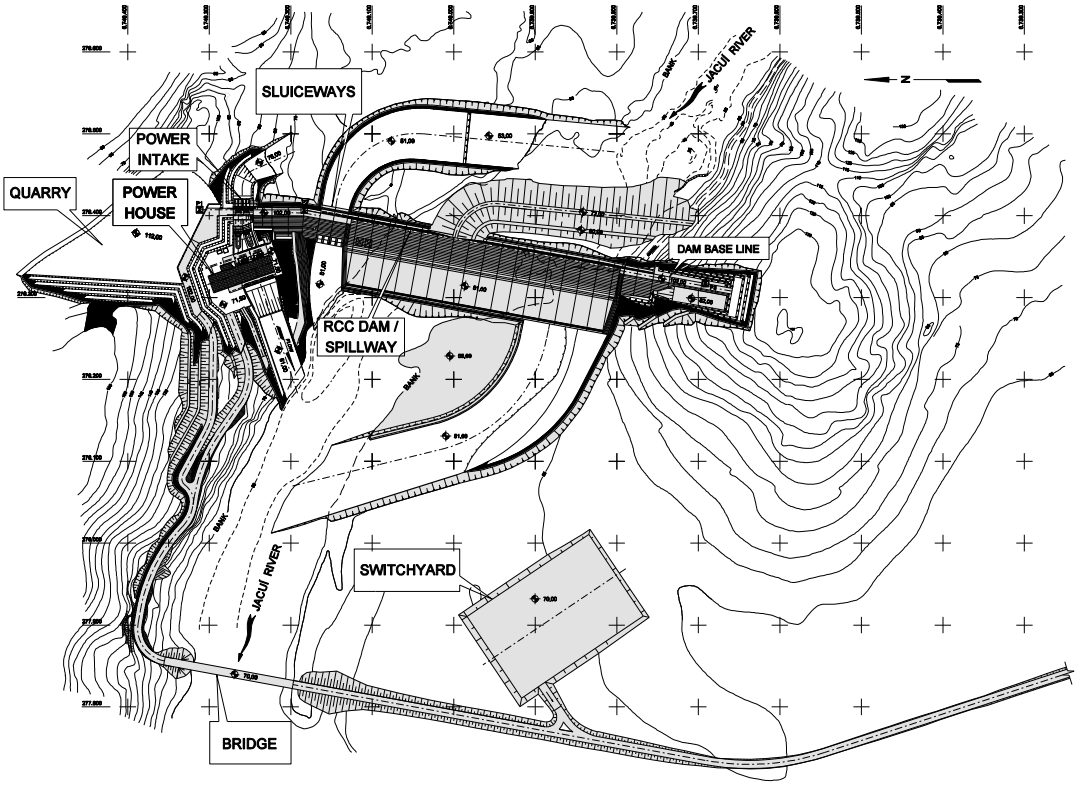

Figure 4 – HPP Dona Francisca General Layout

3. GEOLOGICAL ASPECTS

The dam foundation is constituted by basalt in the banks and by sandstone in the river bed. In the right bank, the basalt was sound and sparsely jointed; in the left bank the basalt presented more fractured and it had been partially removed.

In the river bed, in the spillway section, the foundation is constituted by reddish sandstone, solid or with crossed stratification, with different degrees of lithification. Intercalated in the sandstone, occur sub-horizontal siltstone layers, claystone and intraformational breccia, centimeters thick and a set of ten meters extent. In these layers occur some clay horizons, millimeter to centimeter thick, sub-horizontal, with a set of ten meters extent, with passages of clay intercalated with rock fragments, which was the first conditional for the stability studies of the dam.

4. HYDROLOGY

The long term mean discharge at the Project site is 281 m^3/s. The maximum discharge observed at the site had a peak of 4,447 m^3/s and the lowest discharge was 18.2 m^3/s. As for the flood regime, floods may occur at any time of the year. However, a minor seasonal variation can be observed and more severe floods are expected to occur in the period from May to October.

5. FINITE ELEMENT MODELING

5.1. MATERIALS AND THEIR PHYSICAL CHARACTERISTICS

The construction materials used in the dam and their physical characteristics are:

Sandstone:	-	Poisson´s Ratio:	0,20
	-	Thermal expansion coefficient:	$7 \times 10^{-6}/^{o}C$
	-	Elasticity modulus:	1×10^{6} kN/m^2
Concrete/rock contact:	-	Poisson´s Ratio:	0,20
	-	Thermal expansion coefficient:	$7 \times 10^{-6}/^{o}C$
	-	Elasticity modulus:	1×10^{6} kN/m^2
Roller compacted concrete:	-	Poisson´s Ratio:	0,23
	-	Thermal expansion coefficient:	$7 \times 10^{-6}/^{o}C$
	-	Elasticity modulus:	2×10^{7} kN/m^2

5.2. LOAD CASES

Own weight

The own weight of the structure was considered in the dam modeling, being the concrete weight calculated for a density of 24 kN/m^3 and the rock weight for 23 kN/m^3.

Temperature

The calculation of the load resulting from the temperature increase due to the cement reaction and subsequent cooling was based on the following premises:

- mean air temperature during concrete pouring: 24 ^{o}C;
- concrete production temperature for the dam basis: 30 ^{o}C;
- temperature increase due to chemical reaction of concrete: 9 ^{o}C;
- mean air temperature at start of cooling of the dam core: 14 ^{o}C;
- concrete production temperature for the final portion of the dam: 20 ^{o}C;
- temperature gradient at the dam basis: $30 + 9 - 14 = 25\ ^{o}$C;
- temperature gradient at the dam crest: $20 + 9 - 19 = 10\ ^{o}$C.

The finite element model was used to verify the distance between contraction joints. The model simulates one block of the dam and its foundation. The nodes at the

bottom of the foundation were vertically restricted and those on the sides, horizontally restricted.

As the structural modeling was carried out with SAP2000, in an asolid, a isoparametrical bi-dimensional element, for a plan parallel to the longitudinal axis of the dam, it was not possible to represent the temperature gradient from the dam core to the external air temperature. As such, an average temperature was adopted for a certain range, both upstream and downstream. For the calculation of the average temperature, it was considered that the temperature varies from the external air temperature up to the maximum temperature, from the upstream and downstream ends upon ¼ of the section towards the dam core. In the central $^2/_4$ of the dam core, the temperature will be at the maximum.

The temperature considerations are distinct for the dam basis and the end section, since they were concreted in different seasons, resulting in different temperature of concrete production and air during pouring.

The temperature varies along the dam height. At the basis, it was considered that the environmental temperature at the time of the dam concrete cooling would be constant at the maximum from the foundation up to 9 m above and then would decrease in the direction of the crest. At the crest, the same would occur, but for different temperatures, varying from a maximum to the external air temperature.

The considered temperature gradients were:

Dam basis and core: $\Delta T = (12.5 \times 1 + 25 \times 2 + 12.5 \times 1) / 4 = 18.75\ ^oC$

Dam crest: $\Delta T = (5 \times 1 + 10 \times 2 + 5 \times 1) / 4 = 7.5\ ^oC$

5.3. THERMAL STRESSES RESULTS

The maximum horizontal tension stress resulting in the model simulation was 610 kN/m^2 near the foundation. The maximum allowable horizontal tension stress considered in model was 750 kN/m², resulting a safety factor of 1.23.

The safety factor was considered acceptable since all loads applied in model were conservative. Later, it was confirmed that the allowable horizontal tension stress considered in model was extremely conservative since the average splitting tensile strength of the core test, resulted in 1,600 kN/m^2.

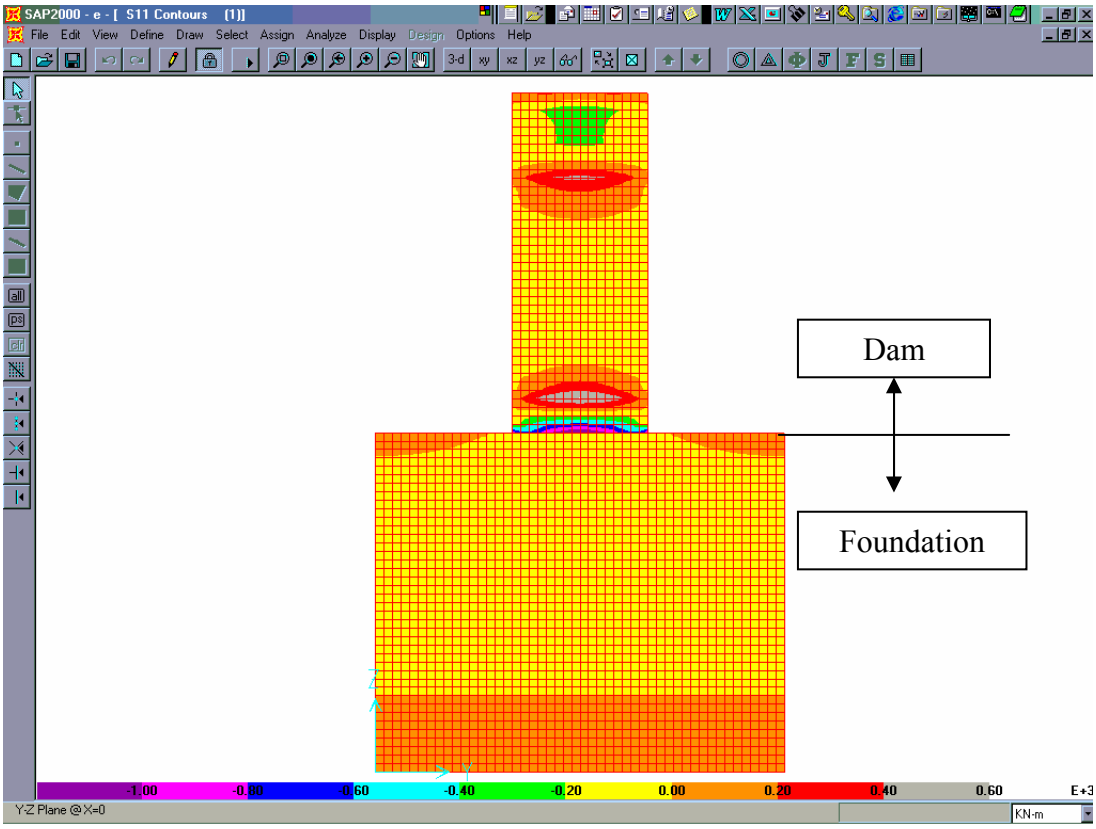

Figure 5 – Stress Results of Thermal Studies

6. EXECUTIVE METHOD FOR THE VERTICAL CONTRACTION JOINTS

Dona Francisca Dam has vertical contraction joints at each 20 m (maximum). The distance between joints was calculated taking into account a fck = 8 MPa and the maximum temperature gradients in the dam. For that, a finite element program simulation model was applied (see next item), and the maximum allowable tensile stresses were computed, considering 10% of fck as tension work stress.

- Materials used in the joints

- High-resistance plastic in rolls

- Naval wood in 6 mm thick plates with a height equal to the poured layer, before compaction. In the case of Dona Francisca, the layer thickness before compaction was 40 cm, and after compaction approximately 30 cm.

- Procedures for execution of the joint

- Wrap the wood plate with the plastic;
- Place the wooden plates wrapped with the plastic at the joint position;
- Pour the mortar bedmix used on all RCC layers;

- Manually place the RCC on both sides of the plate with a shovel in a layer around 30% higher (approximately) than the final compacted layer. In Dona Francisca, the compacted layer has a 30 cm thickness and the poured layer, 40 cm.
- Spread the RCC over the rest of the area;
- Remove the wooden plates, leaving the plastic in the place;
- Compact normally, passing with the roller over the joint where the plastic remained.

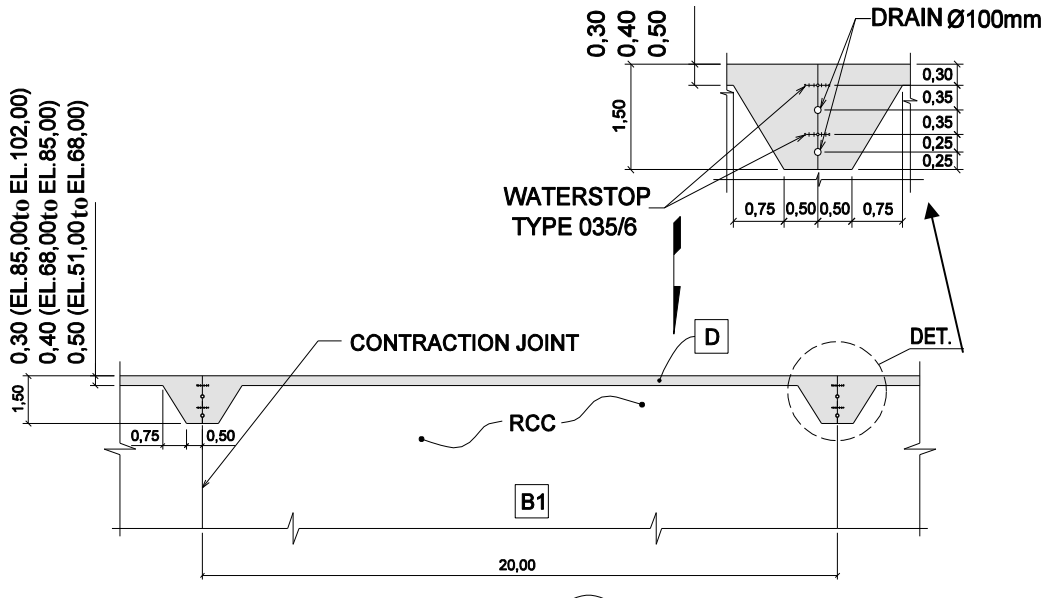

Figure 6 – Spacing between Contraction Joints and Details

7. CONCLUSIONS

The maximum tensile stress in the Y direction – corresponding to the fissure opening direction – for the dam basis, in the region of highest thermal gradient, was 610 kN/m^2. Another high tensile stress point occurs in the same direction at approximately 10 m from the top, were the stress reaches 454 kN/m^2. In the vertical direction, the highest tensile stress found is 85.5 kN/m^2.

Compression stresses in the lateral and vertical directions are, respectively, 1170 kN/m^2 and 1890 kN/m^2.

The vertical tensile stresses are below 90 kN/m^2 and are perfectly compatible with the type of concrete used, including the in joints between layers.

The tensile stresses that might result in thermal fissures in the concrete are higher at the foundation (610 kN/m^2) and lower at the crest (454 kN/m^2). The safety coefficient for the concrete at the dam basis is 1,23 and for the concrete at the crest, 1,32.

The parameters considered in the modeling are conservative. The air temperatures adopted for verification of the temperature gradient in the concrete mass were the maximum and minimum possible temperatures at the site. The allowable tensile stresses

for the roller compacted concrete might be higher than the 10% limit considered in this study.

Given their temporary characteristic, the resulting safety coefficients for the studied loads are considered acceptable.

As such, the minimum spacing of 20 m between joints was considered adequate. Even for the severest conditions foreseen for the site and the seasonal variations during the construction period, the adopted concrete is able to absorb the thermal stresses.

The actual field conditions found during concrete pouring proved that the premises adopted in the modeling were extremely conservative, since the air temperatures were milder than those considered in the studies.

ACKNOWLEDGEMENTS

The authors would like to express their gratitude to the project owner DFESA – Dona Francisca Energética S.A. - and the suppliers construction CONFRAN – Consórcio Fornecedor da UHE Dona Francisca – for allowing the publication of project data and references.

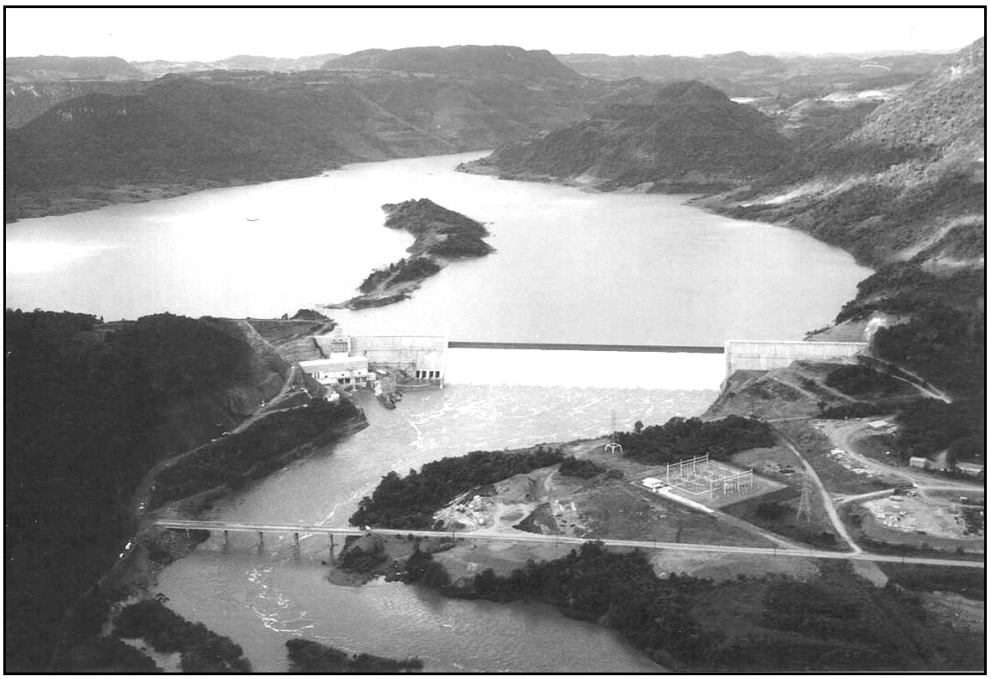

Figure 8 – Downstream View of HPP Dona Francisca after Reservoir Filling

REFERENCES

[1] Franco, S. G. & Margarido, A. F. & Scandiuzzi, L. – DISTÂNCIA ENTRE JUNTAS – Do problema técnico em barragens tipo CCR: determinação da distância entre juntas de retração.

[2] UHE DONA FRANCISCA - TECHNICAL REPORT FOR THE BOARD OF CONSULTANTS – Board Meetings n^{os} 7, 8, 9, Curitiba, Brasil, 2000/2001.

[3] Andriolo, F.R.. THE USE OF ROLLER COMPACTED CONCRETE – São Paulo, Brasil, 1998

[4] Sobrinho, J. A. & Fernandes, A. M. & Foes, P. A. – DONA FRANCISCA HYDROPOWER PLANT – Engevix Engenharia Ltda., Florianópolis, Brasil.

DONA FRANCISCA DAM IN BRAZIL CHALLENGES OF BUILDING A RCC DAM ON A WEAK FOUNDATION

José Antunes Sobrinho, Alexandre Marcon Fernandes, Sérgio de Pauli Basso, Rafael Fernandes Pereira, Leonardo de Bem Silva, and Paulo Afonso Foes

Engevix Engenharia S/A., BRAZIL

SUMMARY: Dona Francisca HPP on the Jacuí River, in the State of Rio Grande do Sul - Southern Region of Brazil - have a total installed capacity of 125 MW. The Gravity Dam is a 660 m long, 50 m high built in roller compacted concrete. The dam foundation is constituted by basalt in the banks and by reddish sandstone, solid or with crossed stratification, with different grade of lithification in the river bed. One of the main concerns during its design and construction was the determination of the stable sections for the dam, particularly of the dam sections laid on fractured sandstone foundation. Safety criteria, classical methods of calculation and mathematical modeling for sliding stability analyses of Dona Francisca gravity dam are the matter of this Report. The computational methods used for the analysis included the software Sap2000.

1. LAY-OUT

The description of the project layout is presented in papers "Critical conditions of seepage under rcc dam on permeable foundation the case of the Dona Francisca Dam" and "Evaluation of thermal stresses in a rcc dam in subtropical region of Brazil the case of the Dona Francisca Dam", in this Workshop. Figure 1 shows the general layout.

2. GEOLOGICAL ASPECTS

The dam foundation is constituted by basalt in the banks and by sandstone in the river bed. In the right bank, the basalt was sound and sparsely jointed; in the left bank the basalt presented more fractured and it had been partially removed.

In the river bed, in the spillway passage, the foundation is constituted by reddish sandstone, solid or with crossed stratification, with different grade of lithification. Intercalated in the sandstone, occur sub-horizontal siltstone layers, claystone and intraformational breccia, centimeters thick and a set of ten meters extent. In these layers occur some clay horizons, millimeter to centimeter thick, sub-horizontal, with a set of

ten meters extent, with passages of clay intercalated with rock fragments, which was the first conditional for the stability studies of the dam.

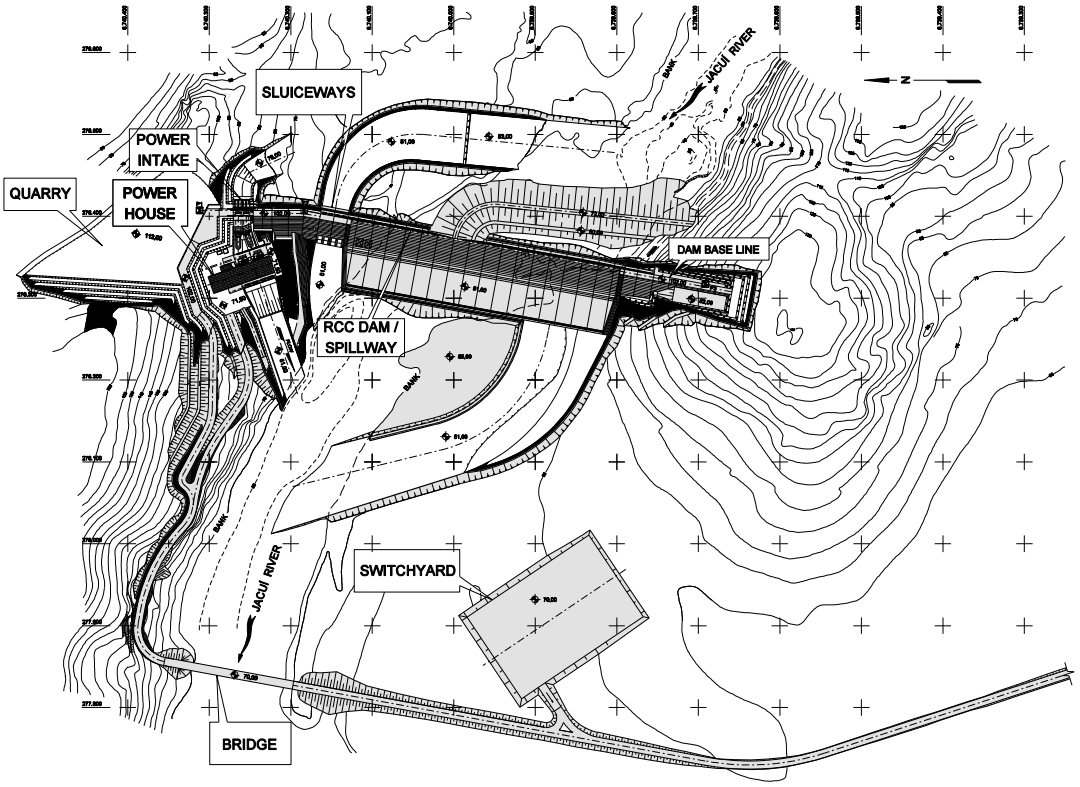

Figure 1 – HPP Dona Francisca General Arrangement

3. HYDROLOGY

The long term mean discharge at the Project site is 281 m^3/s. The maximum discharge observed at the site in the historic gauging period (1940 – 1970) had a peak of 4,447 m^3/s and the minimum discharge was 18.2 m^3/s. As for the flood regime, it may occur at any time of the year. However, a minor seasonal variation can be observed and more severe floods are expected to occur in the period from May to October.

4. RCC STRUCTURES

4.1 GENERAL DETAILS

The main features of the RCC dam/spillway are:

- "Christmas tree" upstream impervious concrete face, 0.50m thick in the bottom to 0.30m thick in the crest;
- Contraction joints each 20 m, maximum;
- RCC layers of 0.30 m;
- Bed mix along the entire contact surface between RCC layers;
- Single drainage gallery;
- Grouting through the upstream slab.

Below are shown some typical details of the dam and spillway construction.

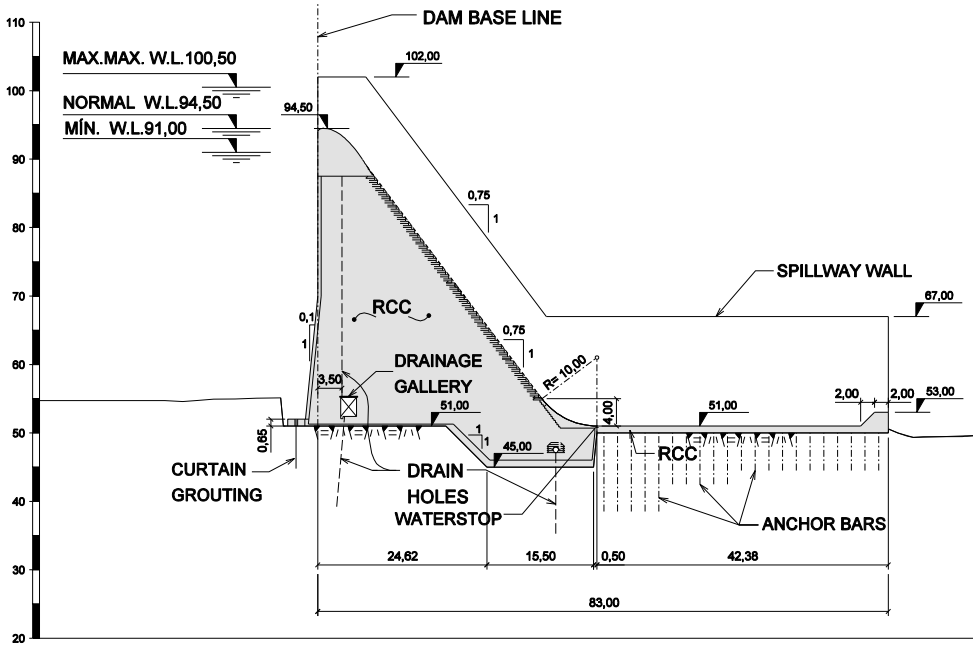

Figure 2 – Typical Dam/Spillway Section

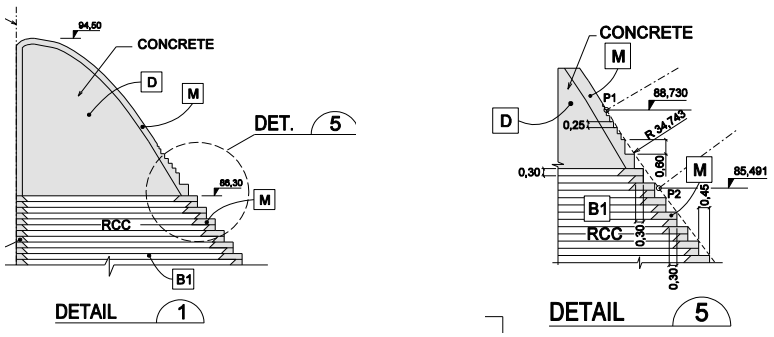

Figure 3 – Crest Spillway Detail

4.2 ROLLER COMPACTED CONCRETE (RCC)

– RCC Materials:

Portland Pozzolanic cement with 30% of pozzolanic material;

Coarse aggregate 25mm;

Coarse aggregate 50mm;

Admixture – retarder and plasticizer;

Crushed sand.

– The mixes used in the dam.

The average mix used during the first stage of the river diversion (blocks B1 to B18) of the dam was the following:

Portland Pozzolanic cement – 90 kg/m^3;

Water – 148 kg/ m^3;

Coarse aggregate 25mm – 691 kg/m^3;

Coarse aggregate 50mm – 565 kg/m^3;

Crushed sand – 1,070 kg/m^3.

For the second stage of the river diversion (blocks B19 to B36) the mix (average) used was the following:

Portland Pozzolanic cement – 85 kg/m^3;

Water – 135 kg/ m^3;

Coarse aggregate 25mm – 693 kg/m^3;

Coarse aggregate 50mm – 567 kg/m^3;

Crushed sand – 1,109 kg/m^3;

Admixture – retarder/plasticizer – 1.02 kg/m^3.

The design required a 9.0 MPa compressive strength for the RCC below the gallery level and a 8.0/7.5 MPa compressive strength for the RCC above the gallery, at the age of 180 days. It was used a lot of mixes along the construction. These mixes, the strength and the age of the concrete are presented in the Figure 4.

Concrete Classification			
Class	fck (MPa)	Type	Cylinder Strength (Days)
A	15	CC	90
B	9	RCC	90
C	15	CC	28
E	12	CC	180
G	15	CC	180
M	24	CC	180
B1	8	RCC	180
D	9	CC	180

Figure 4 – Conventional Concrete and Rolled Compacted Concrete Classification

The use of the admixture was very important for the concrete in the second stage of the river diversion. The summer started in the beginning of the concrete works for the left bank and it was expected high temperatures.

The use of the retarder/plasticizer admixture made possible to reduce the cement and water content, keeping the specified strength, reducing the heat of hydration and increasing the specific gravity (density) of the concrete. Another great benefit is the prolonging of the time RCC can be worked, consequently, compaction by vibrating roller can extend for a longer period of time, after the concrete having been placed.

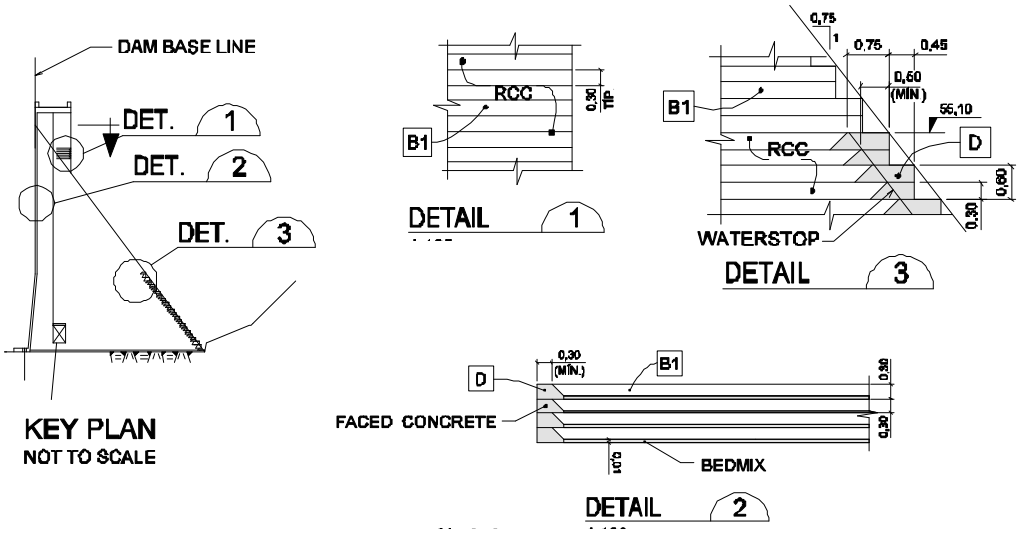

Figure 5 – RCC Construction Detais

5. DAM STABILITY ANALYSIS

5.1 SAFETY CRITERIA

In order to evaluate the sliding safety of concrete dams through the mass concrete or through the conspicuously discontinuity, several classical methods have been used in dam engineering.

The Bureau of Reclamation uses the Shear Friction Factor (SFF) to check the stability against sliding, both through the mass concrete of the concrete and through, or at, the foundation contact.

The SFF is defined as:

$$SFF = \frac{N\,tg\phi + CA}{H}$$, where:

N is the sum of normal forces;

tgϕ is the coefficient of external friction;

C is cohesion;

A is the area;

H is the sum of parallel forces.

In this formulation The SFF value should be upper 3,0 for the Normal Load Conditions, upper 2,0 for Exceptional Load Conditions and upper 1,0 for Limit Load Conditions.

The Corps of Engineers usually apply the Shear Friction Factor to dams over 90m high. For dams below 90m they use the Sliding Factor(SF). which is defined as:

$$SF = \frac{T_f}{T} = \frac{N\,tg\phi + CL}{T}$$, where:

T_f is the resisting shear

T is applied shear

L is the length of base in compression

The SF value should be > 2.00 for Normal Loads and > 1.70 for unusual conditions and 1.3 for extreme load conditions.

In the last three decades large dams were built in Brazil, the engineers have been usually apply in the dams project, for instance: Agua Vermelha (1972), Itaipu (1975), Tucuruí (1980), Xingó (1985), Salto Caxias(1995) etc, the partial coefficient method, computing the Sliding Safety Factor(SFF) to check the stability against the sliding, through the mass concrete, concrete-foundation contact or potential discontinuity site below the surface.

The SSF is defined as:

$$SSF = \frac{\frac{N\,tg\phi}{\gamma\phi} + \frac{CA}{\gamma C}}{H} \rangle 1{,}0$$

Where $\gamma\phi$ and γc are respectively the partial reduction factor for the friction and cohesion.

For Dona Francisca concrete dam or spillway were apply this formulation with the following reduction factors:

Normal Load Conditions:	$\gamma\phi$ =1,5	γc=3,0
Exceptional Load Conditions:	$\gamma\phi$ =1,2	γc=1,5

On the other hand, if the mechanism of rupture consist in the sliding along two or more discontinuities, as shown in Figure 9, the sliding stability analysis involves the determination of the lateral driving force (H1), acting on the plane AB, and the horizontal force (H2), acting against the plane AC, besides all the resisting forces due to cohesion , friction etc. (T1) and the passive wedge resistance Ep.

H=H1+H2

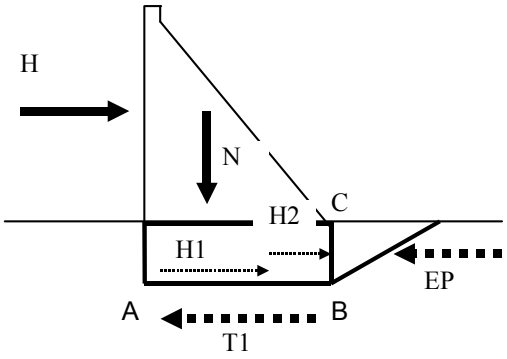

Figure 6 – Forces Acting in a Sliding Plane

In this case two Safety Factors (SF1 and SF2) may be computed, as follows:

SF1=T1/H1 > 1,0 (sliding through discontinuity AB)

SF2=Ep/H2 > 1,0 (sliding through the passive wedge)

As can be seen for the computing both safety factors its necessary the knowing of the H1 and H2 acting forces. The sum of this forces **H=H1+H2** is the only one equation in disposition.

An alternative way to solve this problem is the determination of values of H1 and H2 by a numerical method, in general the Finite Element Method. The answer obtained is relative easy and satisfactory.

5.2 NUMERICAL ANALYSIS

The dimensioning and analysis of the behavior of solid gravity dams including the foundations is usually done by assuming equilibrium to be bidimensional, which as rule is quite satisfactory, and by adopting continuous linear idealization under action of design loading.

Under these conditions, the adequate method for determining the stress and deformations fields of the dam/foundation structure, which is routine in the last three decades, is the Finite Element Method. This method is entirely satisfactory, in terms of accuracy and ability to determine the stress distribution in dam and foundation, including shapes, loading, heterogeneity, anisotropy, etc. In order to determine by the FEM the H1 and H2 values is necessary basically to know the acting forces and the deformability parameters involved. The FEM does not determine the passive resistance. This strength can be evaluated only with knowing of the wedge geometry and its two strength parameters.

For the sliding stability studies of the Dona Francisca spillway structure unit, the relevant strength parameters to be considered were the friction angle and cohesion of the el. 41,50m (average values ϕ=31^o and c=0,5 kgf/cm^2). A two-dimensional finite element model of the dam-foundation system was considered, following the geometry as showed in Figure 8 and incorporating the geomechanical characteristics presented in Figure 7.

Material Description		**Modulus of Elasticity (Kgf/cm^2)**	**Poisson Ratio (ν)**	**Specific Weight (tf/m^3)**
1	Concrete	300,000	0.20	2.45
2	Sandstone (with treatment)	30,000	0.25	2.30
3	Sandstone	10,000	0.25	2.30
4	Concrete-rock / contact	100,000	0.25	2,30
5	Claystone/Siltstone	5,000	0.25	2,30
6	Claystone/Siltstone (with treatment)	10,000	0.25	2,30

Figure 7 – Geomechanical Characteristics of Materials

From the stress values resulting from the finite elements model, added to the subpression loads, the resulting safety factors were calculated, as shown in item 5.1. Nevertheless, more precise safety coefficents, a analysis of the stresses determined in

the model, comparing them to the admissible stresses, was carried out. The resulting stresses, for normal load, are shown in the following figures.

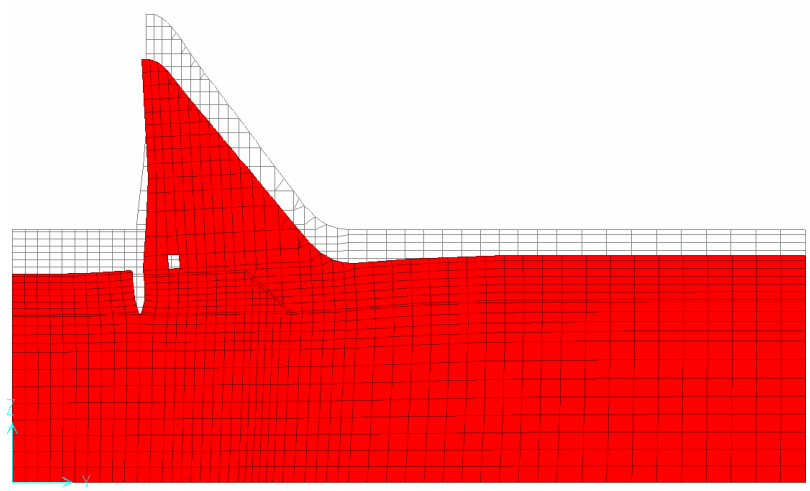

Figure 8 –DEFORMED

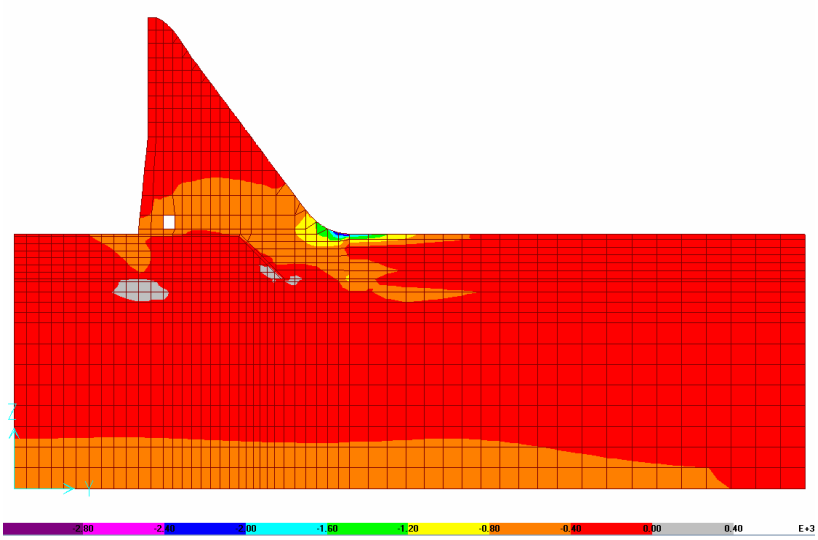

Figure 9 –S11 - NLC

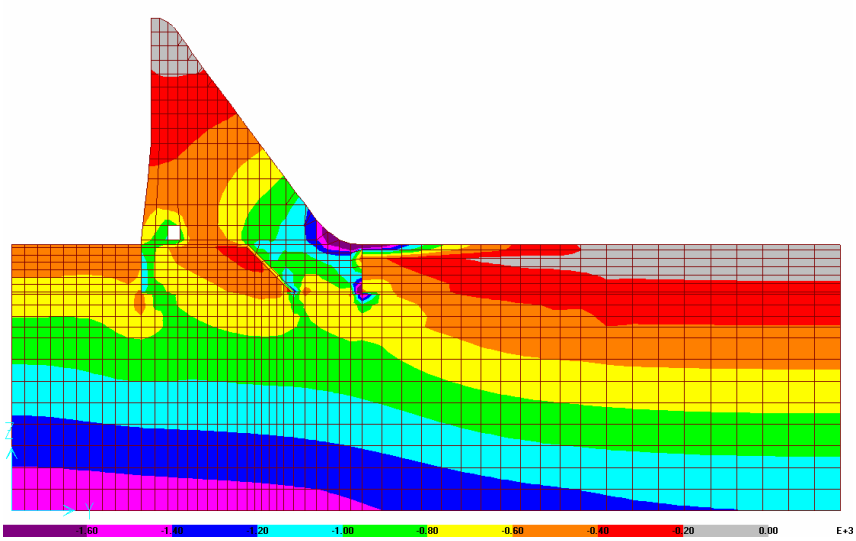

Figure 10 –MIN - NLC

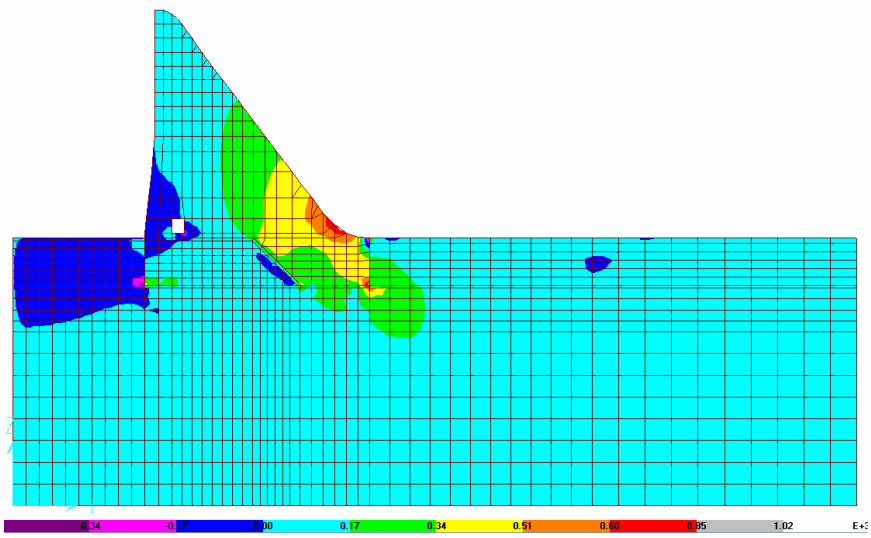

Figure 11 –S12 - NLC

6. CONCLUSIONS

In general, the foundation conditions of the dam are very complex, mainly in its left bank and river bed. The works carried out to comprehend these conditions have demanded a high degree of subjective interpretation of the data of the exploratory drillings. Furthermore, there are three different potential sliding planes for each block of the dam. Because of these conditions, the geologic models are supposed to be very conservative and a great number of protections against sliding were executed. The stability of the dam is assured by:

- a grouting curtain upstream of the dam;
- a grouting curtain near the end sill of the stilling basin, to reduce the amount of seeping water from downstream to the drainage gallery;
- an efficient drainage system;
- a deep toe downstream of the dam, supported by the foundation of the stilling basin;
- ANCHOR bars each 2m in the whole stilling basin to consolidate and to reinforce the foundation downstream of the dam. See Figure 2.

Many blocks of the dam were verified by different methods, due to the complexity of the foundation. Finite element model and classical method were adopted with the following safe factors: 1.5 for friction and 3 for cohesion. Besides, it was also used the US Army Corps of Engineers – Gravity Dam Design, with conservative parameters for the foundation, assuring an adequate margin of safety for the dam.

ACKNOWLEDGEMENT

The authors would like to express their gratitude to the project owner DFESA – Dona Francisca Energética S.A. - and the suppliers construction CONFRAN – Consórcio Fornecedor da UHE Dona Francisca – for allowing the publication of project data and references.

REFERENCES

[1] Tajima, R. & Pereira, R.F. – Mapeamento, Injeção e Drenagem da Fundação da Barragem. Engevix Engenharia Ltda. Florianópolis, Brasil, 2001.

[2] UHE DONA FRANCISCA - TECHNICAL REPORT FOR THE BOARD OF CONSULTANTS – Board Meetings n^{os} 7, 8, 9, Curitiba, Brasil, 2000/2001.

[3] Andriolo, F.R.. THE USE OF ROLLER COMPACTED CONCRETE – São Paulo, Brasil, 1998

[4] Sobrinho, J. A. & Fernandes, A. M. & Foes, P. A. – DONA FRANCISCA HYDROPOWER PLANT – Engevix Engenharia Ltda., Florianópolis, Brasil.

SLOPE STABILITY OF LARGE RESERVOIR BANKS. SLOPE INSTABILITY IN THE SACELE DAM HEIGHTENING CONDITIONS

Dan Stematiu, Dan Păunescu
Technical University of Civil Engineering of Bucharest, ROMANIA

SUMMARY: In the slope instability conditions, previously occurred on the right bank of Sacele reservoir, the dam heightening could aggravate or even trigger a massive landslide putting in danger the intake tower safety. The preventive measures had not the expected effect and a new investigation programme in new conditions required a new stability approach. Each preventive measure has been taken into account in the stability analysis and the own effect on slope stability has been put in evidence in different load hypothesis. The effect of storage level increasing has also been considered. The precarious stability of the entire area has been confirmed by the stability analyses. The reduced efficiency of some preventive measures has been explained and confirmed by parametric analysis. The decision about the more suitable measures to be adopted has been finally taken based on this sensitivity analysis.

RÉSUMÉ: Dans les condition d'instabilité de pante déjà manifestées pour la rive droite du réservoir de Sacele, le surhaussement du barrage peut aggraver ou même déclencher une massive glissement de terrain qui peut péricliter la sûreté de la tour de prise d'eau. Les mesures de prévention déjà prises n'ont pas eu l'effet escompté et un nouvel programme d'investigation dans les nouvelles conditions a nécessite une nouvelle abordation de la stabilité. Chaque mesure de prévention a été considérée avec son propre effet sur la stabilité dans diverses hypothèses de charge. L'effet de l' haussement du niveau normal de retenue a été considérée aussi. La stabilité précaire de toute la pante a été confirmée par l'analyse de stabilité. La décision sur les mesures de stabilité les plus indiquées a été finalement prise en tenant compte de cette analyse de sensitivité.

1. INTRODUCTION

Sacele reservoir is located on the Tarlung River in the Carpathian Mountains, at an average elevation of over 700.00 mASL, and provides the water supply for Brasov city, a town of almost 1 million inhabitants situated in the central region of Romania. Dam heightening has been required by additional water necessity reasons.

Since the first reservoir filling, slope instabilities occurred just in the intake area located on the right bank of the Sacele reservoir, not very far from the earthfill dam. A large amount of remedial works have been achieved during the time but spectacularly effects on stability improvement have not been ascertained.

The general view of the Sacele reservoir and the location of bank instability in the intake vicinity can be seen in Figure 1. In Figure 2 there is an image of the Sacele dam intake on the right bank affected by slope instability.

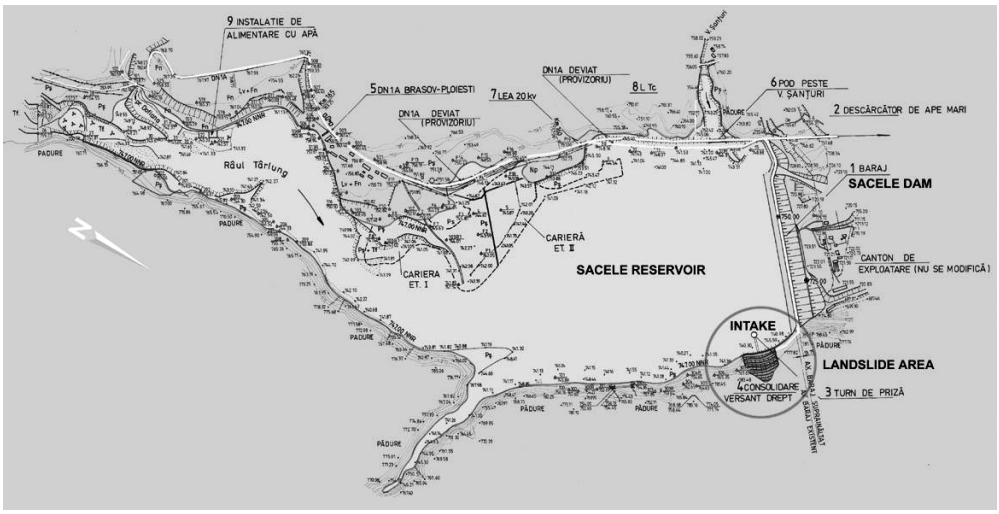

Figure 1. General view of the Sacele reservoir and location of the bank instability

Figure 2. Sacele Dam intake on the right bank affected by slope instability

2. HISTORY OF THE MASS MOVEMENTS AND THE MANMADE INTERVENTIONS

The first active landslide in the area has been recorded since the investigation period for dam construction (1970-1971) when local instabilities, visibly related to the local angle of the slope have been considered as shallow and as less important. Therefore preventive measures have not been adopted at that time. The earth fill dam

has been performed during 1971-1975 and the first reservoir filling begun in 1975. Three years later, in 1978 a reactivation of the landslide affected the access footbridge to the intake tower, proving a real danger even for intake tower safety. Consequently an ample programme of investigation started up. A number of 17 drillings have been achieved and the inclinometers put in evidence the presence of a deep rockslide with clear-cut contour and very unfavorable kinematics. However, a correlation between reservoir level or rainfall intensity and mass movements cannot be found.

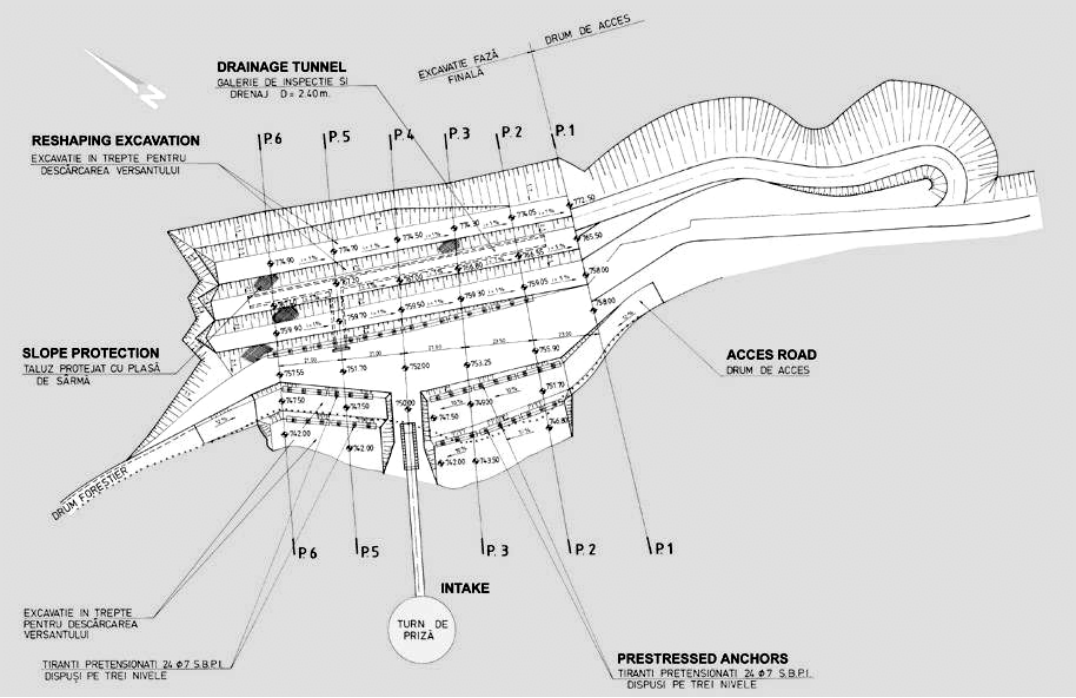

Figure 3. General view of all works expected to be achieved in order to improve the stability

In order to prevent the landslide triggering, several remedial works have been proposed as follows:

- slope reshaping by excavating of about 85.000 m^3 achieving 5 steps and the afferent slope protection;
- slope drainage by performing a drainage gallery of 2.40 m diameter, made from two branches disposed left-right from the main inspection tunnel, provided with radial drains;
- slope reinforcement by achievement of three rows of pre-stressed anchors disposed at different elevations (759.00, 747,50 şi 742.00 mdM) on a front of about 90.00 m large.

A simplified plan viewing all of these works is represented in Figure 3.

From 1980 until 1990 the total measured displacement of the slope was almost 10 cm, the velocity of mass movement decreasing from 1 mm per month to 0.25 mm per month. In 1991 a relative stability has been noticed accrediting the hope of the end of mass movements. Movements of the intake tower have never been recorded. Until 1996 from the list of works presented above the slope reshaping has been adopted as preventive measure and partially accomplished by excavating almost 70.000 m^3 of

deluvium. The slope reshaping has been interrupted because of the retrogressive instabilities advancing to crest. A part of these retrogressive developments can be seen in Figure 4.

Figure 4. Retrogressive instability induced by the slope reshaping

From the drainage tunnel only a part has been achieved too and from the reinforcement works only one row of anchors has been accomplished (see Figure 5). Consequently, the stability improved and a relative calm installed again. Due to this relative stability in the next years the interest for the landslide diminished.

Figure 5. Drainage tunnel portal and the first row of anchors

But the calm was not for ever. After an extreme rainy season long of over two month, in July 2001 several openings between drainage tunnel rings and relative displacements appeared and an increased turbidity of drained water has been noticed certifying the reactivation of landslide (see Figure 6). This time the instability followed

to a very rainy season with intensities exceeding 70-150 l/m^2, i.e. more over the average values recorded.

Taking into account this summary of events, in order to improve the stability and to avoid a possible intake tower damage the problem of the bank instability is reconsidered. Moreover the dam heightening and the rising of storage level with 6.00 m (from 741.00 to 747.00) could induce additional instability on the already unstable slope.

Figure 6. Relative displacements between drainage tunnel rings and drainage holes

3. GEOLOGICAL AND HYDROGEOLOGICAL CONSIDERATIONS

The general slope of the right bank in the intake vicinity is about 35^0 - 45^0.

From the geological point of view, the site presents a series of subsequent layers, strongly disturbed by sliding movements proving again the ever-sliding tendency of this slope. The geological and hydrogeological knowledge in site continuously developed in these last 30 years of investigations. In the following the geology has been simplified in order to keep only the details able to explain the movements and to be of instant interest for the stability analysis. A deluvium layer represents the quaternary with very variable deepness between 1m and 22m, being made from silty clays and clayey silty sands including fragments of rock of wide range of sizes (debris). Several sliding surfaces have been identified in this layer and they are represented in Figure 7. Near the intake tower there is an accumulation of scree slope. The following geotechnical parameters may be considered for this layer:

- Unit weight γ = 18.00-18.50 kN/m^3
- Water content w = 8-12%
- Friction angle unconsolidated, undrained φ_{uu} = 25^0-26^0
- Cohesion c_{uu} = 30 kPa
- Friction angle unconsolidated, undrained, fully saturated φ_{uu} = 18^0-19^0

The bedrock is represented by the complex of cretaceous Sinaia layers and includes gray calcareous sandstone and marl clay shists, both of them fissured and strongly tectonized.

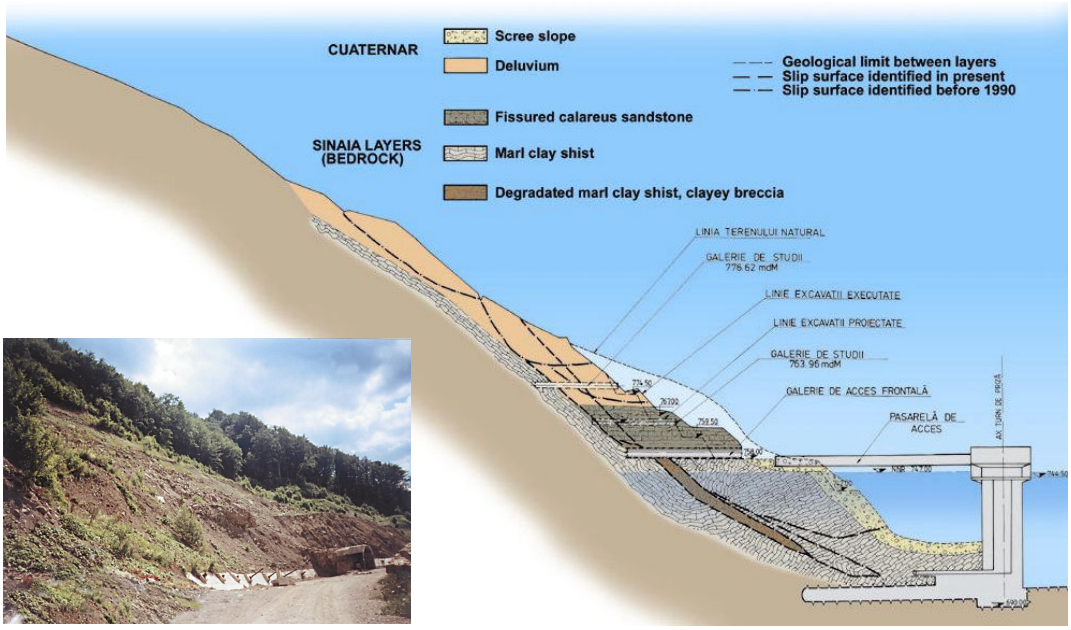

Figure 7. Geological cross section through the unstable slope, main remedial works and the location of the intake tower

The particular shape of the calcareous sandstone volume and its isolated location prove that this volume is not in site. Its actual position could be reached after a sliding process started from another origin located somewhere at a higher elevation. That thing confirms again the historical sliding predisposition of this slope.

Between the calcareous sandstone and the marl clay shist formation a fault of about 0.5-2.0m thicknesses containing a silty clay breccia layer has been identified (see Figure 7). In this layer developed a significant part of the sliding surface. The geotechnical parameters of this material are the following:

- Unit weight γ = 19.5-20.5 kN/m^3
- Water content w = 10-12%
- Friction angle unconsolidated, undrained $\varphi_{uu} = 22^0$
- Cohesion c_{uu} = 40 kPa
- Friction angle unconsolidated, undrained, fully saturate $\varphi_{uu} = 16^0$
- Cohesion c_{uu} = 47 kPa

In the marl clay shists the direction of fissure system is about 25^0-30^0 oriented to the toe slope and almost parallel with it.

From the hydrogeological point of view, the site presents a series of particularities especially related to the alternance of the pervious/impervious layers and of the presence of the reservoir. Intense underground flow has been identified through the entire slope, both through superficial deluvial layers and through the deeper ones. The groundwater level variations have been surveyed until 1992 and recorded from the inclinometers drillings. At the base of the slope especially the reservoir level controls the groundwater level. For the above elevations in the inspection tunnel the groundwater level has been found little above the sliding surface. The rainfalls are the main source of the underground water.

4. STABILITY ANALYSIS

The stability analysis followed an assessment of the remedial works efficiency in the light of the recent investigations in view of storage level increasing. The effect of each remedial measure, both proposed and already adopted, has been modeled in several loading hypotheses able to increase the slope instability.

The analysis made was not based on very sophisticated models because of the inherent uncertainty and insufficiency of the input data. A comparison of situations was of interest in order to put in evidence the efficiency of different measures, single or combined. For these reasons the stability approach is based on the classical limit equilibrium models such as Bishop and Janbu, considered as the most suitable for this shape of sliding surface. The GEOSLOPE software package, module SLOPE/W. Version 4.1 has been successfully used.

For the rocks and soils behavior, the Mohr-Coulomb failure criterion has been adopted. The parameters of the shear strength have been properly calibrated from the condition of obtaining a critical sliding surface similar to the real one, enough determined in site. The calibration has been made related to the parameters of the clay breccia considered as controlling a significant part of the sliding surface. The values of the shear strength parameters such obtained and involved in the stability analysis are brought together in Table 1.

Table 1. Geotechnical parameters used in the stability analysis

Material		Geotechnical parameters		
		γ (kN/m^3)	c (kPa)	φ (^{0})
Deluvium (clyey silty sand with debris)		19 - 22	0	22
Marl clay shists		24	40	27
Clay breccia	fully saturated	24	20	18
	wetted	24	60 (80)	20 (18)
	drained	24	70 (100)	21 (18)

4.1. Hypotheses of analysis

The stability analysis has been organized taking into account several calculus hypotheses.

The presence of the reservoir in view of storage level rising has been modeled by using three hypothesis:

- without reservoir;
- storage level at 741.00 m;
- storage level at 747.00 m.

By slope morphology, two basic hypotheses have been considered:

- natural slope representing the situation before the reshaping excavation (coupled without reservoir and with reservoir level at 741.00 m) and
- reshaped slope after excavation achievement (coupled with the reservoir level at 741.00 m respectively at 747.00 m).

By position of the underground water level and because of the lack of more accuracy records, the stability has been analyzed in another two hypotheses corresponding to: a dry season and a wet season, the difference between them consisting in sensitive level fluctuations.

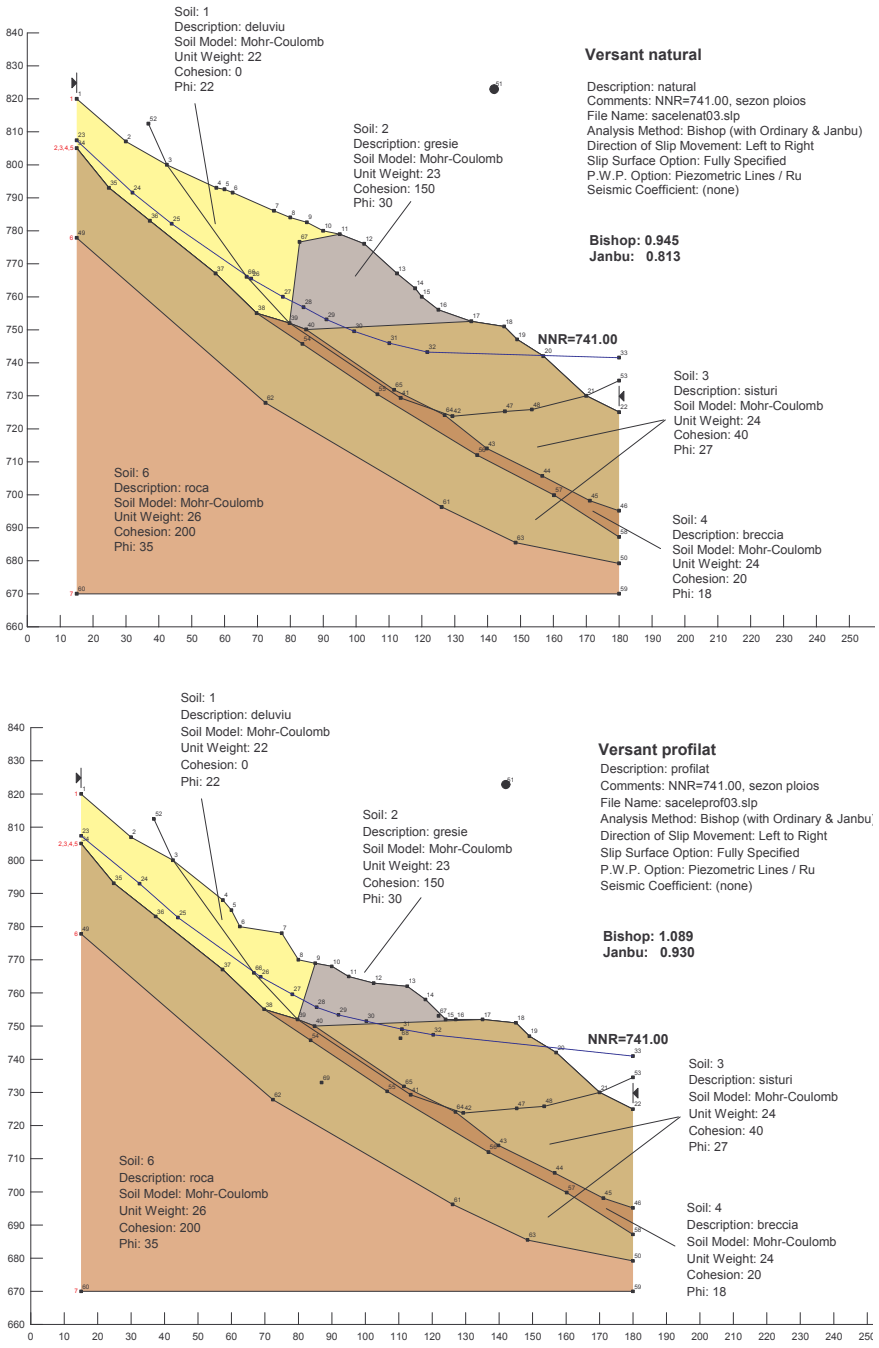

Figure 8. Models adopted for the natural slope and for the excavated one with the reservoir level at 741.00 m. The increased stability is due to slope reshaping

The effects of the anchor rows and of the earthquake have been also put into evidence. The seismic load has been modeled only in the pseudo-static assumption in order to compare the results within different alternatives. As it is well known, the pseudo-static assumption is not the most suitable solution to model the effect of the earthquake on slope stability. Because the instabilities have not been recorded in

seismic conditions, this hypothesis had not particularly developed. In Figure 8 is put in evidence the favorable effect of reshaping excavations and in Figure 9 is represented the model of reshaped slope with the insignificant effect of the 3 rows of anchors.

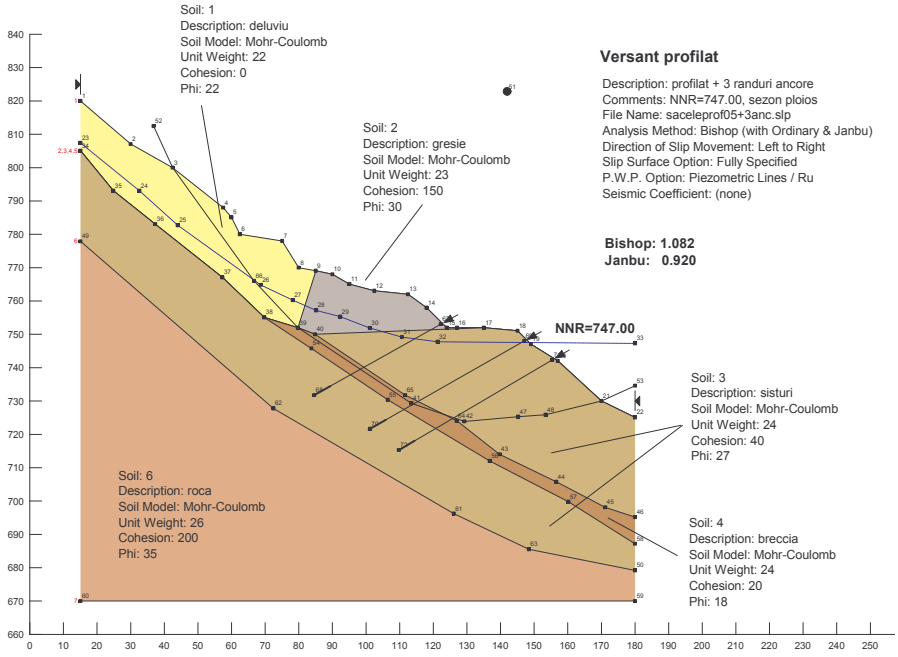

Figure 9. Model adopted for the excavated slope with the reservoir level at 747.00 m. The stability increasing is due to 3 rows of anchors, but it is almost insignificant in comparison with no anchors hypothesis

4.2. Results of stability analysis in the static hypothesis

Accordingly with the hypothesis succinctly presented above, the results of stability analysis have been organized in the next three tables as follows.

Table 2. Factors of safety for the natural slope (before slope reshaping)

Hypothesis	No reservoir	Reservoir level at 741.00 m	
		Dry season	Wet season
FS - Bishop	1,263	1,100	0,945
FS - Janbu	1,072	0,946	0,813

Table 3. Factors of safety for the reshaped slope with reservoir level at 741.00 m

Hypothesis	Dry season No anchors	Wet season			Drained slope
		No anchors	1 row of anchors	3 rows of anchors	
FS-Bishop	1,416	1,089	1,101	1,136	1,470
FS-Janbu	1,208	0,930	0,940	0,964	1,263

Table 4. Factors of safety for the reshaped slope with reservoir level at 747.00 m

Hypothesis	Dry season No anchors	Wet season			Drained slope
		No anchors	1 row of anchors	3 rows of anchors	
FS-Bishop	1,218	1,036	1,048	1,082	1,265
FS-Janbu	1,047	0,887	0,896	0,920	1,087

An overview on the obtained results shows that for a wide range of load hypotheses a narrow range of safety factors is obtained. That thing confirms the precarious stability of the slope and its predisposition to sliding. The values of safety factors presented in Table 2 confirms that for the natural slope the creation of the reservoir was the main cause of the instability, the fluctuations of stable/unstable situations being lead by the level of rainfalls. The slope reshaping excavations, even unfinished, had the most significant positive effect on slope stability (see Table 3). The retrogressive instabilities advancing to crest have been confirmed by the calibration of the model when several of critical surfaces have been tested resulting values of safety factor near by 1.0. The expected storage level increasing from 741.00 m to 747.00 m (see Table 4) proves a not very drastic deterioration of the stability conditions. The slope drainage and especially of the sliding surface remains the most efficient preventive measure, with the most significant effect. The rising of headwater level diminishes in a reduced manner this positive effect because of the immersion the toe slope. On the other hand, the slope reinforcement even with 3 rows of pre-stressed anchors has extremely low effect on the slope stability.

5. CONCLUDING REMARKS

Based on a synthesis of over 30 years of events, investigations and measures, the problem of the instability of the right bank of the Sacele reservoir in the vicinity of the intake tower brings together several concluding remarks.

1. The right bank of the Sacele reservoir at the intake tower vicinity has been affected by severe slope instability induced by the initial rising of reservoir level at 741.00 m.
2. Reshaping excavation of the slope lead to positive effects on the actual landslide but they could induce new retrogressive instabilities.
3. Three rows of pre-stressed anchors had insignificant stabilization effect. For this reason the anchorage works have been interrupted.
4. Excessive rainfalls could induce landslide reactivation.
5. Rising of reservoir level at the additional elevation of 747.00 m has no significant negative effects on the slope stability.
6. Slope drainage, especially of the sliding surface, remains the most suitable solution with significant effect on stability.

Additionally, this study could be a good lesson for the civil engineer in the respect of never adopting a remedial work without a previous thorough analysis.

REFERENCES

[1] Contract U.T.C.B. Supraînălţare baraj Săcele - Etapa I. Analiza stabilitatii versantului drept al acumularii Sacele, 2001.

[2] GEOSLOPE User Manual – Geo-Slope International Calgary, Alberta

Family name	First name	Country	Type of registration	E-mail address	Hotel	Company	Postal address
ABDULAMIT	Altan	Romania	Delegate	altan@hidro.utcb.ro	-	Technical University of Civil Engineering of Bucharest	124 Lacul Tei Bd., sect. 2, 72302 Bucharest, ROMANIA
AMBERG	Francesco	Switzerland	Delegate	francesco.amberg@lombardi.ch	Capitol	Lombardi Ltd.	19 Via R. Simen, 6648 Minusio, SWITZERLAND
ANTOHI	Constantin	Romania	Delegate		UTCB	"Gh. Asachi" University of Iasi	67 D. Mangeron St, Iasi, ROMANIA
ASADI-KHIAVI	Yousef	Iran	Delegate	yousef_asadi@yahoo.co.uk	Capitol	Moshanir Co.	37 Martyr Khoddami St., Vanaq Sq.,5994753486 Tehran, IRAN
KHEDMATI-ZANJANAB	Fatemeh	Iran	accompanying person		Capitol		
ASANACHE	Gheorghe	Romania	Delegate	apasco@xnet.ro	-	Apasco S.A.	293 Tabla Butii, Maneciu, Prahova, ROMANIA
ASMAN	Iulian	Romania	Delegate	iulian.asman@rowater.ro	-	Romanian National Water Administration	6 Edgar Quinet St., sect. 1, 70106 Bucharest, ROMANIA
BOGZIANU	Razvan	Romania	Delegate	razvan.bogzianu@rowater.ro	-	Romanian National Water Administration	6 Edgar Quinet St., sect. 1, 70106 Bucharest, ROMANIA
BOUYGE	Bernard	France	Delegate	bbouyge@razel.fr	Intercontinental	Independent Consulter	Monpellier, FRANCE
BRAND	Bruce	U.S.A.	Delegate	bruce.brand@ferc.gov	Capitol	Federal Energy Regulatory Commission U.S.A	8713 Ramsey Court-Spriegfield, 22151 VA-U.S.A.
BRATIANU	Gheorghe	Romania	Delegate	office@aquaproiect.ro	-	Aquaproiect S.A.	294 Splaiul Independentei, sect. 6, 77703 Bucharest, ROMANIA
CARRÈRE	Alain	France	Delegate	alain.carrere@coyne-et-bellier.fr	Intercontinental	Coyne et Bellier	Coyne et Bellier, 9 Allee des Barbanniers, F-92632 Gennevilliers Cedex, FRANCE
CASOTA	Victor	Romania	Delegate	jiu@hidroconstructia.com	-	Hidroconstructia S.A.	103-105 Calea Dorobantilor, sect. 1, 71223, Bucharest, ROMANIA
COJOCAR	Mihai	Romania	Delegate	udc_productie@hidroconstructia.ro	-	Hidroconstructia S.A.	103-105 Calea Dorobantilor, sect. 1, 71223, Bucharest, ROMANIA
CONSTANTIN	Albert-Titus	Romania	Delegate		UTCB	Polithnica University of Timisoara	1A, George Enescu St.,1900 Timisoara, ROMANIA
DAMIAN	Radu	Romania	delegate	ardeal@hidroconstructia.com	-	Hidroconstructia S.A.	103-105 Calea Dorobantilor, sect. 1, 71223, Bucharest, ROMANIA
DASCALESCU	Nicolae	Romania	delegate	office@rocold.ro	-	Institute of Hyroelectric Studies and Design	5-7 Vasile Lascar St., sect. 2, 79669-Bucharest, ROMANIA

DOBRESCU	Dan	Romania	delegate	dandobrescu_ro@yahoo.com	-	Institute of Hyroelectric Studies and Design S.A.	5-7 Vasile Lascar St., sect. 2, 79669-Bucharest, ROMANIA
FANELLI	Michele	Italy	delegate	michele.fanelli@infinito.it	Intercontinental	Independent Consulter	5 Via L.B. Alberti, 20149-Milano, ITALY
FANELLI	Cesira	Italy	accompanying person		Intercontinental		
FUJII	Kenji	Japan	delegate	afujii@tepco.co.jp	Capitol	Tokyo Electric Power Company	3-3 Higashi-Ueno, 3-Chome, Taito-Ku, 100-0015 Tokyo, JAPAN
FUJIYAMA	Tetsuo	Japan	delegate		Capitol	Maeda Co.	
GABOR	Ovidiu	Romania	delegate	ovidiu.gabor@rowater.ro	-	Romanian National Water Administration	6 Edgar Quinet St., sect. 1, 70106 Bucharest, ROMANIA
GINZBURG	Sofia	Russia	delegate	sonja@concrete.vniig.ru	Capitol	B E Vedeneev Research Institute VNIIG	21 Gzhatskaya 21, 195220 Saint Petersburg, RUSSIA
GLAGOVSKY	Viacheslav	Russia	delegate	glag@ground.vniig.ru	Capitol	B E Vedeneev Research Institute VNIIG	21 Gzhatskaya 21, 195220 Saint Petersburg, RUSSIA
HAPAU-PETCU	Stan	Romania	delegate	office@aquaproiect.ro	-	Aquaproiect S.A.	294 Splaiul Independentei, sect. 6, 77703 Bucharest, ROMANIA
HOFSTETTER	Guenter	Austria	delegate	guenter.hofstetter@uibk.ac.at	Capitol	University of Innsbruck	13 Technikerstrabe, A-6020 Innsbruck, AUSTRIA
HULEA	Dan	Romania	delegate	dan.hulea@hidroelectrica.ro	-	Hidroelectrica S.A.	3 Constantin Nacu St, sect. 2, 70219 Bucharest, ROMANIA
ILIE	Lucian	France	delegate	lucian.ilie@criltechnology.com	-	Cril Technology Co. Paris	6, Square d'Astorg, 78150 Le Chesnay, FRANCE
NECULCE	Luminita	France	accompanying person		-		
ILINCA	Cornel-Dumitru	Romania	delegate	cornel@hidro.utcb.ro	-	Technical University of Civil Engineering of Bucharest	124 Lacul Tei Bd., sect. 2, 72302 Bucharest, ROMANIA
ION	Michael	Romania	delegate	decan@hidro.utt.ro	UTCB	Polithnica University of Timisoara	1A, George Enescu St.,1900 Timisoara, ROMANIA
JIVCOVICI	Adriana	Romania	delegate	iscesucc@isce.ro	-	Institute of Electric Power Studies and Consulting S.A.	293 Calea Vitan St., sect. 3, 74381 Bucharest, ROMANIA
KHOSHRANG	Gholamreza	Iran	delegate	khosrang@mahabghodss.com	Capitol	Mahab Ghodss Co.	17 Takharestan Alley, Zafar st., 15157 Tehran, IRAN
LAZAR	Gheorghe	Romania	delegate	gh_lazar@hidro.utt.ro	UTCB	Polithnica University of Timisoara	1A, George Enescu St.,1900-Timisoara, ROMANIA
MALAI	Marius	Romania	delegate	malai_m@hotmail.com	-	Hidroelectrica S.A. - Cluj Branch	1 Taberei St., 3400 Cluj-Napoca, ROMANIA
MALLA	Sujan	Switzerland	delegate	sujan.malla@ewe.ch	Capitol	ELECTROWATT-EKONO Ltd.	161 Hardturmstr, 8037 Zurich, SWITZERLAND

MATEESCU	Octavian	Romania	delegate	octavian.mateescu@hidroelectrica.ro	-	Hidroelectrica S.A.	3 Constantin Nacu St, sect. 2, 70219 Bucharest, ROMANIA
MAZZA	Guido	Italy	delegate	gmazza@cesi.it	Intercontinental	CESI Milan	54 Via Rubattino, 20134 Milano, ITALY
MEGHELLA	Massimo	Italy	delegate	meghella@cesi.it		CESI Milan	54 Via Rubattino, 20134 Milano, ITALY
MENGA	Roberto	Italy	delegate	roberto.menga@enel.it	Intercontinental	ENEL Hydro S.P.A. ISMES Division	9 Via Pastrengo, 24068 Seriate, ITALY
MIHAESTEANU	Eduard	Romania	delegate	edimihasteanu@yahoo.com	-	Institute of Hyroelectric Studies and Design S.A.	5-7 Vasile Lascar St., sect. 2, 79669-Bucharest, ROMANIA
MOTEA	Iulia	Romania	delegate	iuliam@usa.com	-	Hidroelectrica S.A.	3 Constantin Nacu St, sect. 2, 70219 Bucharest, ROMANIA
NICOARA	Serban	Romania	delegate		UTCB	Polithnica University of Timisoara	1A, George Enescu St.,1900 Timisoara, ROMANIA
NORET-DUCHÈNE	Christine	France	delegate	christine.noret@coyne-et-bellier.fr	Intercontinental	Coyne et Bellier	Coyne et Bellier, 9 Allee des Barbanniers, F-92632 Gennevilliers Cedex, FRANCE
PARVULESCU	Costin	Romania	delegate	iscesucc@isce.ro	-	Institute of Electric Power Studies and Consulting S.A.	293 Calea Vitan St., sect. 3, 74381 Bucharest, ROMANIA
PAUNESCU	Dan	Romania	delegate	paunescu@hidro.utcb.ro	-	Technical University of Civil Engineering of Bucharest	124 Lacul Tei Bd., sect. 2, 72302 Bucharest, ROMANIA
PERNER	Franz	Austria	delegate	franz.perner@verbundplan.at	Capitol	Verbundplan GmbH	29 Rainerstrasse, A-5020 Salzburg, AUSTRIA
POPOVICI	Adrian	Romania	delegate	popovici@hidro.utcb.ro	-	Technical University of Civil Engineering of Bucharest	124 Lacul Tei Bd., sect. 2, 72302 Bucharest, ROMANIA
POPOVICI	Daniela-Irina	Romania	accompanying person		-		
PRUNDEANU	Emil	Romania	delegate	dumitru.prundeanu@hidro-valcea.ro	-	Hidroelectrica S.A.	3 Constantin Nacu St, sect. 2, 70219 Bucharest, ROMANIA
RANDASU	Sorin	Romania	delegate	sorin.randasu@rowater.ro	-	Romanian National Water Administration	6 Edgar Quinet St., sect. 1, 70106 Bucharest, ROMANIA
SAOUMA	Victor	U.S.A.	delegate	saouma@bechtel.colorado.edu		University of Colorado U.S.A / Politecnico di Milano, ITALY	
SARGHIUTA	Radu	Romania	delegate	sarghiut@hidro.utcb.ro	-	Technical University of Civil Engineering of Bucharest	124 Lacul Tei Bd., sect. 2, 72302 Bucharest, ROMANIA
STEMATIU	Dan	Romania	delegate	stematiu@hidro.utcb.ro	-	Technical University of Civil Engineering of Bucharest	124 Lacul Tei Bd., sect. 2, 72302 Bucharest, ROMANIA

STERIAN	Marian	Romania	delegate	apasco@xnet.ro	-	Apasco S.A.	293 Tabla Butii, Maneciu, Prahova, Bucharest, ROMANIA
STERIAN	Alexandrina	Romania	accompanying person		-		
TEODORESCU	Dan	Romania	delegate	dan.teodorescu@rowater.ro	-	Romanian National Water Administration	6 Edgar Quinet St., sect. 1, 70106 Bucharest, ROMANIA
TIMOFTI	Emil	Romania	delegate	office@hidroconstructia.com	-	Hidroconstructia S.A.	103-105 Calea Dorobantilor, sect. 1, 71223, Bucharest, ROMANIA
TOMA	Ion	Romania	delegate	itoma@geodin.ro	-	Institute of Hyroelectric Studies and Design S.A.	5-7 Vasile Lascar St., sect. 2, 79669-Bucharest, ROMANIA
TOUILEB	Bachir	Canada	delegate	touileb.bachir.n@hydro.qc.ca	Intercontinental	Hydro Quebec	855 Sainte-Catherine, est, 19th floor, H2L4P5 Montreal, CANADA
TZENKOV	Anton	Bulgaria	delegate	a.tzenkov@ep-hydro.com	Capitol	Energoprovekt-Hydropower Limited Sofia	
UCHITA	Yoshihisa	Japan	delegate	uchita.y@tepco.co.jp	Intercontinental	Tokyo Electric Power Company	1-1-3 Uchisaiwai-Cho, Chiyoda-Ku, 100-0011 Tokyo, JAPAN
VEILLEUX	Mario	Canada	delegate	veilleux.mario@hydro.qc.ca	Intercontinental	Hydro Quebec	855 Sainte-Catherine, est, 19th floor, H2L4P5 Montreal, CANADA
WOHNLICH	Alexandre	Switzerland	delegate	awohnlich@stucky.ch	Capitol	Stucky Ingenieurs Conseils S.A.	33 Rue du Lac, 1020 Renens, SWITZERLAND
ZENZ	Gerald	Austria	delegate	zenzg@verbundplan.at	Capitol	Verbundplan GmbH	29 Rainerstrasse, A-5020 Salzburg, AUSTRIA

Author index

The Seventh Benchmark Workshop on Numerical Analysis of Dams was held on September 24-26 in Bucharest, Romania. This Workshop was the latest in a series of six workshops successfully organized by the ICOLD Ad-Hoc Committee on Computational Aspects of Analysis and Design of Dams and hosted in Bergamo, Italy (1991 and 1992), Paris, France (1994), Madrid, Spain (1996), Denver-Colorado, U.S.A. (1999) and Salzburg, Austria (2001).

Consistent with previous Workshops, three themes were selected for the 7th Benchnmark-Workshop, referring to concrete dams (Theme A), RCC dams (Theme B) and, respectively embankment dams (Theme C). The problems provided for each of that three themes above mentioned were the followings: evaluation of the ultimate strength of gravity dams with curved shape against sliding (formulator: CESI Milan, Italy), thermal analysis of a RCC gravity dam (formulator: Coyne et Bellier Bureau d'Ingénieurs Conseils Genevilliers, France) and seepage through an earth dam - foundation system and piezometric level variation (formulator: Technical University of Civil Engineering, Bucharest, Romania).

ISBN 973-8165-88-1